Nilotinib Efflux and Resistance Development: The Effects of Combination and Concomitant Therapies on the Transport and Efficacy of Nilotinib

Laura Eadie

The Melissa White Laboratory

Centre for Cancer Biology and

SA Pathology

&

The Faculty of Health Sciences

Department of Medicine and

Centre for Personalised Cancer Medicine

The University of Adelaide

South Australia

A thesis submitted to the University of Adelaide

in candidature for the degree of Doctor of Philosophy

March 2013

Table of Contents

Abstract

Chronic myeloid leukaemia (CML) is characterised by the presence of Bcr-Abl tyrosine kinase. Tyrosine kinase inhibitors (TKIs), such as imatinib, and more recently nilotinib and dasatinib, act by specifically binding to the Bcr-Abl kinase domain. The advent of TKIs resulted in significantly improved treatment outcomes for the majority of patients with CML. However, the focus is now customised treatment regimes employing drug combinations to reduce resistance development and maximise treatment outcomes. The present study investigated the interaction of nilotinib with efflux transporters and 1) assessed how concomitant administration of additional drugs may enhance the effects of nilotinib in patients and 2) how altered expression or inhibition of these transporters affected nilotinib transport and function. Secondly, *in vitro* cell line models of nilotinib resistance were generated in order to replicate modes of nilotinib resistance *in vivo*.

The reported relationship between nilotinib and efflux transporters ABCB1 and ABCG2 is conflicting and nilotinib has previously been reported to inhibit the function of OCT-1. Thus, in order to resolve conjecture, a novel approach was employed to determine the effect of ABCB1/ABCG2 inhibition on nilotinib-mediated Bcr-Abl kinase inhibition. Results demonstrated ABCB1-mediated nilotinib transport was concentration dependent: transport of nilotinib occurred at low concentrations whereas inhibition of both ABCB1 and ABCG2 occurred at high nilotinib concentrations. Additionally, data demonstrated nilotinib had no inhibitory effect on the functional activity of OCT-1 but may reduce intracellular imatinib concentrations by impairing passive influx.

Bcr-Abl dependent modes of resistance relating to kinase domain mutations and Bcr-Abl overexpression are well documented. The mechanisms underlying Lyn-mediated resistance however, require further investigation and Bcr-Abl-independent resistance is even more poorly understood. Accordingly, *in vitro* cell line models of nilotinib resistance were developed. ABCB1 overexpression was consistently

demonstrated as the initiator of nilotinib resistance in all cell lines, however, both Bcr-Abl dependent and Bcr-Abl independent resistance mechanisms were subsequently observed. These results suggest determination of ABCB1 expression levels at diagnosis and 3 months post-therapy, for example, may predict resistance in patients. Furthermore, this is the first reported nilotinib resistant, genuine Bcr-Abl independent cell line model and may provide insight into unexplained TKI resistance observed in patients.

Additionally, both nilotinib resistant cell lines demonstrated ABCC6 overexpression suggesting this transporter may play a role in nilotinib resistance *in vitro*. Further investigation in patient mononuclear cells confirmed nilotinib as a likely substrate of ABCC6. This is the first report of ABCC6 involvement in nilotinib transport and concomitant administration of ABCC6 inhibitors may present an attractive option to enhance TKI efficacy and prevent resistance.

Findings detailed in this thesis may assist in developing new therapeutic strategies using TKIs in combination with other medications in order to enhance the intracellular concentrations of TKI. Additionally, further insight into the modes of resistance to nilotinib, as well as the kinetics of resistance emergence, may assist in identifying patients at risk of developing resistance to TKIs. Finally, ABCB1/ABCC6 mRNA expression levels in *de novo* CML patients at diagnosis may present a novel technique for predicting response to nilotinib at 12 months.

Declaration

I, Laura Eadie, certify that this thesis contains no material which has been accepted for the award of any other degree or diploma in any university or other tertiary institution and, to the best of my knowledge and belief, contains no material previously published or written by another person, except where due reference has been made in the text.

I give consent for this copy of my thesis, when deposited in the University Library, to be available for loan and photocopying, subject to the provisions of the Copyright Act 1968.

I also give permission for the digital version of my thesis to be made available on the web via the University's digital research repository, the Library catalogue, the Australasian Digital Theses Program (ADTP) and also through web search engines, unless permission has been granted by the University to restrict access for a period of time.

Laura Eadie

23rd March 2013

Publications

Manuscripts

Eadie LN, Saunders VA, Hughes TP, White DL. 2013. Degree of kinase inhibition achieved *in vitro* by imatinib and nilotinib is decreased by high levels of ABCB1 but not ABCG2. *Leukemia and Lymphoma*, 54 (3): 569-578. Impact factor: 2.580.

Eadie L, Hughes TP, White DL. 2010. Nilotinib does not significantly reduce imatinib OCT-1 activity in either cell lines or primary CML cells. *Leukemia*, 24 (4): 855-857. Impact factor: 9.561.

Conference Abstracts

Eadie L, Hughes T, White D. New TKI transporter identified that may contribute to nilotinib resistance *in vitro*. *HAA Annual Scientific Meeting*, October 2012. Melbourne, VIC. Oral presentation.

Eadie L, Hughes T, White D. New TKI transporter identified that may contribute to nilotinib resistance *in vitro*. *Postgraduate Research Conference in the Faculty of Health Sciences*, August 2012. Adelaide, SA. Poster presentation.

Eadie L, Hughes T, White D. ABCB1 and Src kinase overexpression may facilitate additional mechanisms of resistance in CML cells treated with nilotinib. *New Directions in Leukaemia Research,* March 2012. Sunshine Coast, QLD. Poster presentation.

Eadie L, Hughes TP, White DL. ABCB1 overexpression may facilitate additional mechanisms of resistance in CML cells treated with nilotinib. *Annual Meeting of the American Society of Hematology*, December 2011. San Diego, California. Online publication.

Eadie L, Hughes T, White D. Bcr-Abl dependent and independent mechanisms of resistance to nilotinib are observed in CML cell lines. *HAA Annual Scientific Meeting*, October 2011. Sydney, NSW. Oral presentation.

Eadie L, Hughes T, White D. Bcr-Abl dependent and independent mechanisms of resistance to nilotinib are observed in CML cell lines. *Postgraduate Research Conference in the Faculty of Health Sciences*, August 2011. Adelaide, SA. Poster presentation.

Eadie L, Saunders V, Hughes, T, White, D. The role of ABCB1 in the transport of nilotinib in CML. *HAA Annual Scientific Meeting*, October 2010. Auckland, New Zealand. Oral presentation.

Eadie L, Saunders V, Hughes T, White D. The role of ABCB1 in the transport of nilotinib in CML. *Postgraduate Research Conference in the Faculty of Health Sciences*, September 2010. Adelaide, SA. Poster presentation.

Eadie L, Saunders V, Hughes T, White D. The role of ABCB1 and ABCG2 in the transport of nilotinib in CML. *New Directions in Leukaemia* Research, March 2010. Sunshine Coast, QLD. Poster presentation.

Scholarships and Awards

Non-Member Travel Grant, HSANZ, 2010–2011

Support for non-members to attend the annual HSANZ conference. Awarded on the basis of submitted abstracts entitled: 'The role of ABCB1 in the transport of nilotinib'; Auckland, New Zealand; 2010 and 'Bcr-Abl dependent and independent mechanisms of resistance to nilotinib are observed in CML cell lines'; Sydney, NSW; 2011.

New Scientist Award for Science and Technology in Society, Golden Key International Honour Society, 2010

One grant was awarded to members from Golden Key chapters Australia and New-Zealand wide, based on academic achievement and submission of an essay analysing and describing how science and technology can have a positive effect on the applicant's area of study.

PhD Scholarship, The Leukaemia Foundation of Australia, 2009–2012

Support for the educational and professional development of researchers and other professionals undertaking a PhD. The award is to support research in Australia into the causes, treatment and care of people with leukaemia, lymphoma, myeloma and related blood disorders and is awarded on the merits of the applicant and project proposal.

Baillieu Supplementary Research Scholarship, Repatriation Fund (Baillieu Gift), 2009–2012

One scholarship is awarded per annum to the highest ranking candidate from the disciplines of medicine, law, commerce, economics or architecture to further support students in receipt of a primary PhD scholarship.

Dawes Top-Up Scholarship, RAH/IMVS Research Committee, 2009–2012

Top-up scholarships are awarded to applicants in receipt of a major external scholarship based on merit and research proposal.

Biomedical Postgraduate Scholarship, NHMRC, 2009

Unable to accept due to acceptance of LFA primary scholarship.

Australian Postgraduate Award, Australian Government, 2009

Unable to accept due to acceptance of LFA primary scholarship.

Abbreviations

µg – Microgram/s

µL – Microlitre/s

µM – Micromolar

7-AAD – 7-Aminoactinomycin D

^{14}C – Carbon-14 radioactive isotope

ABC – ATP Binding Cassette

ACD – Acid Citrate Dextrose Acid

ADME-Tox – Absorption-Distribution-Metabolism-Excretion-Toxicity

AGP – α1 acid glycoprotein

ALL – Acute Lymphoblastic Leukaemia

-AP – Alkaline Phosphatase Conjugated Antibody

AP – Accelerated Phase

APS – Ammonium Persulfate

Ara-C – Arabinofuranosyl Cytidine

ATCC – American Type Tissue Culture Collection

ATP – Adenosine Triphosphate

AZT – Azathioprine

BC – Blast Crisis

BCR-ABL – Breakpoint Cluster Region-Abelson (mRNA)

Bcr-Abl – Breakpoint Cluster Region-Abelson (protein)

BCRP – Breast Cancer Resistance Protein

BM – Bone Marrow

B-P – BODIPY-prazosin

BSA – Bovine Serum Albumin

CCyR – Complete Cytogenetic Remission

cDNA – Complementary DNA

CHR – Complete Haematological Response

CML – Chronic Myeloid Leukaemia

CNS – Central Nervous System

CP –Chronic Phase

CrkI – C1T10 regulator of kinase like

Ct – Cycle Threshold

DAS – Dasatinib

DEPC – Diethylpyrocarbonate

DMEM – Dulbecco's Modified Eagle's Medium

DMSO – Dimethyl Sulphoxide

DNA – Deoxyribonucleic Acid

EDTA – Ethylenediaminetetraacetic Acid

FACS – Fluorescence Activated Cell Sorting

FCS – Foetal Calf Serum

FDA – Food and Drug Administration

g – see rcf

GM-CSFR – Granulocyte Macrophage Colony-Stimulating Factor Receptor

h – Hour/s

HBSS – Hanks Balanced Salt Solution

IC50 – Inhibitory Concentration 50

IFN – Interferon

IM – Imatinib

IUR – Intracellular Uptake and Retention

kD – Kilo Daltons

KD – Kinase Domain

L – Litre/s

M - Molar

MDR – Multidrug Resistance Protein

MFI – Mean Fluorescence Intensity

mg – milligram/s

min – Minutes/s

mL – Millilitre/s

mM – Millimolar

MMR – Major Molecular Response

MNC/s – Mononuclear Cell/s

MQ – Milli-Q

mRNA – messenger RNA

MRP – Multidrug Resistance-Associated Protein

MSR – Membrane Spanning Region

MTX – Methotrexate

MW – Molecular Weight

ND – Not Determined

NEG – Negative Expression Levels

ng – Nanogram/s

NIL – Nilotinib

nM – Nanomolar

OCT-1 – Organic Cation Transporter 1

p- – Phosphorylated Form of Protein

PAGE – Polyacrylamide Gel Electrophoresis

PB – Peripheral Blood

PBMNC/s – Peripheral Blood Mononuclear Cell/s

PBS – Phosphate Buffered Saline

PDGFR – Platelet-Derived Growth Factor Receptor

PE – Phycoerythrin

P-gp – P-Glycoprotein

Ph – Philadelphia Chromosome

P_i – Inorganic Phosphate

PON – Ponatinib

PP – Pantoprazole

PPI/s – Proton Pump Inhibitor/s

PSC – PSC-833

p-value – Probability Value

PVDF – Polyvinylidene Difluoride

rcf – Relative Centrifugal Force

rho-123 – Rhodamine-123

RNA – Ribonucleic Acid

RO – Reverse Osmosis

RQ-PCR – Real Time Quantitative PCR

SD – Standard Deviation

SDS – Sodium Dodecyl Sulphate

sec – second/s

SEM – Standard Error of the Mean

SFK/s – Src Family Kinase/s

SH1/SH2/SH3 – Src Homology Region 1/2/3

S/N – Supernatant

Syk – Spleen Tyrosine Kinase

TBS – Tris Buffered Saline

TBST – Tris Buffered Saline +Tween®20

TKI/s – Tyrosine Kinase Inhibitor/s

TEA – Tetraethylammonium Bromide

TMD – Transmembrane Domain

U/mL – Units Per Millilitre

ver – Verapamil

WCF – White Cell Fluid

Acknowledgements

Undertaking a PhD has single-handedly been the most difficult thing I have ever done in my life. I consider myself a strong person but there have been times during the last four years when I didn't think I would finish. I owe a large part of the fact that I have completed this challenging, often frustrating, yet supremely rewarding journey to a number of people.

Firstly, my supervisors, Tim and Deb, have always been there to offer words of advice and encouragement. Tim, it's great to have a clinician's perspective on data and project direction and your mantra concerning how results will fit into a publication and how we are advancing current knowledge were/will be instrumental both in my PhD as well as in the future. Deb, you are an amazing lady and an invaluable mentor to have. Your unwavering dedication, wisdom, critical appraisals and ability to function on five hours sleep a night have made this thesis possible.

Thanks to past and present members of the Melissa White Lab for providing me with an awesome work environment filled with laughter, nights out (both here and interstate/overseas) and placation (especially concerning one of my numerous rants about missing cutlery in the tearoom!). Special thanks to Bron and Steph for providing me with patient data and persistently chasing up elusive store orders; to Amity and Verity for performing experiments and plying me with chocolate and cake when my stress levels reached critical mass; to Phuong for being a PCR guru and angst sounding-board; to Eva for project and thesis chapter assistance. A special mention must go to Kelvin, whom I consider both a friend and colleague. Hours spent at the bench were so much more enjoyable in your presence (not least of all because of the rockin' playlists you provided). Your happy jigs, J.D-esque reveries and the creepy yet always amusing ways in which you found to scare me, were sorely missed upon your departure.

The PhD journey is so much easier if you have friends who completely understand what you are going through, and I was lucky enough to have two of them! Dance-floor Dale, dwat, Dazzle … so many

laughs, such great memories: the time I think I made you pee in fear a little when I burst out of the cupboard, the time you confessed you would rather be a pretty girl than an ugly boy and the countless times we threw stress balls at each other's heads (sometimes with real malice), form some of my fondest memories of hours spent in the student room. Lisa, what can I say, you are my scientific soul mate. Sometimes I fear we are morphing into the same person, but then I stop and rejoice because, just quietly, how awesome would a Lisa-Laura hybrid be! The involuntary emissions you elicited from me during a good scare, be they vocal or otherwise, the way we are able to speak volumes without uttering a word and the priceless memories made over these last four-odd years will never be forgotten.

I must also make a significant thank-you to the Leukaemia Foundation of Australia, for providing me with a generous scholarship for the duration of my PhD. This scholarship enabled me to attend a large number of prestigious national and international conferences and also eased the financial burden of undertaking full time study while trying to support yourself.

I'm incredibly lucky to have such an amazing group of friends. You guys have been there to share the highs with me, to have a drink with me, dance the night away with me and laugh with me until our faces hurt. You have also distracted me, cooked for me, massaged me, shared a burrito with me and listened to my frustrated ramblings through the lows.

Finally heartfelt thanks to my family. Evonne, you are always on hand to tell me a funny story or send me an inappropriate picture to brighten my day, which was supremely appreciated. Mum and Dad, you guys have also been there for me, in every respect, every step of the way. You have shared in my enthusiasm when I got exciting results (even if you didn't completely understand why I was so excited). You have also been there to pick me up and help keep me going when yet another western blot failed or a supposed conclusive experiment resulted in yet more unanswered questions. I owe a huge part of the perseverance and drive to succeed that resulted in this magnum opus, to you both.

Chapter 1:

Introduction

1.1. Chronic Myeloid Leukaemia (CML)

1.1.1. Philadelphia Chromosome – the Hallmark of CML

CML is a malignant disorder of blood stem cells which is characterised by the presence of the Philadelphia (Ph) chromosome. This small chromosome was first discovered in 1960 by Peter Nowell and David Hungerford. Using a modified method of air-drying metaphase cells cultured on glass[1] this group identified a minute, y-independent chromosome present in all seven cases of CML studied. Interestingly, in most cases, cells possessing normal karyotypes were also observed[2,3]. Concurrent research by a second group confirmed the presence of a CML-specific chromosomal abnormality in cells originating from the bone marrow[4]. Thirteen years after the discovery of the Ph chromosome, Janet Rowely successfully demonstrated the abnormality was due to a reciprocal translocation between the long arms of chromosomes 9 and 22[5]. This balanced translocation results in a fusion oncogene on the Ph chromosome comprising the *ABL* gene from chromosome 9 and the *BCR* gene from chromosome 22[6-8].

1.1.2. The BCR-ABL Fusion Gene gives rise to the Bcr-Abl Oncoprotein

CML comprises approximately one fifth (15–20%) of all leukaemia diagnosed, however it affects a very small percentage of the world's population (249 people/year in Australia). It can affect people from all age groups with the median age of disease onset occurring in the sixth decade[9].

The cytogenetic hallmark of CML is the *BCR-ABL* fusion gene and the resultant Bcr-Abl protein (breakpoint cluster region-Abelson)[10], has constitutively active tyrosine kinase activity. While all CML breakpoints occur within this region[11], the specific point of chromosome breakage differs between CML individuals hence varying sizes of *BCR* are translocated to *ABL*[12]. This results in the inclusion or exclusion of differing exons and the formation of one of four characteristic junctions: e1a2, e13a2, e14a2 or e19a2 (**Figure 1.1**). The specific region in which the breakpoint occurs determines the size of

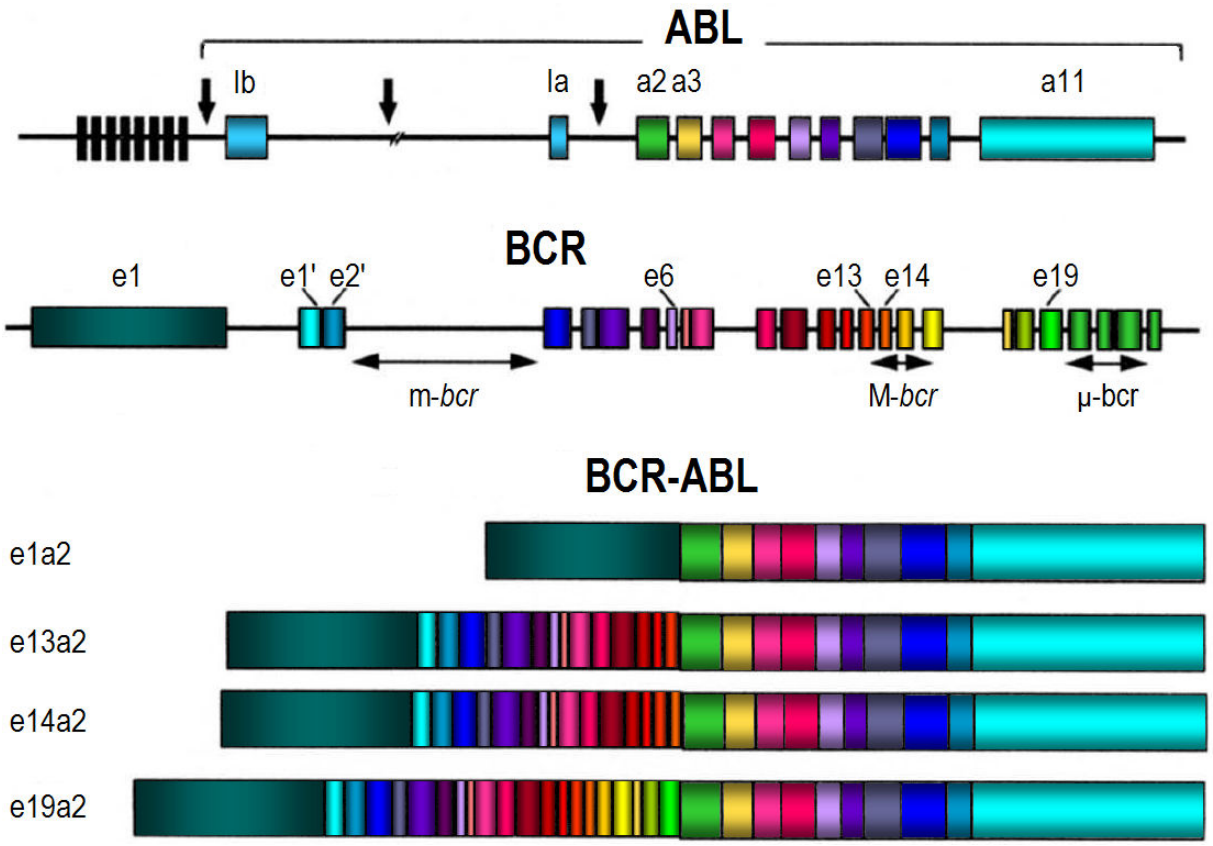

Figure 1.1: Schematic representation of the *BCR-ABL* oncogene (modified from Melo *et al*[13])

Exons are represented by coloured boxes with introns depicted as horizontal lines. The possible breakpoints in *ABL* are denoted by black arrows and although there are several points at which breakage can occur, processing of the transcript results in mRNA of the a2 portion only. The breakpoints in *BCR* occur in three breakpoint cluster regions: m-*bcr*, M-*bcr* and µ-*bcr*. The length of the Bcr-Abl fusion protein is dependent on where the breakpoints occur. Breaks within m-*bcr* result in fusion proteins with an e1a2 junction. Breaks within M-*bcr* result in either e13a2 or e14a2 junctions while breaks in µ-*bcr* form fusion proteins with e19a2 junctions.

Bcr-Abl, with the 210 kDa $p210^{BCR-ABL}$ variant most commonly occurring in CML (**Figure 1.2**). Interestingly, *BCR-ABL* is not found exclusively in CML individuals and may be present in other leukaemias such as Ph+ Acute Lymphoblastic Leukaemia (ALL)[14-18].

1.1.3. $p210^{BCR-ABL}$ – its Role in CML Pathogenesis is due to Increased Tyrosine Kinase Activity

Early *in vitro* experiments in haematopoietic cell lines demonstrated that $p210^{BCR-ABL}$ is both necessary and sufficient for the transformation of bone marrow derived cell lines to lymphoid leukaemic cells[19,20]. This theory was later extended when Daley *et al* showed that the presence of $p210^{BCR-ABL}$ induced a CML-like disease in mice[21] with characteristic splenomegaly and grossly expanded granulocyte population[21,22], a result confirmed by others[23,24]. $p210^{BCR-ABL}$ plays such a critical role in the pathogenesis of CML because of the constitutively active tyrosine kinase it encodes[19,25-27]. Under normal conditions, the Abl protein's nuclear localization and nuclear export signal domains allow migration between nucleus and cytoplasm. However, fusion of *BCR* to *ABL* renders the resultant protein confined to the cytoplasm[27,28]. Here it disrupts numerous signalling pathways critical for normal cellular homeostasis. BCR-ABL has been shown to aberrantly affect cellular signalling via activation of the Ras-ERK, PI3-K/Akt and JAK-STAT pathways[29] (**Figure 1.3**). The increased tyrosine kinase activity leads to unrestricted phosphorylation of tyrosine residues on proteins found in these signal transduction pathways which govern cell proliferation and survival, specifically, growth factor independence and reduced susceptibility to apoptosis[9,30]. Under normal conditions, the Ras pathway reduces cellular proliferation and induces apoptosis, however, in the presence of Bcr-Abl, apoptosis is decreased resulting in accumulation of cells associated with CML[31,32]. The PI3-K/Akt pathway is also affected, as Bcr-Abl indirectly activates PI3-K[33], inducing an Akt signalling cascade leading to the phosphorylation and subsequent activation of other apoptosis related proteins, again reducing apoptosis[34]. Furthermore, Bcr-Abl activates the anti-apoptotic JAK-STAT signalling pathway via directly phosphorylating STAT

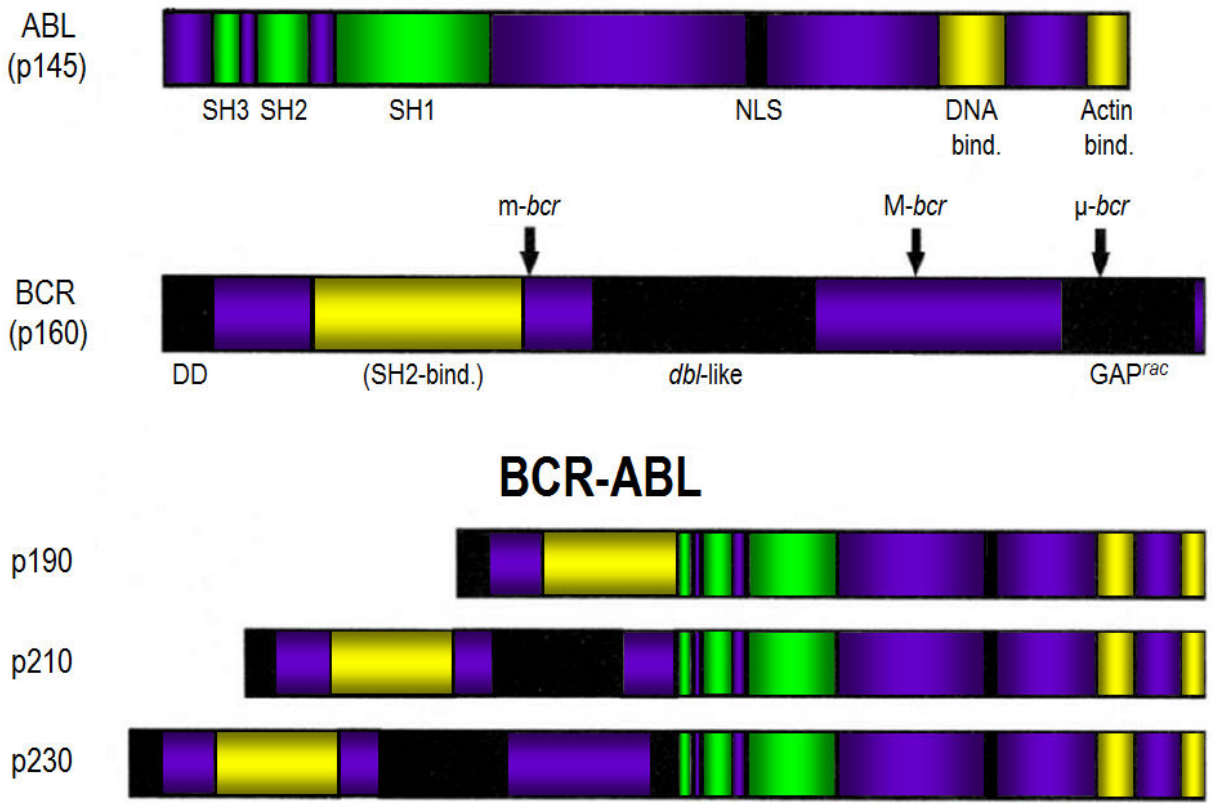

Figure 1.2: Schematic representation of the three major isoforms of the Bcr-Abl oncoprotein (modified from Melo *et al*[13])

The reciprocal translocation of *BCR* and *ABL* genes results in the *BCR-ABL* oncogene. Upon processing, different splicing events give rise to Bcr-Abl proteins of differing lengths and intrinsic tyrosine kinase activity[35]. These Bcr-Abl oncoproteins can consist of three forms depending on where the *BCR* breakpoint occurred: breakages in the m-*bcr* breakpoint region result in the 190 kDa protein $p190^{BCR-ABL}$ which is associated with Ph^{+}ALL[15,17,18]. Breakages in M-*bcr* result in the most common protein $p210^{BCR-ABL}$, associated with CML, while breakages in µ-*bcr* result in the largest protein, the 230 kDa $p230^{BCR-ABL}$ which is associated with chronic neutrophilic leukaemia[14,16].

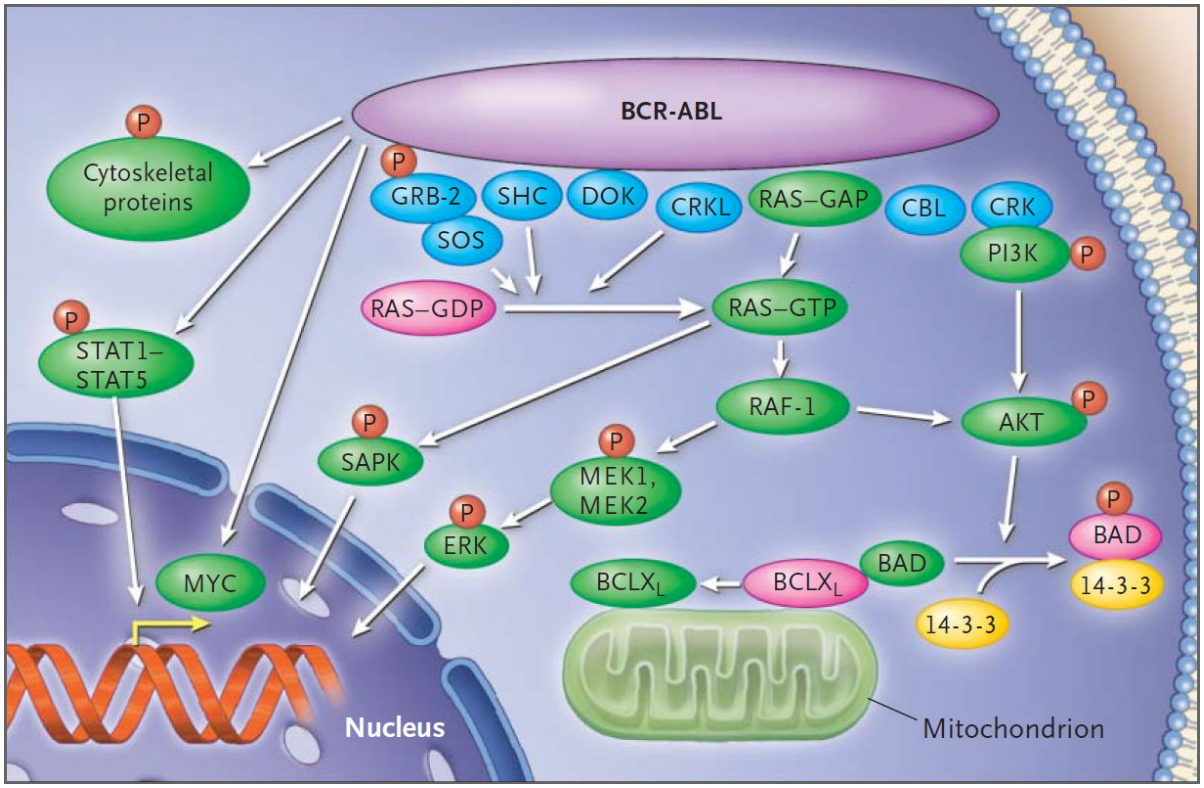

Figure 1.3: Schematic diagram of BCR-ABL signal transduction pathways (Goldman and Melo[36])

Signalling pathways governing cell proliferation and survival are aberrantly activated by BCR-ABL. Key pathways (**GREEN**) include the RAS pathway, the PI-3 kinase pathway and the JAK-STAT pathway. In most instances, BCR-ABL binds to various adaptor proteins (**BLUE**) causing phosphorylation of specific residues (**P**) and subsequent activation.

proteins[34,37,38], specifically, phosphorylation of Stat5 in BCR-ABL expressing cells results in the activation of the anti-apoptotic protein $BCLX_L$[39]. Thus, under the control of Bcr-Abl, and in the subsequent absence of stringent signalling pathway regulation, the myeloid cell population rapidly expands.

However, Bcr-Abl does not only have an effect on cellular signalling, it may also aid the survival of leukaemic cells by influencing cell cycle regulation. CML progenitors appear to cycle more rapidly than their normal counterparts, thus maintaining the primitive population of leukaemic stem cells[9,40-43]. This phenomenon, coupled with reduced apoptosis[30,44] results in leukaemic cells rapidly becoming the dominant cell population.

There is also evidence, from both haematopoietic cell lines as well as CML patients, that Bcr-Abl causes significant post-transcriptional down-regulation of protein complexes involved in DNA repair[45] and surveillance of genome integrity[46-48]. This leads to increased rates of mutation which, when coupled with Bcr-Abl's ability to increase proliferation and reduce apoptosis, results in the survival and replication of cells carrying multiple mutations that further drive the population's expansion[49].

1.1.4. The Haematological Events Associated with Different Phases of CML

CML is tri-phasic in nature consisting of the chronic phase (CP) which, untreated, typically lasts three to six years; the accelerated phase (AP) lasts three to twelve months while the terminal blast crisis (BC) stage generally lasts only a few months before fatal complications develop[9,49,50] (**Figure 1.4**). CP CML is characterised by a massive expansion of the granulocyte population of cells[51]. The myeloid cells retain their ability to differentiate and thus mature normally but due to their growth advantage become the predominant cell population in the bone marrow (BM) and peripheral blood[52]. Transition to AP is marked by an increase in undifferentiated, precursor cells accompanied by resistance to treatment[49,52].

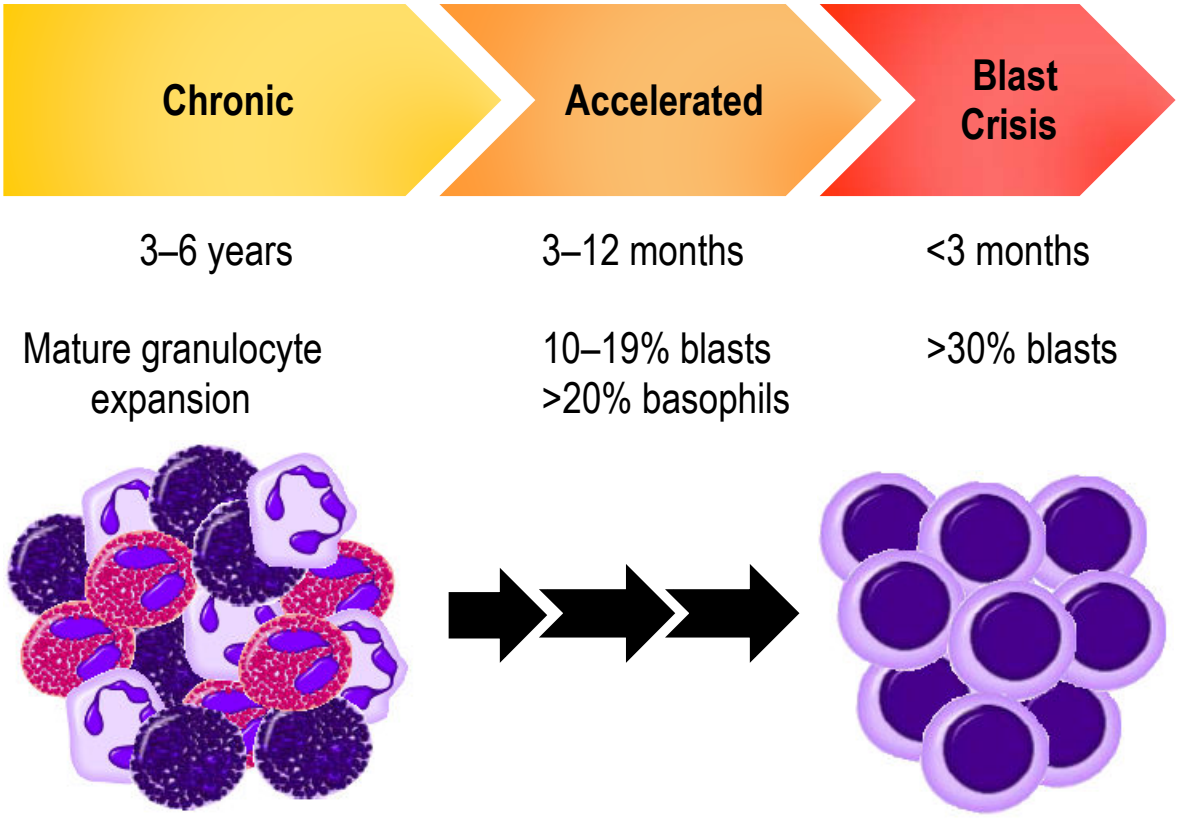

Figure 1.4: Schematic diagram of disease progression in CML

In chronic phase there is a massive expansion of mature granulocytes, mostly neutrophils, basophils and eosinophils. Accelerated phase is marked by an increase in undifferentiated precursor cells. Fatal blast crisis is more representative of an acute leukaemia with a rapid expansion of the immature blast cell population.

Clinically, AP presents with 10-19% myeloblasts in the blood or BM or >20% basophils in BM. The onset of fatal BC results in a substantial and rapid elevation of the number of undifferentiated blast cells[52,53] and more closely resembles an acute leukaemia with >30% blasts in the blood or BM. BC manifests as either myeloid or lymphoid depending on the immunophenotype of the blasts[49].

1.2. Tyrosine Kinase Inhibitors (TKIs)

1.2.1. Development of Imatinib by Novartis Pharmaceuticals

In the late 1980's chemists at Ciba Geigy (now Novartis Pharmaceuticals) began investigating compounds with inhibitory activity against Abl tyrosine kinases. Imatinib mesylate (formerly CGP57148; STI571, Glivec; **Figure 1.5**), acts by competing with ATP for the ATP-binding pocket present in the Bcr-Abl kinase domain (KD)[54] and was found to inhibit proliferation of the Abl tyrosine kinases Bcr-Abl, c-abl and v-abl in cell lines, with IC50 values in the low micromolar range[55-57]. Imatinib also has activity against platelet-derived growth factor receptor (PDGFR), c-kit[58,59], c-fms[60] and ARG[61] as well as the fusion proteins TEL-Abl and TEL-PDGFR[56] without affecting other kinases. Elucidation of the crystal structure of the c-abl-imatinib binding complex revealed that imatinib competitively binds to the inactive conformation of Bcr- Abl preventing ATP from binding and 'freezing' the kinase in this inactive form [62,63]. Following promising results both *in vitro*[57,64,65] and *in vivo*[55,57] imatinib entered Phase I clinical trials.

1.2.2. The Establishment of Imatinib Efficacy in Human CML Patients: Phase I, II and III Clinical Trials

Early experiments in nude mice, investigating the *in vivo* pharmacokinetic inhibition profile of imatinib, demonstrated the need for continuous kinase inhibition[66]. Phase I dose-escalating studies determined the maximally tolerated dose in CP CML patients who had failed previous treatment with interferon (IFN)[67]. No maximally tolerated dose was identified with the most common side effects being nausea, edema, diarrhoea and fatigue with thrombocytopenia and neutropenia in those patients receiving higher

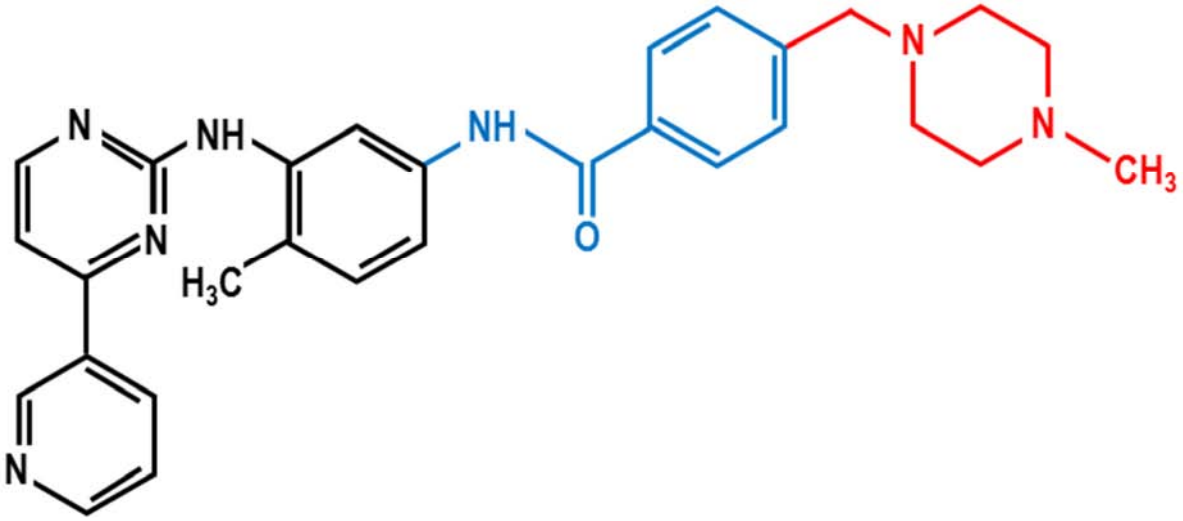

Figure 1.5: The chemical structure of imatinib (modified from Melo *et al*[68])

Following identification of compounds with inhibitory activity against protein kinases, researchers at Ciba Geigy (now Novartis Pharmaceuticals) increased specificity via the addition of a benzamide group (**BLUE**) and improved solubility and bioavailability via adding the N-methylpiperazine (**RED**) group[69]. The resultant molecule, later labelled imatinib, had high specificity for Abl kinase-expressing cells and entered clinical trials for the treatment of CML.

doses[67]. These promising results led to expansion of the study to patients with BC CML and relapsed Ph+ ALL[70] and established the efficacy of imatinib in patients with all phases of disease. Phase II trials confirmed results seen in Phase I[71-74], while results from the highly successful Phase III IRIS trial[75-77](International Randomized Study of Interferon and STI571) led to approval by the Food and Drug Administration (FDA) in 2001, for the use of imatinib as first line therapy in the treatment of patients with all phases of *de novo* CML as well as Ph+ ALL and CML patients who had previously failed IFN therapy[78].

1.2.3. Dasatinib is Over 300 Times More Potent than Imatinib

Second generation TKIs were developed to combat the emergence of imatinib resistant KD mutations and were vastly more effective than imatinib at neutralising Bcr-Abl due to the much greater affinity with which they bound the KD. The first of these compounds, dasatinib (BMS-354825, Sprycel), was developed by Bristol Myers Squibb and functions as a dual ABL/Src kinase inhibitor[79,80] with a potency ~325 fold greater than that of imatinib against leukaemic cells expressing wild-type Bcr-Abl[81] (**Figure 1.6**). Experimental evidence from crystallographic structures[43,82] and solution conformations of the KD-dasatinib complex[82] indicate dasatinib binds the active conformation of Bcr-Abl. Because the active conformation has less stringent binding requirements than the inactive conformation to which imatinib binds, dasatinib is active against many imatinib resistant KD mutations tested *in vitro*[81,83]. Interactions between dasatinib and the highly conserved P-loop region of the Bcr-Abl KD (detailed further in **Section 1.3.2**) are not as critical as for imatinib, further explaining dasatinib's superior activity profile. One notable exception is the T315I mutation, necessary for the formation of a critical hydrogen bond between dasatinib and Bcr-Abl KD[43]. A follow up *in vivo* murine model of disease confirmed *in vitro* results[83] while clinical trials showed dasatinib exhibits superior responses to imatinib as both a first line treatment in CP CML[84] as well as being a safe and effective treatment option for all phases of CML in patients who have failed first line imatinib therapy[85-90].

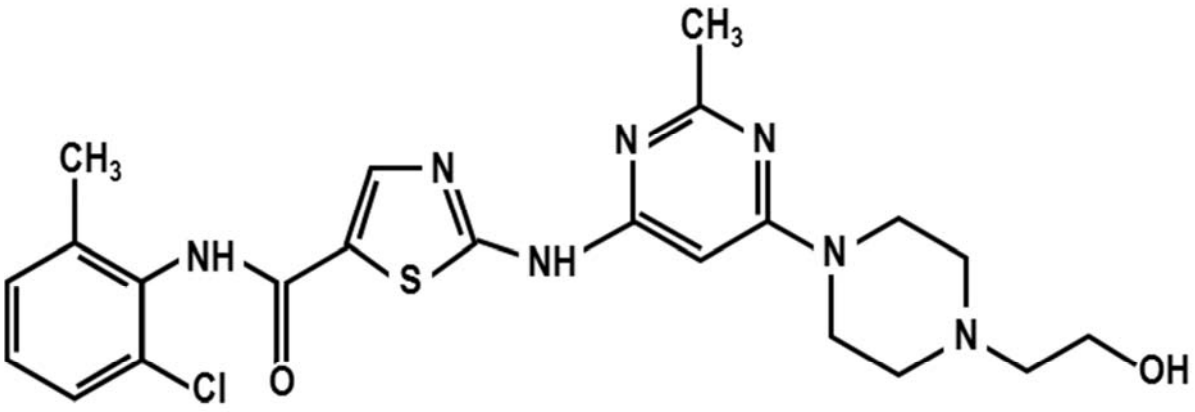

Figure 1.6: The chemical structure of dasatinib (modified from Melo *et al*[68])

Dasatinib binds to and inhibits the active conformation of the Bcr-Abl KD, Src family kinases including Src, Hck, Lyn, Fyn as well as c-kit and PDGF receptor β[91].

1.2.4. Nilotinib is at Least 20 Times More Potent than Imatinib

Novartis Pharmaceuticals developed nilotinib (AMN107, Tasigna) based on the crystal structure of the imatinib-KD complex. Nilotinib is an imatinib derivative and was designed to bind to the Bcr-Abl KD with significantly greater affinity, while still binding the inactive conformation[82,92], via the alteration of particular side groups present on the imatinib molecule[93] (**Figure 1.7**). These side groups give nilotinib a much greater potency than imatinib whilst reducing the number of hydrogen bonds needed for effective engagement of the KD binding pocket[92]. Experimentation *in vitro* found that nilotinib's antiproliferative activity was up to 60 times greater than that of imatinib when used to inhibit imatinib-sensitive cell lines, and at least 20 times greater in imatinib-resistant cell lines (T315I mutation excluded)[92,94]. Nilotinib also has significant anti-proliferative activity against many imatinib-resistant mutations studied *in vitro*[81,92] with subsequent *in vivo* testing confirming these results[92]. The ensuing clinical trials determined nilotinib had a significantly favourable rate of response, disease free progression and overall survival when used to treat patients with many imatinib resistant mutations[89,95-100]. As such, nilotinib received FDA approval in 2011 for use in CP CML patients as a front line therapy option as well as in CP and AP individuals who have failed first line imatinib therapy[101].

1.3. Resistance to TKIs can be Attributed to Numerous Factors

1.3.1. Primary and Secondary Resistance

The use of TKIs has resulted in excellent responses in the majority of CML patients. However, an estimated 20–40% of patients treated with first line imatinib therapy will exhibit primary or secondary resistance[102,103]. Primary resistance occurs when a patient fails to achieve a landmark response in a certain time frame[104], whereas secondary resistance occurs when a previously responsive patient loses response to treatment; progression to a more advanced stage of the disease may also occur[69,105]. More recently, resistance to the second generation TKIs has also been observed. Acquired resistance to TKIs has been investigated in cells lines as well as cells from CML and Ph^+ ALL patients, and most

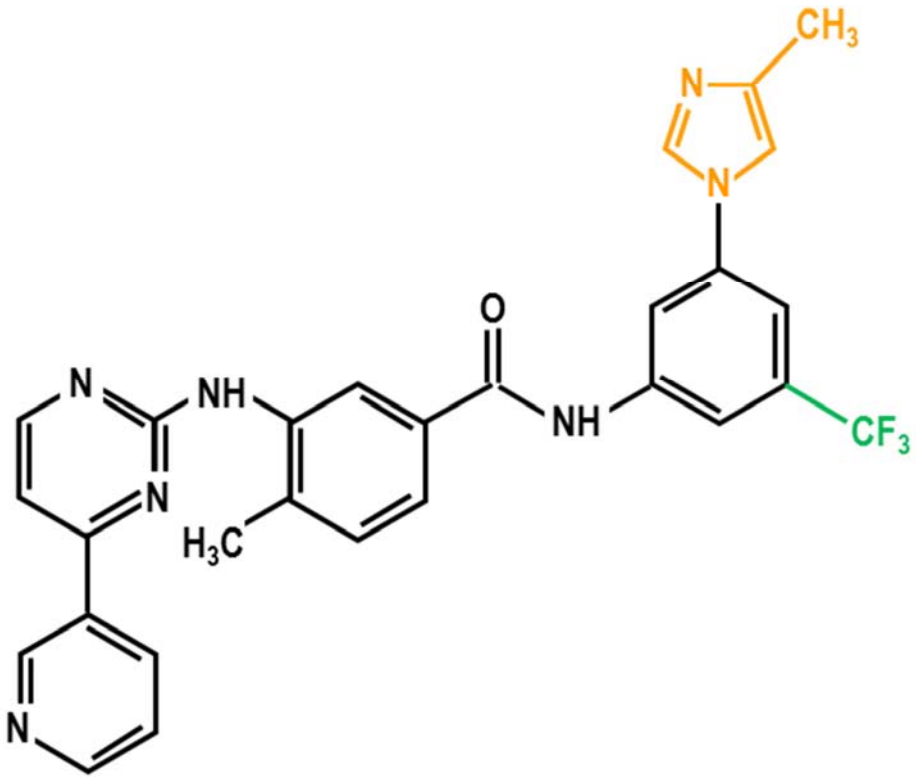

Figure 1.7: The chemical structure of nilotinib (modified from Melo *et al*[68])

Nilotinib binds the inactive conformation of the Bcr-Abl KD, as does imatinib, and while the two TKIs are structurally similar, nilotinib differs in the substitution of the piperazine ring with a trifluoromethyl/ imidazole phenyl moiety (**GREEN**/**ORANGE**) which results in a much greater potency and better topological fit of nilotinib into the KD binding pocket[92].

commonly occurs due to mutation of the Bcr-Abl KD[106-110] and amplification of BCR-ABL[107-109,111-113] at both the genomic and transcript levels. However, resistance to TKIs is a multifactorial process with reductions in bioavailability likely to be a key component of resistance development. Because TKIs are administered orally, variations in gastrointestinal absorption, increased metabolism by the liver and increased sequestration by α1 acid glycoprotein in the plasma have all been attributed to reduced TKI concentrations which may lead to resistance[114]. Resistance may also develop due to events occurring at the cellular level: alterations in expression of cellular proteins can reduce intracellular TKI concentrations as well as activate alternative signalling pathways governing proliferation and survival. Increased expression of drug efflux transporters such as ABCB1 and ABCG2 has been observed during development of resistance *in vitro*[107,111,115-118]; overexpression of Src and other tyrosine kinases[116,119-128] have been observed in imatinib and nilotinib resistant cells; and Bcr-Abl independent mechanisms of resistance[129] have also been described (**Figure 1.8**).

1.3.2. Mutations to the Bcr-Abl Kinase Domain Prevent TKI Binding

Because TKIs bind to the Bcr-Abl KD, interacting in a highly specific manner with a small number of amino acids[62,63], mutations to the KD can either sterically hinder this interaction or prevent the kinase from adopting the conformation necessary for effective TKI binding. Sequencing *BCR-ABL* from patients with secondary imatinib resistance demonstrated that these mutations occur in four distinct clusters within the KD: the ATP-binding (P-) loop, at amino acids T315 and M351 (the catalytic domain) and at the activation (A-) loop[108,131-133] (**Figure 1.9**). Importantly, with the exception of the T315I 'gatekeeper' mutation, the KD mutation profiles for nilotinib and dasatinib are distinct, thus allowing patients who develop a KD mutation while on imatinib therapy the option of subsequent treatment with an alternative second generation TKI (**Figure 1.10**).

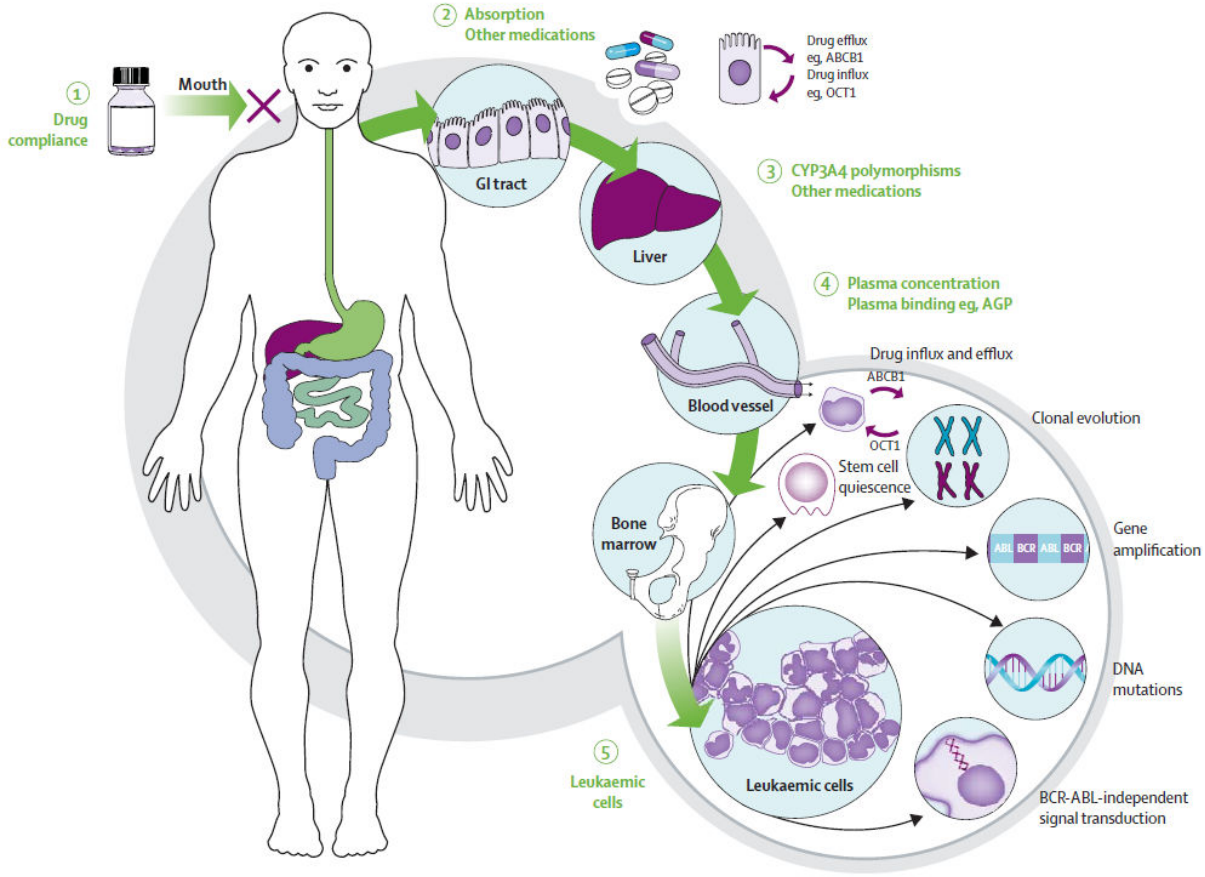

Figure 1.8: Mechanisms of TKI resistance (Apperley[130])

Reduced oral bioavailability, caused by poor compliance, reduced gastrointestinal absorption, increased drug metabolism or binding of TKI by α1 acid glycoprotein in the plasma can lead to lowered concentrations of TKIs available for inhibition of leukaemic cell proliferation. This can result in acquired resistance to TKIs which most commonly occurs due to mutation of the Bcr-Abl KD and amplification of BCR-ABL. However, resistance has also been attributed to increased expression of drug efflux transporters, overexpression of Src and other tyrosine kinases, and more recently, Bcr-Abl independent mechanisms of resistance.

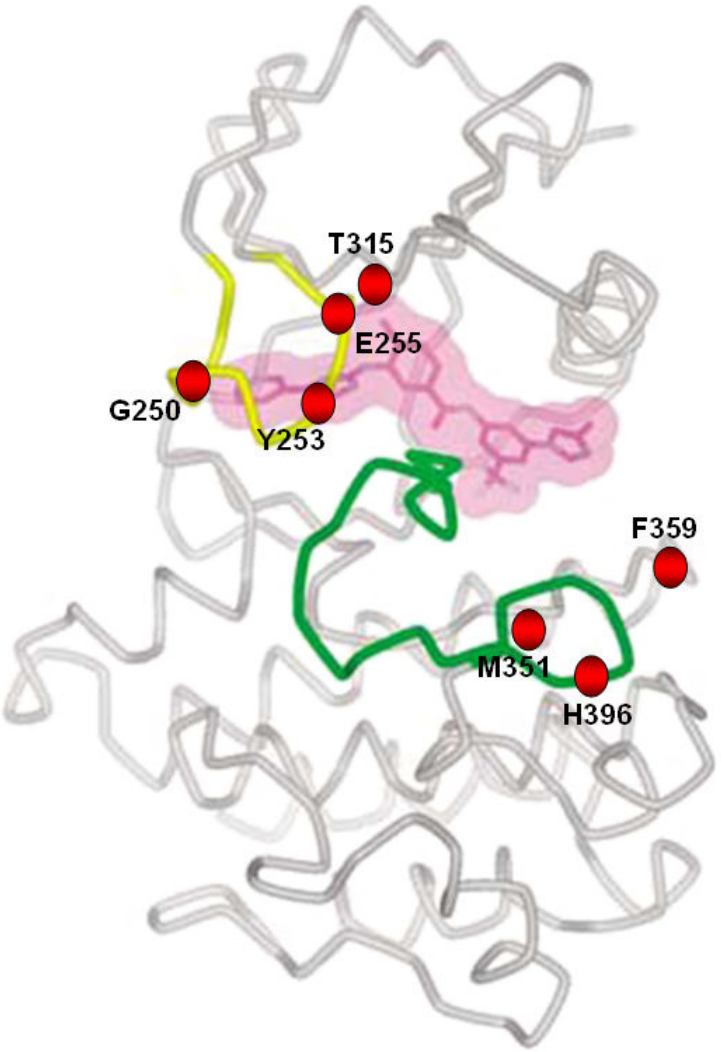

Figure 1.9: The crystal structure of the Bcr-Abl KD with imatinib and common mutations superimposed (modified from Schindler *et al*[63])

Following elucidation of Abl's crystal structure[63] (shown here in complex with imatinib (**PINK**)), point mutations detected in patients were assigned to regions of Bcr-Abl. The seven most common mutations conferring imatinib resistance, depicted in **RED**, cluster in four distinct regions of the KD: P-loop (**YELLOW**) mutations (G250, Y253, E255) affect the induced fit conformation required for satisfactory imatinib binding[136]. Mutations to amino acid T315 abrogate binding of imatinib to Bcr-Abl via disruption of a critical hydrogen bond[63]. Mutations altering amino acids in the catalytic domain (M351, F359) and the A-loop (**GREEN**; H396), prevent Bcr-Abl from adopting the inactive confirmation necessary for effective imatinib binding[69,137].

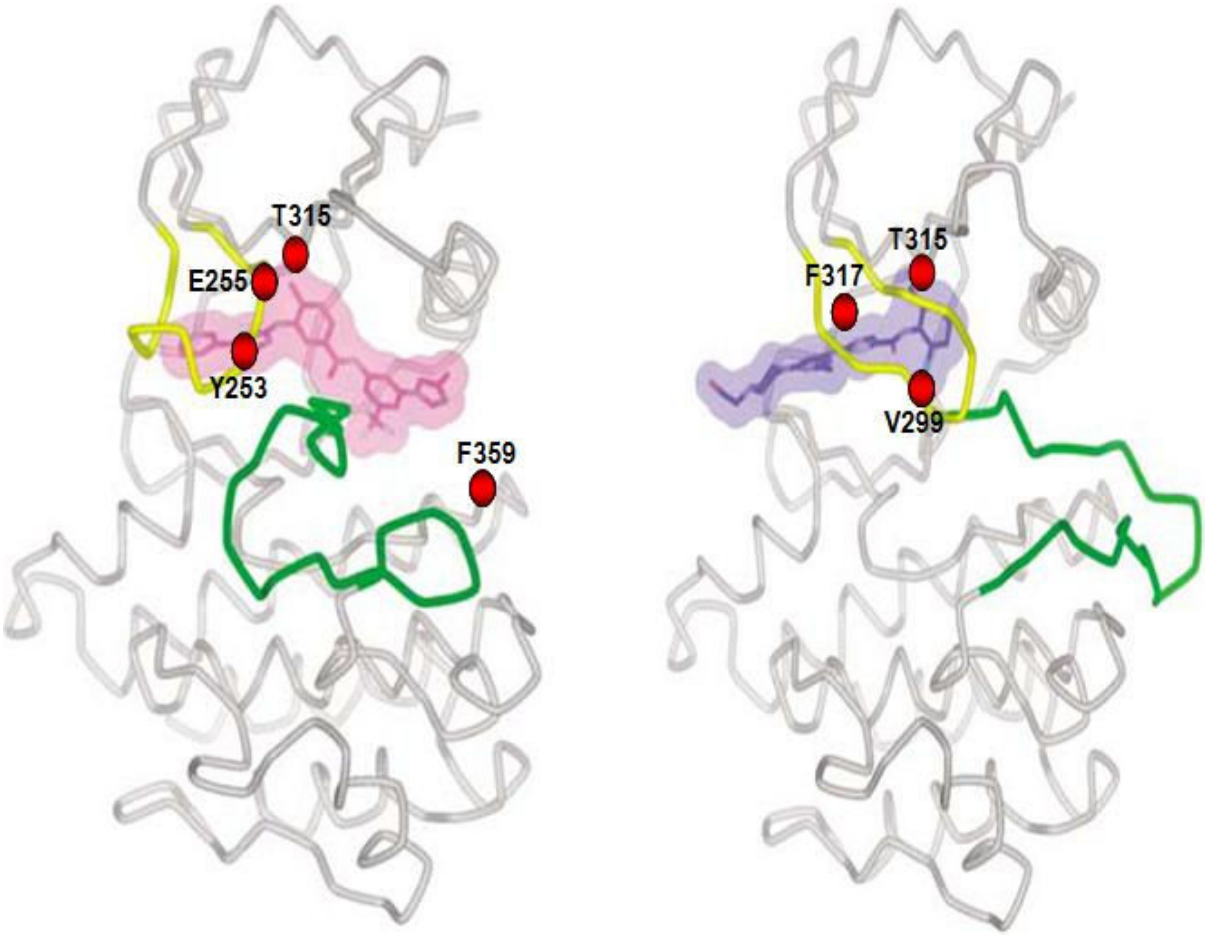

Figure 1.10: The crystal structure of the Bcr-Abl KD with nilotinib and dasatinib and common mutations superimposed (used with permission from Susan Branford)

Nilotinib (**PINK**) binds the inactive conformation of Bcr-Abl while dasatinib (**PURPLE**) binds the active conformation. The most common mutations conferring resistance to each of the TKIs are depicted in **RED**, and with the exception of the T315I mutation, nilotinib and dasatinib have unique mutation profiles.

1.3.3. BCR-ABL Over-Expression

Amplification of the *BCR-ABL* gene, as well as increased expression of Bcr-Abl mRNA transcript, have been demonstrated in both cell lines[107,111,112] and patient cells[108,109,113] resistant to TKIs. It has been hypothesised that an increase in *BCR-ABL* may function as an initial resistance mechanism destabilising the leukaemic cell, thus rendering it susceptible to further damage including KD mutations. Indeed, we have observed overexpression of Bcr-Abl prior to emergence of KD mutations in cell lines resistant to imatinib or dasatinib[107]. This phenomenon has also been noted by others in BC patient cells[109] and cell lines[134]. Conversely, a study in patient progenitor cells, suggests that while increased levels of Bcr-Abl result in increased proliferation and anti-apoptotic signalling, there is no direct effect on imatinib resistance[135], however, evidence for the former notion exceeds that of the latter.

1.3.4. Altered Expression of Drug Efflux Transporters

There is mounting *in vitro* evidence that increased expression of the multidrug resistance protein 1 (MDR1, ABCB1), a cellular efflux pump, leads to decreased intracellular concentrations of imatinib and hence, it has been a suggested mechanism of imatinib resistance. Over-expression of ABCB1 in cell lines resulted in decreased intracellular availability and concentration of imatinib *in vitro*[107,111,115,118,138-140]. Furthermore, increased ABCB1 expression has been observed during development of imatinib resistance in Bcr-Abl positive cell lines[107,111]. However, some conflicting results have been reported with two other studies concluding ABCB1 overexpression confers only minimal resistance to imatinib[141,142]. One possible explanation for this is the large variation in intrinsic imatinib sensitivity of the cell lines utilised in each study. Further confounding this issue is the fact that ABCB1 overexpression was not observed upon analysis of primary BC patient cells[115], although the cohort examined was extremely small. Additionally, neither up-regulation of MDR1 gene nor protein expression was observed in a follow-up *in vivo* study[143]. The contentious nature of these observations remains when MDR1 expression at the blood brain barrier is taken into consideration. *In vivo*

experiments have demonstrated that mdr1a/b (-/-) knockout mice have greater CNS penetration of imatinib when compared with their wildtype counterparts[144,145] thus lending further weight to the argument for over-expression of MDR1 influencing imatinib resistance.

A further study has suggested that over-expression of another common efflux pump, the breast cancer resistance protein (BCRP, ABCG2), can facilitate imatinib resistance in cell lines expressing this transporter[146]. These results further support the notion that drug transporters affect imatinib resistance. In addition to over-expression of efflux transporters, altered expression of the human Organic Cation Transporter 1 (OCT-1) – the major imatinib influx transporter[147] – has also been implicated in imatinib resistance. It has previously been demonstrated that OCT-1 expression is predictive of patient outcome, where those patients with high OCT-1 expression achieve superior imatinib-treatment outcomes[148] and those with low levels of OCT-1 expression respond poorly to treatment[149]. However, our laboratory has shown that OCT-1 activity, rather than expression, is a strong determinant for patient response[150-152]. Patients with low OCT-1 activity fail to achieve treatment milestones, have significantly lower overall survival, as well as event-free survival, and also have a greater chance of developing KD mutations[151]. Thus, while there is consensus for influx of imatinib by OCT-1 and efflux by MDR1, less is known about the interactions of the second generation TKIs with cellular transporters. Recent *in vitro* data has highlighted the importance of drug transporters in the efflux of nilotinib from leukemic cells[153-155] with one study postulating overexpression of MDR1 may contribute to nilotinib resistance[116]. However, reports are conflicting, and the TKI:transporter interactions complicated, hence additional investigations are warranted and further explored and discussed in this thesis (**Chapter 4**).

1.3.5. Over-Expression of Src Family Kinases and other Tyrosine Kinases

The Src family of non-receptor tyrosine kinases consists of the following nine members: Blk, Fgr, Fyn, Hck, Lck, Lyn, Src, Yes and Yrk[156]. Hck and Lyn have been shown to interact with and phosphorylate

Bcr-Abl and have thus been postulated to play a role in Bcr-Abl driven leukaemogenesis[157-159]. More recently it has been suggested that active Hck, Lyn and Fyn are all capable of phosphorylating Bcr-Abl at the SH3-SH2 region of Abl and in doing so hold the kinase domain in its active conformation[123,160]. Increased phosphorylation of Hck and Lyn, as well as overexpression at the mRNA and protein levels, have previously been implicated in resistance to imatinib, nilotinib and dasatinib. Increased expression and activation of Hck and Lyn have been observed in imatinib resistant cell lines[120,121,123,125,128] and those patients who have failed imatinib[121,123,125,161] and dasatinib therapy[161]. More recently, increased Lyn phosphorylation[122,124] and overexpression of Lyn mRNA and protein have also been suggested as a resistance mechanism to nilotinib in both patients[116] and cell lines[116,122].

AXL is a receptor tyrosine kinase that was originally identified in myeloid leukaemia cells[162] and overexpression of mRNA and protein, as well as increased phosphorylation, have been observed in nilotinib resistant patients[126] and cell lines[119,126,127]. Immunoprecipitation assays have recently suggested AXL belongs to a ternary complex with Lyn and Syk which undergoes increased tyrosine phosphorylation in nilotinib resistant cells[126].

A third family of proteins, the Cbl ubiquitin ligases, of which c-Cbl is a member, were originally implicated in acute myeloid leukaemia pathogenesis[163,164]. c-Cbl has been demonstrated to interact with Abl[165] as well as Fyn, Syk[166] and Hck[167], and recently the role of c-Cbl in CML has been investigated yielding preliminary evidence for its involvement in Lyn- and Axl-mediated nilotinib resistance[168].

1.3.6. Direct Versus Indirect Resistance

α1 acid glycoprotein (AGP), a plasma protein, has previously been demonstrated to tightly bind imatinib thus reducing the concentration of drug available for dissemination to the tissues where it exerts its

activity[114]. Co-administration of compounds that compete with imatinib for AGP binding, significantly reduce *in vitro* cell proliferation and *in vivo* disease progression[114] however, it is unlikely AGP is directly responsible for imatinib resistance[169]. Instead, AGP most likely lowers the concentration of imatinib available to leukaemic cells leading to inadequate growth inhibition, disease progression and the emergence of additional mutations which render the patient imatinib-resistant[114,169]. AGP may also play a pivotal role in determining intracellular TKI concentrations. This is particularly evident in the case of nilotinib where, despite its increased potency, this TKI fails to achieve sufficiently high intracellular levels to overcome mutations predicted to be sensitive to this agent. Current nilotinib dosing regimens produce plasma concentrations between 2 μM and 4 μM (steady state trough and peak levels respectively)[170]. However, these levels do not appear to correlate with intracellular drug concentrations given that clinical studies show nilotinib resistant patients harbour mutations[171] with IC50 values predicted to be in the low nanomolar range[81]. Furthermore, when kinase inhibition in patient cells following initiation of nilotinib therapy was correlated with their $IC50^{NIL}$ gradient, we observed substantial kinase inhibition in the presence of sub 150 nM nilotinib. Hence the concentration of intracellular nilotinib required to effectively inhibit Bcr-Abl is significantly lower than steady-state plasma levels. Conversely, imatinib plasma levels are reflective of intracellular drug concentrations, and thus it would be appropriate to explore and compare the *in vivo* kinase inhibition observed in patients receiving up front imatinib versus nilotinib.

1.4. Cellular Transport of TKIs

1.4.1. ATP-Binding Cassette (ABC) Transporter Superfamily

The ABC superfamily contains 49 members which can be grouped into seven smaller subgroups: ABCA–ABCG[172]. In order to be functionally active, ABC transporters must contain at minimum, two cytoplasmic ATP binding domains, which bind and hydrolyse ATP, as well as two trans-membrane domains which interact with the substrate as it crosses the lipid bilayer[172] (**Figure 1.11**). Some of the

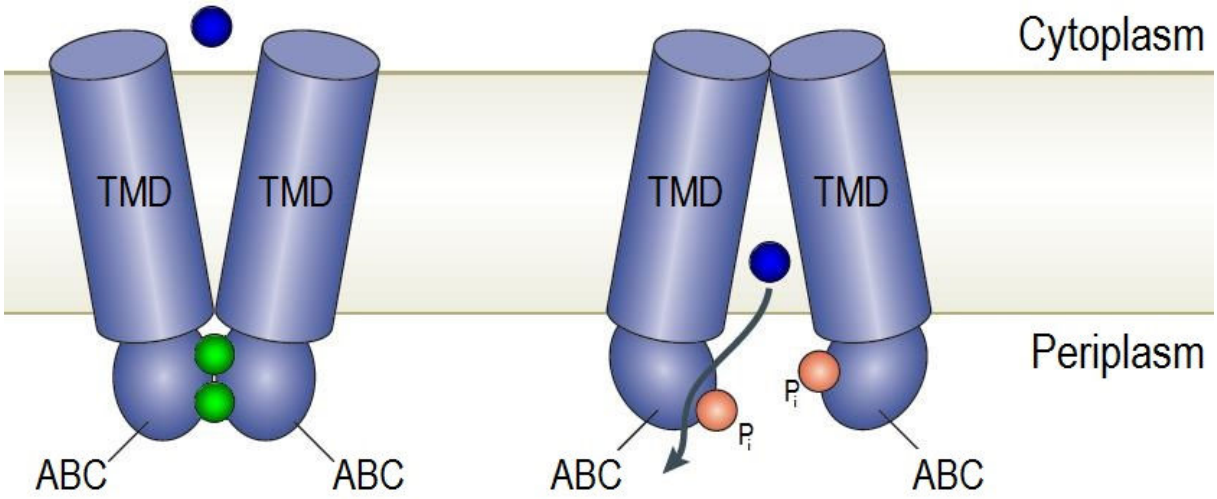

Figure 1.11: Schematic diagram of ABC transporters (modified from Rees *et al* [173])

ABC exporters have at least two trans-membrane domains (TMD) and two ATP-binding domains (ABC) which, upon substrate (**BLUE**) binding, form a closed dimer containing two ATP molecules (**GREEN**) at the interface. Following conformational changes, during which binding affinity is decreased and the substrate is released, ATP hydrolysis occurs. The subsequent release of ADP (**PINK**) and an inorganic phosphate molecule (P_i) returns the dimer to its open conformation to allow additional substrate binding whereby the cycle repeats.

more common members of ABC transporters are ABCB1 (MDR1, P-glycoprotein/P-gp), ABCG2 (BCRP) and ABCC1 (Multidrug Resistance-associated Protein 1/MRP1). ABC transporters naturally function to maintain cholesterol and fatty acid levels in our cells however they are also capable of exporting other lipophilic compounds including xenobiotics and chemotherapeutic agents[173]. For this reason ABC transporters have been implicated in multidrug resistance which can be critical in the treatment of CML and other leukaemia.

The transporters feature different levels of tissue distribution, with ABCB1 and ABCG2 concentrated at points of drug penetration (blood brain barrier, intestine) as well as other sites of drug uptake and excretion (liver, kidney)[172]. Importantly, high expression of these transporters has been demonstrated on primitive haematopoietic stem cells[174,175]. ABCC1 is commonly found in the testes, lungs, kidneys and peripheral blood mononuclear cells (PBMNCs)[172]. Thus, these transporters have key roles in preserving the sanctuary sites (brain and testes) from infiltration by chemotherapeutics such as TKIs. The understanding gained from further investigation of these, and other closely related transporters, may help target CNS disease and residual leukaemic cells present in sanctuary sites that may contribute to the loss of remission observed in some patients[176].

1.4.2. Influx and Efflux of TKIs from the Leukaemic Cell

1.4.2.1. Imatinib and Dasatinib Influx and Efflux

It is well established that imatinib is predominantly actively transported into leukaemic cells via OCT-1[147-150] and that patients with high activity of this cellular protein have better treatment outcomes[151,152,177]. However, much speculation still exists as to the mechanism of export of imatinib as well as the other, more recent, TKIs. It is widely agreed that imatinib is an ABCB1 substrate[138,145,176], hence its overexpression has been implicated as a factor in imatinib resistance[111,115,118,138-140]. There is also agreement that imatinib is not a substrate of ABCC1[176,178].

Conversely, the interaction between imatinib and ABCG2 reported in the literature is far more inconsistent with some studies reporting imatinib as a substrate of ABCG2[138,179], others suggesting imatinib is an ABCG2 inhibitor[146,178,180-182], and further studies indicating imatinib can function as both substrate and inhibitor depending on its concentration[146,153,154]. The disparity observed in the literature with regard to the TKI:transporter relationship can likely be attributed to inconsistencies in methodologies utilised. The differences in model substrates, temperatures and times of incubation, as well as the drug concentrations used in each of the individual studies, are all likely to influence experimental outcome.

In contrast to imatinib, research in our laboratory[183], as well as another's[184], has demonstrated it is unlikely dasatinib utilises OCT-1 to gain access to the cell. In addition, we have demonstrated that dasatinib is a substrate of both ABCB1 and ABCG2[183], with results corroborated by others[154,185,186].

1.4.2.2. Nilotinib Influx and Efflux

We have demonstrated that nilotinib is unlikely to be transported by OCT-1[150] and that it enters the cell in a predominantly passive manner, a theory supported by others[187]. However, the efflux of nilotinib remains controversial with differences in results again appearing to be mainly due to disparities in drug concentrations assayed, a concept discussed in further detail in **Chapter 4**. Initial investigations using the ABCB1 specific inhibitor PSC-833 demonstrated an interaction between nilotinib and ABCB1, while a vanadate sensitive ATPase assay confirmed nilotinib is indeed an ABCB1 substrate at low nanomolar concentrations[155]. Subsequent IC50 experiments revealed ABCB1 overexpressing cell lines exhibit increased resistance which is reversible upon ABCB1 inhibition[154]. However, it has been reported that at high micromolar concentrations nilotinib functions as a potent inhibitor of both ABCB1 and ABCG2[154,155,187-189]. In those studies which concluded that nilotinib was an ABCB1 inhibitor, extremely high concentrations of drug were used based on peak plasma drug levels[170]. However, the high degree

to which nilotinib is protein bound in the plasma[170,190] would significantly lower the concentration of free drug available to the leukaemic cell. Based on *in vitro* experimentation, nilotinib is 98% protein bound[190] and once this is taken into account the concentration of circulating nilotinib available to the leukaemic cell decreases significantly. For example, the plasma concentrations of nilotinib based on a 400 mg twice daily dosing regimen are predicted to be 4270 nM and 1945 nM ($C_{max\ total}$ and $C_{min\ total}$), but once protein binding is allowed for this could decrease to concentrations as low as 85 nM and 39 nM ($C_{max\ free}$ and $C_{min\ free}$)[170]. While the protein interactions determining the concentration of nilotinib available to the cell are complex, this may partly explain why nilotinib resistant patients harbour mutations predicted to be sensitive based on IC50 values determined *in vitro*[81]. Thus, the use of high *in vitro* drug concentrations may not be representative of the *in vivo* situation and as such these results should be viewed with caution.

1.5. The Effect of Combination and Concomitant Therapies on TKI Transport and Efficacy

1.5.1. TKI Combination Therapy versus Single Agent Treatment

Initial TKI combination studies were performed *in vitro* comparing the incidence and type of KD mutations that arise due to single agent treatment versus combination therapy[81,191]. In theory, combination cocktails of TKIs should limit or delay onset of KD mutations since mutations insensitive to one TKI are sensitive to another, with the exception of T315I[81]. Indeed, researchers found that drug combinations using lower concentrations were far more effective at suppressing the growth of resistant clones, suggesting a drug cocktail may be equipotent to higher dose single agents[191]. This strategy would also limit dose related toxicity and the occurrence of adverse events associated with higher concentrations of TKI necessary in some single agent regimens. Furthermore, recent preliminary evidence utilising preclinical models suggests that removal of one of the drugs, once substantial

inhibition of the leukaemic clone has occurred, has no detrimental effect on long term disease progression[192].

More recent experimentation assessing the efficacy of imatinib and nilotinib against cell lines expressing wildtype and imatinib resistant Bcr-Abl confirmed previous results. Both *in vitro* and *in vivo* assays demonstrated the combination of imatinib and nilotinib resulted in additive to synergistic impairment of cell growth and disease burden respectively, without adverse toxicity in normal bone marrow[193]. These results are in accord with *in vitro* studies performed in our laboratory assessing the simultaneous administration of imatinib and nilotinib which demonstrated a significant, imatinib-mediated increase in intracellular concentrations of nilotinib. Conversely, we have also demonstrated that nilotinib decreases the intracellular concentration of imatinib[194] which others have reported to be due to inhibition of OCT-1[187]. However, the most likely mechanism by which imatinib increases intracellular nilotinib concentrations is by inhibition of efflux transporters. It has previously been demonstrated that imatinib can act as both substrate[138,145,176] and inhibitor of ABCB1[118,154]. Thus, as it is likely nilotinib is also transported by ABCB1[153,154,176], imatinib-mediated inhibition of, or competitive transport though ABCB1, would result in an increase in intracellular nilotinib.

Combination studies involving imatinib and dasatinib have also been conducted *in vitro* with results demonstrating a reduction in both the number of resistant clones and the range of mutations emerging, although the concentration of imatinib used is unlikely to be clinically achievable[195]. This observed synergy is likely due, at least in part, to interactions with efflux transporters since dasatinib is also a reported substrate of ABCB1 and ABCG2[154,183,185,186]. However, the fact that dasatinib and imatinib bind different conformations of Bcr-Abl may also contribute to the synergy observed[195].

Sequential treatment with nilotinib following failure of imatinib therapy has highlighted the clinical relevance of combination TKI therapy[196]. Taken together with *in vitro* data demonstrating the synergistic effect of these TKIs, and the fact that lower doses are required when used in combination compared with single agent treatment, up front combination nilotinib:imatinib therapy may provide superior response in terms of adverse toxicity and suppression of mutation development.

1.5.2. Effect of Concomitant Medications on TKI Therapy

In addition to TKIs interacting with efflux transporters, other commonly administered medications are also known to modulate ABCB1 and ABCG2 function, by direct inhibition or through indirect conformational changes. Proton pump inhibitors (PPIs), such as pantoprazole and esomeprazole, reduce gastric acid production and are readily prescribed to CML patients to combat imatinib-mediated gastric side effects. PPIs have previously been shown to inhibit both ABCB1 and ABCG2[197-199] and as such may potentially affect transport of TKIs. Indeed, *in vitro* investigations within our laboratory with simultaneously administered nilotinib and PPIs, demonstrate a significantly decreased IC50 in the presence of PPI. Concurrent experimentation assessing intracellular nilotinib levels revealed this is most likely due to an increase in intracellular nilotinib[200].

Simvastatin and lovastatin are two commonly prescribed drugs used to lower cholesterol and treat cardiovascular disease. Growing evidence suggests that the statin class of drugs is able to modulate ABCB1-mediated transport both directly and indirectly. Initial *in vitro* experiments demonstrated the statins' ability to inhibit ABCB1-mediated rhodamine-123 effflux[201]. More recently, these results were confirmed using the fluorescent ABCB1 substrate calcein, with results demonstrating the addition of simvastatin directly inhibits ABCB1[202]. However, it has also been reported that statins are capable of indirectly inhibiting ABCB1 function through a reduction in glycosylation and subsequent alteration in protein conformation. The reduction in glycosylation may also adversely affect protein half-life as down

regulation of ABCB1 protein in the presence of simvastatin has also been observed[202]. A recent *in vitro* study using imatinib in combination with lovastatin provides preliminary evidence for statins increasing the cytotoxic effect of imatinib[203]. Thus concomitant administration of drugs such as PPIs and statins, which are already widely prescribed with human pharmacology well understood, make these medications attractive options with the potential to further enhance the efficacy of TKIs.

1.6. Summary and Project Aims

TKIs have resulted in significantly improved treatment outcomes for the majority of patients with CML. However, there still remains a group of patients who demonstrate primary resistance, and a further group who develop secondary resistance following a successful treatment phase. The underlying mechanisms of resistance to nilotinib remain poorly understood and with nilotinib now a front line therapy option, improvement of treatment outcomes is necessary for these patients. It is also important to understand the cellular transport of nilotinib in order to elucidate possible interactions with other TKIs and drug efflux pumps, as well as investigate the effect of concomitant therapies on intracellular nilotinib concentrations. This information will assist in tailoring treatment strategies to individual patients which is particularly important as we move into the era of customised therapeutics in CML. Therefore, this thesis addresses two primary aims:

- To study the interaction of nilotinib with the major cellular drug transporters and assess
    a) how concomitant administration of other drugs could be used to enhance the effects of nilotinib in patients; and
    b) how altered expression or inhibition of these transporters affects nilotinib transport and function
- To generate an *in vitro* cell line model of nilotinib resistance to recapitulate and study modes of nilotinib resistance *in vivo*

Results from this research will provide a greater understanding of nilotinib transport, particularly with respect to ABC transporters. The findings presented here may assist in developing new therapeutic strategies using TKIs in combination with other medications in order to enhance intracellular concentrations of TKI. Additionally, further insight into the modes of resistance to nilotinib, as well as the kinetics of resistance mechanism emergence, may assist in determining treatment options for CML patients and predicting patients at risk of losing response to therapy.

Chapter 2

Materials and Methods

2.1. Commonly Used Reagents

Table 2.1: Suppliers and catalogue numbers of commonly used reagents

Reagent	Supplier	Catalogue Number
4G10-PE Antibody	Millipore	FCMAB232PE
7-Aminoactinomycin D (7-AAD)	Invitrogen	A1310
^{14}C-Tetraethylammonium Bromide (TEA)	Perkin Elmer	NEC298050UC
Acetic Acid	Fisher Scientific	0400
Ammonium Persulfate (APS)	Sigma	A9164
Annexin V-PE	BD Biosciences	556421
Axl Antibody (138 kDa)	Cell Signalling	4977
β-Actin Antibody (43 kDa)	Santa Cruz	sc-130656
BD Cytofix	BD Biosciences	554655
BD Phosflow Fix Buffer I	BD Biosciences	557870
BD Phosflow Perm Buffer III	BD Biosciences	558050
β-mercaptoethanol	Sigma	M6250
Benchmark Protein Ladder	Invitrogen	10748-010
Bis-Acrylamide solution 37.5:1 (40% Acrylamide)	Biorad	161-0149
BODIPY-Prazosin	Invitrogen	B-7433
Bovine Serum Albumin (BSA) Powder	Sigma	49418
Bromophenol Blue	Sigma	114391
c-Abl Antibody (Bcr-Abl 210 kDa)	Cell Signalling	2862
Calcium Chloride ($CaCl_2$)	Sigma	449709
CD243-PE (ABCB1) Antibody	Beckman Coulter	PN IM 2370U
cdc25C Antibody (60 kDa)	Cell Signalling	4688
Chk2 Antibody (62 kDa)	Cell Signalling	2662
Chloroform	Merck	100776B
Crkl Antibody (Crkl 36 kDa; p-Crkl 39 kDa)	Santa Cruz	SC-319
Cyclosporin A	RAH Pharmacy	
DEPC H_2O	MP Biomedicals Inc.	821739
D-Glucose	Sigma	G7528
Dimethyl Sulphoxide (DMSO)	Merck	K39661852
Dulbecco's Modified Eagle's Medium (DMEM)	Sigma	D6046
dNTP Set (N=A, C, G, T)	GE Healthcare	27-2035-02
DTT 0.1 M	Invitrogen	18064-014
ECF Substrate	GE Healthcare	RPN 5785
Ethylenediaminetetraacetic Acid (EDTA)	APS	180-500G
Ethanol	Merck	4.10230.2511
Foetal Calf Serum (FCS)	JRH Biosciences	12003-500M

Formaldehyde	BDH	10113
G-418, Geneticin	Invitrogen	10131-027
Glycerol	Ajax Finechem	242
Glycine	Sigma	G8898
Glycogen	Roche	901393
Hanks Balanced Salt Solution (HBSS)	Sigma	H9394
hBCRP-PE (ABCG2) Antibody	R&D Systems	FAB995P
HEPES 1 M	Sigma	H0887
Hydrochloric Acid (HCl, 35%)	Fisher Scientific	1100
Indomethacin (MW=357.79)	Sigma	I7378
Isopropanol	Ajax Finechem	425-2.5L PL
Kaleidoscope Prestained Standards	Biorad	161-0375
L-glutamine 200 mM	SAFC Biosciences	SAFC 59202C
Lymphoprep	Axis Shield	1114547
Lyn Antibody (56 kDa)	Cell Signalling	2732
MAP3K5 (ASK1) Antibody (155 kDa)	Cell Signalling	3762
Methanol	Chem Supply	MA004-P
Methyl Violet	BDH	34033
MICROSCINT-20 Scintillation Fluid	Perkin Elmer	6013621
Mouse IgG Antibody (AP-conjugated)	Cell Signalling	7056
Mouse IgG1-AF488 Antibody	BD Biosciences	557782
Mouse IgG1-PE Antibody	R&D Systems	IC002P
Mouse IgG2a-PE Antibody	DakoCytomation	X095001
Mouse IgG2b-PE Antibody	DakoCytomation	X095101
p-Akt-PE (pT308) Antibody	BD Biosciences	558275
Pantoprazole (MW=383.4)	RAH Pharmacy	
Paraformaldehyde (16%)	ProSciTech	15710
p-Axl Antibody (pY779; 140 kDa)	R&D Systems	AF2228
p-c-Abl Antibody (p-Bcr-Abl pY245; 210 kDa)	Cell Signalling	2861
p-CrkL-PE (pY207) Antibody	BD Biosciences	560788
p-Erk 1&2-PE (pT202/pY204) Antibody	BD Biosciences	612566
p-Lyn Antibody (pY396; 61 kDa)	abcam	ab40660
p-Stat5-PE (pY694) Antibody	BD Biosciences	612567
p-Syk Antibody (pY525/526; 72 kDa)	Cell Signalling	2711
PDGFR-β Antibody (190 kDa)	Cell Signalling	3175
Penicillin 5000 U/mL Streptomycin 5000 µg/mL	Sigma	P4458
Phosphate Buffered Saline (PBS)	SAFC Biosciences	59331C
Prazosin Hydrochloride (MW=419.9)	Sigma	P7791
Probenecid (MW=285.4)	Sigma	P8761

PSC-833 (MW=1214.7)	Novartis	
PVDF (Western Blot Membrane)	GE Healthcare	PRN 303F
Rabbit IgG Antibody (AP-conjugated)	Santa Cruz	SC2007
Random Hexamer Primer	Geneworks	RP-6
Rhodamine-123	Invitrogen	R-302
RPMI-1640 Medium w/o L-glutamine	Sigma	R0883
SDS (Sodium Dodecyl Sulphate)	Sigma	L4509
Sodium Azide (NaN_3)	Sigma	S2002
Sodium Chloride (NaCl)	Ajax Finechem	1128
Sodium Fluoride (NaF)	Sigma	S7920
Sodium (ortho) Vanadate (Na_3VO_4)	Sigma	S6508
Superscript II Reverse Transcriptase	Invitrogen	18064-014
SYBR Green Supermix	SA Biosciences	PA-012-24
Syk Antibody (72 kDa)	Cell Signalling	2712
Taqman Master Mix	Applied Biosystems	4318157
TEMED	Sigma	T7024
Tris (hydroxymethyl) Aminomethane	Merck	1083870500
TRIzol Reagent	Invitrogen	15596-018
Trypan Blue Solution (0.4%)	Sigma	T8154
Trypsin	SAFC Biosciences	59417C
Tween®20	Sigma	P9416
Verapamil Hydrochloride (MW=491.1)	RAH Pharmacy	
Western Blot Recycling Kit	Alpha Diagnostic	90100

2.2. Solutions, Buffers, Media & Inhibitors

2.2.1. Adherent Cell Line Wash Buffer

HBSS – 500 mL

0.53 mM EDTA (1 M) – 530 µL

0.25% Trypsin (2.5%) – 1 mL

2.2.2. phospho-Flow Wash Buffer

1×PBS – 500 mL

1% FCS – 5 mL

0.1% NaN_3 – 0.5 g

The solution can be stored at 4°C indefinitely.

2.2.3. Cell Culture Media

RPMI-1640 medium – 500 mL for suspension cells

DMEM – 500 mL for adherent cells

2 mM L-Glutamine (200 mM) – 5 mL

25000 Units Penicillin (5000 U/mL) – 5 mL

25000 µg Streptomycin sulphate (5000 µg/mL) – 5 mL

10% FCS – 50 mL

The media was stored at 4°C and preheated to 37°C in a water bath prior to use.

2.2.4. Cytotoxicity Assay Staining Buffer

HBSS – 47.5 mL

100 mM $CaCl_2$ – 2.5 mL

2.2.5. dNTP Set (N=A, C, G, T)

Stock: 25 mM = 40 µL of each dNTP

Working stock: 5 mM = 20 µL of 25 mM stock in 80 µL DEPC water

2.2.6. Flow Cytometry Fixative (FACS Fixative)

1×PBS – 500 mL

40% w/v Formaldehyde – 5 mL

D-glucose – 10 g

0.02% NaN_3 – 0.1 g

The solution was stored at 4°C for ~6 months.

2.2.7. Freeze Mix

70% HBSS

20% FCS

10% DMSO

The solution was made up fresh for each batch of samples to be cryopreserved.

2.2.8. Imatinib Mesylate, MW=589.72

Imatinib mesylate (imatinib; Glivec; formerly STI-571) was provided by Novartis Pharmaceuticals (Basel, Switzerland). Stock solutions of this compound were prepared at 10 mM with distilled water, sterile filtered and stored at -70°C.

2.2.9. 50% ^{14}C-Imatinib (100 µM)

^{14}C-Imatinib (1695.72 µM) – 29.5 µL

10 mM imatinib – 5 µL

RPMI-1640 medium – 966 µL

^{14}C-imatinib (specific activity 3.394 MBq) was provided by Novartis Pharmaceuticals. Stock solutions were prepared at 1 mg/mL with distilled water and stored at -70ºC.

2.2.10. Inhibitors of ABC Transporters

2.2.10.1. Cyclosporin A – Inhibits ABCB1, ABCB4, ABCB11, ABCC1, ABCC2, ABCC3, ABCG2

Cyclosporin A (RAH Pharmacy, Adelaide, Australia) was used at 10 µM from a 4.15 mM stock.

41.5 mM stock = 250 mg/5 mL 5% glucose solution

Further dilute this stock 1:10 in 5% glucose solution

2.2.10.2. Indomethacin – Inhibits ABCC1, ABCC2, ABCC4, ABCC6, ABCC11

Indomethacin (Sigma) was used at 100 µM from a 10 mg/mL stock.

10 mg/mL = 10 mg/1 mL DMSO

2.2.10.3. Ko143 – Inhibits ABCG2

Ko143 is an analogue of fumitremorgin C kindly provided by Dr John Allen, Centenary Institute, Sydney, Australia. 1 mM stock solutions and 10 µM working solutions were prepared in sterile water and stored at -70ºC.

2.2.10.4. Pantoprazole – Inhibits ABCB1, ABCC6, ABCG2

Pantoprazole (RAH Pharmacy) was used at 200 µM from a 10 mM stock.

10 mM stock = 40 mg dissolved in 10 mL 0.9% NaCl

2.2.10.5. Probenecid – Inhibits ABCC1, ABCC2, ABCC3, ABCC4, ABCC5, ABCC6, ABCC11

Probenecid (Sigma) was used at 1 mM from a 175 mM stock.

175 mM stock = 125 mg dissolved in 2.5 mL DMSO

2.2.10.6. PSC-833 – Inhibits ABCB1, ABCB4, ABCC1, ABCC4

PSC-833 is a Cyclosporin A derivative kindly provided by Novartis Pharmaceuticals and was used at 10 µM from 8.23 mM stock.

8.23 mM stock = 10 mg/mL = 10 mg/500 µL 9:1 Ethanol:Tween®20, +500 µL water

2.2.10.7. Verapamil – Inhibits ABCB1, ABCB4, ABCC1, ABCC3, ABCC4, ABCG2, OCT-1

Verapamil (RAH Pharmacy) was used at 50 µM from a 2.5 mg/mL stock dissolved in H_2O.

2.5 mg/mL = 5.091 mM

2.2.11. Laemmli's Buffer

50 mM Tris-HCl (pH 6.8)

10% Glycerol

2% SDS

5% β-Mercaptoethanol

0.1% Bromophenol Blue

1 mM Na_3VO_4

10 mM NaF

The buffer was stored in 1 mL aliquots at -20 ºC and thawed before use.

2.2.12. Membrane Blocking Solutions

2.2.12.1. 2.5% Skim Milk

Non-fat milk powder – 12.5 g

1×TBST – 500 mL

The following proteins require blocking in 2.5% non-fat milk powder: p-Crkl.

2.2.12.2. 5% Skim Milk

Non-fat milk powder – 25 g

1×TBST – 500 mL

The following proteins require blocking in 5% non-fat milk powder: β-actin, Chk2, p-Axl.

2.2.12.3. 2% BSA

BSA – 10 g

1×TBST – 500 mL

The following proteins require blocking in 2% BSA: Axl, Syk, p-Syk.

2.2.12.4. 5% BSA

BSA – 25 g

1×TBST – 500 mL

The following proteins require blocking in 5% BSA: c-Abl, cdc25C, Lyn, MAP3K5, p-c-Abl, p-Lyn.

2.2.13. Nilotinib, MW = 529.5

Nilotinib (Tasigna; formerly AMN107) was provided by Novartis Pharmaceuticals. Stock solutions were prepared at 10 mM in DMSO and stored at 4°C.

2.2.14. ^{14}C-Nilotinib (10 µM)

2.2.14.1. 50% ^{14}C-Nilotinib

^{14}C-Nilotinib (1882 µM) – 2.66 µL

1 mM nilotinib – 5 µL

RPMI-1640 medium – 992.3 µL

2.2.14.2. 100% ^{14}C-Nilotinib

^{14}C-Nilotinib (1882 µM) – 5.32 µL

RPMI-1640 medium – 994.7 µL

^{14}C-nilotinib (specific activity 3.31 MBq) was provided by Novartis Pharmaceuticals. Stock solutions were prepared at 1 mg/mL with methanol and stored at -70°C.

2.2.15. Ponatinib (Free Base), MW=532.56

Ponatinib was provided by Ariad Pharmaceuticals (Cambridge, Massachusetts). Stock solutions were prepared at 10 mM with DMSO, sterile filtered and stored at 4°C.

2.2.16. Prazosin Hydrochloride – Inhibits OCT-1, OCT-2, OCT-3

Prazosin hydrochloride (Signma) was used at 100 µM from a 10 mM stock.

10 mM stock = 4.2 mg in 1 mL of methanol

2.2.17. Random Hexamer Primer (100 mg stock)

Working stock: 250 ng/mL = 100 mg in 400 µL DEPC water

2.2.18. 1×SDS-PAGE Running Buffer

25 mM Tris-HCl – 3.026 g (pH 8.3)

192 mM Glycine – 14.413 g

0.1% SDS – 1 g

Reagents were dissolved in 750 mL RO H_2O and then made up to 1 L.

2.2.19. SDS-Polyacrylamide Gel

2.2.19.1. Specific for Hoefer Ruby SE600 Tank

	Resolving gel (12%)	Stacking gel (5%)
H_2O	12.9 mL	6 mL
40% Acrylamide	9 mL	1.26 mL
1.5 M Tris Buffer A	7.5 mL	
1.5 M Tris Buffer B		2.52 mL
10% SDS	300 µL	100 µL
10% APS	300 µL	100 µL
TEMED	8 µL	10 µL

2.2.19.2. Specific for Hoefer SE260 Tank

	Resolving gel (14%)	Stacking gel (5%)
H_2O	3.8 mL	3 mL
40% Acrylamide	3.5 mL	630 µL
1.5 M Tris A	2.5 mL	
1.5 M Tris B		1.26 mL
10% SDS	100 µL	50 µL
10% APS	100 µL	50 µL
TEMED	6 µL	5 µL

2.2.20. 10× Tris Buffered Saline (TBS)

200 mM Tris-HCl – 24.2 g (pH 7.5)

1.5 M NaCl – 87.6 g

Reagents were dissolved in 750 mL RO H_2O, the pH adjusted to 7.5 with HCl and the solution made up to 1 L.

2.2.20.1. 1×TBS

10×TBS stock – 100 mL

RO H_2O – 900 mL

2.2.20.2. 1×TBST

10×TBS stock – 100 mL

0.1% Tween®20 – 1 mL

RO H_2O – 900 mL

2.2.21. 100% ^{14}C-Tetraethylammonium Bromide (TEA; 2500 µM)

^{14}C-TEA (28600 µM) – 87.4 µL

RPMI-1640 medium – 912.6 µL

^{14}C-TEA (specific activity 1.85 MBq) was purchased from Perkin Elmer and stored at 4ºC; working solutions were prepared as required.

2.2.22. Thaw Solution

HBSS – 500 mL

5% FCS – 25 mL

5% ACD – 25 mL

HEPES – 5 mL

The solution (without ACD) was stored at 4°C. ACD was added and the solution heated to 37°C in a water bath prior to use.

2.2.23. 1×SDS-PAGE Transfer Buffer

25 mM Tris-HCl – 3.026 g (pH 8.3)

192 mM Glycine – 14.413 g

20% Methanol – 200 mL

Reagents were dissolved in 750 mL RO H_2O and then made up to 1 L.

2.2.24. Tris Buffer A

Milli-Q® H_2O – 500 mL

1.5 M Tris-HCl – 90.855 g (pH 8.8)

2.2.25. Tris Buffer B

Milli-Q® H_2O – 500 mL

0.5 M Tris-HCl – 30.285 g (pH 6.8)

2.2.26. White Cell Fluid

Glacial Acetic Acid – 2 mL

Milli-Q® H_2O – 98 mL

Methyl Violet – a few crystals

Acetic acid was added slowly to Milli-Q® H_2O. The methyl violet (Gurr®, BDH) was then added, and the solution mixed well to ensure that the crystals dissolved completely. The solution was filtered using a

0.2 µm bottle top filter, and stored at room temperature.

2.3. General Techniques

2.3.1. Lymphoprep Isolation of Peripheral Blood Mononuclear Cells (PBMNCs)

Peripheral blood (PB) from patients with CML (40–60 mL) was collected in lithium heparin tubes. All samples were collected with informed consent in accordance with the Institutional Ethics approved protocols and with reference to the Declaration of Helsinki. A white cell count was performed using white cell fluid and a maximum of 1×10^8 cells (maximum of 15 mL of blood) were transferred into a 50 mL polypropylene conical tube (Falcon tube). The blood volume was brought to 35 mL using HBSS +1% HEPES and underlain with 15 mL of lymphoprep. Tubes were centrifuged at 306 × *g* for 30 min with no brake. The interface containing the PBMNCs was then transferred to another 50 mL Falcon tube and washed once in HBSS +1% HEPES.

2.3.2. Cell Counts and Viability

Patient PBMNC concentration was determined by diluting the cell suspension in white cell fluid (WCF). Viability of patient PBMNCs and cell lines was assessed by diluting samples with trypan blue solution. 10 µL of these suspensions was transferred to a haemocytometer counting chamber (Neubauer Improved, Assistant, Germany) and cell concentration and viability calculated accordingly.

2.3.3. Maintenance of Cell Lines

2.3.3.1. Cell Line Specifications

K562 cells were originally derived from the pleural effusion of a 53 year old female with blast crisis CML[204] and were obtained from the American Type Tissue Culture Collection (ATCC, Manassas, VA). K562 cells were transfected by electroporation with pcDNA3 vector containing full length ABCG2 (kindly provided by Prof. Douglas Ross, University of Maryland, Baltimore, MD). The resultant K562-ABCG2

cells were cultured in 500 µg/mL G418 (Invitrogen, Carlsbad, CA) and assessed for appropriate ABCG2 expression by quantitative PCR and flow cytometry[183]. K562-Dox cells stably overexpress ABCB1 following continuous passage of K562 cells in doxorubicin (kindly provided by Prof. Leonie Ashman, University of Newcastle, Callaghan, NSW). KCL22 cells were originally derived from the pleural effusion of a blast crisis CML patient[205] (kindly provided by Prof. Junia Melo, Centre for Cancer Biology, University of Adelaide, Adelaide, SA). KU812 cells were established from the peripheral blood of a 38 year old male with blast crisis CML[206] and were obtained from the ATCC. VBL-100 cells stably overexpress ABCB1 following the continuous passage of CEM cells in vinblastine (kindly provided by Leonie Ashman). HeLa cells were originally derived from a 31 year old female with cervical cancer[207] (kindly provided by Dr Bruce Lyons, School of Medicine, University of Tasmania, Hobart, TAS). HepG2 cells were originally derived from the liver tissue of a 15 year old male with hepatocellular carcinoma[208] (kindly provided by Prof. Andrew Zannettino, Centre for Cancer Biology and Centre for Stem Cell Research/Robinson Institute, University of Adelaide, Adelaide, SA).

2.3.3.2. Culture of General Cell Lines

All appropriate tissue culture techniques were performed in a Class two "biohazard" laminar flow hood (Gelman Sciences). Suspension cell lines (K562, K562-ABCG2, K562-Dox, KCL22, KU812, VBL100) were maintained at a cell density between 1×10^5–1×10^6 cells/mL in 25cm^2, 75cm^2 or 175cm^2 tissue culture flasks (Greiner). Media was pre-warmed to 37°C prior to use. Cultures were incubated in a 37°C/5% CO_2 incubator. Cell cultures were checked every second day for contamination, counted and recultured at the above concentrations. Adherent cell lines (HeLa, HepG2) were maintained in 75cm^2 tissue culture flasks at a cell density of 1×10^7 cells in 20 mL media. Prior to reculture, cells were rinsed twice with pre-warmed adherent cell wash buffer and trypsinised at 37ºC for ~10 min with 0.25% trypsin. Cell aggregates were separated by pipetting and resuspended in fresh media devoid of trypsin.

2.3.3.3. Culture of Nilotinib Resistant Cell Lines

K562 and K562-Dox cell lines were gradually exposed to increasing concentrations of nilotinib to yield one nilotinib resistant K562 cell line and two nilotinib resistant K562-Dox cell lines. Nilotinib culture was initiated at 15 nM and the concentration increased at a rate of 25–500 nM every 10–20 days depending on cell proliferation and viability until reaching 2 μM (approximately 6 months duration for K562 cells and 7 and 8 months duration for the two K562-Dox cell lines). Serial dilutions of nilotinib (in DMSO) were prepared from 10 mM stocks such that no more that 0.1% DMSO was present in culture. Control cell lines cultured in 0.1% DMSO were maintained in parallel. Prior to nilotinib escalation, cells were harvested as follows:

3× 1×10^7 aliquots of cells for TRIzol preparations, frozen for later RNA extraction

3× 1×10^7 aliquots of cells for cryopreservation

2.3.4. Cryopreservation of Cells

Cells were pelleted at the desired concentration, resuspended in 1 mL of Freeze Mix per 1×10^7 cells and quickly transferred to cryo-ampoules (Nalgene). Patient PBMNCs were frozen to -80ºC using a Controlled Rate Freezer (Planer KRYO10 Series II) at a rate of 1°C per min. Cell lines were cryopreserved using a 'Mr Frosty' container (Nalgene) for a minimum of 4 h at -70ºC. Samples were stored for up to 10 years in liquid nitrogen (-196°C).

2.3.5. Thawing of Cells

Cells were removed from liquid nitrogen and thawed rapidly in a 37°C water bath. In a laminar flow hood, the cell suspension was quickly transferred to a 50 mL Falcon tube, and approximately 20 mL of thaw solution (warmed to 37°C) was added drop-wise with constant mixing. The sample volume was then increased to 30 mL with thaw solution and the cells pelleted by centrifugation at 306 × *g* for 10 min. The supernatant was aspirated and the procedure repeated to remove all residual DMSO.

2.3.6. Cytotoxicity Assay

Cells were washed and resuspended in fresh culture media to remove traces of drug before being cultured in a 24-well plate. To ensure accurate concentrations of drug in each replicate, TKI was added in increasing concentrations as detailed in **Appendix 1A** to 4 mL of cell suspension at 2×10^5 cells/mL. The 24-well plates were seeded with 1 mL of cell suspension in triplicate, then placed in sterilised cake boxes and incubated for 72 h before staining with Annexin V/7-AAD and trypan blue to observe cell death.

2.3.7. Fluorescence Activated Cell Sorting (FACS) for ABCG2 Positive Cells

2.5×10^7 cells were aliquoted into 10× 5 mL polystyrene round bottom tubes (Falcon, FACS tubes) at a concentration of 2.5×10^6 cells/tube and each tube stained with 100 µL ABCG2-PE. Test cells were sorted for ABCG2 positivity on a Becton Dickinson Aria, using FACS Diva Software version 6.1.3 (BD Biosciences). Only the top 20% of positive cells were selected for reculture.

2.3.8. Antibody Staining for Flow Cytometric Analysis

2.3.8.1. Visualisation of Surface Proteins

2×10^5–1×10^6 cells were transferred to 5 mL FACS tubes and following suspension in approximately 250 µL of buffer, PE-conjugated antibodies were added to tubes as specified (**Table 2.2**). Cells were incubated for a period of 40 min on ice in the dark, washed twice with buffer and re-suspended in FACS fixative. Samples were stored at 4°C in the dark until analysis was performed. Control tubes were stained with isotype control IgG-PE antibodies and these were used to define the gates for positive and negative expression. The fluorescence intensity of cell suspensions was examined using an FC500 flow cytometer (Beckman Coulter, Miami, FL) and FCS Express 4 software (De Novo Software, Los Angeles, CA). Cell populations were analysed based on the forward and side light scattering properties and the fluorescence intensity of PE fluorochromes.

Table 2.2: Antibody staining for surface flow cytometry

Antibody	Cell Number	Concentration	Volume	Buffer
IgG2a-PE	5×10^5	100 µg/mL	5 µL	HBSS +1% HEPES
ABCB1-PE	1×10^6	25 µg/mL	20 µL	HBSS +1% HEPES
IgG2b-PE	5×10^5	100 µg/mL	5 µL	HBSS +1% HEPES
ABCG2-PE	1×10^6	25 µg/mL	20 µL	HBSS +1% HEPES

2.3.8.2. Visualisation of Phospho-Proteins

5×10^5–1×10^6 cells were transferred to 5 mL FACS tubes and 500 µL phospho-flow wash buffer added (**Section 2.2.2**). Cells were washed twice and the supernatant aspirated. 250 µL BD Cytofix was added to each tube while vortexing and cells incubated on ice for 30 min. Following incubation, cells were washed in 500 µL phospho-flow wash buffer and then permeabilised in 250 µL ice cold BD Phosflow Perm Buffer III while vortexing. Following 30 min incubation on ice, cells were washed 3× in 500 µL phospho-flow wash buffer and supernatant aspirated. Cells were then resuspended in 100 µL phospho-flow wash buffer and stained with antibodies in line with manufacturers' instructions according to **Table 2.3** at room temperature for 1 h in the dark.

Table 2.3: Antibody staining for phospho-flow cytometry

Antibody	Volume
IgG2b-PE	5 µL
4G10-PE (1:10 in PBS)	10 µL
IgG1-PE	5 µL
p-Akt-PE (pT308)	5 µL
IgG2a-PE	5 µL
p-CrkL-PE (pY207)	5 µL
IgG1-PE	5 µL
p-Erk-PE (T202/Y204)	5 µL
IgG1PE	5 µL
p-Stat5-PE (Y694)	5 µL

Cells were then washed in 500 µL phospho-flow wash buffer, supernatant aspirated and resuspended in 200 µL phospho-flow wash buffer. Samples were stored at 4°C in the dark until analysis was performed. Control tubes were used to define the gates for positive and negative expression. The fluorescence intensity of cell suspensions was examined using an FC500 flow cytometer and FCS Express 4 software. Cell populations were analysed based on the forward and side light scattering properties and the fluorescence intensity of PE fluorochromes.

2.3.8.3. Determination of Cell Viability

Cell viability was measured by staining cells with both 7-Amino-actinomycin (7-AAD) and Annexin V-PE and analysing using a flow cytometer. 7-AAD is excluded by viable cells but can penetrate the membranes of dying or dead cells where it intercalates into double stranded nucleic acids. Annexin V is a Ca^{++}-dependent phospholipid-binding protein that binds to phosphatidlyserine residues of the cell membrane. In normal cells, these residues are located in the inner surface of the cell membrane and are therefore inaccessible to Annexin V. However, at an early stage of apoptosis, the phosphatidlyserine residues are translocated to the outside of the cell making them subsequently available for binding by Annexin V[209].

Following cytotoxicity assays, cells were mixed thoroughly and transferred from 24-well plates to 5 mL round bottom FACS tubes (one tube per plate well). A 20 µL aliquot per tube was deposited in a 96-well plate for trypan blue viability determination then cells were centrifuged at 845 × *g* for 2 min and the supernatant removed (all centrifugation in this method is at 845 × *g* for 2 min). 7-AAD and Annexin V were thawed in darkness on ice before being diluted in staining buffer (**Section 2.2.4**). 7-AAD was used at 0.5 µL of 1 mM stock diluted in 39.5 µL staining buffer (40 µL per sample), while Annexin V was used at 1 µL of stock diluted in 9 µL staining buffer (10 µL per sample). To make the Annexin V positive control, 500 µL of zero drug culture was added to an equal volume of DMSO in a 5 mL FACS tube and

incubated at room temperature for 20 min. To make the 7-AAD positive control, 500 µL of zero drug culture were added to 2 mL cold ethanol (70%) in a 5 mL FACS tube and incubated on ice for 20 min. To make the negative control, 500 µL zero drug culture was washed with 1 mL staining buffer in a 5 mL FACS tube and then stored on ice. 7-AAD and Annexin V control cells were washed twice in 2 mL PBS then both control and experimental cells washed once in staining buffer. Supernatants were removed by aspiration leaving ~50 µL, Annexin V and/or 7-AAD added as per **Table 2.4** and cells incubated at room temperature in the dark for 15 min. Cells were then resuspended in 400 µL staining buffer and the tube stored on ice for a maximum of 1 h prior to flow cytometric analysis.

Table 2.4: Staining for cell viability

	Annexin V	7-AAD
Negative Control	–	–
Annexin V Positive Control	10 µL	–
7-AAD Positive Control	–	40 µL
Experimental Samples	10 µL	40 µL

2.3.9. Fluorescent Substrate Efflux Studies

2.3.9.1. Rhodamine-123 Efflux for ABCB1 Function

During the accumulation period, 1 mL of K562-Dox cells were resuspended at 1×10^6/mL in 5 mL round bottom FACS tubes. Cells were then incubated for 30 min at 37°C in the absence or presence of rhodamine-123 as per **Table 2.5a**. PSC-833 was used as a positive control for ABCB1 inhibition. K562 cells, which do not express ABCB1, were used as negative controls and incubated under the same conditions. Following the accumulation period, efflux was initiated by centrifuging cells twice at 845 × *g* for 2 min in cold PBS. Cells were then resuspended in warm RPMI-1640 medium supplemented with 10% FCS as per **Table 2.5b** and incubated at 37ºC for 60 min to allow efflux to take place. Following the efflux period, cells were again washed twice in PBS and resuspended in 400 µL PBS supplemented

with 5% BSA before flow cytometric analysis. Assessment of ABCB1 expression (**Section 2.3.3.1**) was conducted simultaneously to ensure appropriate expression levels.

Table 2.5a: Incubation conditions for rhodamine-123 accumulation

K562-Dox/K562	Rhodamine-123 (0.5 µg/mL)	PSC-833 (10 µM)
Unstained	–	–
Rhodamine-123 Efflux	✓	–
No Efflux	✓	✓

Table 2.5b: Incubation conditions for rhodamine-123 efflux

K562-Dox/K562	Rhodamine-123 (0.5 µg/mL)	PSC-833 (10 µM)
Unstained	–	–
Rhodamine-123 Efflux	–	–
No Efflux	–	✓

2.3.9.2. BODIPY-Prazosin Efflux for ABCG2 Function

During the accumulation period, 1 mL of K562-ABCG2 cells were resuspended at 1×10^6/mL in 5 mL round bottom FACS tubes. Cells were then incubated for 30 min at 37ºC in the absence of presence of BODIPY-prazosin as per **Table 2.6a**. Ko143 was used as a positive control for ABCG2 inhibition. K562 cells, which do not express ABCG2, were used as negative controls and incubated under the same conditions. Following the accumulation period, efflux was initiated by centrifuging cells twice at 845 × *g* for 2 min in cold PBS. Cells were then resuspended in warm RPMI-1640 medium supplemented with 10% FCS as per **Table 2.6b** and incubated at 37ºC for 60 min to allow efflux to take place. Following the efflux period, cells were again washed twice in PBS and resuspended in 400 µL PBS supplemented with 5% BSA before flow cytometric analysis. Assessment of ABCG2 expression (**Section 2.3.3.1**) was conducted simultaneously to ensure appropriate expression levels.

Table 2.6a: Incubation conditions for BODIPY-prazosin accumulation

K562-ABCG2/K562	BODIPY-Prazosin (250 nM)	Ko143 (1 µM)
Unstained	–	–
BODIPY-prazosin Efflux	✓	–
No Efflux	✓	✓

Table 2.6b: Incubation conditions for BODIPY-prazosin efflux

K562-ABCG2/K562	BODIPY-Prazosin (250 nM)	Ko143 (1 µM)
Unstained	–	–
BODIPY-prazosin Efflux	–	–
No Efflux	–	✓

2.4. Specialised Techniques

2.4.1. Imatinib/Nilotinib Intracellular Uptake and Retention (IUR) Assay

The IUR and OCT-1 activity assays were performed as previously described by White *et al*.[150]. All assay points were performed in triplicate. 2×10^5 viable cells were incubated in 2 mL of RPMI-1640 medium +10% FCS in the presence or absence of varying concentrations of ^{14}C-imatinib or -nilotinib ranging from 0–4 µM. Inhibitors of influx and efflux (prazosin, verapamil and Ko143) were also added as required. Cells and reagents were incubated for 2 h at 37°C/5% CO_2. Following incubation the cellular and aqueous phases were separated by centrifugation at 4300 × *g* for 5 min, then pulse spun to 16000 × *g* for 30 sec. A 20 µL aliquot of supernatant (S/N) from each tube was then added to 100 µL of Microscint-20 in a 96-well flat bottomed plate. The remaining supernatant was aspirated from the tubes and 50 µL of Microscint-20 was added. The tubes were vortexed thoroughly, and pulse spun for 15 sec at 16000 × *g*. The lysed cells were transferred to a 96-well plate with wells containing 50 µL of Microscint-20. The plate was covered with an adhesive plastic seal and was then counted on a Top Count scintillation counter (Perkin Elmer) as counts per minute (cpm). The incorporation of ^{14}C-imatinib or -nilotinib in ng/200 000 cells was then calculated using the formula below:

$$\frac{\text{(cpm cells – background)}}{\text{[(cpm cells – background) + (cpm S/N – background)]}} \times \text{ng of } {}^{14}\text{C-TKI added}$$

2.4.1.1. OCT-1 Activity

The OCT-1 inhibitor prazosin was used in the $IUR^{imatinib}$ assay at 100 µM. The OCT-1 activity was calculated as the difference between the $IUR^{imatinib}$ in the absence of prazosin and the $IUR^{imatinib}$ in the presence of prazosin. Where IUR values in the presence of prazosin were equal or higher than the values in the absence of prazosin, these patients were scored as having negligible (0 ng/200 000 cells) OCT-1 activity.

2.4.2. IC50 Assay Specific for phosphorylated-Crkl (p-Crkl) Inhibition

2×10^5 Bcr-Abl positive cell lines and 2×10^6 patient PBMNCs were incubated for 2 h at 37ºC with concentrations of nilotinib ranging 0–100 000 nM, imatinib ranging 0–100 µM and dasatinib ranging 0–5000 nM. To determine the effect of cellular transporters such as ABCB1, ABCG2 and ABCC6 on TKI transport, IC50 experiments were incubated in the absence and presence of various inhibitors of transport (**Section 2.2.10**). Following incubation cells were washed once with cold PBS and lysed in Laemmli's buffer (**Section 2.2.11**) by boiling for 12 min. Lysates were clarified by microfugation and stored at -20ºC before resolution by SDS-PAGE.

2.4.3. SDS-PAGE and Western Blot

2.4.3.1. Specific for p-Crkl

Western blotting for p-Crkl was performed as previously described by White *et al*.[210]. 2×10^5 cells (cell lines) or 2×10^6 cells (patient PBMNCs) were placed into a 1.5 mL microtube (Eppendorf), and pelleted by centrifugation for 5 min at 4300 × *g*. All supernatant was removed and cells were lysed in 20 µL of Laemmli's buffer, by boiling in a 100°C heat block for 12 min. Cell lysates were stored at -20°C.

Protein lysate (corresponding to 1×10^5 cell lines or 2×10^6 patient PBMNCs) was resolved on an SDS 12% polyacrylamide gel, and the protein electrophoretically transferred to a PVDF membrane (GE Healthcare) at 65 mA overnight. The membrane was incubated for 1 h at room temperature with 2.5% skim milk powder. The membrane was then probed for 2 h at room temperature with 1:500 anti-Crkl antibody (Santa Cruz) in 2.5% skim milk powder. Following this, the membrane was rinsed in 1×TBST buffer (**Section 2.2.20.2**), and then washed for 3× 5 min with 1×TBST buffer. The membrane was then incubated with 1:2000 alkaline-phosphatase conjugated anti-rabbit immunoglobulin antibody (SantaCruz) in 2.5% skim milk powder for 1 h at room temperature. The membrane was rinsed in 1×TBST buffer, washed for 3× 5 min in 1×TBST buffer and then washed for 3× 5 min in 1×TBS buffer (**Section 2.2.20.1**). Bound antibodies were detected with ECF substrate (Amersham Biosciences) by FluorImager analysis (Molecular Dynamics).

2.4.3.2. Specific for High Molecular Weight Proteins (>100 kDa)

Western blotting for the high molecular weight proteins Axl, p-Axl, c-ABL, p-c-ABL, and MAP3K5 was performed using the BIO-RAD Trans-Blot® Turbo™ Blotting System according to the manufacturer's instructions. Briefly, lysates of 1×10^6 cells were made as described in **Section 2.4.3.1**, resolved on a BIO-RAD 4-15% Criterion™TGX™ Precast Gel and transferred to PVDF membrane using Midi Transfer Packs (BIO-RAD) at 2.5 A for 10 min. Membranes were then incubated in blocking solution for 1 h at room temperature before being probed with primary antibody as per **Table 2.7**. Following overnight incubation at 4ºC, membranes were rinsed in 1×TBST buffer, and then washed for 3× 5 min with 1×TBST buffer. The membrane was then incubated with secondary antibody as per **Table 2.7** for 1 h at room temperature. Following incubation, the membrane was rinsed in 1×TBST buffer, washed for 3× 5 min with 1×TBST buffer and then washed in 1×TBS buffer for 3× 5 min. Bound antibodies were detected with ECF substrate by FluorImager analysis. For Bcr-Abl IC50 determination (**Section 6.3.6**), membranes were initially probed for p-Bcr-Abl and then stripped with Western Stripping Buffer (Alpha

Diagnostic). Following stripping, membranes were probed for Bcr-Abl. Membranes were also probed for the control protein β-actin following the same incubation conditions as described for primary proteins. Detected proteins were quantified using ImageQuant software and expression normalised to control.

Table 2.7: Incubation conditions for high molecular weight western blot

1° Antibody	Diluent	Concentration	2° Antibody	Diluent	Concentration
Axl	2% BSA/TBST	1:1000	α-rabbit-AP	2% BSA/TBST	1:2000
p-Axl	5% skim milk powder/TBST	1:200	α-rabbit-AP	5% skim milk powder/TBST	1:2000
c-Abl	5% BSA/TBST	1:1000	α-rabbit-AP	5% BSA/TBST	1:2000
p-c-Abl	5% BSA/TBST	1:500	α-rabbit-AP	5% BSA/TBST	1:2000
MAP3K5	5% BSA/TBST	1:1000	α-rabbit-AP	5% BSA/TBST	1:2000

2.4.3.3. Specific for Low Molecular Weight Proteins (<100 kDa)

Western blotting for the low molecular weight proteins β-actin, cdc25C, Chk2, Lyn, p-Lyn, Syk and p-Syk was performed using the BIO-RAD Trans-Blot® Turbo™ Blotting System according to the manufacturer's instructions. Briefly, lysates of 4×10^5–1×10^6 were made as described in **Section 2.4.3.1**, resolved on a BIO-RAD 4-15% Criterion™TGX™ Precast Gel and transferred to PVDF membrane using Midi Transfer Packs (BIO-RAD) at 2.5 A for 7 min. Membranes were then incubated in blocking solution for 1 h at room temperature before being probed with primary antibody as per **Table 2.8**. Following overnight incubation at 4ºC, membranes were rinsed in 1×TBST buffer, and then washed for 3× 5 min with 1×TBST buffer. The membrane was then incubated with secondary antibody as per **Table 2.8** for 1 h at room temperature. Following incubation, the membrane was rinsed in 1×TBST buffer, washed for 3× 5 min with 1×TBST buffer and then washed in 1×TBS buffer for 3× 5 min. Bound antibodies were detected with ECF substrate by FluorImager analysis. Detected proteins were quantified using ImageQuant software and expression normalised to control.

Table 2.8: Incubation conditions for lower molecular weight western blot

1° Antibody	Diluent	Concentration	2° Antibody	Diluent	Concentration
β-actin	5% skim milk powder/TBST	1:1000	α-rabbit-AP	5% skim milk powder/TBST	1:2000
cdc25C	5% BSA/TBST	1:1000	α-rabbit-AP	5% BSA/TBST	1:2000
Chk2	5% skim milk powder/ TBST	1:1000	α-rabbit-AP	5% skim milk powder/TBST	1:2000
Lyn	5% BSA/TBST	1:1000	α-rabbit-AP	5% BSA/TBST	1:2000
p-Lyn	5% BSA/TBST	1:1000	α-rabbit-AP	5% BSA/TBST	1:2000
Syk	2% BSA/TBST	1:1000	α-rabbit-AP	2% BSA/TBST	1:2000
p-Syk	2% BSA/TBST	1:1000	α-rabbit-AP	2% BSA/TBST	1:2000

2.4.3.4. Densitometry Analysis using ImageQuant Software

Phosphorylated and non-phophorylated CrkI bands were quantified using ImageQuant software (Molecular Dynamics) and p-CrkI as a percentage of the total CrkI protein calculated. The average signal for each protein band was determined and background signal from blank membrane deducted. Bands of p-CrkI were measure and graphed as a percentage of the intensity of the total CrkI (ie: p-CrkI +CrkI=100%). The percentages were then normalised with 0 nM TKI representative of 100% p-CrkI and the highest concentration of TKI (eg 100 μM imatinib) representative of 0% p-CrkI. The IC50 value was then taken as the concentration of TKI when normalised p-CrkI reached 50%.

2.4.4. Full Moon BioSystems Antibody Microarray

The antibody microarrays utilise fluorescent detection of proteins and provide a high-throughput system for expression profiling and comparison between treated and untreated samples. For full details of the proteins contained in each array see **Appendix 1B**. The arrays were carried out according to the manufacturer's instructions. Briefly, 2.5×10^6 K562 and K562-Dox cells were harvested, placed in a 50 mL Falcon tubes and centrifuged for 5 min at 417 × *g*. Supernatant was aspirated and cells washed 3× in cold PBS. Cells were transferred to clean 1.7 mL tubes before addition of lysis beads and 200 μL

extraction buffer. Cells were vortexed vigorously for 1 min before incubation on ice for 10 min. The vortexing step was repeated at 10 min intervals for the next 60 min.

Following this, cells were centrifuged at 16000 × *g* for 20 min at 4°C and transferred to clean tubes. Supernatant was applied to spin columns 100 µL at a time, the columns placed in collection tubes and tubes centrifuged for 2 min at 750 *g*. The UV absorptions of resultant protein lysates were measured using a NanoDrop Spectrophotometer (Thermo scientific). Subject to satisfactory absorbance and concentration readings in line with the manufacturer's instructions, 45 µg of lysates were mixed with labelling buffer and 3 µL Biotin/DMF solution. The mixture was incubated at room temperature for 2 h before addition of 35 µL stop reagent. After incubation at room temperature for 30 min, lysates were combined with 6 mL coupling solution and poured over pre-blocked microarray slides. Slides were incubated for 2 h at room temperature on an orbital shaker before washing twice for 10 min in wash solution. Slides were rinsed extensively in Milli-Q® H_2O before detection with detection buffer containing 60 µL Cy3-Streptavidin (0.5 mg/mL). Completed slides were sent to Full Moon BioSystems Array Scanning Service for analysis.

2.4.5. Real Time Quantitative PCR (RQ-PCR)

2.4.5.1. RNA Extraction

1×10^6–1×10^7 cells were lysed in 1 mL of TRIzol reagent and incubated at room temperature for 5 min. 200 µL of chloroform was added, tubes then shaken vigorously for 15 sec and incubated at room temperature for 2–3 min. Following this time, the tubes were centrifuged at 12000 × *g* for 15 min at 4°C. The aqueous phase (top layer) was transferred to a fresh RNase/DNase free 1.5 mL tube. RNA was precipitated by the addition of 1 µL glycogen (20 µg) and 500 µL isopropanol. The samples were gently mixed and incubated at room temperature for 10 min. RNA was pelleted by centrifugation at 12000 × *g* for 10 min at 4°C. The supernatant was removed from the RNA pellet, and the pellet washed

in 1 mL of 75% ethanol and centrifuged at 7500 × *g* for 5 min at 4°C. Supernatant was removed and tubes pulse spun to facilitate removal of excess ethanol. The RNA pellet was briefly dried then dissolved in 20–100 µL DEPC water (depending on size of pellet) at 55°C for 10 min. RNA was quantified using a NanoDrop Spectrophotometer and samples diluted with DEPC water to achieve the desired concentration of between 250 ng–1 µg/µL and stored at -70°C.

2.4.5.2. cDNA Synthesis

1 µg of RNA was added to 1 µL of random hexamers (250 ng/µL) and total volume taken to 11 µL with DEPC water. The mixture was heated to 70°C for 10 min and chilled briefly at 4°C. The first strand synthesis reagent mix was prepared as described below in **Table 2.9**.

Table 2.9: First strand synthesis reagent mix

Reagent	Volume (Per Sample)
5× First strand buffer	4 µL
0.1 M DTT	2 µL
5 mM dNTPs	2 µL
Superscript II	1 µL

9 µL of the reagent mix was then added to each tube, contents gently mixed and placed in a Mastercycler (Eppendorf). Incubation conditions were as follows:

Hold 1 @ 25°C for 10 min

Hold 2 @ 42°C for 50 min

Hold 3 @ 70°C for 10 min

Hold 4 @ 4°C ∞

At the completion of this cycle, 20 µL DEPC water was added to each tube, and the cDNA stored at -20°C.

2.4.5.3. RQ-PCR for Transporter and Src Family Kinase mRNA Expression

RQ-PCR for transporter mRNA expression was performed as previously described by White *et al*.[177]. Primers (see **Table 2.10**) were designed using Primer Express software v2.0 (Applied Biosystems, Foster City, CA), and were diluted to a working stock of 100 ng/µL in DEPC water. PCR master mix was prepared as per **Table 2.11** for each primer set to be tested.

Table 2.10: Primer sequences for transporter PCR

Primer Name	Sequence 5' to 3'
Genes of interest	
ABCA9 forward	CCT TCC ACG AAA CAA GGA AA
ABCA9 reverse	CAG TTC CCA CGG GTA ACT TTT
ABCB1 forward	AGA CAT GAC CAG GTA TGC CTA T
ABCB1 reverse	AGC CTA TCT CCT GTC GCA TTA
ABCC1 forward	AGG TGG ACC TGT TTC GTG AC
ABCC1 reverse	AGG TGA TCC TCG ACA GGA AG
ABCC2 forward	CTG GGA ACA TGA TTC GGA AGC
ABCC2 reverse	GAG GAT TTC CCA GAG CCG AC
ABCC4 forward	GGT TCC CCT TGG AAT CAT TT
ABCC4 reverse	ATC CTG GTG TGC ATC AAA CA
ABCC6 forward	ACA CTT CAA TTG GGG AGC AG
ABCC6 reverse	TGT TGT TCC CTG GAG TAG CC
ABCC12 forward	CTC AGT AGG GGA ACG TCA GC
ABCC12 reverse	TCG CAG TTG AGA ACT GTG TTG
ABCG2 forward	CAC CTT ATT GGC CTC AGG AA
ABCG2 reverse	CCT GCT TGG AAG GCT CTA TG
AQP1 forward	ATT AAC CCT GCT CGG TCC TT
AQP1 reverse	CAT CCA GGT CAT ACT CCT CCA
AXL forward	TGC ATG AAG GAA TTT GAC CA
AXL reverse	TCG TTC AGA ACC CTG GAA AC
CBL forward	GCA GCC CAT TAG TAG GTC CA
CBL reverse	TAA ATG GCA TTG GCA GAT GA
FYN forward	ACG GGA GGT TCA CAA TCA AG
FYN reverse	TTG GTG ACC AGC TCT GTG AG
LYN forward	AAG TTG GTG AAA AGG CTT GG
LYN reverse	GCC ACC TTG GTA CTG TTG TTA

SLC10A1 forward	CCA TAG GGA TCG TCC TCA AA
SLC10A1 reverse	AGG TGG CAA TCA AGA GTG GT
SLC28A3 forward	CTT CGG TGG GCT CAT AAT GT
SLC28A3 reverse	TGA AGC ACC AGC ATC TGT GTA
SYK forward	CAC CAA GGA GGG CAA ATA GA
SYK reverse	TCC CAG CTT CCC AAA TGT AG

Standard	
hRANKL-D Forward	TCA GCC TTT TGC TCA TCT CAC TAT
hRANKL-G Reverse	CCA CCC CCG ATC ATG GT
House-keeping genes	
BCR Forward	CCT TCG ACG TCA ATA ACA AGG AT
BCR Reverse	CCT GCG ATG GCG TTC AC
GUSB forward	CTG AAC AGT CAC CGA CGA GA
GUSB reverse	GAA CGC TGC ACT TTT TGG TT

Table 2.11: Preparation of PCR master mix

Reagent	Volume (per sample)
SYBR Green	5 µL
Forward Primer (100 ng/µL)	0.5 µL
Reverse Primer (100 ng/µL)	0.5 µL
DEPC H_2O	2 µL

8 µL of appropriate Master Mix was added to each tube. The standard used in RQ-PCR is Receptor Activator of Nuclear Factor Kappa-B Ligand (RankL). This was originally supplied by Peter Diamond as a plasmid and serial dilutions made to achieve 10 000 copies per µL. 1 µL of RankL standard cDNA was added to RANKL tubes and 2 µL of unknown or cell line control cDNA was added to the allocated tubes. Tubes were then placed into a 72 well Rotor-Gene (Corbett Research). Results were analysed using Rotor-Gene 6000 Series software (Corbett Research) and transporter expression was calculated as a percentage of house-keeping gene expression (BCR for transporter genes, GUSB for Src kinase genes).

Profile settings on the Rotor-Gene were as follows:

Hold 1 @ 50°C, 2 min

Hold 2 @ 95°C, 15 min

Cycling (48 repeats) Step 1 @ 95°C, hold 15 sec

Step 2 @ 60°C, hold 26 sec

Step 3 @ 72°C, hold 10 sec, acquiring to Cycling A (Sybr)

Hold 3 @ 72°C, 30 sec

2.4.5.4. RQ-PCR for BCR-ABL mRNA Expression

Previously designed primers and probes[211] (see **Table 2.12**) for the b3a2 Bcr-Abl transcript contained in K562 and K562-Dox cells were used. Standards for each transcript (copy number 10–10^6 for b3a2 and 10^3–10^6 for BCR) were prepared and run in every batch. The Hammersmith Hospital supplied the standard as a plasmid containing a modified b3a2 transcript derived from the K562 cell line. Approximately 200 bases are removed from ABL exons 2 and 3 and 100 bases of a different sequence ligated in that region. The resultant plasmid contains an intact sequence in the region of the b3a2 Taqman target sequence. Master mixes were made using the TaqMan Universal PCR Master Mix (Applied BioSystems) as per **Table 2.13**.

Table 2.12: Primer sequences for Bcr-Abl PCR

Primer Name	Sequence 5' to 3'
BCR forward	CCT TCG ACG TCA ATA ACA AGG AT
BCR reverse	CCT GCG ATG GCG TTC AC
TaqMan BCR probe	*TCC ATC TCG CTC ATC ATC ACC GAC A*
b3a2 forward	GGG CTC TAT GGG TTT CTG AAT G
b3a2 reverse	CGC TGA AGG GCT TTT GAA CT
TaqMan b3a2 probe	*CAT CGT CCA CTC AGC CAC TGG ATT TAA GC*

Table 2.13: Preparation of PCR master mix

Reagent	Volume (per sample)
TaqMan Universal PCR Master Mix	12.5 µL
DEPC H_2O	9.55 µL

Forward Primer (50 µM)	0.1 µL
Reverse Primer (50 µM)	0.1 µL
Probe	0.25 µL

22.5 µL of master mix was pipetted into the appropriate wells of a 96-well PCR plate (on ice), before adding 2.5 µL of standards in duplicate (see Setup sheet in **Appendix 1C**). Standard wells were capped before addition of 2.5 µL cDNA to corresponding wells. HeLa cells were used as a negative control and were included in every experiment along with a no template control. High and low quality control samples at two different levels of Bcr-Abl were also included to ensure consistency between assays. The PCR was run on the ABI Prism 7500 Sequence Detection System (Applied Biosystems) with the following cycler conditions:

Hold 1 @ 50°C, 2 min

Hold 2 @ 95°C, 10 min

Cycling (45 repeats) Step 1 @ 95°C, hold 15 sec

Step 2 @ 60°C, hold 1 min

After completion of the run, wells were checked for evaporation and the plate discarded. Results were analysed using the ABI Prism 7500 software (Applied Biosystems).

2.4.6. Taqman Transporter Array

The transporter arrays utilise gene-specific primer and probe sets in order to compare gene expression between treated and untreated samples. For full details of the genes contained the arrays see **Appendix 1D**. The arrays were carried out according to the manufacturer's instructions. Briefly, 6 tubes of cDNA per experimental condition were synthesised as per **Section 2.4.5.2** but the 20 µL DEPC water was not added. cDNA was pooled in a UV cabinet and master mixes made as per **Table 2.14**.

Table 2.14: Preparation of Taqman array master mix

Reagent	Volume (per plate)
TaqMan Universal PCR Master Mix	1040 µL
DEPC H_2O	936 µL
cDNA	104 µL

20 µL master mix was added to each well of the Taqman array plate and the PCR run on the ABI Prism 7500 Sequence Detection System with the following cycler conditions:

Hold 1 @ 50°C, 2 min

Hold 2 @ 95°C, 10 min

Cycling (40 repeats) Step 1 @ 95°C, hold 15 sec

Step 2 @ 60°C, hold 1 min

After completion of the run, wells were checked for evaporation and the plate discarded. Results were analysed using the ABI Prism 7500 software (Applied Biosystems).

2.4.7. Long PCR and BCR-ABL Kinase Domain Sequencing

Previously designed primers (**Table 2.15**) were used for Long PCR and a master mix made as per **Table 2.16**.

Table 2.15: Primer sequences for Bcr-Abl Long PCR

Primer Name	Sequence 5' to 3'
LongF 0810	ACT ATG AGC GTG CAG AGT GGA
LongR 0510	GAG GGA GCA ATG GAG ACA CG

Table 2.16: Preparation of sequencing master mix

Reagent	Volume (per sample)
dNTP (25 mM)	0.75 µL
DEPC H_2O	18.325 µL
10× Buffer 3	2.5 µL

MgCl (25 mM)	0.75 µL
Forward or Reverse Primer	0.15 µL
Expand Enzyme Mix	0.375 µL

Expand enzyme mix and 10× Buffer 3 were used from the Expand Long Template PCR System kit (Roche Diagostics). 23 µL of master mix was pipetted into a flat top PCR tube and 2 µL cDNA added per corresponding sample. The PCR was then run according to the following cycler conditions:

Hold 1 @ 94°C, 2 min

Cycling (10 repeats) Step 1 @ 94°C, hold 10 sec

Step 2 @ 60°C, hold 30 sec

Step 3 @ 68°C, hold 2 min

Cycling (30 repeats) Step 1 @ 94°C, hold 10 sec

Step 2 @ 60°C, hold 30 sec

Step 3 @ 68°C, hold 2 min – increase by 20 sec every cycle

Hold 2 @ 68°C, 7 min

Hold 3 @ 4°C, ∞

After completion of the run, PCR products were visualised on a 2% agarose gel (stained with ethidium bromide) to confirm success of the reaction. The PCR products were then cleaned using an UltraClean™ PCR clean-up DNA purification kit (Mo Bio Laboratories) and diluted 1:4 before being used as a template for sequencing as described previously[212].

The primers for forward and reverse sequencing reactions are as detailed in **Table 2.17** and the master mixes were made as per **Table 2.18**.

Table 2.17: Primer sequences for Bcr-Abl kinase domain sequencing

Primer Name	Sequence 5' to 3'
ABL Kinase F	CGC AAC AAG CCC ACT GTC T
Nest R 1010	CAA GGT ACT CAC AGC CCC ACG GA

Table 2.18: Preparation of PCR master mix

Reagent	Volume (per sample)
Big Dye	1 µL
Sequencing Buffer	2 µL
Forward Primer (50 µM)	0.15 µL
Reverse Primer (50 µM)	0.15 µL
DEPC H_2O	5.85 µL

9 µL of master mix was pipetted into a flat top PCR tube and 1 µL of purified long PCR product added before cycling as follows:

Cycling (25 repeats) Step 1 @ 99°C, hold 10 sec

Step 2 @ 50°C, hold 5 sec

Step 3 @ 60°C, hold 4 min

Hold 1 @ 4°C, ∞

The sequencing reaction was cleaned using the BigDye®XTerminator™ Purification Kit (Applied Biosystems) as follows: 45 µL SAM™ solution and 10 µL XTerminator™ solution were added to each sample and vortexed for 30 min. Tubes were then centrifuged for 2 min at 1000 *g* before being sent to the sequencing department for in-house sequencing. Results were analysed using Mutation Surveyor version 3.24 (SoftGenetics).

2.5. Clinical Details of CML Patients

Newly diagnosed chronic phase CML patients who had not received prior TKI therapy were used in this study. Patients may have been enrolled in the TIDEL II or ENESTxtnd trials. TIDEL II is a phase II

study in adult patients of initial intensified imatinib therapy (600 mg once daily), and sequential dose-escalation (800 mg once daily) followed by treatment with nilotinib (400 mg twice daily) in suboptimal responders to determine the rate and duration of major molecular response. ENESTxtnd is a phase III study in adult patients to evaluate efficacy of initial nilotinib therapy (300 mg twice daily) using molecular response.

2.6. Statistical Analyses

Figures were constructed using GraphPad Prism 5.01© software (GraphPad Software Inc.) and Microsoft Excel 2010 software. Column graphs represent the mean plus the standard error of the mean (SEM) except where specified. Box plots display the median value, the upper 25th and lower 75th percentiles and the whiskers encompass the 10th and 90th percentiles; points outside this range are depicted as individual dots. All statistical analyses were performed using SigmaStat 3.0© software (SPSS Inc.). Normality tests were performed on each data set using a Kolmogorov-Smirnov test. The Levene Median Test was used to assess for equal variance when appropriate. The Mann-Whitney Rank Sum or the Student's *t*-test were used to determine differences between experimental groups. Where the data sets passed the normality and equal variance tests a *t*-test was applied, where the data failed either test a Mann-Whitney Rank Sum was used. Differences were considered to be statistically significant when the probability value (*p*-value) was <0.05.

Chapter 3

Nilotinib is Imported Passively and has no Significant Effect on Imatinib OCT-1 Activity

3.1. Introduction

We, and others, have previously demonstrated that imatinib is predominantly imported into the leukaemic cell via active transport through the organic cation transporter 1 (OCT-1)[147-150]. OCT-1 activity is determined by the difference between imatinib Intracellular Uptake and Retention (IUR) in the absence and presence of the specific OCT-1 inhibitor prazosin and is highly predictive of patient response[151,177]. Conversely, nilotinib does not require OCT-1 to gain entry to leukaemic cells[150] and instead this drug appears to enter cells in a predominantly passive manner[187]. Previous research from our laboratory has demonstrated that the addition of nilotinib to radiolabelled imatinib reduced the intracellular concentrations of imatinib, however this reduction failed to reach statistical significance[194]. More recently it was proposed that the nilotinib-mediated reduction of intracellular imatinib was due to inhibition of OCT-1[187]. This suggestion could have significant implications for imatinib/nilotinib combination therapies as well as an adversely affecting the action of concomitantly administered medications transported by OCT-1, such as the diabetes drug metformin[213,214] and ranitidine[215] which inhibits the production of stomach acid. This chapter aims to assess the effect of nilotinib on imatinib OCT-1 activity as this measurement is the key predictor of long term patient response[151].

3.2. Approach

IUR experiments were performed as described (**Section 2.4.1**) on CML cell lines as well as thawed CML patient mononuclear cells (MNCs) (**Section 2.3.5**) isolated from peripheral blood diagnosis samples. OCT-1 activity was measured using the OCT-1 inhibitor prazosin (**Section 2.4.1.1**). The IUR and OCT-1 activity are expressed as ng of TKI per 200 000 cells. To investigate the transport kinetics of nilotinib compared with imatinib, K562 cells were incubated with either ^{14}C-imatinib or -nilotinib (2 μM) at 37°C versus 4°C for timepoints ranging from 2 min to 2 h. At 37°C all modes of cellular transport are functional whereas at 4°C active transport in the cell is inhibited and any alterations in intracellular drug concentrations are predominantly due to passive transport. To investigate the effect of nilotinib on

imatinib OCT-1 activity, patient cells were incubated with ^{14}C-imatinib at 1 μM and 2 μM for 2 h at 37°C alone and in combination with prazosin (100 μM) and non-radiolabelled nilotinib (1 μM and 2 μM). Imatinib was used at 1 and 2 μM as these concentrations accurately reflect trough levels seen in patient plasma. Nilotinib was used at 1 and 2 μM as we have previously shown a nilotinib-mediated decrease in intracellular imatinib at these concentrations[194] and it has been postulated that this is due to inhibition of OCT-1 by nilotinib[187]. Thus, in order to distinguish the effects of nilotinib on passive versus active (OCT-1-mediated) imatinib import, experiments were performed in K562 cells at both 37°C and 4°C. Additionally, it has previously been suggested that higher concentrations of nilotinib could abolish uptake of OCT-1 substrates such as imatinib and tetraethylammonium bromide (TEA). Thus, in order to investigate this hypothesis, IUR experiments were performed with ^{14}C-imatinib and -TEA in the absence and presence of 4 μM nilotinib. The analyses discussed in this chapter were used to determine how nilotinib uptake kinetics differ from those of imatinib and whether there is any detrimental effect on imatinib OCT-activity when used in combination with nilotinib.

3.3. Results

3.3.1. The Uptake Kinetics of Nilotinib are Different to Imatinib and Provide a Strong Indication for ATP-Dependent Efflux

K562 cells were incubated in the presence of 2 μM ^{14}C-labelled TKI at differing temperatures and time points. Results demonstrated that after 15 min incubation with ^{14}C-nilotinib there was no significant difference in the IUR of nilotinib at 4°C versus 37°C (p=0.972; **Table 3.1**), arguing against an active mode of influx. However, after 2 h incubation the IUR of nilotinib was significantly less at 37°C than at 4°C (p<0.001; **Figure 3.1**) providing a strong indication for this drug undergoing ATP-dependent efflux. Conversely, the IUR of imatinib was significantly higher at 37°C than at 4°C for both timepoints (p=0.008 and p=0.024 respectively; **Figure 3.2**). Thus, data demonstrate that the kinetics of intracellular drug accumulation of nilotinib is statistically different to that of imatinib and indicates that

Table 3.1: The uptake kinetics of nilotinib are significantly different to imatinib

	15 min (ng/200 000 cells)	2 h (ng/200 000 cells)	
^{14}C-nilotinib at 37°C	279 ± 88	89 ± 22	***p*<0.001**
^{14}C nilotinib at 4°C	283 ± 75	283 ± 94	*p*=0.951
	p=0.972	***p*<0.001**	
^{14}C-imatinib at 37°C	44 ± 10	35 ± 10	*p*=0.342
^{14}C-imatinib at 4°C	22 ± 8	21 ± 6	*p*=0.576
	***p*=0.008**	***p*=0.024**	

K562 cells were incubated in the presence of 2 μM ^{14}C-labelled TKI as indicated. Data suggest that nilotinib is actively pumped out of the cell at 37°C but not at 4°C indicating passive influx and an ATP-dependent efflux mechanism. Conversely, imatinib IUR remains stable over 2 h at both 37°C and 4°C confirming imatinib enters the cell in an active manner. The data represent the median of at least five separate experiments performed in triplicate ±SD. Statistical analyses were performed using Student's *t*-test with statistically significant *p*-values highlighted in bold.

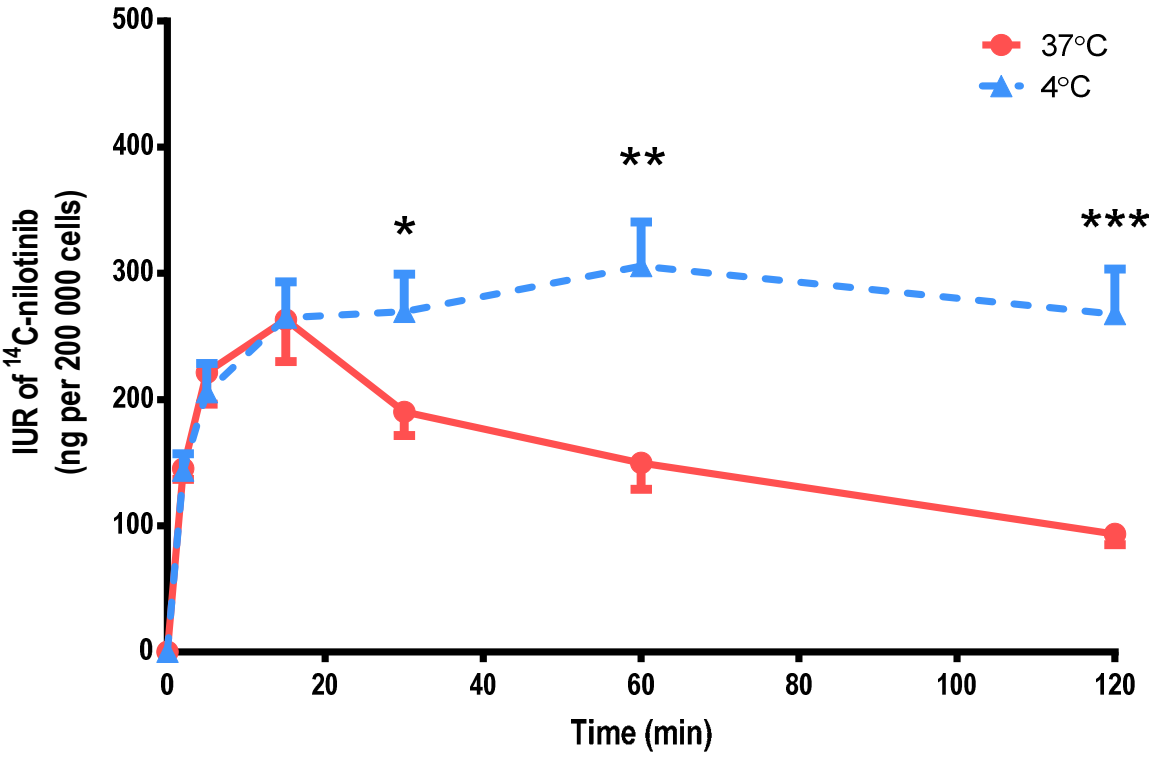

Figure 3.1: Nilotinib enters K562 cells passively followed by active efflux at 37°C

K562 cells were incubated in the presence of 2 μM ^{14}C-nilotinib at differing temperatures for 2 min to 2 h. Data indicate uptake of ^{14}C-nilotinib within the first 15 min of incubation is efficient and predominantly passive; however a temperature dependent, ATP-related efflux mechanism subsequently predominates resulting in a reduction in IUR at 37°C but not at 4°C. The data represent the mean of seven separate experiments performed in triplicate. Statistical analyses were performed using Student's *t*-test with statistically significant *p*-values denoted by asterisks at the corresponding time points (* $p<0.05$; ** $p<0.01$; *** $p<0.001$). Error bars represent SEM.

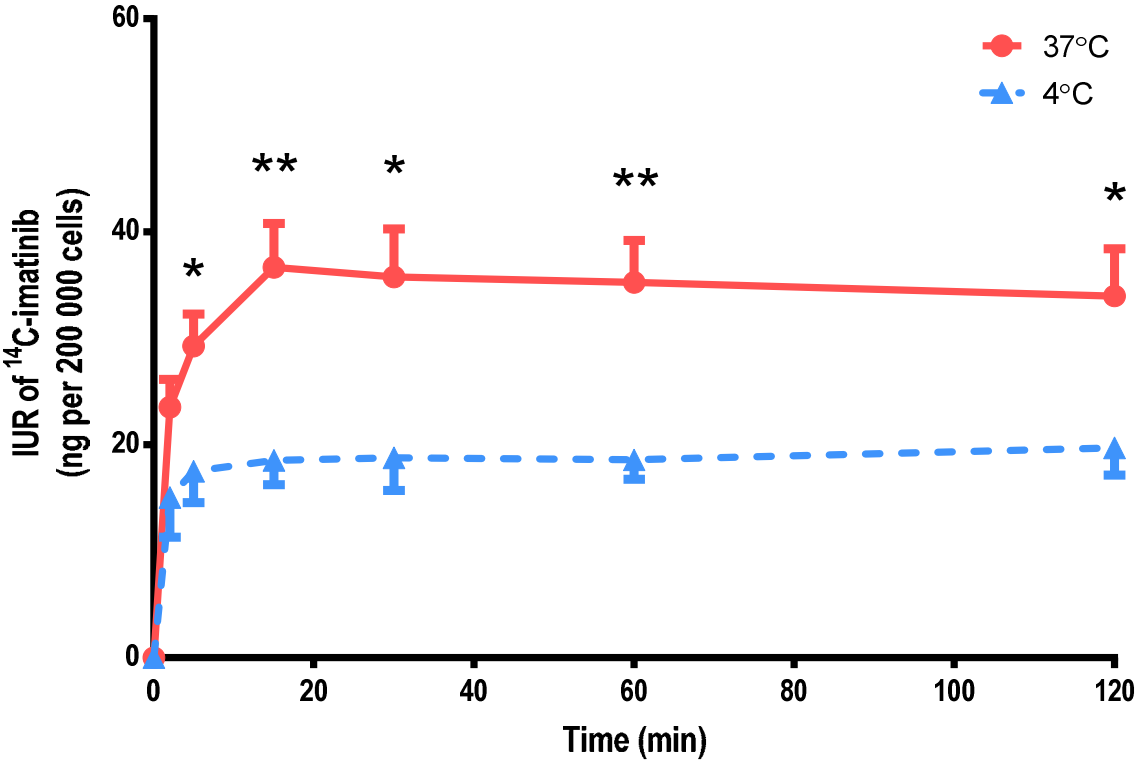

Figure 3.2: Imatinib enters K562 cells via active transport and is retained for at least two hours

K562 cells were incubated in the presence of 2 μM ^{14}C-imatinib at differing temperatures for 2 min to 2 h. Data indicate OCT-1 mediated active uptake of ^{14}C-imatinib contributing to the stability of intracellular concentrations over the 2 h time period assayed. The data represent the mean of five separate experiments performed in triplicate. Statistical analyses were performed using Student's *t*-test with statistically significant *p*-values denoted by asterisks at the corresponding time points (* $p<0.05$; ** $p<0.01$). Error bars represent SEM. Imatinib IUR experiments were conducted by Amity Frede who had no role in the analysis of the data.

nilotinib is rapidly taken into cells in an ATP-independent manner. This is in contrast to active influx of imatinib via OCT-1. Once equilibrium between influx and efflux of imatinib was established over the two hour time period, a balance occurred between active import by OCT-1 and efflux, resulting in the characteristically stable intracellular imatinib concentrations observed. However, since the uptake of nilotinib is most likely passive, along a concentration gradient, the same pattern of transport kinetics did not occur. Instead, the active efflux component predominated resulting in the export of nilotinib from the cell and the subsequent reduction observed in intracellular concentrations.

3.3.2. Nilotinib has No Significant Effect on OCT-1 Activity in CML Patient Cells

In order to examine the effects of nilotinib on intracellular imatinib concentrations, as well as the functional activity of the OCT-1 protein, patient MNCs were incubated with nilotinib and imatinib in combination. While intracellular concentrations of ^{14}C-imatinib in patient cells were reduced in the presence of 1 μM and 2 μM nilotinib when the two TKIs were incubated simultaneously at 37°C, this reduction failed to reach statistical significance at either concentration: 1 μM imatinib alone=8.1, +1 μM nilotinib=7.6, +2 μM nilotinib=7.6 ng/200 000 cells; 2 μM imatinib alone=17.1, +1 μM nilotinib=15.1, +2 μM nilotinib=15.1 ng/200 000 cells; p>0.05 for all data points (**Figure 3.3**). There was also no significant effect of 1 μM and 2 μM nilotinib when used in conjunction with the OCT-1 inhibitor prazosin, and therefore no effect on imatinib OCT-1 activity in this patient cohort (n=7, p=0.710 and 0.974 respectively). Similar experiments were performed with K562 cells, with results confirming those observed in patient cells (**Figure 3.4**). Again, addition of nilotinib to ^{14}C-imatinib decreased imatinib IUR without this reduction reaching statistical significance: 1 μM imatinib alone=12.9, +1 μM nilotinib=11.1, +2 μM nilotinib=11.2 ng/200 000 cells; 2 μM imatinib alone=26.9, +1 μM nilotinib=21.0, +2 μM nilotinib=21.2 ng/200 000 cells; p>0.05 for all data points. It is important to note that while the reductions observed in imatinib IUR upon addition of nilotinib and prazosin in most patients and cell lines are not statistically significant, these reductions occur consistently in every experiment performed.

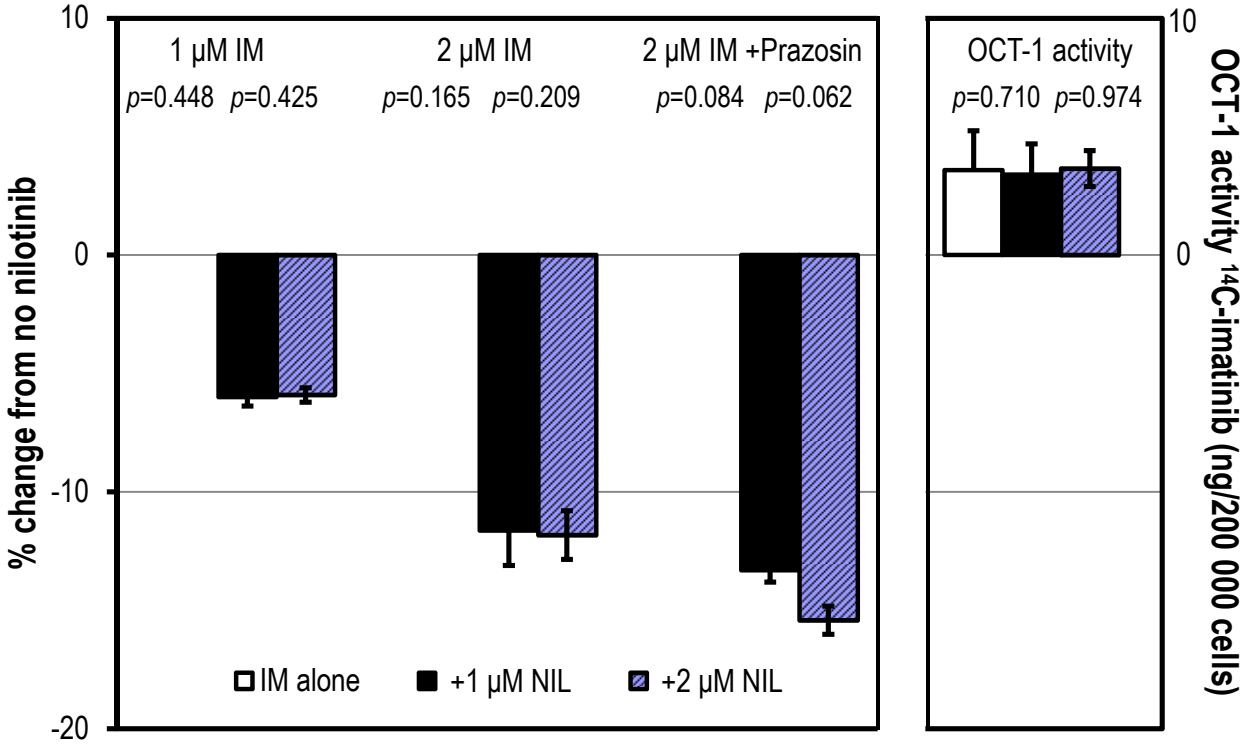

Figure 3.3: Nilotinib reduces imatinib IUR without affecting OCT-1 activity in patient cells

Patient MNCs were incubated with ^{14}C-imatinib and the IUR determined by scintillation counting. The percentage change in the presence of 1 µM and 2 µM nilotinib was calculated when compared with cells incubated in the absence of nilotinib. OCT-1 activity is a read out for the functional activity of the OCT-1 protein and data demonstrate that the addition of nilotinib has no significant effect on the OCT-1 activity of imatinib. Data represent the mean from experiments performed in triplicate from seven different patients. Statistical analyses were performed using Student's *t*-test. *p*-values on the left correlate with MNCs incubated with 1 µM nilotinib while *p*-values on the right correlate with MNCs incubated with 2 µM nilotinib. Error bars represent SEM. IM=imatinib; NIL=nilotinib.

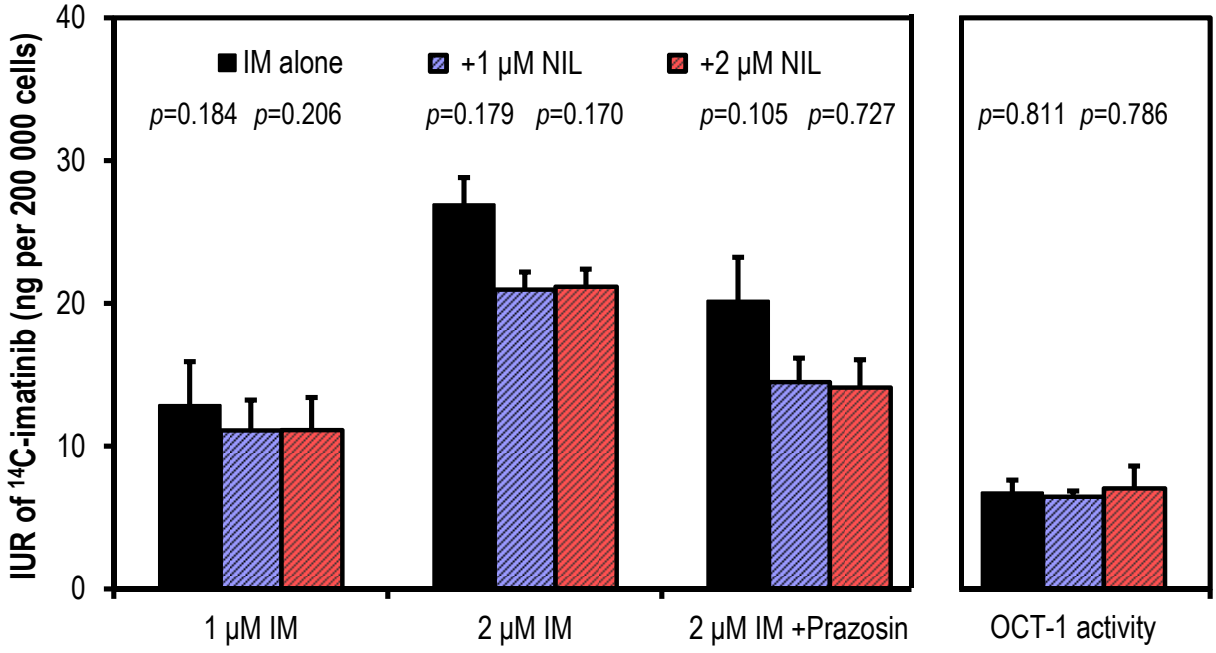

Figure 3.4: Nilotinib reduces imatinib IUR without affecting OCT-1 activity in cell lines

K562 cells were incubated with ^{14}C-imatinib at 37ºC in the absence and presence of prazosin and the IUR determined by scintillation counting. Data demonstrate that the addition of 1 μM and 2 μM nilotinib consistently reduces the IUR of imatinib (1 and 2 μM). The addition of prazosin further reduces imatinib IUR while having no effect on OCT-1 activity. Data represent the mean from three separate experiments performed in triplicate. Statistical analyses were performed using Student's *t*-test. Error bars represent SEM. IM=imatinib; NIL=nilotinib.

Thus, it is possible that even though nilotinib does not adversely affect the major mode of imatinib uptake (OCT-1), it is able to exert influence over a minor efflux mode. Consistent with this reasoning is the fact that the most notable reduction in intracellular imatinib concentrations in CML patient MNCs is observed in the 2 μM imatinib +prazosin arm of the experiment, in which the OCT-1 independent, most likely passive, influx of imatinib is measured (**Figure 3.3**). While uptake of imatinib is primarily active, a passive component also contributes to intracellular drug levels. Thus, these data suggest that nilotinib is affecting this mode of imatinib transport rather than the OCT-1-mediated import upon which patient response is dependent.

3.3.3. Nilotinib Hinders Passive Imatinib Uptake

In order to investigate the effect of nilotinib on passive imatinib uptake further, IUR experiments with K562 cells performed at 37ºC and 4ºC were compared. As detailed above, at 37ºC a reduction in intracellular ^{14}C-imatinib in the presence of 1 μM and 2 μM nilotinib was observed, confirming results from patient cells. Importantly, there was no effect on OCT-1 activity (**Figure 3.4**). Similar experiments conducted at 4ºC (**Figure 3.5**), a temperature at which OCT-1 mediated uptake of imatinib is inhibited, demonstrated that the level of 2 μM imatinib alone is reduced to levels comparable to those observed in the 37ºC +prazosin arm of the experiment (16.8 vs 20.2 ng per 200 000 cells respectively; p=0.368). Furthermore, at 4ºC there was an additional reduction in the intracellular concentration of imatinib in the presence of 1 μM and 2 μM nilotinib (13.1 and 13.7 ng per 200 000 cells respectively) suggesting that the effect of nilotinib is mediated through passive, and not active, ATP-dependent mechanisms such as inhibition of OCT-1. As anticipated, there was no measurable effect of prazosin at 4ºC.

It has previously been suggested that high micromolar concentrations of nilotinib are capable of reducing uptake of OCT-1 substrates[187]. Thus, in order to further examine the effect of nilotinib on OCT-1 mediated drug uptake, the experiments of Davies *et al.*, in which 4 μM nilotinib reduced the

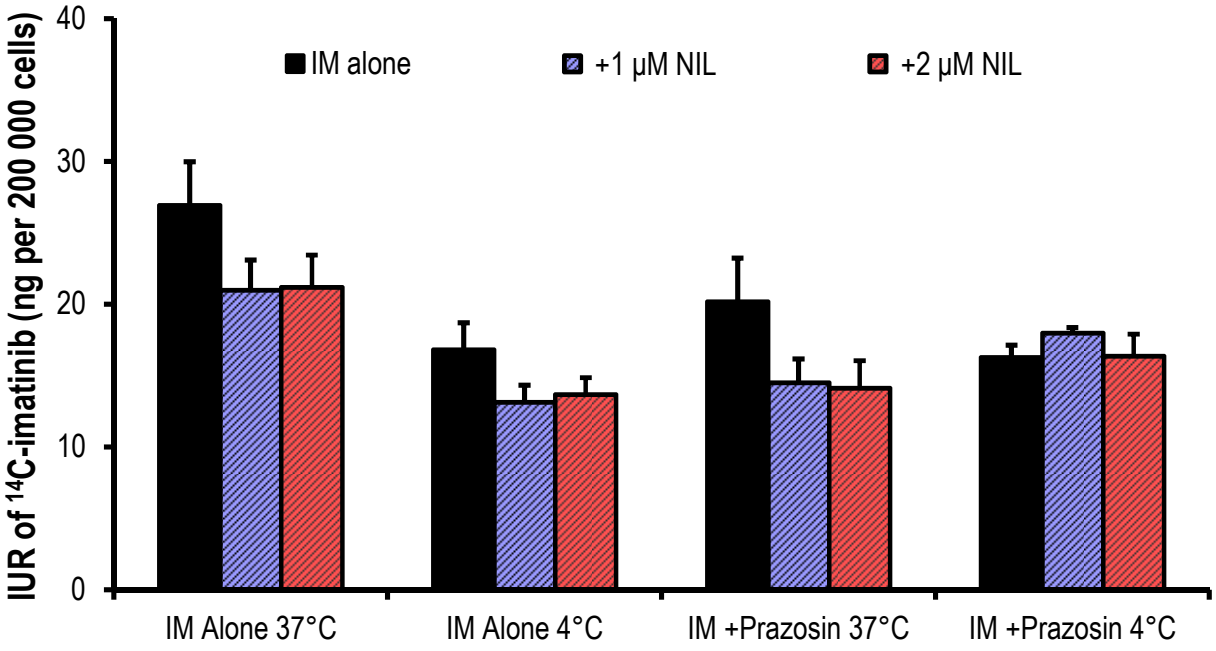

Figure 3.5: Nilotinib reduces imatinib IUR by inhibiting passive uptake

K562 cells were incubated with 2 µM ^{14}C-imatinib at 37ºC and 4ºC in the absence and presence of prazosin and IUR determined by scintillation counting. Data demonstrate that the IUR of imatinib at 4ºC in the absence and presence of nilotinib is comparable to that seen at 37ºC in the presence of prazosin. Addition of 1 µM and 2 µM nilotinib consistently reduces the IUR of imatinib. The addition of prazosin further reduces imatinib IUR while having no effect on OCT-1 activity. Data represent the mean from four separate experiments performed in triplicate. Error bars represent SEM. IM=imatinib; NIL=nilotinib.

uptake of both imatinib and the model OCT-1 substrate TEA, were recapitulated. In contrast to this previous report, we found that 4 μM nilotinib did not reduce the intracellular concentrations of either imatinib (**Table 3.2**) or TEA (**Table 3.3**).

3.4. Discussion

While much is known about the transport kinetics of imatinib, to date, little has been published on those of nilotinib. A better understanding of how nilotinib is transported into and out of the leukaemic cell may allow enhancement of drug uptake and retention via modulation of any drug transporters involved. Additionally, increased knowledge of nilotinib transport may also lead to new advances regarding the efflux of this TKI, with the possibility of inhibition of any drug transporters involved. The findings described in this chapter strongly suggest that nilotinib enters the leukaemic cell in a passive manner which is in contrast to the active OCT-1-dependent influx of imatinib. Maximum intracellular concentrations of ^{14}C-nilotinib are reached within 15 min of incubation, followed by a rapid, temperature-sensitive decrease. The kinetics of imatinib uptake demonstrate that at 37ºC equilibrium exists between active/passive influx and active/passive efflux resulting in the high stable intracellular levels observed. At 4ºC, there is again equilibrium between influx and efflux, however, at this temperature transport is predominantly passive resulting in the lowered stable intracellular levels observed. The kinetics of nilotinib differ to those of imatinib in that influx is likely due to passive mechanisms only. Thus, at 37ºC, active efflux predominates resulting in intracellular levels that decline over time. However, at 4ºC the equilibrium that exists between passive influx and efflux results in the stable intracellular levels observed (**Figure 3.6**).

One might wonder why the decline in intracellular nilotinib occurs after fifteen minutes rather than immediately following drug exposure. There are two possible explanations for this: the first being that nilotinib may up-regulate expression of its own transporter, a phenomenon observed previously with

Table 3.2: High concentrations of nilotinib have no effect on the IUR of imatinib

	0.5 μM imatinib	+nilotinib	1 μM imatinib	+nilotinib	2 μM imatinib	+nilotinib
K562	7.5 ± 0.5	7.0 ± 1.3	13.0 ± 2.5	13.1 ± 2.8	26.7 ± 3.4	23.3 ± 4.4
p-values		0.738		0.982		0.575
KCL22	7.4 ± 0.4	7.6 ± 0.3	14.6 ± 1.3	15.6 ± 0.2	30.1 ± 3.2	27.4 ± 3.2
p-values		0.715		0.467		0.595

K562 and KCL22 cells were incubated for 2 h at 37ºC in the presence of the indicated drug combinations. The IUR of imatinib in the absence and presence of 4 μM nilotinib was then determined via scintillation counting. Data demonstrate that nilotinib has no significant effect on imatinib IUR at concentrations previously reported to abolish ^{14}C-imatinib uptake. All values were calculated in ng per 200 000 cells. Data represent the mean from three separate experiments performed in triplicate ±SEM. Statistical analyses were performed using Student's *t*-test.

Table 3.3: High concentrations of nilotinib have no effect on the IUR of TEA

Time points (min)	0	2	15	30	60	120
TEA alone	0	9.9 ± 1.2	9.6 ± 0.6	9.2 ± 0.9	10.1 ± 0.5	11.3 ± 0.7
+4 μM nilotinib	0	9.9 ± 0.8	10.9 ± 1.3	10.5 ± 0.7	11.1 ± 0.7	11.3 ± 1.2
p-values	N/A	0.982	0.422	0.316	0.300	0.973

K562 cells were incubated for time periods ranging from 2 min to 2 h at 37ºC with ^{14}C-TEA (5 μM) in the absence and presence of 4 μM nilotinib. The concentration of TEA per 200 000 cells was then determined via scintillation counting. Data demonstrate that the addition of nilotinib has no significant effect on the IUR of TEA as previously reported. Data represent the mean of four separate experiments performed in triplicate ±SEM. Statistical analyses were performed using Student's *t*-test.

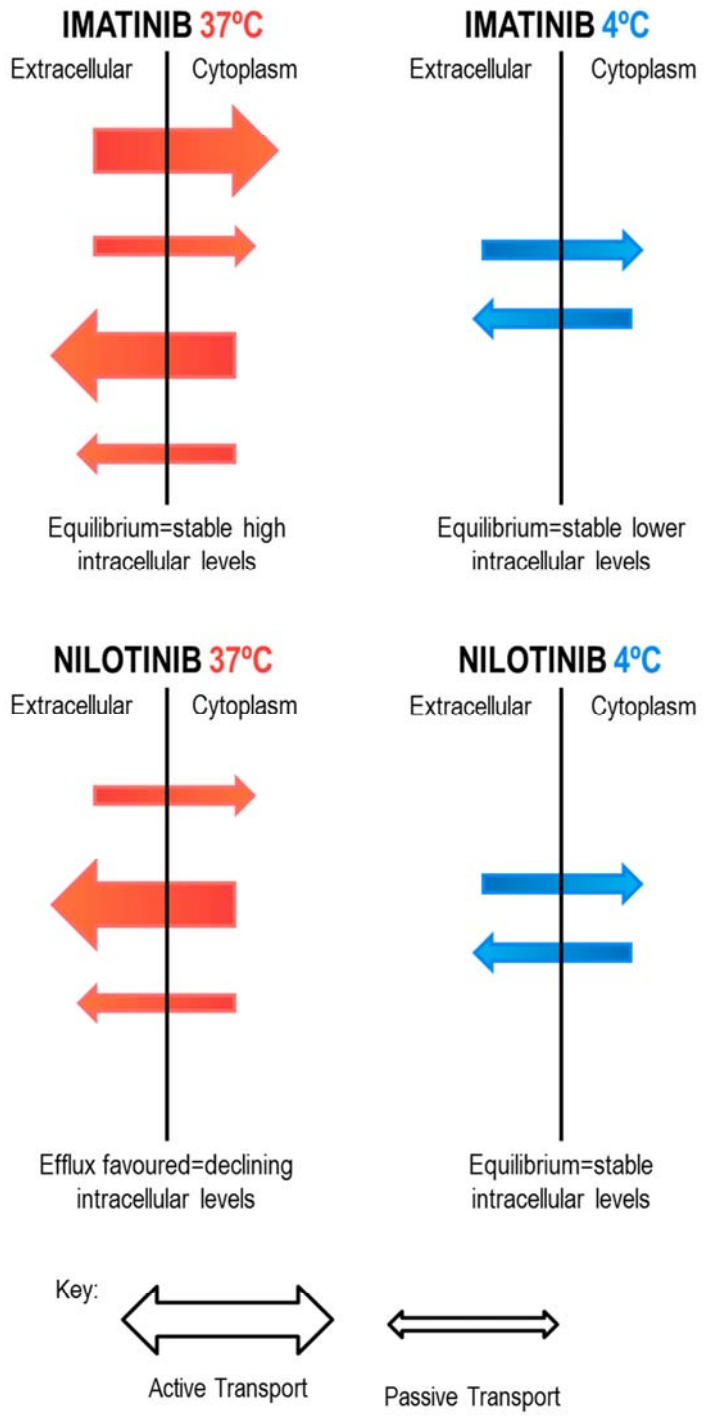

Figure 3.6: Schematic representation of the net effect of temperature on TKI transport

At 37ºC, the equilibrium between imatinib influx and efflux results in a stable high intracellular concentration. At 4ºC the intracellular levels remains stable but are lower due to the absence of active transport. Conversely, at 37ºC active efflux of nilotinib predominates over passive influx resulting in intracellular levels that decline over time. Whereas at 4ºC, passive transport of nilotinib results in stable intracellular levels analogous to those of imatinib.

other xenobiotics[138,216-219] and further discussed in **Chapter 7**. Secondly, movement of substrates through transporters is not instantaneous with prior research demonstrating that substrate traversal of the lipid bilayer via ABCB1 can take from minutes (doxorubicin) up to an hour (rhodamine-123)[220]. Therefore, it is possible that nilotinib requires approximately fifteen minutes to move through its efflux transporter/s whereby explaining the delay before intracellular levels begin to decline. Because efflux transporters appear to play such a critical role in the determination of intracellular nilotinib concentrations, it is unlikely that accumulation of nilotinib can be further improved by alteration of drug influx, but instead, potentially by inhibition of efflux transporters as discussed in further chapters.

OCT-1 activity is defined as the functional activity of the OCT-1 protein and is determined by assessing the levels of imatinib in the absence and presence of the OCT-1 inhibitor, prazosin. Our laboratory has previously demonstrated this measure is highly predictive of long term patient response to imatinib[151,177]. We[194] and others[187] have observed a decrease in intracellular imatinib in the presence of nilotinib and this has been postulated to be due to inhibition of the OCT-1 protein[187]. Thus, determining whether nilotinib adversely affects imatinib OCT-1 activity is crucial, especially given the increasing emphasis on combination and individualised therapy regimes in the treatment of CML. The data described here provide no evidence of a nilotinib-mediated effect on imatinib OCT-1 activity. Although the addition of nilotinib to imatinib does result in a decrease in the intracellular concentration of imatinib, this reduction fails to reach statistical significance. No evidence was found that this decrease is mediated through OCT-1 or any other active process, suggesting that nilotinib may interfere with the passive uptake of imatinib. It is well established that nilotinib is more lipophilic than imatinib, offering the possible explanation that nilotinib is more likely to be trapped in the plasma membrane resulting in steric hindrance of the passive import of imatinib through the cell membrane (**Figure 3.7**).

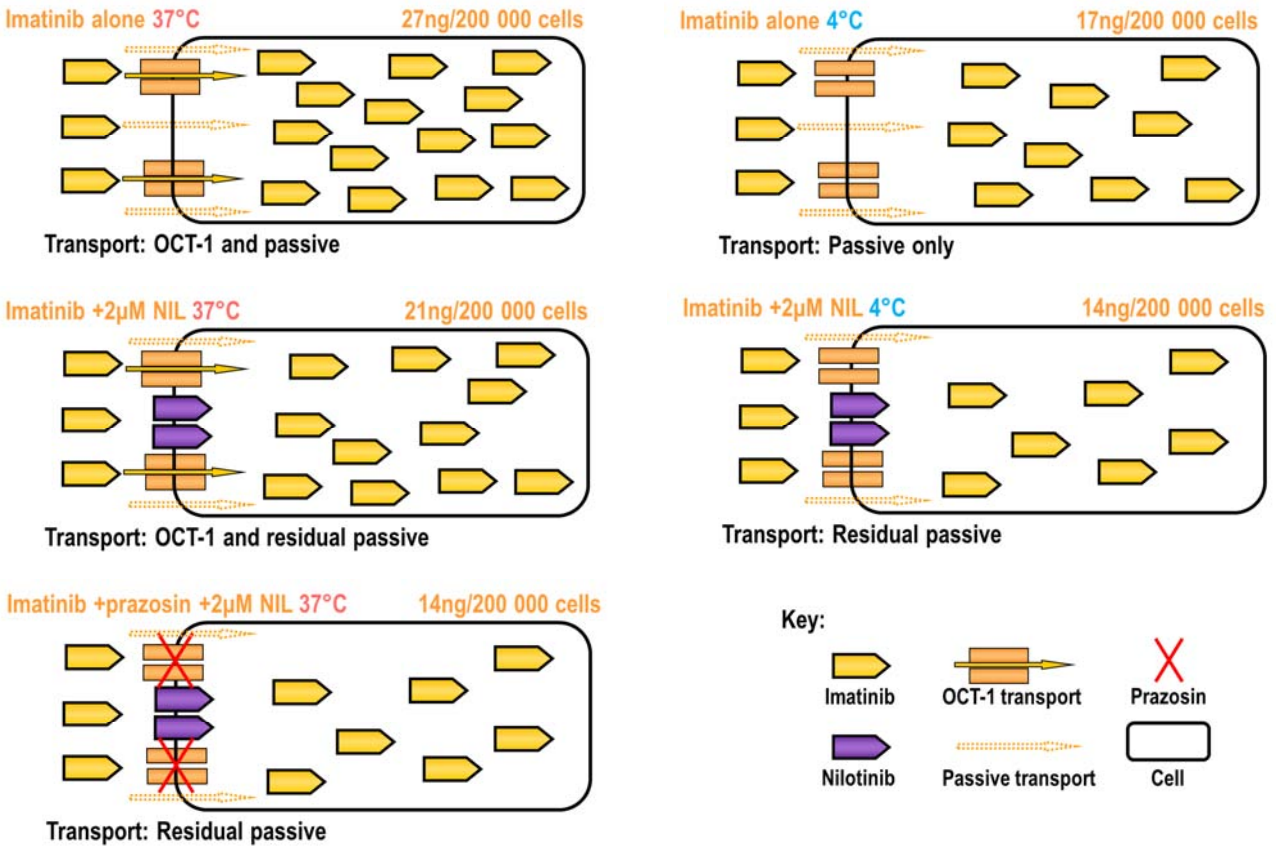

Figure 3.7: Schematic summary of the effects of nilotinib and temperature on imatinib influx

At 37ºC both active and passive influx of imatinib occurs, whereas at 4ºC only passive influx occurs resulting in a lowered IUR (upper figures). Passive influx of imatinib is blocked in the presence of nilotinib at both 37ºC and 4ºC but the IUR at 4ºC is significantly decreased due to the additional inhibition of active influx at this temperature (middle figures). In the presence of both prazosin and nilotinib, the IUR is comparable to that in the 4ºC imatinib +nilotinib arm of the experiment as here both active and passive transport is also inhibited (lower figure).

OCT-1 has a large extracellular substrate binding domain containing multiple binding sites, hence we wanted to determine whether the influx of other OCT-1 substrates was also affected by nilotinib. Studies performed by Davies *et al.*[187] suggest that nilotinib is able to reduce uptake of the model OCT-1 substrate, tetraethylammonium bromide (TEA), and the authors conclude this is due to nilotinib disrupting the function of OCT-1. However, as we did not observe any effect of nilotinib on OCT-1 activity, we sought to replicate these experiments. In agreement with data from the imatinib and nilotinib combination experiments described, we found the uptake of TEA was unaffected by addition of nilotinib after two hours co-incubation. Davies *et al.* performed timecourse experiments assessing the effect of nilotinib on the uptake of TEA over a period of 10 min–2 h. Results demonstrated an initial inhibition of TEA uptake in the presence of 4 μM nilotinib, however, the difference was abolished by later time points. In fact, results confirmed those described here with no difference in intracellular TEA concentrations apparent following two hours incubation with nilotinib. Moreover, the extremely high micromolar concentrations of nilotinib used in their studies are unlikely to be achieved intracellularly in patients, demanding caution in interpretation of their results. Thus, while we conclude it is unlikely that OCT-1-mediated transport of drugs such as imatinib and metformin would be blocked when co-administered with nilotinib, due to the multiple binding sites within the OCT-1 protein, it is not possible to infer from experiments performed with one OCT-1 substrate a universal effect on all substrates. The interaction of different substrates must be independently assessed as binding regions within the extracellular domain may or may not overlap or interact.

In conclusion, data presented here demonstrates that the transport kinetics of nilotinib differ from those of imatinib and suggest that transport of this drug is mediated by passive influx and active efflux. The findings presented in this chapter also illustrate that while nilotinib does decrease what is most likely passive imatinib uptake, albeit insignificantly, it has no effect on OCT-1 activity. Nilotinib also has no significant effect on the uptake of the model OCT-1 substrate TEA. No evidence was found that nilotinib

would result in significant reductions in the intracellular concentration of co-administered drugs, such as imatinib, metformin or ranitidine, which are also transported through OCT-1.

Chapter 4

Nilotinib-Mediated Kinase Inhibition is Decreased by High Levels of ABCB1 but not ABCG2

4.1. Introduction

Intracellular drug concentrations are dependent on numerous parameters including absorption, distribution, metabolism, excretion and toxicity (ADME-Tox). One of the major groups of transporters involved in ADME-Tox is the ATP-Binding Cassette (ABC) superfamily. These transporters are capable of transporting chemotherapeutics and other xenobiotics across cell membranes and have been identified as a cause of multidrug resistance[172]. ABC transporters are expressed at points of drug penetration and hence play a key role in the removal of a wide variety of toxic agents from cells as well as the prevention of such compounds from traversing tissue barriers and penetrating 'sanctuary' sites such as the brain and testes. ABC transporters are comprised of, at minimum, four characteristic domains: two helical transmembrane regions embedded within the cell membrane and two cytoplasmic ATP-binding domains. While the ATP-binding domains are highly conserved, the transmembrane domains vary, thus allowing interaction with, and transport of, a diverse range of compounds[173]. Two prominent members of the ABC superfamily, ABCB1 and ABCG2 have previously been implicated in the efflux of tyrosine kinase inhibitors (TKIs) from Chronic Myeloid Leukaemia (CML) cells[115,140,146]. However, much conjecture exists concerning the TKI:ABC transporter relationship. Some studies suggest TKIs are ABC transporter substrates[145,153,154,176,179], while others suggest the TKIs have an inhibitory function[155,180-182,187,189]. Furthermore, the reported TKI:ABC transporter relationships vary with each TKI and transporter, as well as with the specific concentration of TKI tested in individual studies.

ABCB1 (multidrug resistance protein 1, MDR1; P-glycoprotein, PgP) is a 170 kDa protein primarily expressed at blood-tissue barriers such as blood-brain and blood-testis as well as at the apical surface of cells found in the liver, intestine, kidney and importantly, primitive haematopoietic stem cells[172]. The transporter consists of twelve membrane spanning regions and two ATP-binding domains[221] (**Figure 4.1**) which hydrolyse molecules of ATP in two separate reactions in order to transport a substrate; usually a hydrophobic molecule of neutral or positive charge[222]. The first hydrolysis reaction provides

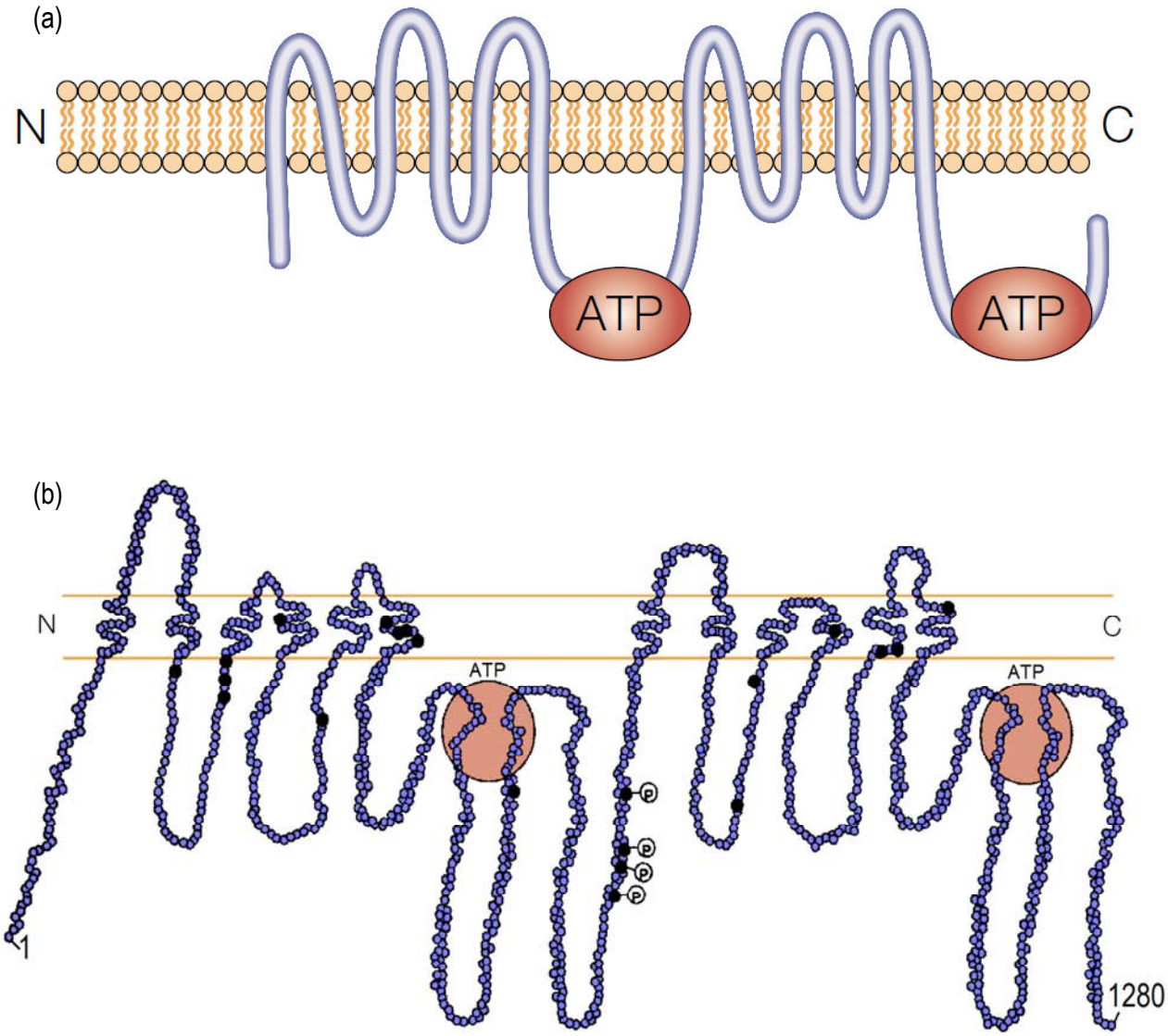

Figure 4.1: Structure of ABCB1

a) Schematic representation showing the protein's twelve transmembrane regions and two ATP-binding sites[223]. b) A two-dimensional model of ABCB1 showing the 1280 amino acid sequence (**PURPLE**) with key point mutations altering substrate specificity shown in **BLACK** and sites of phosphorylation designated (**P**) (modified from Ambudkar *et al*.[222]).

energy for substrate transportation while the second is required to transform the transporter back to its original conformation ready for substrate binding[224]. It has been proposed that ABCB1 contains at least three drug binding sites which interact to cooperatively transport substrate[225-228], (**Figure 4.2a**). However, more recent studies suggest a single large, flexible binding region containing subsites for binding of multiple drug molecules simultaneously. These distinct but over lapping domains allow induced fit of numerous substrates through hydrogen bonding and hydrophobic interactions with the amino acids lining the binding pocket. Additionally, the number, magnitude and specificity of these interactions determine the strength of drug binding (**Figure 4.2b**)[229,230].

ABCG2 (breast cancer resistance protein, BCRP) is a 72 kDa protein which is also primarily expressed at blood-tissue barriers with mRNA analysis indicating this transporter is most prevalent in placental tissue[231,232]. ABCG2 is also expressed to a lesser extent at the apical surface of brain, liver, prostate, intestinal and stem cells[172,231]. Unlike ABCB1, ABCG2 exists as a half-transporter consisting of six transmembrane regions and one ATP-binding domain (**Figure 4.3a**) that dimerises to form a functional homodimer[223,233]. In addition, it has been suggested that ABCG2 subunits are also capable of assembling into a functional tetrameric structure with a central aqueous region bridged by disulphide bonds[234-236]. To date, no crystal structure is available for ABCG2, however, computational modelling based on closely related bacterial transporters combined with predicted secondary structures have resulted in a hypothetical structure[237] . Images from high resolution electron microscopy confirm that ABCG2 most likely functions as a tetrameric complex comprised of four ABCG2 homodimers[234-236] transporting diverse substrates of both positive and negative charge, sulphate conjugates as well as organic anions (**Figure 4.3b**)[232]. In contrast to most other ABC transporters, ABCG2 contains the ATP-binding domain at the N-terminal of the protein. However, like ABCB1, ABCG2 is also predicted to have multiple binding sites with over lapping specificities[238].

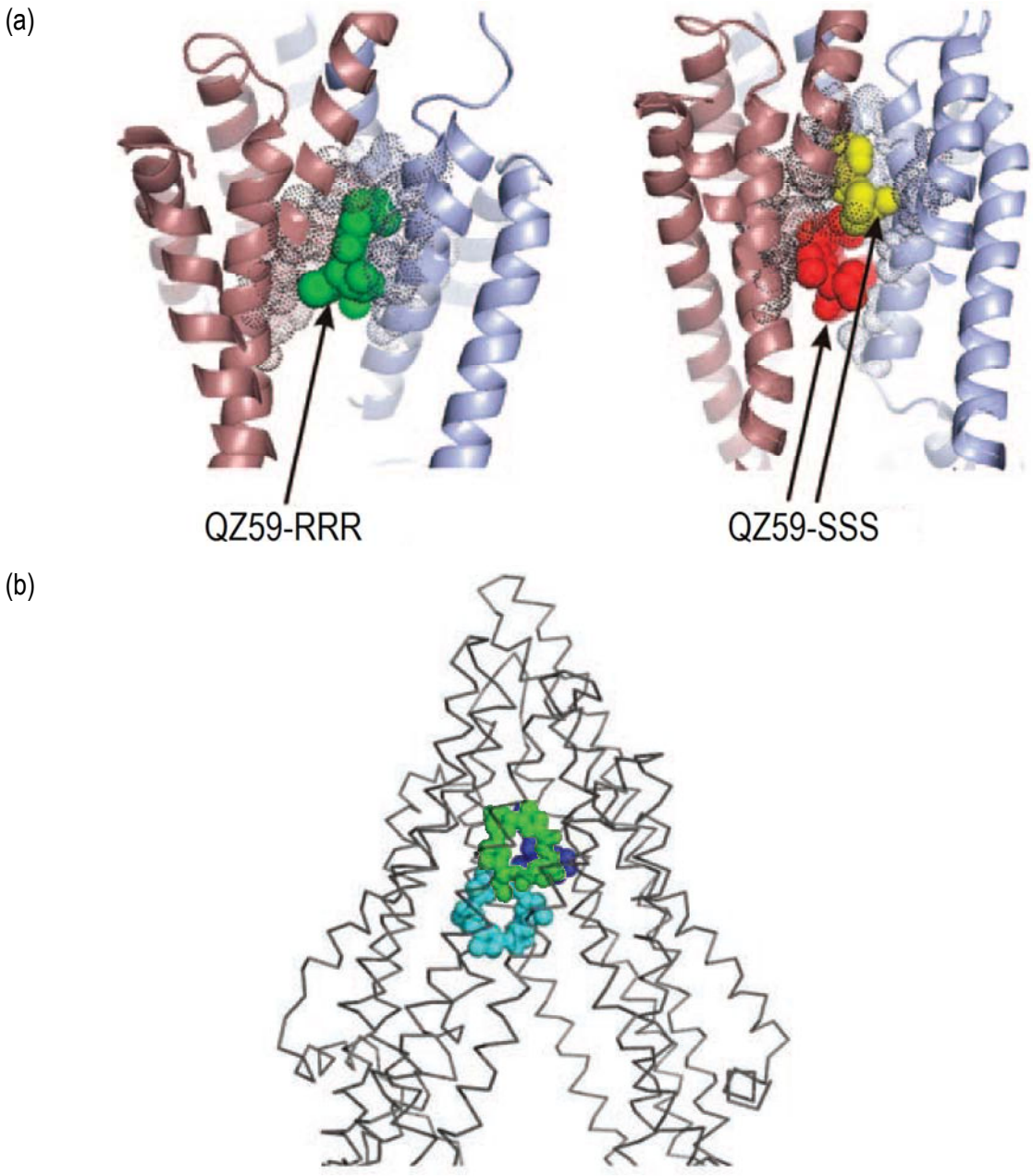

Figure 4.2: High resolution crystal structures of ABCB1 bound to different peptide molecules

a) One possible model of ABCB1 binding sites suggests three distinct sites operate cooperatively: one molecule of QZ59-RRR (**GREEN**, a cyclic peptide) binds to the middle site of the drug binding region; two molecules of QZ59-SSS (a steroisomer of QZ59-RRR) are able to bind to the upper (**YELLOW**) and lower (**RED**) binding sites in different orientations (adapted from Eckford et al[233]). b) Another possible model suggests a single binding site able to accommodate multiple molecules: one QZ59-RRR molecule (**GREEN**) and two QZ59-SSS molecules (**BLUE** and **CYAN**) bind simultaneously (modified from Aller *et al*[229]).

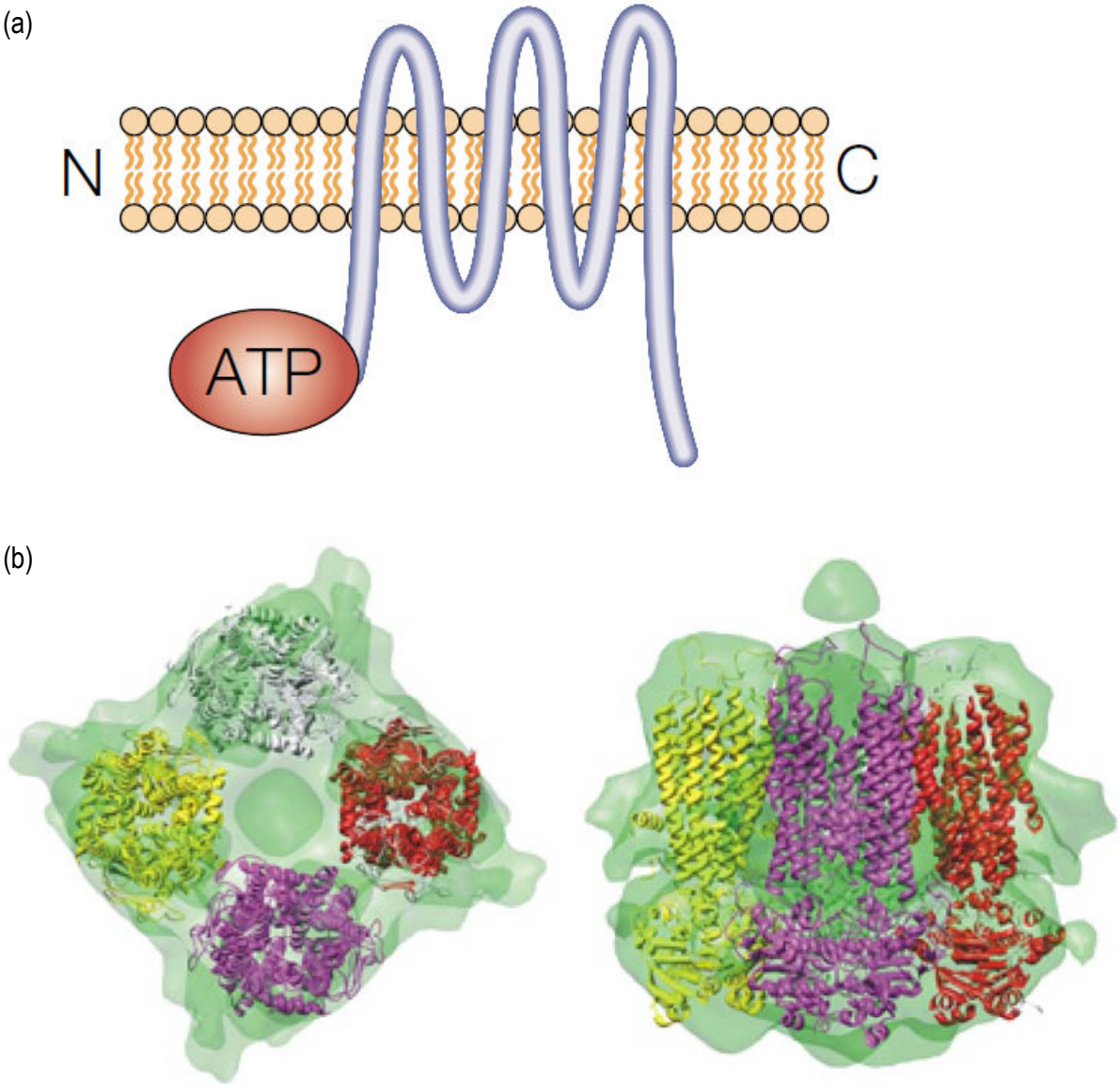

Figure 4.3: Schematic diagram of ABCG2 and the predicted structure of an ABCG2 homotetramer

a) Schematic representation showing the half-transporter's six transmembrane regions and single ATP-binding site[223]. b) A central (left) and side (right) view of a hypothetical ABCG2 homo-tetramer predicted by computational modelling[235].

Numerous inhibitors of both ABCB1 and ABCG2 that reverse the multi-drug resistance phenotype have been identified. While these compounds do not result in cell death directly, when co-administered with certain cytotoxic drugs known to be transported by ABCB1 and/or ABCG2, the efflux of the cytotoxic drug is prevented resulting in increased concentrations within the cell. Competitive inhibitory compounds bind to the transporter with high affinity, preventing the transport of other substrates. Alternatively, these inhibitors may induce a conformational change upon binding consequently preventing substrate binding and/or ATP-hydrolysis. Inhibitors can also be substrates; these compounds lock the transporter in a futile and repetitive transport cycle resulting in a much slower rate of transport of the cytotoxic substrate resulting in increased intracellular concentrations and subsequent cell death[233].

The concentration at which transport modulators and cytotoxic compounds are used appears to be extremely important. It has been demonstrated that the small molecule sulfinpyrazone can function as both an enhancer[239] and inhibitor[240] of ABC transporter-mediated export depending on the sulfinpyrazone concentration and experimental system utilised. Similarly, the disparity observed in the literature with regard to the TKI:transporter relationship may also be explained by variations in methodologies used in individual studies, with differences in model substrates, temperatures and times of incubation and, importantly, drug concentrations all likely to influence experimental outcome. Conflicting reports exist identifying nilotinib as both a substrate and inhibitor of ABCB1 and ABCG2. Generally, it appears that at high micromolar concentrations (>1 μM) nilotinib functions as an inhibitor of both ABCB1 and ABCG2[153-155,187-189] whereas at lower, nanomolar concentrations nilotinib is a substrate of these transporters[153-155] (**Tables 4.1a and b**). Indeed, Hegedus *et al*. aptly demonstrated that vanadate-sensitive ATPase activity varied with TKI concentration[155]. Similarly, utilisation of this colorimetric assay has revealed that at concentrations below 10 μM, verapamil acts as a stimulator of ABCB1 ATPase activity whereas at higher concentrations it functions as an inhibitor[241].

Table 4.1a: Different nilotinib:ABCB1 interactions occur at different TKI concentrations

Substrate	Inhibitor	Concentration	Reference
✓		<100 nM	Dohse *et al.*[154]
✓		500 nM–1 μM	Hegedus *et al.*[155]
	✓	5 μM	Davies *et al.*[187]
	✓	500 nM–2.5 μM	Dohse *et al.*[154]
	✓	>1 μM	Hegedus *et al.*[155]
	✓	>1 μM	Hiwase *et al.*[188]
	✓	>2.5 μM	Tiwari *et al.*[189]

Table 4.1b: Different nilotinib:ABCG2 interactions occur at different TKI concentrations

Substrate	Inhibitor	Concentration	Reference
✓		10 and 25 nM	Brendel *et al.*[153]
✓		<100 nM	Dohse *et al.*[154]
✓		10 nM–1 μM	Hegedus *et al.*[155]
	✓	100–200nM	Brendel *et al.*[153]
	✓	2.5 μM	Davies *et al.*[187]
	✓	500 nM–2.5 μM	Dohse *et al.*[154]
	✓	>1 μM	Hegedus *et al.*[155]
	✓	>1 μM	Tiwari *et al.*[189]

To overcome the discrepancies observed previously due to differences in methodologies, in this study we have used Bcr-Abl kinase inhibition as the confirmatory readout for drug:transporter interactions. We have previously demonstrated that the degree of kinase inhibition achieved is linked to patient response[210]. The amount of TKI which enters and is retained in the target leukaemic cells influences the degree of kinase inhibition. High drug efflux results in lower intracellular drug concentrations, hence lower kinase inhibition and a greater concentration of TKI required to inhibit kinase activity by 50% (higher IC50 value). The C1T10 regulator of kinase like (CrkI) protein is an immediate downstream effector molecule of Bcr-Abl, with levels of its phosphorylated form (p-CrkI) directly proportional to Bcr-Abl kinase activity. Thus, by measuring alterations of CrkI phosphorylation status in the presence of TKIs and high or low ABCB1 and ABCG2 expression, the differences in calculated IC50 values provide direct evidence for TKI:transporter interactions. The use of a range of TKI concentrations selected to span the IC50 value also provides insight into these interactions at pharmacologically relevant TKI concentrations. Thus, because the level of kinase inhibition is a key determinant of patient response, the approach described is both clinically applicable, and the most relevant approach for assessment of the effect of ABC transporters on TKI mode of action.

4.2. Approach

To investigate the role of ABCB1 and ABCG2 in the transport of nilotinib, TKI-mediated kinase inhibition was used as the key readout for determining TKI:transporter interactions. This enabled a direct assessment of TKI-mediated kinase inhibition over a large concentration range, thus resolving current conjecture within the literature pertaining to clinically relevant dosages. IC50 experiments (**Section 2.4.2**) and western blot assays specific for p-CrkI inhibition (**Section 2.4.3.1**) were performed on the parental K562 cell line, as well as ABCB1/ABCG2 over-expressing variants, in the absence and presence of specific inhibitors of efflux (**Section 2.2.10**). Verapamil was used at a concentration of 50 μM as this has previously been demonstrated to specifically inhibit ABCB1 activity[242] whereas at higher

concentrations inhibition of ABCG2 and/or ABCC1 may also occur[174,243]. PSC-833 is also known to be a potent inhibitor of ABCB1 and was used at 10 μM[244,245]. If nilotinib is a substrate for ABCB1/ABCG2, one would expect that in the presence of efflux inhibition nilotinib will be more effectively retained within the cell leading to increased kinase inhibition which reads out as a decreased IC50 value. Expression levels of ABCB1 and ABCG2 were assessed prior to each experiment using flow cytometric analysis (**Section 2.3.8.1**). Additionally, efflux studies (**Section 2.3.9**) were performed to confirm that transporters were functionally active. Fluorescently labelled rhodamine-123 was used as a probe for ABCB1 function while BODIPY-prazosin was used as a probe for both ABCB1 and ABCG2 function. In these experiments, low levels of probe indicate high expression and function of ABCB1 or ABCG2. Upon addition of ABCB1/ABCG2 inhibitors levels of probe should increase due to export being prevented. Efflux studies were also performed in the presence of five different concentrations of nilotinib: 150 nM, 500 nM, 1 μM, 2 μM and 5 μM in order to determine whether low versus high nilotinib concentrations have differing inhibitory effects on ABCB1 and ABCG2 function.

In a separate series of experiments, cell lines were incubated in the absence and presence of ABCB1 and ABCG2 specific inhibitors using 150 nM nilotinib in order to determine whether this lower concentration caused sufficient inhibition of Bcr-Abl kinase activity as measured by p-Crkl protein levels. To investigate the effect of ABCB1 and ABCG2 inhibition on intracellular concentrations of radiolabelled nilotinib, Intracellular Uptake and Retention (IUR) assays (**Section 2.4.1**) were performed for time points ranging from 2 min to 2 h on cell lines in the absence and presence of ABCB1/ABCG2 specific inhibitors. In these experiments, inhibitors were added for 30 min prior to addition of radiolabelled TKI to allow sufficient inhibition of the transporter to take place. To determine whether nilotinib:ABC transporter interactions were concentration specific, intracellular ^{14}C-nilotinib levels were assessed following incubation with both 150 nM and 2 μM nilotinib. A secondary set of $IC50^{NIL}$ experiments were conducted in parallel using various concentrations of the proton pump inhibitor pantoprazole. Proton

pump inhibitors, such as pantoprazole, are frequently prescribed to CML patients to alleviate gastric side effects experienced as a result of TKI therapy or as ongoing therapy. Thus it was pertinent to evaluate whether concomitant administration of pantoprazole had an effect on nilotinib-mediated kinase inhibition. The analyses discussed in this chapter were used to determine the impact of high levels of ABCB1 and ABCG2 on nilotinib-mediated kinase inhibition. This approach enabled resolution of current discrepancies as a result of differences in methodologies between studies. In addition, these analyses emphasised the importance of concentration when studying TKI:ABC transporter relationships and highlighted the possibility of ABC transporters other than ABCB1/ABCG2 playing a role in nilotinib transport.

4.3. Results

4.3.1. High Levels of ABCB1 but not ABCG2 Decrease Nilotinib-Mediated Kinase Inhibition

Flow cytometric analyses were performed on all cell lines prior to each experiment to confirm levels of ABCB1 and ABCG2 expression. The mean fluorescence intensity (MFI) for each cell line was compared with the corresponding isotype control. K562 and KU812 cells had characteristically low expression of both ABCB1 and ABCG2 (<3% and 2–7% respectively). K562-Dox cells demonstrated very high ABCB1 expression 92–99% and negligible ABCG2 expression, while K562-ABCG2 cells demonstrated 55–70% ABCG2 expression and negligible expression of ABCB1 (**Figure 4.4**).

ABCB1 and ABCG2 substrate efflux studies were also performed to confirm the functional activity of transporters. In the K562-Dox and K562-ABCG2 cell lines where there is 99% and >50% expression (ABCB1 and ABCG2 respectively), addition of specific inhibitors resulted is near complete inhibition of the transporters' functional activity as assessed by rhodamine-123 and BODIPY-prazosin. Results for all cell lines were consistent with expression levels of ABCB1/ABCG2 and are summarised in **Figure 4.5** and **Table 4.2**. K562 cells demonstrated high levels of rhodamine-123 and BODIPY-prazosin in the

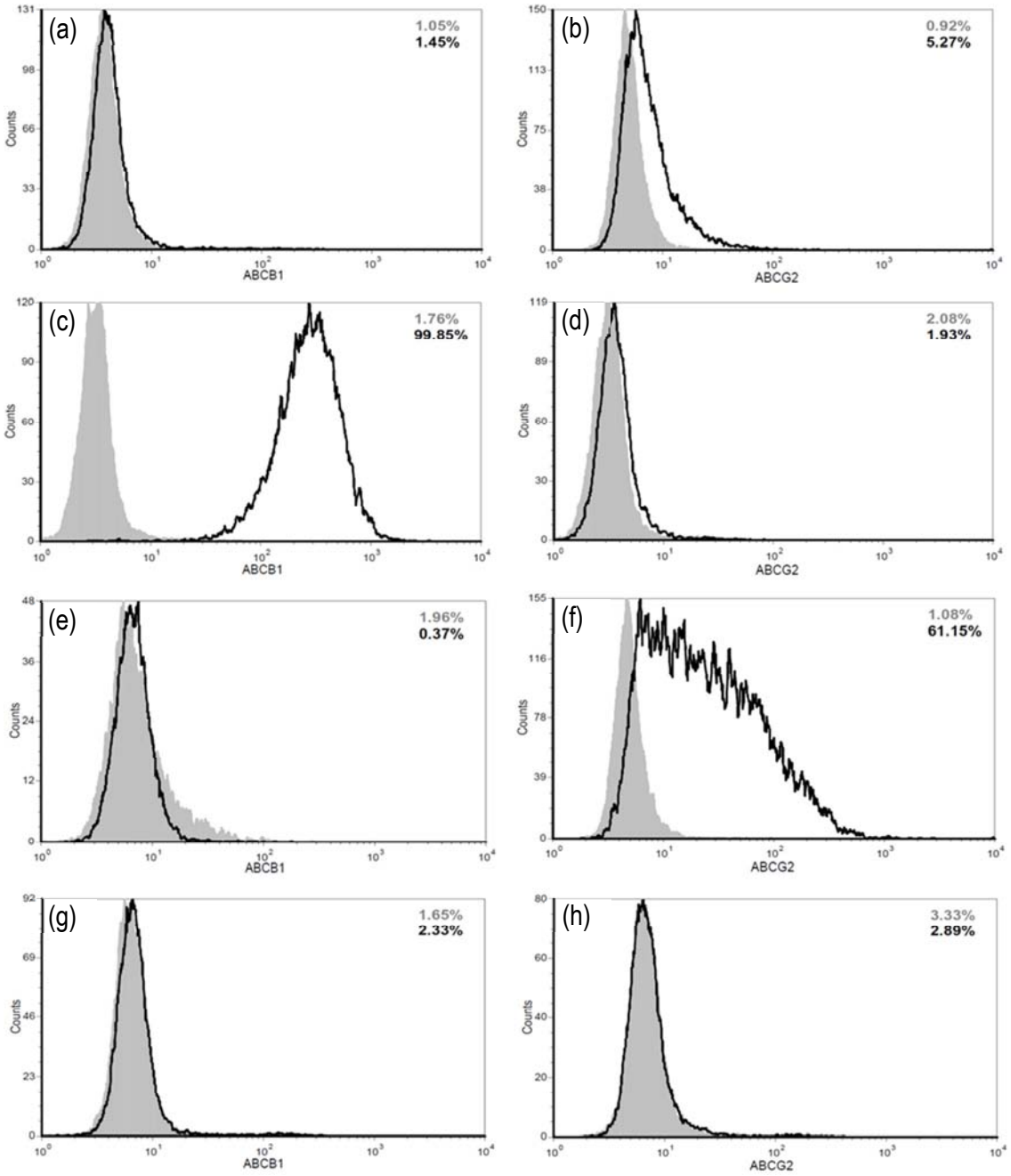

Figure 4.4: ABCB1 and ABCG2 protein expression in Bcr-Abl positive cell lines

K562 (a, b), K562-Dox (c, d), K562-ABCG2 (e, f) and KU812 (g, h) cells were stained with fluorescently labelled antibodies for ABCB1 (a, c, e, g) and ABCG2 (b, d, f, h) and transporter protein expression levels determined by flow cytometric analysis. The bold **BLACK** lines represent cells stained with either **ABCB1-PE** or **ABCG2-PE** antibodies, while the **GREY** filled histograms represent cells stained with corresponding **isotype** control antibodies. The percentages displayed denote cells positive for transporter expression. Data are representative of typical expression levels.

Table 4.2: Summary of the MFI depicted by the histograms in Figure 4.5

Cell Line	rho-123	rho-123 + PSC-833	B-P	B-P +Ko143	B-P	B-P +PSC-833
K562	770.5	1236.0	128.29	134.05	128.29	71.53
K562-Dox	9.42	855.4	10.65	11.54	10.65	120.68
K562-ABCG2	903.9	1239.0	77.41	147.73	77.41	56.73

Figure 4.5: Functional studies with rhodamine-123 and BODIPY-prazosin in Bcr-Abl positive cell lines

Cells were stained with fluorescent substrates and fluorescence determined in the absence and presence of specific inhibitors of ABCB1 (PSC-833) and ABCG2 (Ko143). K562 cells demonstrated characteristically high levels of rhodamine-123 (rho-123) and BODIPY-prazosin (B-P) in the absence and presence of inhibitors, consistent with the low expression levels of ABCB1 and ABCG2 observed. K562-Dox cells demonstrated high levels of rhodamine-123 and BODIPY-prazosin in the presence of PSC-833, consistent with ABCB1 inhibition resulting in retention of substrates. In the absence of inhibitors, rhodamine-123 and BODIPY-prazosin levels were low, consistent with efflux of substrates from cells. K562-ABCG2 cells demonstrated high levels of BODIPY-prazosin in the presence of Ko143, and lower levels in its absence; high levels of rhodamine-123 in both the absence and presence of inhibitors. These results are consistent with high levels of ABCG2 and low levels of ABCB1. The values displayed in the table denote the MFI of cells positive for fluorescent substrate. Data are representative of typical MFI levels. The **GREY** filled histograms represent **unstained control**, the **BLACK** lines represent **fluorescent substrate alone** and the **BLUE** and **RED** lines represent fluorescent substrate in the presence of **PSC-833** and **Ko143** respectively.

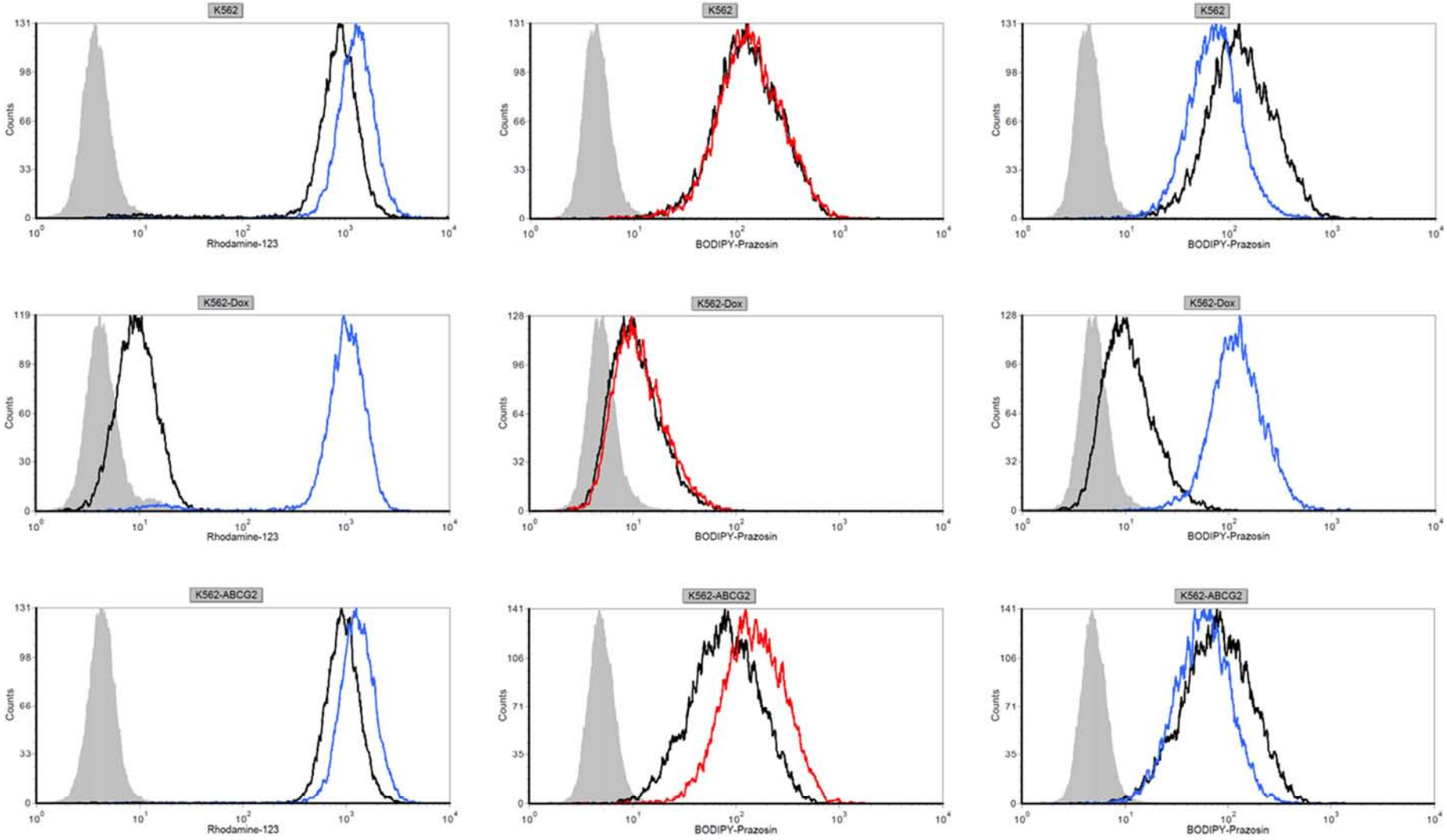

Figure 4.5 (continued): Functional studies with rhodamine-123 and BODIPY-prazosin in Bcr-Abl positive cell lines

absence and presence of ABCB1/ABCG2 inhibition consistent with the low expression levels of these transporters in this cell line. K562-Dox cells demonstrated low levels of rhodamine-123 and BODIPY-prazosin in the absence of ABCB1 inhibition, however upon addition of the ABCB1 inhibitor PSC-833 levels of both fluorescent substrates increased (rhodamine-123 MFI from 9.42 to 855.4; BODIPY-prazosin MFI from 10.65 to 120.68). Similarly, K562-ABCG2 cells demonstrated low levels of BODIPY-prazosin in the absence of ABCG2 inhibition, however, upon addition of Ko143, levels increased from an MFI of 77.41 to 147.73. Importantly, there was no change in BODIPY-prazosin levels in K562-Dox cells in the presence of Ko143 or in K562-ABCG2 cells in the presence of PSC-833 demonstrating specificity of inhibition.

To assess the effects of ABCB1 on nilotinib-related kinase inhibition, K562 and the ABCB1 over-expressing variant K562-Dox were incubated in increasing concentrations of nilotinib. Cells were cultured for 2 h in increasing concentrations of nilotinib and over-expression of ABCB1 resulted in a significant increase in $IC50^{NIL}$ (219 nM to 411 nM, n>4, p=0.011; **Figure 4.6**). Additionally, in the presence of PSC-833, the $IC50^{NIL}$ in K562-Dox cells was reduced by 69% (K562-Dox alone: 411 nM; +PSC-833 129 nM; n=4, p=0.016; **Figure 4.6**). In contrast, no significant change was observed in the K562 cells (negligible ABCB1 expression) with only a 7% decrease in $IC50^{NIL}$ measured (K562 alone: 219 nM; +PSC-833 204 nM; n>4, p=0.787; **Figure 4.6**). These data strongly suggest that ABCB1 has a role in nilotinib mediated kinase inhibition and nilotinib transport.

It is now well documented that PSC-833 has an unexplained effect on nilotinib uptake[150,187]. For this reason a second ABCB1 inhibitor, verapamil, was used at a concentration previously demonstrated to be specific for ABCB1 inhibition (50 μM)[174,242,243]. Results observed for K562-Dox cells incubated with verapamil were similar to those observed with PSC-833; the $IC50^{NIL}$ reduced by 71% in the presence of inhibitor ($IC50^{NIL}$: 121 nM; n=4, p=0.018, **Figure 4.6**) adding further support for ABCB1 involvement in

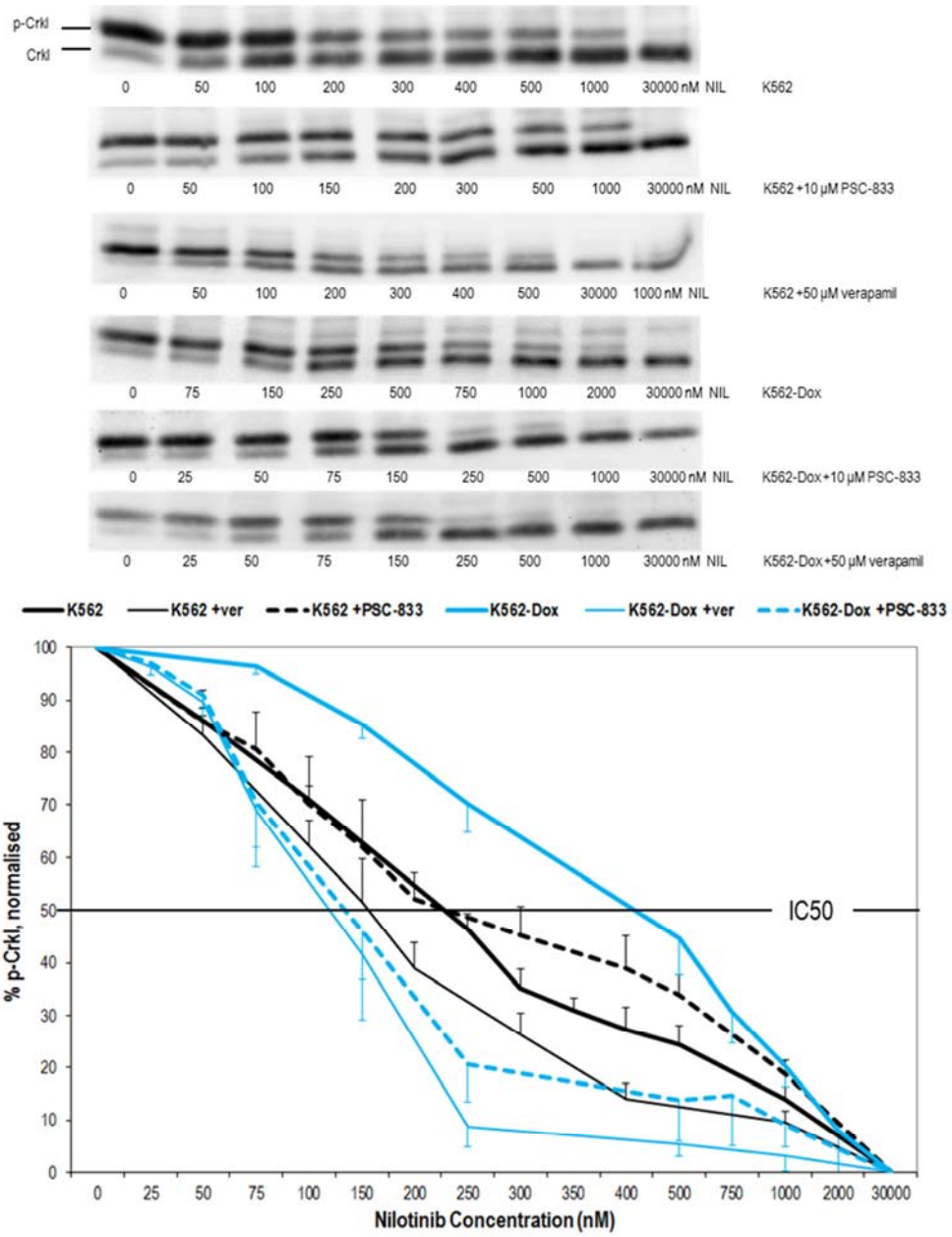

Figure 4.6: ABCB1 overexpression increases $IC50^{NIL}$

IC50 was determined via incubating cells for 2 h at 37°C in the absence and presence of 10 μM PSC-833 and 50 μM verapamil. Crkl western blot was performed to determine the concentration of nilotinib required to inhibit Bcr-Abl kinase activity by 50%. Data demonstrate that the high levels of ABCB1 in K562-Dox cells significantly increase $IC50^{NIL}$. Similarly, $IC50^{NIL}$ significantly decreases upon ABCB1 inhibition in K562-Dox cells but not K562 control cells. The western blot analysis shown is representative of at least three separate experiments with densitometry analysis shown below. IC50 values were calculated separately for individual experiments and the mean values for each nilotinib concentration plotted. Error bars represent SEM. NIL=nilotinib; ver=verapamil; PSC=PSC-833.

nilotinib transport. Verapamil had no significant effect on $IC50^{NIL}$ in K562 cells (K562 alone: 219 nM; +verapamil 162 nM; 26% decrease; n>7, *p*=0.071; **Figure 4.6**).

In contrast, overexpression of ABCG2 did not result in a significant increase in $IC50^{NIL}$ (K562: 219 nM; K562-ABCG2: 221 nM, n>5, *p*=0.710; **Figure 4.7**). Additionally, when K562-ABCG2 cells were treated with Ko143 no significant change in $IC50^{NIL}$ was observed: (K562-ABCG2 alone: 221 nM; +Ko143: 180 nM; n=5, *p*=0.222, 18% decrease). Again, no significant change was observed in K562 control cells (K562 alone: 219 nM; +Ko143: 268 nM; n>4, *p*=0.231, 22% increase) indicating ABCG2 has minimal impact on nilotinib-related kinase inhibition and an insignificant role in nilotinib transport at clinically relevant dosages (**Figure 4.7**).

4.3.2. Nilotinib Likely Inhibits Efflux Transporters at 2 µM

The $IC50^{NIL}$ experiments highlighted an important trend indicating substantial kinase inhibition occurs in the presence of 2 µM nilotinib (80–90% p-Crkl reduction). Thus near maximal kinase inhibition occurs at concentrations often specified as clinically relevant. However, because nilotinib is highly plasma protein bound, this concentration of nilotinib is unlikely to be clinically relevant with respect to mediating kinase inhibition. Additionally, concentrations in the high micromolar range are likely to saturate any transporters involved in nilotinib efflux causing an inhibitory effect. Indeed, IUR experiments performed with 2 µM nilotinib in four cell lines known to express disparate levels of ABCB1 and ABCG2 (**Figure 4.4**) demonstrated no significant difference in intracellular nilotinib concentrations at any of the time points assayed (*p*>0.05; **Figure 4.8**). Thus, it is likely that at 2 µM, nilotinib acts as an inhibitor of both ABCB1 and ABCG2 resulting in the similar patterns of transport kinetics seen for K562, K562-Dox, K562-ABCG2 and KU812 cells. Supporting this hypothesis are data from rhodamine-123 and BODIPY-prazosin efflux experiments performed in K562-Dox and K562-ABCG2 cells in the presence of nilotinib. As expected, nilotinib had no significant effect on rhodamine-123 efflux in K562, K562-ABCG2 or

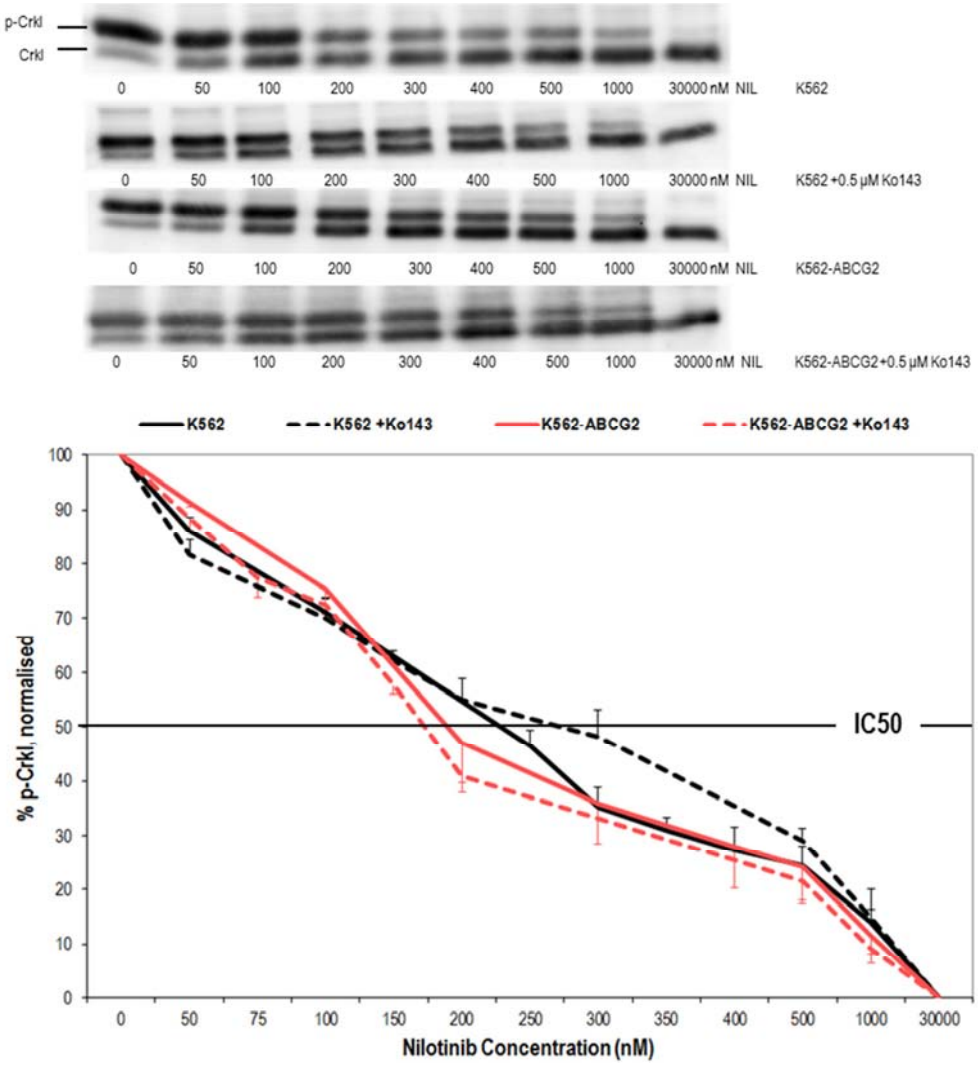

Figure 4.7: High levels of ABCG2 have no significant effect on $IC50^{NIL}$ in CML cell lines

IC50 was determined via incubating cells for 2 h at 37°C in the absence and presence of 0.5 µM Ko143. Crkl western blot was performed to determine the concentration of nilotinib required to inhibit Bcr-Abl kinase activity by 50%. Data demonstrate that high levels of ABCG2 do not significantly increase $IC50^{NIL}$. Similarly, $IC50^{NIL}$ does not significantly decrease upon ABCG2 inhibition in either K562-ABCG2 cells or K562 control cells. The western blot analysis shown is representative of three separate experiments with the corresponding densitometry analysis representing the mean. NIL=nilotinib.

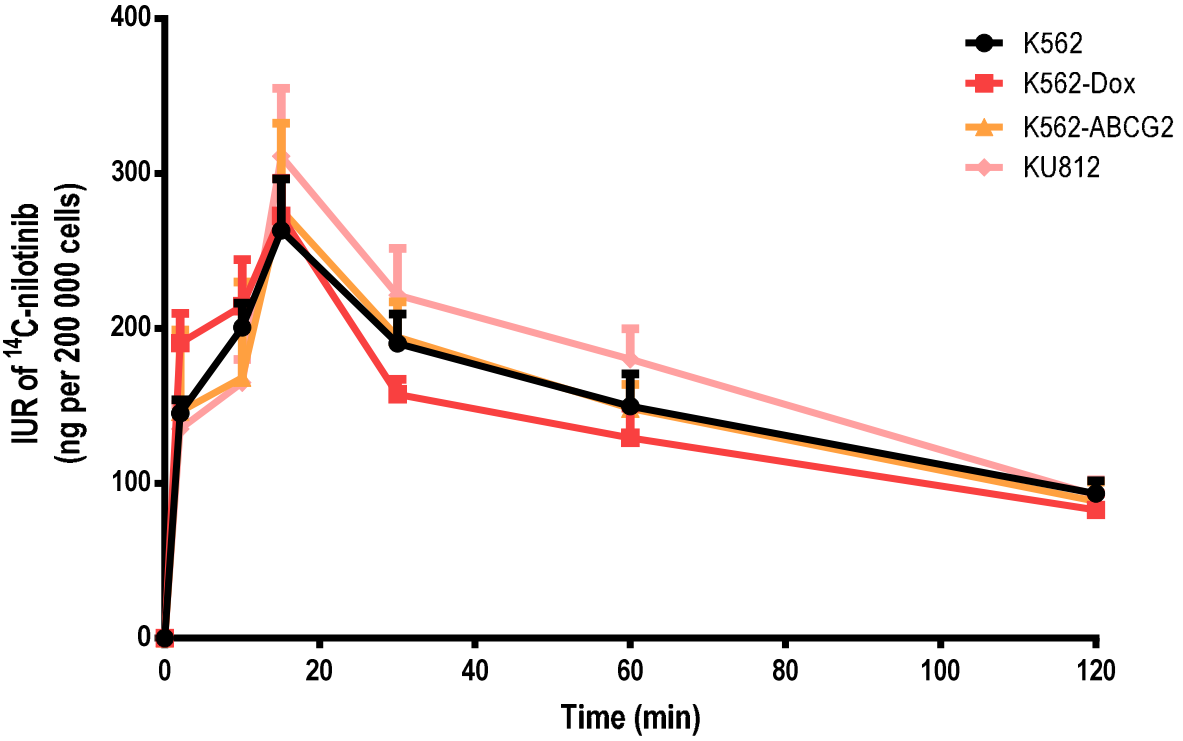

Figure 4.8: No difference is observed in 2 µM nilotinib transport kinetics in cell lines expressing varying levels of ABCB1 and ABCG2

K562, K562-Dox, K562-ABCG2 and KU812 cells were incubated in the presence of 2 µM ^{14}C-nilotinib for time points ranging 2 min to 2 h. Data demonstrate that there is no significant difference in the uptake of ^{14}C-nilotinib regardless of ABCB1 and ABCG2 expression levels indicating that at 2 µM nilotinib is likely acting as an inhibitor of both of these transporters. The data represent the mean of at least three separate experiments performed in triplicate. Statistical analyses were performed using Student's *t*-test. Error bars represent SEM.

KU812 cells. However, in K562-Dox cells, addition of high micromolar concentrations of nilotinib (2 μM and 5 μM) resulted in inhibition of ABCB1 and a corresponding increase in intracellular rhodamine-123 levels (**Figure 4.9a**). Again, as expected, addition of nilotinib to K562 and KU812 cells had no effect on BODIPY-prazosin efflux. In K562-ABCG2 cells micromolar concentrations of nilotinib (1 μM and 2 μM) inhibited BODIPY-prazosin efflux to the same extent as the known ABCG2 inhibitor Ko143. Similarly, in K562-Dox cells, addition of nilotinib at concentrations above 500 nM resulted in dose dependent inhibition of BODIPY-prazosin efflux via ABCB1. Interestingly, 1 μM and 2 μM nilotinib was more effective than PSC-833 at inhibiting BODIPY-prazosin efflux (**Figure 4.9b**). Importantly 150 nM nilotinib had no significant effect on either ABCB1 or ABCG2 function and thus this concentration was chosen for further *in vitro* investigations.

4.3.3. ABCB1 Inhibition Increases Intracellular ^{14}C-Nilotinib at 150 nM but not at 2 μM

In light of the results observed with 2 μM nilotinib, the interaction of nilotinib with ABCB1 at a concentration of 150 nM was subsequently assessed. While the reported plasma concentration for nilotinib falls between 2 μM and 4 μM (steady state trough and peak levels respectively)[170], it has previously been demonstrated, both *in vitro*[81] and *in vivo*[171], that clinically relevant Bcr-Abl kinase domain mutations known to cause resistance to nilotinib have $IC50^{NIL}$ values in the low nanomolar range. Thus evaluating nilotinib:transporter interactions at a lower concentration was an appropriate next step. However, it was first necessary to determine that 150 nM was a suitable concentration to achieve measurable kinase inhibition in cell lines. Hence a series of experiments were performed over a 48 h time period where K562, K562-Dox and K562-ABCG2 cells were incubated with 150 nM nilotinib in the absence and presence of PSC-833, verapamil and Ko143. Within 2 h, in the absence of transport inhibition, 28–47% kinase inhibition occurred (**Figure 4.10**). Upon addition of 10 μM PSC-833 or 50 μM verapamil there was no significant change in kinase inhibition in K562 cells at any of the time points investigated ($p>0.05$; **Figure 4.10a**), however, in K562-Dox cells these inhibitors increased the level of

Figure 4.9: High micromolar concentrations of nilotinib inhibit the function of both ABCB1 and ABCG2

Cells were stained with fluorescent substrates a) rhodamine-123 and b) BODIPY-prazosin and fluorescence determined in the absence and presence of increasing concentrations of nilotinib. K562 and KU812 cells demonstrated characteristically high levels of rhodamine-123 and BODIPY-prazosin in the absence and presence of nilotinib, consistent with low expression levels of ABCB1 and ABCG2. K562-Dox cells demonstrated higher levels of rhodamine-123 and BODIPY-prazosin in the presence of high micromolar concentrations of nilotinib, consistent with ABCB1 inhibition resulting in retention of substrates. In the absence of inhibition, rhodamine-123 and BODIPY-prazosin levels were low, consistent with efflux of substrates from cells. K562-ABCG2 cells demonstrated higher levels of BODIPY-prazosin in the presence of >150 nM nilotinib and lower levels in its absence. These results are consistent with nilotinib functioning as an inhibitor of both ABCB1 and ABCG2 at high micromolar concentrations but not at low nanomolar concentrations. Data are representative of typical MFI levels with the geometric mean of the peaks detailed. The **GREY** filled histograms represent **fluorescent substrate alone**, the **BLUE** histograms represent control inhibitors (either **PSC-833** or **Ko143** depending on substrate and cell line) while the coloured histograms represent **150 nM**, **500 nM**, **1 µM**, **2 µM** and **5 µM** nilotinib respectively.

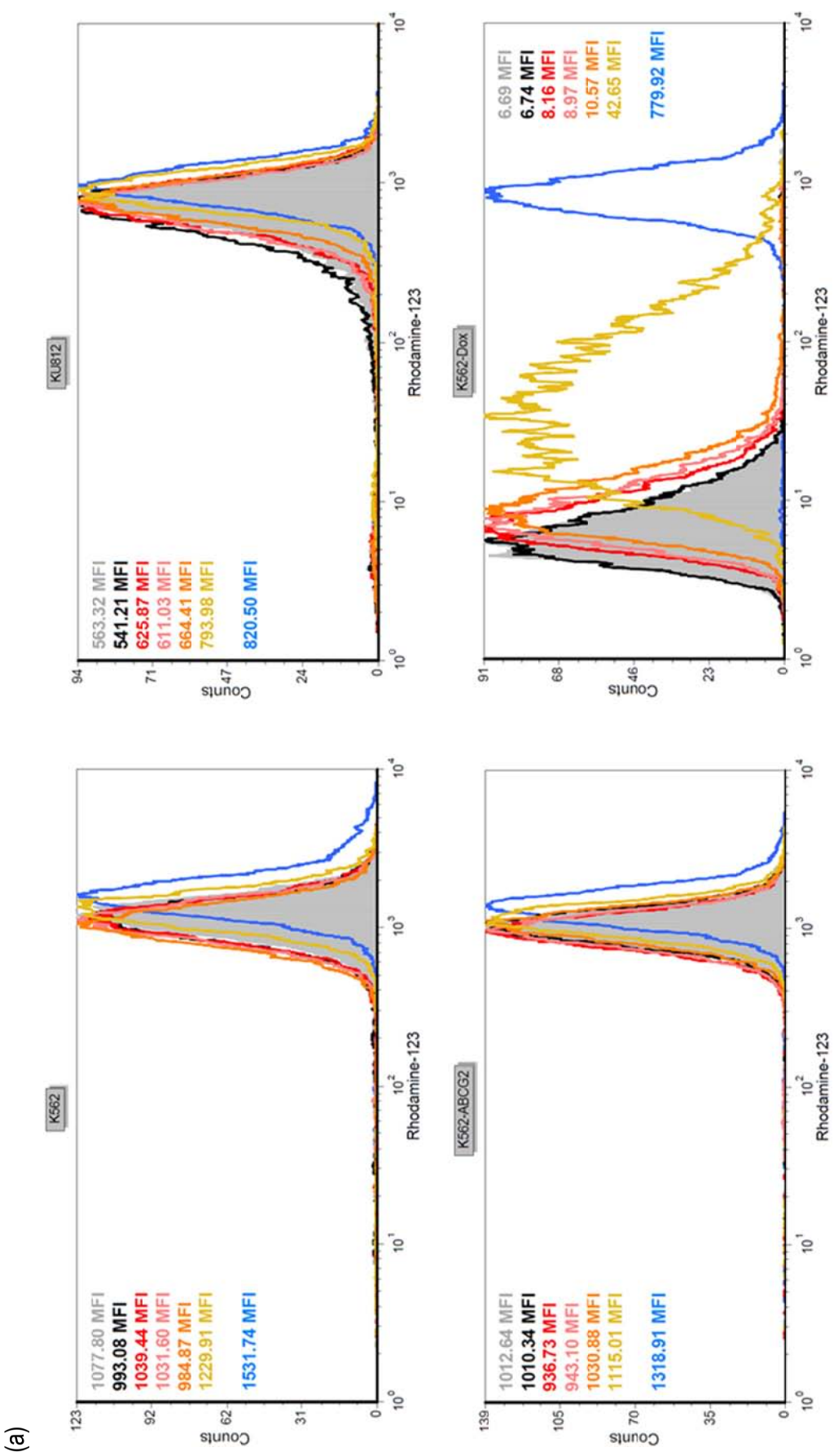
(a)
K562
1077.80 MFI
993.08 MFI
1039.44 MFI
1031.60 MFI
984.87 MFI
1229.91 MFI
1531.74 MFI
K562-ABCG2
1012.64 MFI
1010.34 MFI
936.73 MFI
943.10 MFI
1030.88 MFI
1115.01 MFI
1318.91 MFI
KU812
563.32 MFI
541.21 MFI
625.87 MFI
611.03 MFI
664.41 MFI
793.98 MFI
820.50 MFI
K562-Dox
6.69 MFI
6.74 MFI
8.16 MFI
8.97 MFI
10.57 MFI
42.65 MFI
779.92 MFI
Counts
Rhodamine-123

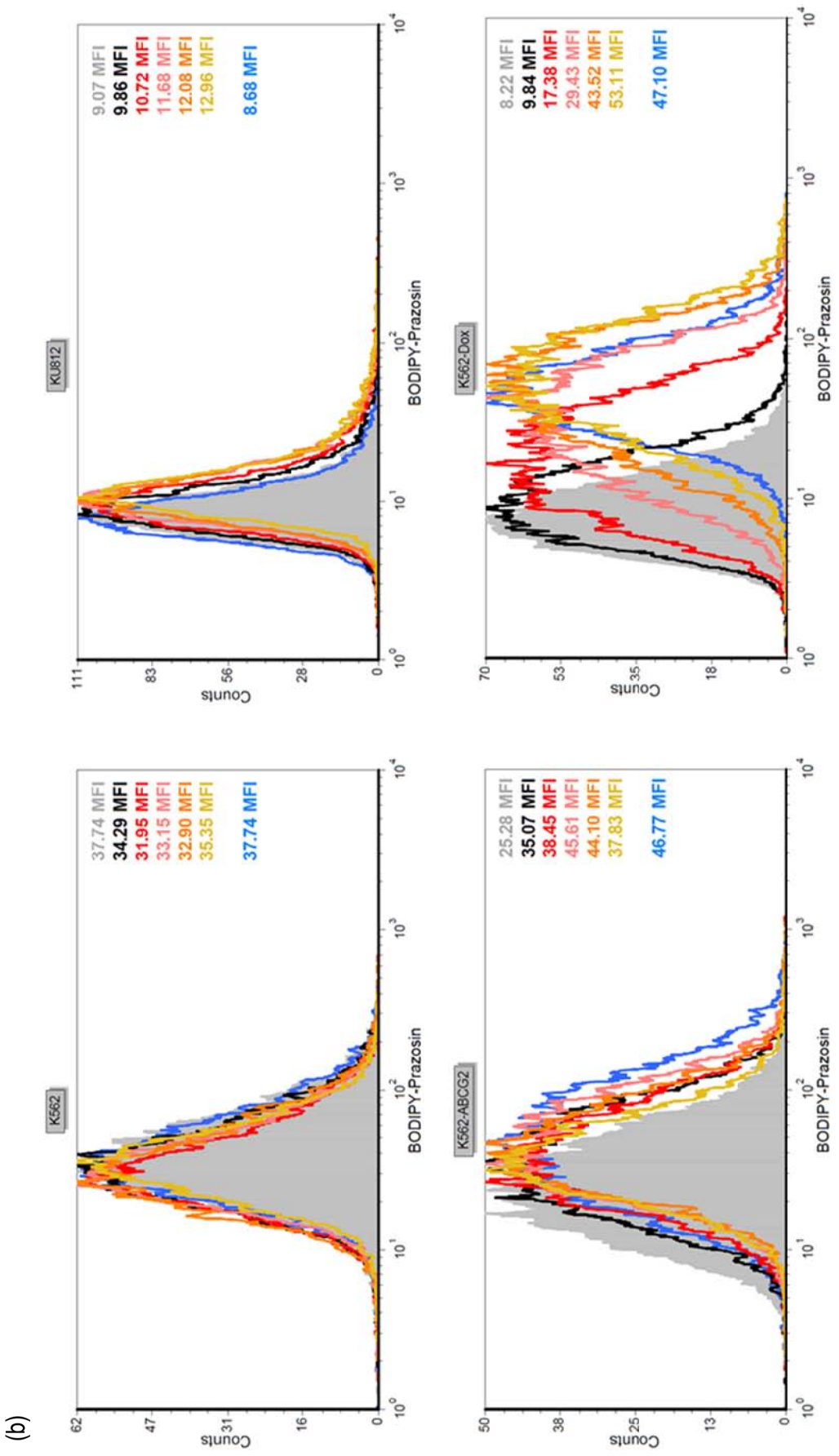
(b)
KU812
9.07 MFI
9.86 MFI
10.72 MFI
11.68 MFI
12.08 MFI
12.96 MFI
8.68 MFI
K562-Dox
8.22 MFI
9.84 MFI
17.38 MFI
29.43 MFI
43.52 MFI
53.11 MFI
47.10 MFI
K562
37.74 MFI
34.29 MFI
31.95 MFI
33.15 MFI
32.90 MFI
35.35 MFI
37.74 MFI
K562-ABCG2
25.28 MFI
35.07 MFI
38.45 MFI
45.61 MFI
44.10 MFI
37.83 MFI
46.77 MFI
Counts
BODIPY-Prazosin

Figure 4.10: 150 nM nilotinib results in sufficient kinase inhibition in Bcr-Abl positive cell lines

a) K562 b) K562-Dox c) K562-ABCG2 cells were incubated in the absence and presence of ABCB1 and ABCG2 inhibitors over a 48 h time period. Cells were incubated for 2–48 h at 37°C in the absence and presence 10 μM PSC-833, 50 μM verapamil and 0.5 μM Ko143 and % kinase activity determined. Data demonstrate that 150 nM nilotinib causes sufficient inhibition of kinase activity within 2 h and inhibition of ABCB1, but not ABCG2 causes a consistent increase in kinase inhibition which reaches significance at 24 h. The western blot analyses shown are representative of three separate experiments with the corresponding densitometry analysis representing the mean. Statistical analyses were performed using Student's *t*-test with statistically significant *p*-values denoted by asterisks (* $p<0.05$). Error bars represent SEM. % kinase activity was normalised and activity at 0 h denoted as 100%.

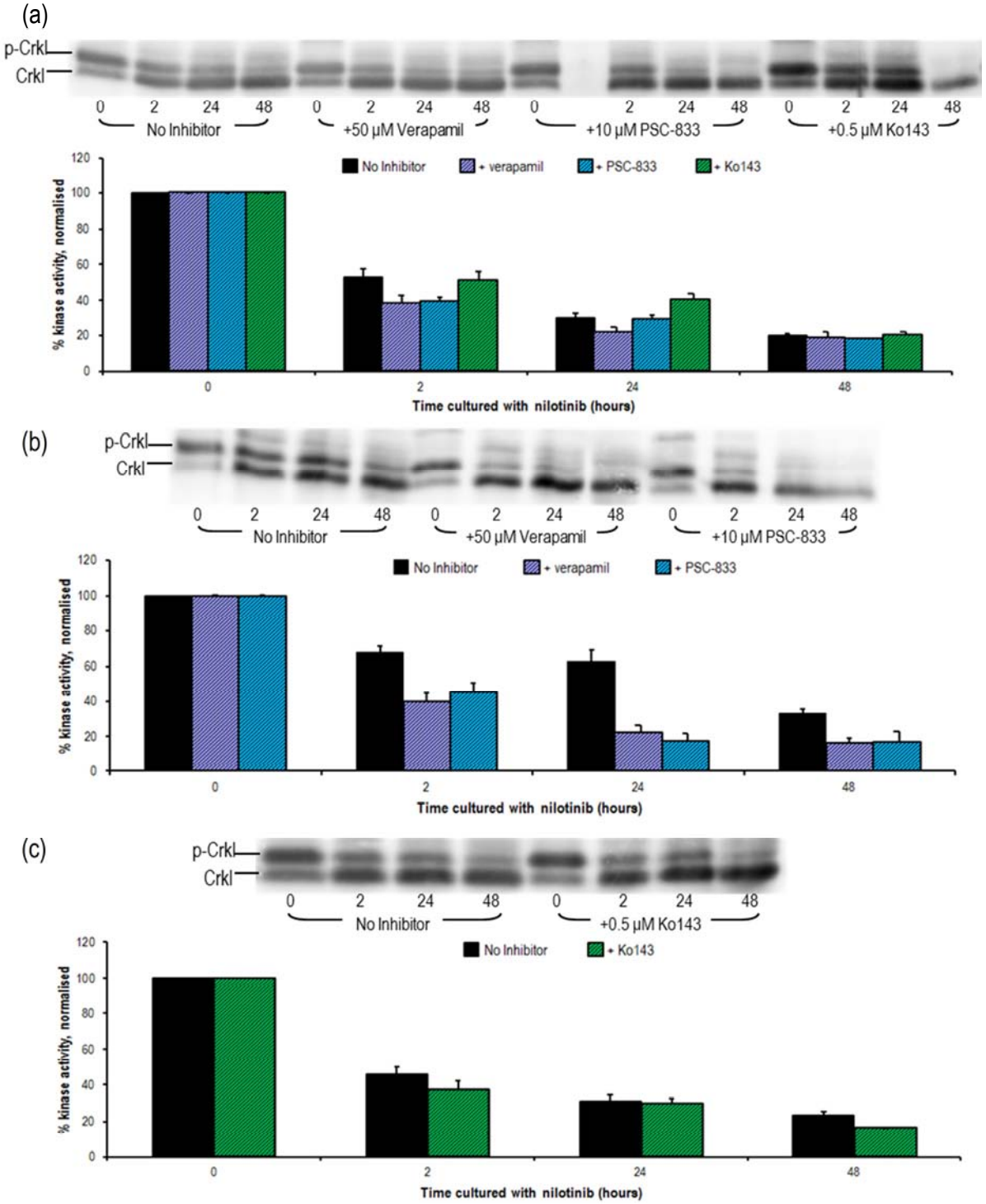
(a)
p-Crkl
Crkl
0 2 24 48 0 2 24 48 0 2 24 48 0 2 24 48
No Inhibitor
+50 µM Verapamil
+10 µM PSC-833
+0.5 µM Ko143
No Inhibitor
+ verapamil
+ PSC-833
+ Ko143
% kinase activity, normalised
Time cultured with nilotinib (hours)
(b)
p-Crkl
Crkl
0 2 24 48 0 2 24 48 0 2 24 48
No Inhibitor
+50 µM Verapamil
+10 µM PSC-833
No Inhibitor
+ verapamil
+ PSC-833
% kinase activity, normalised
Time cultured with nilotinib (hours)
(c)
p-Crkl
Crkl
0 2 24 48 0 2 24 48
No Inhibitor
+0.5 µM Ko143
No Inhibitor
+ Ko143
% kinase activity, normalised
Time cultured with nilotinib (hours)

kinase inhibition at all time points reaching significance at 24 h (p<0.004; **Figure 4.10b**). The addition of 0.5 μM Ko143 had no significant effect on nilotinib kinase inhibition in either K562 or K562-ABCG2 cells (p>0.05; **Figure 4.10a, c**). These results are consistent with $IC50^{NIL}$ experiments, further supporting the notion of nilotinib acting as an ABCB1 substrate at clinically relevant concentrations.

Since both PSC-833 and verapamil have similar effects on nilotinib kinase inhibition and rhodamine-123 efflux (**Appendix 2A**) we believe verapamil to be a reliable and selective ABCB1 inhibitor for use in IUR experiments in lieu of the more widely used PSC-833. The use of verapamil eliminates the confounding interference of PSC-833 on nilotinib uptake[187]. Thus, verapamil was used to investigate the effect of ABCB1 inhibition on nilotinib IUR over a 2 h period in K562-Dox cells. IUR assays were initially performed using 2 μM ^{14}C-nilotinib and no difference in IUR was observed when cells were pre-incubated with verapamil at any of the time points investigated (p>0.05, n=4; **Figure 4.11a**). However, when experiments were replicated using the much lower concentration of 150 nM ^{14}C-nilotinib, there was a clear increase in IUR in the presence of verapamil at all time points (n=5; **Figure 4.11b**). These data indicate that nilotinib transport via ABCB1 may be concentration dependent with efflux taking place at lower concentrations that are likely to be more clinically relevant[81,171]. Importantly, K562 control cells also showed no significant difference in nilotinib IUR in the presence of verapamil (p>0.05, n=3; **Figure 4.12b**).

Conversely nilotinib does not appear to exhibit a strong interaction with ABCG2 at low nanomolar concentrations. IUR experiments performed with 150 nM ^{14}C-nilotinib in K562-ABCG2 cells in the absence or presence of 0.5 μM Ko143 demonstrated no significant difference in intracellular levels of nilotinib (p>0.05, n=3; **Figure 4.12a**).

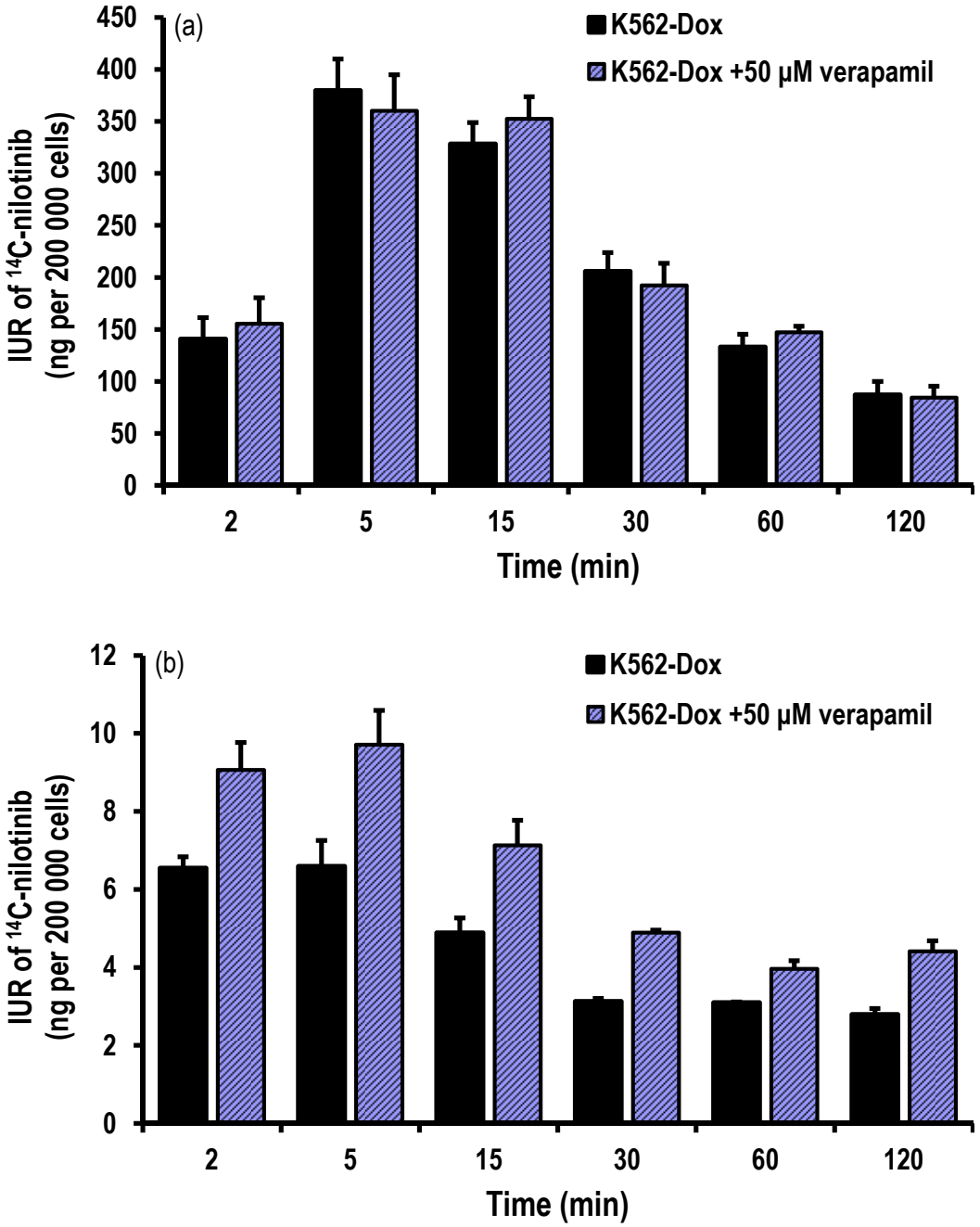

Figure 4.11: ABCB1 inhibition increases IUR when nilotinib is used at 150 nM but not at 2 µM

IUR experiments were performed with a) 2 µM and b) 150 nM ^{14}C-nilotinib in K562-Dox cells. Cells were incubated for 2 min–2 h at 37°C in the absence and presence of 50 µM verapamil and ng of incorporated nilotinib determined. Data demonstrate inhibition of ABCB1 causes a consistent increase in nilotinib IUR when 150 nM but not 2 µM nilotinib concentration is used. Experiments were performed in triplicate at least four times with data representing the median. Statistical analyses were performed using Student's *t*-test. Error bars represent SEM. NIL=nilotinib.

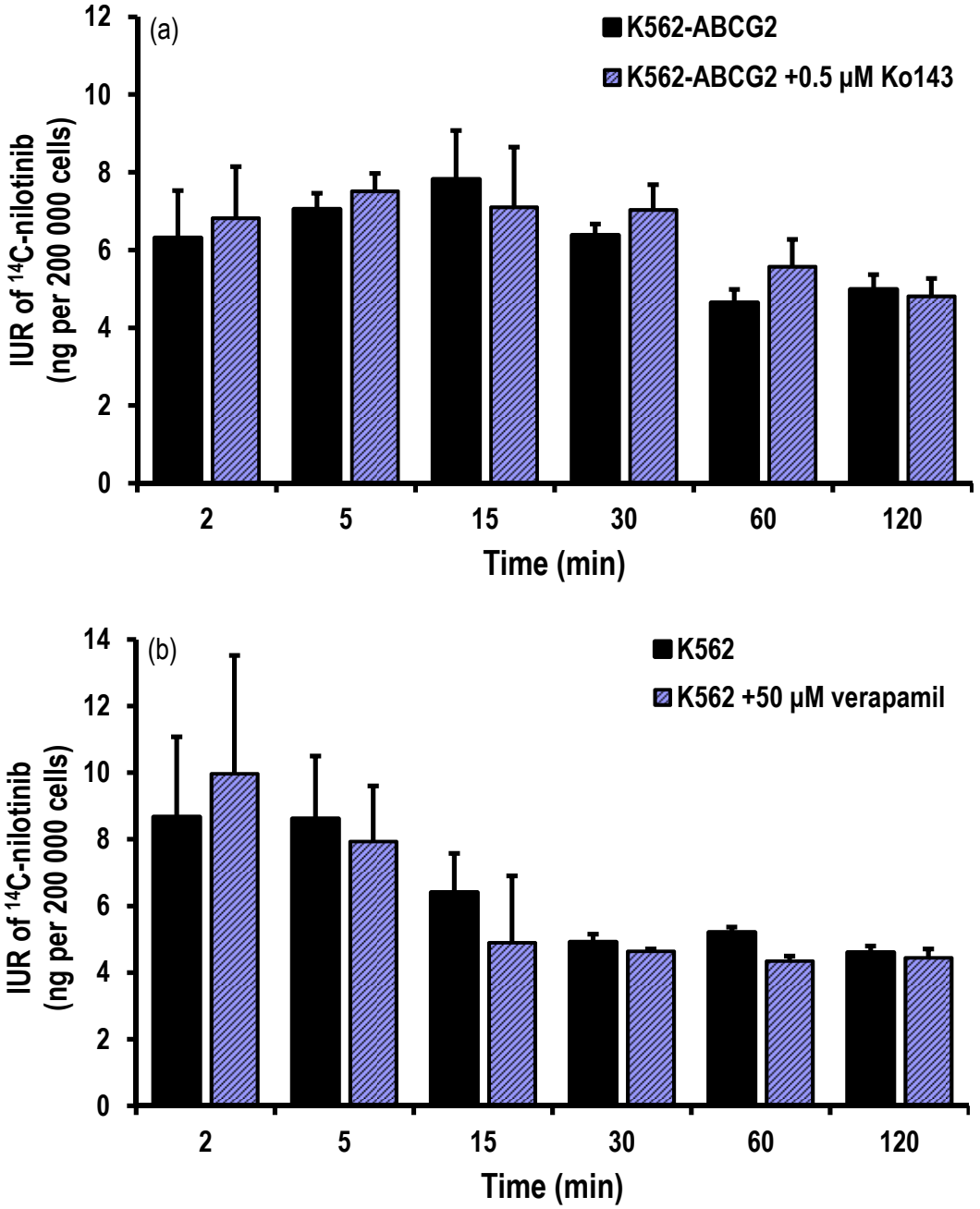

Figure 4.12: ABCG2 inhibition has no effect on nilotinib IUR

IUR experiments were performed with 150nM ^{14}C-nilotinib in a) K562-ABCG2 and b) K562 cells. Cells were incubated for 2 min–2 h at 37°C with 150nM ^{14}C-nilotinib in the absence and presence of a) 0.5 µM Ko143 or b) 50 µM verapamil and ng of incorporated nilotinib determined. Data demonstrate inhibition of ABCG2 has no significant effect on nilotinib IUR at 150 nM nilotinib. Data also demonstrate no significant effect of ABCB1 inhibition on nilotinib IUR in K562 control cells. Experiments were performed in triplicate at least three times with data representing the median. Statistical analysis was performed using Student's *t*-test. Error bars represent SEM. NIL=nilotinib.

4.3.4. Nilotinib may be Effluxed by other ABC Transporters

IC50 experiments, analogous to those performed in cell lines with ABCB1/ABCG2 inhibitors, were used to investigate effects of the commonly prescribed medication pantoprazole on nilotinib-mediated kinase inhibition. K562, K562-Dox, K562-ABCG2 and KU812 cells were incubated in increasing concentrations of nilotinib in the absence and presence of various concentrations of pantoprazole, an inhibitor of both ABCB1 and ABCG2. Results demonstrated that pantoprazole had a significant effect on nilotinib mediated kinase inhibition in all four cell lines. $IC50^{NIL}$ was significantly decreased in the presence of as little as 50 μM pantoprazole with the percentage reduction increasing correspondingly with the concentration of pantoprazole (**Figure 4.13** and **Table 4.4**). In K562-Dox cells addition of 50 μM pantoprazole resulted in a 56% decrease in $IC50^{NIL}$ while addition of 200 μM and 500 μM pantoprazole resulted in 57% and 69% decrease respectively ($n>3$, $p<0.05$). Similar results were observed in K562-ABCG2, KU812 and K562 control cells. These data suggest that there may be other efflux transporter/s, closely related to ABCB1 and ABCG2 and expressed in all four cell lines, also involved in nilotinib transport.

4.4. Discussion

ABCB1 and ABCG2 are expressed at points of drug penetration (blood brain barrier, intestine) as well as other sites of drug uptake and excretion (liver, kidney)[172], indicating an essential role in tissue absorption, distribution and excretion, and ultimately in the plasma level of drug achieved. Importantly, expression of these transporters has been demonstrated on primitive hematopoietic stem cells[174,175] as well as CML CD34+ cells[181,187], and here they are likely to impact the efficacy of TKI therapy. Clinically, interactions of TKIs with these ABC transporters may be further exacerbated by drug:drug interactions resulting from the use of concomitant therapies (for example pantoprazole, esomeprazole and sildenafil) which also associate with ABC transporters[174,175,199,246-249]. Gaining a better understanding of TKI:ABC transporter interactions may provide important insights into the mechanism of TKI resistance in CML

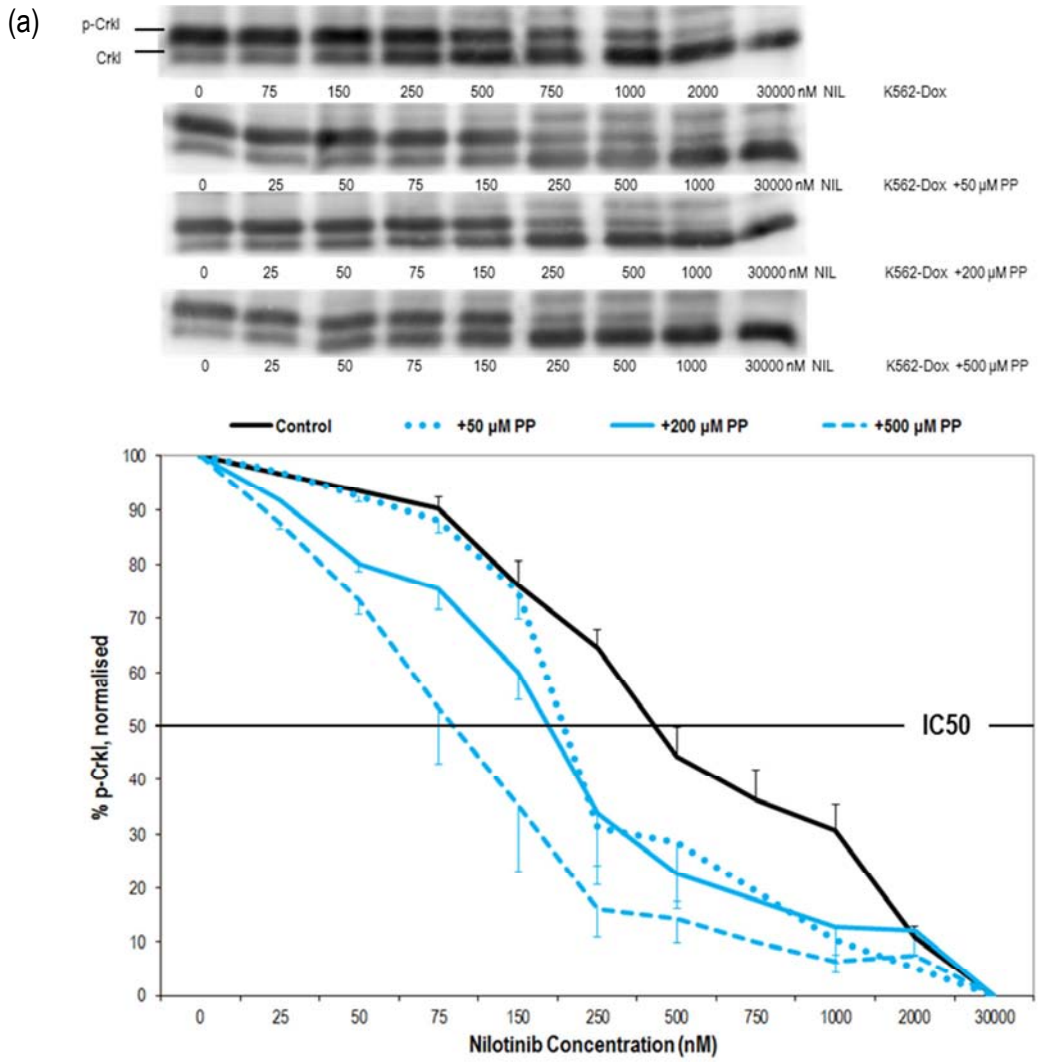

Figure 4.13: Pantoprazole significantly decreases $IC50^{NIL}$ in CML cell lines

IC50 was determined via incubating a) K562-Dox, b) K562-ABCG2, c) KU812 and d) K562 cells for 2 h at 37°C in the absence and presence of various concentrations of pantoprazole ranging 50–500 µM. CrkI western blot was performed to determine the concentration of nilotinib required to inhibit Bcr-Abl kinase activity by 50%. Data demonstrate that addition of pantoprazole significantly decreases $IC50^{NIL}$. The western blot analyses shown are representative of at least three separate experiments with the corresponding densitometry analysis representing the mean. NIL=nilotinib; PP=pantoprazole.

(b)

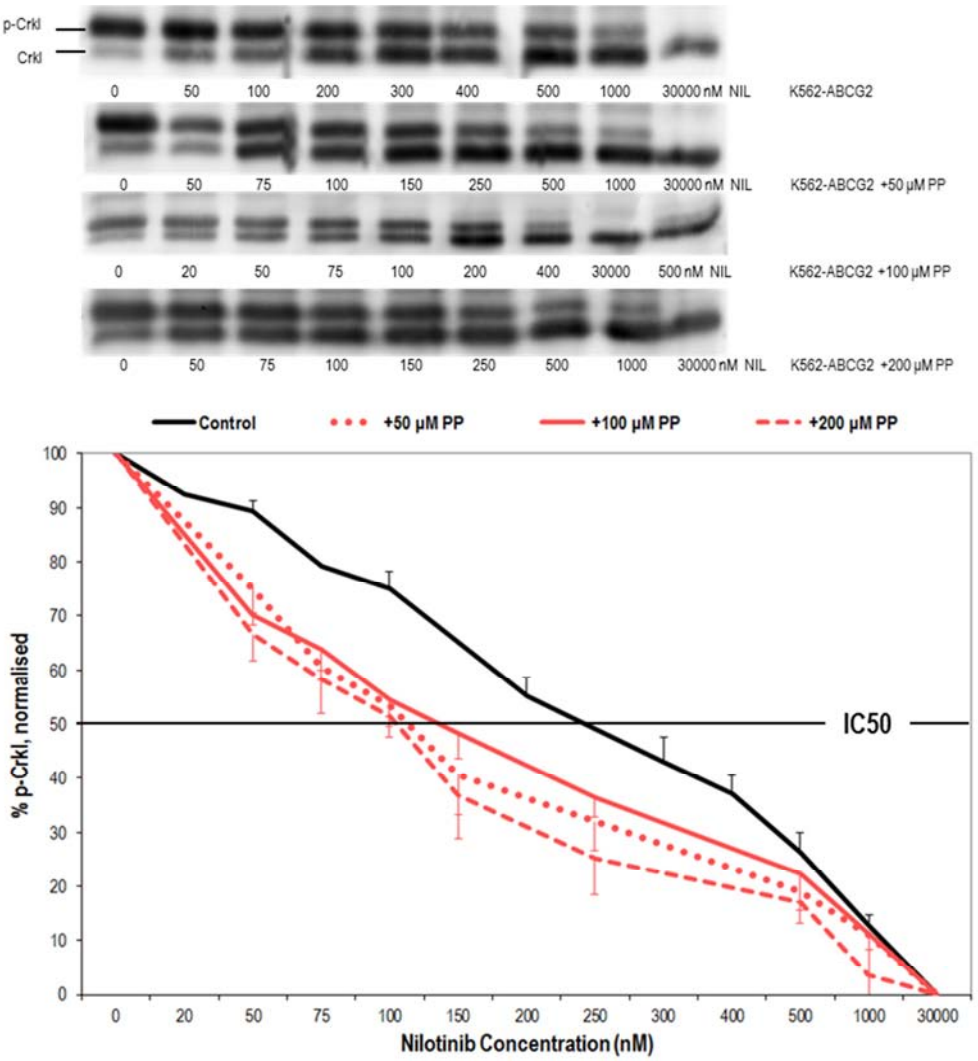
p-Crkl
Crkl
0 50 100 200 300 400 500 1000 30000 nM NIL
K562-ABCG2
0 50 75 100 150 250 500 1000 30000 nM NIL
K562-ABCG2 +50 µM PP
0 20 50 75 100 200 400 30000 500 nM NIL
K562-ABCG2 +100 µM PP
0 50 75 100 150 250 500 1000 30000 nM NIL
K562-ABCG2 +200 µM PP
Control
+50 µM PP
+100 µM PP
+200 µM PP
% p-Crkl, normalised
IC50
Nilotinib Concentration (nM)

(c)

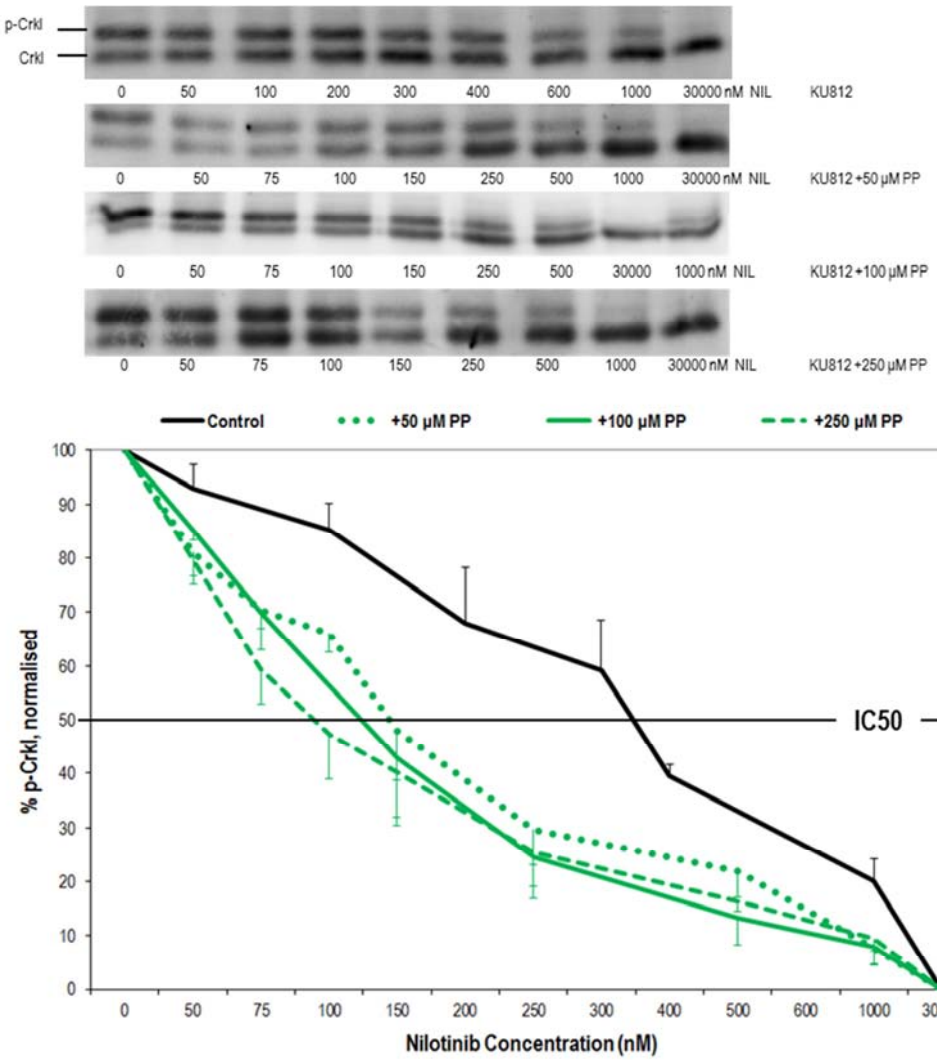
p-Crkl
Crkl
0 50 100 200 300 400 600 1000 30000 nM NIL
KU812
0 50 75 100 150 250 500 1000 30000 nM NIL
KU812 +50 µM PP
0 50 75 100 150 250 500 30000 1000 nM NIL
KU812 +100 µM PP
0 50 75 100 150 250 500 1000 30000 nM NIL
KU812 +250 µM PP
Control
+50 µM PP
+100 µM PP
+250 µM PP
% p-Crkl, normalised
IC50
Nilotinib Concentration (nM)

(d)

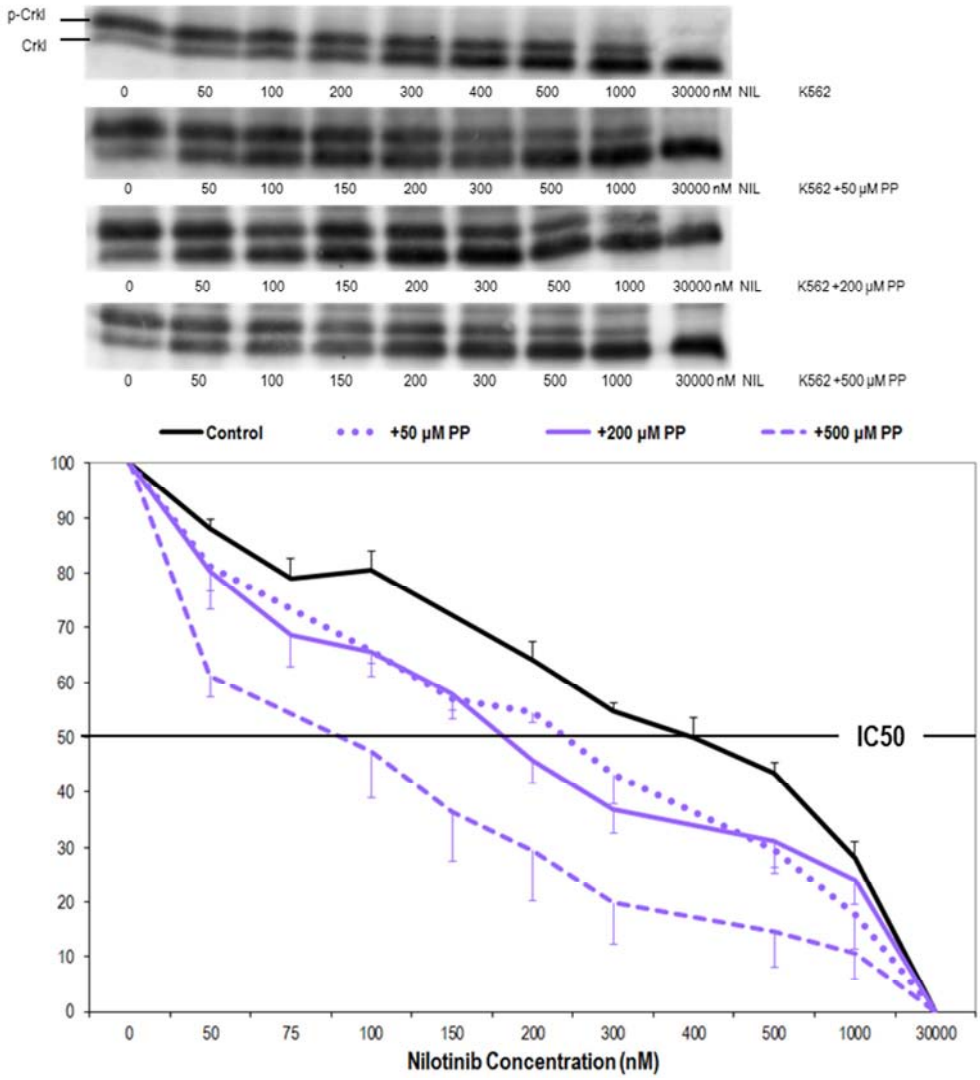
p-CrkI
CrkI
0 50 100 200 300 400 500 1000 30000 nM NIL K562
0 50 100 150 200 300 500 1000 30000 nM NIL K562 +50 µM PP
0 50 100 150 200 300 500 1000 30000 nM NIL K562 +200 µM PP
0 50 100 150 200 300 500 1000 30000 nM NIL K562 +500 µM PP
Control
+50 µM PP
+200 µM PP
+500 µM PP
IC50
Nilotinib Concentration (nM)

Table 4.4: The effect of increasing concentrations of pantoprazole on $IC50^{NIL}$ in cell lines

K562-Dox	$IC50^{NIL}$ (nM)	% decrease	n value	*p*-value
Control	463		n=5	
+50 μM PP	202	56%	n=3	*p*=0.021
+200 μM PP	201	57%	n=4	*p*=0.010
+500 μM PP	145	69%	n=3	*p*=0.010

K562-ABCG2	$IC50^{NIL}$ (nM)	% decrease	n value	*p*-value
Control	261		n=6	
+50 μM PP	122	53%	n=5	*p*=0.007
+100 μM PP	157	40%	n=5	*p*=0.041
+200 μM PP	120	54%	n=5	*p*=0.011

KU812	$IC50^{NIL}$ (nM)	% decrease	n value	*p*-value
Control	305		n=5	
+50 μM PP	149	51%	n=5	*p*=0.010
+100 μM PP	146	62%	n=5	*p*=0.011
+250 μM PP	96	69%	n=5	*p*=0.004

K562	$IC50^{NIL}$ (nM)	% decrease	n value	*p*-value
Control	388		n=6	
+50 μM PP	254	34%	n=3	*p*=0.012
+200 μM PP	217	44%	n=5	*p*=0.001
+500 μM PP	114	71%	n=4	*p*<0.001

Statistical analyses were performed using Student's *t*-test; NIL=nilotinib, PP=pantoprazole.

and may assist clinical decision making regarding the use of concomitant medications which may also interact with ABCB1 and/or ABCG2.

To resolve the disparity seen in the literature Bcr-Abl kinase inhibition was utilised to determine the interaction of nilotinib with the cellular efflux transporters ABCB1 and ABCG2. This is the first study to do so and because this approach measures actual target inhibition by nilotinib over a large concentration range, the conjecture surrounding clinically relevant dosages can be better addressed.

It has previously been demonstrated that increased expression of ABCB1[111,115,118,138-140] and ABCG2[146] *in vitro* leads to decreased intracellular concentrations of imatinib and hence has been a suggested mechanism of imatinib resistance. Furthermore, *in vivo* studies have demonstrated that ABCB1(-/-) knockout mice have greater imatinib penetration of the central nervous system when compared with their wildtype ABCB1 counterparts[144,145]. Similarly, there is mounting evidence that over-expression of ABCB1 can lead to resistance to nilotinib in cell lines[116] (discussed further in **Chapters 5** and **6**). However, transport of nilotinib reported in the literature is controversial, with differences in results appearing to be mainly due to disparities in concentrations assayed. It is reported that at high micromolar concentrations nilotinib functions as a potent inhibitor of both ABCB1 and ABCG2[116,155,187,189,250,251] however at lower nanomolar concentrations nilotinib may be a substrate of these transporters[116,153,155,250]. In many of the studies which conclude that nilotinib is an inhibitor, extremely high concentrations were used based on the peak plasma drug levels of 4 μM[170]. However, due to the fact that in the plasma, nilotinib is greater than 95% protein bound[170,190], the concentration of free drug available to the leukaemic cell is likely to be significantly lower. Furthermore, the finite number of transporters present on the cell surface means that at high concentrations *in vitro*, nilotinib may saturate the transporter[252] and thus mask any subtle interactions that may take place *in vivo*. Therefore the use of high drug concentration *in vitro* and nilotinib's purported inhibitory effects may not be

representative of the *in vivo* situation and as such these results should be viewed with caution.

This investigation demonstrated that nilotinib-mediated kinase inhibition is impacted by high expression of ABCB1 but not ABCG2. Inhibition of ABCB1 resulted in decreased $IC50^{NIL}$ prompting the postulation that this is most likely due to increased intracellular levels of TKI, thus indicating this transporter plays a clinically relevant role in nilotinib efflux. Conversely, nilotinib does not appear to have a strong interaction with ABCG2. It could be postulated that the mixed population of cells present in the K562-ABCG2 culture is interfering with the analysis and leading to the erroneous conclusion that ABCG2 overexpression has no effect on nilotinib-mediated kinase inhibition. Thus it was necessary to re-sort the K562-ABCG2 cells at a later date to attain a pure population of overexpressing cells (**Section 2.3.7**). Additional $IC50^{NIL}$ and $IC50^{IM}$ experiments were performed, again in the absence and presence of ABCB1/ABCG2 inhibitors, to confirm that the mixed population of cells used in initial experimentation was not causing misleading artefacts in the analysis. Importantly, this additional experimentation demonstrated that overexpression of ABCG2 did not significantly increase $IC50^{NIL}$ thus confirming initial results (**Appendix 2B**). Furthermore, while the specific $IC50^{NIL}$ values have decreased, the trend observed mimicked that of prior experiments whereby addition of Ko143 had no effect on nilotinib-mediated kinase inhibition. The tendency for cell line IC50 values to drift over time is not a new concept with our laboratory observing a decrease in IC50 as passage number increases. Thus, experiments performed a year or more apart may have different absolute IC50 values but because the decrease is uniform, the trends observed upon addition of inhibitors remains the same.

Unfortunately, assessment of the effect of ABCB1 and ABCG2 inhibition was not possible in primary cells due to the low expression levels of these transporters in patient mononuclear cells. While it has previously been demonstrated that ABCB1 and ABCG2 are expressed at higher levels in CML CD34+ cells[181,187,244], the large numbers of cells required to perform IC50s in the absence and presence of

inhibitors prevented these experiments from being conducted. However, the relevance of ABC transporters in the patient setting remains, with our laboratory previously demonstrating a connection between high expression of ABCB1 and the development of kinase domain mutations and/or disease resistance in a small cohort of patients[253]. There is also evidence in cell line models to suggest that increasing levels of ABCB1 (at both the mRNA and protein level) are frequently associated with the development of TKI resistance[107,111,116,244] (discussed further in **Chapters 5** and **6**).

IC50 experiments in the presence of the proton pump inhibitor pantoprazole demonstrated a consistent decrease in $IC50^{NIL}$ in Bcr-Abl positive cell lines irrespective of ABCB1/ABCG2 overexpression status. These data raise the possibility that there is another, pantoprazole-inhibitable, transporter expressed in all four cell lines also involved in nilotinib transport (discussed further in **Chapter 7**).

The results detailed here clarify some inconsistencies present in the current literature concerning the nilotinib:ABC transporter relationship. This approach uses kinase inhibition as the key readout for the interaction of nilotinib with ABCB1 and ABCG2 whereas previous publications utilise methods that do not assess the direct action of TKIs. Additionally, our laboratory has demonstrated a direct correlation between kinase inhibition and patient response[210] and has previously employed this technique to ascertain the dasatinib:ABCB1/ABCG2 interaction with results confirming the work of others[155,183,186,210,250]. Interestingly, $IC50^{NIL}$ experiments emphasised the fact that at high micromolar concentrations, maximum kinase inhibition occurred thus alluding to the possibility that concentrations of nilotinib in excess of 2 μM may mask subtle TKI:transporter interactions and may not accurately reflect the *in vivo* situation. Adding further weight to this hypothesis are data from IUR assays in Bcr-Abl positive cell lines expressing low and high levels of ABCB1 and ABCG2. These data demonstrated no significant difference in intracellular concentrations of nilotinib when used at 2 μM. However, experiments repeated using nilotinib at lower nanomolar concentrations supported the results from

kinase inhibition studies. Inhibition of ABCB1 but not ABCG2 resulted in a consistent and substantial increase in intracellular levels of radiolabelled nilotinib. Additionally, efflux studies utilising high and low concentrations of nilotinib demonstrated that at concentrations in excess of 2 μM, nilotinib functions as an inhibitor of both ABCB1 and ABCG2 *in vitro*. The clear evidence of the concentration dependence of ABCB1-mediated nilotinib efflux provided here likely explains the lack of consensus on this question in previous studies. From the clinical perspective, these findings suggest that nilotinib is likely to be susceptible to resistance mediated by over-expression of ABCB1. Hence, as this will be particularly evident in patients with low plasma concentrations of TKIs, these patients may benefit from combination TKI:ABCB1 inhibitor therapy. While limited clinical data is available on patients receiving up front nilotinib who go on to develop resistance, future studies assessing ABCB1 levels in such patients may be of value.

In conclusion, the findings detailed in this chapter strongly suggest that ABCB1 but not ABCG2 is involved in nilotinib efflux. We have demonstrated that high levels of ABCB1 significantly decrease nilotinib-mediated kinase inhibition resulting in a significantly increased $IC50^{NIL}$. Inhibition of ABCB1 significantly decreases $IC50^{NIL}$, most likely due to an increase in intracellular nilotinib concentrations. Nilotinib may also be effluxed by another ABC transporter, closely related to ABCB1, and combination TKI:ABC transporter inhibitor therapy may present an attractive option to enhance TKI efficacy.

Chapter 5

ABCB1 Overexpression is the Initiator of Resistance in K562 Cells

5.1. Introduction

The synthesis and clinical development of small molecule inhibitors designed to block the kinase activity of Bcr-Abl has revolutionised the treatment of chronic myeloid leukaemia (CML). Imatinib, the first of these tyrosine kinase inhibitors (TKIs), has induced complete cytogenetic remissions (CCyR) in over 87% of newly diagnosed CML patients by five years[254]. More recently the second generation of TKIs, nilotinib and dasatinib, have resulted in significantly better treatment outcomes for the majority of patients with CML. However, there still exists a group of patients who demonstrate primary resistance to TKI therapy and a second group who develop secondary resistance following an initially successful treatment phase. Primary resistance is observed in 15–25% of patients and occurs once they fail to achieve a landmark response, for example a complete haematological response (CHR) by 3 months or a CCyR by 18 months[254]. Secondary resistance is recognised when a patient loses cytogenetic or molecular remission or undergoes disease progression while on treatment. Primary resistance to imatinib may be due, in part, to decreased OCT-1 activity resulting in inadequate imatinib uptake and function[177], however, the cause of primary nilotinib resistance remains unclear. Primary resistance is usually overcome by alteration of TKI therapy, either by dose increase or use of a more potent TKI. In contrast, it may be possible to identify patients at risk of developing secondary nilotinib resistance and intervene before this occurs. In order to determine which patients are more likely to develop TKI resistance following a successful treatment phase, it is necessary to understand the kinetics of resistance emergence. In previous studies in which nilotinib resistant cell lines were generated, resistance mechanisms were determined only once cells demonstrated overt resistance to the final concentration of nilotinib; however, researchers failed to examine modes of resistance in the intermediary cells created during incremental increases of nilotinib. In this study, cultured cells were sampled at every stage of resistance generation allowing the dynamics of resistance development and the interplay between resistance mechanisms to be studied. This may allow the identification of early warning signs in patients who are more likely to develop overt resistance later.

There are several overlapping modes of resistance to the first and second generation TKIs which can be broadly classified as Bcr-Abl *dependent* and *independent*. Bcr-Abl overexpression has been observed both *in vitro* and *in vivo* and has been attributed to duplication of the Ph chromosome[109,255], mutations in the promoter region of *BCR-ABL*[256] and the presence of double minutes carrying *BCR-ABL*[107,257]. Double minutes are small, circular fragments of extra chromosomal DNA which lack centromeres. This means that they segregate randomly into daughter cells during mitosis giving these cells a potential growth advantage[258]. *BCR-ABL* amplification by any of these mechanisms presumably leads to an increase in transcription and translation causing a substantial increase in the amount of Bcr-Abl protein within the cell thus rendering clinically achievable concentrations of TKI ineffective.

The most common mode of secondary TKI resistance observed clinically is mutation of the Bcr-Abl kinase domain (KD) with up to 40% of resistant patients developing mutations while undertaking TKI therapy[171,212,259,260]. Imatinib and nilotinib bind the inactive conformation of the KD while dasatinib binds the active conformation and spontaneous mutations in key regions of the binding pocket can prevent TKI binding. With the exception of the T315I mutation which disrupts a critical KD:TKI hydrogen bond, nilotinib and dasatinib have complementary inhibition profiles such that a patient with a nilotinib-resistant mutation will still be sensitive to dasatinib and vice versa (**Figure 5.1**).

Overexpression of the drug efflux transporters ABCB1[107,111,115,116,118,138-140] and ABCG2[146] have been implicated in resistance to imatinib, nilotinib and dasatinib *in vitro*. Additionally, as described in **Chapter 4**, ABCB1 overexpression leads to significantly increased $IC50^{NIL}$ which is negated upon ABCB1 inhibition suggesting ABCB1-mediated nilotinib transport. Thus, the interplay between ABCB1/ABCG2 overexpression and other resistance mechanisms was investigated and is discussed in the current chapter.

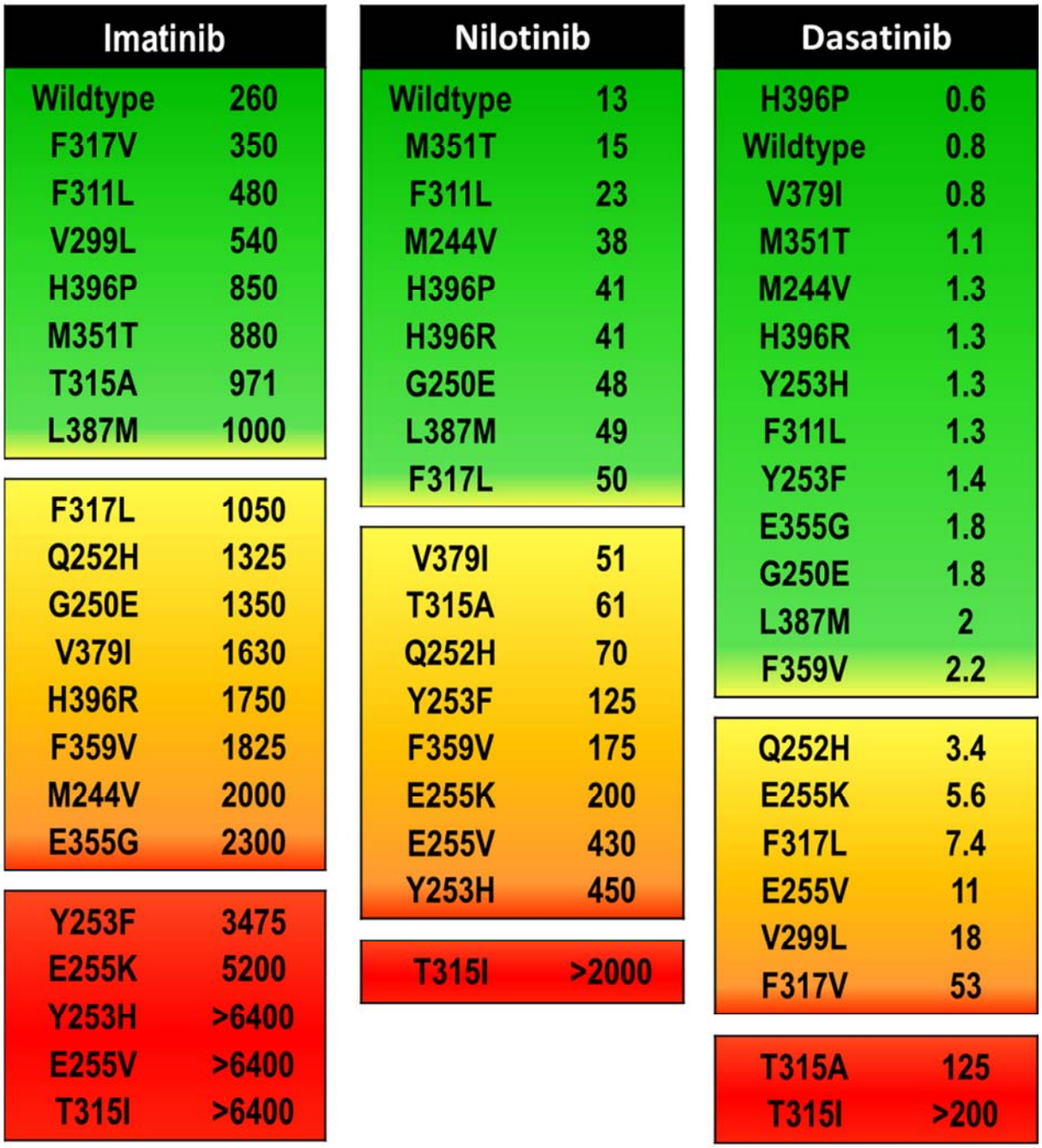

Imatinib	
Wildtype	260
F317V	350
F311L	480
V299L	540
H396P	850
M351T	880
T315A	971
L387M	1000
F317L	1050
Q252H	1325
G250E	1350
V379I	1630
H396R	1750
F359V	1825
M244V	2000
E355G	2300
Y253F	3475
E255K	5200
Y253H	>6400
E255V	>6400
T315I	>6400

Nilotinib	
Wildtype	13
M351T	15
F311L	23
M244V	38
H396P	41
H396R	41
G250E	48
L387M	49
F317L	50
V379I	51
T315A	61
Q252H	70
Y253F	125
F359V	175
E255K	200
E255V	430
Y253H	450
T315I	>2000

Dasatinib	
H396P	0.6
Wildtype	0.8
V379I	0.8
M351T	1.1
M244V	1.3
H396R	1.3
Y253H	1.3
F311L	1.3
Y253F	1.4
E355G	1.8
G250E	1.8
L387M	2
F359V	2.2
Q252H	3.4
E255K	5.6
F317L	7.4
E255V	11
V299L	18
F317V	53
T315A	125
T315I	>200

Figure 5.1: Sensitivity of Bcr-Abl KD mutants to imatinib, nilotinib and dasatinib as determined by *in vitro* cell proliferation assays (modified from O'Hare *et al.*[110])

The IC50 values in nM indicate the concentration of inhibitor required to reduce cell viability by 50%. GREEN shading represents sensitive mutations, YELLOW shading represent intermediate sensitivity and RED shading represents resistant mutations.

Dasatinib is a dual Bcr-Abl-Src family kinase (SFK) inhibitor whereas imatinib and nilotinib are not active against SFKs. Accordingly, overexpression and activation of SFK are often observed in imatinib and nilotinib resistant cells, both *in vitro*[116,119-123,125,128] and *in vivo*[116,121,123,125,161].

The SFKs consist of Fyn, Src and Yes which are ubiquitously expressed as well as Blk, Fgr, Hck, Lck, Lyn and Yrk which are expressed in cells of the haematopoietic lineage[156]. These proteins are structurally related, with each member consisting of a highly variable 'unique' domain at the N-terminal containing a myristoyl moiety; the SH1, or kinase, domain which is responsible for the enzymatic activity; an SH2 domain which allows the protein to interact with phosphotyrosine motifs; and the SH3 domain which allows autoregulation of kinase activity through intramolecular interactions as well as direct binding to adapter proteins[261,262] (**Figure 5.2**).

SFKs are involved in numerous signalling pathways governing cell proliferation and survival as well as homeostasis (**Figure 5.3**) and have previously been implicated in a variety of human cancers[262]. For this reason, activation of SFKs is tightly regulated via intramolecular interactions. Phosphorylation of a tyrosine residue in the kinase domain results in activation of the kinase. However, phosphorylation of a tyrosine residue in the carboxy terminal by negative regulators such as the tyrosine kinase CSK[263], coupled with interactions between the SH3 domain and the kinase linker region, results in the catalytically inactive, closed conformation (**Figure 5.4**). Autophosphorylation at the amino terminal supersedes inhibitory phosphorylation at the carboxy end making the kinase insensitive to negative regulation by CSK[264,265]; however, there is some evidence that additional SFK members as well as other tyrosine kinases, including Bcr-Abl, are also capable of phosphorylating amino terminal residues[159]. Overexpression of Lyn is common in the development of imatinib and nilotinib resistance and is usually referred to as a Bcr-Abl *independent* resistance mechanism[57,116,121,126]. However, it has been demonstrated that SFKs and Bcr-Abl engage in reciprocal phosphorylation[123,158,160]. Indeed, it has been

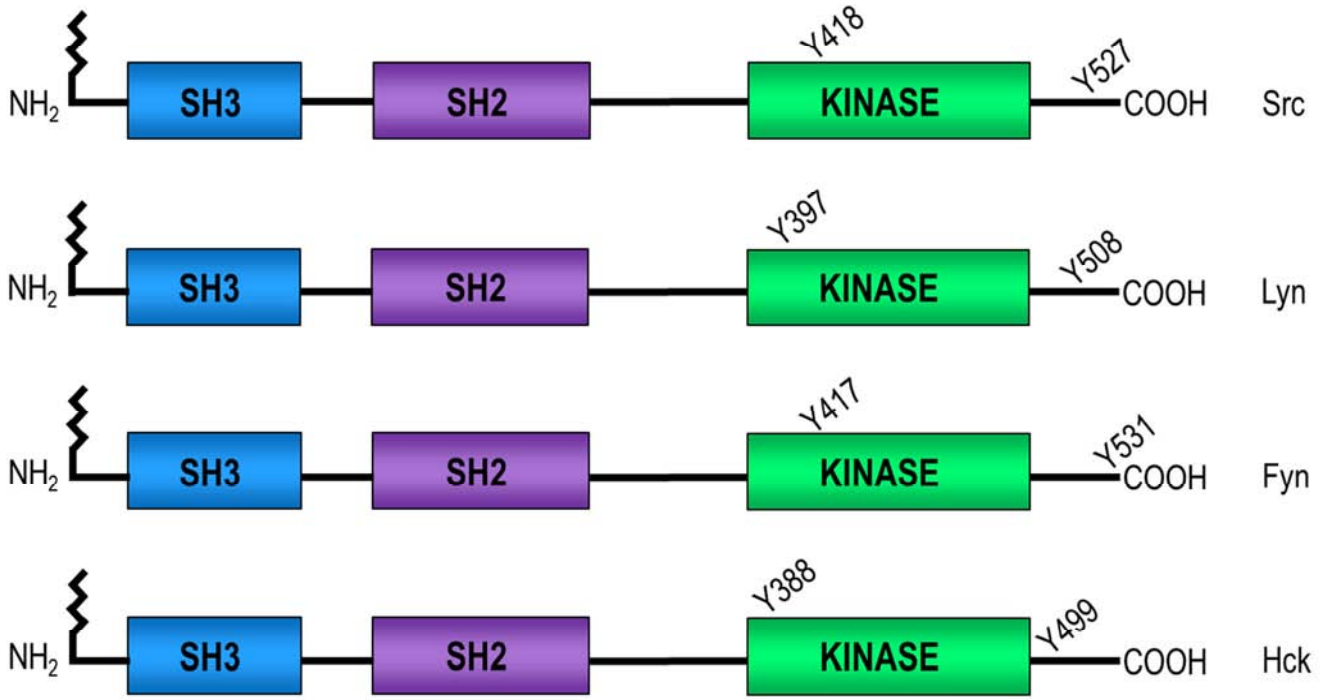

Figure 5.2: Schematic diagram of the protein domains of four commonly studied SFKs (modified from Ingley *et al*. and Tegtmeyer *et al*.[261,266])

SFK members contain a poorly conserved, myristoylated 'unique' region of 50–70 residues at the N-terminal, an SH1 (kinase) domain of ~300 residues which provides enzymatic activity, an SH2 domain of ~100 residues which allows intramolecular phosphotyrosine interactions and an SH3 domain of ~50 residues which interacts with the protein's own kinase linker region as well as other adapter proteins. Phosphorylatable tyrosine (Y) residues are indicated which, while varying slightly in position, are conserved between members and govern the activity of the kinase.

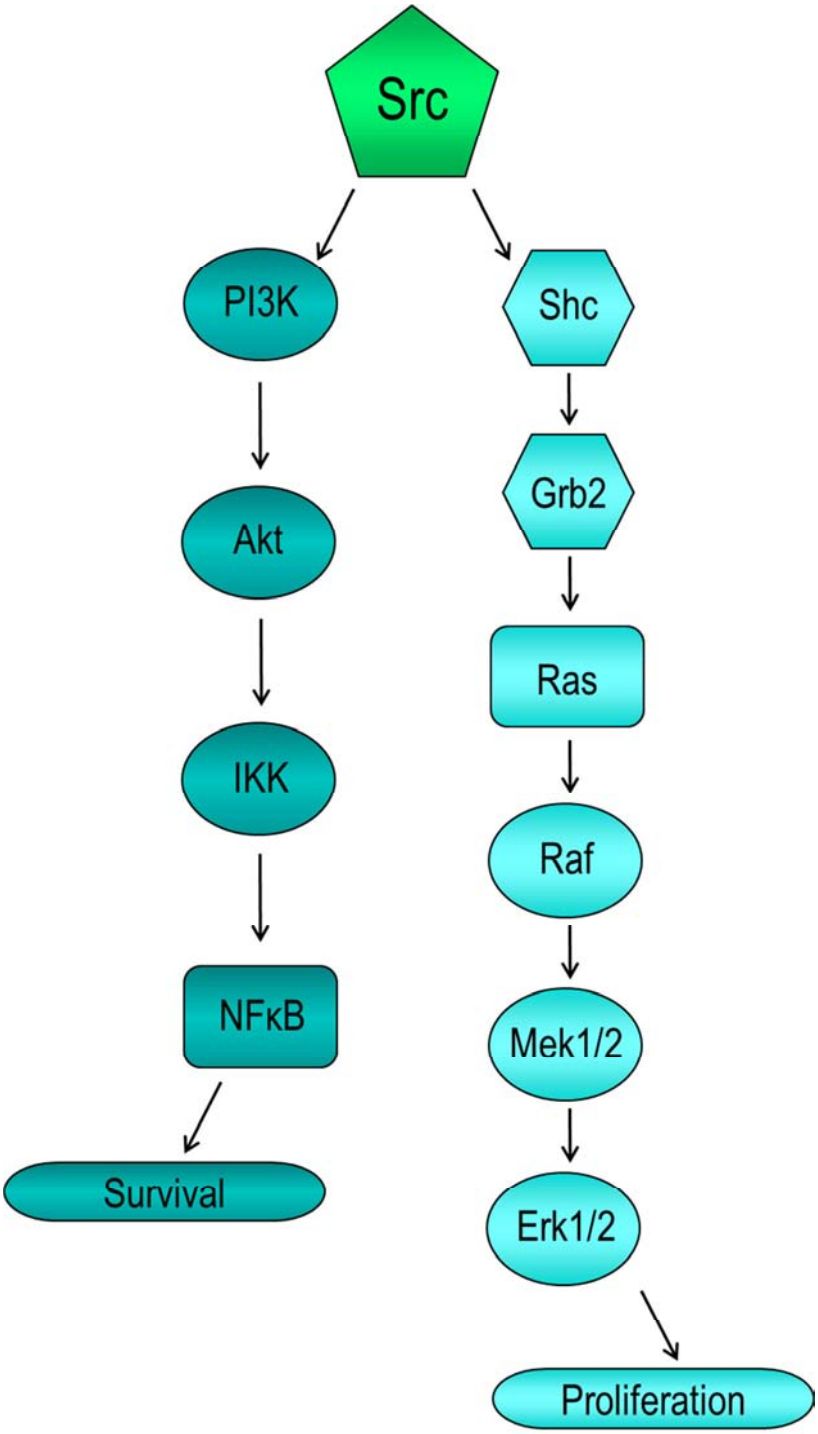

Figure 5.3: Schematic summary of signalling pathways involving SFKs (modified from Summy *et al.*[262])

SFKs have been implicated in signalling pathways involved in cell survival and proliferation as well as having a role in cellular homeostasis (not shown). Two key signalling pathways important in the pathogenesis of CML are highlighted here with kinases represented by ovals and adapter proteins represented by hexagons.

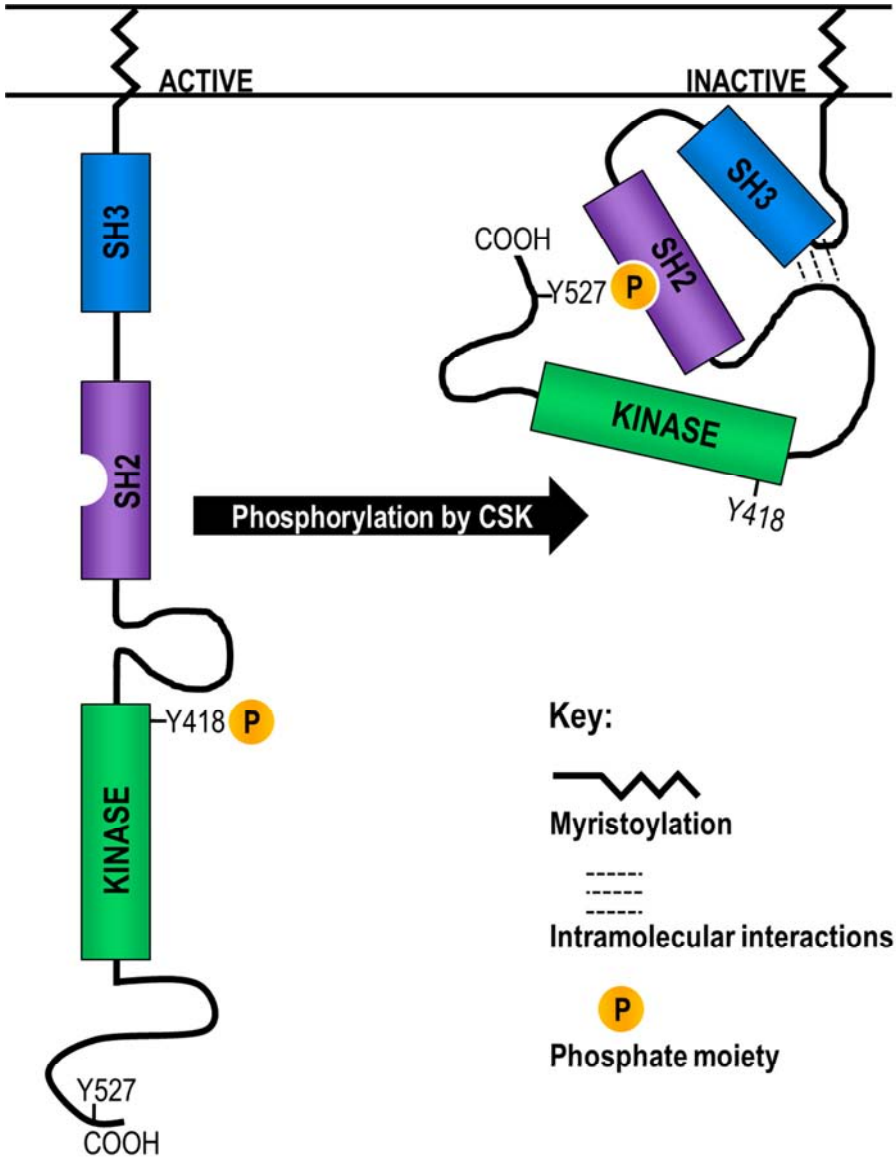

Figure 5.4: Schematic representation of the transition from active to inactive SFK as a result of differential phosphorylation (adapted from Ingley *et al*. and Tegtmeyer *et al*.[261,266])

The active kinase on the left demonstrates the open conformation with the SH2 and SH3 domains available for substrate and regulatory molecule binding. The carboxy terminal is dephosphorylated leaving the substrate binding site exposed while autophosphorylation results in phosphorylation of a tyrosine (Y) residue and maximal kinase activity (Y418 in the case of Src depicted here). Upon phosphorylation of a tyrosine in the carboxy terminal (Y527 for Src) by negative regulators such as CSK, the kinase adopts the catalytically inactive, closed conformation facilitated by intramolecular interactions between the SH3 domain and the kinase linker region.

recently suggested that active Fyn, Hck and Lyn are all capable of phosphorylating Bcr-Abl at the SH3-SH2 region of Abl and, in doing so, hold the kinase domain in its active conformation such that dasatinib is able to bind but imatinib and nilotinib are not[123,160]. Thus, it is likely that resistance due to Lyn overexpression is not independent of Bcr-Abl but instead favours the active conformation of the kinase in the presence of nilotinib and imatinib.

Another kinase implicated in TKI resistance is the receptor tyrosine kinase Axl. Axl was originally described in patients with CML[162,267,268] and other myeloproliferative disorders[268,269] but is detected ubiquitously in a wide variety of organs and cells[162]. This 140 kDa protein is comprised of two Ig repeats coupled with two fibronectin type III repeats in the extracellular region and a tyrosine kinase domain in the intracellular region[270] (**Figure 5.5**). Axl overexpression and/or increased phosphorylation has been described in both patients and Bcr-Abl positive cell lines resistant to imatinib and nilotinib[119,126,127] as well as several other types of cancer including colon[271] and breast[272]. Yeast two hybrid experiments demonstrated that Axl interacts with proteins from the PI3-K and Ras-ERK signalling pathways indicating a role in cell survival, proliferation and migration (**Figure 5.6**). Because many of the binding partners of Axl contain an SH2 domain, which likely forms the Axl:binding protein interface[273], it is expected that Axl binds to SFK members. However, this was not demonstrated until recently when immunoprecipitation experiments using resistant CML cell lines revealed that Lyn and Axl interact within a ternary complex also containing spleen tyrosine kinase (Syk)[126].

Syk is a non-receptor tyrosine kinase primarily expressed in haematopoietic cells[274] with overexpression initially observed in AML[275], and more recently, a role in CML proposed[126]. Syk is a 72 kDa cytoplasmic protein containing a kinase domain and two tandem SH2 domains[276] (**Figure 5.7**). Its activity, like SFKs, is regulated via autophosphorylation of tyrosine residues in the activation loop of the kinase domain[277,278] as well as phosphorylation of tyrosines 342 and 352 by other kinases such as Lyn[126,279].

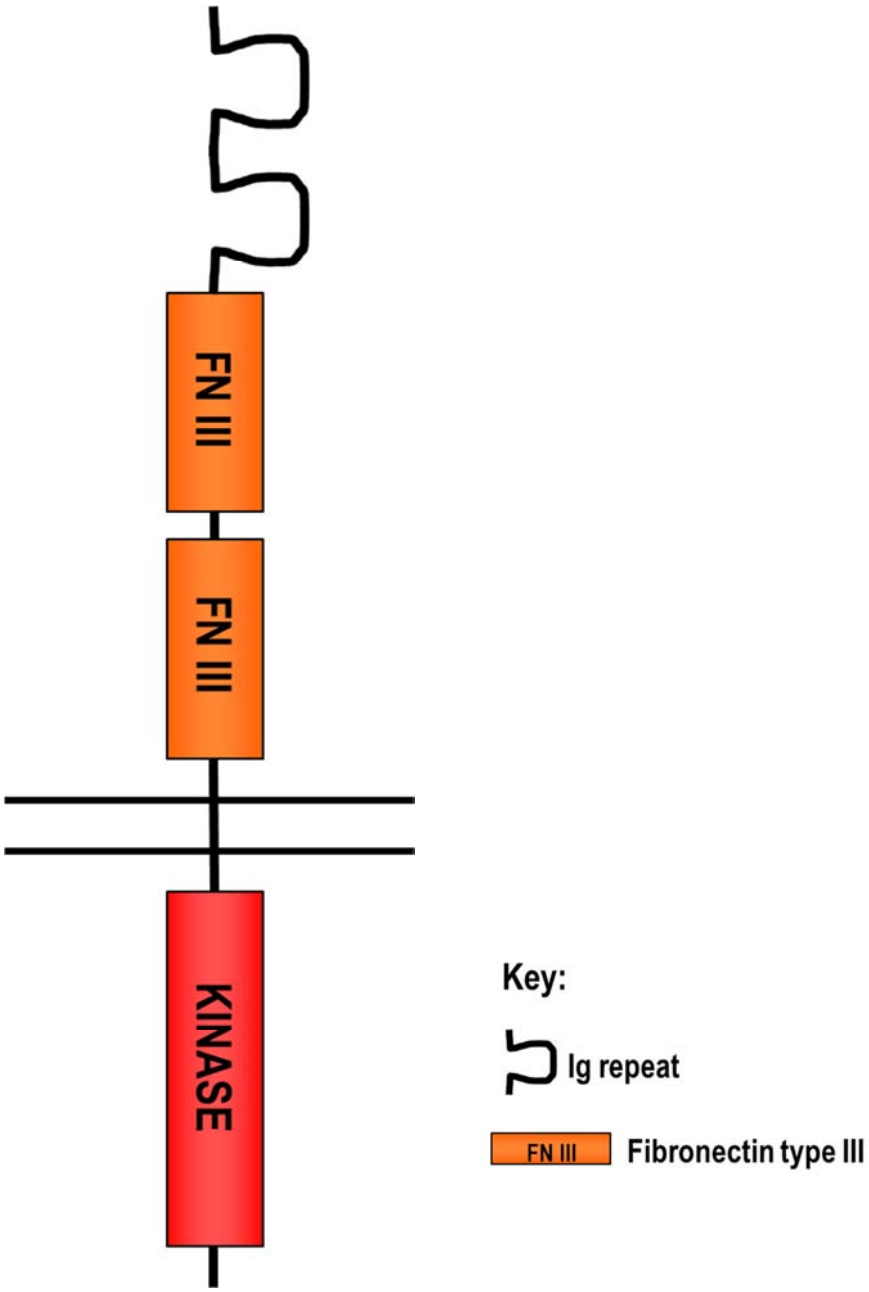

Figure 5.5: Schematic representation of the Axl receptor tyrosine kinase (modified from Hafizi *et al.*[270]

Axl is composed of two Ig repeats and two fibronectin type III repeats in the extracellular region and a tyrosine kinase domain in the intracellular region. The kinase domain is capable of constitutive activation in the absence of extracellular stimulation and thus gives the kinase oncogenic potential.

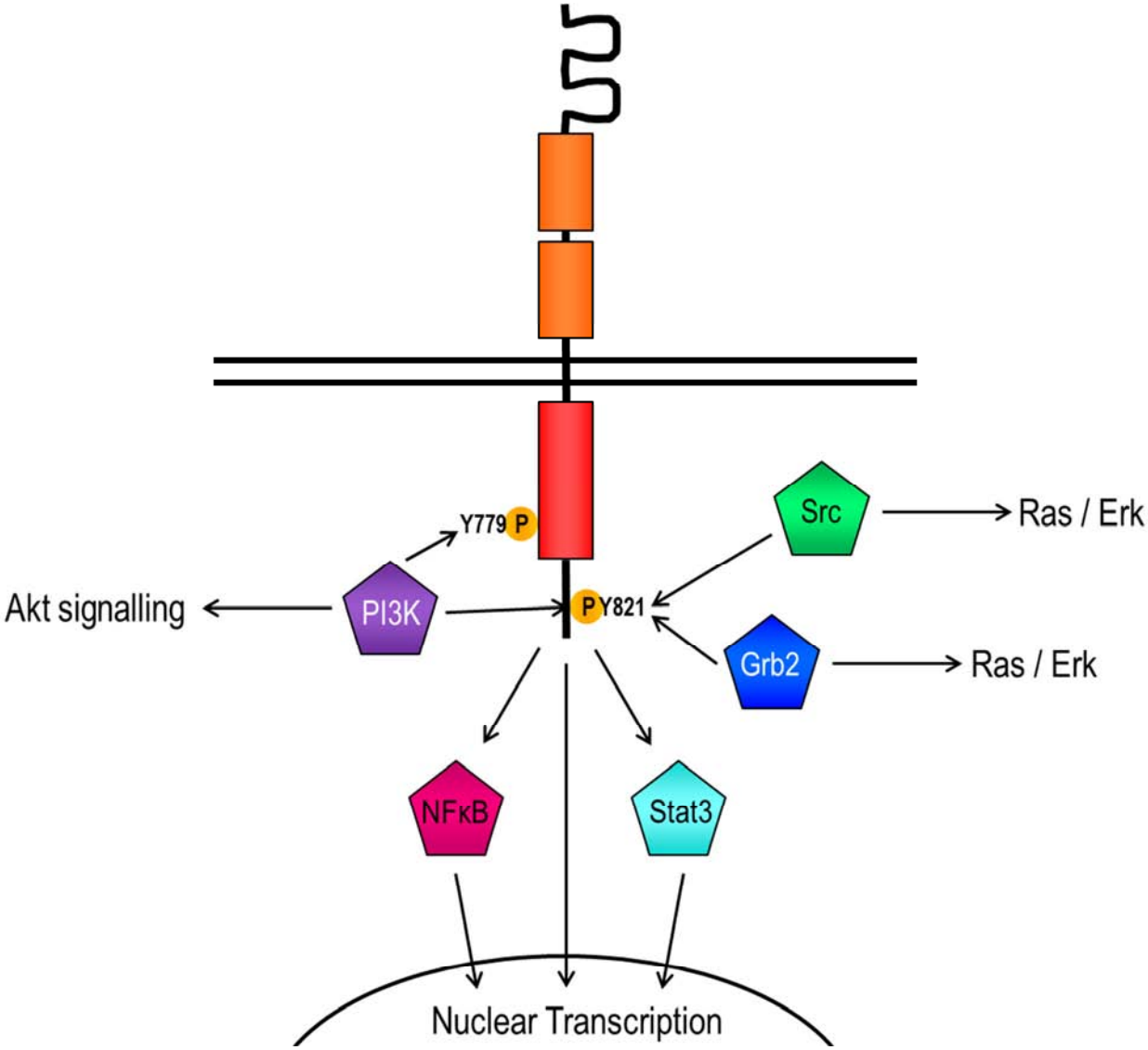

Figure 5.6: Schematic summary of signalling pathways involving Axl (modified from Hafizi *et al.*[270])

Phosphorylated tyrosine residues Y779 and Y821, on Axl's intracellular kinase domain, act as docking sites for proteins involved in signalling pathways governing cell proliferation and survival. Axl interacts with binding partners, such as Src, Grb2 and various subunits of PI3-K through SH2 domains.

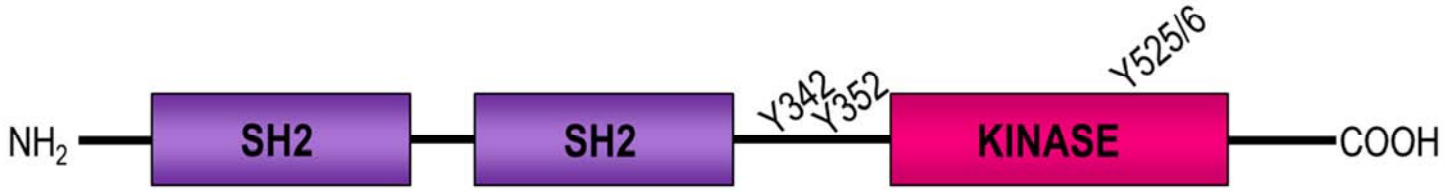

Figure 5.7: Schematic representation of Syk protein domains (adapted from Efremov *et al.*[276])

Syk comprises of two tandem SH2 domains which facilitate interaction with SFK members. Activation of Syk occurs via autophosphorylation of tyrosine (Y) residues Y525 and Y526 in the kinase domain activation loop in conjunction with phosphorylation of Y342 and Y352 by SFKs such as Lyn.

In addition to regulating the phosphorylation of Axl[126], Syk has also been demonstrated to interact with Fyn and the ubiquitin ligase c-Cbl[166,280]. Accordingly, c-Cbl may be a 'master regulator' with recent evidence suggesting an inverse relationship exists between c-Cbl and Lyn/Axl whereby low levels of c-Cbl facilitate increased levels of Lyn and Axl leading to imatinib and nilotinib resistance *in vitro*[123,168]. The interactions between these cellular kinases are extremely complex, with many signalling pathways and phosphorylation targets overlapping making dissecting the causative event leading to overexpression and activation of SFKs difficult. Thus, while much is known about the Bcr-Abl dependent modes of resistance relating to KD mutations and Bcr-Abl overexpression, the mechanisms underlying Lyn-mediated resistance require further investigation. Consequently, there is much need for an *in vitro* system in which to study TKI resistance and this forms the basis of the analyses detailed in the current chapter.

5.2. Approach

The Bcr-Abl positive cell line K562 was cultured long term in gradually increasing concentrations of nilotinib starting with 15 nM and increasing to 2 μM (**Section 2.3.3.3**; **Table 5.1**). Control cells were cultured in parallel in a constant diluent concentration of 0.1% DMSO to control for the DMSO present in cell cultures containing nilotinib. Cell growth was monitored visually, while cell viability was monitored by trypan blue exclusion of dead cells (**Section 2.3.2**). The concentration of nilotinib was increased once >80% of cells demonstrated survival (nilotinib tolerance) in culture for at least 10 consecutive days. At each stage of nilotinib escalation, ampoules of cells were frozen (**Section 2.3.4**) to allow thawing and re-culture at a later time point (**Section 2.3.5**). In addition, aliquots of cells were lysed in TRIzol reagent for RNA extraction and cDNA synthesis (**Section 2.4.5**). Concentrations of nilotinib up to 100 nM were tolerated easily, however growth and viability substantially reduced upon exposure to 125 nM nilotinib (**Table 5.1**). Once cells demonstrated ~80% survival in 125 nM nilotinib, the level of resistance was determined via IC50 assays based on p-Crkl protein expression (**Section 2.4.2**).

Table 5.1: Summary of nilotinib concentrations to which cell line resistance intermediates were exposed and the corresponding number of days before dose was increased

K562		
Nilotinib Concentration	% Live Cells	Days in Culture
15 nM NIL	95.0	10
25 nM NIL	99.1	11
50 nM NIL	96.7	10
75 nM NIL	93.7	14
100 nM NIL	94.6	12
125 nM NIL	83.6	**28**
140 nM NIL	87.4	17
200 nM NIL	85.2	13
300 nM NIL	93.3	12
400 nM NIL	90.8	14
1 μM NIL	83.9	12
2 μM NIL	94.1	Ongoing

Resistance was confirmed by cytotoxicity assays (**Section 2.3.6**). Nilotinib dose escalation continued until a concentration of 2 μM was reached to reflect plasma levels achieved *in vivo* in nilotinib treated patients[170] and resistance was again determined by cytotoxicity assays and p-Crkl IC50. Modes of resistance were investigated as summarised in **Figure 5.8**. Briefly, because ABCB1 and ABCG2 overexpression has previously been linked to TKI resistance[115,116,118,138,139], cell surface expression of these transporters was assessed routinely during resistance development and prior to each IC50 and cytotoxicity assay using flow cytometric analysis (**Section 2.3.8.1**). Cell lines were screened for increased BCR-ABL expression, and overexpression of the kinases LYN, AXL and SYK (**Sections 2.4.3** and **2.4.5**). Cells were also assessed for kinase domain mutations (**Section 2.4.7**).

5.3. Results

5.3.1. K562 Cells Cultured in 125 nM Nilotinib Demonstrate Resistance to TKIs *In Vitro*

Nilotinib resistant K562 2 μM NIL cells were generated through exposure to gradually increasing concentrations of nilotinib. Nilotinib concentrations up to 100 nM were easily tolerated, however, upon exposure to 125 nM nilotinib, cell growth stalled and viability significantly decreased (**Table 5.2**). After approximately one month exposure to 125 nM nilotinib, cell viability increased to >80% and resistance to nilotinib was evaluated by IC50 specific for p-Crkl protein expression. These assays rely on Bcr-Abl kinase inhibition as the key readout and thus enable a distinction between Bcr-Abl *dependent* and Bcr-Abl *independent* mechanisms of resistance; an increase in IC50 value indicates on target, Bcr-Abl *dependent* resistance. K562 125 nM NIL cells demonstrated significantly increased $IC50^{NIL}$ when compared with control cells: $IC50^{NIL}$ increased from 199 nM to 1826 nM, $p<0.001$ (**Figure 5.9a**). Resistance was confirmed by cytotoxicity assay with K562 125 nM NIL cells demonstrating significantly increased survival compared with control cells when exposed to 1000 nM nilotinib for 72 h: 69% vs 100% survival, $p<0.001$ (**Figure 5.10a**).

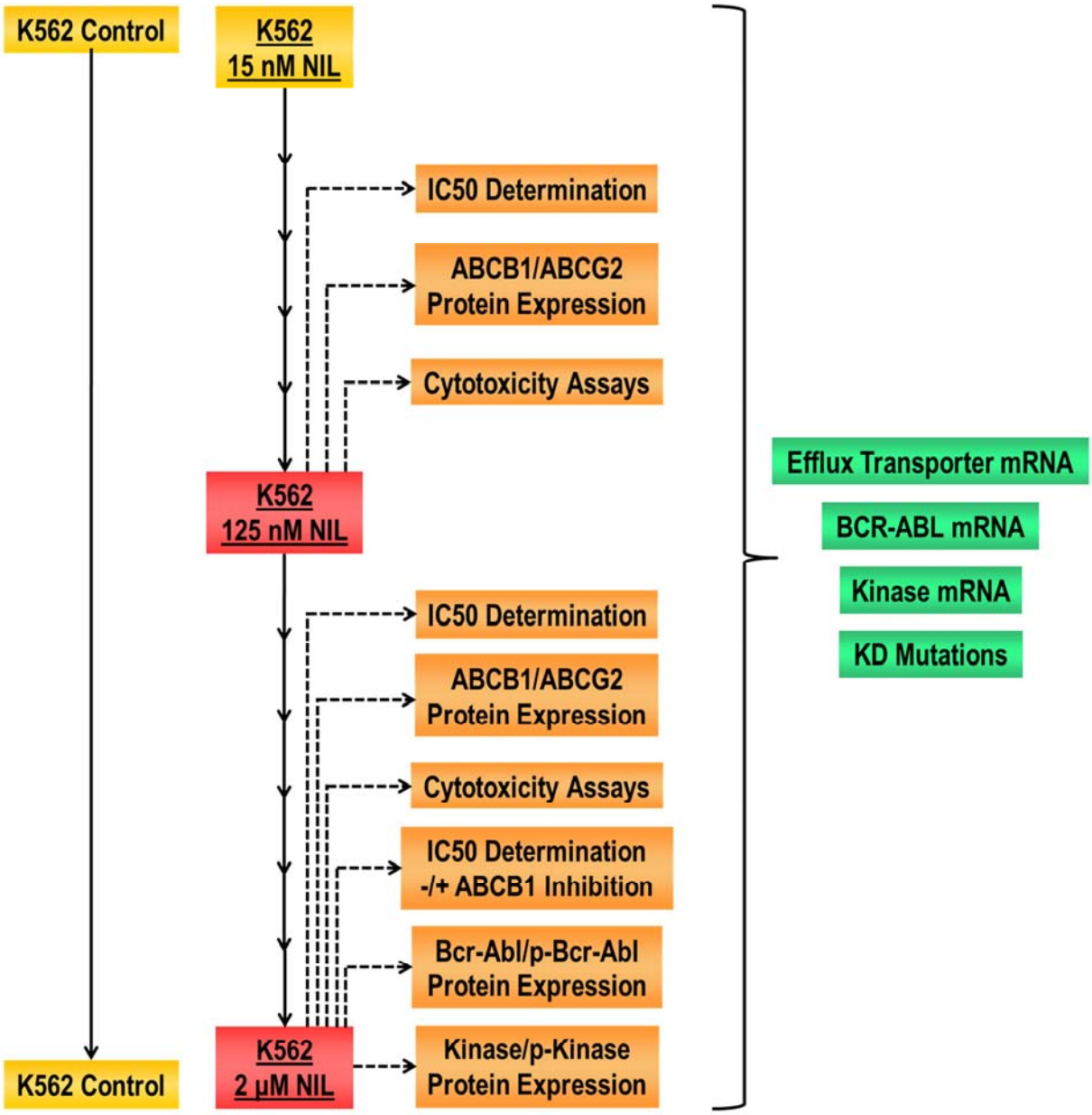

Figure 5.8: Schematic summary of generation and determination of nilotinib resistance in K562 cells

K562 cells were cultured in gradually increasing concentrations of nilotinib. At nilotinib concentrations 125 nM and 2 µM, resistance was assessed by various *in vitro* methods (**ORANGE BOXES**). In addition, mRNA levels and KD mutations were determined in all resistance intermediates (**GREEN BOXES**). All assays were also performed on K562 control cells for comparison. Bold arrows represent steps in escalation of nilotinib. Dashed arrows denote which assays were performed on each intermediate. NIL=nilotinib; KD=kinase domain.

Table 5.2: Summary of live K562 cells after exposure to 125 nM nilotinib for the corresponding number of days

Days in Culture	% Live Cells
2	96.9
4	70.9
7	39.3
22	73.4
25	80.6
28	83.6

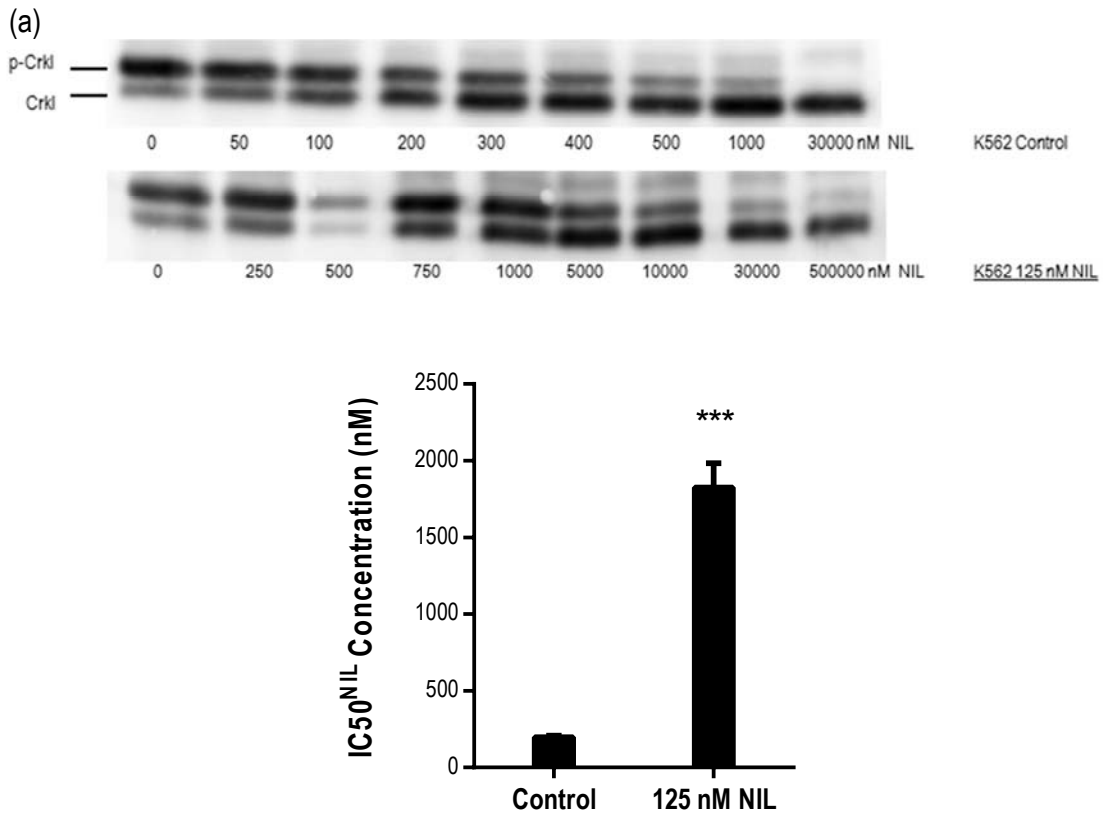

Figure 5.9: <u>K562 125 nM NIL</u> cells are significantly resistant to TKI-mediated kinase inhibition

IC50 was determined via incubating cells for 2 h at 37°C in the presence of increasing concentrations of a) nilotinib, b) imatinib and c) dasatinib. Crkl western blot was performed to determine the concentration of TKI required for 50% Bcr-Abl kinase inhibition. Data demonstrate that <u>K562 125 nM NIL</u> cells have a significantly increased IC50 when compared with control cells; for example at 30 000 nM nilotinib, p-Crkl is completely inhibited in K562 control cells but this is not the case in <u>K562 125 nM NIL</u> cells. The western blot analyses shown are representative of at least three separate experiments with the corresponding densitometry analysis representing the mean. Statistical analyses were performed using Student's *t*-test with statistically significant *p*-values denoted by asterisks (* $p<0.05$; *** $p<0.001$). Error bars represent SEM. NIL=nilotinib; IM=imatinib; DAS=dasatinib.

(b)

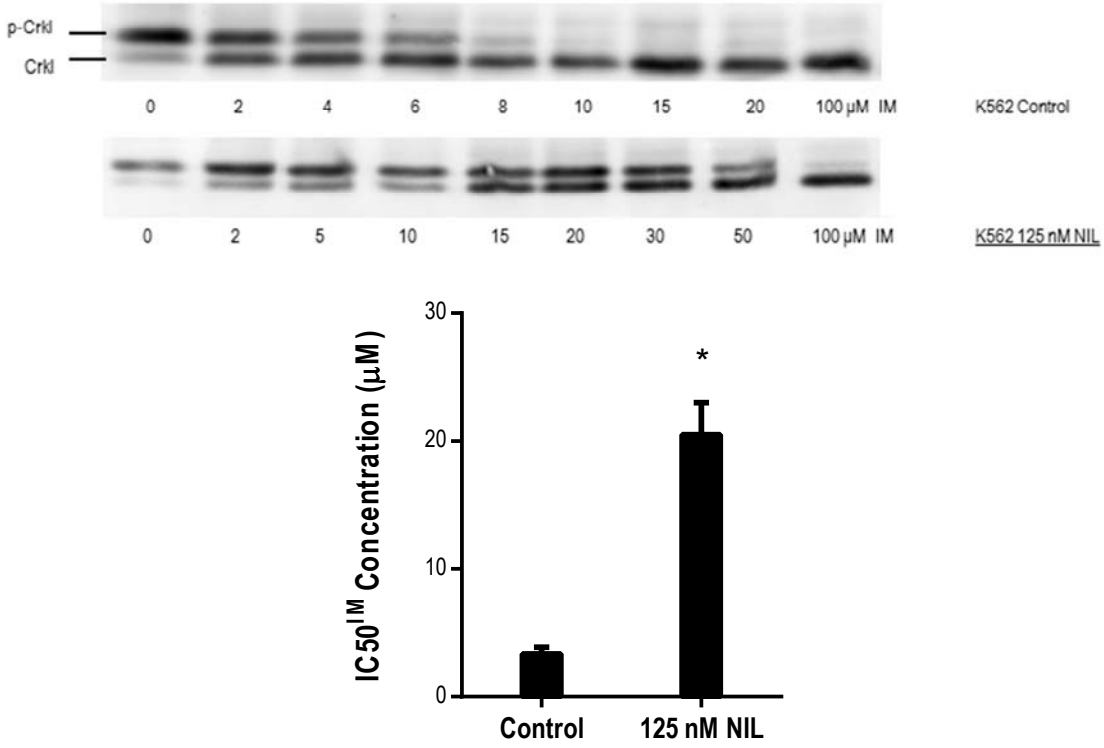
p-Crkl
Crkl
0 2 4 6 8 10 15 20 100 µM IM
K562 Control
0 2 5 10 15 20 30 50 100 µM IM
K562 125 nM NIL
IC50IM Concentration (µM)
30
20
10
0
*
Control
125 nM NIL

(c)

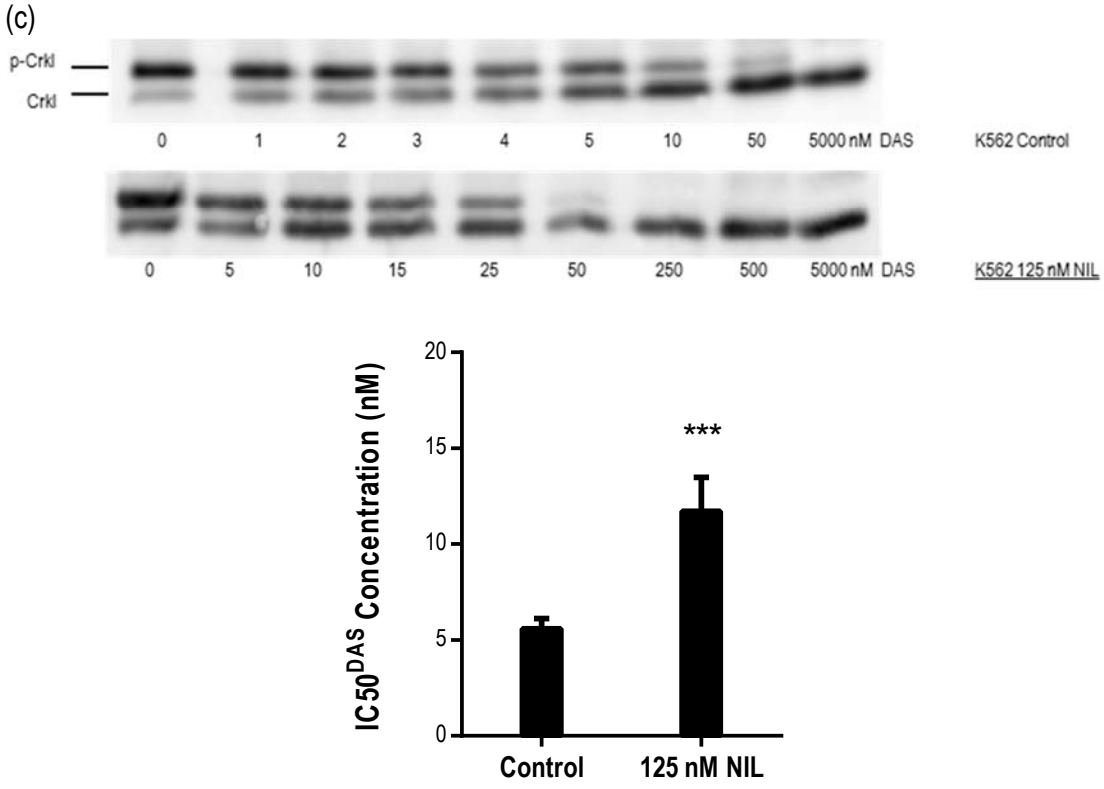
p-Crkl
Crkl
0 1 2 3 4 5 10 50 5000 nM DAS
K562 Control
0 5 10 15 25 50 250 500 5000 nM DAS
K562 125 nM NIL
IC50DAS Concentration (nM)
20
15
10
5
0
***
Control
125 nM NIL

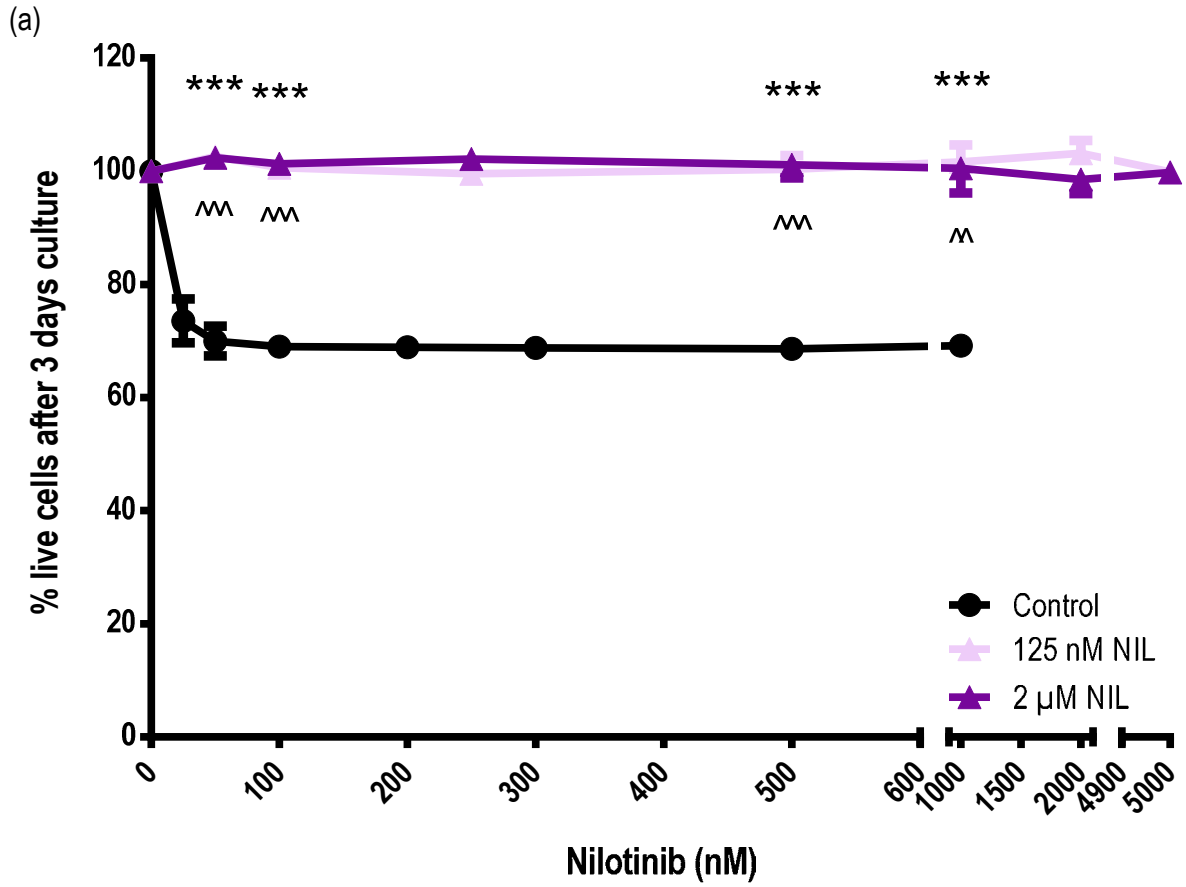

Figure 5.10: K562 125 nM NIL and K562 2 µM NIL cells have decreased TKI-mediated cell death

Cells were cultured for 72 h in increasing concentrations of a) nilotinib b) imatinib and c) dasatinib and cell death determined by Annexin V/7-AAD staining. Data demonstrate that K562 125 nM NIL cells and K562 2 µM NIL cells have significantly increased survival in the presence of TKIs when compared with control cells. Results were confirmed visually and with trypan blue staining (**Appendices 3A** and **3B**). It is important to note that trypan blue staining demonstrates near complete cell death, while Annexin V/7-AAD staining results in a maximum of 40% cell death even at the highest TKI concentrations. The FACS plots shown are representative of at least three separate experiments performed in triplicate with the corresponding survival curves representing the mean. Data were normalised to 0 nM TKI with the number of live cells in the absence of TKI set at 100%. Statistical analyses were performed using Student's *t*-test with statistically significant *p*-values denoted by asterisks and carets, representing K562 125 nM NIL and K562 2 µM NIL cell lines respectively (* $p<0.05$; ** $p<0.01$; *** $p<0.001$). Error bars represent SEM. NIL=nilotinib; IM=imatinib; DAS=dasatinib.

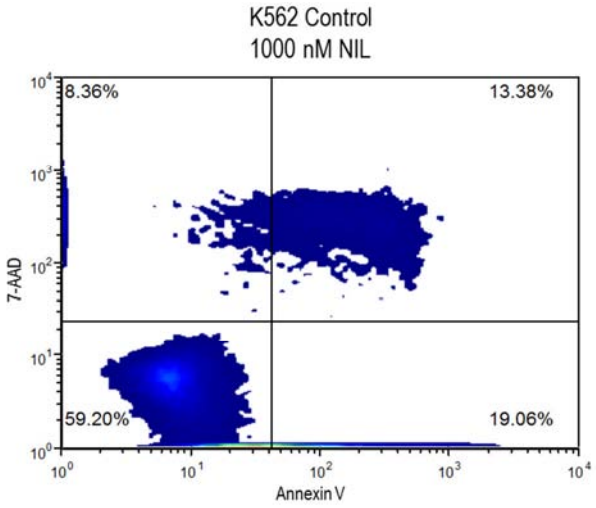
K562 Control
1000 nM NIL
8.36%
13.38%
59.20%
19.06%
7-AAD
Annexin V

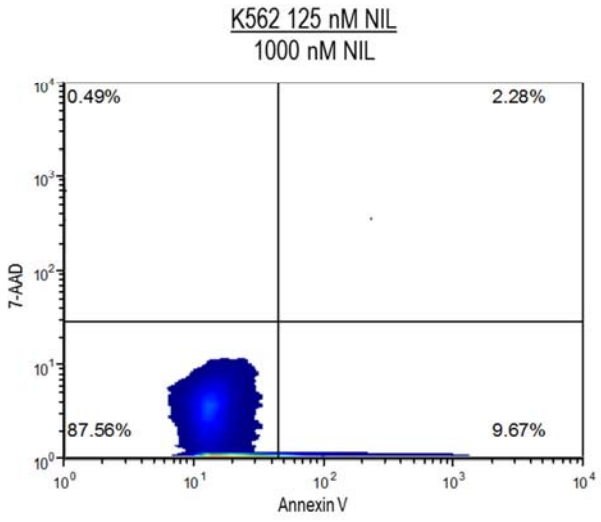
K562 125 nM NIL
1000 nM NIL
0.49%
2.28%
87.56%
9.67%
7-AAD
Annexin V

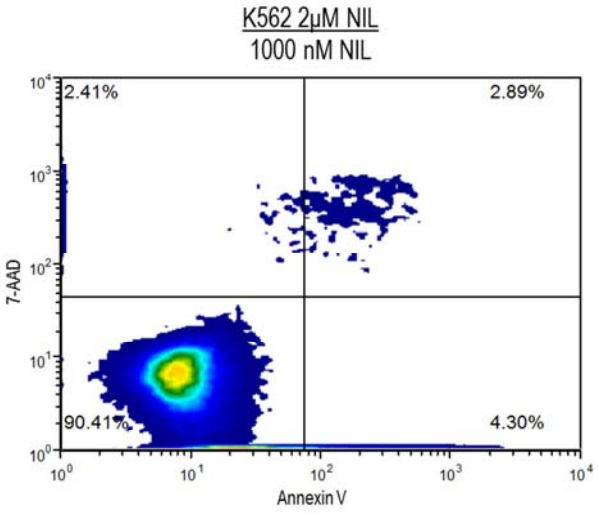
K562 2μM NIL
1000 nM NIL
2.41%
2.89%
90.41%
4.30%
7-AAD
Annexin V

(b)

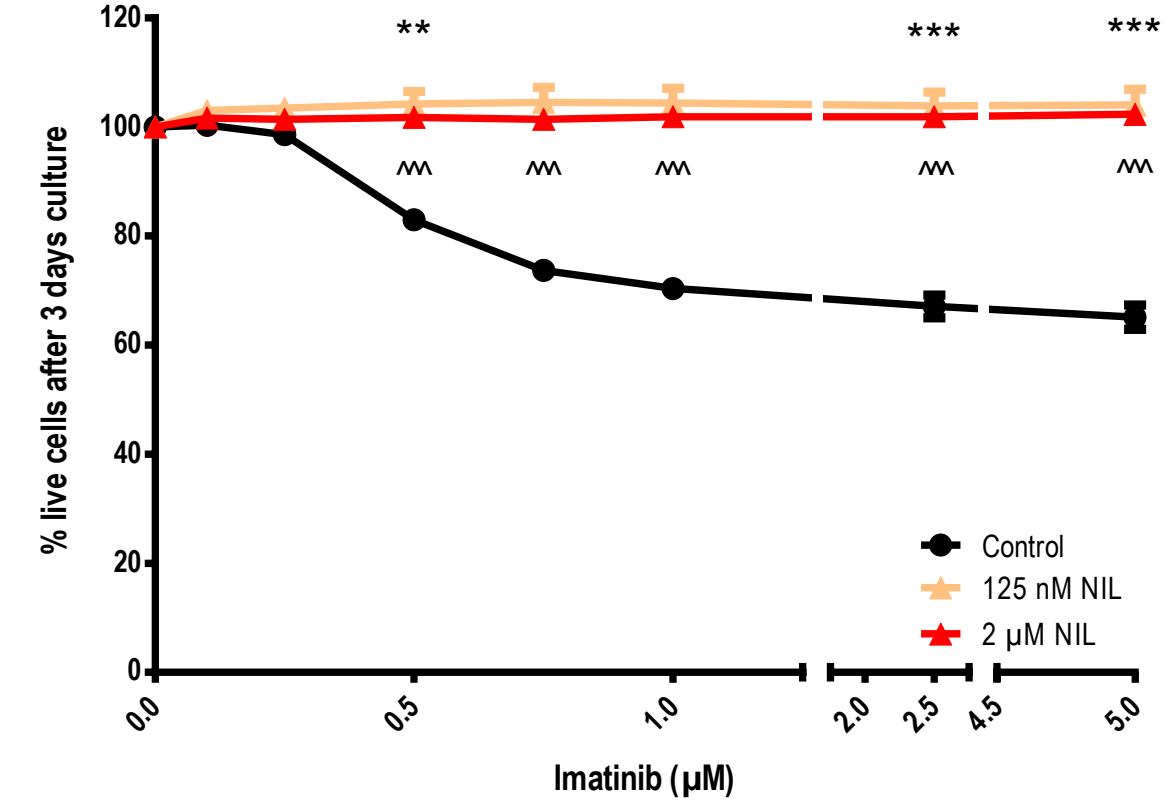
120
100
80
60
40
20
0
% live cells after 3 days culture
**
***
***
Control
125 nM NIL
2 µM NIL
0.0
0.5
1.0
2.0
2.5
4.5
5.0
Imatinib (µM)

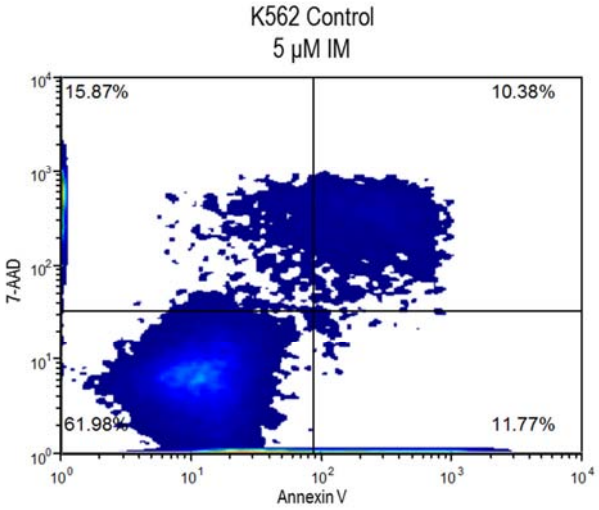
K562 Control
5 µM IM
15.87%
10.38%
61.98%
11.77%
7-AAD
Annexin V

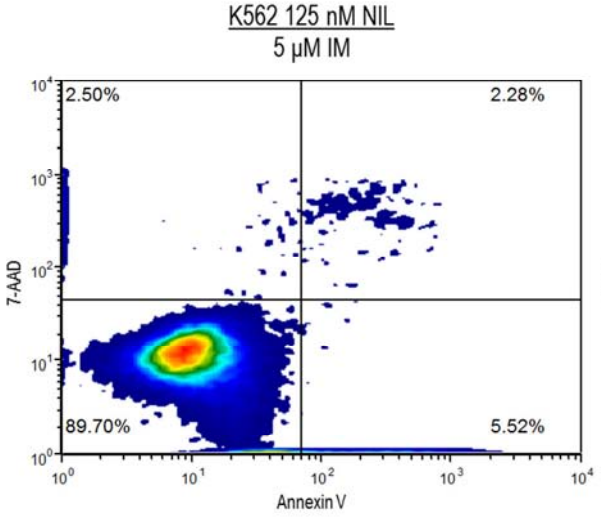
K562 125 nM NIL
5 µM IM
2.50%
2.28%
89.70%
5.52%
7-AAD
Annexin V

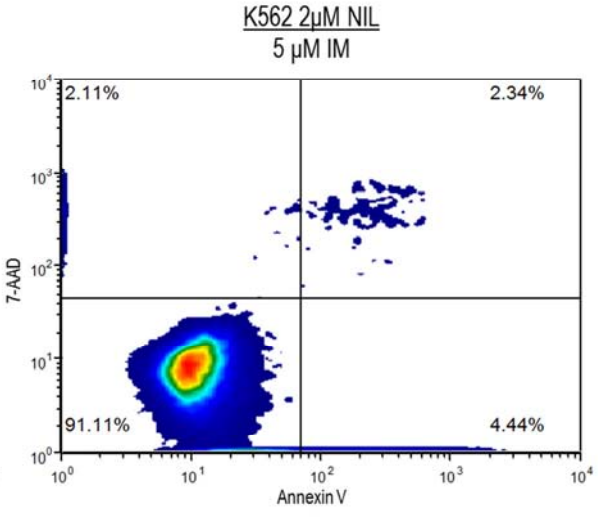
K562 2µM NIL
5 µM IM
2.11%
2.34%
91.11%
4.44%
7-AAD
Annexin V

(c)

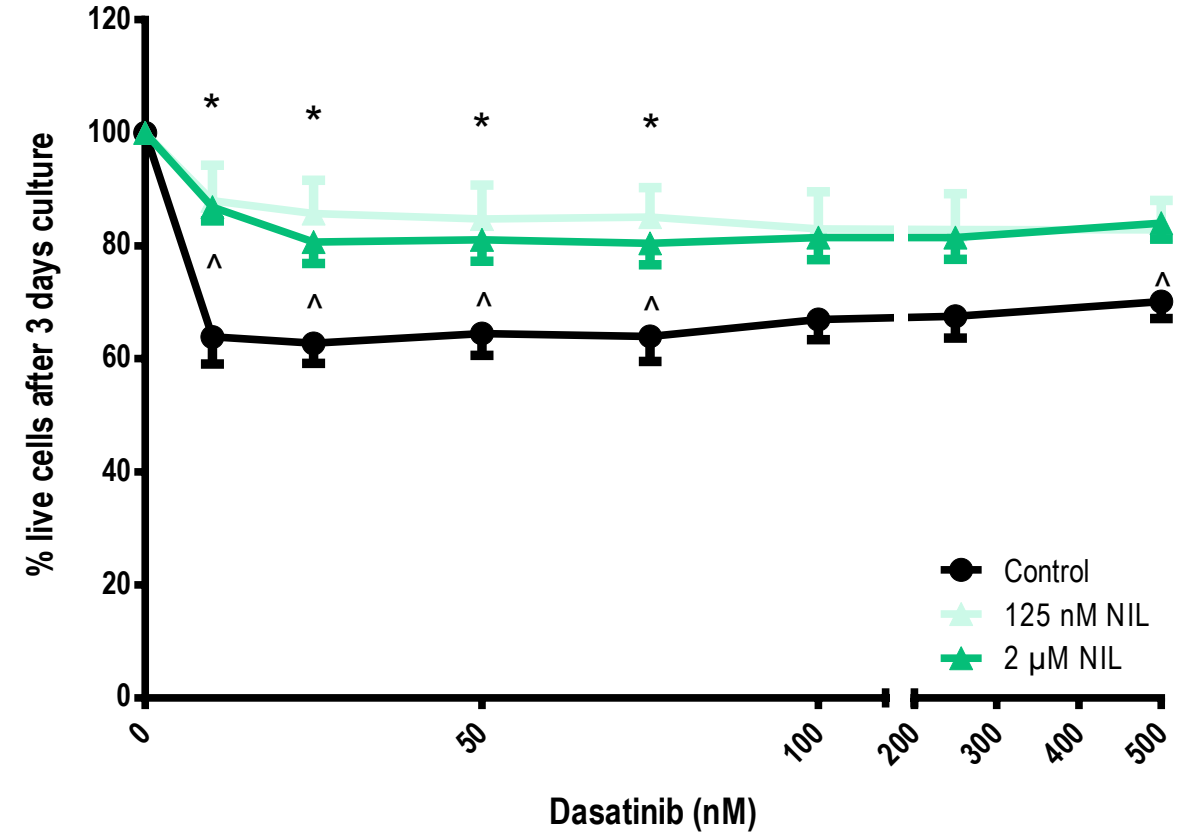
% live cells after 3 days culture
120
100
80
60
40
20
0
*
*
*
*
^
^
^
^
^
0
50
100
200
300
400
500
Dasatinib (nM)
Control
125 nM NIL
2 µM NIL

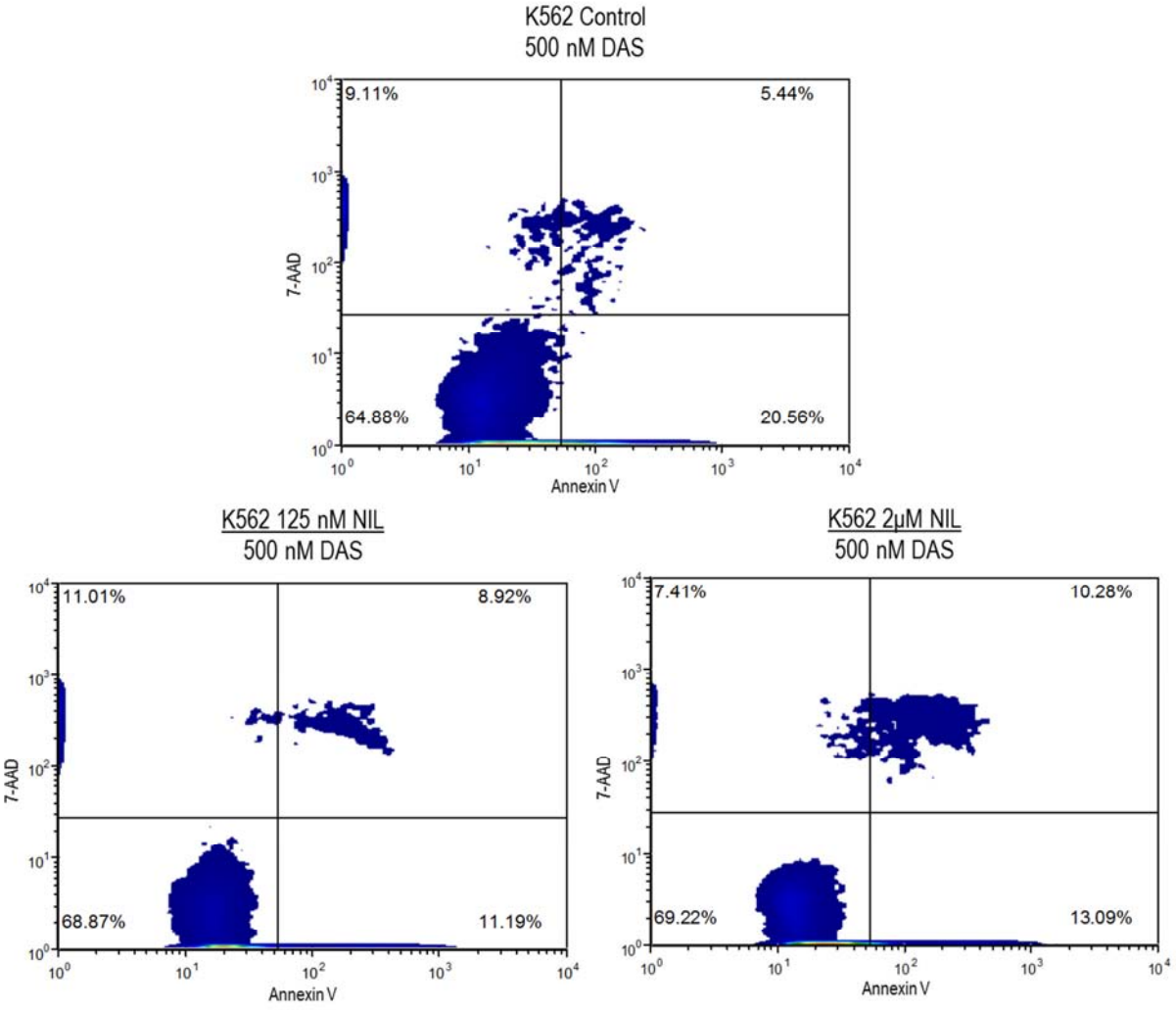
K562 Control
500 nM DAS
9.11%
5.44%
64.88%
20.56%
7-AAD
Annexin V
K562 125 nM NIL
500 nM DAS
11.01%
8.92%
68.87%
11.19%
K562 2µM NIL
500 nM DAS
7.41%
10.28%
69.22%
13.09%

K562 125 nM NIL cells were also assessed for resistance to two other TKIs currently available: imatinib and dasatinib. Again, K562 125 nM NIL cells demonstrated significantly increased IC50 when compared with control cells: $IC50^{IM}$ increased from 3.3 μM to 20.5 μM, p=0.011; $IC50^{DAS}$ increased from 5.6 nM to 11.7 nM, p<0.001 (**Figure 5.9b and c**). These results were confirmed by cytotoxicity assay with cells demonstrating increased survival in the presence of TKI when compared with control cells: 65% vs 100% survival in the presence of 5 μM imatinib, p<0.001; 70% vs 83% survival in the presence of 500 nM dasatinib (**Figure 5.10b and c**).

5.3.2. K562 Cells Cultured in 2 μM Nilotinib Demonstrate Resistance to TKIs *In Vitro*

Culture of K562 cells in nilotinib was continued to a concentration of 2 μM in order to reflect the trough plasma levels observed in patients[170]. Once this concentration was tolerated, the resultant K562 2 μM NIL cells were assessed for maintenance of increased $IC50^{NIL}$ compared with control cells: 199 nM vs 1661 nM, p<0.001 (**Figure 5.11a**). Again, this resistance was confirmed by cytotoxicity assay with K562 2 μM NIL cells demonstrating significantly increased survival compared with control cells when exposed to 1000 nM nilotinib for 72 h: 69% vs 100% survival, p=0.002 (**Figure 5.10a**).

K562 2 μM NIL cells were assessed for resistance to three other TKIs currently available: imatinib, dasatinib and ponatinib. Cells demonstrated significantly increased IC50 when compared with control cells for imatinib and ponatinib: $IC50^{IM}$ increased from 3.3 μM to 21.3 μM, p<0.001; $IC50^{PON}$ increased from 4.6 nM to 12.2 nM, p=0.004 (**Figure 5.11b** and **d**). Interestingly, cells were not as resistant to dasatinib demonstrating only a marginal increase in IC50: K562 control $IC50^{DAS}$=6.3 nM, K562 2 μM NIL $IC50^{DAS}$=7.6 nM, p=0.021 (**Figure 5.11c**). These results were confirmed by cytotoxicity assay: survival increased from 65% to 100% in the presence of 5 μM imatinib, p<0.001; from 70% to 84% survival in the presence of 500 nM dasatinib, p=0.030 (**Figure 5.10b and c**). These data indicate the presence of additional resistance mechanism/s which allow discrimination between imatinib/nilotinib resistance

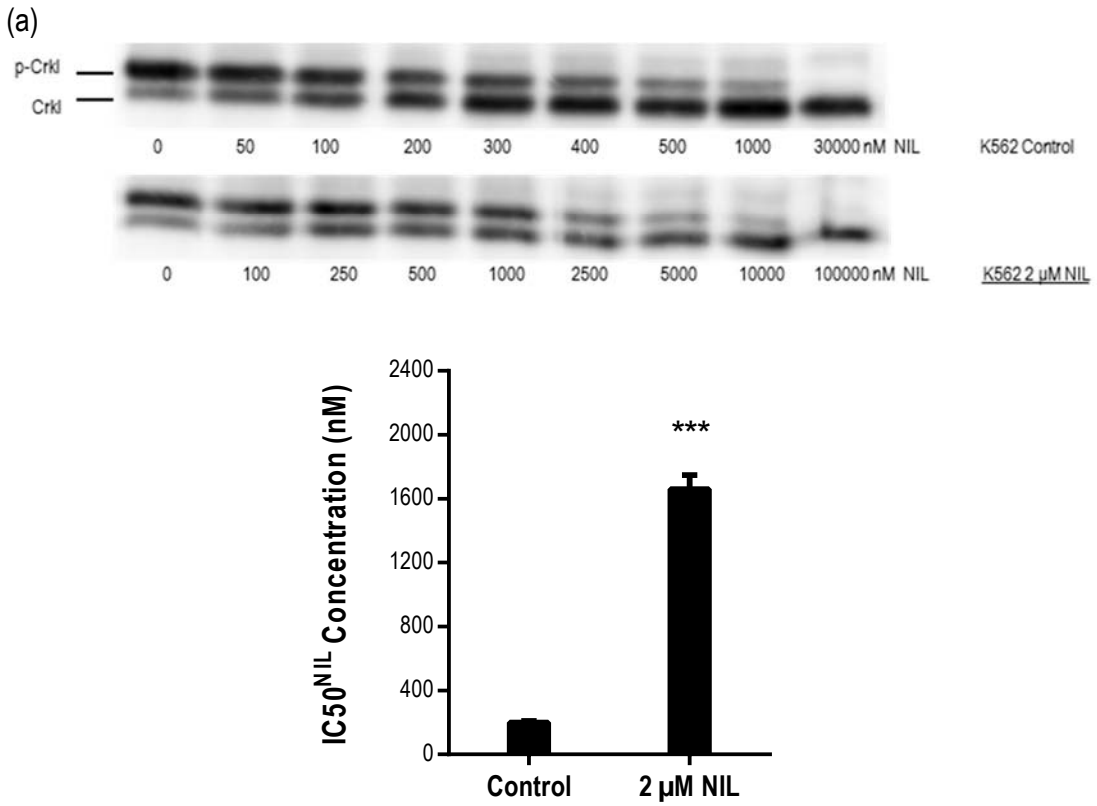

Figure 5.11: <u>K562 2 µM NIL</u> cells are significantly resistant to TKI-mediated kinase inhibition

IC50 was determined via incubating cells for 2 h at 37°C in the presence of increasing concentrations of a) nilotinib, b) imatinib, c) dasatinib and d) ponatinib. Crkl western blot was performed to determine the concentration of TKI required for 50% Bcr-Abl kinase inhibition. Data demonstrate that <u>K562 2 µM NIL</u> cells have a significantly increased $IC50^{NIL, IM, DAS, PON}$ when compared with control cells. The western blot analyses shown are representative of at least three separate experiments with the corresponding densitometry analysis representing the mean. Statistical analyses were performed using Student's *t*-test with statistically significant *p*-values denoted by asterisks (* $p<0.05$; ** $p<0.01$; *** $p<0.001$). Error bars represent SEM. NIL=nilotinib; IM=imatinib; DAS=dasatinib; PON=ponatinib.

(b)

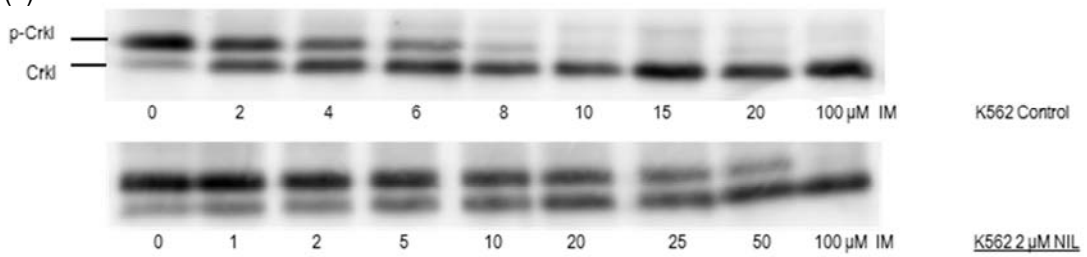
p-Crkl
Crkl
0 2 4 6 8 10 15 20 100 µM IM
K562 Control
0 1 2 5 10 20 25 50 100 µM IM
K562 2 µM NIL

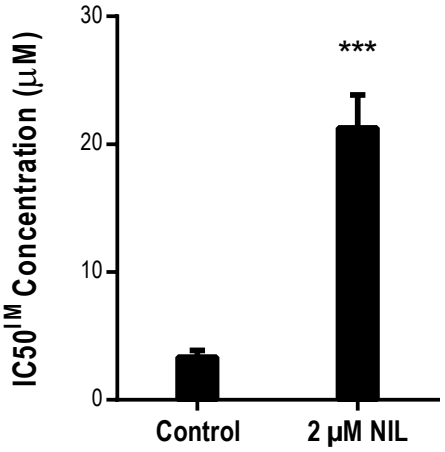
IC50IM Concentration (µM)
30
20
10
0
***
Control
2 µM NIL

(c)

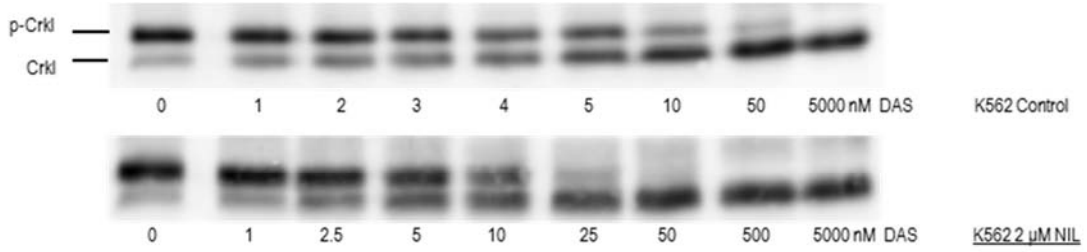
p-Crkl
Crkl
0 1 2 3 4 5 10 50 5000 nM DAS
K562 Control
0 1 2.5 5 10 25 50 500 5000 nM DAS
K562 2 µM NIL

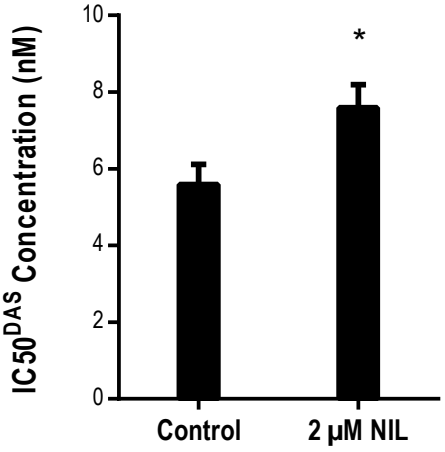
IC50DAS Concentration (nM)
10
8
6
4
2
0
*
Control
2 µM NIL

(d)

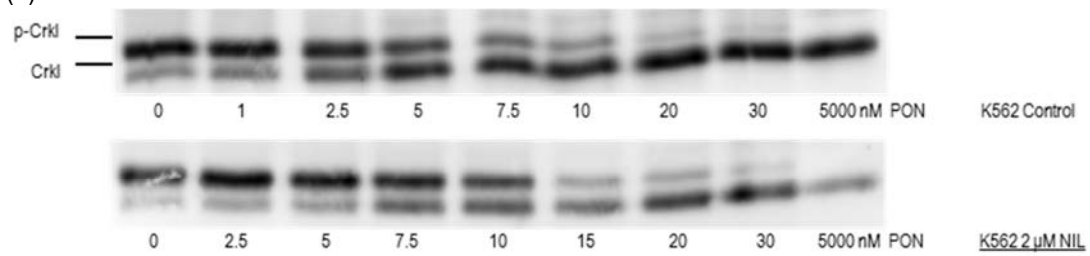
p-Crkl
Crkl
0 1 2.5 5 7.5 10 20 30 5000 nM PON
K562 Control
0 2.5 5 7.5 10 15 20 30 5000 nM PON
K562 2 µM NIL

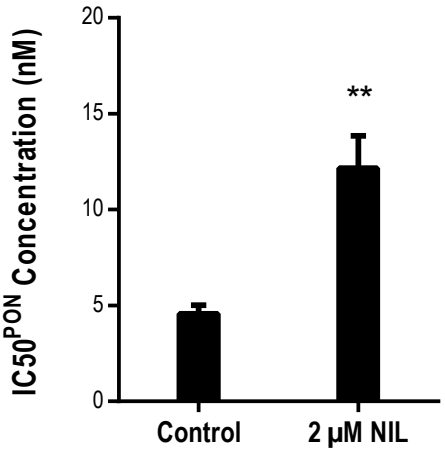
IC50PON Concentration (nM)
20
15
10
5
0
**
Control
2 µM NIL

compared with dasatinib resistance. Possible candidate mechanisms include overexpression of SFKs and/or overexpression of efflux transporters and are discussed later in this current chapter and in further detail in **Chapter 7**.

5.3.3. Onset of Resistance to Nilotinib in K562 Cells Coincides with ABCB1 Overexpression

Once overt resistance had been established, it was necessary to determine the mechanism/s by which this resistance occurred. Firstly, cells were assessed for increased expression of three ABC transporters previously implicated in multidrug resistance in leukaemia[281]: ABCB1, ABCG2 and ABCC1. The onset of resistance at 125 nM nilotinib coincided with a significant increase in ABCB1 mRNA expression with resistant cells demonstrating up to 5-fold greater levels when compared with control cells (p<0.001; **Figure 5.12a**). Surface protein expression was also significantly increased with K562 125 nM NIL cells demonstrating up to 15-fold greater levels when compared with control cells (**Figure 5.12b**). Interestingly, ABCG2 mRNA levels peaked earlier suggesting that ABCB1 and ABCG2 may work in concert (**Figure 5.13a**). However, this increase in mRNA failed to translate to an increase in protein (**Figure 5.13b**) suggesting ABCG2 is unlikely to play a role in the development of nilotinib resistance. There was no significant change in mRNA levels of ABCC1 in any nilotinib resistance intermediates compared with control cells, indicating ABCC1 is also unlikely to be involved in development of nilotinib resistance (p>0.05; **Figure 5.14**).

5.3.4. Sustained Culture of K562 Cells in Nilotinib Results in Decreased ABCB1 Expression and Continued TKI Resistance

Continued culture in concentrations of nilotinib up to 2 μM resulted in decreased levels of ABCB1 mRNA and protein (**Figure 5.12**), however $IC50^{NIL}$, $IC50^{IM}$ and $IC50^{PON}$ remained high (**Figure 5.11**). It was also observed that ABCB1 protein expression decreased as passage number in the same concentration of nilotinib increased: K562 125 nM NIL passage 33=42% ABCB1, compared with passage 69=2.2%

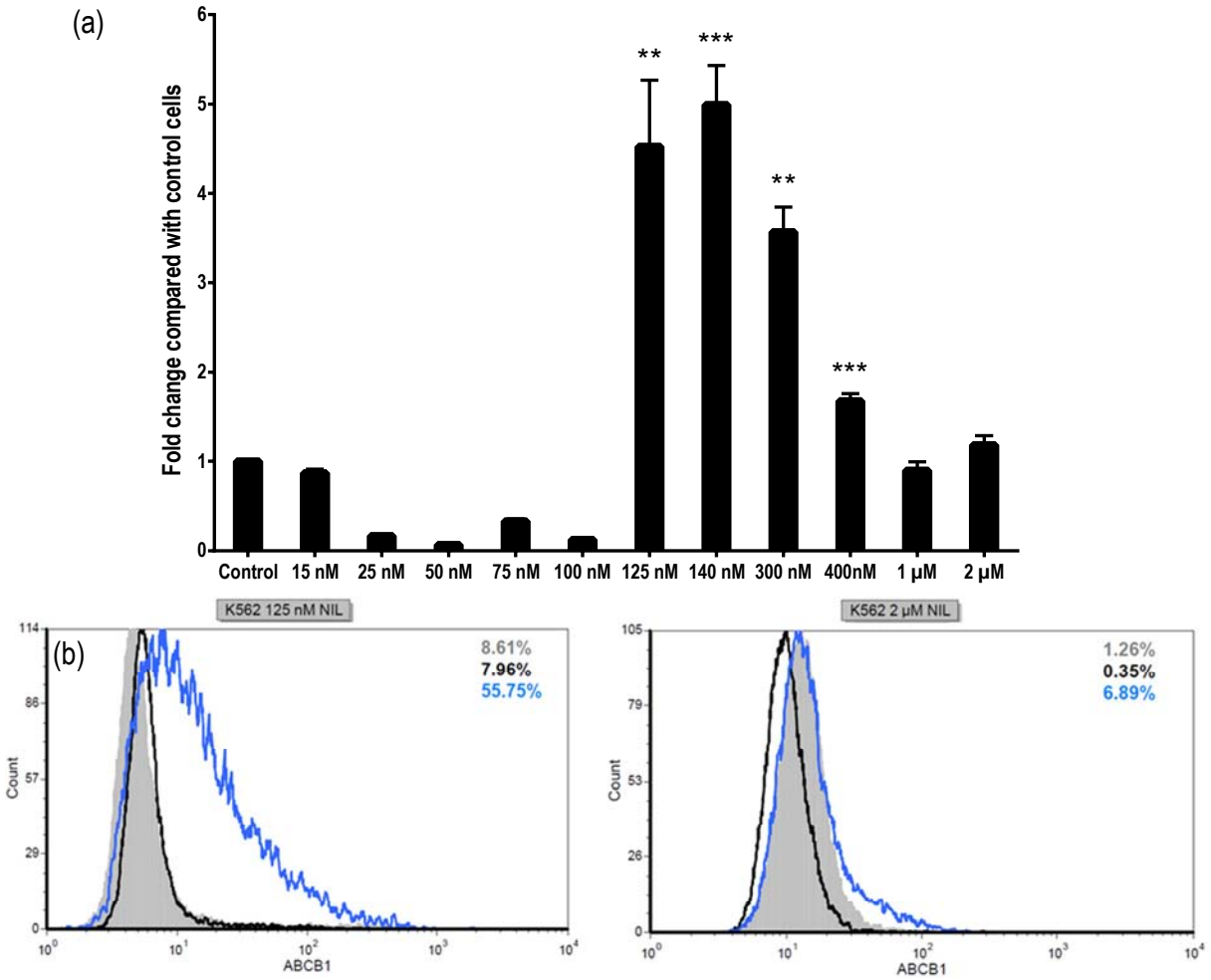

Figure 5.12: Onset of nilotinib resistance in K562 cells coincides with ABCB1 overexpression with levels decreasing upon continued nilotinib exposure

Expression levels of ABCB1 a) mRNA and b) protein were assessed in K562 NIL cells. Data demonstrate overexpression of ABCB1 at the onset of resistance in K562 125 nM NIL cells. This is followed by a steady decline upon continued exposure to nilotinib back to levels comparable with those observed in control cells. mRNA expression represents the mean of six independent experiments performed in triplicate while the histograms shown are representative of typical expression levels. The percentages displayed in the histograms denote cells positive for ABCB1 expression. The bold **BLACK** and **BLUE** lines represent **control** and **resistant** cells stained with ABCB1 antibody while the **GREY** filled histograms represent cells stained with **isotype control** antibody. Statistical analyses were performed on mRNA levels as a percentage of BCR using Student's *t*-test. Statistically significant *p*-values are denoted by asterisks (** $p<0.01$; *** $p<0.001$). Error bars represent SEM.

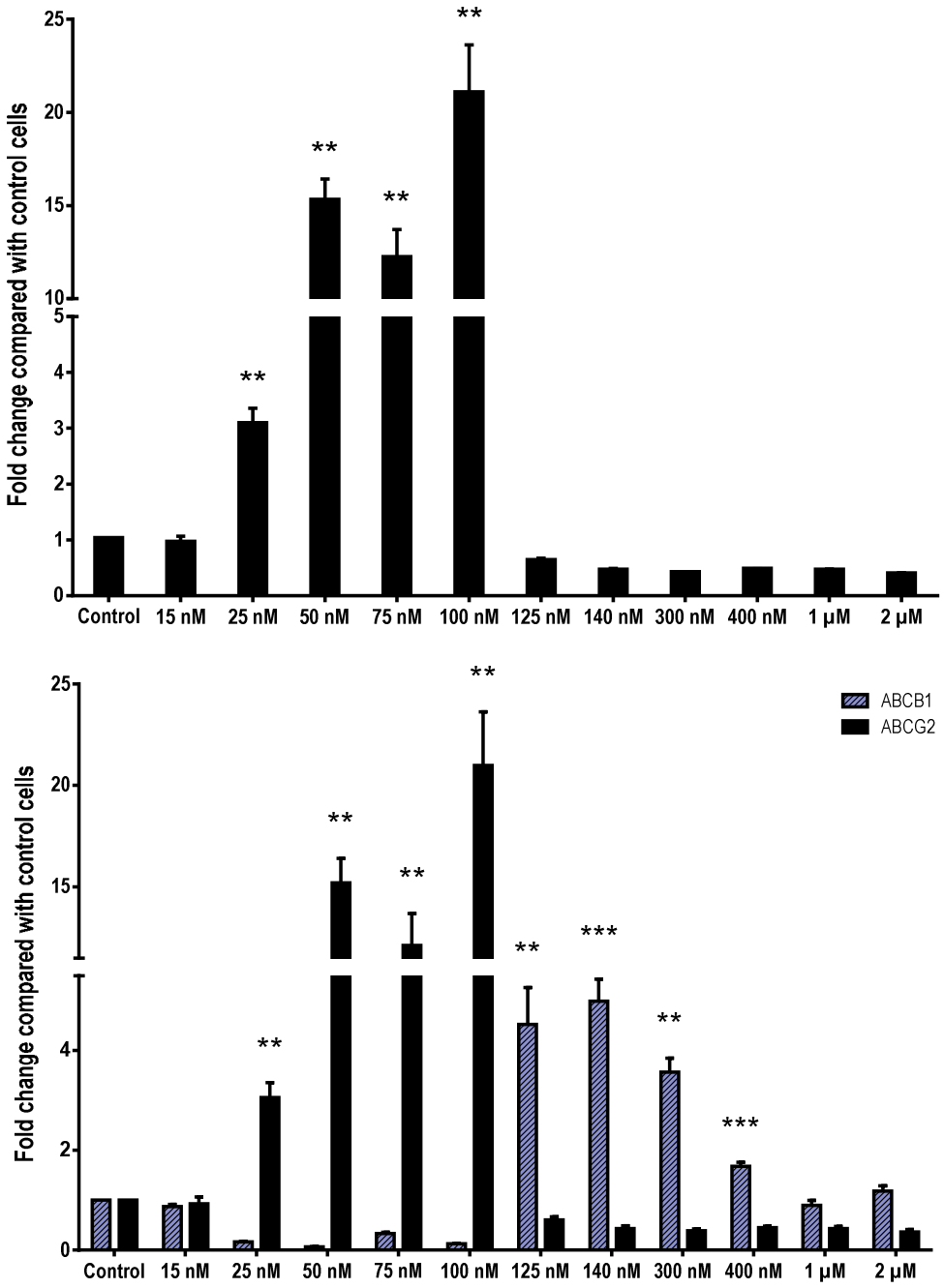

Figure 5.13a: ABCG2 mRNA levels increase upon exposure to low levels of nilotinib

Expression levels of ABCG2 mRNA were assessed in K562 nilotinib resistance intermediates. Data demonstrate increased ABCG2 expression prior to the onset of resistance with levels decreasing as ABCB1 levels increase. mRNA expression represents the mean of six independent experiments performed in triplicate. Statistical analyses were performed on mRNA levels as a percentage of BCR using Student's *t*-test. Statistically significant *p*-values are denoted by asterisks (** $p<0.01$; *** $p<0.001$). Error bars represent SEM.

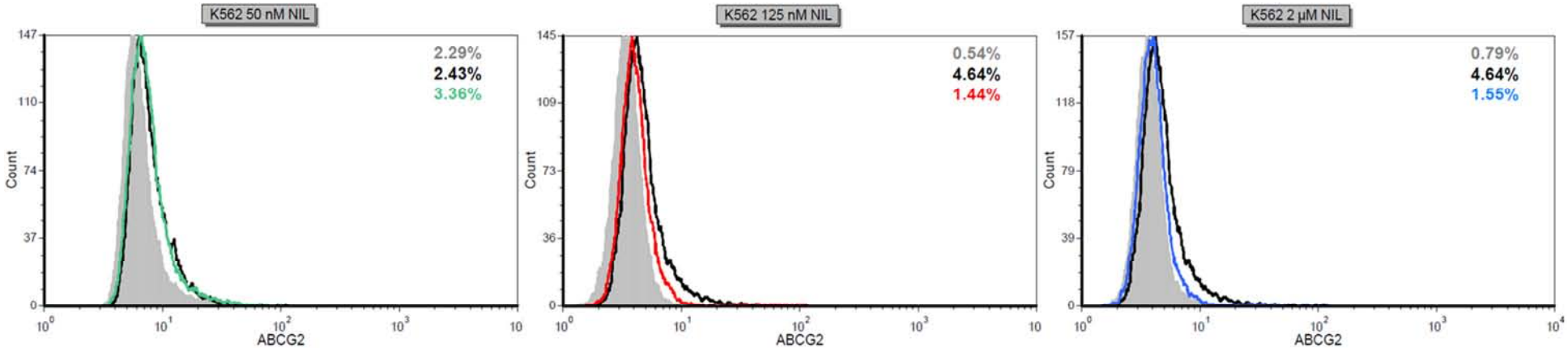

Figure 5.13b: ABCG2 protein levels do not increase upon exposure to nilotinib

Expression levels of ABCG2 protein were assessed in K562 nilotinib resistance intermediates. Data demonstrate no increase in ABCG2 protein expression prior to the onset of resistance (50 nM) nor in cells following the onset of resistance (125 nM and 2 µM) when compared with control cells. The histograms shown are representative of typical expression levels. The percentages displayed in the histograms denote cells positive for ABCG2 expression. The bold **BLACK** lines represent **control** cells while the bold **GREEN**, **RED** and **BLUE** lines represent **50 nM**, **125 nM** and **2 µM** resistant cells respectively, stained with ABCG2 antibody. The **GREY** filled histograms represent cells stained with isotype control antibody.

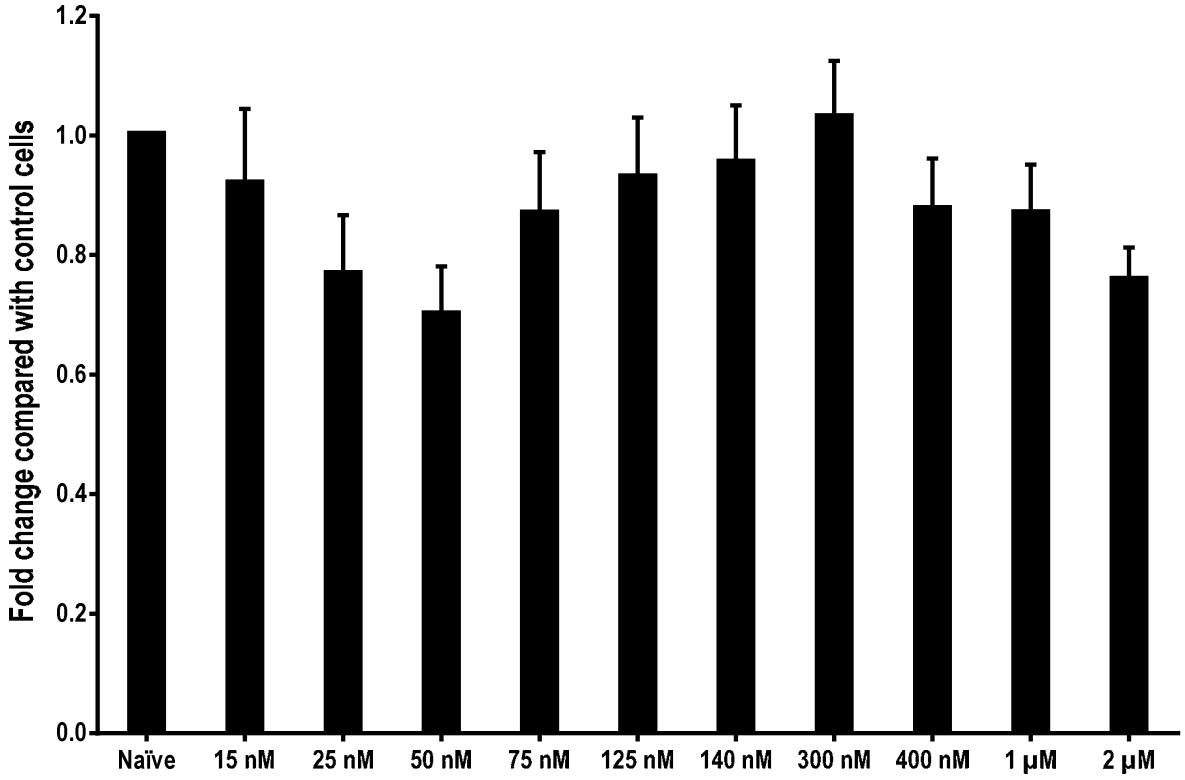

Figure 5.14: ABCC1 levels do not increase during development of nilotinib resistance in K562 cells

Expression levels of ABCC1 mRNA were assessed in K562 nilotinib resistance intermediates. Data demonstrate no increase in ABCC1 expression at any time during development of nilotinib resistance. mRNA expression represents the mean of six independent experiments performed in triplicate. Statistical analyses were performed on mRNA levels as a percentage of BCR using Student's *t*-test. Error bars represent SEM.

ABCB1 (**Table 5.3**). Additionally, ABCB1 expression directly impacted $IC50^{NIL}$: over a period of seven days ABCB1 expression decreased from 85% to 72% to 61% with a corresponding decrease in $IC50^{NIL}$ from 2700 nM to 2120 nM to 1570 nM (**Figure 5.15**). This raised the important question as to whether ABCB1 overexpression was necessary for the initiation of nilotinib resistance or whether it was simply a cellular stress response that would occur in the presence of any xenobiotic. Hence, $IC50^{NIL}$ experiments were performed in the absence and presence of cyclosporin A; an ABCB1 inhibitor[282]. Results demonstrated a decrease in the $IC50^{NIL}$ in the presence of cyclosporin A: 2030 nM to 1530 nM. This decrease was not observed in control cells: 203 nM to 285 nM in the absence and presence of cyclosporin A respectively (**Figure 5.16**). If ABCB1 overexpression was the sole mechanism of resistance, one would expect ABCB1 inhibition to increase the intracellular concentration of nilotinib resulting in an increase in Bcr-Abl kinase inhibition and a subsequent reduction in p-Crkl levels and $IC50^{NIL}$ back to levels observed in control cells. Intriguingly however, inhibition of ABCB1 in resistant cells did not reduce $IC50^{NIL}$ to levels comparable to those seen control cells, thus it was postulated these cells harbour further resistance mechanism/s.

5.3.5. Nilotinib Resistant K562 Cells have Additional Resistance Mechanisms

Because Bcr-Abl overexpression is a common form of TKI resistance observed in patients[109], resistant K562 cells were screened for increased expression of Bcr-Abl mRNA and protein. Results demonstrated this possibility was unlikely since no overexpression of Bcr-Abl mRNA was observed in any of the resistance intermediates (**Figure 5.17a**). Furthermore, there was no increase in Bcr-Abl protein in early or late stage resistance intermediates (**Figure 5.17b**).

The fact that K562 2 µM NIL cells were resistant to nilotinib and imatinib, while maintaining sensitivity to dasatinib, indicated these cells may have developed a mutation such as Y253H, E255K or F359V which are known to confer resistance to both nilotinib and imatinib, but not dasatinib (**Figure 5.1**). Thus all

Table 5.3: ABCB1 protein expression decreases as passage number in the same concentration of nilotinib increases

Passage Number	ABCB1 Expression in K562 125 nM NIL
33	47.0%
52	36.5%
56	25.0%
58	17.2%
64	5.4%
69	2.1%

Passage Number	ABCB1 Expression in K562 2 µM NIL
5	15.4%
13	14.1%
15	9.4%
17	7.1%
21	4.7%

ABCB1 % expression was determined by flow cytometry.

Figure 5.15: ABCB1 expression levels decrease over time with $IC50^{NIL}$ values decreasing proportionally

In order to determine the effect of continued cell culture on ABCB1 expression, the K562 50 nM NIL cell line was freshly thawed and, over a period of seven days, ABCB1 expression and $IC50^{NIL}$ examined. IC50 was determined via incubating cells for 2 h at 37°C in the presence of increasing concentrations of nilotinib. CrkI western blot was performed to determine the concentration of TKI required for 50% Bcr-Abl kinase inhibition. Simultaneously, expression levels of ABCB1 protein were assessed by flow cytometric analysis. Data demonstrate that K562 cells cultured in 50 nM nilotinib for a period of seven days lose expression of ABCB1 exhibiting a corresponding decrease in $IC50^{NIL}$. The western blot analyses shown are representative of one experiment with the corresponding ImageQuant analyses also depicted and the corresponding $IC50^{NIL}$ values shown above. The percentages displayed in the histograms denote cells positive for ABCB1 expression. The bold **BLUE** and **BLACK** lines represent **resistant** and **control** cells respectively, stained with ABCB1 antibody while the **GREY** filled histograms represent cells stained with **isotype control** antibody.

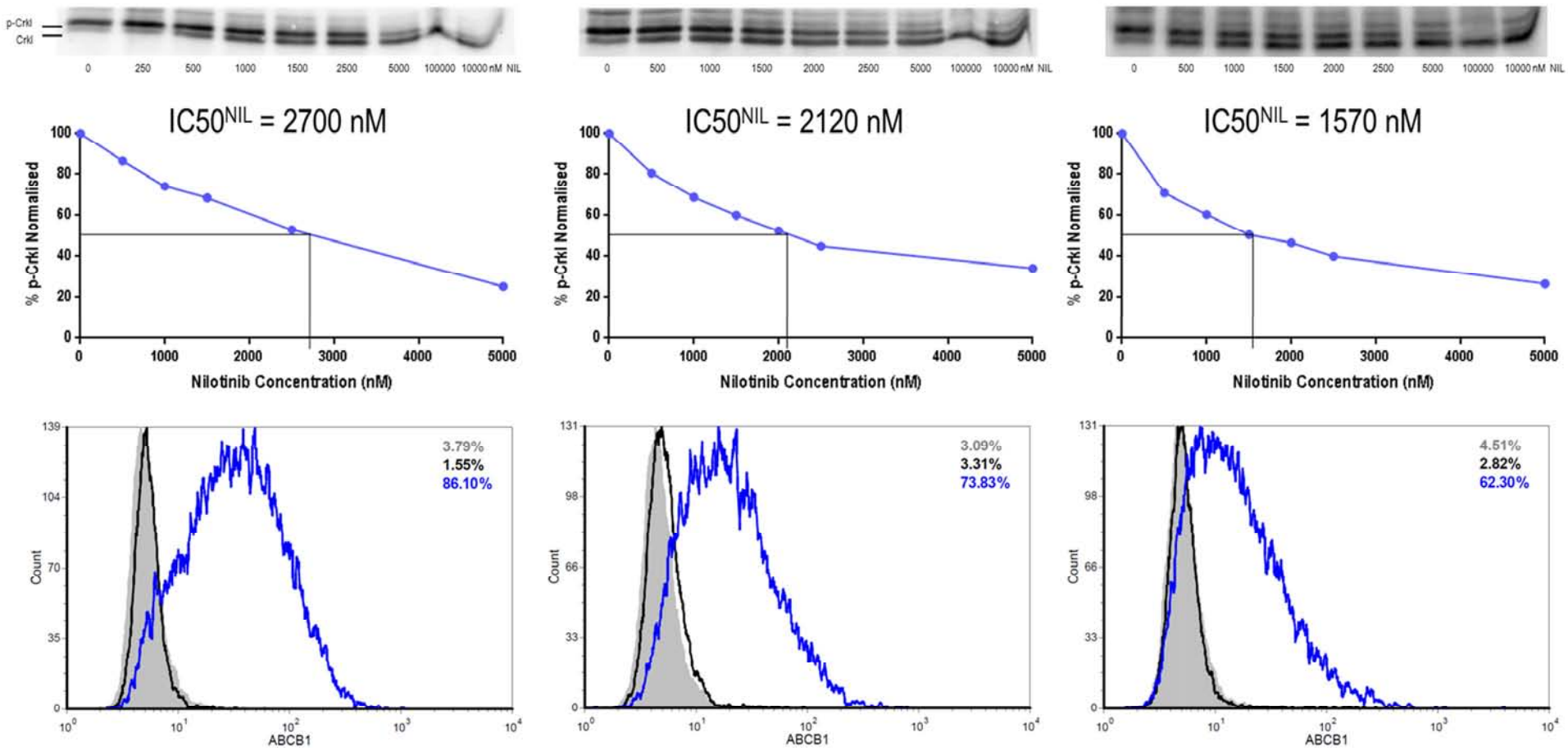
p-Crkl
Crkl
0 250 500 1000 1500 2500 5000 100000 10000 nM NIL
0 500 1000 1500 2000 2500 5000 100000 10000 nM NIL
0 500 1000 1500 2000 2500 5000 100000 10000 nM NIL
IC50NIL = 2700 nM
IC50NIL = 2120 nM
IC50NIL = 1570 nM
% p-Crkl Nomalised
Nilotinib Concentration (nM)
Count
ABCB1
3.79%
1.55%
86.10%
3.09%
3.31%
73.83%
4.51%
2.82%
62.30%

Figure 5.16: ABCB1 inhibition decreases p-Crkl protein levels in resistant K562 2 μM NIL cells

IC50 was determined via incubating cells for 2 h at 37°C in the presence of increasing concentrations of nilotinib. Crkl western blot was performed to determine the concentration of TKI required for 50% Bcr-Abl kinase inhibition. Simultaneously, expression levels of ABCB1 protein were assessed by flow cytometric analysis. Data demonstrate that K562 2 μM NIL cells have a decreased $IC50^{NIL}$ in the presence of ABCB1 inhibition compared with $IC50^{NIL}$ in the absence of ABCB1 inhibition. Cyclosporin A is PSC-833 analogue and was used in lieu of PSC-833 due to its commercially availability. A concentration of 10 μM was demonstrated to effectively inhibit ABCB1-mediated rhodamine-123 efflux from K562-Dox cells (**Appendix 3C**). The western blot analyses shown represent one experiment with the corresponding ImageQuant analyses also depicted. The histograms shown are representative of typical expression levels. The percentages displayed in the histograms denote cells positive for ABCB1 expression. The bold **BLUE** and **BLACK** lines represent **resistant** and **control** cells respectively, stained with ABCB1 antibody while the **GREY** filled histograms represent cells stained with **isotype control** antibody. NIL=nilotinib.

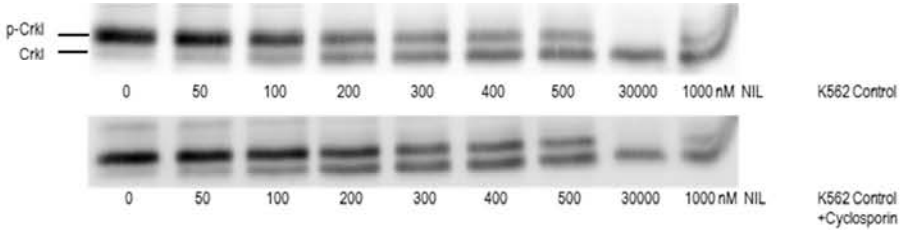
p-Crkl
Crkl
0 50 100 200 300 400 500 30000 1000 nM NIL
K562 Control
0 50 100 200 300 400 500 30000 1000 nM NIL
K562 Control +Cyclosporin

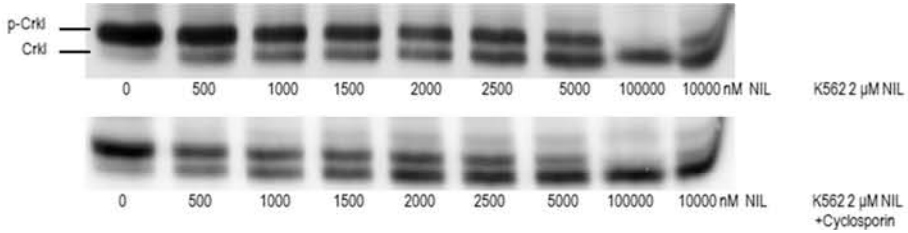
p-Crkl
Crkl
0 500 1000 1500 2000 2500 5000 100000 10000 nM NIL
K562 2 µM NIL
0 500 1000 1500 2000 2500 5000 100000 10000 nM NIL
K562 2 µM NIL +Cyclosporin

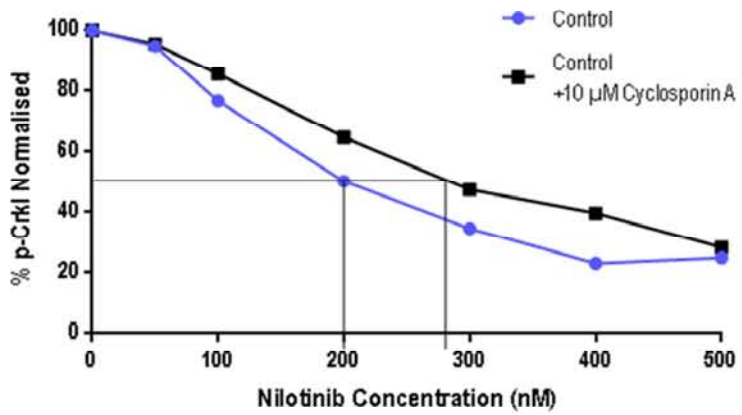
% p-Crkl Normalised
Nilotinib Concentration (nM)
Control
Control +10 µM Cyclosporin A

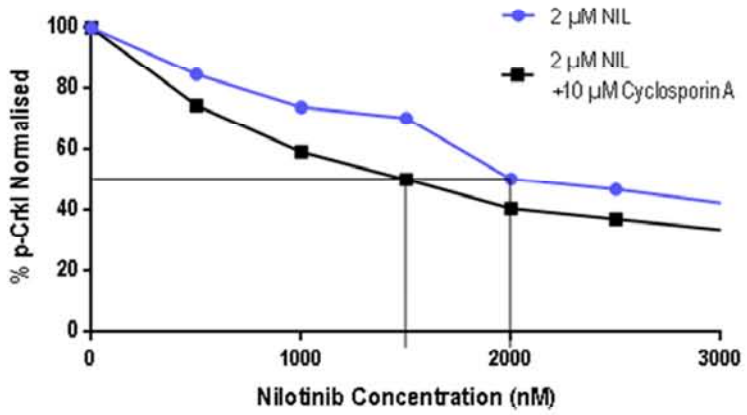
% p-Crkl Normalised
Nilotinib Concentration (nM)
2 µM NIL
2 µM NIL +10 µM Cyclosporin A

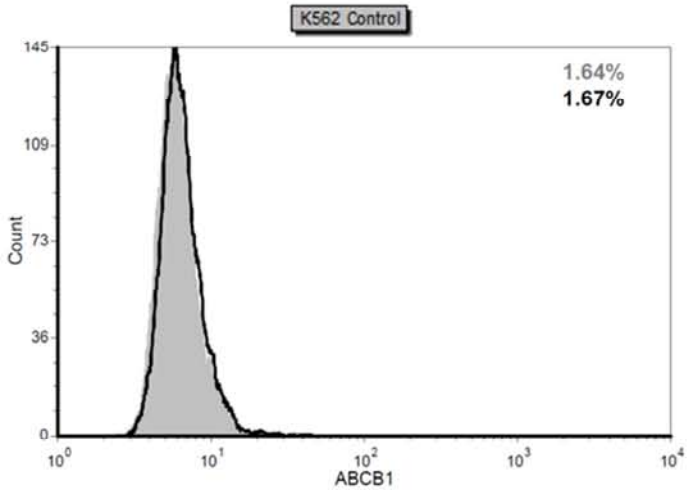
K562 Control
1.64%
1.67%
Count
ABCB1

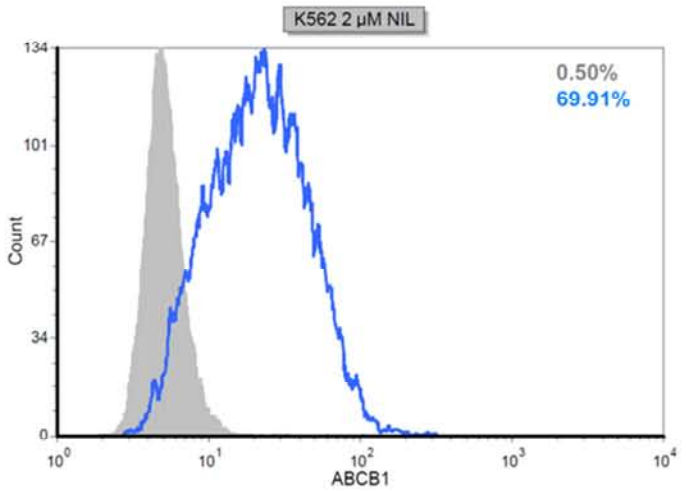
K562 2 µM NIL
0.50%
69.91%
Count
ABCB1

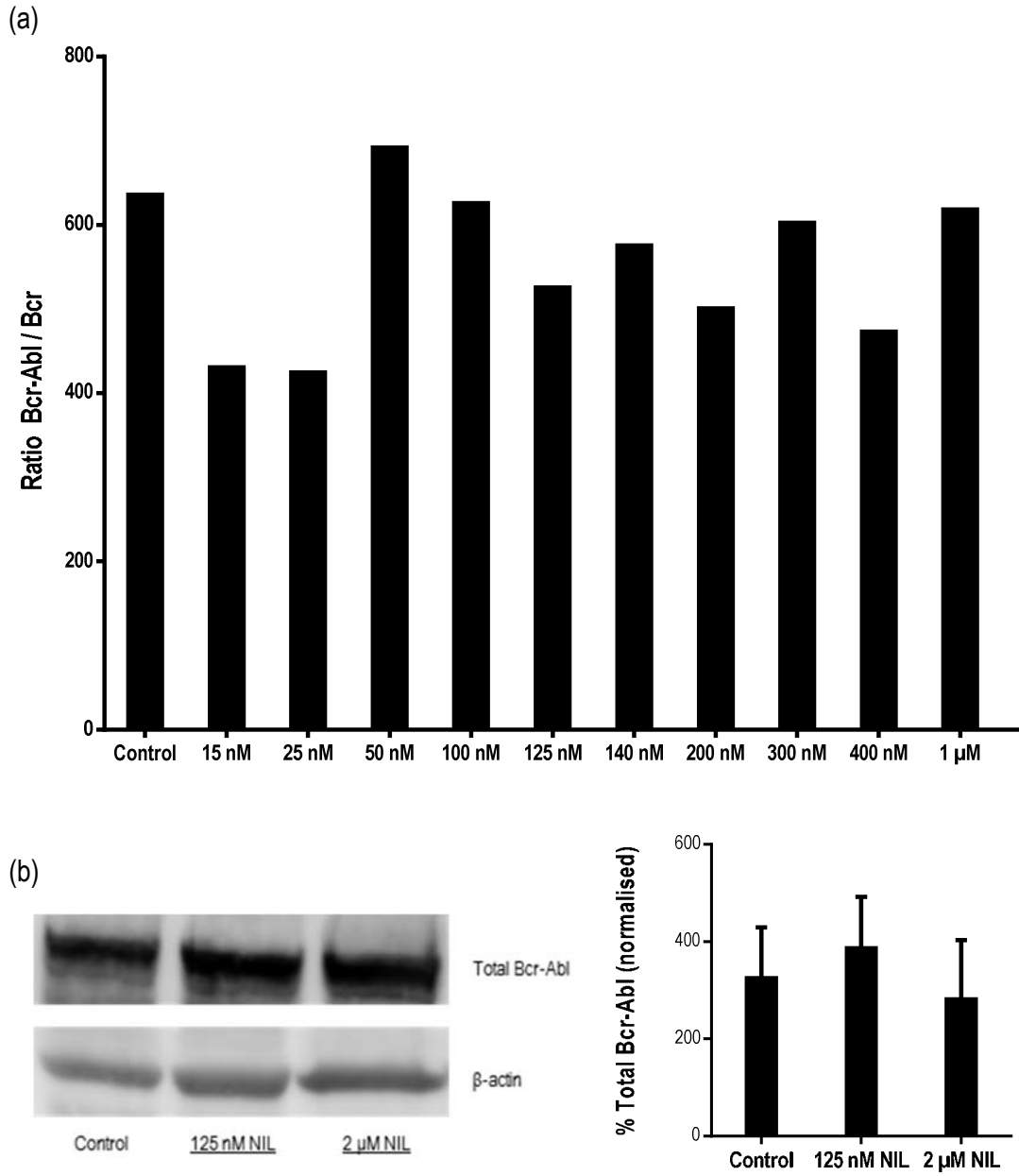

Figure 5.17: No Bcr-Abl overexpression was observed during development of nilotinib resistance in K562 cells

Expression levels of Bcr-Abl a) mRNA and b) protein were assessed in K562 nilotinib resistance intermediates. Data demonstrate no increase in Bcr-Abl mRNA or protein expression during development of nilotinib resistance. The error bars in b) represent SEM. No error bars are plotted in a) as the mRNA expression shown is the mean of two independent experiments. Western blot analyses shown are representative of at least three separate experiments with the quantitation representing the mean. Bcr-Abl protein levels were normalised to β-actin control. NIL=nilotinib.

K562 resistance intermediates were screened for Bcr-Abl kinase domain mutations. However, results indicated that no mutations were present (**Appendix 3D**).

5.3.6. Nilotinib Resistant K562 Cells have Increased Expression of Src Family Kinases

In addition to inhibiting tyrosine kinases such as Bcr-Abl, dasatinib also has activity against Src Family Kinases (SFKs) including Fyn, Lyn and Src[80,91]. Hence, in the absence of a kinase domain mutation, SFK overexpression offers a potential explanation for the differential sensitivity to TKIs observed in K562 2 µM NIL cells. Thus, expression levels of SFKs Lyn and Fyn, as well as Syk and Axl, two cellular kinases demonstrated to interact with SFKs[126,166,280] and previously linked to TKI resistance[119,125-127,168], were determined. Results demonstrated that upon development of nilotinib resistance in K562 125 nM NIL cells, mRNA expression of Lyn, Fyn, Axl and Syk increased and remained high for the remainder of nilotinib culture. The most striking increase was observed for Lyn expression with resistant cells exhibiting 15–18 fold greater levels when compared with control cells (p<0.05). Resistant cells also demonstrated significantly increased levels of Axl (7–10 fold increase, p<0.01), Fyn (up to 4 fold increase, p<0.001) and Syk (~3.5 fold increase, p<0.05; **Figure 5.18**).

While total protein levels for Lyn and Axl did not increase, the level of phosphorylation of both of these proteins increased in resistant cells (**Figure 5.19a and b**). Activation of Lyn increased significantly and there was also a trend for increased phosphorylation of Axl, however, this failed to reach statistical significance. Autophosphorylation of Lyn at tyrosine 396 (Y396) results in catalytic activation of the kinase. Resistant K562 cells demonstrated a significant increase in phosphorylation of this residue corresponding with onset of resistance at 125 nM nilotinib and Lyn mRNA overexpression (p=0.008). Phosphorylation of Axl at Y779 is associated with activation of PI3-K/Akt signalling. Resistant K562 cells demonstrated a possible increase in phosphorylation of Axl Y779 indicating a potential role for this signalling pathway in the reduced apoptosis and increased cell proliferation observed.

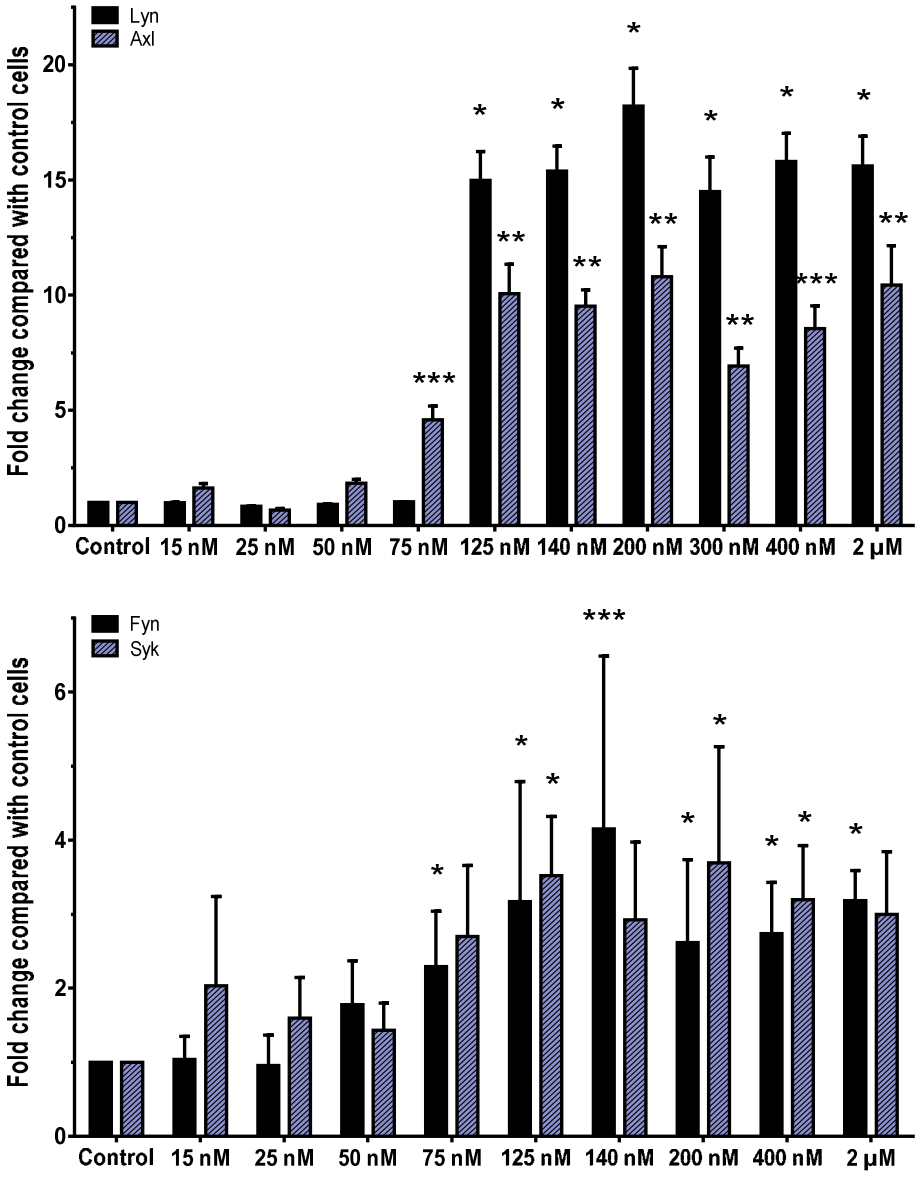

Figure 5.18: Nilotinib resistant K562 cells exhibit increased mRNA expression of Lyn, Axl, Fyn and Syk kinases

Expression levels of Lyn, Axl, Fyn and Syk mRNA were assessed in K562 nilotinib resistance intermediates. Data demonstrate a significant increase in Lyn, Axl and Fyn expression coinciding with the onset of resistance at 125 nM nilotinib. Data also demonstrate a marked increase in Syk mRNA levels reaching significance at 125 nM, 200 nM and 400 nM nilotinib. mRNA expression represents the mean of at least four independent experiments performed in triplicate. Statistical analyses were performed on mRNA levels as a percentage of GusB using Student's *t*-test. Statistically significant *p*-values are denoted by asterisks (* $p<0.05$; ** $p<0.01$; *** $p<0.001$). Error bars represent SEM.

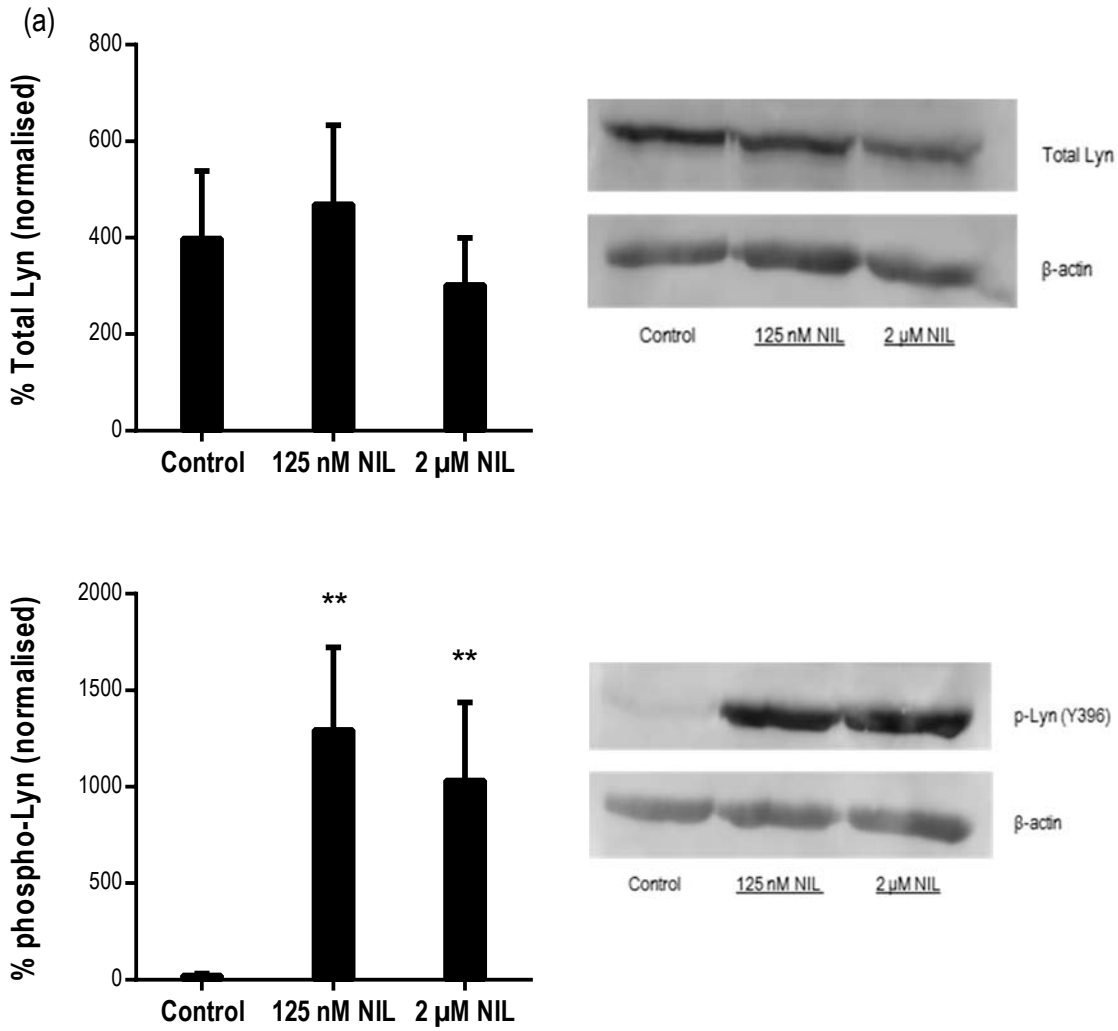

Figure 5.19: Nilotinib resistant K562 cells exhibit increased phosphorylation of Lyn and Axl proteins

Protein expression levels of a) Lyn and b) Axl and c) Syk were assessed in K562 control and resistant cells. Data demonstrate that there is no increased expression of Lyn or Axl protein; however, the level of p-Lyn (Y396) and p-Axl (Y779) increased significantly indicating high levels of activated kinases. Conversely, levels of Syk but not p-Syk (Y525/526) are elevated in resistant cells. Western blot analyses shown are representative of at least three separate experiments with the corresponding quantitation representing the mean. Protein levels were normalised to β-actin control. Statistical analyses were performed using Student's *t*-test with statistically significant *p*-values denoted by asterisks (** $p<0.01$). Error bars represent SEM. Ramos cells stimulated with goat anti-human IgM provide the positive control for Syk protein.

(b)

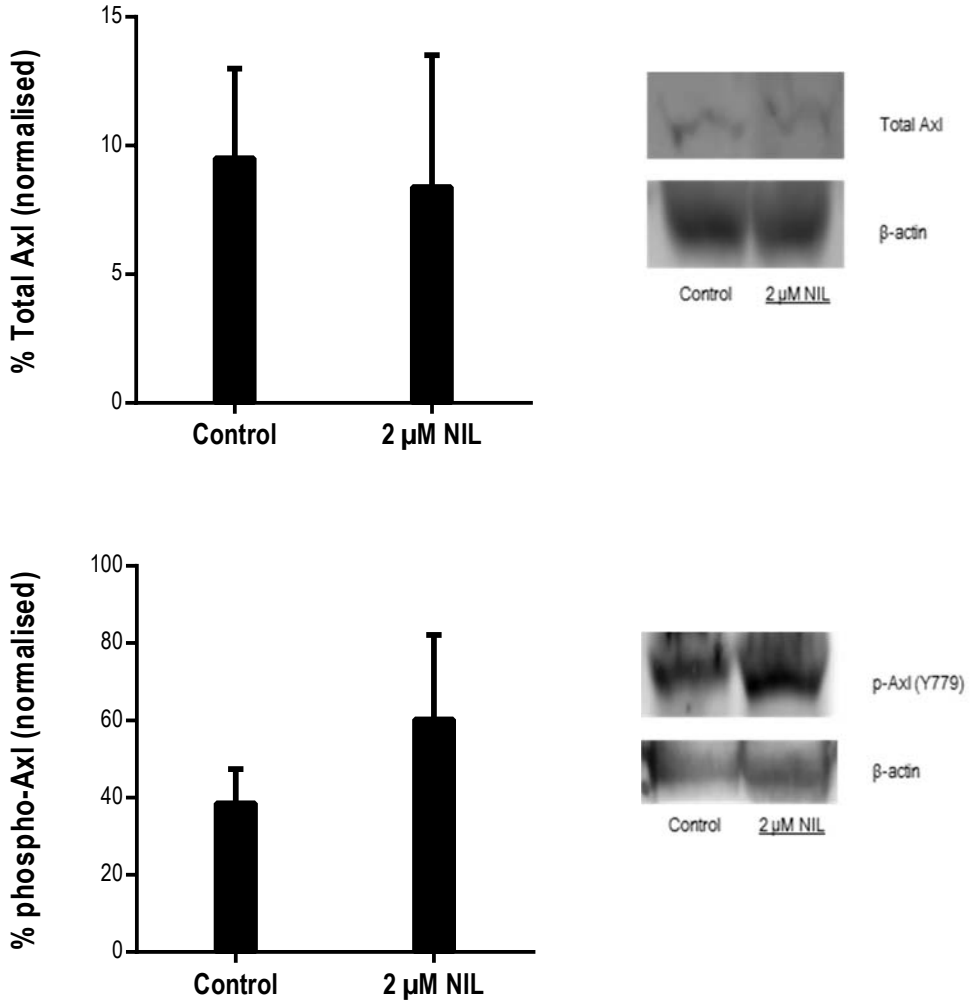
% Total Axl (normalised)
15
10
5
0
Control
2 µM NIL
Total Axl
β-actin
Control
2 µM NIL
% phospho-Axl (normalised)
100
80
60
40
20
0
Control
2 µM NIL
p-Axl (Y779)
β-actin
Control
2 µM NIL

(c)

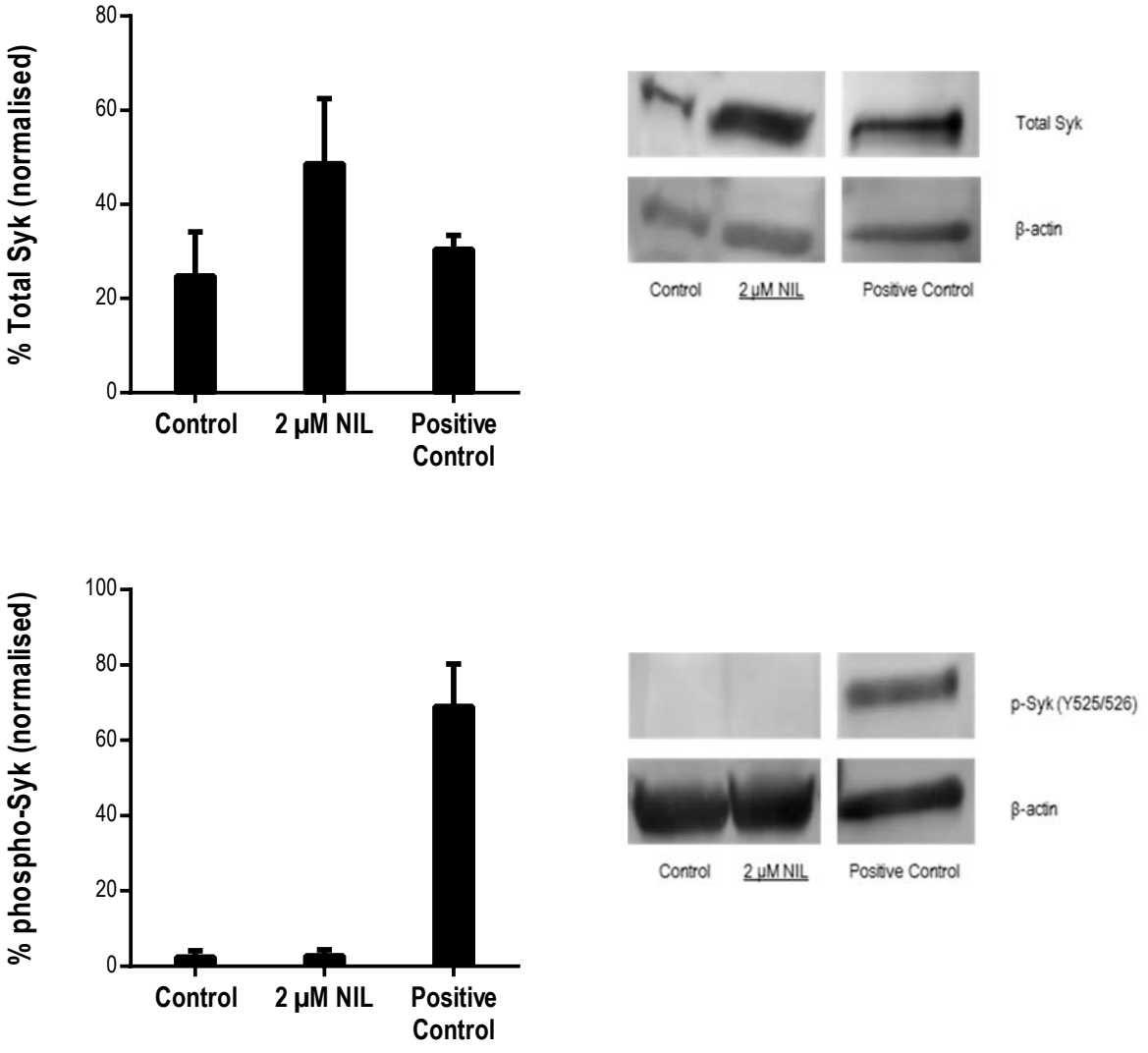
% Total Syk (normalised)
80
60
40
20
0
Control
2 µM NIL
Positive Control
Total Syk
β-actin
Control
2 µM NIL
Positive Control
% phospho-Syk (normalised)
100
80
60
40
20
0
Control
2 µM NIL
Positive Control
p-Syk (Y525/526)
β-actin
Control
2 µM NIL
Positive Control

Conversely, there appears to be an increase in levels of total Syk protein, although this failed to reach statistical significance; however, there was no detectable expression of p-Syk (Y525/526) (**Figure 5.19c**). Syk has previously been implicated in the regulation of Axl phosphorylation[126], hence the increased levels of Syk observed here may explain the increased phosphorylation of Axl.

c-Cbl has been hypothesised as the master regulator of the Lyn-Axl-Syk ternary complex[126], targeting the proteins for ubiquitination and degradation[123]. Hence, levels of c-Cbl mRNA were assessed in K562 nilotinib resistance intermediates. Results demonstrated a modest, yet significant decrease in c-Cbl which may be responsible for the increased levels of Syk observed in resistant cells; although this requires further investigation (**Figure 5.20**).

Thus, during development of nilotinib resistance in K562 cells, ABCB1 overexpression precedes increased activation of cellular kinases such as Lyn and Axl. This renders cells resistant to both nilotinib and imatinib, however, a degree of sensitivity to dasatinib is retained.

5.4. Discussion

The introduction of imatinib revolutionised the treatment of CML, however, 30–40% of patients develop resistance to imatinib therapy with Bcr-Abl kinase domain (KD) mutations the most common cause of resistance[283]. The second generation TKIs, nilotinib and dasatinib, have activity against many imatinib resistant mutations although a group of patients who develop resistance remains. As we move into the era of customised treatment regimes, it becomes important to predict which patients are likely to respond to a given TKI such that treatment plans are tailored to the individual. Thus, *in vitro* cell line models are key in determining, not only common modes of TKI resistance, but also kinetics of resistance development and interplay of resistance mechanisms. In this study, a K562 cell line model resistant to 2 μM nilotinib was generated and the resistance emergence extensively examined.

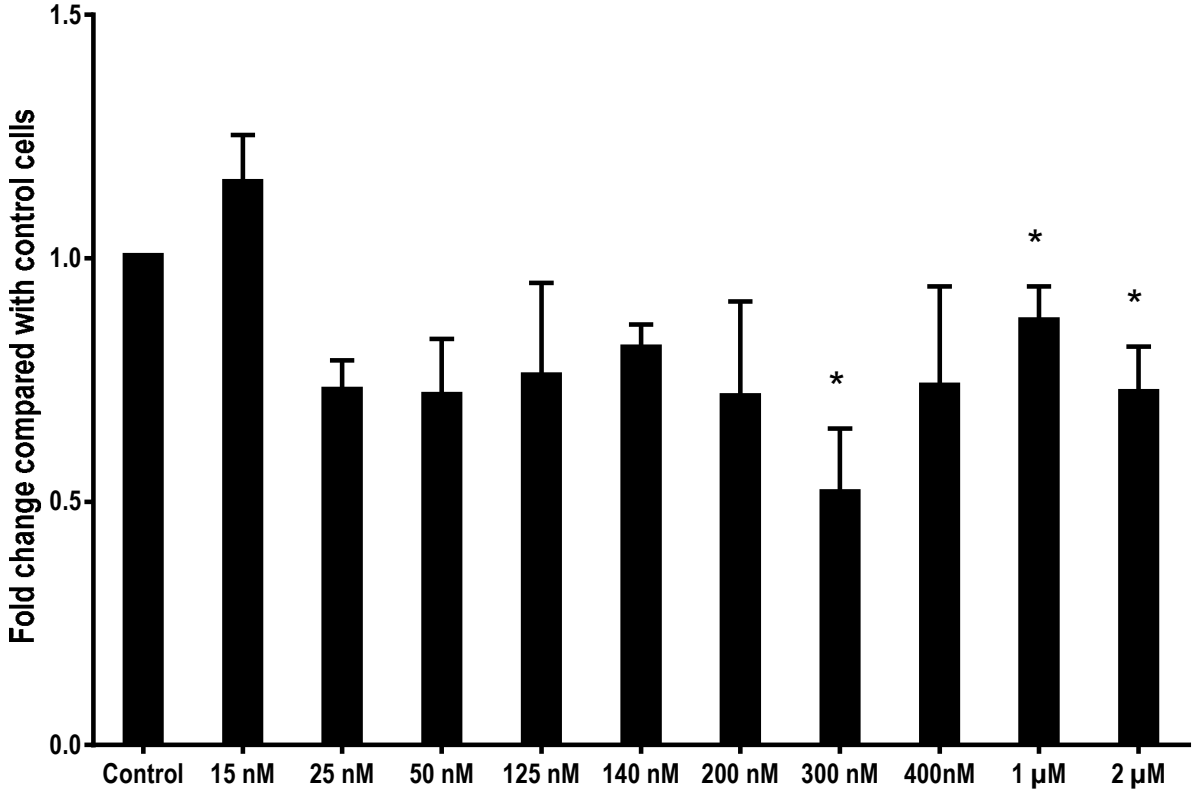

Figure 5.20: c-Cbl levels decrease during development of nilotinib resistance in K562 cells

Expression levels of c-Cbl mRNA were assessed in K562 nilotinib resistance intermediates. Data demonstrate a decrease in c-Cbl expression during development of nilotinib resistance that reaches significance at 300nM, 1 µM and 2 µM. mRNA expression represents the mean of six independent experiments performed in triplicate. Statistical analyses were performed on mRNA levels as a percentage of GusB using Student's *t*-test. Statistically significant *p*-values are denoted by asterisks (* $p<0.05$). Error bars represent SEM.

5.4.1. ABCB1 Overexpression is the Initiator of Resistance to Nilotinib *In Vitro*

ABCB1 overexpression was the mechanism utilised to initiate resistance in K562 cells. Notably, this is the first report of ABCB1 overexpression, at both the mRNA and protein levels, in the K562 cell line in response to exposure to nilotinib. Importantly, $IC50^{NIL}$ was demonstrated to directly correlate with ABCB1 expression confirming the notion that nilotinib is an ABCB1 substrate thus supporting results detailed in **Chapter 4**. Continued culture in increasing concentrations of nilotinib resulted in a loss of ABCB1 expression back to control levels, prior to additional resistance mechanisms predominating.

Intriguingly, ABCG2 mRNA overexpression was also observed in early K562 resistance intermediates. One potential explanation for this increase is the level of redundancy that exists between closely related transporters, such as those from the ABC superfamily. Indeed, it has previously been noted in knockout studies that the reduction of one transporter modifies the expression of another, closely related, efflux pump: ABCB1 knockout mice have up-regulated levels of ABCG2[284]. Additionally, a similar phenomenon has been observed in our laboratory with Oct-1 specific siRNA: levels of Oct-2, Oct-3 and Oct-6 mRNA increased significantly in response to Oct-1 knockdown (Jane Engler, unpublished results). Thus, it is possible that the presence of nilotinib directly impacts levels of ABCB1 mRNA which in turn impact ABCG2 mRNA levels, independently of nilotinib. Data described in **Figure 5.13a** is in keeping with this theory: ABCB1 expression initially decreased when compared with control levels and this corresponded with an increase in ABCG2 expression. However, upon ABCB1 overexpression, ABCG2 expression decreased. Importantly, the increase in ABCG2 mRNA failed to translate to overexpression of ABCG2 protein; hence it is unlikely that ABCG2 plays a role in development of nilotinib resistance. Similarly, levels of ABCC1 mRNA also did not increase significantly during development of nilotinib resistance also making it highly unlikely this transporter plays a role in nilotinib resistance.

5.4.2. ABCB1 Overexpression Precedes Bcr-Abl Dependent Mechanisms of Resistance in K562 Cells

Following ABCB1 overexpression in nilotinib resistant K562 cells, additional mechanisms of resistance predominated. $IC50^{NIL}$ and $IC50^{IM}$ remained significantly higher in K562 2 µM NIL resistant cells compared with control cells; however, a degree of sensitivity to dasatinib was maintained. The fact that $IC50^{NIL}$ and $IC50^{IM}$ values remained elevated suggested the TKIs were no longer effectively inhibiting Bcr-Abl which is indicative of a Bcr-Abl *dependent* mechanism of resistance. In addition to inhibiting Bcr-Abl, dasatinib also has activity against members of the Src family of tyrosine kinases (SFKs)[80,91] while nilotinib and imatinib do not. Bcr-Abl and SFKs have been demonstrated to phosphorylate each other favouring the active conformation of Bcr-Abl, to which nilotinib and imatinib are unable to bind[123,160]. Thus, cells which exhibit resistance to nilotinib and imatinib, but retain sensitivity to dasatinib, are likely to harbour SFK-related resistance mechanisms. Indeed, K562 2 µM NIL cells demonstrated mRNA overexpression of the SFKs Lyn and Fyn. These cells also demonstrated mRNA overexpression of two other cellular kinases reportedly involved in development of nilotinib resistance: Axl[119,126,127] and Syk[126]. Although increased expression of Lyn and Axl proteins were not observed, there was increased tyrosine phosphorylation of Lyn relating to increased activity of the kinase. There was also a trend for increased phosphorylation of Axl, although this failed to reach statistical significance. Thus, in order to confirm a role for Axl in the development of nilotinib resistance in K562 cells, further investigations are required. Additionally, resistant cells had increased levels of Syk protein even though phosphorylation of this protein was not observed. Determination of Fyn protein levels was attempted; however, failure to optimise the assay necessitates additional experimentation in order to confirm a functional role for Fyn in the development of resistance in K562 cells.

The current study investigated the emergence of resistance in K562 cells upon exposure to nilotinib (**Table 5.4**). Based on the results described, one possible scenario by which K562 cells develop

Table 5.4: Summary of resistance mechanisms in K562 cells

	K562 125 nM NIL	K562 2 µM NIL
Resistance by cytotoxicity to all TKIs	✓	✓
$IC50^{NIL}$	↑↑↑	↑↑↑
$IC50^{IM}$	↑↑↑	↑↑↑
$IC50^{DAS}$	↑↑↑	↑
KD mutations	×	×
ABCB1 protein overexpression	✓	×
ABCG2 protein overexpression	×	×
Increased Bcr-Abl protein	×	×
Increased Lyn protein	×	×
Increased p-Lyn	✓	✓
Increased Axl protein	×	×
Increased p-Axl	ND	✓
Increased Syk protein	ND	✓
Increased p-Syk	ND	No phosphorylation

✓=yes; ×=no; ↑=increase; ↓=decrease; ↔=no change; ND=not determined.

nilotinib resistance involves decreased levels of intracellular nilotinib caused by ABCB1-mediated efflux creating favourable conditions for increased activity of Lyn. Constitutively activated Lyn, which exists in a ternary complex with Syk and Axl[126], causes phosphorylation of Bcr-Abl stabilising it in the active conformation. Nilotinib and imatinib are no longer able to bind effectively resulting in inadequate inhibition and the observed increase in $IC50^{NIL}$ and $IC50^{IM}$. Phosphorylated Bcr-Abl subsequently activates effector molecules in downstream signalling pathways governing apoptosis, growth and survival, leading to resistant cells capable of proliferating in the presence of TKI. Syk regulates the phosphorylation of Axl[126], thus, overexpression of Syk leads to increased phosphorylation of Axl at Y779. This residue then forms the docking site for effector molecules involved in signalling pathways governing apoptosis and proliferation[273], allowing resistant cells to survive in the presence of TKI. The causative event/s resulting in Lyn activation may involve down regulation of c-Cbl as previously suggested[123,168], although this requires further investigation including analysis of c-Cbl protein levels (**Figure 5.21**).

It is likely that the events following ABCB1 up regulation, while dependent on the cell line studied, are stochastic in nature and thus the same modes of resistance may not be observed if the process was repeated. Also of interest, is the fact that K562 2 μM NIL cells still exhibit a degree of resistance to dasatinib, despite dasatinib-mediated inhibition of both Bcr-Abl and Lyn. This suggests there is a third mechanism of resistance present; a concept discussed further in **Chapter 7**.

In conclusion, the findings detailed in this chapter strongly suggest that, in K562 cells, ABCB1 overexpression provides the initial catalyst required for additional Bcr-Abl *dependent* mechanisms of resistance to occur. Results detailed here demonstrate that ABCB1 overexpression not only provides a favourable intracellular environment for the manifestation of other mutations/aberrant protein activation but that it is also directly responsible for nilotinib resistance. Subsequently, additional modes of

Figure 5.21: Schematic representation of the interplay existing between resistance mechanisms in K562 cells

Lyn, Axl and Syk have previously been demonstrated to exist in a ternary complex in CML cells that is targeted for degradation by c-Cbl[126]. Decreased levels of c-Cbl may result in the increased levels of phosphorylated Lyn (p-Lyn) present in the K562 2 µM NIL resistant cell line. An increase in levels of Syk protein was also observed in resistant cells compared with control cells possibly explaining the increased phosphorylation of Axl[126] which has previously been demonstrated to interact with proteins from the PI3-K and Ras signalling pathways[270]. Active p-Lyn and Bcr-Abl then engage in reciprocal phosphorylation leading to greatly increased levels of p-Bcr-Abl such that imatinib and nilotinib are no longer able to effectively inhibit its activity. Thus, constitutive activation of downstream signalling pathways governing cell survival and apoptosis occurs. Adapter proteins are depicted in **PURPLE**, transcription factors in **BLUE**, kinases in **GREEN** and apoptosis related proteins in **RED**. IM=imatinib; NIL=nilotinib.

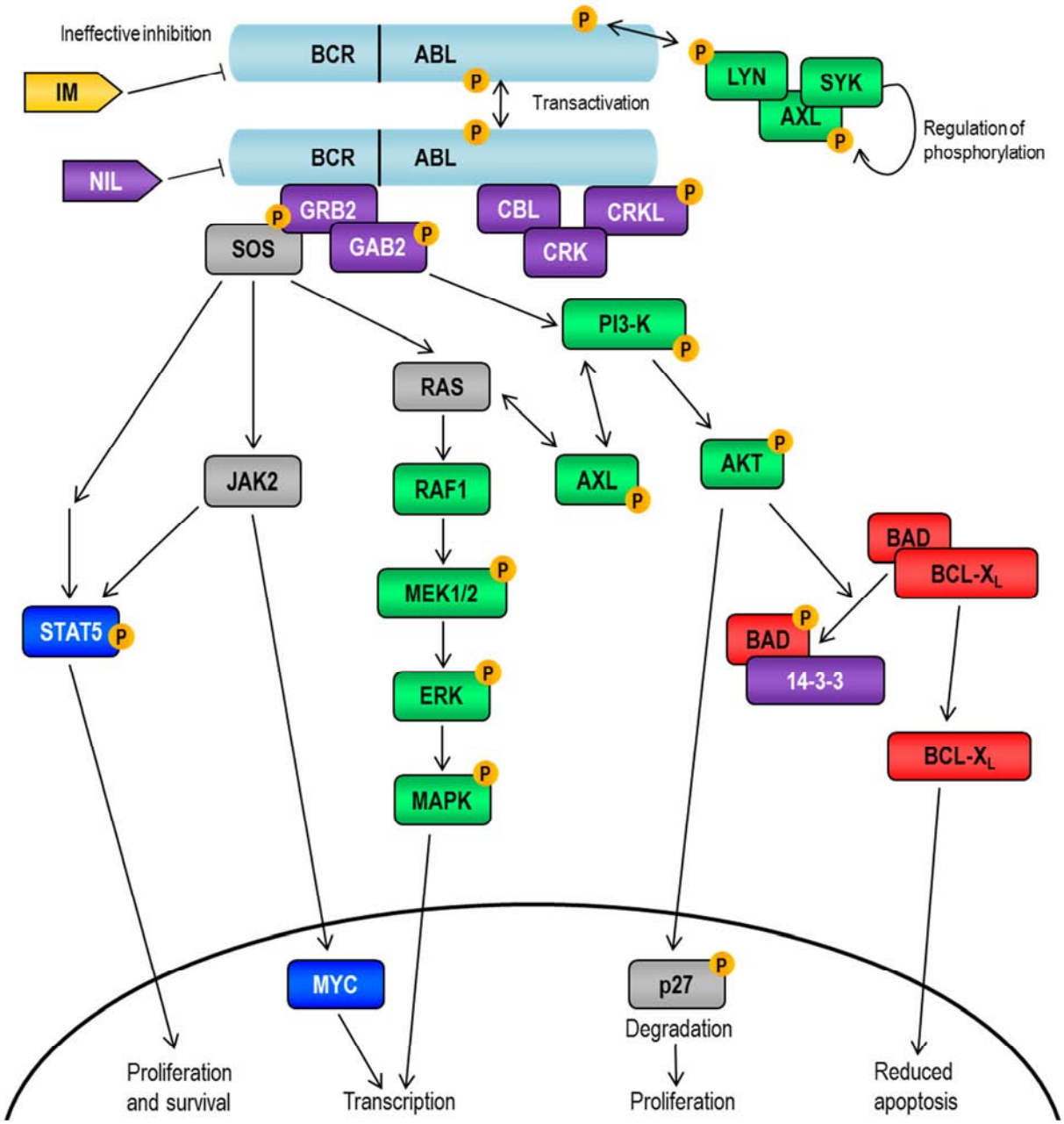
Ineffective inhibition
IM
BCR
ABL
P
Transactivation
LYN
SYK
AXL
Regulation of phosphorylation
NIL
GRB2
SOS
GAB2
CBL
CRKL
CRK
PI3-K
RAS
JAK2
RAF1
AXL
AKT
BAD
BCL-XL
MEK1/2
STAT5
BAD
14-3-3
ERK
BCL-XL
MAPK
MYC
p27
Degradation
Proliferation and survival
Transcription
Proliferation
Reduced apoptosis

resistance occurred: activation of Lyn was observed and potentially activation of Axl. Overall, the *in vitro* model of resistance described presents a valuable tool for studying resistance in patients.

Chapter 6

ABCB1 Overexpression Precedes Bcr-Abl Independent Resistance in K562-Dox Cells

6.1. Introduction

As described in **Chapter 5**, the most common form of secondary resistance observed in CML patients is kinase domain (KD) mutations (**Figure 5.1**). However, approximately 50% of patients who relapse do not have detectable KD mutations. These patients are also at high risk of failing to respond to second-line TKI therapy and usually relapse a second time, again without detectable KD mutations[171,285]. Additionally, a group of frankly resistant, relapsed patients exist who still have adequate inhibition of Bcr-Abl activity[108]. In these patients a Bcr-Abl *independent* mechanism is most likely driving resistance, with a number of signalling pathways postulated to be the cause: JAK-STAT[286,287] and PI3-K signalling[129,288], for example. While these signalling pathways function in cells containing non-mutated, wildtype *BCR-ABL,* in the context of Bcr-Abl independent resistance, it is likely that the need for signalling through Bcr-Abl is circumvented through other receptors such as PDGFR or GM-CSFR[289] (**Figure 6.1**). In addition, TKIs also have activity against other cellular kinases, for example c-kit and PDGFR and additionally, in the case of dasatinib, non-receptor tyrosine kinases such as Src family kinases (SFK). Therefore, if kinase activity is key to disease pathogenesis, it is possible for somatic mutations in these targets to cause Bcr-Abl independent resistance to TKIs; although the evidence for this in CML patients is limited. There is currently a very poor understanding of the cellular events leading to Bcr-Abl-independent resistance and unfortunately, those patients resistant to TKIs in the absence of KD mutations will not be effectively targeted by TKIs alone. Thus, better understanding of the initiating mechanisms leading to Bcr-Abl independent resistance is required before rational therapeutic interventions can take place. Consequently, there is much need for an *in vitro* system in which to study TKI resistance in the Bcr-Abl *independent* setting and this forms the basis of the analyses detailed in the current chapter.

Our laboratory has previously observed a stochastic emergence of resistance both within and between cell lines exposed to the same TKI[107]. Exposure of K562 cells to gradually increasing concentrations of

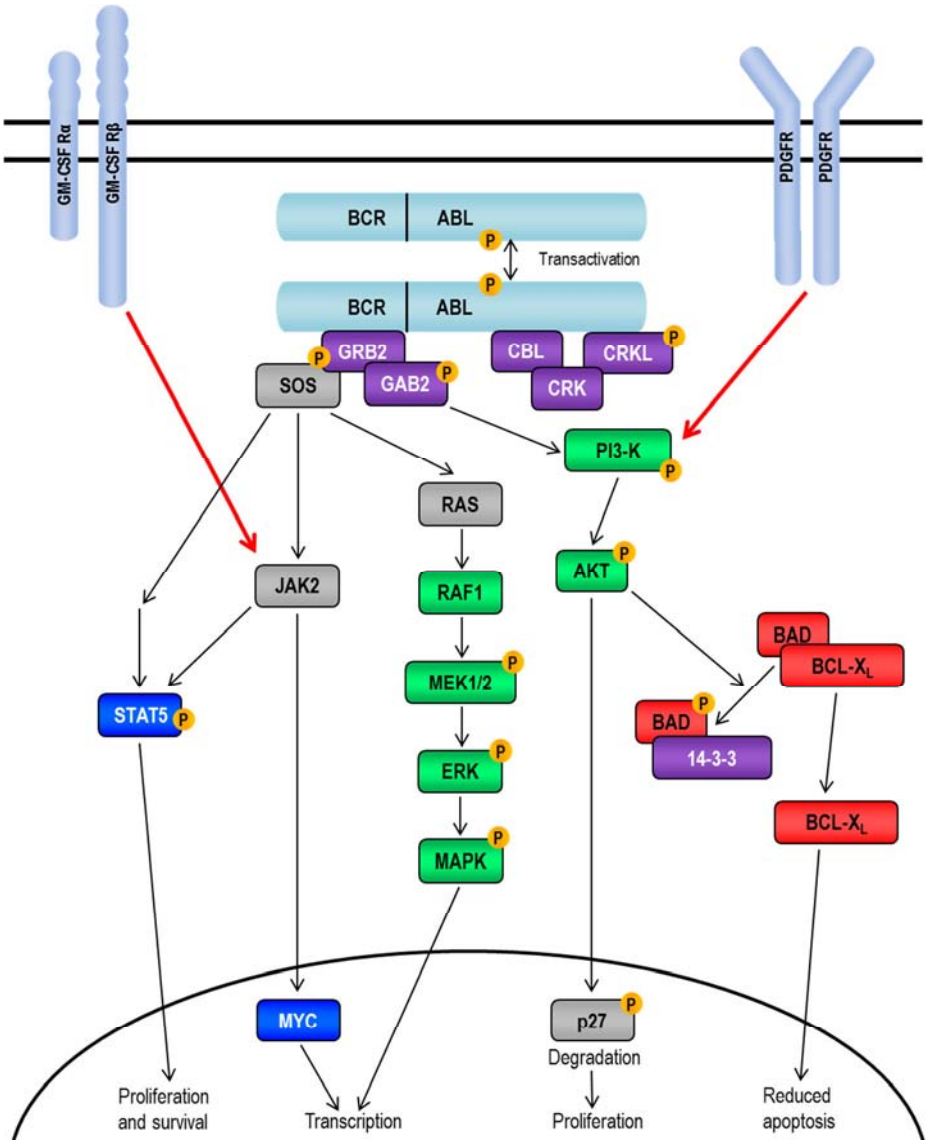

Figure 6.1: Schematic representation of Bcr-Abl signalling pathways aberrantly activated in CML (modified from O'Hare *et al*.[290])

Upon Bcr-Abl dimerization, trans autophosphorylation causes activation of the kinase and formation of docking sites for adapter proteins (**PURPLE**) such as Grb2 and Crkl. In the context of Bcr-Abl *dependent* signalling, subsequent activation of downstream pathways facilitates enhanced proliferation and survival as well as reduced apoptosis. Selected pathways such as JAK-STAT, PI3-K and Ras-ERK are depicted with transcription factors shown in **BLUE**, kinases in **GREEN** and apoptosis related proteins in **RED**, however many other pathways not depicted have also been reported. In the context of Bcr-Abl *independent* signalling, activation of downstream pathways in the absence or inhibition of Bcr-Abl may occur through activation of these pathways by alternate receptors (bold **RED** arrows).

nilotinib resulted in the initial overexpression of ABCB1 followed by the predomination of over active Lyn and Axl kinases (**Chapter 5**). Additionally, we have previously demonstrated in a small cohort of chronic phase CML patients, that high ABCB1 expression at diagnosis may be associated with the development of KD mutations and/or disease resistance in patients receiving imatinib therapy[253]. In accord with these observations, in the current study, we sought to investigate resistance emergence in K562-Dox cells. K562-Dox cells have stably overexpressed ABCB1 for many years as a result of continued passage in doxorubicin and thus provide a suitable model in which to study the association between ABCB1 expression and nilotinib resistance.

The cell lines generated and subsequent analyses discussed in this chapter were used to investigate the onset and interplay of nilotinib resistance mechanisms *in vitro* thus allowing possible identification of and early intervention for patients at risk of developing resistance to TKI therapy. Additionally, the two cell lines generated harbour resistance mechanisms *independent* of Bcr-Abl. This is the first description of an *in vitro* model in which cells retain kinase inhibition yet are completely resistant to TKIs and may provide explanation for patients who lose response to TKI therapy in the absence of KD mutations and other known mechanisms of resistance.

6.2. Approach

The Bcr-Abl positive cell line K562-Dox (ABCB1 overexpressing) was cultured long term in gradually increasing concentrations of nilotinib starting with 15 nM and increasing to 2 μM (**Section 2.3.3.3**; **Table 6.1**). Control cells were cultured in parallel in a constant diluent concentration of 0.1% DMSO to control for the DMSO present in cell cultures containing nilotinib. Cell growth was monitored visually, while cell viability was monitored by trypan blue exclusion of dead cells (**Section 2.3.2**). The concentration of nilotinib was increased once ~70% of cells demonstrated survival (nilotinib tolerance) in culture for at least 10 consecutive days. At each stage of nilotinib escalation, ampoules of cells were frozen (**Section**

Table 6.1: Summary of nilotinib concentrations to which cell line resistance intermediates were exposed and the corresponding number of days before dose was increased

K562-Dox

Nilotinib Concentration	% Live Cells	Days in Culture
15 nM NIL	99.6	11
30 nM NIL	96.9	10
60 nM NIL	98.5	11
100nM NIL #1	91.3	12
125 nM NIL #1	73.6	**81**
200 nM NIL #1	76.6	16
300 nM NIL #1	63.2	11
1 µM NIL #1	75.8	19
2 µM NIL #1	90.7	Ongoing
50 nM NIL #2	86.4	**39**
100 nM NIL #2	85.7	23
125 nM NIL #2	87.9	13
200 nM NIL #2	90.0	18
1 µM NIL #2	61.0	26
2 µM NIL #2	87.0	Ongoing

2.3.4) to allow thawing and re-culture at a later time point (**Section 2.3.5**). In addition, aliquots of cells were lysed in TRIzol reagent for RNA extraction and cDNA synthesis (**Section 2.4.5**). Concentrations of nilotinib up to 100 nM were tolerated easily, however growth and viability substantially reduced upon exposure to 125 nM nilotinib (**Table 6.1**). For this reason a second line (termed #2) of K562-Dox cells was created from the K562-Dox 100 nM NIL #1 line. A frozen ampoule of cells cultured in 100 nM nilotinib was thawed and re-escalation of nilotinib began at 50 nM. Once cells demonstrated ~80% survival in 125 nM nilotinib, the level of resistance was determined via IC50 assays based on p-Crkl protein expression (**Section 2.4.2**) and confirmed by cytotoxicity assays (**Section 2.3.6**). Nilotinib dose escalation continued until a concentration of 2 μM was reached to reflect plasma levels achieved *in vivo* in nilotinib treated patients[170] and resistance was again determined by cytotoxicity assays and p-Crkl IC50. Modes of resistance were investigated as summarised in **Figure 6.2**. Briefly, because ABCB1 and ABCG2 overexpression has previously been linked to TKI resistance[115,116,118,138,139], cell surface expression of these transporters was assessed routinely during resistance development and prior to each IC50 and cytotoxicity assay using flow cytometric analysis (**Section 2.3.8.1**). ABCB1 function was also assessed by rhodamine efflux studies (**Section 2.3.9.1**). Cell lines were screened for total tyrosine phosphorylation status (**Section 2.3.8.2**) and phosphorylation status of Bcr-Abl, Lyn, Axl and Syk (**Section 2.4.3**), as well as altered levels of other cellular kinases and cancer signalling proteins when compared with control cells (**Section 2.4.4**). Levels of ABCB1 mRNA were also determined in *de novo* CML patients prior to initiation of nilotinib therapy.

6.3. Results

6.3.1. K562-Dox Cells Cultured in 125 nM Nilotinib Demonstrate Resistance to TKIs *In Vitro*

Initially, one line of nilotinib resistant K562-Dox cells was generated through exposure to gradually increasing concentrations of nilotinib (K562-Dox NIL #1). Nilotinib concentrations up to 100 nM were easily tolerated, however, upon exposure to 125 nM nilotinib, cell growth stalled and viability

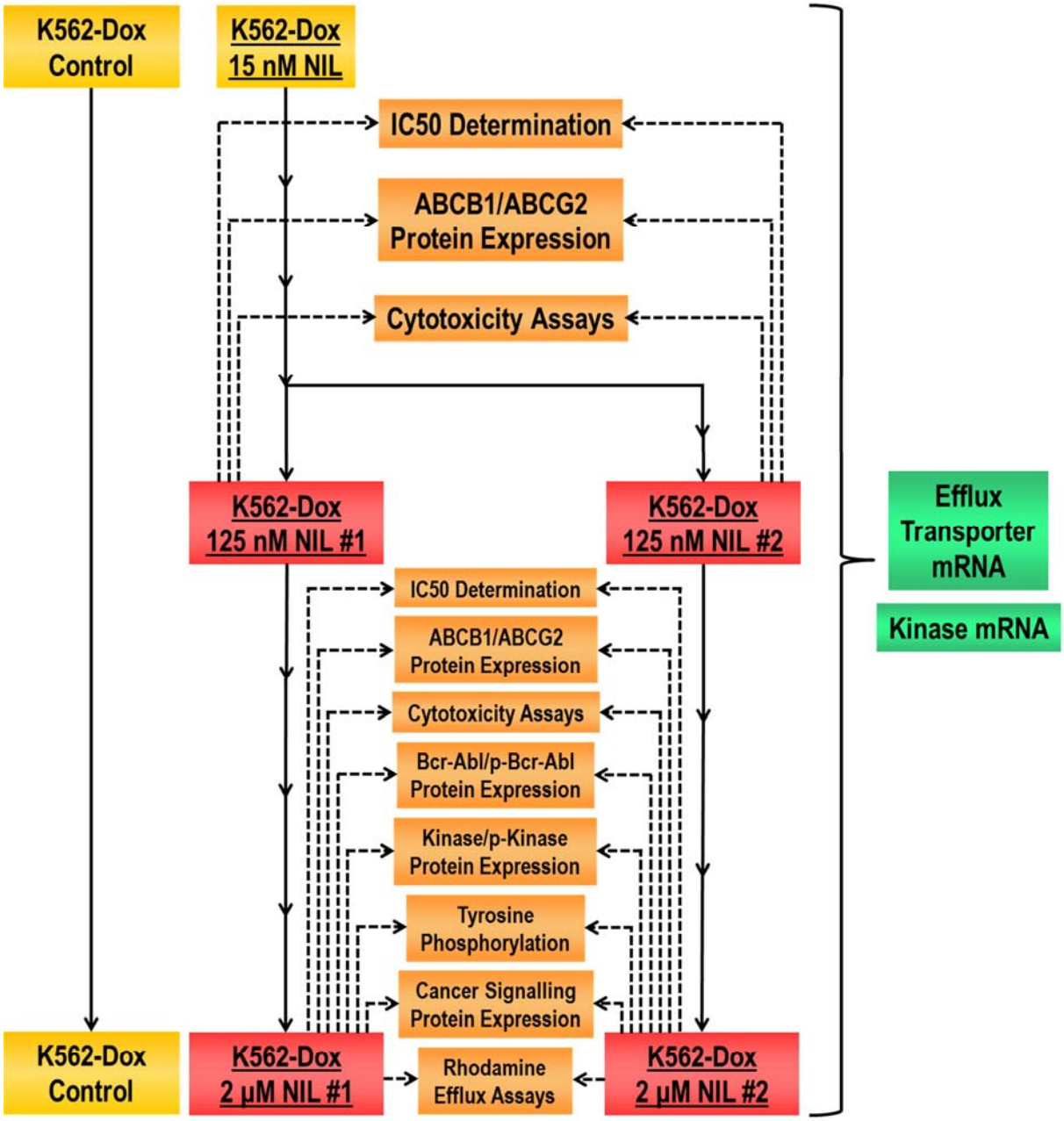

Figure 6.2: Schematic summary of generation and determination of nilotinib resistance in K562-Dox cells

K562-Dox cells were cultured in gradually increasing concentrations of nilotinib. At nilotinib concentrations 125 nM and 2 µM, resistance was assessed by various *in vitro* methods (**ORANGE BOXES**). In addition, mRNA levels were determined in all resistance intermediates (**GREEN BOXES**). All assays were also performed on K562 control cells for comparison. Bold arrows represent steps in escalation of nilotinib. Dashed arrows denote which assays were performed upon each intermediate. NIL=nilotinib.

significantly decreased (**Table 6.2a**). However, after approximately three months exposure to 125 nM nilotinib, cell viability increased to >60%. Because growth of K562-Dox NIL #1 cells in 125 nM nilotinib was so laboured, culture of a second K562-Dox cell line (K562-Dox NIL #2) was initiated from a frozen ampoule of 100 nM NIL #1 cells and re-escalation in nilotinib commenced. These cells were also slow growing, however, after approximately two and a half months, were able to tolerate 125 nM nilotinib with cell viability reaching 88% (**Table 6.2b**). Thus, resistance to nilotinib in both K562-Dox 125 nM NIL #1 and K562-Dox 125 nM NIL #2 cells was evaluated by cytotoxicity assay. K562-Dox 125 nM NIL #1 cells demonstrated increased survival compared with control cells when exposed to 1000 nM nilotinib for 72 h: 42% vs 98% survival. K562-Dox 125 nM NIL #2 also demonstrated increased survival compared with control cells when exposed to 1000 nM nilotinib for 72 h: 42% vs 98% survival (**Figure 6.3a**).

Resistance to imatinib and dasatinib were assessed with resistant cells demonstrating increased survival when compared with control cells. In the presence of 5 μM imatinib: K562-Dox control=31% survival, K562-Dox 125 nM NIL #1=92% survival, K562-Dox 125 nM NIL #2=93% survival. In the presence of 500 nM dasatinib: K562-Dox control=11% survival, K562-Dox 125 nM NIL #1=95% survival, K562-Dox 125 nM NIL #2=77% survival (**Figure 6.3b and c**).

6.3.2. K562-Dox 125 nM NIL #1 and K562-Dox 125 nM NIL #2 Cells Demonstrate Differential IC50

$IC50^{NIL}$, $IC50^{IM}$ and $IC50^{DAS}$ specific for p-Crkl protein expression were determined for both K562-Dox 125 nM NIL #1 and K562-Dox 125 nM NIL #2 cells. Interestingly, while both cell lines demonstrated resistance via cytotoxicity assays, only K562 125 nM NIL #2 cells demonstrated significantly increased $IC50^{NIL}$ when compared with control cells: 507 nM vs 888 nM, $p<0.001$ (**Figure 6.4a**). $IC50^{DAS}$ also increased from 108 nM to 210 nM, p=0.018; however, $IC50^{IM}$ demonstrated no change from 10.4 μM to 10.1 μM, p=0.953 which was unexpected (**Figure 6.4b and c**).

Table 6.2a: Summary of live K562-Dox NIL #1 cells after exposure to 125 nM nilotinib for the corresponding number of days

Days in Culture	% Live Cells
2	94.0
6	68.1
9	46.2
12	44.8
16	56.5
55	45.5
74	58.8
76	54.4
79	62.7
81	73.6
83	62.4
88	62.3

Table 6.2b: Summary of live K562-Dox NIL #2 cells after exposure to increasing concentrations of nilotinib for the corresponding number of days

[Nilotinib]	Days in Culture	% Live Cells
50 nM	2	58.7
	4	29.1
	14	65.0
	18	84.9
	21	58.5
	23	39.6
	25	44.3
	28	53.5
	31	79.1
	33	79.4
	35	88.2
	39	86.4
100 nM	9	64.5
	12	69.4
	23	85.7
125 nM	2	91.3
	6	75.0
	9	87.2
	13	87.9

(a)

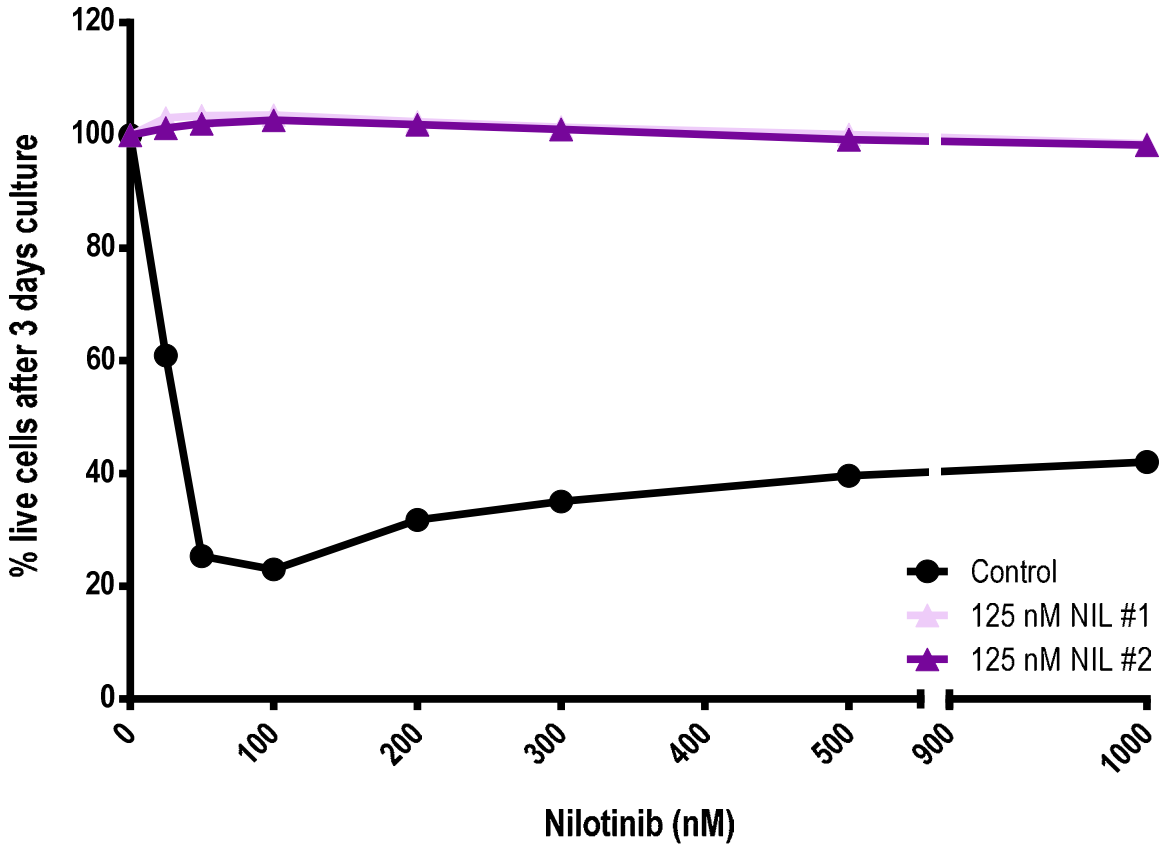

Figure 6.3: K562-Dox 125 nM NIL #1 and K562-Dox 125 nM NIL #2 cells have significantly decreased TKI-mediated cell death

Cells were cultured for 72 h in increasing concentrations of a) nilotinib b) imatinib and c) dasatinib and cell death determined by Annexin V/7-AAD staining. Data demonstrate that K562-Dox 125 nM NIL #1 and K562-Dox 125 nM NIL #2 cells have increased survival in the presence of TKIs when compared with control cells. Results were confirmed with trypan blue staining (**Appendix 4A**). The FACS plots shown represent one experiment performed in triplicate with the corresponding survival curves representing the mean. Data were normalised to 0 nM TKI with the number of live cells in the absence of TKI set at 100%. NIL=nilotinib; IM=imatinib; DAS=dasatinib.

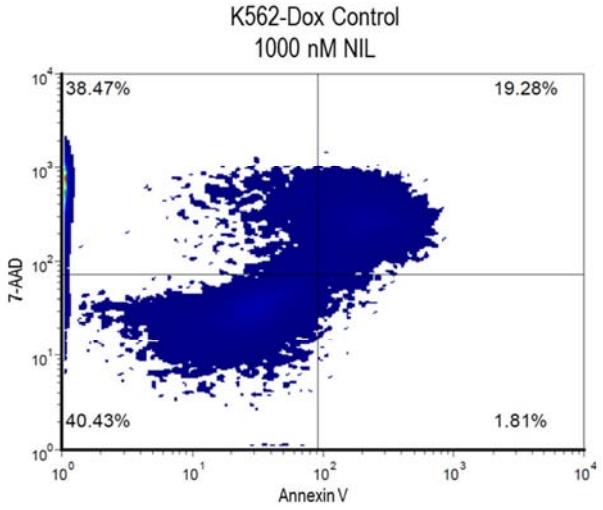
K562-Dox Control
1000 nM NIL
38.47%
19.28%
40.43%
1.81%
7-AAD
Annexin V

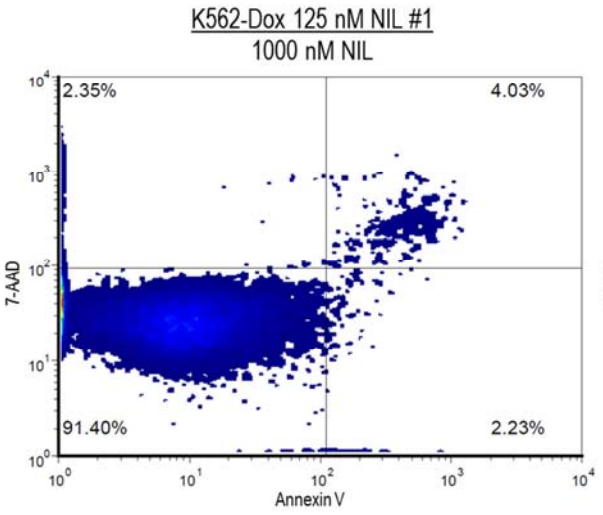
K562-Dox 125 nM NIL #1
1000 nM NIL
2.35%
4.03%
91.40%
2.23%
7-AAD
Annexin V

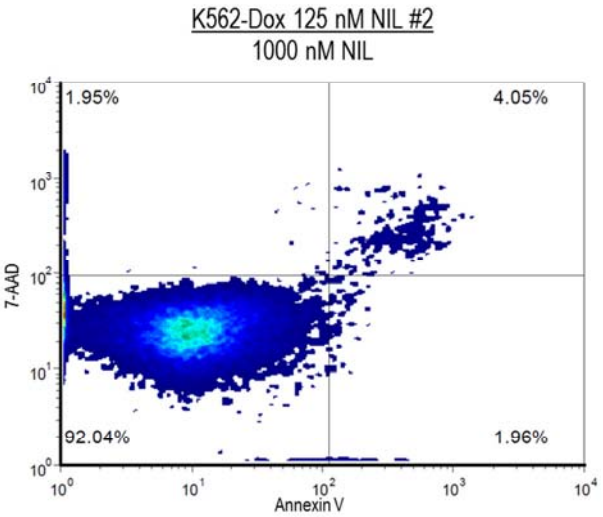
K562-Dox 125 nM NIL #2
1000 nM NIL
1.95%
4.05%
92.04%
1.96%
7-AAD
Annexin V

(b)

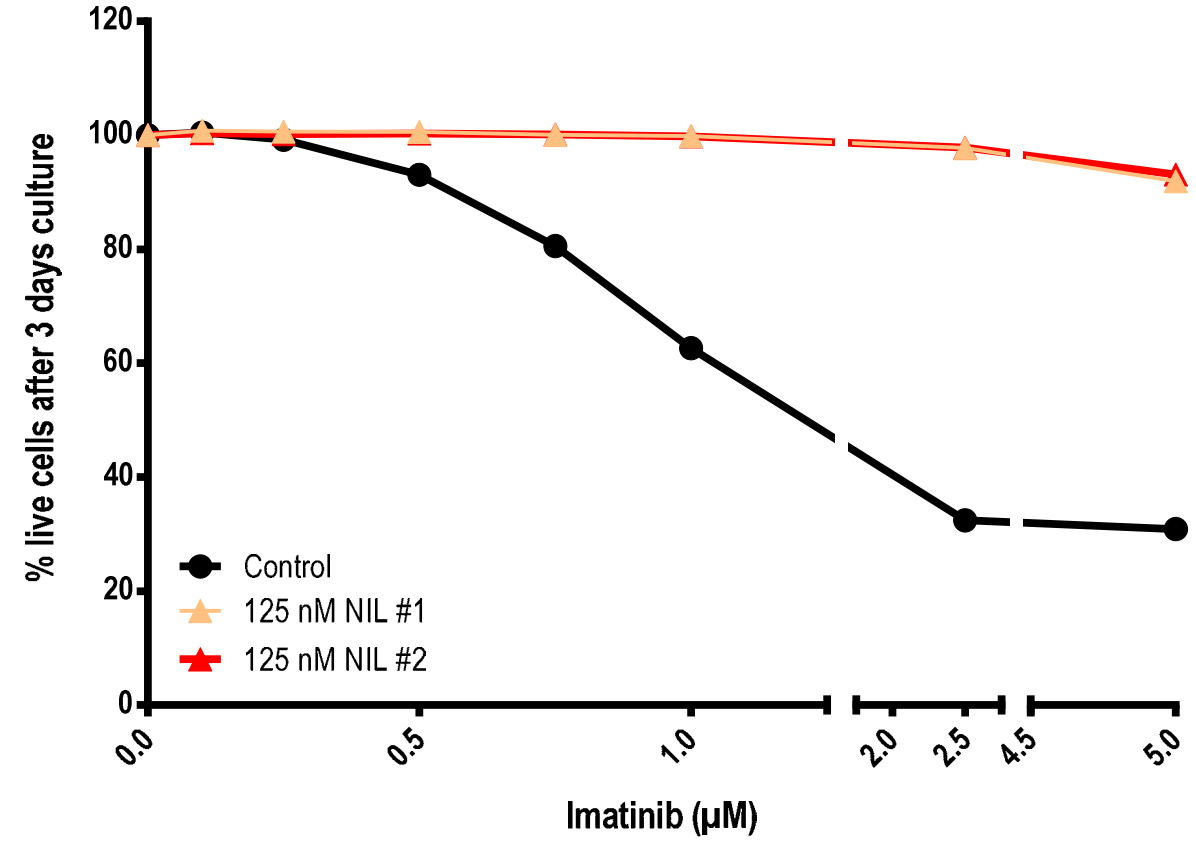
120
100
80
60
40
20
0
% live cells after 3 days culture
Control
125 nM NIL #1
125 nM NIL #2
0.0
0.5
1.0
2.0
2.5
4.5
5.0
Imatinib (μM)

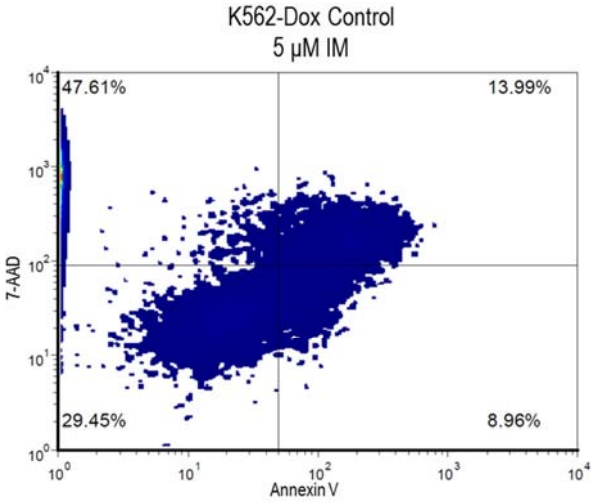
K562-Dox Control
5 μM IM
47.61%
13.99%
29.45%
8.96%
7-AAD
Annexin V

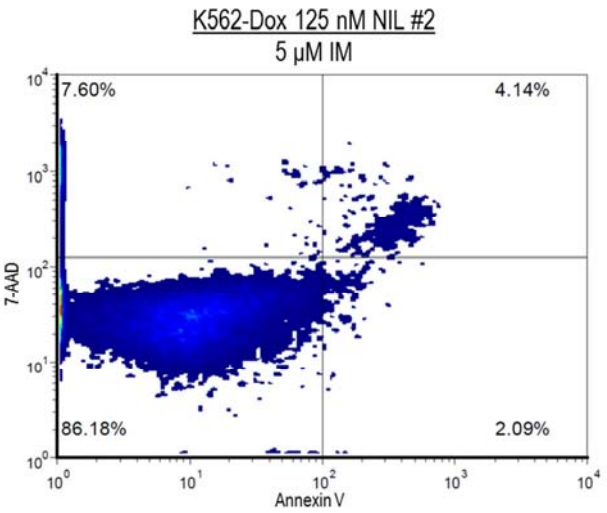
K562-Dox 125 nM NIL #2
5 μM IM
7.60%
4.14%
86.18%
2.09%
7-AAD
Annexin V

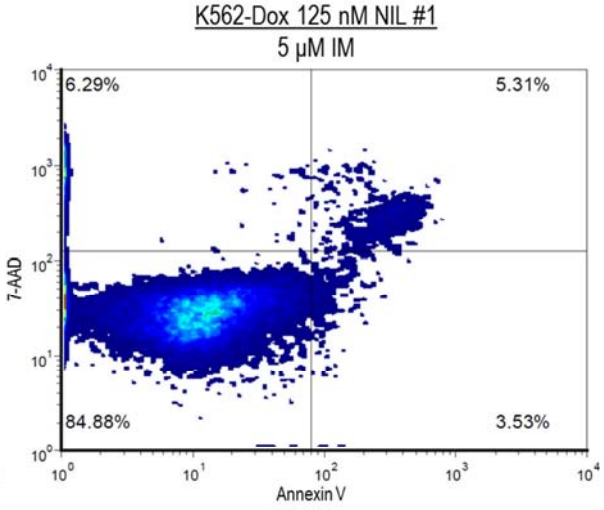
K562-Dox 125 nM NIL #1
5 μM IM
6.29%
5.31%
84.88%
3.53%
7-AAD
Annexin V

(c)

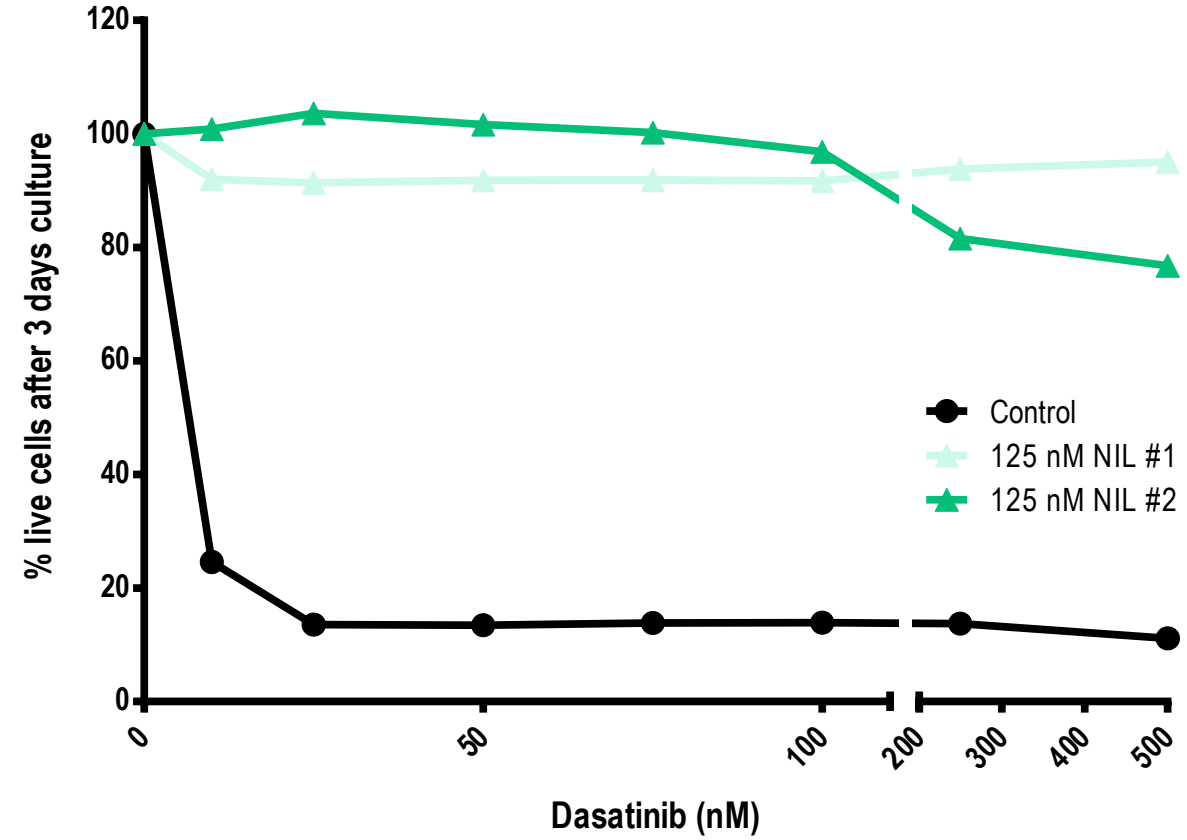
% live cells after 3 days culture
120
100
80
60
40
20
0
0
50
100
200
300
400
500
Dasatinib (nM)
Control
125 nM NIL #1
125 nM NIL #2

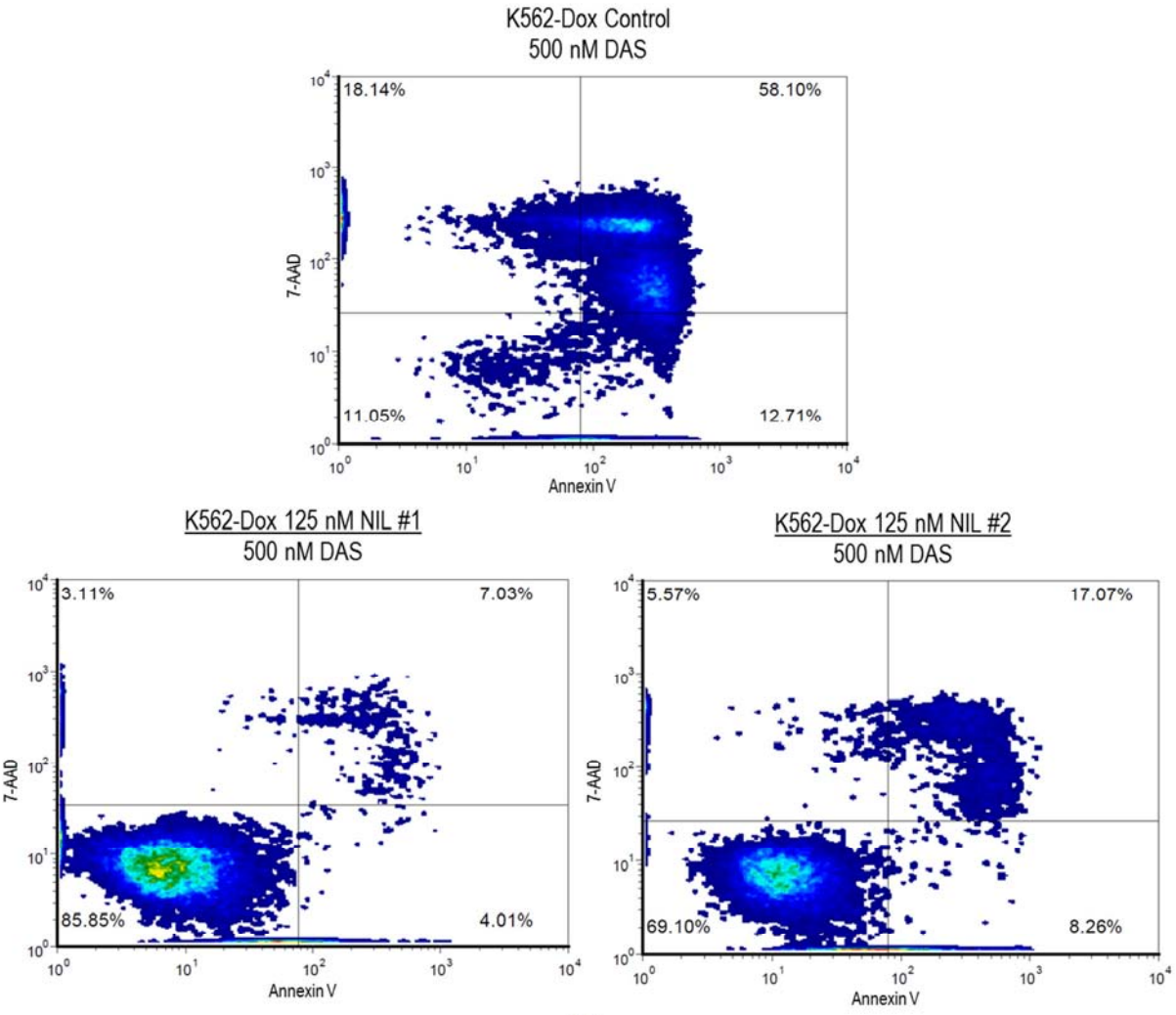
K562-Dox Control
500 nM DAS
18.14%
58.10%
11.05%
12.71%
7-AAD
Annexin V
K562-Dox 125 nM NIL #1
500 nM DAS
3.11%
7.03%
85.85%
4.01%
7-AAD
Annexin V
K562-Dox 125 nM NIL #2
500 nM DAS
5.57%
17.07%
69.10%
8.26%
7-AAD
Annexin V

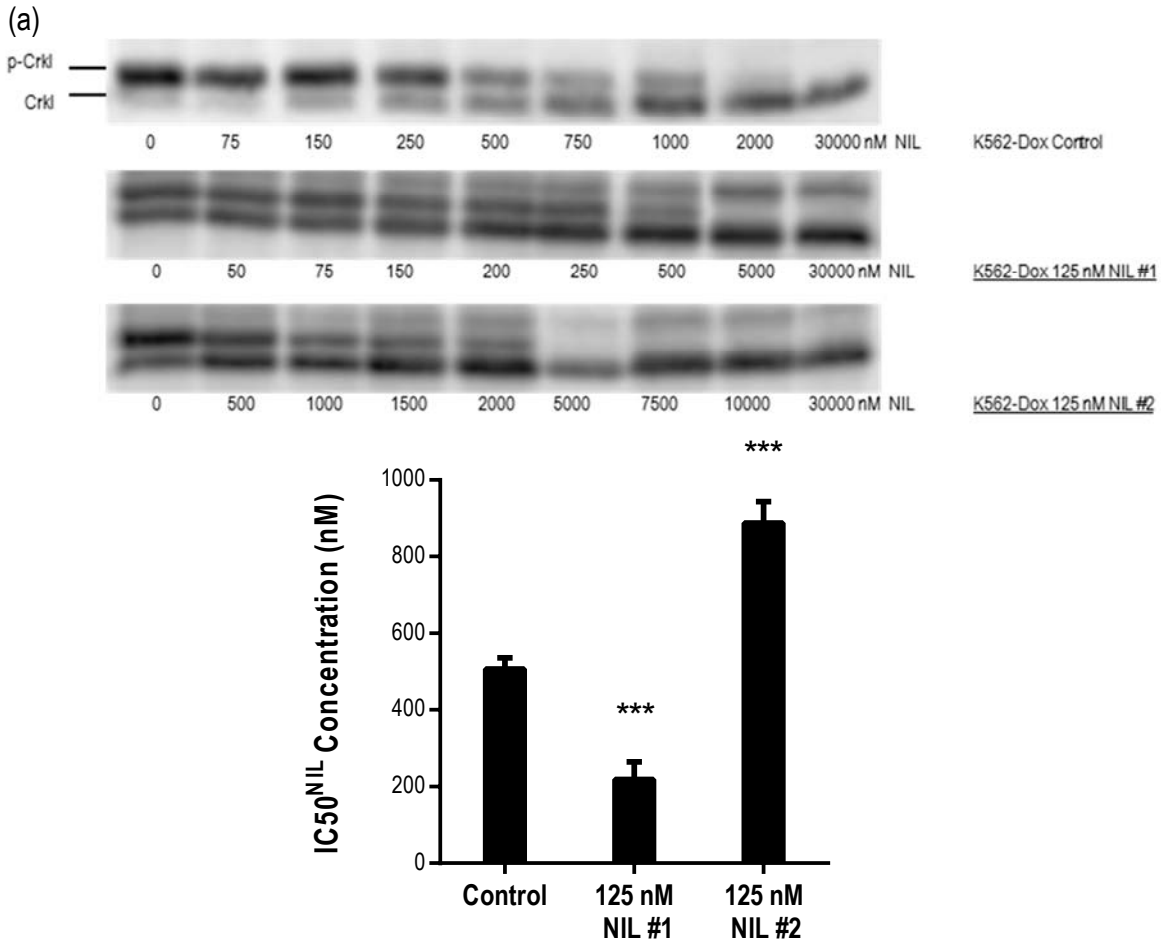

Figure 6.4: K562-Dox 125 nM NIL #1 and K562-Dox 125 nM NIL #2 cells have contrasting levels of Bcr-Abl kinase inhibition

IC50 was determined via incubating cells for 2 h at 37°C in the presence of increasing concentrations of a) nilotinib, b) imatinib and c) dasatinib. Crkl western blot was performed to determine the concentration of TKI required for 50% Bcr-Abl kinase inhibition. Data demonstrate that K562-Dox 125 nM NIL #1 cells have significantly decreased IC50 when compared with control cells whereas K562-Dox 125 nM NIL #2 cells have significantly increased IC50 when compared with control cells. The western blot analyses shown are representative of at least three separate experiments with the corresponding densitometry analysis representing the mean. Statistical analyses were performed using Student's *t*-test with statistically significant *p*-values denoted by asterisks (* $p<0.05$; ** $p<0.01$; *** $p<0.001$). Error bars represent SEM. NIL=nilotinib, IM=imatinib, DAS=dasatinib.

(b)

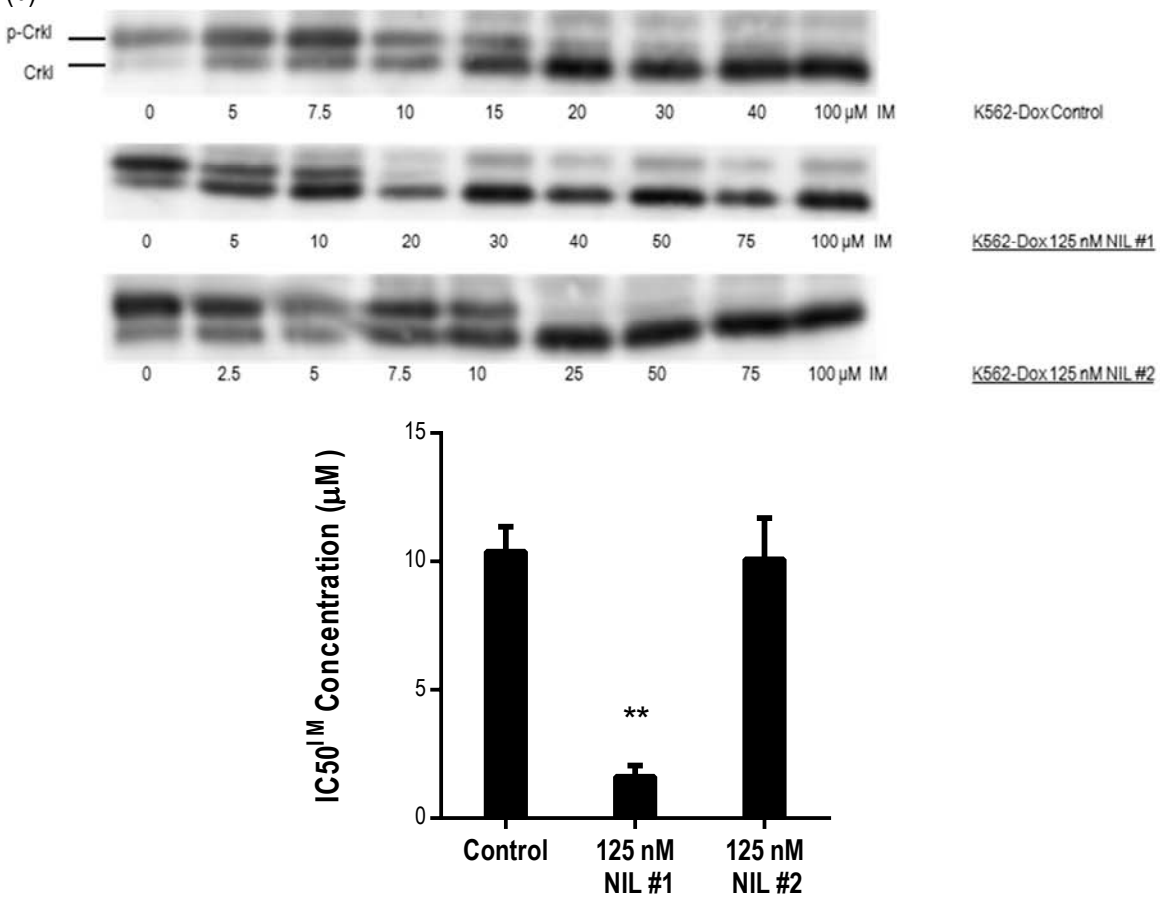
p-Crkl
Crkl
0 5 7.5 10 15 20 30 40 100 µM IM
K562-Dox Control
0 5 10 20 30 40 50 75 100 µM IM
K562-Dox 125 nM NIL #1
0 2.5 5 7.5 10 25 50 75 100 µM IM
K562-Dox 125 nM NIL #2
IC50IM Concentration (µM)
15
10
5
0
**
Control
125 nM NIL #1
125 nM NIL #2

(c)

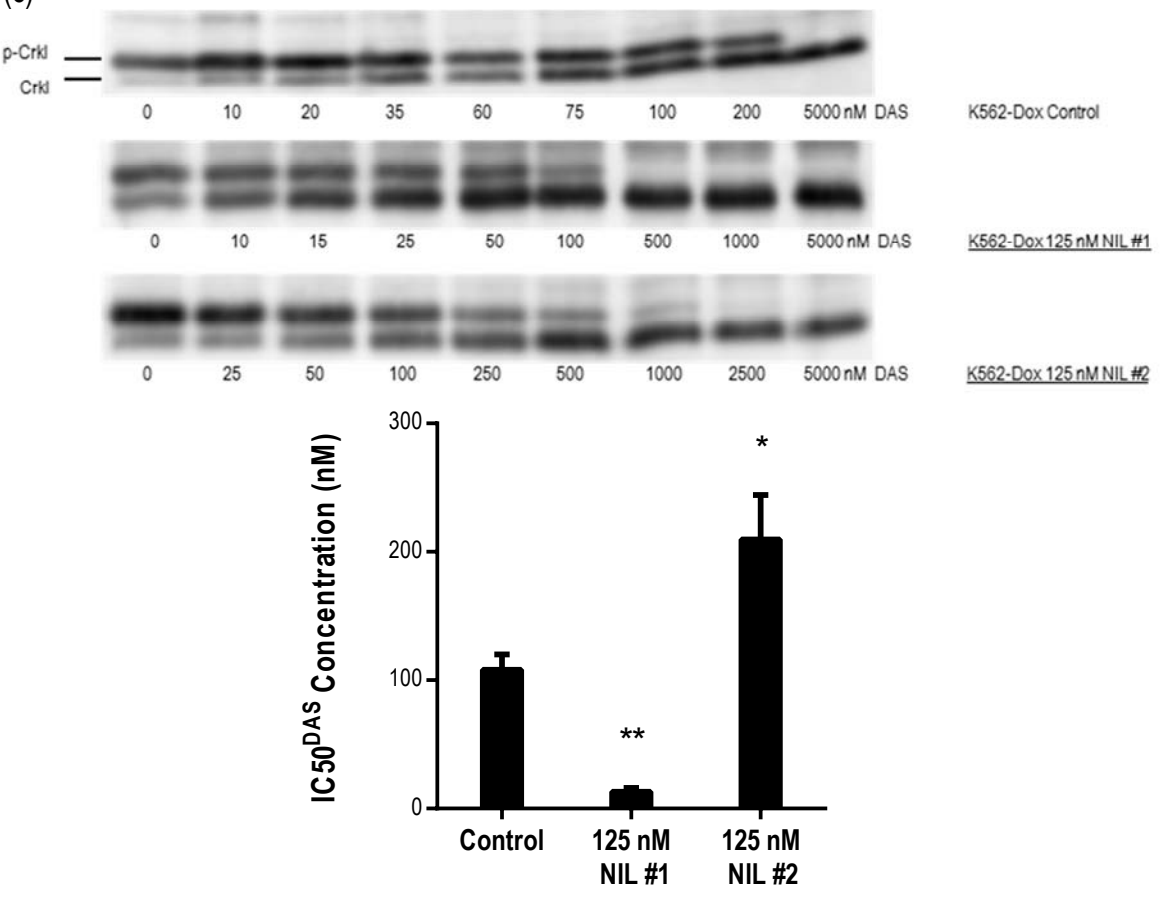
p-Crkl
Crkl
0 10 20 35 60 75 100 200 5000 nM DAS
K562-Dox Control
0 10 15 25 50 100 500 1000 5000 nM DAS
K562-Dox 125 nM NIL #1
0 25 50 100 250 500 1000 2500 5000 nM DAS
K562-Dox 125 nM NIL #2
IC50DAS Concentration (nM)
300
200
100
0
**
*
Control
125 nM NIL #1
125 nM NIL #2

Intriguingly, K562 125 nM NIL #1 cells demonstrated a significantly decreased $IC50^{NIL}$, $IC50^{IM}$ and $IC50^{DAS}$ when compared with control cells, despite being fully resistant via cytotoxicity assays. $IC50^{NIL}$ decreased from 507 nM to 219 nM, $p<0.001$; $IC50^{IM}$ decreased from 10.4 μM to 1.3 μM, $p=0.003$; and $IC50^{DAS}$ decreased from 108 nM to 13 nM, $p=0.003$ (**Figure 6.4**).

6.3.3. IC50 in Resistant K562-Dox Cells is Dependent on ABCB1 Expression

ABCB1 expression was assessed to investigate whether overexpression also played a role in resistance development in K562-Dox cells. Data demonstrated that ABCB1 mRNA and protein expression directly correlated with IC50. In K562-Dox 125 nM NIL #2 cells, in which $IC50^{NIL}$ and $IC50^{DAS}$ were high, ABCB1 protein expression increased from 274 MFI in control cells to 515 MFI in resistant cells ($p=0.002$; **Figure 6.5a**). Additionally, ABCB1 mRNA also increased 2.2-fold when compared with control cells ($p=0.003$; **Figure 6.6a**). However, in K562-Dox 125 nM NIL #1 cells, in which $IC50^{NIL}$, $IC50^{IM}$ and $IC50^{DAS}$ were low, two populations of cells were present: ABCB1-positive cells and an ABCB1-negative population. Interestingly the ABCB1-negative population increased in size, with a corresponding decrease in the ABCB1-positive population, as time elapsed (**Figure 6.5b**). Likewise, ABCB1 mRNA was decreased by 3.8-fold when compared with control cells ($p=0.002$; **Figure 6.6a**).

6.3.4. Sustained Culture of K562-Dox Cells in Nilotinib Results in Decreased ABCB1 Expression and Loss of ABCB1 Function

Continued culture in concentrations of nilotinib up to 2 μM resulted in decreased levels of ABCB1 mRNA and protein (**Figure 6.6**) in both K562-Dox NIL #1 and K562-Dox NIL #2 cell lines. In K562-Dox 2 μM NIL #1 cells expression levels of ABCB1 protein and mRNA decreased by 33- and 200-fold respectively ($p<0.001$ and $p=0.002$ respectively). Similarly, in K562-Dox 2 μM NIL #2 cells, expression levels of ABCB1 protein and mRNA decreased by 97- and 250-fold respectively ($p<0.001$ and $p=0.002$ respectively; **Figure 6.6**).

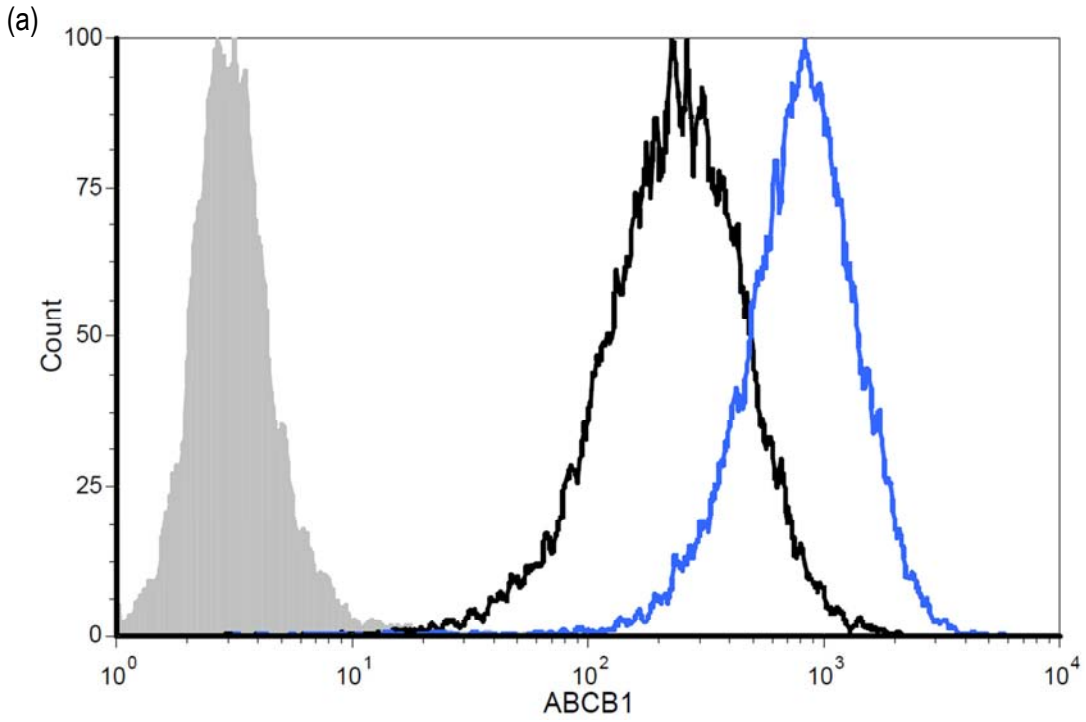

Figure 6.5: ABCB1 protein expression directly correlates with IC50 in K562-Dox NIL resistant cells

Expression levels of ABCB1 protein were assessed in a) K562-Dox 125 nM NIL #2 and b) K562-Dox 125 nM NIL #1 cells. Data demonstrate K562-Dox 125 nM NIL #2 cells have increased expression levels of ABCB1 protein when compared with control cells and this correlates with the increased $IC50^{NIL}$ and $IC50^{DAS}$. Data also demonstrate K562-Dox 125 nM NIL #1 cells comprise two distinct populations: ABCB1-positive and ABCB1-negative cells. The ABCB1-negative cell population increased over time with a corresponding decrease in ABCB1-positive cells. K562-Dox 125 nM NIL #1 cells had decreased $IC50^{NIL}$, $IC50^{IM}$ and $IC50^{DAS}$ when compared with control cells. The histograms displayed in a) represent typical ABCB1 MFI levels. The percentages displayed in b) denote cells positive for ABCB1 expression. The bold **BLACK** and **BLUE** lines represent **control** and **resistant** cells respectively, stained with ABCB1 antibody. The **GREY** filled histograms represent cells stained with **isotype control** antibody.

(b)

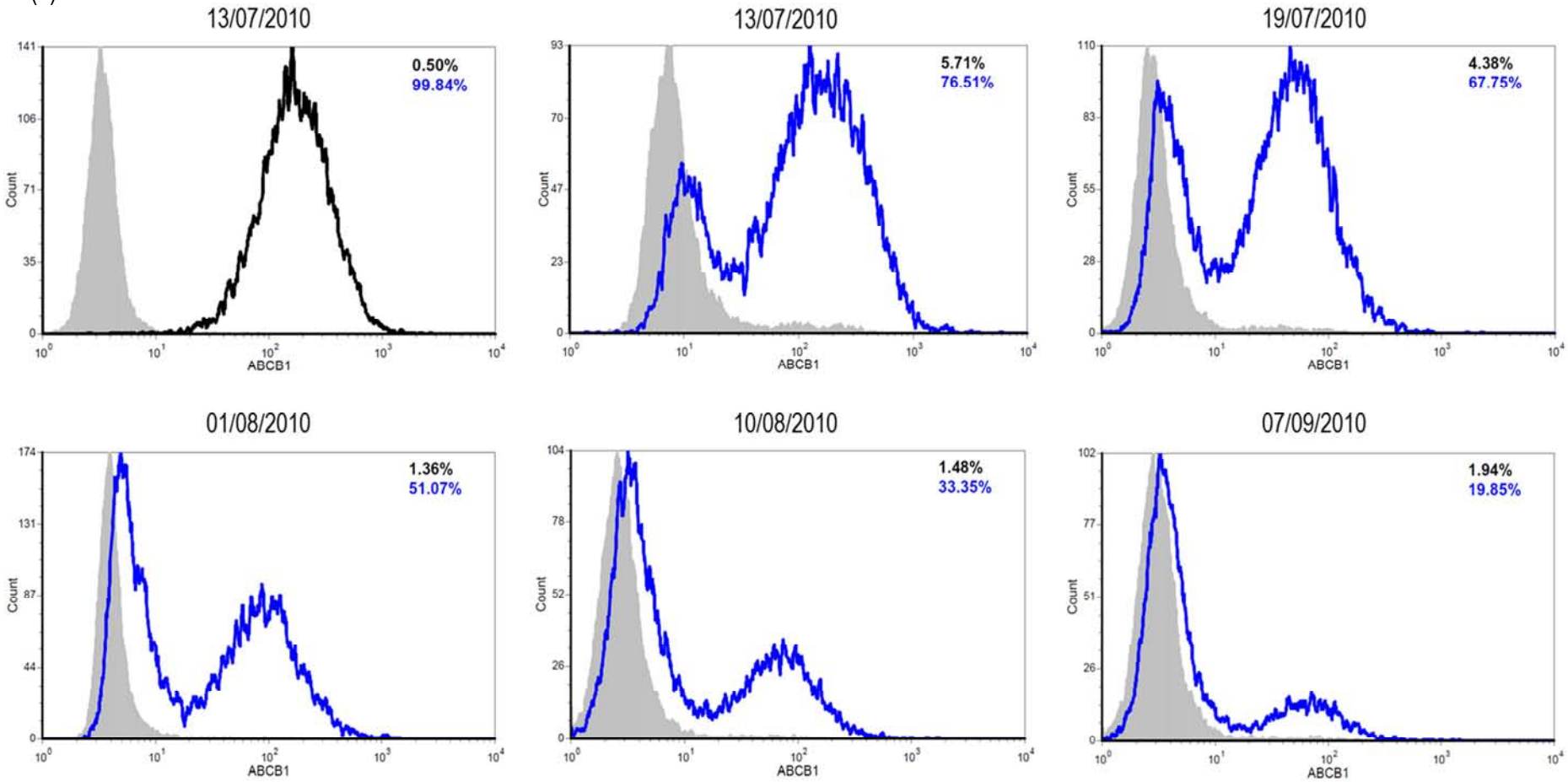

Figure 6.5 (continued): ABCB1 protein expression directly correlates with IC50 in <u>K562-Dox NIL</u> resistant cells

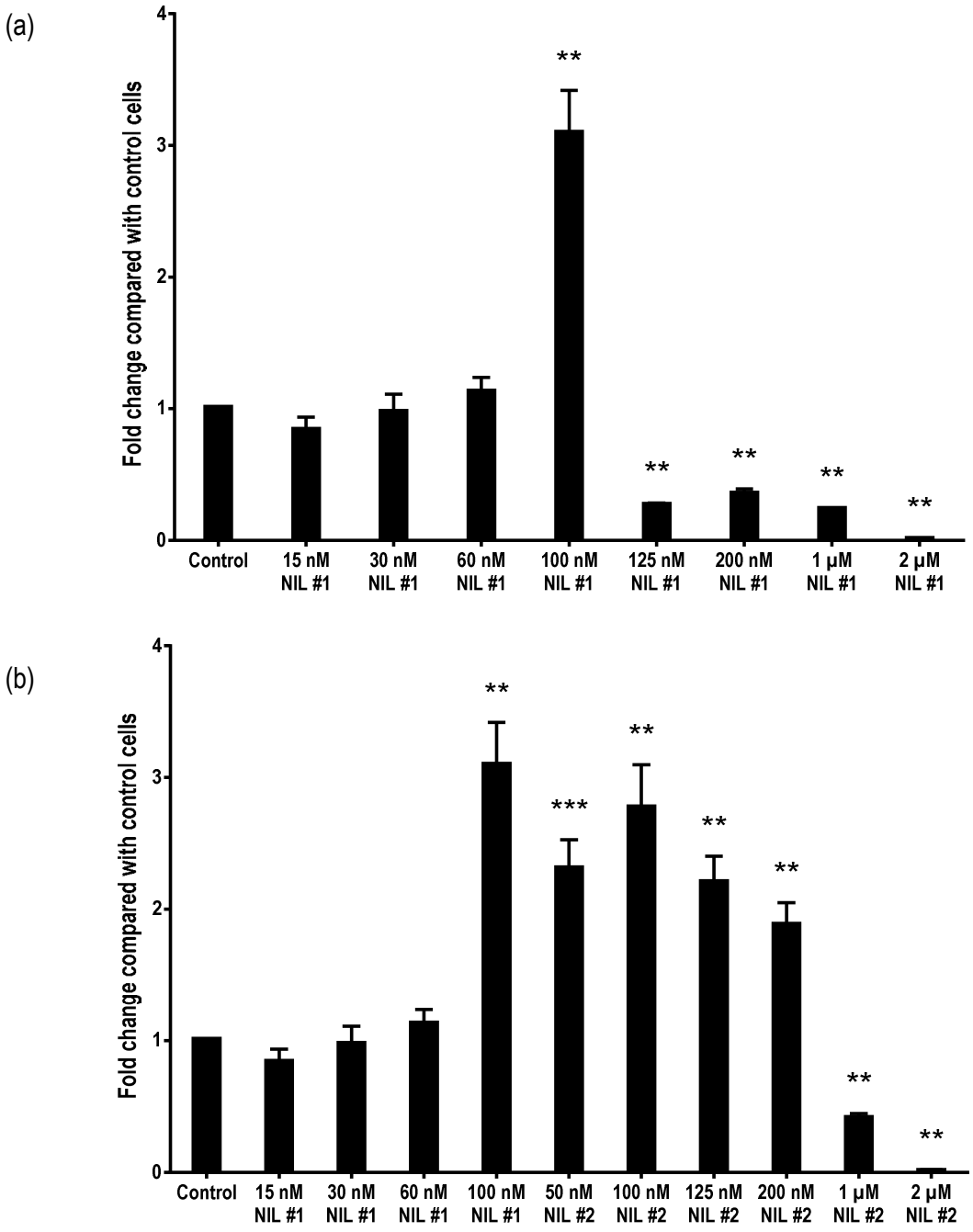

Figure 6.6a: Culture of K562-Dox cells in 2 µM nilotinib causes complete loss of ABCB1 mRNA

Expression levels of ABCB1 mRNA were assessed in a) K562-Dox NIL #1 and b) K562-Dox NIL #2 resistance intermediates. Data demonstrate a significant decrease in ABCB1 expression when cells are cultured in concentrations of nilotinib up to 2 µM. The mRNA expression represents the mean of six independent experiments performed in triplicate. Statistical analyses were performed on mRNA levels as a percentage of BCR using Student's *t*-test. Statistically significant *p*-values are denoted by asterisks (** $p<0.01$; *** $p<0.001$). Error bars represent SEM. NIL=nilotinib.

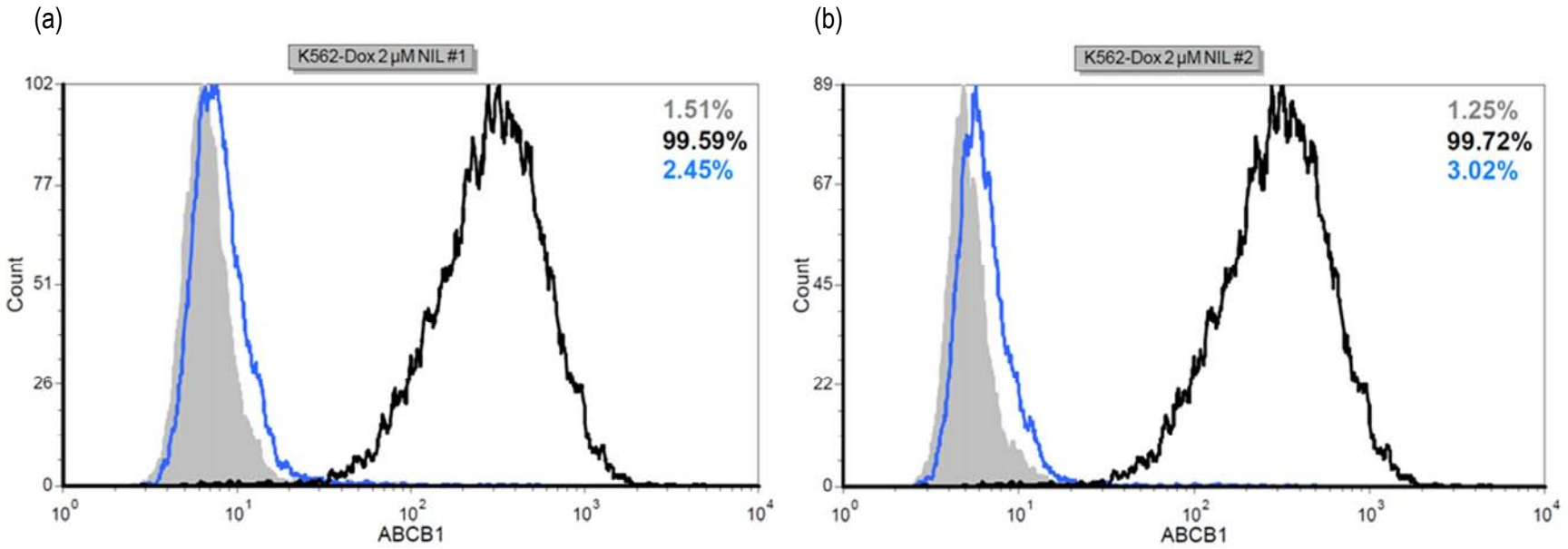

Figure 6.6b: Culture of K562-Dox cells in 2 µM nilotinib causes complete loss of ABCB1 protein

Expression levels of ABCB1 protein were assessed in a) K562-Dox 2 µM NIL #1 and b) K562-Dox 2 µM NIL #2 cells. Data demonstrate a significant decrease in ABCB1 expression. The histograms shown are representative of typical expression levels. The percentages displayed in the histograms denote cells positive for ABCB1. The bold **BLACK** and **BLUE** lines represent **control** and **resistant** cells respectively, stained with ABCB1 antibody. The **GREY** filled histograms represent cells stained with **isotype control** antibody.

Following long term exposure of K562 cells to the ABCB1 substrate doxorubicin, resultant K562-Dox cells have stably expressed ABCB1 for over a decade. This is the first time loss of ABCB1 expression in K562-Dox cells due to continued culture in TKI has been described. Thus, it was important to determine whether there was also a loss of ABCB1 function. Therefore, K562-Dox 2 μM NIL #1 and K562-Dox 2 μM NIL #2 cells were assessed for ability to effectively efflux the ABCB1 substrate rhodamine-123. Results demonstrated a complete loss of ABCB1 function with both resistant cell lines demonstrating comparable rhodamine-123 levels to the parental K562 cell line. Rhodamine-123 levels in K562-Dox control cells were as expected (**Figure 6.7**).

No significant increase in levels of ABCG2 mRNA was observed in any K562-Dox NIL #1 resistance intermediates; there was, however, a significant decrease. Furthermore, no significant increase in ABCG2 protein was observed in either K562-Dox 125 nM NIL #1 or K562-Dox 2 μM NIL #1 cells (**Figure 6.8a**). However, in early K562-Dox NIL #2 resistance intermediates, a significant increase in ABCG2 mRNA was observed although this failed to translate to a significant increase in ABCG2 protein and it was not maintained within later resistance intermediates (**Figure 6.8b**). Thus, because no functional ABCG2 protein was present, it is unlikely this transporter plays a role in resistance to nilotinib in K562-Dox cells.

Similarly, no significant increase in ABCC1 mRNA was observed in K562-Dox NIL #2 resistant cells. However, a slight increase in ABCC1 levels was observed in K562-Dox NIL #1 cells, although this increase was inconsistent and non-substantial (**Figure 6.9**). Thus, while it is unlikely ABCC1 plays a role in nilotinib resistance in K562-Dox cells, this possibility cannot be completely ruled out.

Figure 6.7: K562-Dox 2 µM NIL #1 and K562-Dox 2 µM NIL #2 cells lose the ability to effectively efflux rhodamine-123 when cultured in 2 µM nilotinib

Cells were stained with the fluorescent substrate rhodamine-123 and fluorescence determined in the absence and presence of the specific ABCB1 inhibitor PSC-833. K562-Dox control cells demonstrated characteristically high levels of rhodamine-123 in the presence of PSC-833 consistent with ABCB1 inhibition resulting in retention of substrate. In the absence of inhibition, rhodamine-123 levels were low, consistent with efflux of substrate from cells. Parental K562 cells demonstrated characteristically high levels of rhodamine-123 in the absence and presence of PSC-833 consistent with negligible levels of ABCB1. Similarly, K562-Dox 2 µM NIL #1 and K562-Dox 2 µM NIL #2 cells also demonstrated high levels of rhodamine-123 in the absence and presence of PSC-833 indicating these cells had lost all functional ABCB1 protein. Data are representative of typical MFI levels with the geometric mean of the peaks detailed. The **BLACK** histograms represent **fluorescent substrate alone** while the **BLUE** histograms represent **PSC-833-mediated inhibition** of ABCB1.

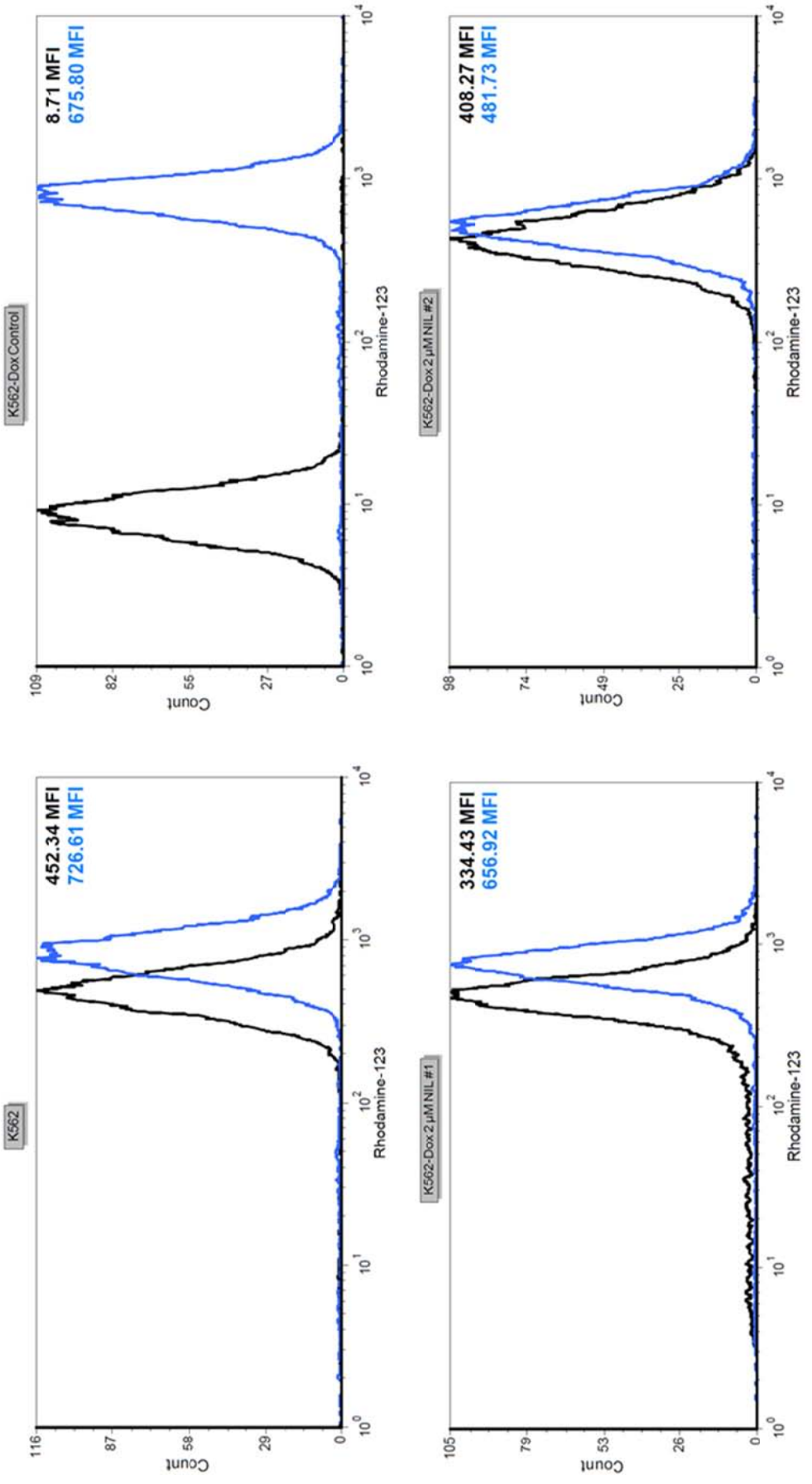
K562-Dox Control
8.71 MFI
675.80 MFI
K562-Dox 2 µM NIL #2
408.27 MFI
481.73 MFI
K562
452.34 MFI
726.61 MFI
K562-Dox 2 µM NIL #1
334.43 MFI
656.92 MFI
Count
Rhodamine-123

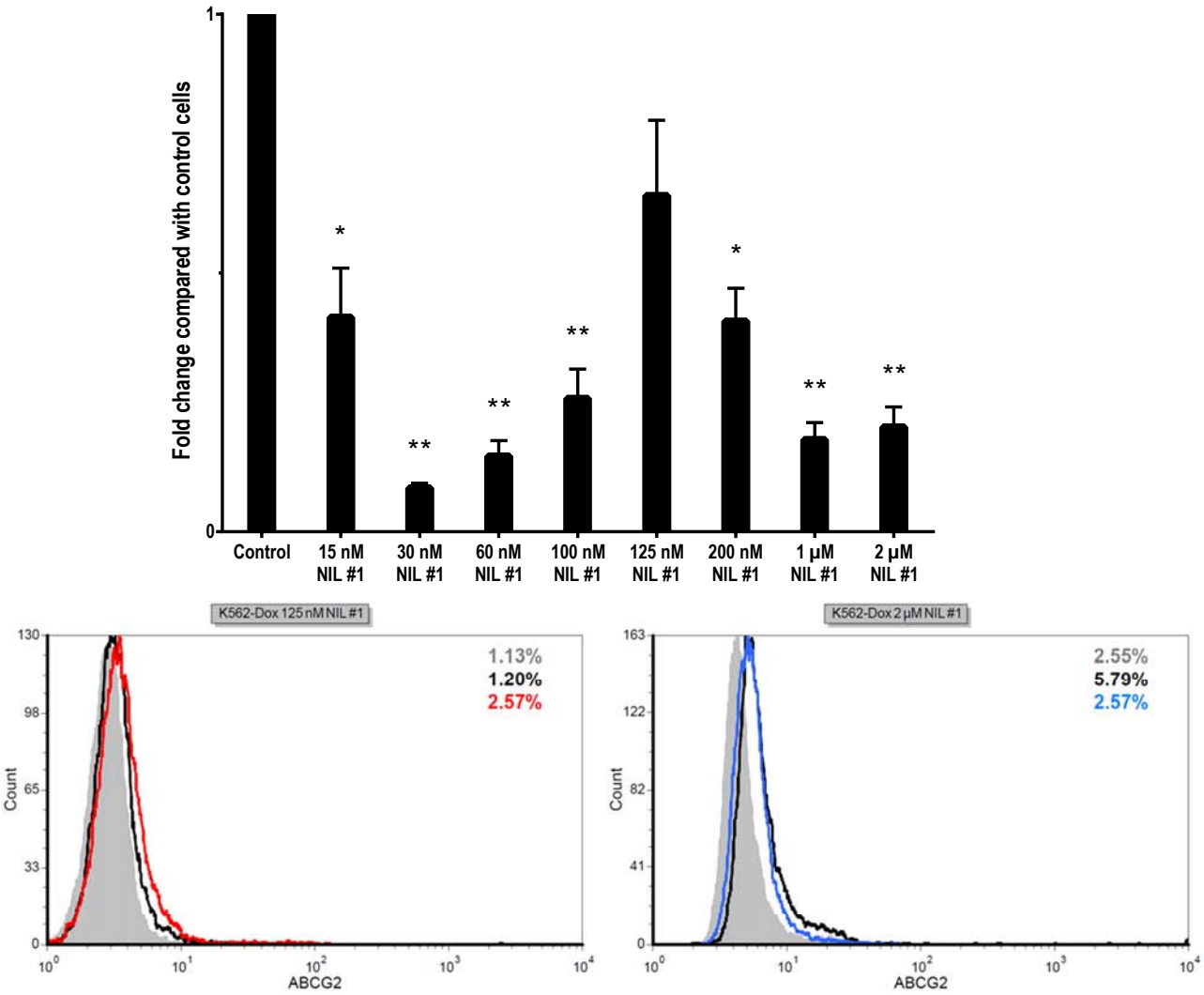

Figure 6.8a: ABCG2 levels do not increase in K562-Dox NIL #1 cells

Expression levels of ABCG2 mRNA and protein were assessed in K562-Dox NIL #1 nilotinib resistance intermediates. Data demonstrate no increase in ABCG2 expression during development of nilotinib resistance: a significant decrease in mRNA expression and no change in protein levels were observed. mRNA expression represents the mean of six independent experiments performed in triplicate while the histograms shown are representative of typical expression levels. The bold **BLACK** lines represent **control cells** while the bold **RED** and **BLUE** lines represent **K562-Dox 125 nM NIL #1** and **K562-Dox 2 µM NIL #1** cells respectively, stained with ABCG2 antibody. The **GREY** filled histograms represent cells stained with **isotype control** antibody. Statistical analyses were performed on mRNA levels as a percentage of BCR using Student's *t*-test. Statistically significant *p*-values are denoted by asterisks (* $p<0.05$; ** $p<0.01$). Error bars represent SEM. NIL=nilotinib.

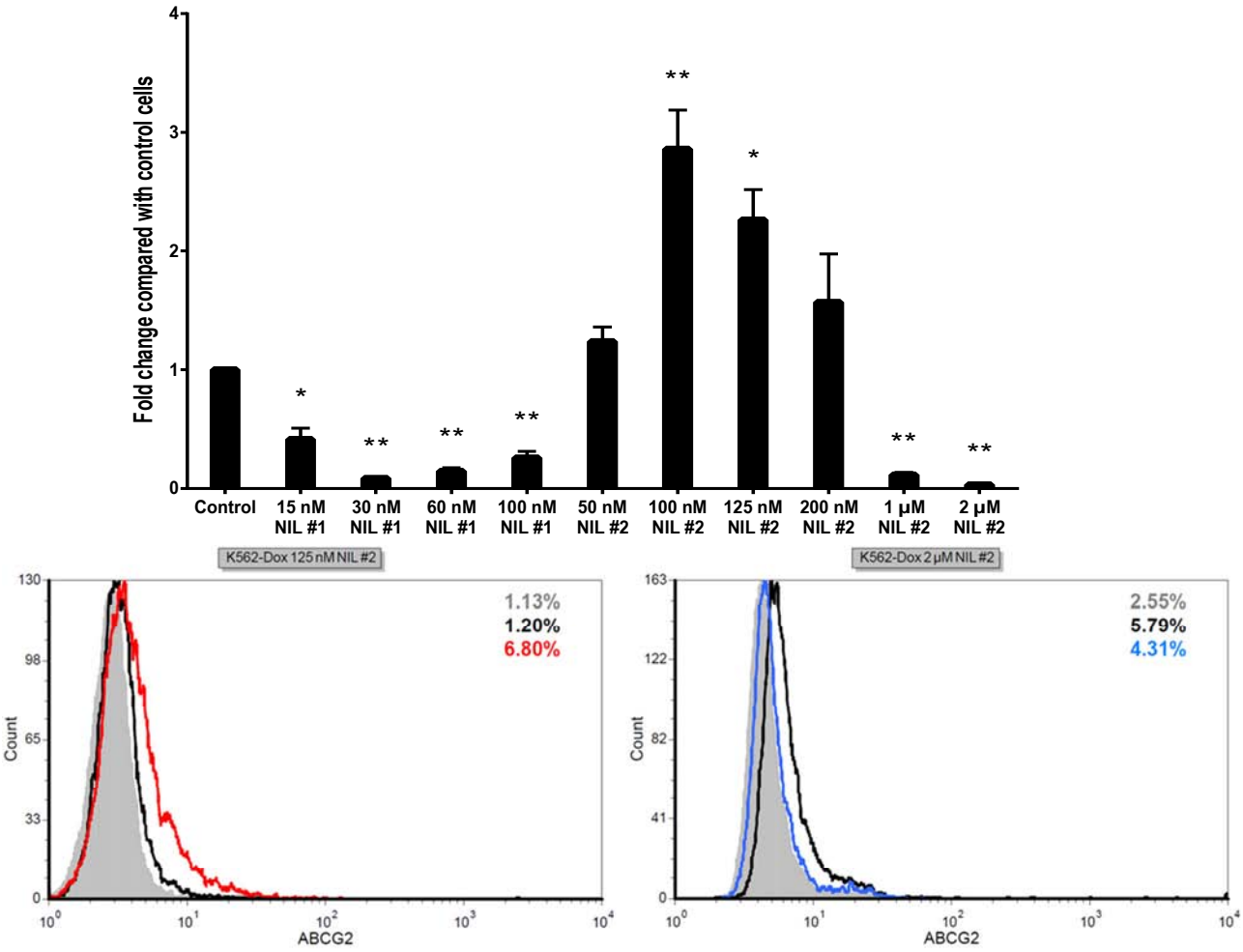

Figure 6.8b: ABCG2 protein levels do not increase in K562-Dox NIL #2 cells

Expression levels of ABCG2 mRNA and protein were assessed in K562-Dox NIL #2 cells. Data demonstrate an increase ABCG2 mRNA in early stage K562-Dox NIL #2 resistance intermediates but this decreases in later stage nilotinib resistance Importantly, this increase in mRNA fails to translate to an increase in ABCG2 protein levels in either K562-Dox 125 nM NIL #2 or K562-Dox 2 µM NIL #2 cells. mRNA expression represents the mean of six independent experiments performed in triplicate while the histograms shown are representative of typical expression levels. The bold **BLACK** lines represent **control** cells while the bold **RED** and **BLUE** lines represent **K562-Dox 125 nM NIL #2** and **K562-Dox 2 µM NIL #2** cells respectively, stained with ABCG2 antibody. The **GREY** filled histograms represent cells stained with **isotype control** antibody. Statistical analyses were performed on mRNA levels as a percentage of BCR using Student's *t*-test. Statistically significant *p*-values are denoted by asterisks (* $p<0.05$; ** $p<0.01$). Error bars represent SEM. NIL=nilotinib.

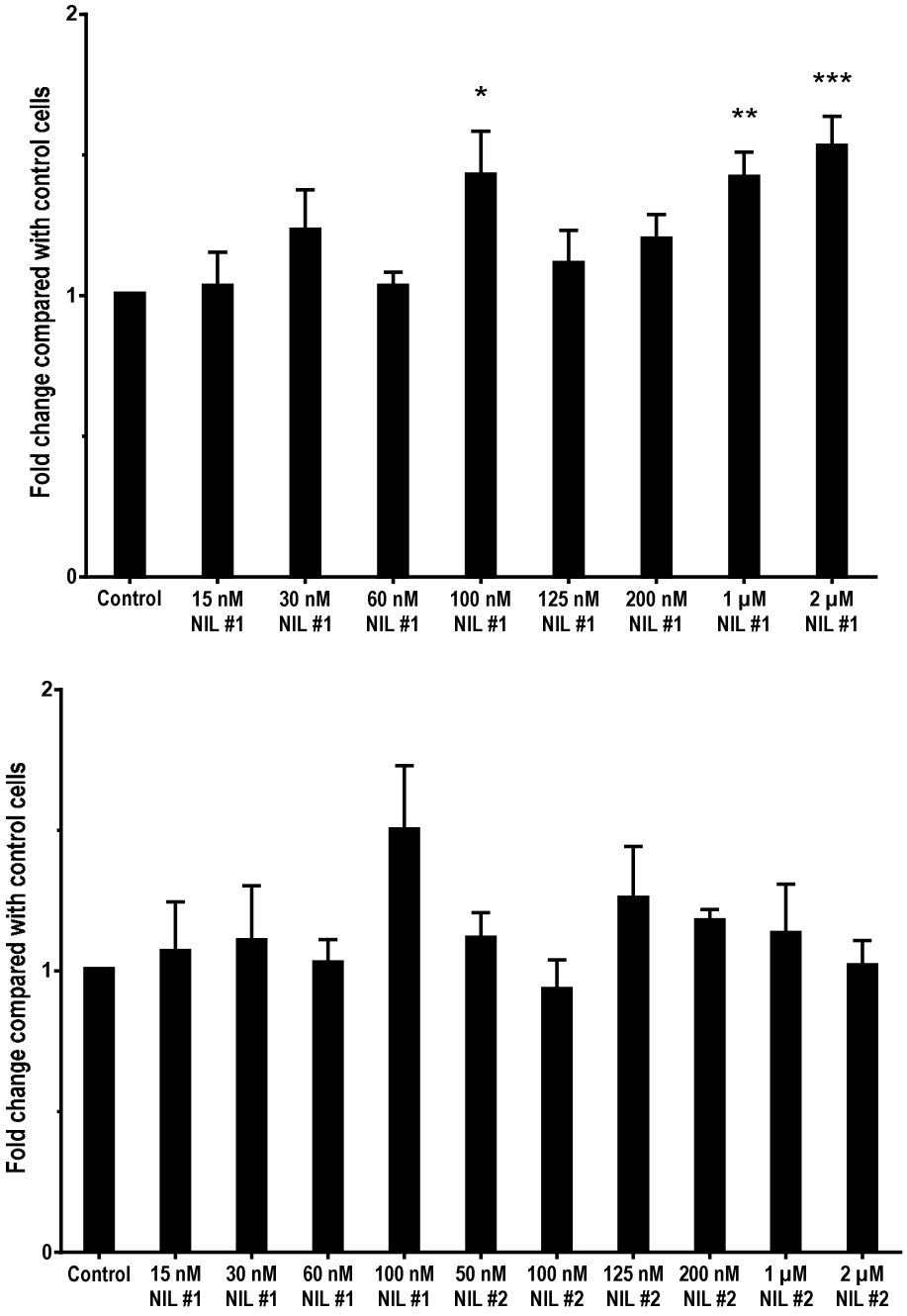

Figure 6.9: ABCC1 levels do not increase in K562-Dox NIL #2 cells

Expression levels of ABCC1 mRNA were assessed in a) K562-Dox NIL #1 and b) K562-Dox NIL #2 cells. Data demonstrate no consistent increase in ABCC1 expression during development of nilotinib resistance. mRNA expression represents the mean of six independent experiments performed in triplicate. Statistical analyses were performed on mRNA levels as a percentage of BCR using Student's *t*-test. Statistically significant *p*-values are denoted by asterisks (* $p<0.05$; ** $p<0.01$; *** $p<0.001$). Error bars represent SEM. NIL=nilotinib.

6.3.5. K562-Dox Cells Cultured in 2 μM Nilotinib Demonstrate Bcr-Abl Independent Resistance to TKIs *In Vitro*

Importantly, while K562 2 μM NIL #1 and K562 2 μM NIL #2 cells demonstrated negligible levels of ABCB1, they were still completely resistant to three currently available TKIs. K562-Dox 2 μM NIL #1 cells demonstrated significantly increased survival compared with control cells when exposed to 1000 nM nilotinib for 72 h: 44% vs 120% viable cells (p=0.002; **Figure 6.10a**). Survival also increased in the presence of 5 μM imatinib with viable cells increasing from 39% to 103% (p<0.001) and in the presence of 500 nM dasatinib from 37% to 102% (p<0.001; **Figure 6.10b and c**). Similar results were observed in K562 2 μM NIL #2 cells: the percentage of viable cells in the presence of 1000 nM nilotinib increased from 44% to 112% (p<0.001), viable cells in the presence of 5 μM imatinib increased from 39% to 109% (p<0.001), and viable cells in the presence of 500 nM dasatinib increased from 37% to 106% (p<0.001; **Figure 6.10a–c**).

Interestingly, the $IC50^{NIL}$, $IC50^{IM}$ and $IC50^{DAS}$ were all significantly decreased in both cell lines indicating a Bcr-Abl *independent* mode of resistance. In K562-Dox 2 μM NIL #1 cells, the $IC50^{NIL}$ decreased significantly when compared with control cells (507 nM to 106 nM, p<0.001). Similar results were observed for K562-Dox 2 μM NIL #2 cells: $IC50^{NIL}$=159 nM, p<0.001 (**Figure 6.11a**). Likewise, $IC50^{IM}$ decreased significantly in both K562-Dox 2 μM NIL #1 (760 nM, p=0.001) and K562-Dox 2 μM NIL #2 (1.1 μM, p=0.003) when compared with control cells (10.4 μM, **Figure 6.11b**). $IC50^{DAS}$ decreased from 108 nM in control cells to 2.3 nM and 2.4 nM, K562-Dox 2 μM NIL #1 and K562-Dox 2 μM NIL #2 respectively (p=0.001, **Figure 6.11c**). $IC50^{PON}$ decreased from 10.1 nM in control cells to 4.2 nM in K562 2 μM NIL #2 cells (p<0.001, **Figure 6.11d**).

6.3.6. p-Crkl Protein Levels Provide an Accurate Surrogate for Bcr-Abl Kinase Activity

It has recently been proposed that p-Crkl protein levels may not accurately reflect Bcr-Abl activity[291].

(a)

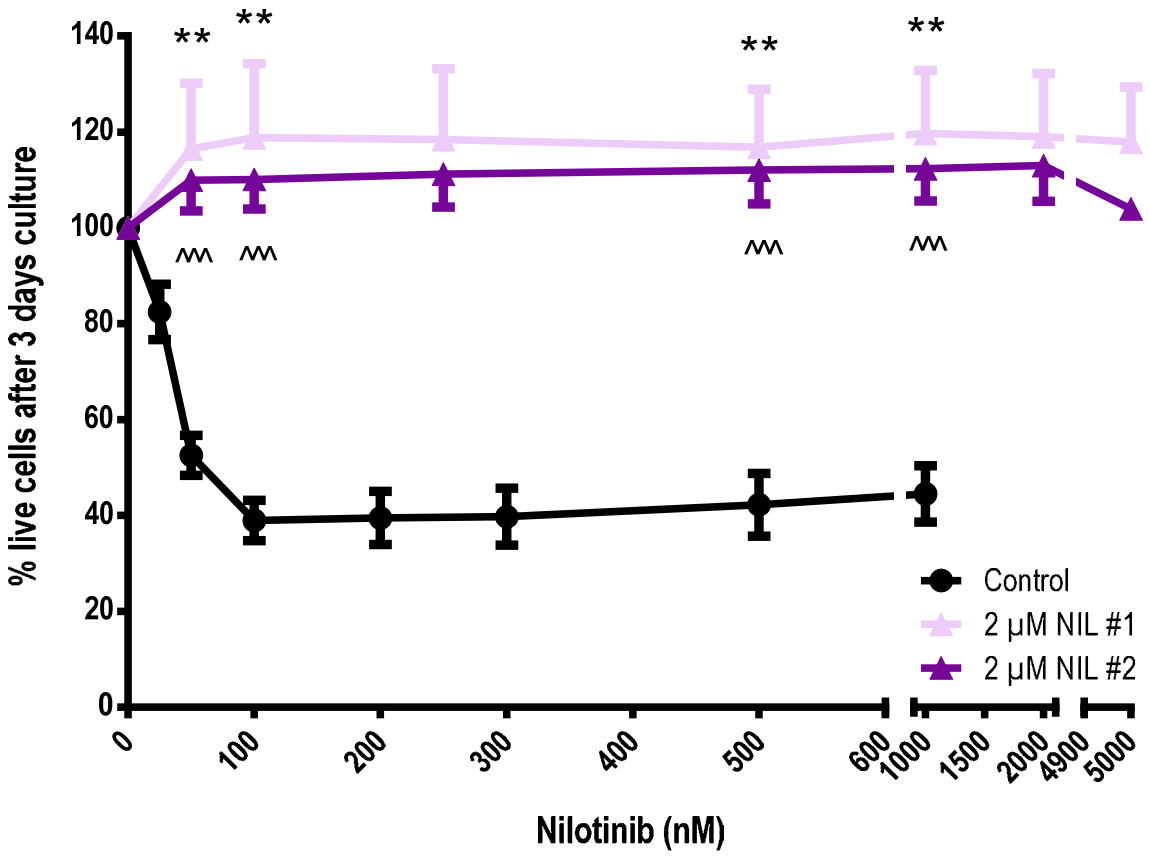

Figure 6.10: K562-Dox 2 µM NIL #1 and K562-Dox 2 µM NIL #2 cells have significantly decreased TKI-mediated cell death

Cells were cultured for 72 h in increasing concentrations of a) nilotinib b) imatinib and c) dasatinib and cell death determined by Annexin V/7-AAD staining. Data demonstrate that K562-Dox 2 µM NIL #1 and K562-Dox 2 µM NIL #2 cells have increased survival in the presence of TKIs when compared with control cells. Results were confirmed visually and with trypan blue staining (**Appendices 4B** and **4C**). The FACS plots shown are representative of at least three separate experiments performed in triplicate with the corresponding survival curves representing the mean. Data were normalised to 0 nM TKI with control values set at 100% live cells. Statistical analyses were performed using Student's *t*-test with statistically significant *p*-values denoted by asterisks and carets representing K562-Dox 2 µM NIL #1 and K562-Dox 2 µM NIL #2 cell lines respectively (** $p<0.01$; *** $p<0.001$). Error bars represent SEM. NIL=nilotinib; IM=imatinib; DAS=dasatinib.

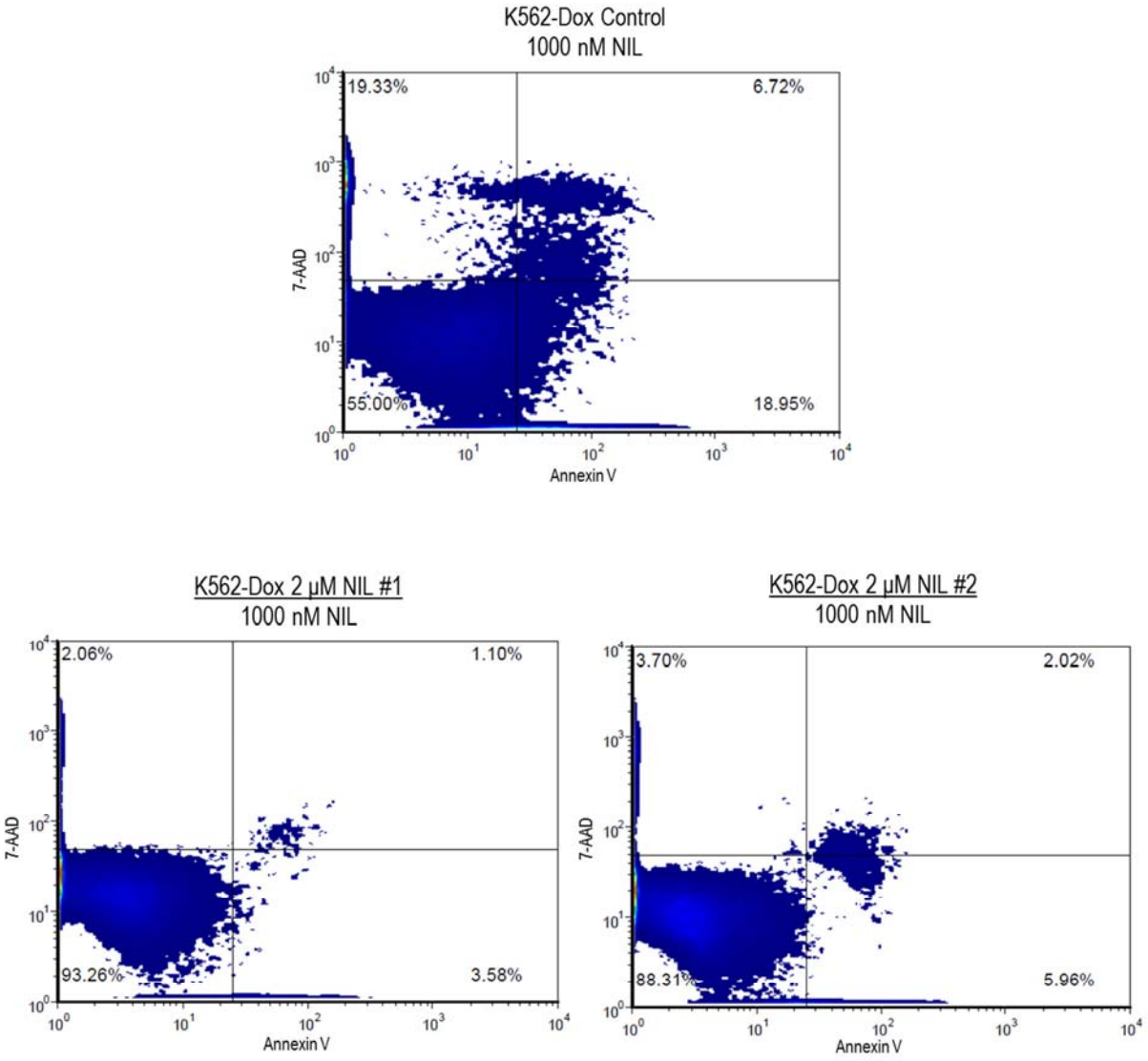
K562-Dox Control
1000 nM NIL
19.33%
6.72%
55.00%
18.95%
7-AAD
Annexin V
K562-Dox 2 µM NIL #1
1000 nM NIL
2.06%
1.10%
93.26%
3.58%
7-AAD
Annexin V
K562-Dox 2 µM NIL #2
1000 nM NIL
3.70%
2.02%
88.31%
5.96%
7-AAD
Annexin V

(b)

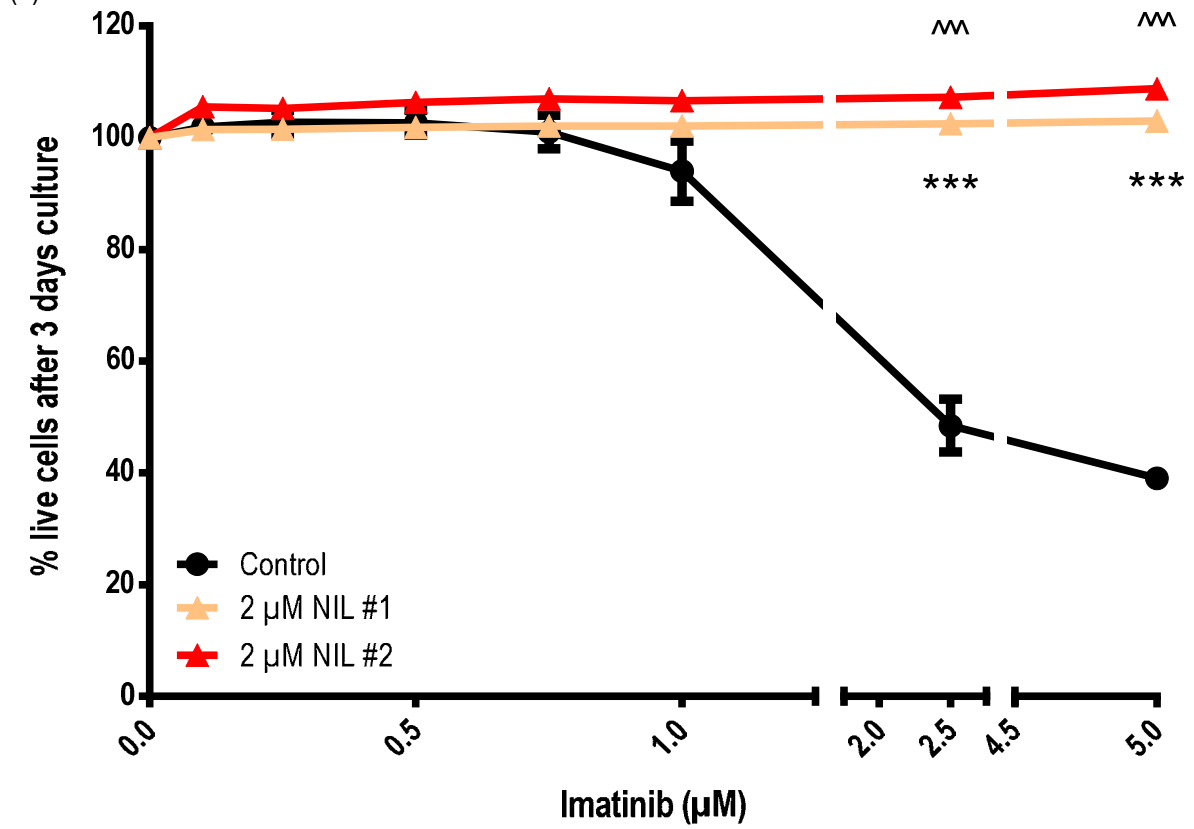
120
100
80
60
40
20
0
% live cells after 3 days culture
***
***
Control
2 μM NIL #1
2 μM NIL #2
0.0
0.5
1.0
2.0
2.5
4.5
5.0
Imatinib (μM)

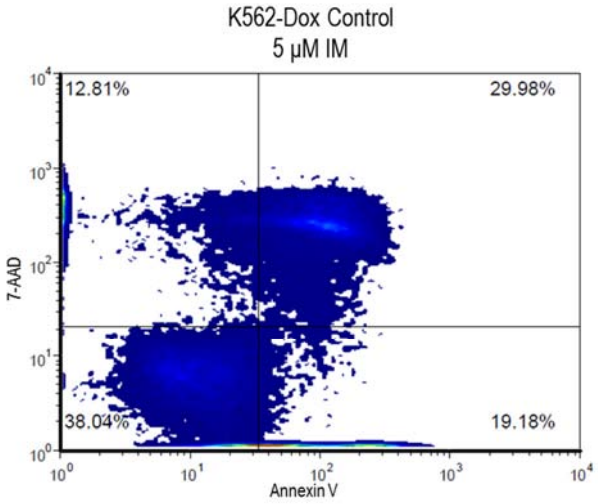
K562-Dox Control
5 μM IM
12.81%
29.98%
38.04%
19.18%
7-AAD
Annexin V

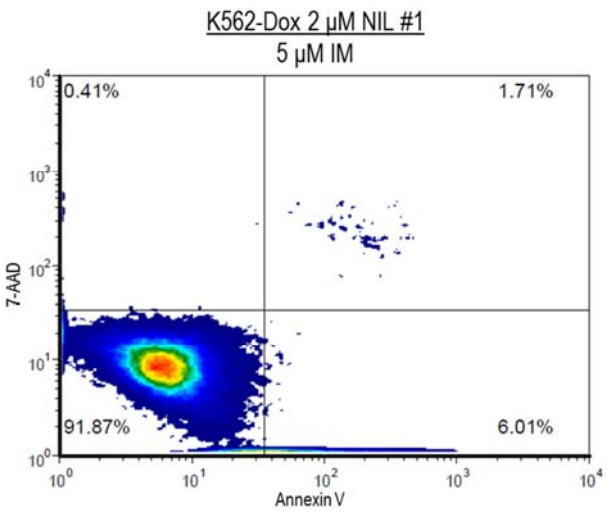
K562-Dox 2 μM NIL #1
5 μM IM
0.41%
1.71%
91.87%
6.01%
7-AAD
Annexin V

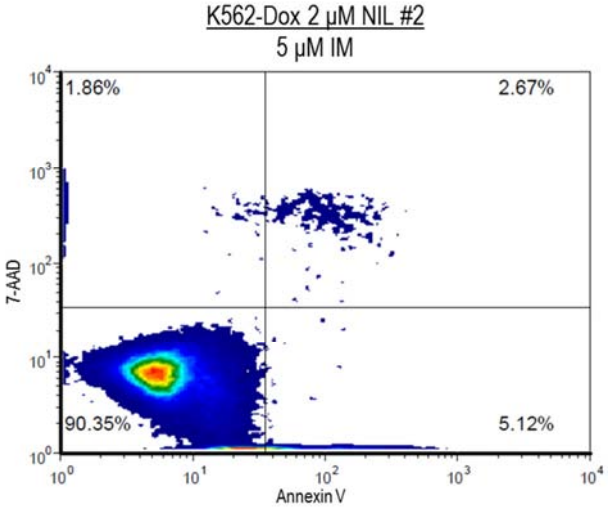
K562-Dox 2 μM NIL #2
5 μM IM
1.86%
2.67%
90.35%
5.12%
7-AAD
Annexin V

(c)

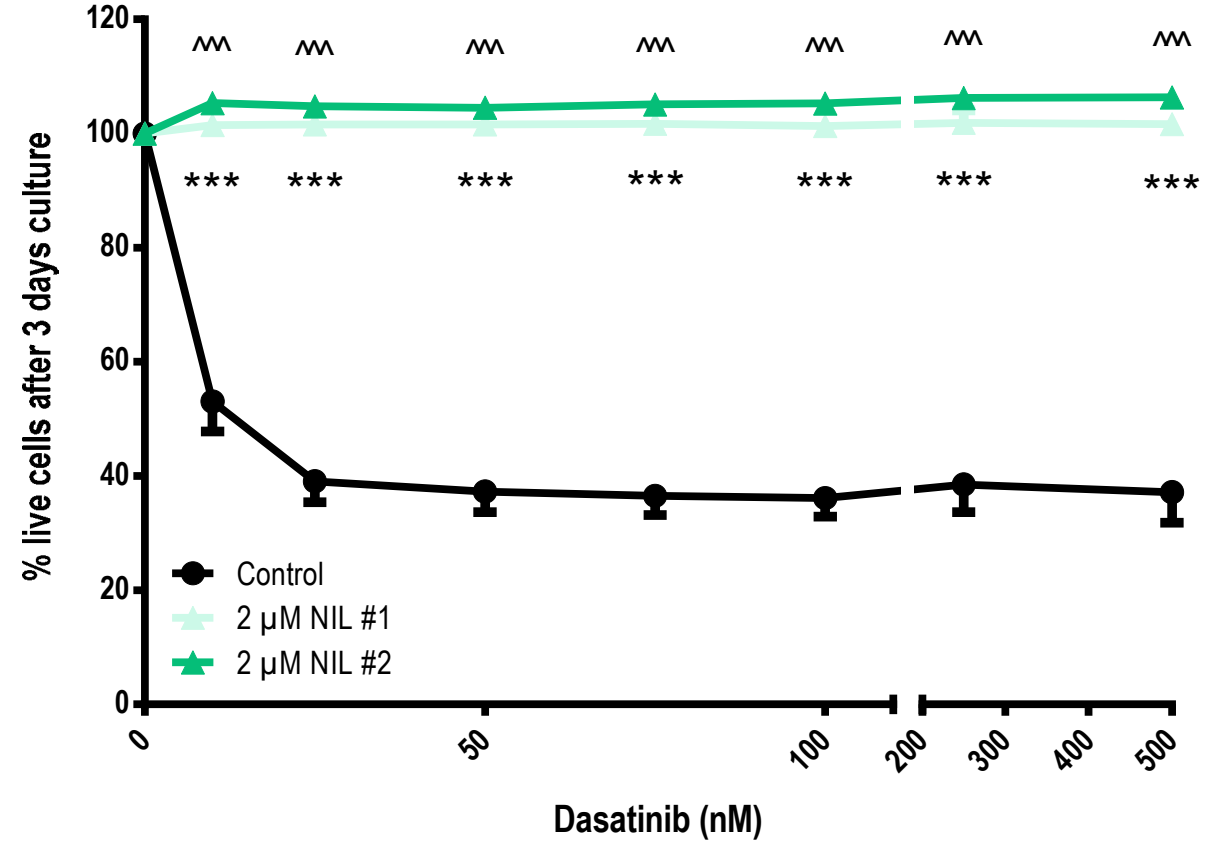
% live cells after 3 days culture
120
100
80
60
40
20
0
***
Control
2 µM NIL #1
2 µM NIL #2
0
50
100
200
300
400
500
Dasatinib (nM)

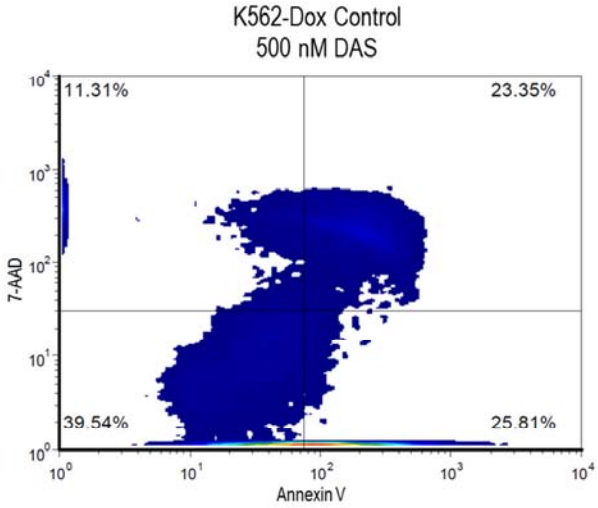
K562-Dox Control
500 nM DAS
11.31%
23.35%
39.54%
25.81%
7-AAD
Annexin V

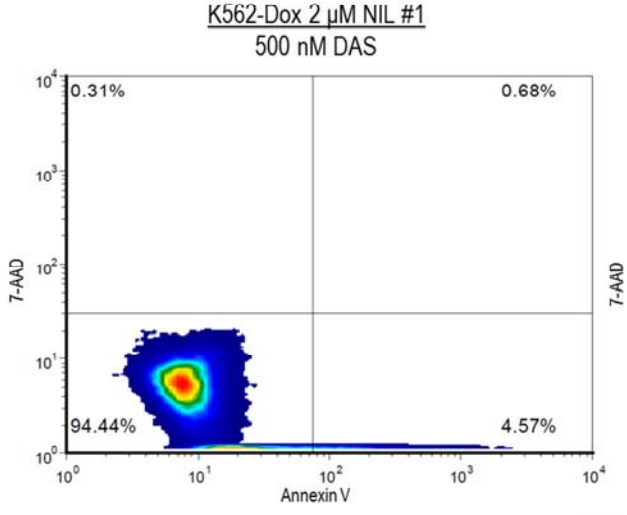
K562-Dox 2 µM NIL #1
500 nM DAS
0.31%
0.68%
94.44%
4.57%
7-AAD
Annexin V

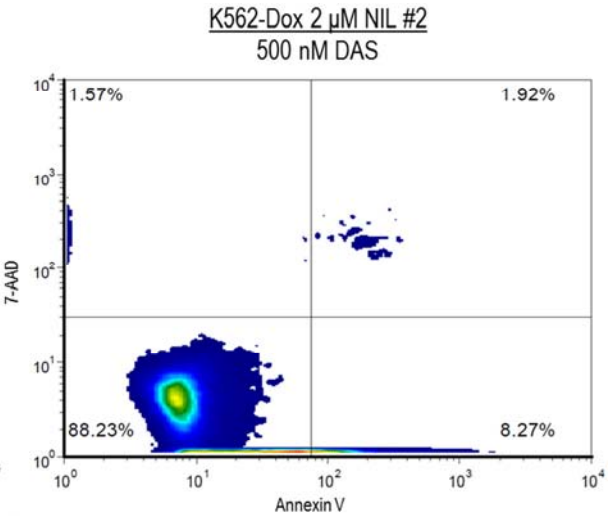
K562-Dox 2 µM NIL #2
500 nM DAS
1.57%
1.92%
88.23%
8.27%
7-AAD
Annexin V

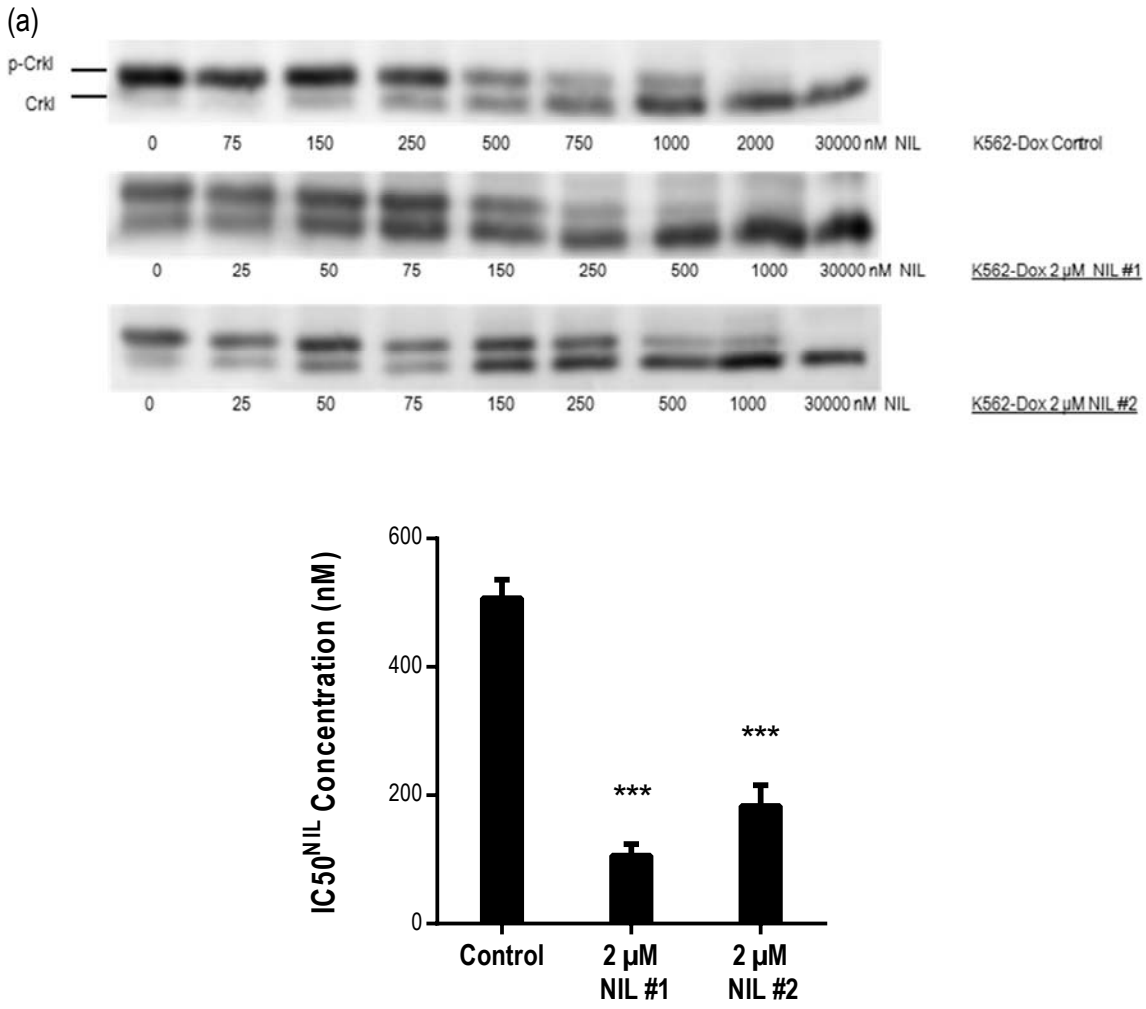

Figure 6.11: K562-Dox 2 µM NIL #1 and K562-Dox 2 µM NIL #2 cells have significantly decreased IC50

IC50 was determined via incubating cells for 2 h at 37°C in the presence of increasing concentrations of a) nilotinib, b) imatinib, c) dasatinib and d) ponatinib. Crkl western blot was performed to determine the concentration of TKI required for 50% Bcr-Abl kinase inhibition. Data demonstrate that both K562-Dox 2 µM NIL #1 and K562-Dox 2 µM NIL #2 cells have significantly decreased IC50 when compared with control cells. The western blot analyses shown are representative of at least three separate experiments with the corresponding densitometry analysis representing the mean. Statistical analyses were performed using Student's *t*-test with statistically significant *p*-values denoted by asterisks (*** $p<0.001$). Error bars represent SEM. NIL=nilotinib; IM=imatinib; DAS=dasatinib; PON=ponatinib.

(b)

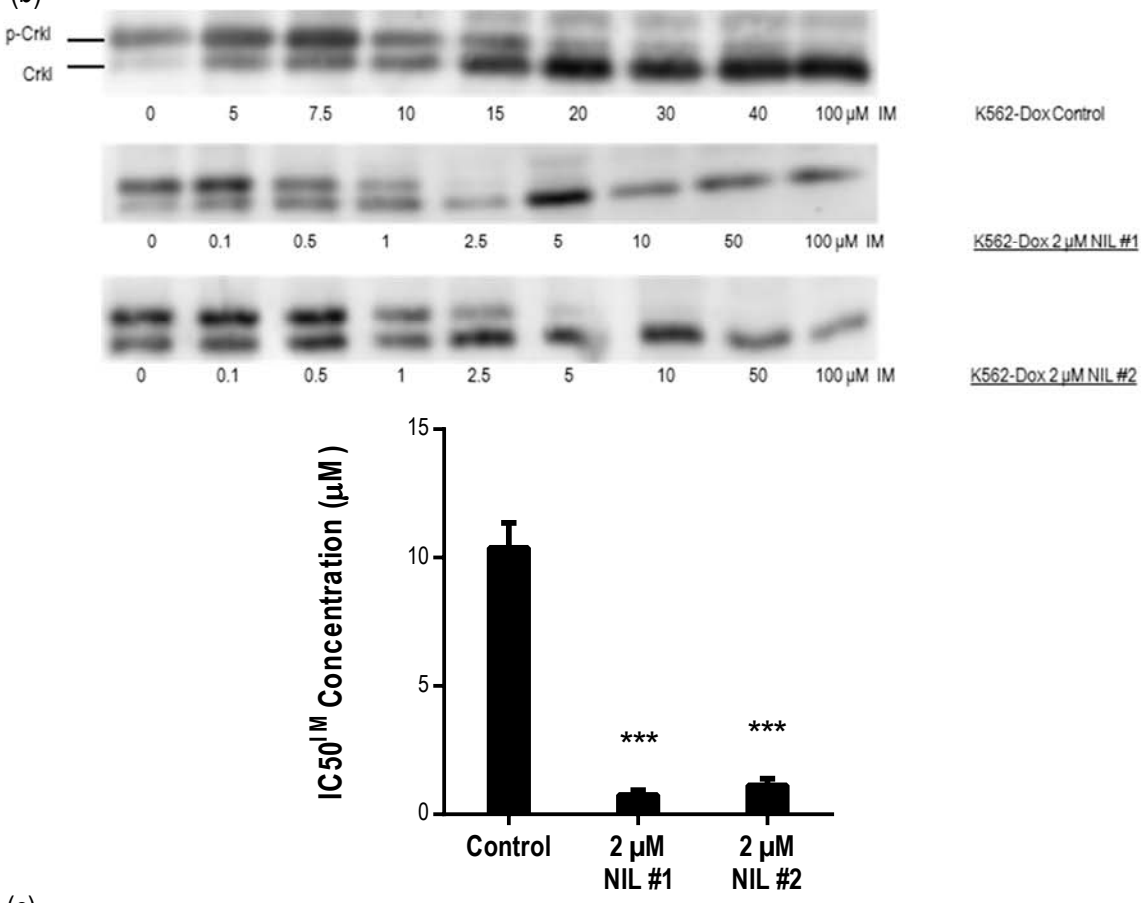
p-Crkl
Crkl
0 5 7.5 10 15 20 30 40 100 µM IM
K562-Dox Control
0 0.1 0.5 1 2.5 5 10 50 100 µM IM
K562-Dox 2 µM NIL #1
0 0.1 0.5 1 2.5 5 10 50 100 µM IM
K562-Dox 2 µM NIL #2
IC50IM Concentration (µM)
15
10
5
0
***
***
Control
2 µM NIL #1
2 µM NIL #2

(c)

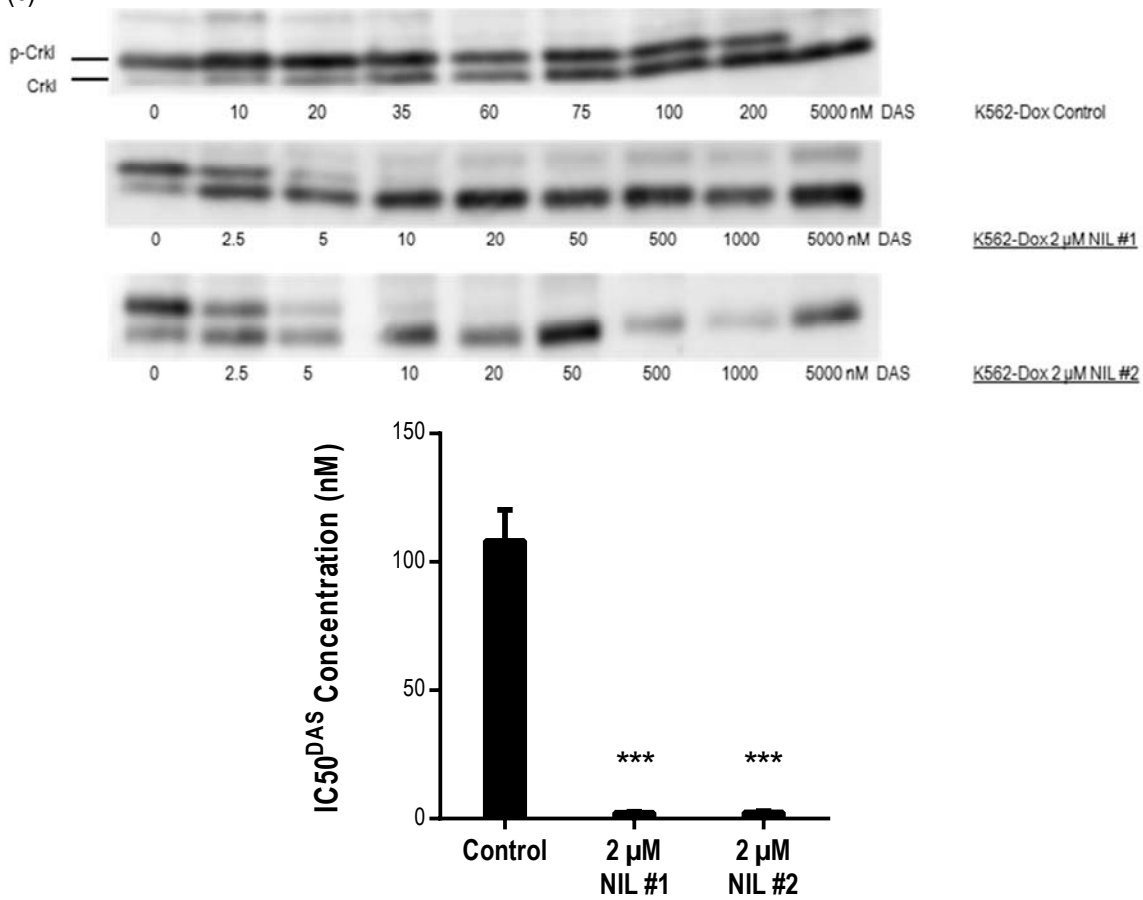
p-Crkl
Crkl
0 10 20 35 60 75 100 200 5000 nM DAS
K562-Dox Control
0 2.5 5 10 20 50 500 1000 5000 nM DAS
K562-Dox 2 µM NIL #1
0 2.5 5 10 20 50 500 1000 5000 nM DAS
K562-Dox 2 µM NIL #2
IC50DAS Concentration (nM)
150
100
50
0
***
***
Control
2 µM NIL #1
2 µM NIL #2

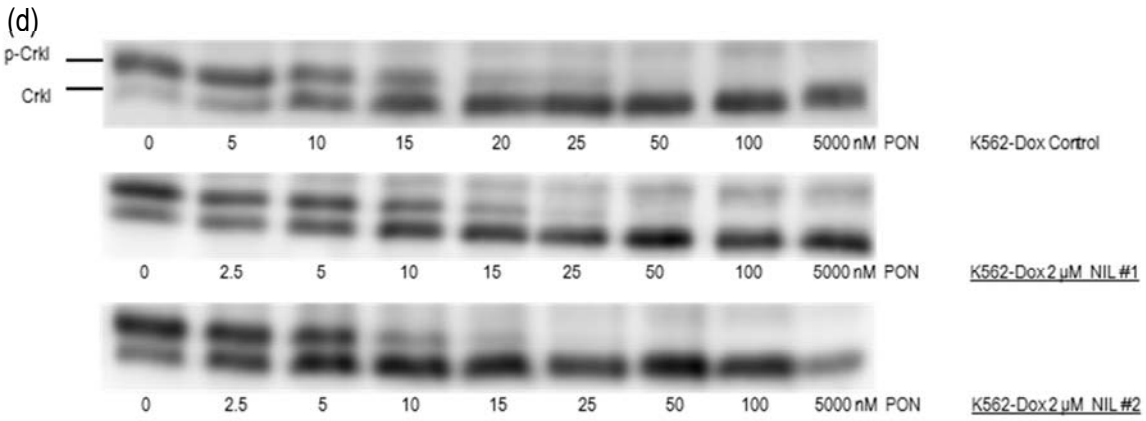
(d)
p-Crkl
Crkl
0 5 10 15 20 25 50 100 5000 nM PON
K562-Dox Control
0 2.5 5 10 15 25 50 100 5000 nM PON
K562-Dox 2 µM NIL #1
0 2.5 5 10 15 25 50 100 5000 nM PON
K562-Dox 2 µM NIL #2

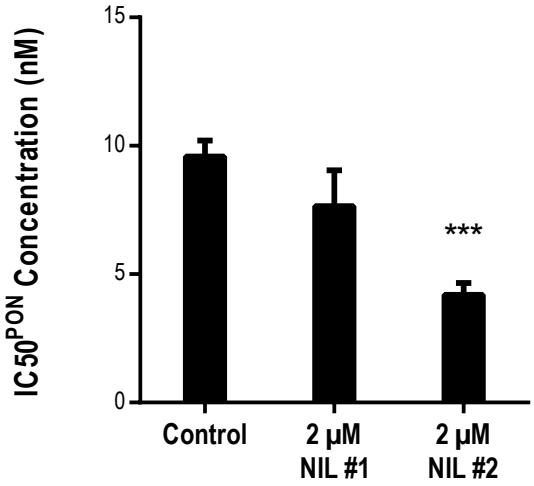
IC50PON Concentration (nM)
15
10
5
0
***
Control
2 µM NIL #1
2 µM NIL #2

Thus, in order to determine whether p-Crkl protein constitutes a valid surrogate marker for Bcr-Abl activity, protein levels of p-Crkl as well as Bcr-Abl and phosphorylated Bcr-Abl (p-Bcr-Abl) were assessed in cells incubated in increasing concentrations of nilotinib. Indeed, results demonstrated that p-Crkl inhibition parallels Bcr-Abl kinase inhibition with a steady decrease in levels of both p-Crkl and p-Bcr-Abl in the presence of increasing concentrations of nilotinib. Importantly, levels of total Bcr-Abl protein remained constant Furthermore, levels of p-Bcr-Abl in nilotinib resistant cells demonstrated sufficient inhibition of Bcr-Abl kinase activity despite resistance to 2 µM nilotinib thus confirming results from p-Crkl specific $IC50^{NIL}$ (**Figure 6.12**).

6.3.7. Bcr-Abl Inhibition in K562-Dox 2 µM NIL #1 and K562-Dox 2 µM NIL #2 cells is Reversed upon Drug Washout

Following the validation of p-Crkl as an indicator of Bcr-Abl kinase activity, it was necessary to confirm that the resistance mechanism present in these cells was Bcr-Abl independent. Thus nilotinib was removed from the culture media by thorough washing and K562-Dox 2 µM NIL #1 and K562-Dox 2 µM NIL #2 cells allowed equilibrate overnight. Total Bcr-Abl levels and p-Bcr-Abl levels were then determined and compared with the levels in cells that remained in culture with nilotinib. Results demonstrated that in both cell lines kinase activity was completely inhibited in the presence of nilotinib causing a significant decrease in p-Bcr-Abl protein levels when compared with control cells ($p<0.05$). However, upon drug washout, reactivation of the Bcr-Abl kinase occurred resulting in similar levels of p-Bcr-Abl in both resistant and control cells ($p>0.05$). Importantly, total Bcr-Abl levels remained unaffected in the absence and presence of nilotinib (**Figure 6.13**). Thus, while nilotinib was effective at inhibiting Bcr-Abl kinase activity, both cell lines demonstrated complete resistance indicating the presence of a genuine Bcr-Abl independent resistance mechanism.

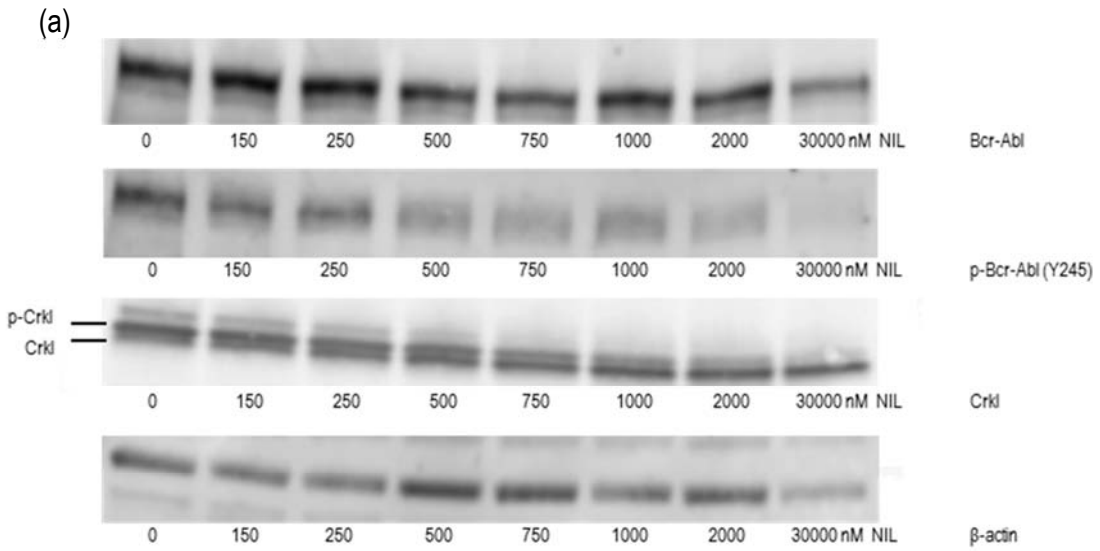

Figure 6.12: p-Crkl protein levels reflect Bcr-Abl kinase activity in the presence of nilotinib

a) K562-Dox control, b) K562-Dox 2 μM NIL #1 and c) K562-Dox 2 μM NIL #2 cells were incubated for 2 h at 37°C in the presence of increasing concentrations of nilotinib. Western blot for total Bcr-Abl, p-Bcr-Abl, Crkl and β-actin were performed. Data demonstrate that levels of total Bcr-Abl remain constant in the presence of nilotinib, however, levels of p-Bcr-Abl decrease as nilotinib concentration increases. Levels of p-Crkl decrease concordantly indicating this protein is a valid surrogate for Bcr-Abl kinase activity. The western blot analyses shown are representative of three separate experiments. NIL=nilotinib.

(b)

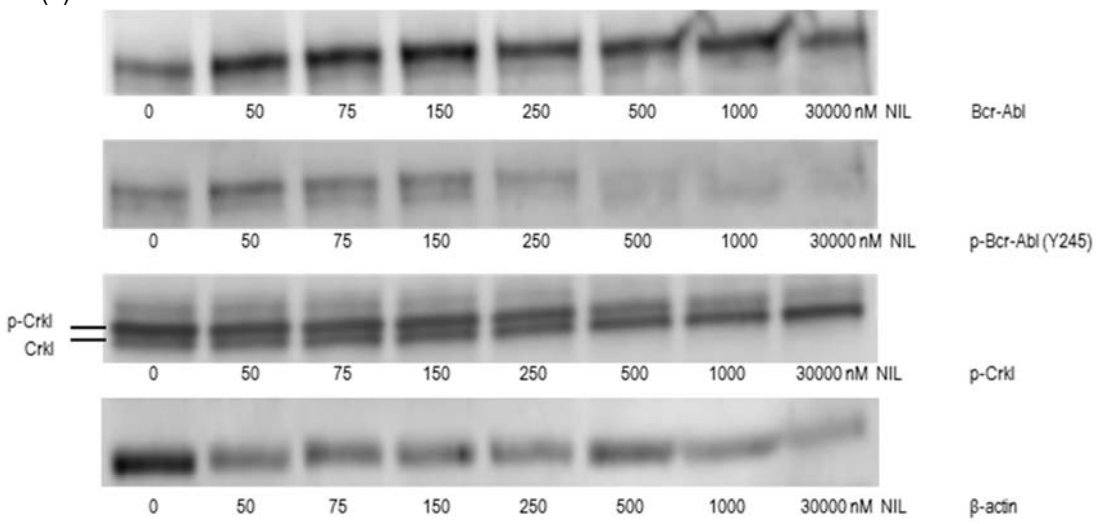
0 50 75 150 250 500 1000 30000 nM NIL
Bcr-Abl
0 50 75 150 250 500 1000 30000 nM NIL
p-Bcr-Abl (Y245)
p-Crkl
Crkl
0 50 75 150 250 500 1000 30000 nM NIL
p-Crkl
0 50 75 150 250 500 1000 30000 nM NIL
β-actin

(c)

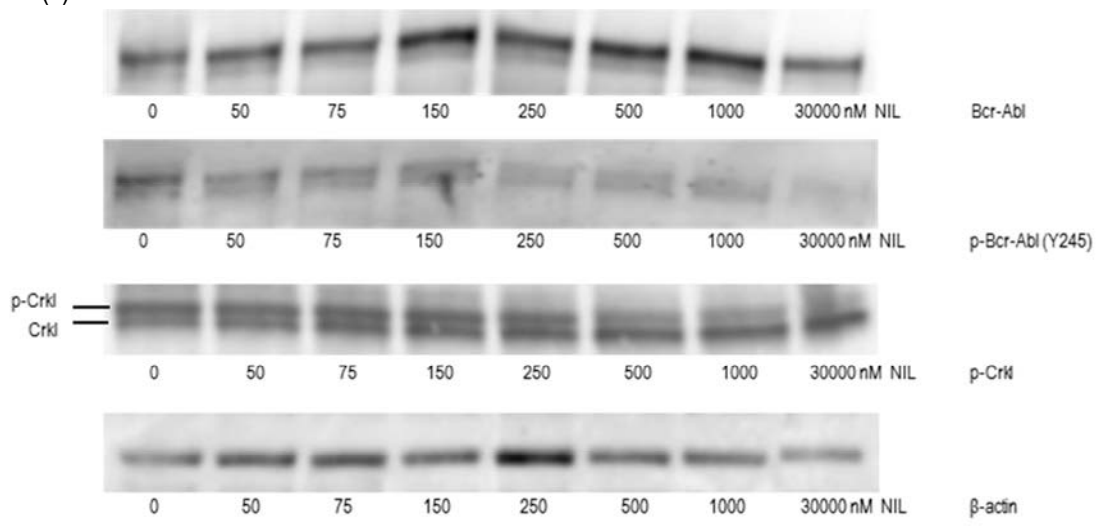
0 50 75 150 250 500 1000 30000 nM NIL
Bcr-Abl
0 50 75 150 250 500 1000 30000 nM NIL
p-Bcr-Abl (Y245)
p-Crkl
Crkl
0 50 75 150 250 500 1000 30000 nM NIL
p-Crkl
0 50 75 150 250 500 1000 30000 nM NIL
β-actin

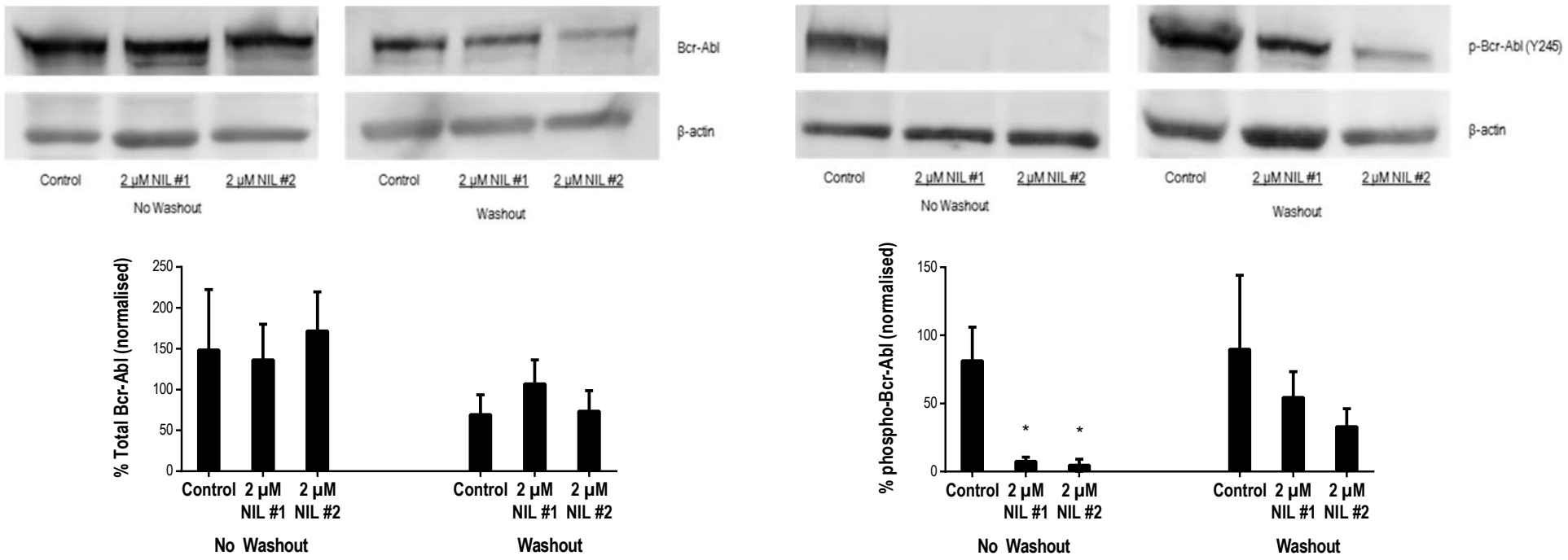

Figure 6.13: Bcr-Abl activity is inhibited in <u>K562-Dox 2 μM NIL #1</u> and <u>K562-Dox 2 μM NIL #2</u> cells; kinase reactivation occurs upon drug washout

Total Bcr-Abl and p-Bcr-Abl protein levels were determined in K562-Dox cells either cultured continuously in 2 μM nilotinib or thoroughly washed and cultured overnight in the absence of nilotinib. Data demonstrate that total Bcr-Abl levels remain constant in the absence or presence nilotinib. Conversely, levels of p-Bcr-Abl, which are significantly reduced in the presence of nilotinib, increase to levels comparable with those in control cells upon nilotinib washout, thus indicating Bcr-Abl *independent* resistance. Western blot analyses shown are representative of three separate experiments with the corresponding quantitation representing the mean. Bcr-Abl levels were normalised to β-actin control. Statistical analyses were performed using Student's *t*-test with statistically significant *p*-values denoted by asterisks (* $p<0.05$). Error bars represent SEM. NIL=nilotinib.

6.3.8. No Increase in Lyn or Axl Expression or Activity was Observed in Nilotinib Resistant K562-Dox Cells

While it has already been established that Lyn and Bcr-Abl engage in reciprocal phosphorylation thus rendering Lyn overexpression and/or activation a Bcr-Abl *dependent* mechanism of resistance[123,158,160], persistent activation of Lyn may be the result of a conformational change induced by a point mutation[125]. Hence, mRNA and protein levels of Lyn and Axl, two common tyrosine kinases involved in nilotinib resistance, were determined. However, results demonstrated that neither mRNA (**Figure 6.14a**) nor protein (**Figure 6.15a**) levels of Lyn increased significantly; in fact, Lyn levels decreased, although this failed to reach statistical significance. There was also no increase in Lyn activity, with p-Lyn (Y396) levels in both K562-Dox 2 µM NIL #1 and K562-Dox 2 µM NIL #2 cells slightly reduced when compared with those in control cells, although again, this failed to reach statistical significance (**Figure 6.15a**). Similarly, there was also no increase in Axl mRNA (**Figure 6.14b**) nor in total and p-Axl (Y779) protein levels (**Figure 6.15b**). Levels of total Axl protein appeared decreased when compared with control cell levels, although this also failed to reach statistical significance. Levels of Syk and p-Syk (Y525/526) were undetectable in both control and resistant cells (**Figure 6.15c**).

6.3.9. Total Tyrosine Phosphorylation is Decreased in Nilotinib Resistant K562-Dox Cells

In the case of Bcr-Abl independent resistance, activation of alternative signalling pathways such as JAK-STAT[286,287] and PI3-K[129,288] may occur. For this reason, total tyrosine phosphorylation in K562-Dox 2 µM NIL #1 and K562-Dox 2 µM NIL #2 cells was assessed via flow cytometry. Results demonstrated that, in both resistant cell lines, tyrosine phosphorylation significantly decreased when compared with control cells. The percentage of cells staining positive for 4G10 antibody deceased significantly from 78.1% in control cells to 2.2% and 4.1% in K562-Dox 2 µM NIL #1 and K562-Dox 2 µM NIL #2 cells respectively ($p<0.001$, **Figure 6.16a**). Further investigation into specific effector molecules contained in these pathways (**Figure 6.1**) demonstrated a reduction in phosphorylation of Akt (T308), Erk

(a)

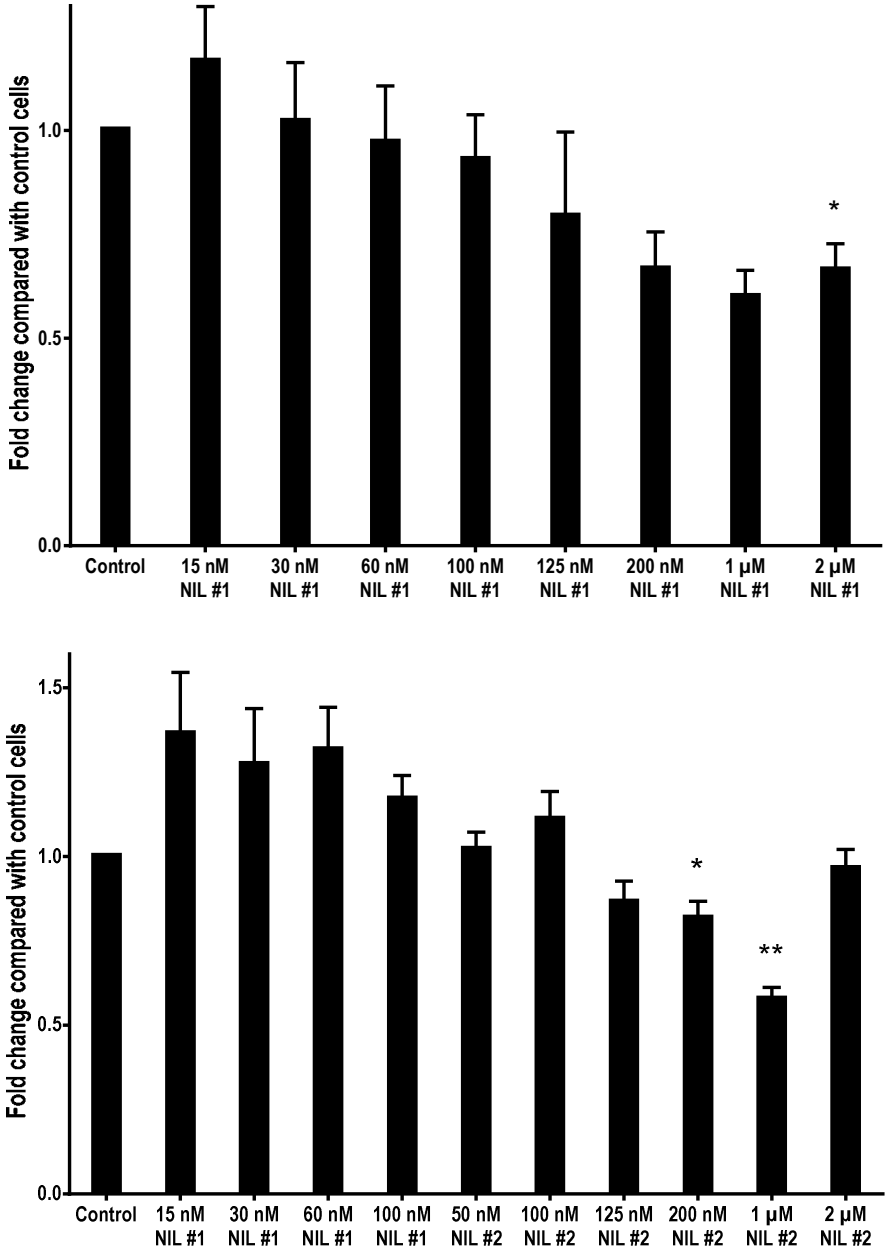

Figure 6.14: Lyn and Axl mRNA levels do not increase during development of nilotinib resistance in K562-Dox Cells

Expression levels of a) Lyn and b) Axl mRNA were assessed in K562-Dox nilotinib resistance intermediates. Data demonstrate no increase in either Lyn or Axl expression at any time during development of resistance. mRNA expression represents the mean of at least three independent experiments performed in triplicate. Statistical analyses were performed on mRNA levels as a percentage of GusB using Student's *t*-test with statistically significant *p*-values denoted by asterisks (* $p<0.05$; ** $p<0.01$). Error bars represent SEM. NIL=nilotinib.

(b)

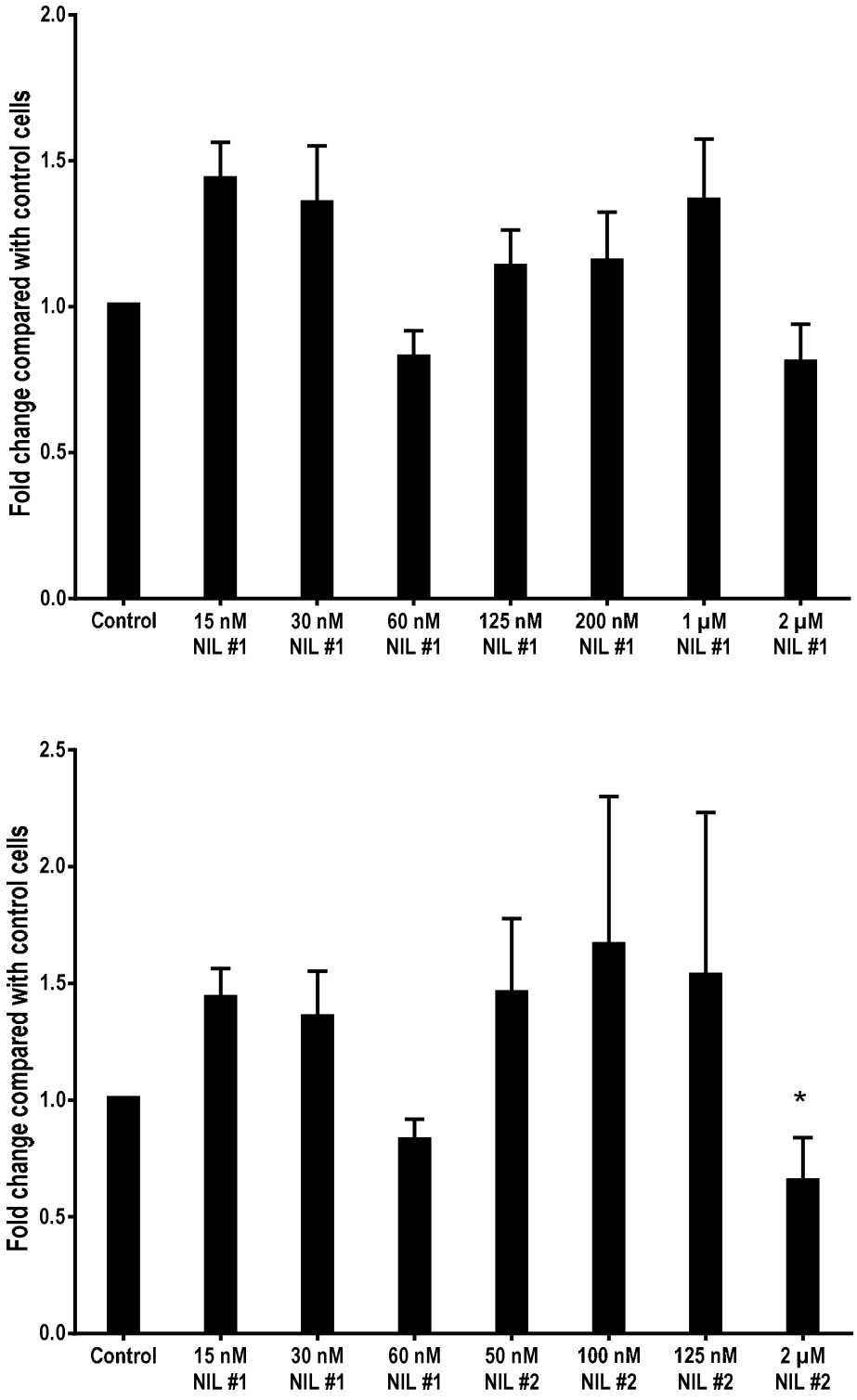

Figure 6.14 (continued): Lyn and Axl mRNA levels do not increase during development of nilotinib resistance in K562-Dox Cells

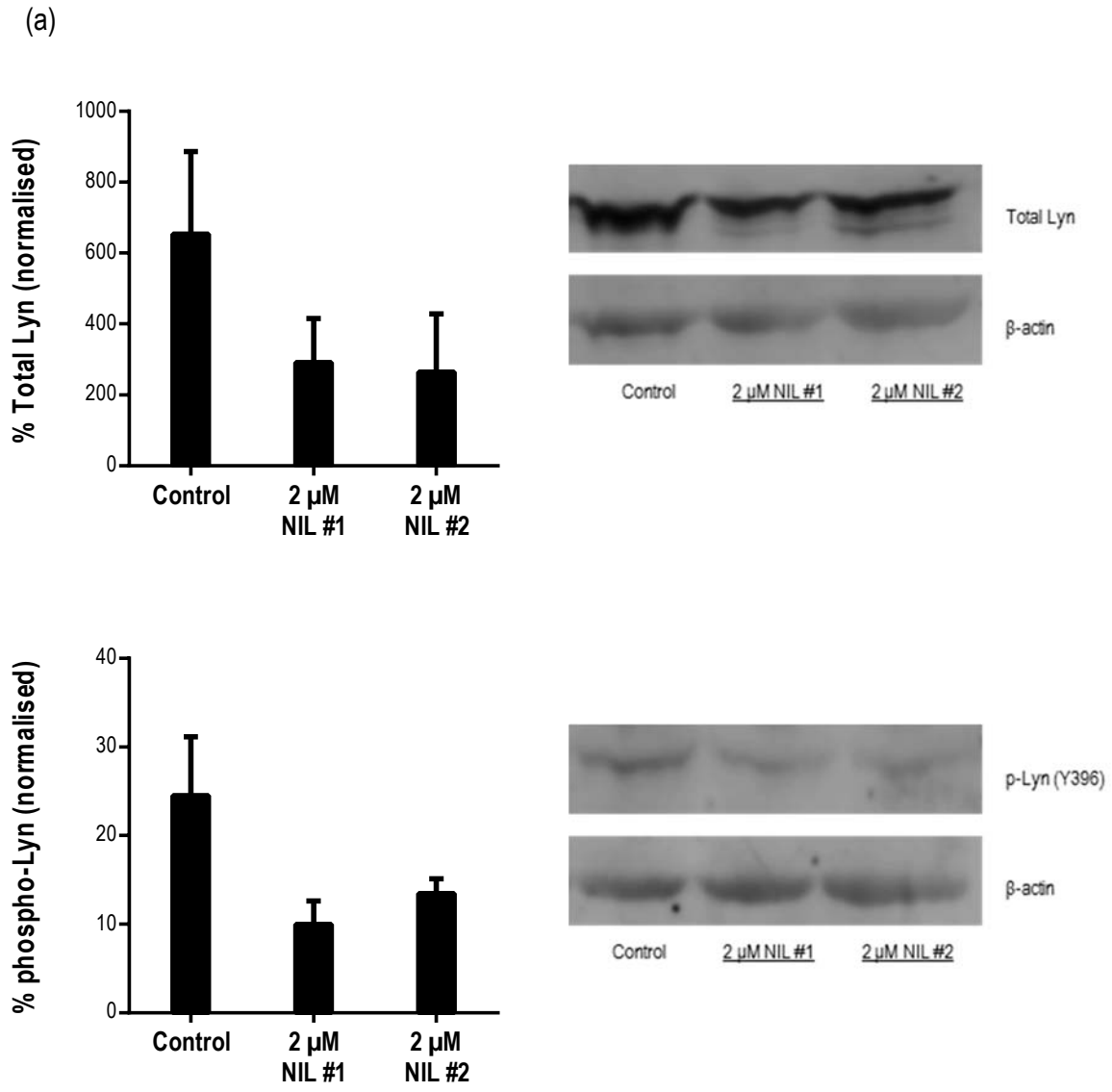

Figure 6.15: Nilotinib resistant K562-Dox cells do not exhibit increased expression or activity of Lyn, Axl or Syk proteins

Protein expression levels of a) Lyn, b) Axl and c) Syk were assessed in K562-Dox control and resistant cells. Data demonstrate that there is no increase in expression of Lyn, Axl or Syk proteins; importantly there is also no increase in levels of p-Lyn (Y396), p-Axl (Y779) or p-Syk (Y525/526) indicating no increase in activity of these proteins. Western blot analyses shown are representative of at least three separate experiments with the corresponding quantitation representing the mean. Protein levels were normalised to β-actin control. Error bars represent SEM. Ramos cells stimulated with goat anti-human IgM provide the positive control for Syk protein. NIL=nilotinib.

(b)

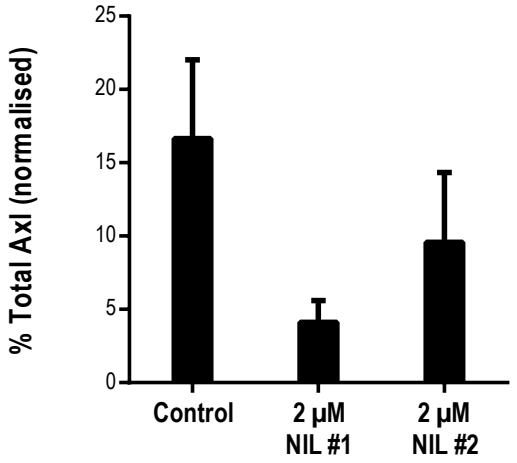
% Total Axl (normalised)
25
20
15
10
5
0
Control
2 µM NIL #1
2 µM NIL #2

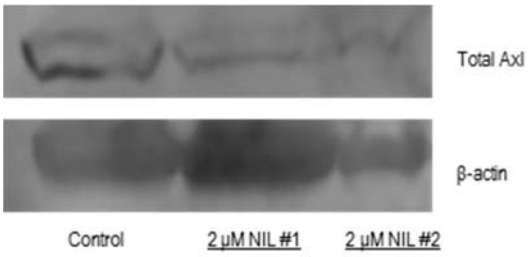
Total Axl
β-actin
Control
2 µM NIL #1
2 µM NIL #2

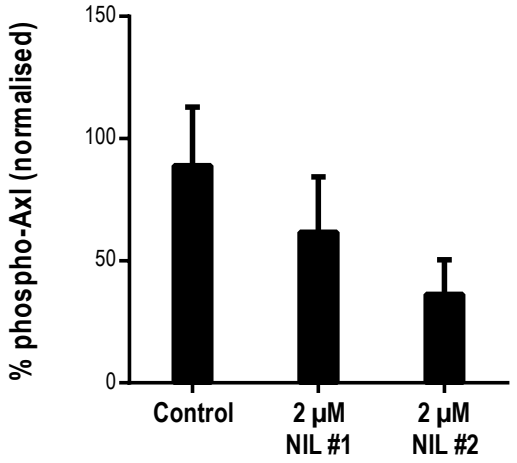
% phospho-Axl (normalised)
150
100
50
0
Control
2 µM NIL #1
2 µM NIL #2

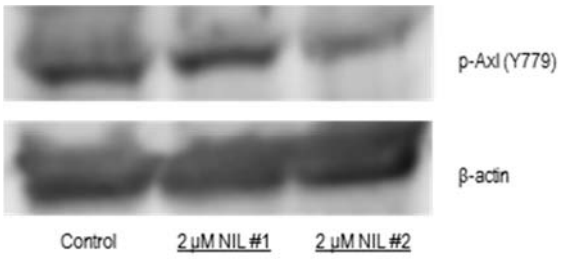
p-Axl (Y779)
β-actin
Control
2 µM NIL #1
2 µM NIL #2

(c)

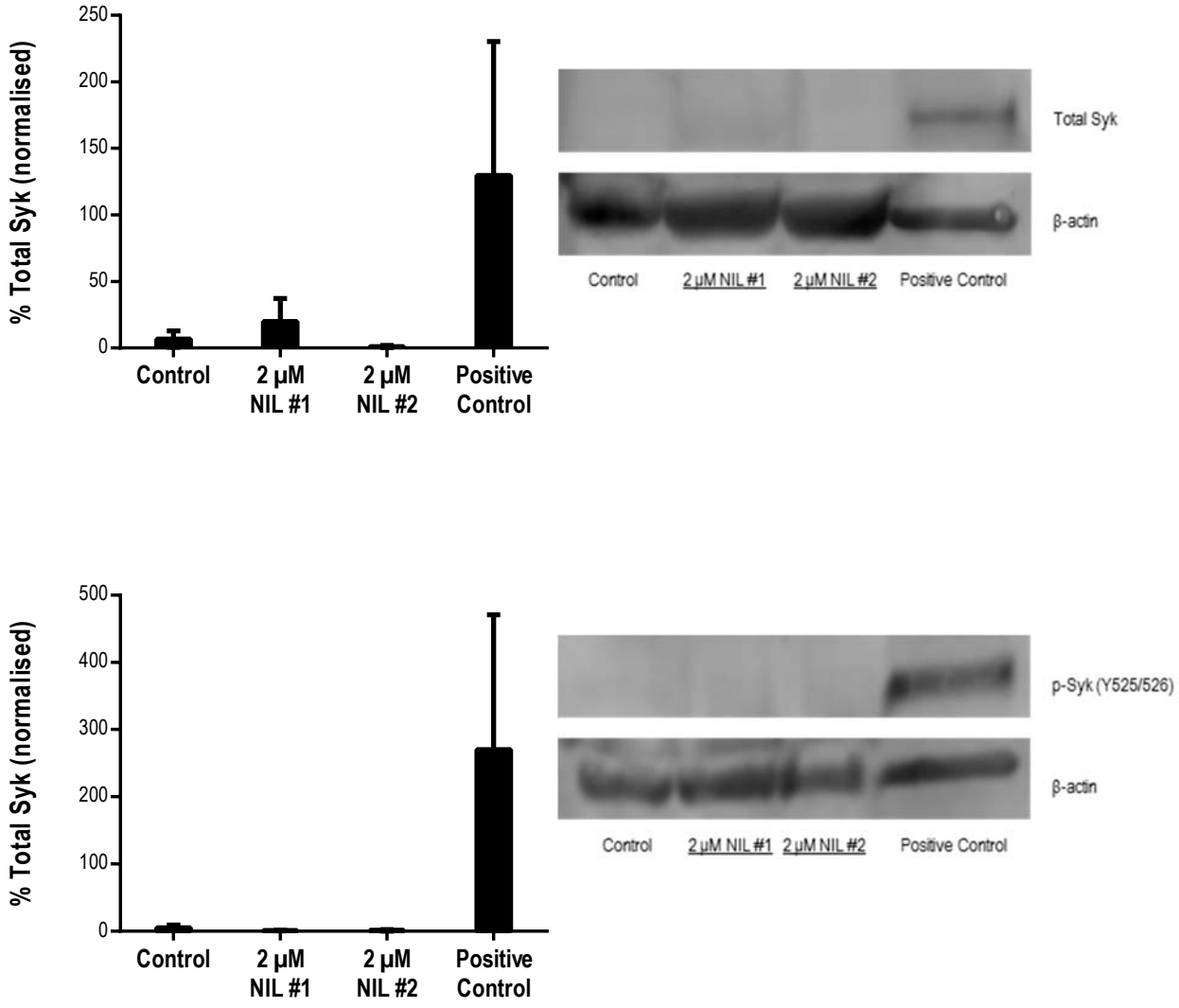
% Total Syk (normalised)
250
200
150
100
50
0
Control
2 µM NIL #1
2 µM NIL #2
Positive Control
Total Syk
β-actin
Control
2 µM NIL #1
2 µM NIL #2
Positive Control
% Total Syk (normalised)
500
400
300
200
100
0
Control
2 µM NIL #1
2 µM NIL #2
Positive Control
p-Syk (Y525/526)
β-actin
Control
2 µM NIL #1
2 µM NIL #2
Positive Control

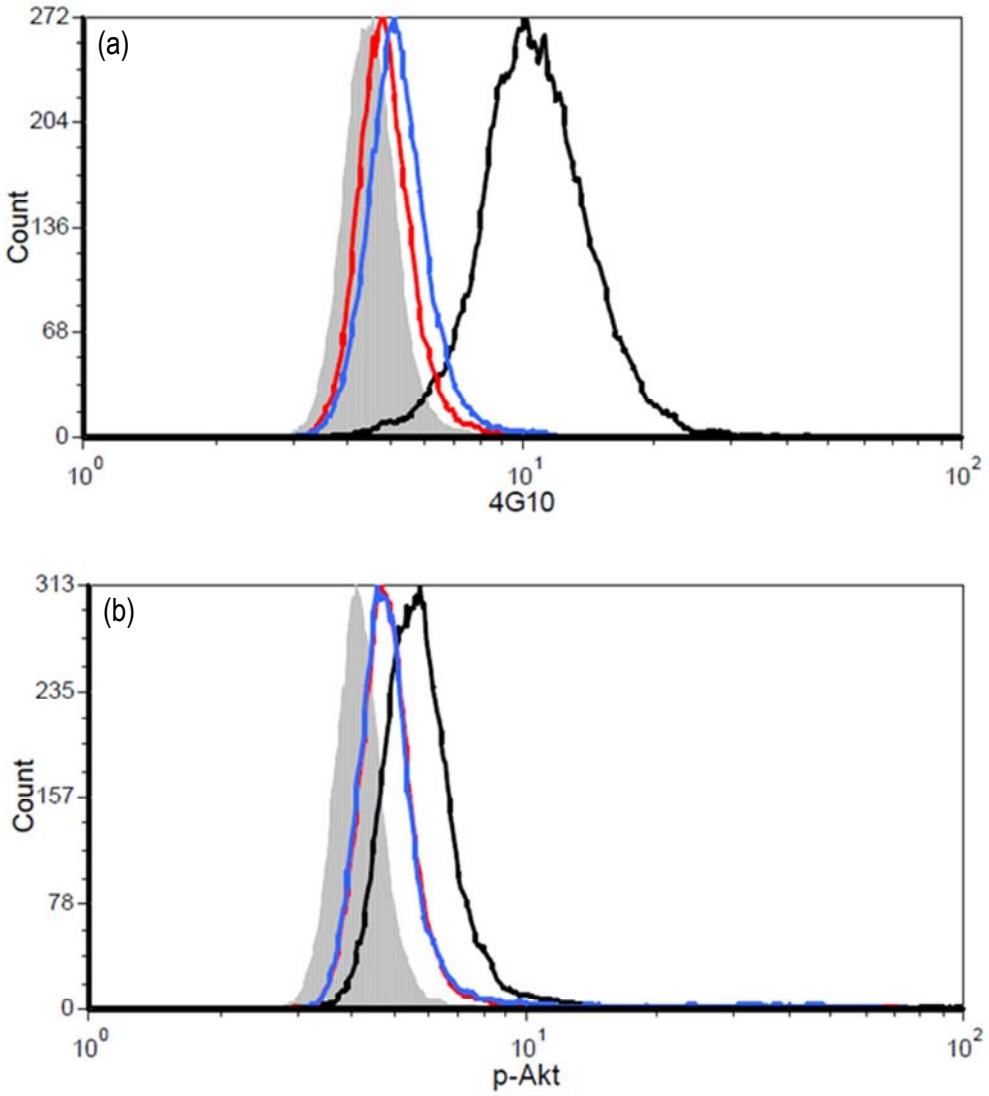

Figure 6.16: Total tyrosine phosphorylation is decreased in nilotinib resistant K562-Dox cells

K562-Dox control and K562-Dox 2 µM NIL resistant cells were stained with a) 4G10 antibody to assess total tyrosine phosphorylation status. Phosphorylation status of the oncoproteins b) Akt, c) Erk, d) Stat5 and e) Crkl was also determined. Data demonstrate a significant decrease in total tyrosine phosphorylation in resistant cells when compared with control cells. Additionally, there was no increase in phosphorylation of the oncoproteins. Data are representative of typical MFI levels. The **GREY** filled histograms represent cells stained with **isotype control** antibody. The bold **BLACK**, **RED** and **BLUE** histograms represent **K562-Dox control**, **K562-Dox 2 µM NIL #1** and **K562-Dox 2 µM NIL #2** cells respectively, stained with the antibodies detailed on the histograms. Flow cytometry was conducted by Amity Frede who had no role in the analysis of the data.

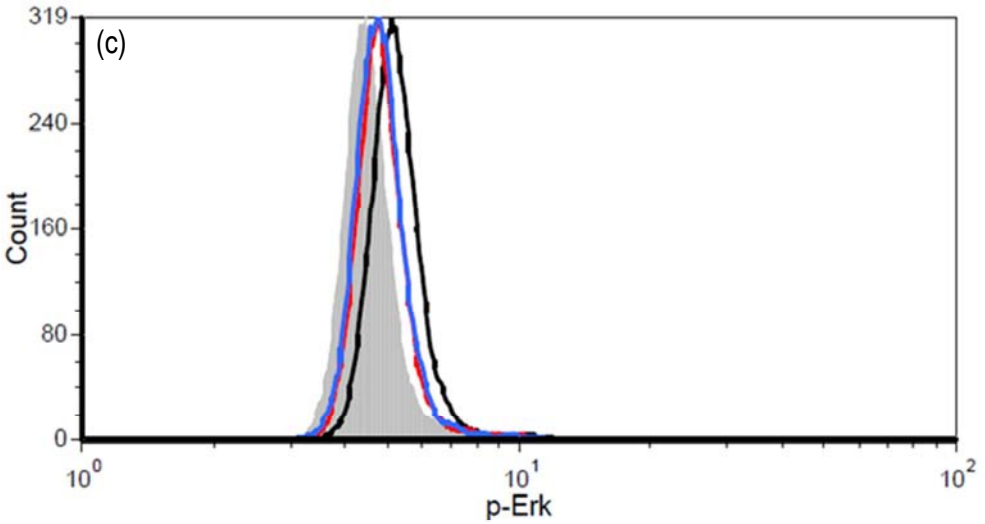
(c)
319
240
160
80
0
Count
10^0
10^1
10^2
p-Erk

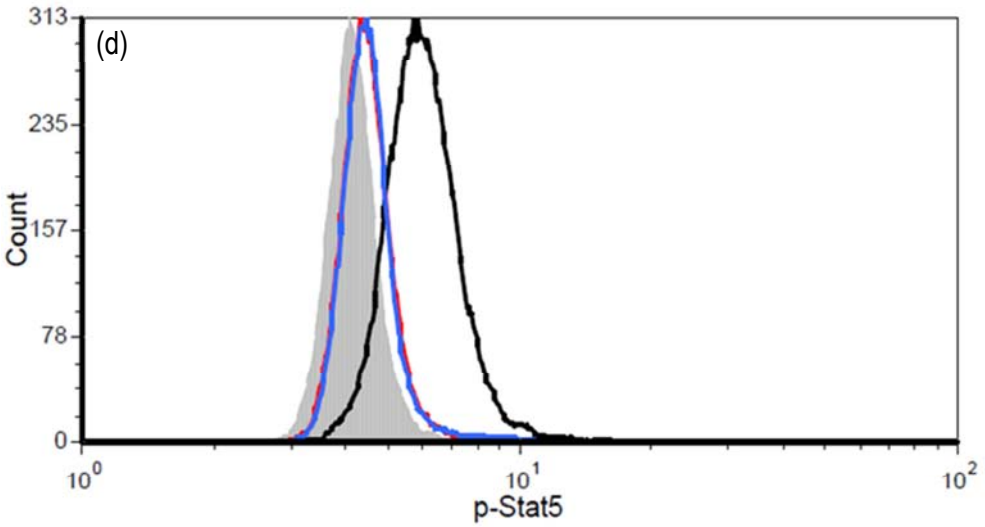
(d)
313
235
157
78
0
Count
10^0
10^1
10^2
p-Stat5

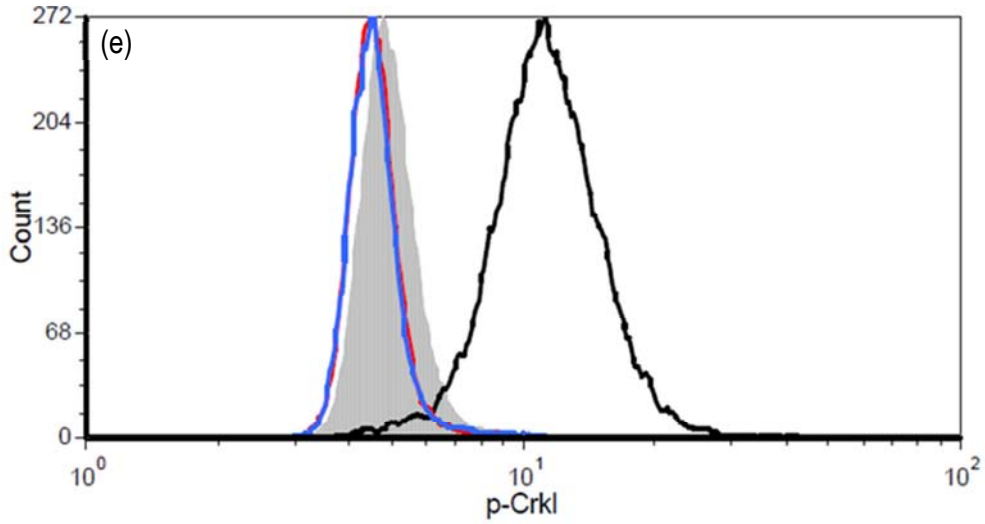
(e)
272
204
136
68
0
Count
10^0
10^1
10^2
p-Crkl

(T202/Y204) and Stat5 (Y694) although this failed to reach statistical significance; phosphorylation of Crkl was also reduced, confirming results from western blot (**Figure 6.16b-e**).

6.3.10. Nilotinib Resistance in K562-Dox Cells may be due to Aberrant Expression of Proteins Governing Cell Survival and Apoptosis

None of the previously reported causes of Bcr-Abl independent resistance in CML appeared to be the source of resistance to nilotinib in the K562-Dox cells here, thus a more global approach was employed in an attempt to determine the resistance mechanism/s present. Commercially available micro array plates (Fullmoon Biosystems) were used to compare protein expression levels of various cellular kinases and proteins involved in cancer signalling in resistant cells versus control cells. The arrays were analysed by Fullmoon Biosystems and the percentage change in expression levels determined (**Appendix 4D**). A smaller selection of interesting candidate proteins exhibiting large percentage changes were then validated by western blot where possible: PDGFR-β, MAP3K5, cdc25C and Chk2 (unfortunately western blot for PDGFR-β was unable to be optimised).

Platelet-derived growth factor receptors (PDGFR), such as PDGFR-β, are receptor tyrosine kinases involved in signalling pathways governing cell growth, differentiation and migration[292]. Additionally, overactivity of these receptors caused by abnormal gene rearrangement has previously been implicated in various malignancies including CML[293]. Upon comparison of protein levels in K562-Dox cells, array data demonstrated a 109% and 98% increase in expression of PDGFR-β in K562-Dox 2 μM NIL #1 and K562-Dox 2 μM NIL #2 cells respectively when compared with control cells (**Table 6.3**).

Mitogen-activated protein kinase kinase kinase 5 (MAP3K5) is a cellular kinase involved in stress-related apoptosis. Activation of this protein induces cell death; conversely decreased expression and/or reduced activity promotes cell survival. Array results demonstrated a 57% and 54% decrease in K562-

Table 6.3: Summary of proteins yielding large changes in expression in K562-Dox NIL resistant versus K562-Dox control cells

Cell Line	Protein	Fold Change	% Change
K562-Dox 2 µM NIL #1	PDGFR-β	1.09	+109
	MAP3K5	-0.57	-57
	cdc25C	1.45	+145
	Chk2	0.98	+98
K562-Dox 2 µM NIL #2	PDGFR-β	0.98	+98
	MAP3K5	-0.54	-54
	cdc25C	-0.47	-47
	Chk2	1.04	+104

Dox 2 μM NIL #1 and K562-Dox 2 μM NIL #2 cells respectively when compared with control cells (**Table 6.3**). These data were confirmed by western blot with resistant cells demonstrating a clear reduction in MAP3K5 protein levels (**Figure 6.17a**).

Chk2 and cdc25C are proteins involved in DNA damage repair pathways. cdc25C is a protein phosphatase that regulates the entry of cells into mitosis while Chk2 acts by inhibiting cdc25C thus preventing premature mitosis from occurring. Array results demonstrated an increase in expression of both cdc25C and Chk2 in K562-Dox 2 μM NIL #1 cells of 145% and 98% respectively (**Table 6.3**). However, western blot results did not confirm this with data showing a clear decrease in levels of cdc25C and no significant change in levels of Chk2 (**Figure 6.17b and c**). Array results demonstrated an increase in Chk2 expression in K562-Dox 2 μM NIL #2 cells of 104% which was confirmed by western, although this failed to reach statistical significance (**Table 6.3**, **Figure 6.17c**). However, the decrease in cdc25C expression observed in the array for K562-Dox 2 μM NIL #2 cells (47%, **Table 6.3**) was confirmed by western blot (**Figure 6.17b**).

6.3.11. Newly Diagnosed CML Patients Exhibit a Range of ABCB1 mRNA Expression Levels

Our laboratory has previously demonstrated a correlation between high levels of ABCB1 expression at diagnosis and loss of response to imatinib therapy[253]. Accordingly, ABCB1 mRNA levels were determined in 83 newly diagnosed CML patients receiving 300 mg upfront nilotinib twice daily to investigate whether the same is true for nilotinib. Peripheral blood diagnosis samples were used prior to therapy commencement such that baseline ABCB1 levels were determined. Data demonstrate a large variation in ABCB1 mRNA levels from <1% to 78% with a median level of 9.6% (**Figure 6.18**). Patients were divided in half about the median and early molecular response at three months assessed (<10% Bcr-Abl). However, because nilotinib has a far greater potency compared with imatinib, the majority of patients achieved this landmark reduction in Bcr-Abl levels by three months making this time frame

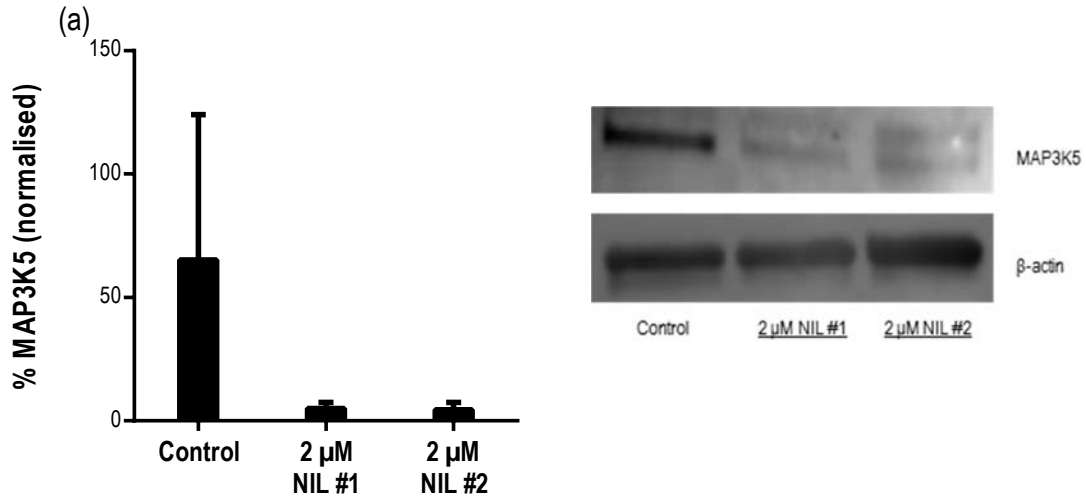

Figure 6.17: Nilotinib resistant K562-Dox cells exhibit differing levels of cellular proteins when compared with control cells

Expression levels of a) MAP3K5 b) cdc25C and c) Chk2 proteins were assessed in K562-Dox control and resistant cells. Data demonstrate that resistant cells exhibit decreased levels of MAP3K5 and cdc25C, but no significant change in Chk2. Western blot analyses shown are representative of at least three separate experiments with the corresponding quantitation representing the mean. Protein levels were normalised to β-actin control. Statistical analyses were performed using Student's *t*-test with statistically significant *p*-values denoted by asterisks (* $p<0.05$). Error bars represent SEM. NIL=nilotinib.

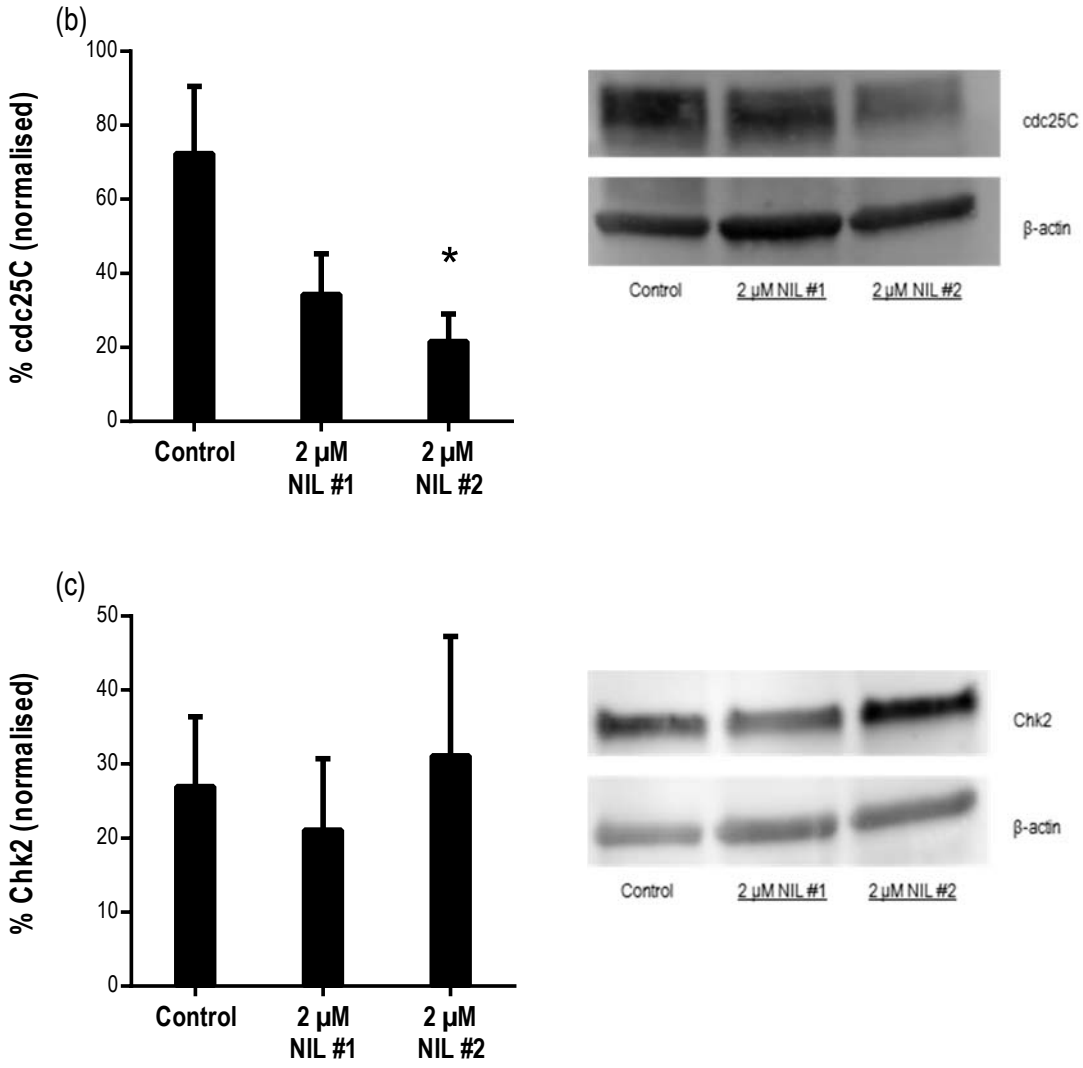
(b)
% cdc25C (normalised)
100
80
60
40
20
0
*
Control
2 µM NIL #1
2 µM NIL #2
cdc25C
β-actin
Control
2 µM NIL #1
2 µM NIL #2
(c)
% Chk2 (normalised)
50
40
30
20
10
0
Control
2 µM NIL #1
2 µM NIL #2
Chk2
β-actin
Control
2 µM NIL #1
2 µM NIL #2

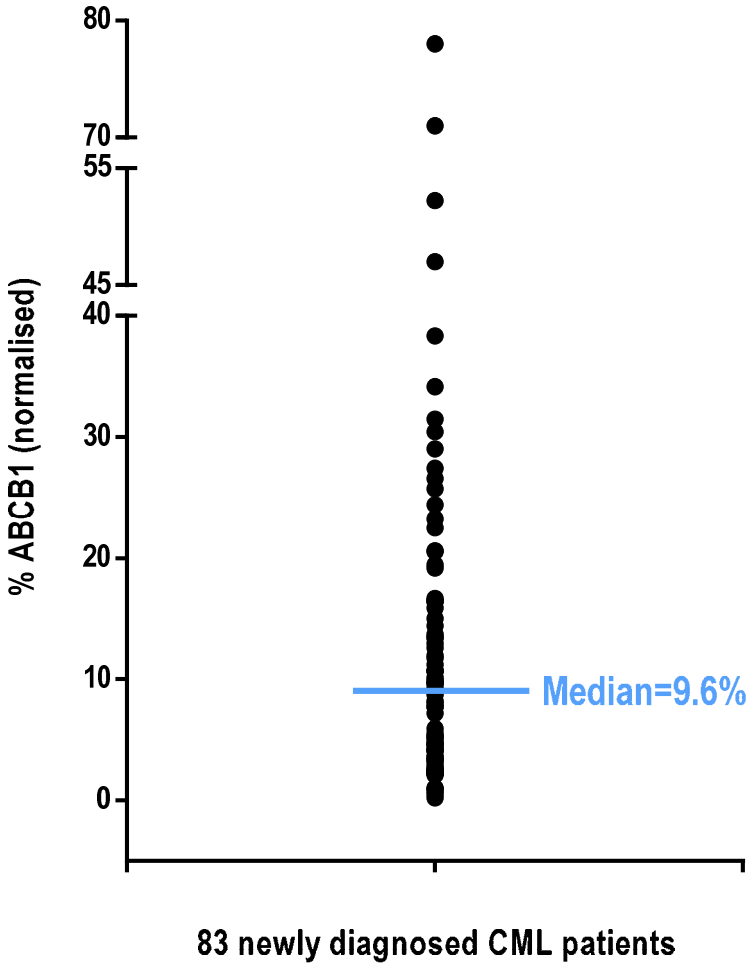

Figure 6.18: *De novo* CML patients exhibit diverse levels of ABCB1 mRNA

ABCB1 mRNA levels were assessed in the peripheral blood of 83 *de novo* CML patients prior to commencement of nilotinib therapy. Data demonstrate a wide variation in expression. Patients were divided in half about the median based on ABCB1 expression. mRNA expression was determined as a percentage of BCR and represents the mean of three independent experiments performed in triplicate. VBL100 (ABCB1 over expressing) cells were used as a control for reproducibility in all assays. Experiments in which control results were inconsistent were repeated and the results were not included in the analysis.

unsatisfactory for predicting long term response. Unfortunately, 12 month data is not yet available on a large enough cohort of patients for any conclusions to be drawn regarding long term response. As an alternative, patients were assessed for ability to achieve a major molecular response (MMR) of <1% Bcr-Abl at three months. However, results demonstrated no correlation between ABCB1 overexpression and achievement of MMR at three months: 64.3% of patients with low ABCB1 expression achieved MMR compared with 85.4% of patients with high ABCB1 expression. Although again, 3 months may be too short a time frame for meaningful predictions of long term response to be drawn.

6.4. Discussion

TKIs such as imatinib, and more recently nilotinib and dasatinib, have resulted in significantly better treatment outcomes for the majority of patients with CML. However, a substantial group remains (up to 35%) that develops secondary resistance; most commonly due to kinase domain (KD) mutations[102,103]. Furthermore, there are some patients who relapse following a successful imatinib treatment phase with an absence of KD mutations. These patients are also at risk of failing to respond to treatment with either of the second generation TKIs and usually relapse a second time, again without detectable KD mutations[171,285]. Additionally, a group of frankly resistant, relapsed patients exist who still have adequate inhibition of Bcr-Abl activity[108], although this study utilised a small cohort of patients undergoing imatinib treatment and there have been no confirmatory results in the ensuing years. However, the long term treatment outcomes of nilotinib are yet to be defined and Bcr-Abl independent resistance may be applicable here. Accordingly, a greater understanding of the kinetics of resistance development, especially in the Bcr-Abl *independent* setting, is required. For this reason, two nilotinib resistant K562-Dox cell lines were generated so that resistance emergence could be observed in the presence of ABCB1 overexpression.

6.4.1. ABCB1 Overexpression is the Initiator of Resistance to Nilotinib *In Vitro*

ABCB1 overexpression was established as an important initiator of nilotinib resistance in K562 cells (**Chapter 5**). Importantly, further overexpression of ABCB1 was also observed in K562-Dox cells with expression levels directly correlating with $IC50^{NIL}$. Interestingly, continued culture in increasing concentrations of nilotinib resulted in a loss of ABCB1 expression back to parental K562 levels as additional resistance mechanisms emerged. It is likely that ABCB1 overexpression caused increased export of nilotinib leading to lower intracellular nilotinib concentrations. This then resulted in suboptimal Bcr-Abl inhibition which presumably created a favourable environment for development of other resistance mechanisms (**Figure 6.19**).

Our laboratory has previously demonstrated a correlation between high levels of ABCB1 mRNA at diagnosis and subsequent development of KD mutations in patients receiving imatinib therapy[253]. We have also demonstrated a significant reduction in $IC50^{NIL}$ in CML patient mononuclear cells incubated in the presence of the ABCB1 inhibitor pantoprazole compared with those incubated in the absence of pantoprazole[294]. These results were supported by clinical *in vivo* data[295]: retrospective analyses were performed in newly diagnosed, chronic phase CML patients receiving up front nilotinib as well as those patients with imatinib resistant disease being treated with nilotinib as a second line therapy. Molecular and cytogenetic responses were assessed in patients receiving concomitant pantoprazole (or another similar proton pump inhibitor, PPI) compared with those patients who did not receive any co-medication. Results demonstrated that concurrent use of PPIs had no adverse effect on nilotinib efficacy; in fact, a modest increase in molecular and cytogenetic responses was observed. Accordingly, ABCB1 mRNA levels were assessed in 83 *de novo* CML patients receiving up front nilotinib therapy. Results demonstrated large variation in ABCB1 expression which will later be correlated with response at 12 months once this data becomes available. Dependent on these data, patients exhibiting high levels of ABCB1 at diagnosis may benefit from combination ABCB1 inhibitor:TKI therapy.

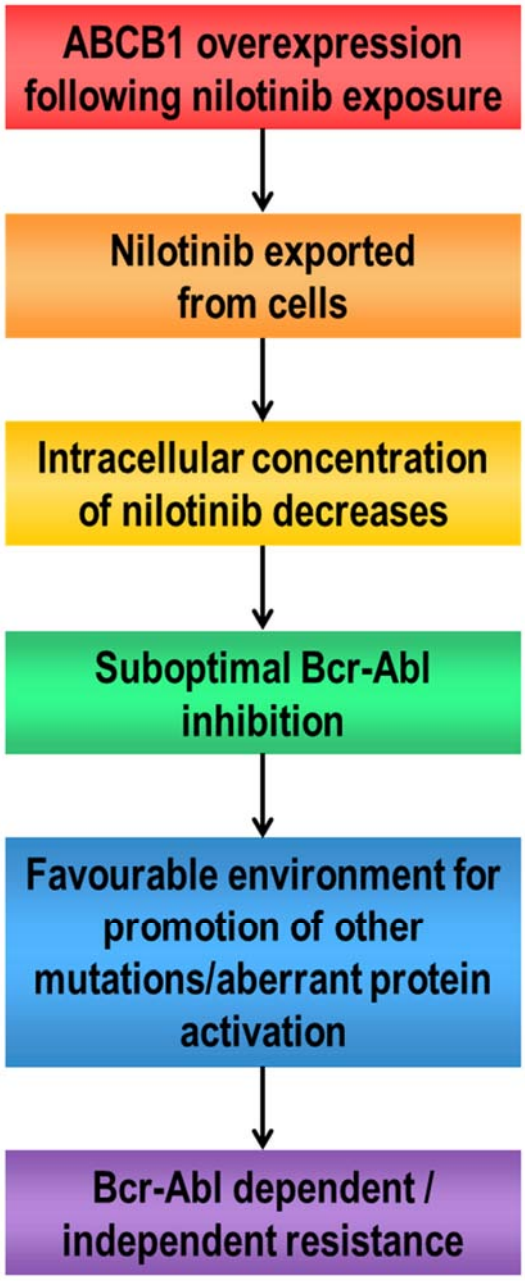

Figure 6.19: Schematic summary of resistance generation in cell lines

ABCB1 overexpression is the initiating event facilitating nilotinib resistance *in vitro*. This was observed in resistant K562, as well as K562-Dox cell lines, and was thus not dependent on ABCB1 expression status at the start of resistance generation. ABCB1-mediated nilotinib efflux presumably occurred resulting in a decreased level of intracellular nilotinib. This then resulted in inferior Bcr-Abl inhibition leading to a cellular environment that promoted further mutations/aberrant activation of proteins ultimately resulting in the Bcr-Abl *dependent* (K562 cells) and Bcr-Abl *independent* (K562-Dox cells) resistance observed.

ABCG2 mRNA overexpression was also observed in early resistance intermediates from K562-Dox NIL #2 cells. However, this failed to translate to an overexpression in ABCG2 protein and thus data described here does not support a role for ABCG2 in development of nilotinib resistance. As discussed in the previous chapter, this is most likely due to the level of redundancy that exists between closely related transporters, such as those from the ABC superfamily. It is likely the presence of nilotinib directly impacts levels of ABCB1 mRNA, which in turn impact ABCG2 mRNA levels independently of nilotinib, as was demonstrated in ABCB1 knockout mice[284].

Importantly, whereas ABCB1 mRNA overexpression occurred consistently and incrementally with increasing nilotinib concentration in all resistant cell lines generated, ABCG2 overexpression did not. Similarly, levels of ABCC1 mRNA were also inconsistent, both within and between cell lines. Thus, even though the difference in levels of ABCC1 mRNA in resistant versus control cells may have reached significance in the late stage K562-Dox resistance intermediates, it is unlikely this transporter plays a role in nilotinib resistance.

6.4.2. ABCB1 Overexpression Precedes Bcr-Abl Independent Resistance in K562-Dox Cells

Following ABCB1 overexpression in nilotinib resistant K562-Dox cells, a Bcr-Abl *independent* mechanism of resistance predominated, which, to date, remains undetermined. Interestingly, K562-Dox 2 μM NIL #1 cells lost ABCB1 expression at an earlier time point (125 nM) than K562-Dox 2 μM NIL #2 cells (1 μM). As mentioned previously, IC50 correlated with ABCB1 expression: low ABCB1 expression, low IC50; high ABCB1 expression, high IC50. However, once cultured in 2 μM nilotinib, both K562-Dox 2 μM NIL #1 and K562-Dox 2 μM NIL #2 cells had negligible levels of ABCB1 mRNA and protein. $IC50^{NIL}$, $IC50^{IM}$ and $IC50^{DAS}$ were all significantly decreased yet both resistant cells lines demonstrated significantly increased survival in the presence of all three TKIs when compared with control cells. K562-Dox cells have been stably expressing ABCB1 for over a decade and this is the first report of

complete loss of ABCB1 expression back to levels observed in parental K562 cells. Importantly, loss of expression was accompanied by loss of function as demonstrated by inability to efflux the ABCB1 substrate rhodamine-123.

Intriguingly, investigation of other common modes of TKI resistance failed to determine the cause of resistance in these cell line models (**Table 6.4**). There was no overexpression of Lyn or Axl mRNA in any of the resistance intermediates from either K562-Dox 2 μM NIL #1 or K562-Dox 2 μM NIL #2 cells. There was also no overexpression of Lyn, Axl or Syk proteins nor increased phosphorylation of these proteins in 2 μM nilotinib resistant cells. Total tyrosine phosphorylation was reduced, as was phosphorylation of Akt, Erk and Stat5, which are all important effector molecules in pathways governing cell proliferation and survival[290]. IC50 data demonstrated that Bcr-Abl kinase activity was sufficiently inhibited in resistant cells and this was confirmed by flow cytometry specific for p-Crkl. It is important to note that the growth rates of the resistant cells did not differ from that of the control cells thus excluding decreased growth as a potential explanation for the decreased cytotoxicity observed in spite of Bcr-Abl inhibition. Taken together, these data suggest a Bcr-Abl *independent* mode of resistance and thus these cell lines may offer an *in vitro* model for those frankly resistant, relapsed patients who maintain sufficient Bcr-Abl inhibition[108].

6.4.3. Crkl Phosphorylation Status Provides an Adequate Surrogate for Bcr-Abl Activity

Due to the unstable nature of Bcr-Abl upon disruption of patient cells[290], a surrogate marker of Bcr-Abl kinase activity was required. Crkl is the major tyrosine-phosphorylated protein in neutrophils from patients with CML but is unphosphorylated in Bcr-Abl negative cells[296] and thus p-Crkl is considered the most specific readout of Bcr-Abl activity. Importantly, we[210,297], and others[298,299], have demonstrated that the degree of Crkl phosphorylation is strongly predictive of molecular response in patients treated with imatinib. Conversely, it has recently been suggested that p-Crkl may not accurately represent Bcr-

Table 6.4: Summary of resistance mechanisms in K562-Dox NIL #1 and K562-Dox NIL #2 cells

	K562-Dox 125 nM NIL #1	K562-Dox 2 µM NIL #1	K562-Dox 125 nM NIL #2	K562-Dox 2 µM NIL #2
Resistance by cytotoxicity to all TKIs	✓	✓	✓	✓
$IC50^{NIL}$	↓↓↓	↓↓↓	↑↑↑	↓↓↓
$IC50^{IM}$	↓↓	↓↓↓	↔	↓↓↓
$IC50^{DAS}$	↓↓	↓↓↓	↑	↓↓↓
ABCB1 protein overexpression	×	×	✓	×
ABCG2 protein overexpression	×	×	×	×
Increased Bcr-Abl protein	ND	×	ND	×
Increased Lyn protein	ND	×	ND	×
Increased p-Lyn	ND	×	ND	×
Increased Axl protein	ND	×	ND	×
Increased p-Axl	ND	×	ND	×
Increased Syk protein	ND	No expression	ND	No expression
Increased p-Syk	ND	No phosphorylation	ND	No phosphorylation
Increased total tyrosine phosphorylation	ND	×	ND	×
Increased PDGFR-β protein	ND	✓	ND	✓
Decreased MAP3K5 protein	ND	✓	ND	✓

✓=yes; ×=no; ↑=increase; ↓=decrease; ↔=no change; ND=not determined.

Abl kinase activity. *In vitro* experiments with dasatinib, employing a rigorous washing technique in which residual TKI was washed out, demonstrated p-Crkl levels did not correlate with presence or absence of TKI, although this may be cell type specific[291]. However, for the purposes detailed in this current study, in which CML cells are continuously exposed to nilotinib, results clearly demonstrate levels of p-Bcr-Abl (Y245) mimic those of p-Crkl thus confirming p-Crkl as an accurate and sensitive surrogate for Bcr-Abl kinase activity.

6.4.4. Activation of Signalling Pathways Governing Growth and Survival May Occur Via PDGFR-β Circumventing Bcr-Abl

Determination of p-Bcr-Abl levels in K562-Dox 2 μM resistant cells demonstrated near complete inhibition in the presence of nilotinib which was reversible upon drug washout. Thus, TKI-mediated inhibition is taking place yet the cells remain resistant indicating a Bcr-Abl *independent* mechanism of resistance. In order to ascertain a contributing signalling pathway, global protein arrays assessing levels of cellular kinases and cancer signalling proteins in resistant versus control cells were conducted. Results indicated a potential role for PDGFR-β, MAP3K5 and the DNA damage checkpoint proteins cdc25C and Chk2.

Western validation confirmed array results for MAP3K5 in both K562-Dox 2 μM NIL #1 and K562-Dox 2 μM NIL #2 cells. Western results also validated array results for cdc25C and Chk2 in K562-Dox 2 μM NIL #2 cells but were not as convincing for cdc25C and Chk2 in K562-Dox 2 μM NIL #1 cells (**Table 6.5**). This is most likely due to the stage of the cell cycle at which the cells were sampled for array processing (K562-Dox 2 uM NIL #1 cells were growing at a higher concentration than that of K562-Dox 2 uM NIL #2 cells). cdc25C is constitutively phosphorylated during interphase and thus the antibody on the array would not have recognised a modified protein. Therefore, if cells were no longer in the exponential growth phase, feasibly this may have affected the levels of cdc25C observed. However,

Table 6.5: Comparison of protein levels in resistant K562-Dox cells versus control cells as determined by protein array and western blot

Cell Line	Protein	Array	Western
K562-Dox 2 µM NIL #1	PDGFR-β	↑	N/A
	MAP3K5	↓	↓
	cdc25C	↑	↓
	Chk2	↑	↔
K562-Dox 2 µM NIL #2	PDGFR-β	↑	N/A
	MAP3K5	↓	↓
	cdc25C	↓	↓
	Chk2	↑	↑

↑=increase; ↓=decrease; ↔=no change; N/A=western unable to be optimised.

upon validation by western, which was repeated five times, cells were sampled and lysed during the growth phase giving a more realistic depiction of cdc25C levels in resistant cells.

Collectively, the array results, in conjunction with western validation, indicate that DNA damage has occurred in resistant cells resulting in up regulation of Chk2 and a corresponding down regulation of cdc25C. This DNA damage may be related to an activating mutation of PDGFR-β causing aberrant activation of the PI3-K/Akt pathway in the absence of Bcr-Abl signalling ultimately leading to increased proliferation and reduced apoptosis (**Figure 6.20**). Activating mutations of PDGFR-α have previously been reported in the pathology of gastrointestinal tumours (GIST)[300], however, activating mutations in PDGFR-β are yet to be described in myeloproliferative disorders such as CML. Alternatively, it has also been demonstrated that binding of PDGFR-β, for example, with abnormal binding partners can cause constitutive activation and aberrant overexpression of the receptor[301]. While fusions of different genes with PDGFR-α have already been reported in atypical CML[302] and other diseases[303,304], the abnormal overexpression and/or activation of PDGFR-β described here could provide a novel mode of Bcr-Abl *independent* resistance in CML in response to nilotinib; a line of investigation we intend to pursue in the future. Further to this, PDGFR-β has been demonstrated to interact with other downstream effector molecules in signalling pathways governing cellular proliferation. PDGFR-β is capable of directly activating proteins downstream of Erk[305] which may explain why no increased phosphorylation of Erk was observed in these cell lines.

Additionally, the reduced levels of MAP3K5 observed, which under normal conditions is activated in response to external stress[306], may also be involved in the reduced apoptosis and increased survival exhibited by resistant cells. MAP3K5 has previously been demonstrated to play a role in the inactivation of members of the Bcl-2 family of proteins resulting in apoptosis (**Figure 6.21**). However, *in vitro* experimentation demonstrated that a dominant-negative form of MAP3K5 was unable to correctly

Figure 6.20: Schematic representation of the interplay existing between resistance mechanisms in K562-Dox cells

Abnormal expression and/or activity of PDGFR-β in nilotinib resistant K562-Dox cells may cause aberrant growth and survival. Activating mutations of PDGFR-α, which is closely related to PDGFR-β, have previously been implicated in disease phenotypes[300]. Additionally, binding of PDGFR-β to abnormal binding partners has been demonstrated to cause constitutive activation of the receptor leading to deregulation of downstream signalling pathways[301]. This, coupled with decreased levels of MAP3K5 leading to reduced apoptosis, may be responsible for the uncontrolled growth and survival exhibited by resistant K562-Dox 2 μM cells in the presence of adequate Bcr-Abl inhibition. Adapter proteins are depicted in **PURPLE**, transcription factors in **BLUE**, kinases in **GREEN** and apoptosis related proteins in **RED**.

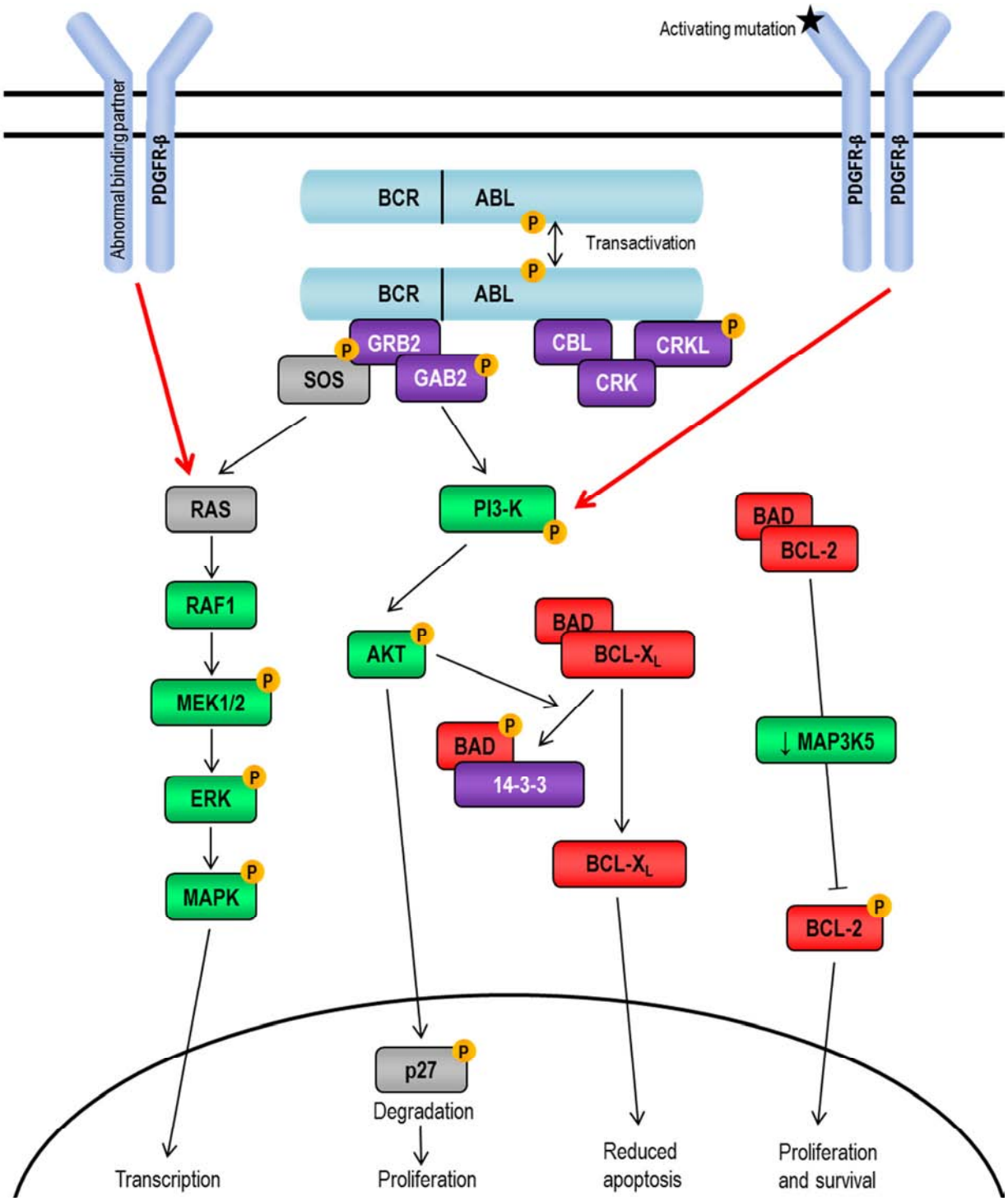
Activating mutation
Abnormal binding partner
PDGFR-β
PDGFR-β
PDGFR-β
BCR
ABL
P
Transactivation
P
BCR
ABL
GRB2
P
SOS
GAB2
P
CBL
CRKL
P
CRK
RAS
PI3-K
P
BAD
BCL-2
RAF1
AKT
P
BAD
BCL-XL
MEK1/2
P
BAD
P
14-3-3
↓ MAP3K5
ERK
P
BCL-XL
MAPK
P
BCL-2
P
p27
P
Degradation
Transcription
Proliferation
Reduced apoptosis
Proliferation and survival

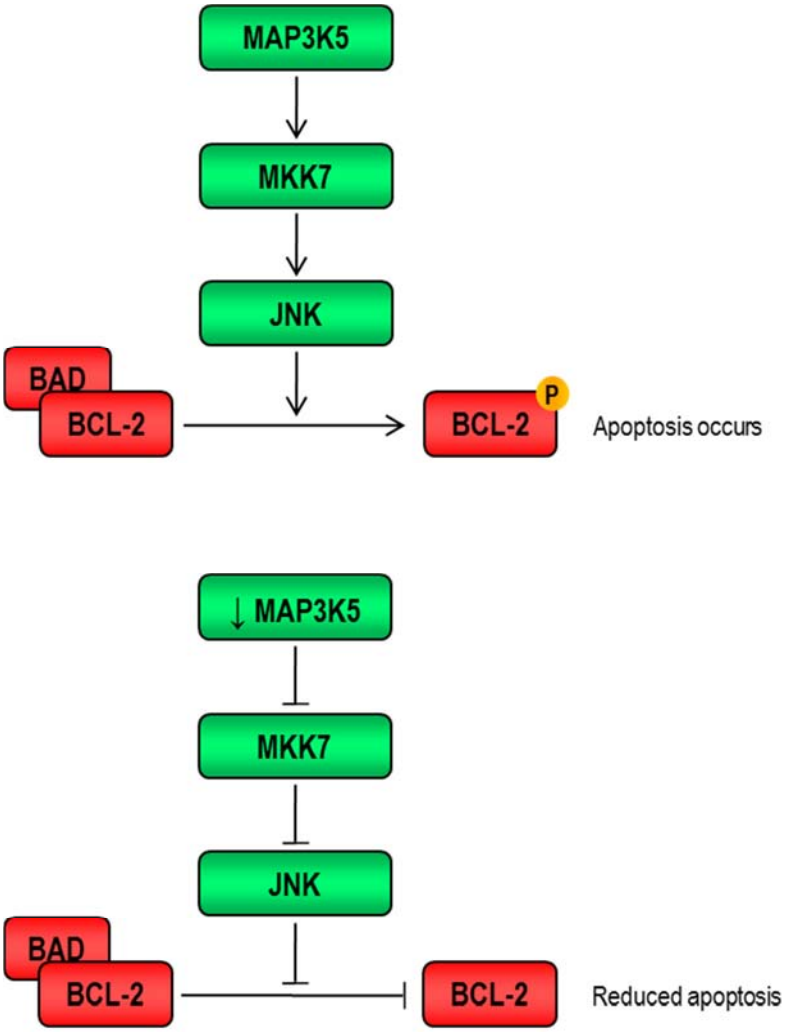

Figure 6.21 Schematic representation of the role of MAP3K5 in the regulation of apoptosis

Bcl-2 family members such as Bcl-2 and Bcl-X_L are involved in regulation of apoptosis. Phosphorylation of the anti-apoptotic Bcl-2 protein causes its inactivation, resulting in apoptosis. MAP3K5 has been demonstrated to promote Bcl-2 phosphorylation (upper diagram), however, dominant-negative versions of the kinase result in decreased apoptosis *in vitro*[307] (lower figure). Presumably, decreased levels of MAP3K5, as apparent in K562-Dox 2 µM NIL #1 and K562-Dox 2 µM NIL #2 cells, would have the same effect, offering a potential explanation for the reduced apoptosis observed in these cell lines.

phosphorylate Bcl-2 leading to reduced apoptosis[307]. Thus, it is likely that the decreased levels of MAP3K5 present in K562-Dox 2 μM NIL #1 and K562-Dox 2 μM NIL #2 cells are responsible, in part, for the reduced apoptosis observed in the presence of nilotinib (**Figure 6.20**). Supporting this notion, array results demonstrated reduced phosphorylation of Bcl-2 in both K562-Dox 2 μM NIL #1 and K562-Dox 2 μM NIL #2 cells: decreases of 19% (-0.19 fold change) and 23% (-0.23 fold change) were observed respectively (**Appendix 4D**).

In conclusion, the findings detailed in this chapter strongly suggest that ABCB1 overexpression provides the initial platform required for additional Bcr-Abl *dependent* and *independent* mechanisms of resistance to occur. The results described here demonstrate that ABCB1 overexpression not only provides a favourable intracellular environment for the manifestation of other mutations/aberrant protein activation but that it is also directly responsible for nilotinib resistance. Subsequently, different modes of resistance occurred in different cell lines. In K562 2 μM NIL resistant cells increased activation of Lyn and Axl was observed, whereas in K562-Dox 2 μM NIL resistant cells Bcr-Abl *independent* resistance predominated. Thus, patients in whom ABCB1 expression is initially high may be predisposed to developing Bcr-Abl *independent* resistance while others may develop alternative forms of resistance. Overall, the *in vitro* models of resistance described present a valuable tool for studying resistance in patients.

Chapter 7

ABCC6 is Involved in Nilotinib Transport and Resistance Development

7.1. Introduction

Through thorough investigation, ABCB1 and ABCG2 have been implicated in the efflux of tyrosine kinase inhibitors (TKIs) from Chronic Myeloid Leukaemia (CML) cells[115,140,146]. However, the relationship between TKIs and other closely related transporters, such as those belonging to the Multidrug Resistance Protein (MRP) subfamily, has not been as widely studied.

The MRP family consists of nine transporters (MRP1-9) that have been implicated in the efflux of chemotherapeutic compounds from cancer cells. MRPs are capable of extruding a wide variety of substrates from cells[308]. MRPs are expressed in different tissues and can be divided into two groups depending on the number of membrane spanning regions (**Table 7.1**). ABCC6 (MRP6) is a 160 kDa protein that was first identified in human tissues and cancer cell lines[309]. ABCC6 is primarily expressed in the liver and kidney[309-311] and has previously been shown to confer resistance to a number of anti-cancer agents such as etoposide, doxorubicin and daunorubicin[312]. Additionally, ABCC6 bears striking sequence homology to ABCC1[309]. ABCC6 consists of seventeen transmembrane domains and two ATP-binding domains which hydrolyse ATP in order to transport substrates, usually lipophilic molecules of negative charge[221,312] (**Figure 7.1**).

As detailed previously (**Chapter 4**), $IC50^{NIL}$ experiments were performed in four cell lines with different expression levels of ABCB1 and ABCG2, in the absence and presence of pantoprazole, a dual ABCB1/ABCG2 inhibitor. However, results demonstrated a significant reduction in $IC50^{NIL}$ in the presence of pantoprazole in all cell lines regardless of ABCB1 or ABCG2 expression status (**Table 7.2**). These data suggest that there may be other ABC efflux transporter/s expressed in all four cell lines, also involved in nilotinib transport.

Members of the ABC family of transporters have overlapping substrate specificities due to the high

Table 7.1: Summary of properties of transporters from the MRP family (modified from Chen *et al.*[313]

MRP	Alternate Name	Number of MSRs	Tissue Expression	Resistance Profile*
MRP1	ABCC1	3	ubiquitous	anthracyclines, camptothecins, MTX, etoposide, irinotecan
MRP2	ABCC2	3	liver, kidney, intestine	anthracyclines, camptothecins, MTX, etoposide, cisplatin, irinotecan
MRP3	ABCC3	3	small intestine, pancreas, colon, kidneys, placenta, adrenal gland	MTX, tenoposide, etoposide
MRP4	ABCC4	2	prostate, testis, ovary, lung, hepatocytes, intestine, pancreas	MTX, irinotecan, topotecan, AZT
MRP5	ABCC5	2	all major tissues	MTX, cisplatin, AZT, daunorubicin, doxorubicin, gemcitabine, Ara-C
MRP6	ABCC6	3	kidney, liver	doxorubicin, daunorubicin, etoposide, teniposide, cisplatin, actinomycin-D
MRP7	ABCC10	3	most tissues	paclitaxel, docetaxel, vincristine, vinblastine, Ara-C, gemcitabine
MRP8	ABCC11	2	testis, breasts	MTX, Ara-C
MRP9	ABCC12	2	testis, breasts, ovary, brain, skeletal muscles	unknown

* selected anticancer drugs

MSR=Membrane Spanning Region; MTX=methotrexate; AZT=azathioprine; Ara-C=arabinofuranosyl cytidine

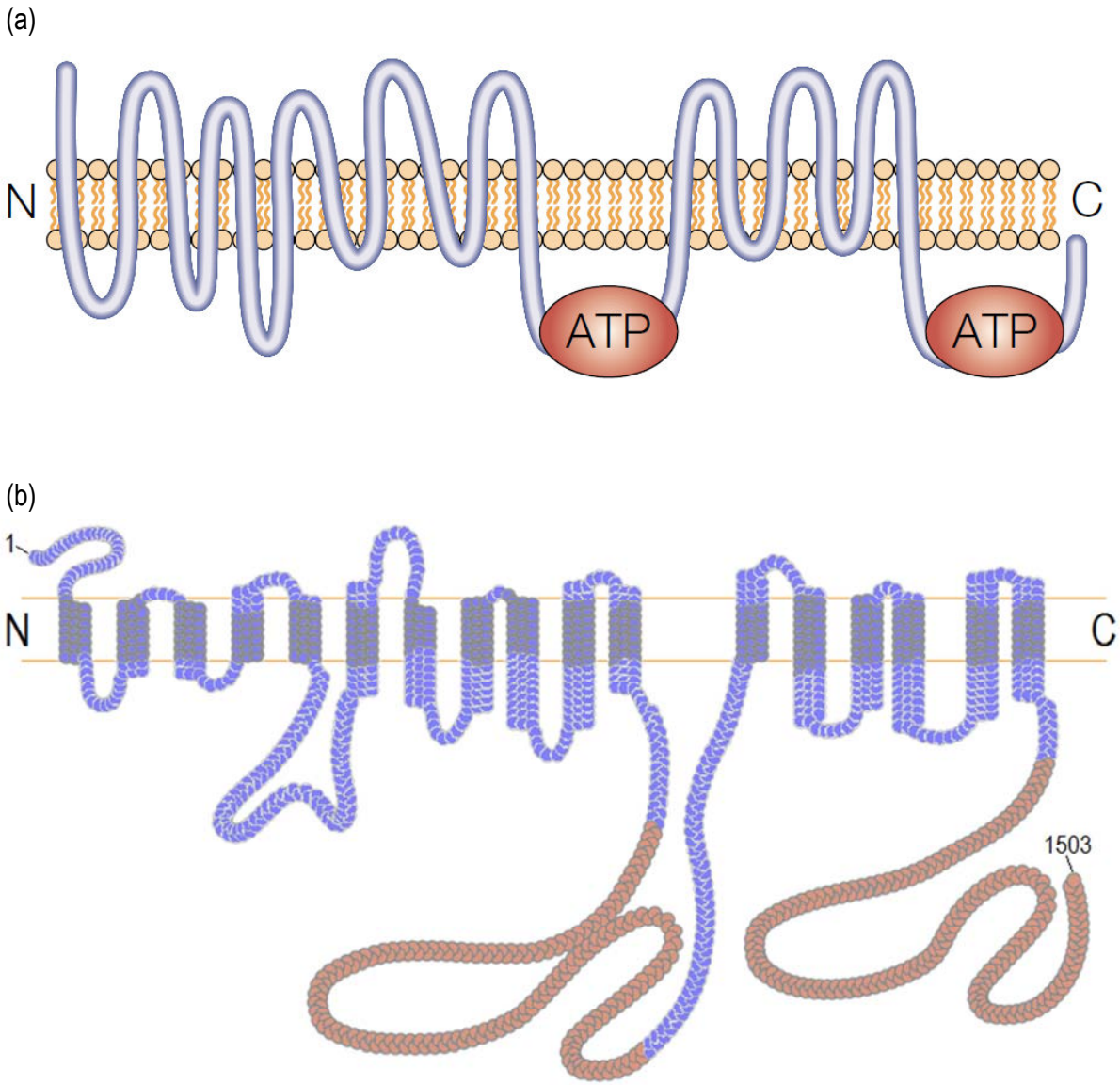

Figure 7.1: Structure of ABCC6

a) Schematic representation showing the protein's seventeen transmembrane domains and two ATP-binding sites[223]. b) A two dimensional model of ABCC6 based on structure of ABCC1 showing the 1503 amino acid sequence (**PURPLE**). The ATP binding domains are also indicated (**BROWN**), modified from Fulop *et al.*[314].

Table 7.2: The effect of pantoprazole on $IC50^{NIL}$ in cell lines

Cell Line	ABCB1	ABCG2	% decrease	*p*-value
K562-Dox				
Control	✓	–		
+200 μM PP	✓	–	57%	*p*=0.010
K562-ABCG2				
Control	–	✓		
+200 μM PP	–	✓	54%	*p*=0.011
KU812				
Control	–	–		
+250 μM PP	–	–	69%	*p*=0.004
K562				
Control	–	–		
+200 μM PP	–	–	44%	*p*=0.001

Statistical analyses were performed using Student's *t*-test; PP=pantoprazole.

degree of homology observed both within and between the seven subgroups (ABCA–ABCG)[315]. Additionally, many inhibitors of ABC transport also have overlapping specificities which makes it difficult to determine which transporter a given inhibitor is acting on (**Table 7.3**). For this reason, a panel of inhibitors was utilised to ascertain the involvement of various ABC transporters in the transport of nilotinib; an approach that has been successfully employed previously to eliminate those transporter unlikely to interact with imatinib[147]. Proton pump inhibitors (PPIs) such as pantoprazole, esomeprazole and omeprazole, are frequently prescribed to CML patients to alleviate gastric side effects experienced as a results of TKI therapy or as ongoing therapy. The effect of concomitant administration of PPIs in patients receiving nilotinib therapy has been investigated with no adverse effect on TKI efficacy described; in fact a modest, yet statistically insignificant improvement in major molecular response (MMR) was observed[295]. Indeed, we have demonstrated *in vitro* that PPIs significantly increase the intracellular concentration of nilotinib in both cell lines and primary patient cells[294].

PPIs can be divided into two groups based on structure although all contain the timoprazole backbone. Omeprazole, esomeprazole and pantoprazole belong to the same group containing benzimidazole moieties (**Figure 7.2**). Omeprazole was the first drug of this class, however, considerable inter-patient variability led to development of the *S*-isomer, esomeprazole. Esomeprazole is a mirror image of omeprazole and both have been implicated in the inhibition of ABCC6-mediated efflux of cisplatin *in vitro* and *in vivo*[197,312,316]. Pantoprazole shares considerable structural similarities with esomeprazole but addition of a difluoromethyl moiety resulted in increased half-life and greater solution stability[317]. Esomeprazole and pantoprazole are often cited as a dual ABCB1/ABCG2 inhibitors[197,198,318] and thus, while not studied directly, it is possible that pantoprazole is also capable of ABCC6 inhibition. Indeed, two separate *in vitro* studies investigating the interaction of PPIs with ABCB1 and ABCG2 confirmed the likelihood of pantoprazole inhibiting other transporters in addition to ABCB1 and ABCG2[198,319].

Table 7.3: Summary of inhibitors used in this study and the corresponding cellular transporters upon which they are active

Transporter	Inhibitor					
	PSC-833			**Verapamil**		
	Reference	[Inhibitor]	% Inhibition	Reference	[Inhibitor]	% Inhibition
Oct-1				[213][213] [320][320]	50 µM 100 µM	69–100% 80%
ABCB1	[321][321] [322][322] [323][323]	10 µM 41 µM 5 µM	75% 100% 67%	[243][243] [282][282] [323][323] [324][324]	100 µM 100 µM 20 µM 234 µM	51% 70% 30% 50%
ABCB4	[323][323]	5 µM	62%	[323][323]	20 µM	42%
ABCC1	[325][325]	27 µM	50%	[326][326]	8 µM	36%
ABCC2						
ABCC3				[327][327]	111 µM	13.1%
ABCC4	[328][328]	10 µM	44%	[328][328] [329][329]	30 µM 25 µM	46% 39%
ABCC5						
ABCC6						
ABCC11						
ABCG2				[174][174] [178][178]	153 µM 100 µM	90% 21%

Inhibitor								
Pantoprazole			**Indomethacin**			**Probenecid**		
Reference	[Inhibitor]	% Inhibition	Reference	[Inhibitor]	% Inhibition	Reference	[Inhibitor]	% Inhibition
[197][197] [198][198]	290 µM 250 µM	50% ~75%						
			[330][330] [331][331]	10 µM 100 µM	29% 25%	[330][330] [331][331] [332][332] [333][333]	1 mM 1 mM 1 mM 5 mM	29% 90% 95% 65%
			[331][331] [332][332]	100 µM 600 µM	5% 50%	[331][331] [332][332] [334][334] [335][335] [336][336]	1 mM 1 mM 1 mM 1 mM 260 µM	78% 25% 90% 90% 60%
						[327][327] [336][336]	333 µM 260 µM	65% 70%
			[329][329] [335][335] [337][337]	50 µM 100 µM 50 µM	26% 95% 89%	[328][328] [335][335] [338][338] [339][339] [340][340]	300 µM 1 mM 1 mM 100 µM 1 mM	51% 80% 40% 48% 90%
						[338][338] [341][341]	1 mM 50 µM	>80% 68%
[197][197] [197][197]	138 µM* 145 µM^	69% 80%	[331][331]	100 µM	83%	[331][331]	1 mM	30%
			[342][342]	10 µM	36%	[342][342]	10 µM	24%
[144][144] [199][199] [247][247]	100 µM 100 µM 250 µM	55% 95% 90%						

Results from *omeprazole and ^esomeprazole. Pantoprazole demonstrated similar results but data was not shown.

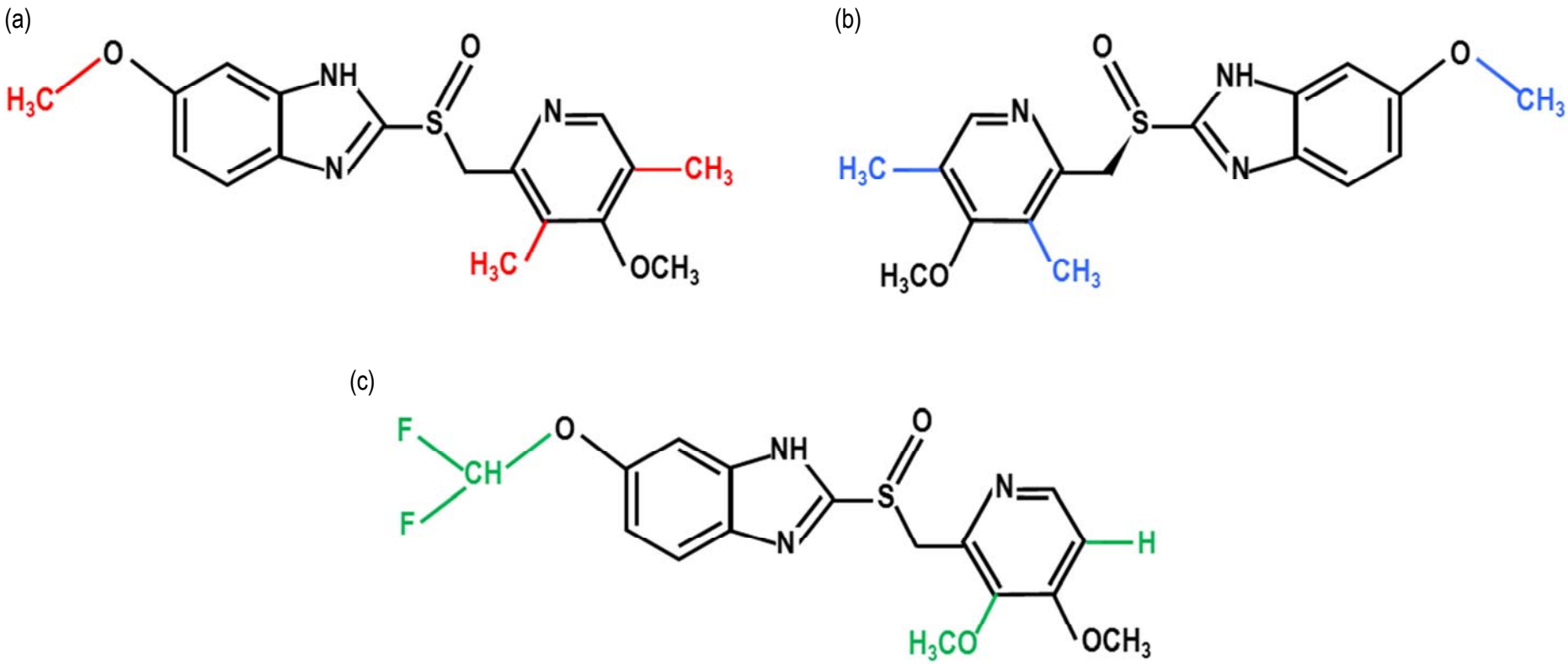

Figure 7.2: Structure of three common PPIs (modified from Jain *et al.*[343])

The chemical structures of a) omeprazole, b) esomeprazole and c) pantoprazole are depicted. All PPIs contain the timoprazole backbone (**BLACK**); esomeprazole is an analogue of omeprazole with both drugs containing the same terminal groups extending from the benzimidazole moieties (**BLUE** and **RED** respectively). Pantoprazole differs slightly in that it contains a difluoromethyl group which increases its half-life and solution solubility (**GREEN**).

Concomitant administration of inhibitors of ABC transporters have previously been demonstrated to increase the efficacy of various cytotoxic agents *in vitro* and *in vivo*[344,345]. While some Phase III studies have demonstrated an association between increased toxicity and the combined usage of ABCB1 inhibitors with cancer therapy[346,347], other reports confirm results observed *in vitro*; increased response rates as well as overall survival have been observed in patients receiving conventional therapy combined with adjunct ABC transporter inhibitors in the treatment of solid tumours[348,349], myelodysplastic syndromes[350] and leukaemia[351]. Administration of TKIs with such inhibitors may also present an attractive therapy option in order to enhance TKI efficacy in CML. Thus, this chapter aims to assess the effect of concomitant administration of ABC inhibitors on *in vitro* intracellular concentrations of TKIs in patient mononuclear cells (MNCs).

7.2. Approach

Previous studies have demonstrated that exposure of cells to xenobiotics results in an increase in mRNA expression of relevant transporters[138,216-219]. Thus, in order to identify other candidate transporters potentially involved in the transport of nilotinib, mRNA expression levels in Bcr-Abl positive cell lines exposed to nilotinib were compared with those in cells incubated in the absence of nilotinib (**Figure 7.3**). Commercially available Taqman Transporter Arrays (Applied Biosystems) containing primer and probe sets specific for 84 human transporters as well as 12 controls were utilised (**Section 2.4.6**; **Appendix 1D**). Based on previous studies, K562 and KU812 cells were initially exposed to varying concentrations of nilotinib (25 nM–500 nM) for time points ranging 12–48 h in order to determine the greatest length of time resulting in minimal cell death. Once these variables had been determined, K562 cells were incubated with 75 nM nilotinib for 24 h and KU812 cells were incubated with 100 nM nilotinib for 12 h. Additionally, K562 cells that had been growing long term in 300 nM and 2 µM nilotinib, as part of the resistance development detailed in **Chapter 5**, were also assessed for alterations in transporter expression compared with control cells. This allowed identification of 'transporters of

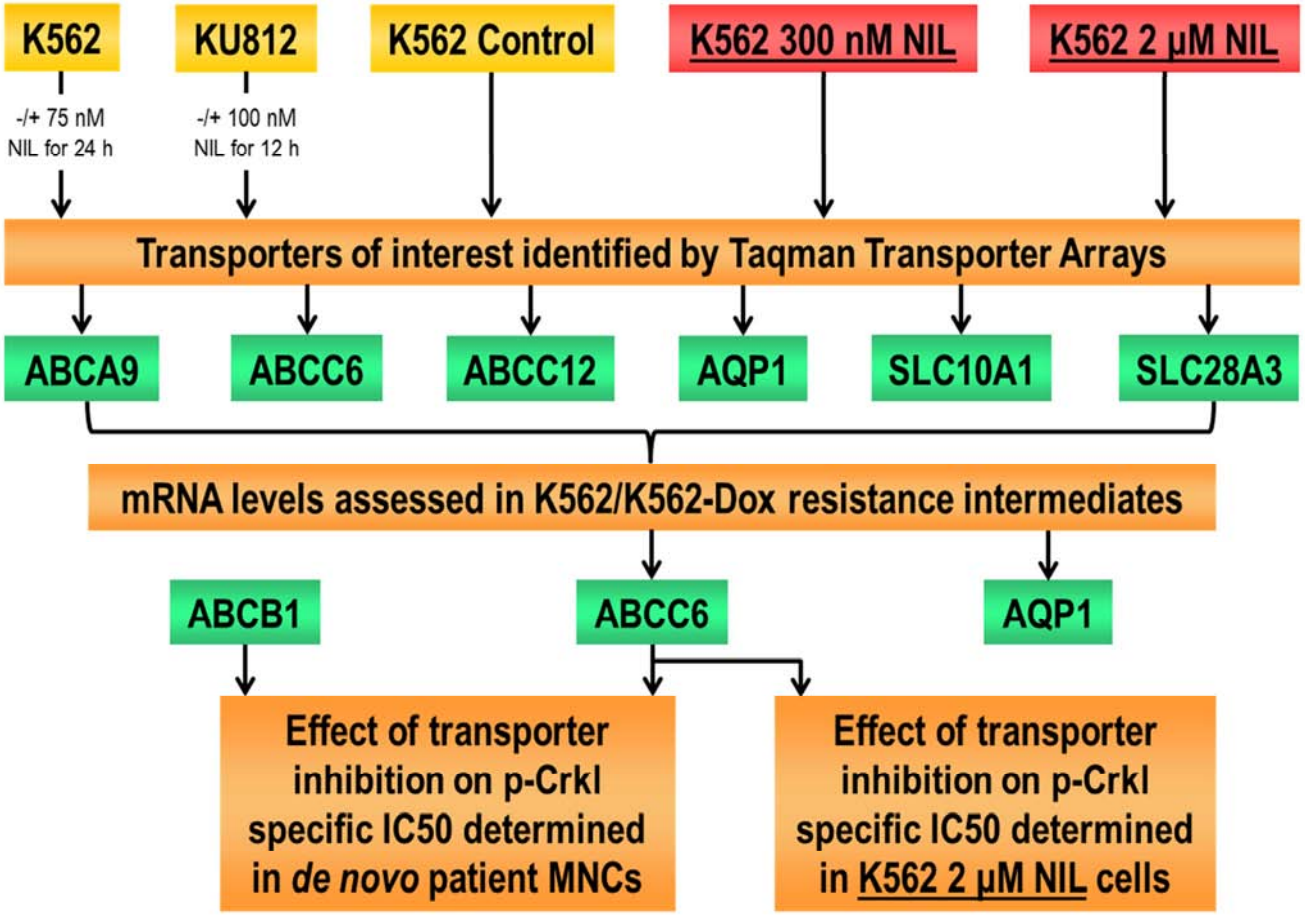

Figure 7.3: Schematic summary of approach used to ascertain relevant nilotinib transporters

Cells were cultured in the absence or presence of nilotinib and transporter mRNA expression determined. Relevance to nilotinib transport was confirmed in K562 and K562-Dox resistance intermediates. The effect of ABCC6 inhibition on nilotinib-, imatinib- and dasatinib-mediated Bcr-Abl kinase inhibition was then assessed in *de novo* CML patient MNCs. The effect of ABCC6 inhibition on $IC50^{NIL}$ was also determined in K562 2 µM NIL resistant cells. NIL=nilotinib.

interest' demonstrating overexpression in all four instances. Resistance intermediates for K562 and K562-Dox nilotinib resistant cells were then interrogated for changes in mRNA expression of these transporters of interest by RQ-PCR (**Section 2.4.5**). The number of PCR cycles required for amplification of product above threshold indicated extremely low expression levels for the majority of the transporters of interest thus making it unlikely these transporters were involved in nilotinib transport or resistance development. However, levels of ABCC6 mRNA increased proportionally with increasing nilotinib concentration (and increasing nilotinib resistance) in K562 cells, making investigation of the effect of inhibition of this transporter warranted in patient MNCs.

The involvement of ABCB1 in transport of, and resistance to, nilotinib has previously been discussed in **Chapters 4, 5** and **6**. Thus, the effect of ABCB1 inhibition on intracellular concentrations of nilotinib in MNCs isolated from peripheral blood samples of *de novo* CML patients was assessed by p-Crkl specific IC50 (**Section 2.4.2**) prior to the onset of TKI therapy. Three ABCB1 inhibitors were selected for use: PSC-833, verapamil and pantoprazole. PSC-833 was used at 10 μM as previous publications have deemed this concentration sufficient to inhibit ABCB1[321-323]. Additionally, rhodamine-123 efflux assays have demonstrated 10 μM PSC-833 completely inhibits ABCB1 function (**Chapter 4**). Verapamil was used at 50 μM as this concentration is thought to be ABCB1 specific; higher concentrations (150 μM) may inhibit ABCG2 as well[174]. 50 μM verapamil is also sufficient to inhibit ABCB1-mediated rhodamine-123 efflux (**Chapter 4**). While 200 μM pantoprazole exceeds the reported C_{max}[352], this concentration was chosen based on *in vitro* data[197,198] as well as experimentation from our laboratory demonstrating the degree of kinase inhibition in patient MNCs in the presence of 200 μM pantoprazole mimics that observed in the presence of 10 μM pantoprazole[294]. Pantoprazole was favoured over other well studied PPIs, esomeprazole and omeprazole, as it has been demonstrated *in vivo*, that pantoprazole has a greater half-life as well as greater stability at neutral pH[353].

The effect of ABCC6 inhibition on intracellular concentrations of nilotinib, imatinib and dasatinib in *de novo* CML patient PBMNCs was assessed by p-Crkl specific IC50. In addition to pantoprazole, two extra inhibitors of ABCC6 were selected for use: indomethacin and probenecid, which were used at 100 µM and 1 mM respectively, based on previously published *in vitro* studies (**Table 7.3**). Importantly, neither inhibitor has been demonstrated to interact with ABCB1. Additionally, levels of ABCC6 mRNA were determined in 83 *de novo* CML patients prior to initiation of nilotinib therapy (**Section 2.4.5**) such that ABCC6 expression can be correlated with response once this data becomes available.

IC50 experiments were also conducted on K562 2 µM NIL resistant cells (**Section 2.3.3.3**) in the absence and presence of the ABCC6 inhibitor indomethacin. These cells exhibit overexpression of ABCB1 and ABCC6 mRNA. Thus, as pantoprazole inhibits both ABCB1 and ABCC6, this was not deemed a specific inhibitor since inhibition of ABCB1 may have complicated results. Similarly, probenecid exhibits less transporter specificity than indomethacin (**Table 7.3**) and was also omitted from this line of *in vitro* testing.

7.3. Results

7.3.1. Exposure to Nilotinib Causes Alterations in mRNA Levels of Cellular Transporters

Previous studies have demonstrated that >8 h incubation with various cytotoxic agents results in mRNA up regulation of transporters known to be relevant for those drugs[217,218]. Thus, K562 and KU812 cells were cultured for 12–48 h in the presence of increasing concentrations of nilotinib (0–500 nM) to determine the optimum conditions at which minimal cell death occurred while in the presence of sufficient nilotinib to induce changes in mRNA. Following incubation, cell death was determined by Annexin V/7-AAD flow cytometry and confirmed by trypan blue staining. Results demonstrated minimal K562 cell death occurred when cells were cultured with 75 nM of nilotinib for 24 h; similarly minimal KU812 cell death occurred when cells were cultured with 100 nM nilotinib for 12 h (**Appendix 5A**).

Accordingly, cells were cultured under these conditions, the mRNA expression of cellular transporters assessed and compared with expression in cells incubated in the absence of nilotinib. The fold changes in expression levels were calculated (**Appendix 5B a–b**) with those demonstrating greater than 8-fold increase of transporters in the presence of nilotinib summarised in **Table 7.4**.

7.3.2. Cellular Transporter mRNA Expression is Different in Nilotinib Sensitive and Resistant Cells

Once it was established that transient exposure to nilotinib induced changes in transporter mRNA expression, it was next determined whether long term exposure resulted in similar alterations. Consequently, nilotinib resistant K562 cells cultured long term in two different concentrations of nilotinib (300 nM and 2 μM) were assessed for changes in mRNA expression when compared with control cells. Again, the fold changes in mRNA expression were calculated (**Appendix 5B c–d**) and those demonstrating a greater than 5-fold increase in transporter expression in the presence of nilotinib determined (**Table 7.5**).

7.3.3. ABCC6 mRNA Increases During Development of Nilotinib Resistance *In Vitro*

Results from all four experiments were compared and transporters exhibiting consistent up regulation were further examined in the intermediates generated during development of nilotinib resistance in K562 cells (**Chapter 5**). Unfortunately expression levels for ABCA9, ABCC12, SLC10A1 and SLC28A3 were extremely low thus making it less likely that these transporters play a role in development of nilotinib resistance (**Appendix 5C**). However, ABCC6 and Aquaporin 1 (AQP1) demonstrated significant up regulation of mRNA upon development of nilotinib resistance. AQP1 mRNA levels reached a maximum of 5.4-fold greater in K562 125 nM NIL cells when compared with control cells (p<0.001; **Figure 7.4a**). The increase observed in ABCC6 mRNA levels was more marked with mRNA expression levels reaching a maximum of 57-fold greater in K562 300 nM NIL cells compared with

Table 7.4a: mRNA levels of cellular transporters in K562 cells cultured in the absence and presence of 75 nM nilotinib demonstrating greater than 8-fold increase in expression

Transporter Gene	0 nM NIL (Ct)	+75 nM NIL (Ct)	Fold Change
ABCA1	37.2	34.3	8.7
ABCA9	**36.9**	**32.8**	**20.7**
ABCB5	36.9	33.0	17.9
ABCC11	37.3	34.4	8.5
ABCC12	**40.0**	**37.0**	**9.1**
ABCC6	**40.0**	**36.9**	**9.7**
AQP1	**27.0**	**23.9**	**10.0**
AQP7	37.1	33.9	10.3
SLC10A1	**36.1**	**29.9**	**86.9**
SLC10A2	40.0	37.0	9.4
SLC28A3	**37.2**	**34.0**	**10.7**
SLC5A1	40.0	37.0	9.3
SLCO1A2	30.9	28.0	8.7

Table 7.4b: mRNA levels of cellular transporters in KU812 cells cultured in the absence and presence of 100 nM nilotinib demonstrating greater than 8-fold increase in expression

Transporter Gene	0 nM NIL (Ct)	+100 nM NIL (Ct)	Fold Change
ABCA9	**37.0**	**21.5**	**53879.0**
ABCC12	**37.2**	**33.2**	**17.8**
ABCC6	**40.0**	**37.0**	**9.5**
AQP1	**33.0**	**29.0**	**18.6**
SLC28A3	**37.0**	**33.0**	**18.6**

Common transporters requiring further investigation are shown in **BOLD**.

NIL=nilotinib; Ct=cycle threshold (the number of cycles required for the fluorescent signal to exceed background level).

Table 7.5a: mRNA levels of cellular transporters in K562 cells cultured long term in the absence and presence of 300 nM nilotinib demonstrating greater than 5-fold increase in expression

Transporter Gene	Control (Ct)	+300 nM NIL (Ct)	Fold Change
ABCA13	29.7	27.4	5.2
ABCA9	**37.0**	**34.5**	**5.9**
ABCB1	29.6	25.4	19.9
ABCC3	38.4	36.1	5.2
ABCC6	**37.4**	**31.6**	**64.5**
AQP1	**30.8**	**26.9**	**16.2**
SLC10A1	**40.0**	**34.3**	**58.2**
SLC16A3	30.7	27.3	11.2
SLC28A3	**37.9**	**33.7**	**20.3**
SLCO2B1	31.1	26.7	22.7

Table 7.5b: mRNA levels of cellular transporters in K562 cells cultured long term in the absence and presence of 2 µM nilotinib demonstrating greater than 5-fold increase in expression

Transporter Gene	Control (Ct)	+2 µM NIL (Ct)	Fold Change
ABCC6	**37.0**	**33.9**	**8.1**
AQP1	**30.0**	**27.0**	**7.9**
SLC10A1	**40.0**	**32.0**	**248.3**
SLC16A3	33.0	29.0	16.0
SLC19A3	40.0	13.2	119997543.9
SLC22A8	37.0	7.7	621847739.5
SLCO2B1	29.0	26.0	8.3

Common transporters requiring further investigation are shown in **BOLD**.

NIL=nilotinib; Ct=cycle threshold (the number of cycles required for the fluorescent signal to exceed background level).

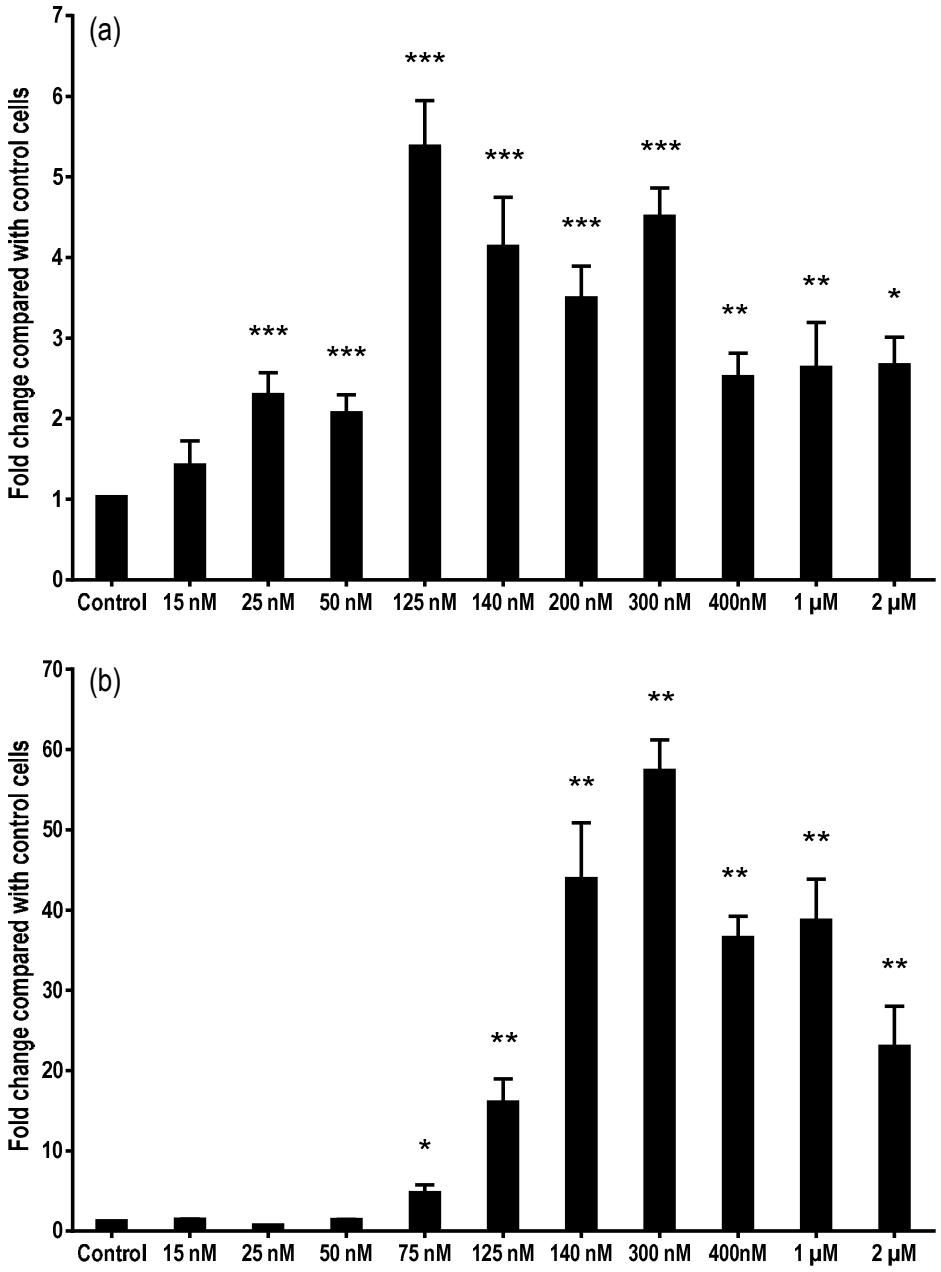

Figure 7.4: Onset of nilotinib resistance in K562 cells coincides with overexpression of AQP1 and ABCC6

Expression levels of a) AQP1 and b) ABCC6 were assessed in K562 nilotinib resistance intermediates. Data demonstrate overexpression of both AQP1 and ABCC6 at the onset of resistance in K562 125 nM NIL cells. Levels remain high as the concentration of nilotinib increases. mRNA expression represents the mean of six independent experiments performed in triplicate. Statistical analyses were performed on mRNA levels as a percentage BCR using Student's *t*-test. Statistically significant *p*-values are denoted by asterisks (* $p<0.05$; ** $p<0.01$; *** $p<0.001$). Error bars represent SEM.

control cells (p=0.002; **Figure 7.4b**). ABCC6 mRNA expression also increased in K562-Dox NIL #1 and K562-Dox NIL #2 cells during development of nilotinib resistance. Levels peaked in K562-Dox 1 μM NIL #1 and K562-Dox 1 μM NIL #2 cells, reaching 33- and 23-fold greater levels respectively than those in control cells (p=0.002; **Figure 7.5**).

ABCC1, ABCC2 and ABCC4 are all inhibited by both indomethacin and probenecid and are expressed at points of drug extrusion (liver, kidney). Thus, mRNA levels of these transporters were also assessed in order to exclude them as potential candidates in the development of nilotinib resistance. Importantly, there was no significant change in expression levels of ABCC1, ABCC2 or ABCC4 in any of the resistance intermediates from K562 cells making them unlikely candidates in the transport of, or development of resistance to, nilotinib (**Figure 7.6**).

7.3.4. ABCB1 Inhibition Does Not Significantly Affect Nilotinib-Mediated Kinase Inhibition in Patient Mononuclear Cells

ABCB1 expression has been implicated in the transport of nilotinib (**Chapter 4**); additionally, overexpression has been associated with development of nilotinib resistance *in vitro* (**Chapters 5** and **6**). Thus, the role of ABCB1 in nilotinib-mediated kinase inhibition was determined in patient MNCs. $IC50^{NIL}$ experiments were performed with the MNCs of *de novo* CML patients prior to the start of TKI therapy in the absence and presence of three ABCB1 inhibitors: PSC-833, verapamil and pantoprazole. It was expected that if ABCB1 is involved in nilotinib transport in patient MNCs, inhibition of this transporter should increase concentrations of intracellular nilotinib resulting in a reduction in $IC50^{NIL}$ (**Figure 7.7**). However, a significant decrease in $IC50^{NIL}$ was observed only in those cells incubated in the presence of 200 μM pantoprazole: 41 nM versus 71 nM in control cells (p<0.001). The addition of 10 μM PSC-833 and 50 μM verapamil had no effect on $IC50^{NIL}$: 76 nM and 80 nM respectively (p>0.05; **Figure 7.8**) suggesting ABCB1 may not play a critical role in the efflux of nilotinib from patient MNCs.

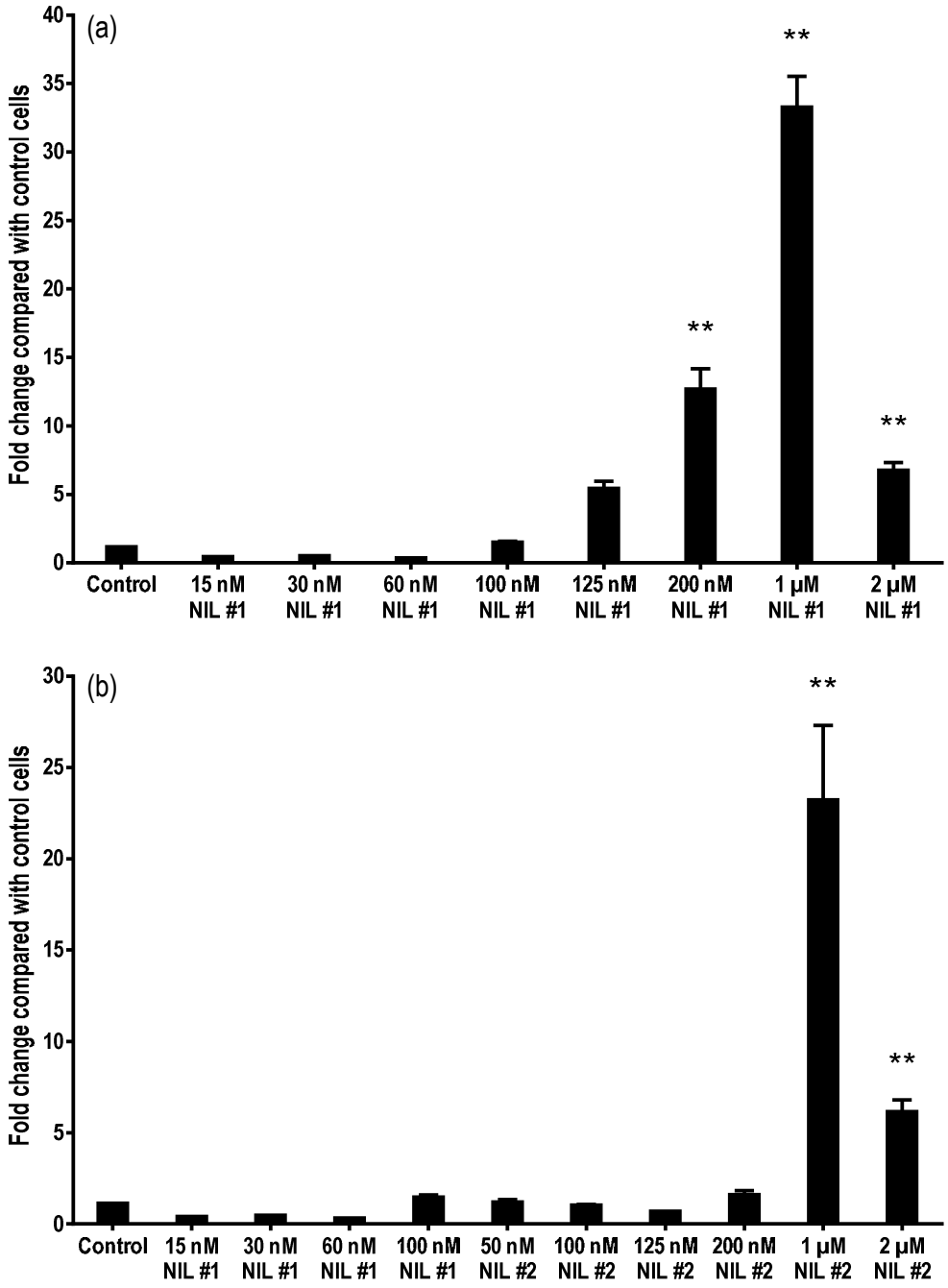

Figure 7.5: ABCC6 expression in K562-Dox cells increases with resistance

Expression levels of ABCC6 mRNA were assessed in a) K562-Dox NIL #1 and b) K562-Dox NIL #2 cells. Data demonstrate overexpression of ABCC6 in both cell lines which reached a maximum in the 1 µM NIL intermediates. mRNA expression represents the mean of six independent experiments performed in triplicate. Statistical analyses were performed on mRNA levels as a percentage of BCR using Student's *t*-test. Statistically significant *p*-values are denoted by asterisks (** $p<0.01$). Error bars represent SEM. NIL=nilotinib.

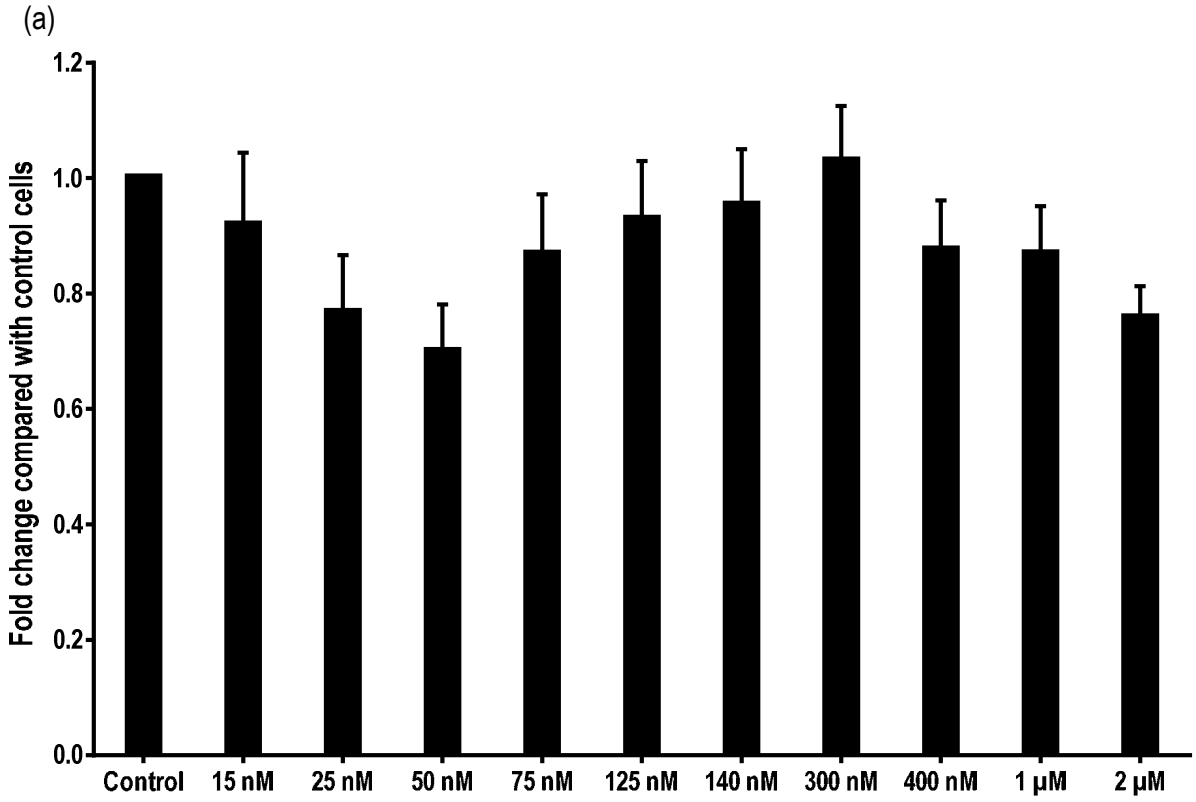

Figure 7.6: Neither ABCC1, ABCC2 nor ABCC4 levels increase during development of nilotinib resistance in K562 cells

Expression levels of a) ABCC1, b) ABCC2 and c) ABCC4 mRNA were assessed in K562 nilotinib resistance intermediates. Data demonstrate no increase in levels of ABCC1, ABCC2 or ABCC4 expression at any time during development of nilotinib resistance. mRNA expression represents the mean of at least three independent experiments performed in triplicate. Statistical analyses were performed on mRNA levels as a percentage of BCR using Student's *t*-test. Error bars represent SEM.

(b)

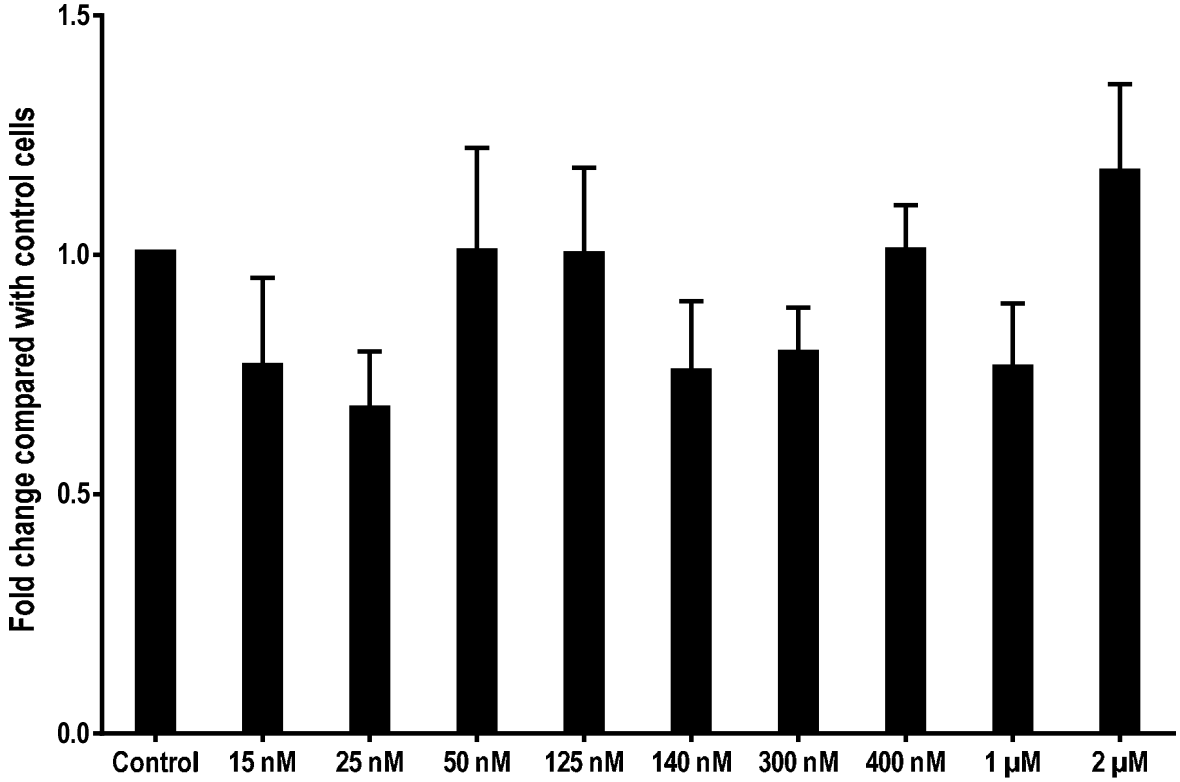
Fold change compared with control cells
1.5
1.0
0.5
0.0
Control
15 nM
25 nM
50 nM
125 nM
140 nM
300 nM
400 nM
1 µM
2 µM

(c)

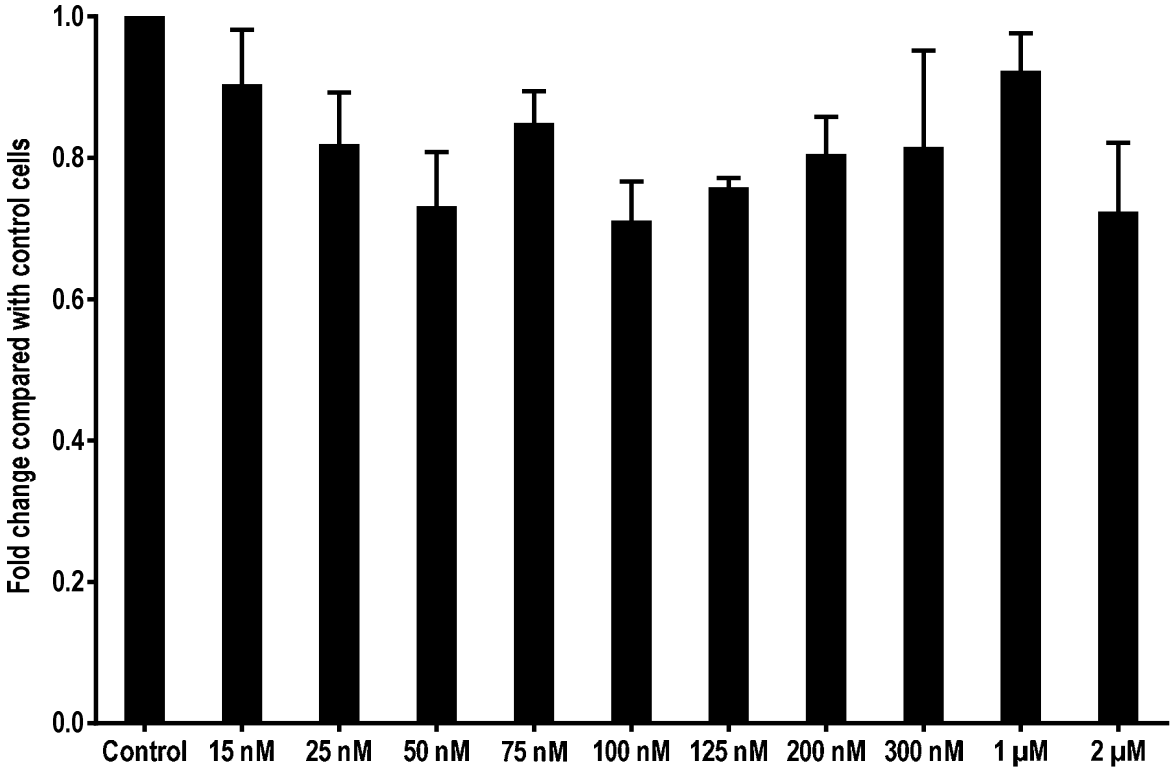
Fold change compared with control cells
1.0
0.8
0.6
0.4
0.2
0.0
Control
15 nM
25 nM
50 nM
75 nM
100 nM
125 nM
200 nM
300 nM
1 µM
2 µM

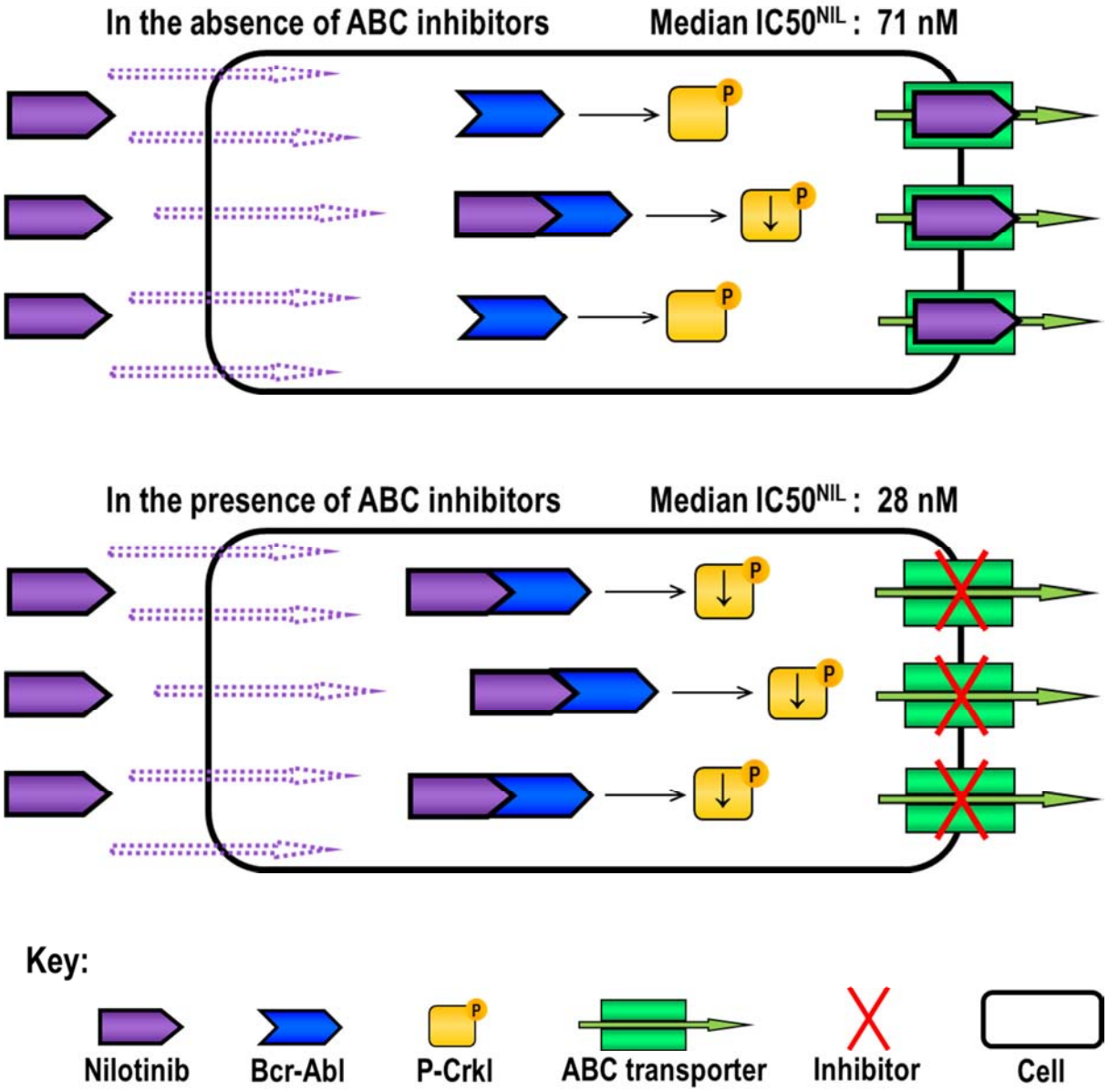

Figure 7.7: Schematic summary of p-Crkl specific IC50 experiments

TKIs enter the cell (in the case of nilotinib by passive transport) and bind to Bcr-Abl inhibiting its kinase activity. This results in a reduction of downstream effector molecules such as p-Crkl allowing calculation of an IC50 value. In the absence of ABC inhibitors (upper figure), nilotinib is exported from the cell by efflux transporters. If nilotinib is transported by ABCB1 for example, in the presence of ABCB1 inhibitors such as PSC-833, verapamil and pantoprazole (lower figure) nilotinib is retained within the cell to a greater degree resulting in increased kinase inhibition and reduced IC50.

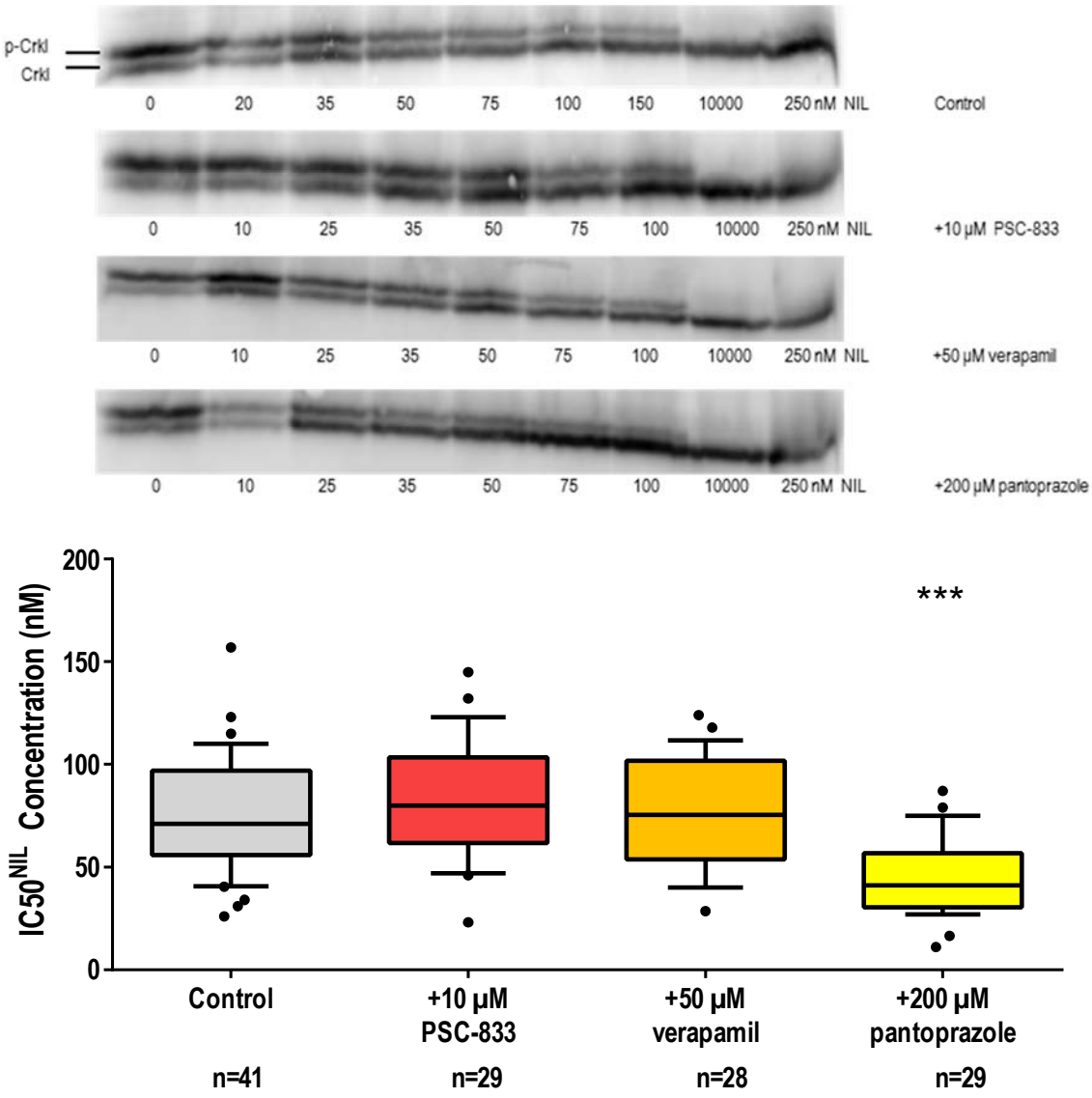

Figure 7.8: Inhibition of ABCB1 does not significantly decrease $IC50^{NIL}$ in patient MNCs

IC50 was determined via incubating patient MNCs for 2 h at 37°C with increasing concentrations of nilotinib in the absence and presence of three ABCB1 inhibitors: 10 µM PSC-833, 50 µM verapamil and 200 µM pantoprazole. Crkl western blot was performed to determine the concentration of nilotinib required to inhibit Bcr-Abl kinase activity by 50%. Data demonstrate that $IC50^{NIL}$ is significantly reduced in the presence of pantoprazole but no effect is observed in the presence of PSC-833 or verapamil. The western blot analyses shown depict one patient and are representative of typical results. The corresponding box plots depict the median, the upper 25th and the lower 75th percentiles while the whiskers encompass the 10th and 90th percentiles. Statistical analyses were performed using Student's *t*-test with statistically significant *p*-values denoted by asterisks (*** $p<0.001$). NIL=nilotinib.

7.3.5. ABCC6 Inhibition Significantly Increases Nilotinib-Mediated Kinase Inhibition in Patient Mononuclear Cells

Because pantoprazole has inhibitory activity against other ABC transporters (**Table 7.3**), $IC50^{NIL}$ experiments were repeated in the presence of two additional ABCC6 inhibitors: indomethacin and probenecid. Results demonstrated a significant reduction in $IC50^{NIL}$ in the presence of both indomethacin and probenecid ($IC50^{NIL}$ in the absence of inhibitor=71 nM; +100 μM indomethacin=38 nM; +1 mM probenecid=28 nM; $p<0.001$; **Figure 7.9**). These results indicate it is likely ABCC6 plays a role in the transport of nilotinib.

7.3.6. ABCC6 Inhibition Has No Significant Effect on Imatinib-Mediated Kinase Inhibition in Patient Mononuclear Cells

Once the interaction between nilotinib and ABCC6 had been established, we sought to determine whether a similar interaction occurred between ABCC6 and the two other TKIs currently approved for treatment of CML: imatinib and dasatinib. $IC50^{IM}$ experiments in the absence and presence of pantoprazole, indomethacin and probenecid were conducted in a cohort of 23 *de novo* CML patients prior to therapy. Data demonstrated no significant reduction in $IC50^{IM}$ upon addition of any of the ABCC6 inhibitors ($IC50^{IM}$ in the absence of inhibitor=0.96 μM; +200 μM pantoprazole=1 μM; +100 μM indomethacin=1 μM; +1 mM probenecid=1.08 μM; $p>0.05$; **Figure 7.10**). Thus, it is unlikely ABCC6 plays a role in the transport of imatinib in patient MNCs.

7.3.7. ABCC6 Inhibition Significantly Increases Dasatinib-Mediated Kinase Inhibition in Patient Mononuclear Cells

Similarly, the role of ABCC6 in the transport of dasatinib within CML patient MNCs was also investigated. Again, $IC50^{DAS}$ experiments were performed in the absence and presence of pantoprazole, indomethacin and probenecid. Results demonstrated a significant decrease in $IC50^{DAS}$ in

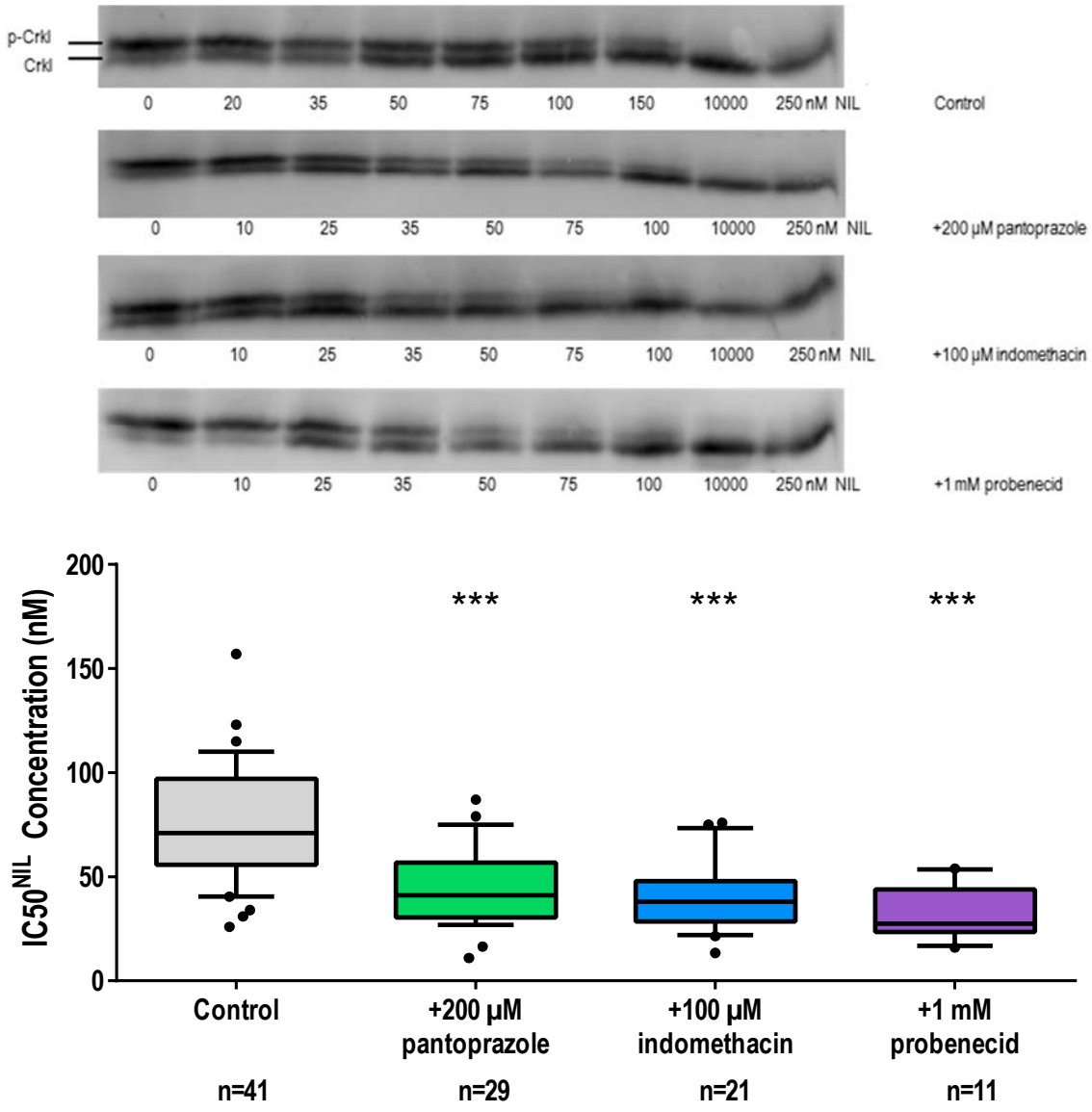

Figure 7.9: Inhibition of ABCC6 significantly reduces $IC50^{NIL}$ in patient MNCs

IC50 was determined via incubating patient MNCs for 2 h at 37°C with increasing concentrations of nilotinib in the absence and presence of three ABCC6 inhibitors: 200 µM pantoprazole, 100 µM indomethacin and 1 mM probenecid. Crkl western blot was performed to determine the concentration of nilotinib required to inhibit Bcr-Abl kinase activity by 50%. Data demonstrate that $IC50^{NIL}$ is significantly reduced in the presence of all three inhibitors. The western blot analyses shown depict one patient and are representative of typical results. The corresponding box plots depict the median, the upper 25th and the lower 75th percentiles while the whiskers encompass the 10th and 90th percentiles. Statistical analyses were performed using Student's *t*-test with statistically significant *p*-values denoted by asterisks (*** $p<0.001$). NIL=nilotinib.

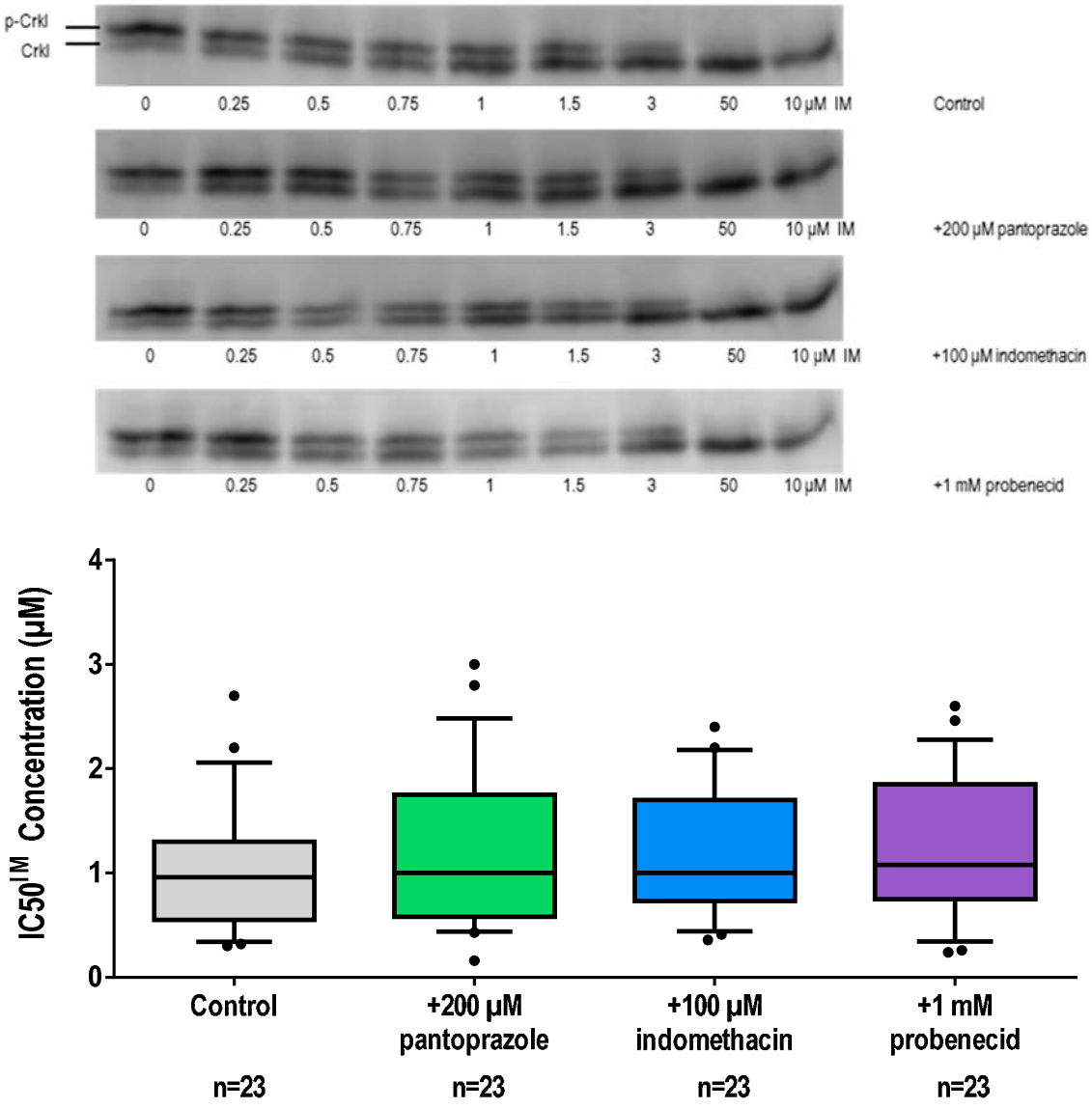

Figure 7.10: Inhibition of ABCC6 has no significant effect on $IC50^{IM}$ in patient MNCs

IC50 was determined via incubating patient MNCs for 2 h at 37°C with increasing concentrations of imatinib in the absence and presence of three ABCC6 inhibitors: 200 µM pantoprazole, 100 µM indomethacin and 1 mM probenecid. Crkl western blot was performed to determine the concentration of imatinib required to inhibit Bcr-Abl kinase activity by 50%. Data demonstrate there is no significant change in $IC50^{IM}$ in the presence of any of the inhibitors. The western blot analyses shown depict one patient and are representative of typical results. The corresponding box plots depict the median, the upper 25th and the lower 75th percentiles while the whiskers encompass the 10th and 90th percentiles. Statistical analyses were performed using Student's *t*-test. IM=imatinib.

the presence of all three inhibitors ($IC50^{DAS}$ in the absence of inhibitor=4.3 nM; +200 μM pantoprazole=3.2 nM, p=0.014; +100 μM indomethacin=2.5 nM, p<0.001; +1 mM probenecid=2.2 nM, p<0.001; **Figure 7.11**). Thus, it is likely ABCC6 plays a role in the efflux of dasatinib from patient MNCs.

7.3.8. ABCC6 Inhibition in K562 2 μM NIL Resistant Cells Reduces $IC50^{NIL}$ and $IC50^{DAS}$ but has No Effect on $IC50^{IM}$

In order to confirm whether ABCC6 overexpression played a role in resistance to TKIs *in vitro*, $IC50^{NI}$ $IC50^{IM}$ and $IC50^{DAS}$ were evaluated in K562 2 μM NIL resistant cells in the absence and presence of indomethacin. It is important to remember that this cell line harbours additional resistance mechanisms which may also contribute to the increased $IC50^{NIL}$, $IC50^{IM}$ and $IC50^{DAS}$ observed (**Chapter 5**). Unfortunately, determination of $IC50^{NIL}$ was not possible due to incomplete inhibition of Bcr-Abl kinase activity at the highest nilotinib concentration (100 000 nM), although a decrease in $IC50^{NIL}$ in the presence of indomethacin was still observed in K562 2 μM NIL resistant cells (**Figure 7.12a**). Importantly, data from $IC50^{IM}$ and $IC50^{DAS}$ experiments, in which complete kinase inhibition was apparent, supported results observed in patients MNCs. In the presence of 100 μM indomethacin, K562 2 μM NIL $IC50^{DAS}$ was decreased to levels comparable to those observed in control cells (K562 control=5.6 nM; K562 2 μM NIL=7.6 nM; K562 2 μM NIL +100 μM indomethacin=6.3 nM; **Figure 7.12b**). This is presumably due to inhibition of Lyn kinase by dasatinib and ABCC6 inhibition by indomethacin. Conversely, addition of indomethacin had no effect on $IC50^{IM}$ in K562 2 μM NIL cells, however the $IC50^{IM}$ value was not decreased to levels observed in control cells most likely due to overexpression of Lyn, against which imatinib has no activity. As expected, the addition of indomethacin had no effect on $IC50^{IM}$ nor $IC50^{DAS}$ in K562 control cells (**Figure 7.12c**).

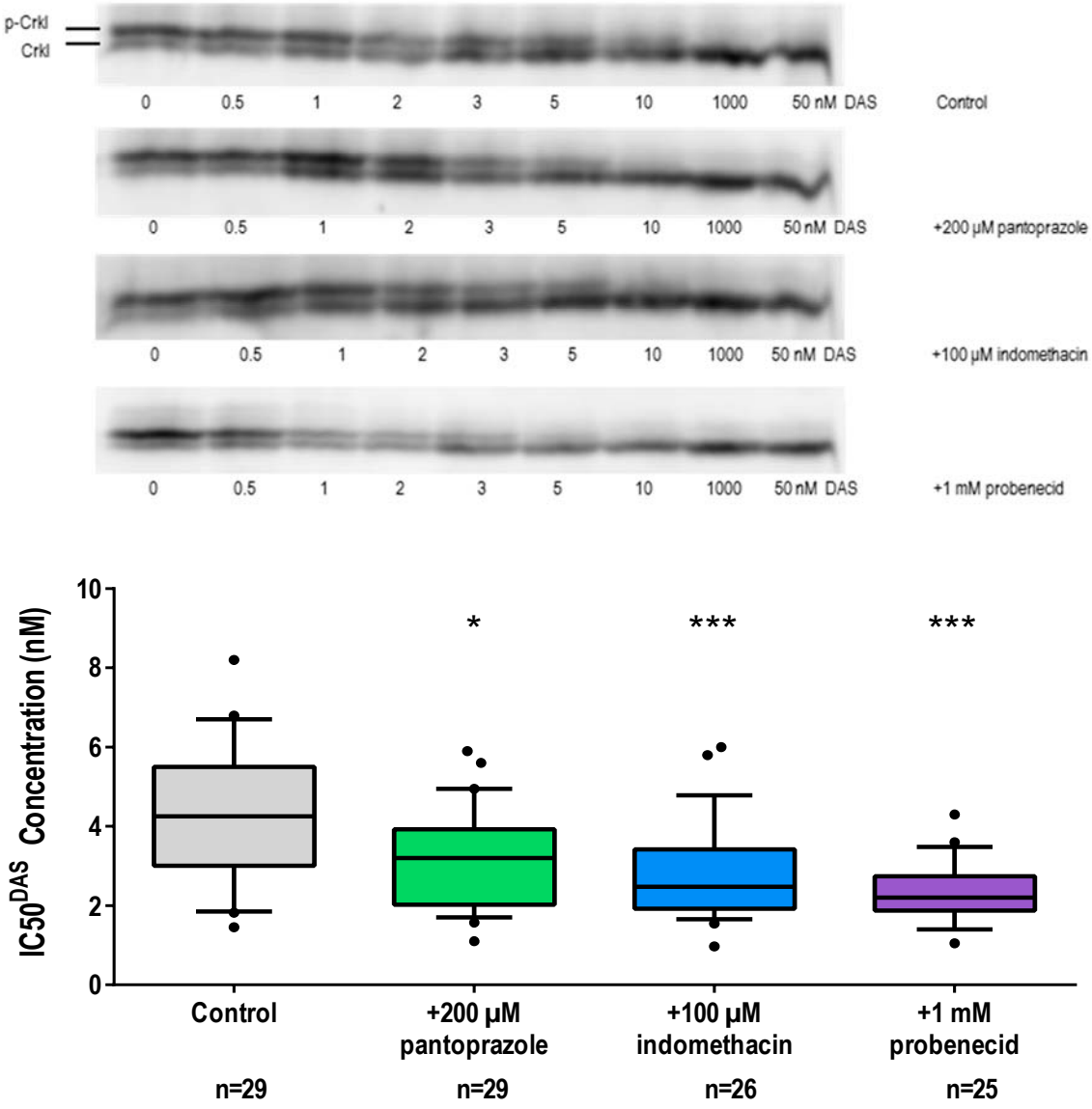

Figure 7.11: Inhibition of ABCC6 significantly reduces IC50^{DAS} in patient MNCs

IC50 was determined via incubating patient MNCs for 2 h at 37°C with increasing concentrations of dasatinib in the absence and presence of three ABCC6 inhibitors: 200 µM pantoprazole, 100 µM indomethacin and 1 mM probenecid. Crkl western blot was performed to determine the concentration of dasatinib required to inhibit Bcr-Abl kinase activity by 50%. Data demonstrate a significant decrease in IC50^{DAS} in the presence of all three inhibitors. The western blot analyses shown depict one patient and are representative of typical results. The corresponding box plot depicts the median, the upper 25th and the lower 75th percentiles while the whiskers encompass the 10th and 90th percentiles. Statistical analyses were performed using Student's *t*-test with statistically significant *p*-values denoted by asterisks ($p<0.05$; *** $p<0.001$). DAS=dasatinib.

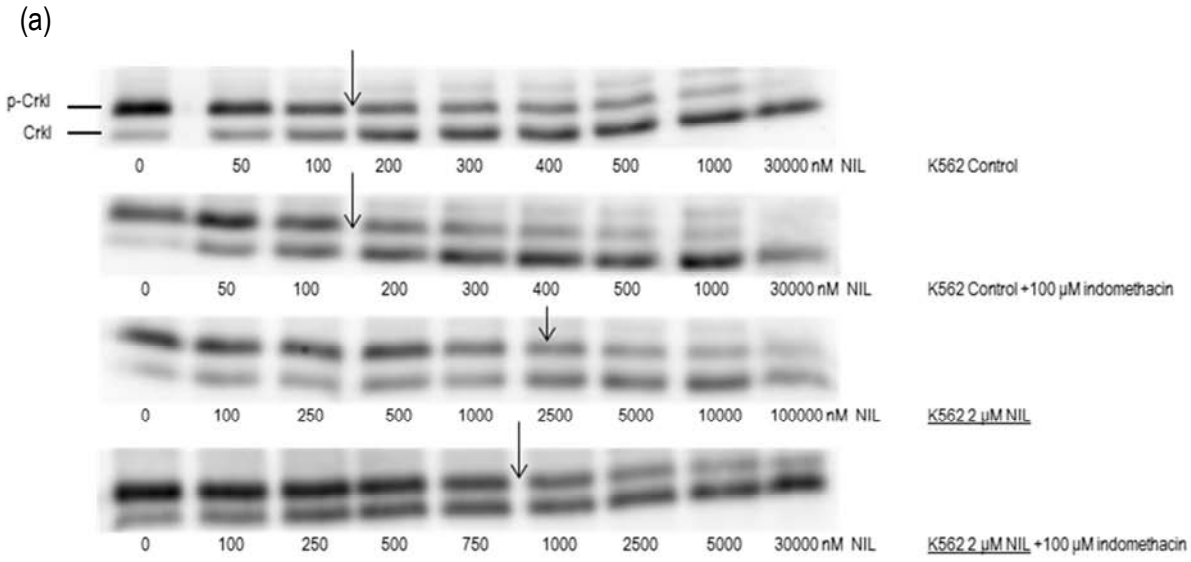

Figure 7.12: ABCC6 inhibition reduces $IC50^{DAS}$ in K562 2 µM NIL cells

IC50 was determined via incubating cells for 2 h at 37°C in the presence of increasing concentrations of a) nilotinib, b) imatinib and c) dasatinib in the absence and presence of the ABCC6 inhibitor, indomethacin. Crkl western blot was performed to determine the concentration of TKI required for 50% Bcr-Abl kinase inhibition. Data demonstrate that K562 2 µM NIL cells have a significantly increased $IC50^{DAS}$ which is negated upon ABCC6 inhibition. $IC50^{NIL}$ is unable to be determined and $IC50^{IM}$ remains unaffected by ABCC6 inhibition. These results support those observed in patient MNCs. The western blot analyses shown are representative of at least three separate experiments with the corresponding densitometry analysis representing the mean. Statistical analyses were performed using Student's t-test with statistically significant *p*-values denoted by asterisks (* $p<0.05$). Error bars represent SEM. The arrows depict approximate nilotinib concentration required for achievement of equal levels of Crkl and p-Crkl proteins. NIL=nilotinib; IM=imatinib; DAS=dasatinib; indo=indoemthacin.

(b)

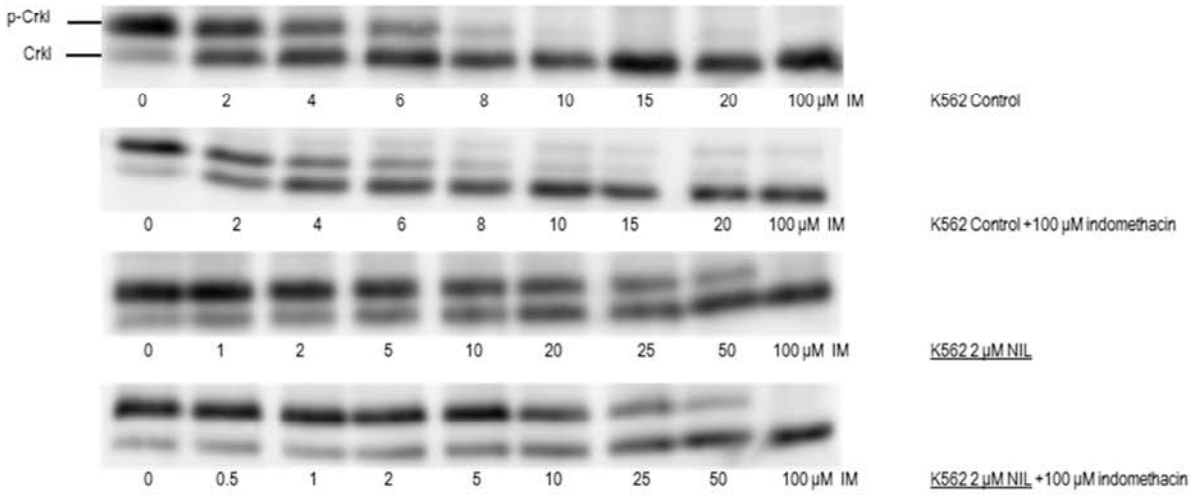
p-Crkl
Crkl
0 2 4 6 8 10 15 20 100 µM IM
K562 Control
0 2 4 6 8 10 15 20 100 µM IM
K562 Control +100 µM indomethacin
0 1 2 5 10 20 25 50 100 µM IM
K562 2 µM NIL
0 0.5 1 2 5 10 25 50 100 µM IM
K562 2 µM NIL +100 µM indomethacin

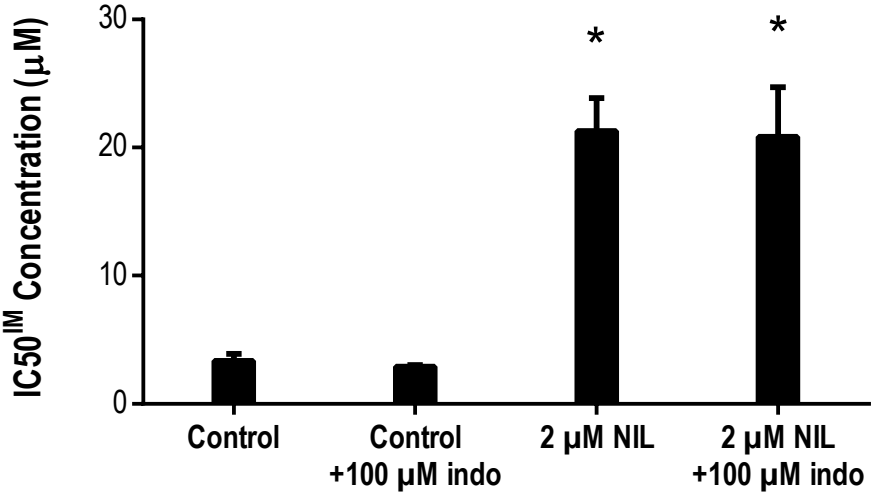
IC50IM Concentration (µM)
30
20
10
0
*
*
Control
Control +100 µM indo
2 µM NIL
2 µM NIL +100 µM indo

(c)

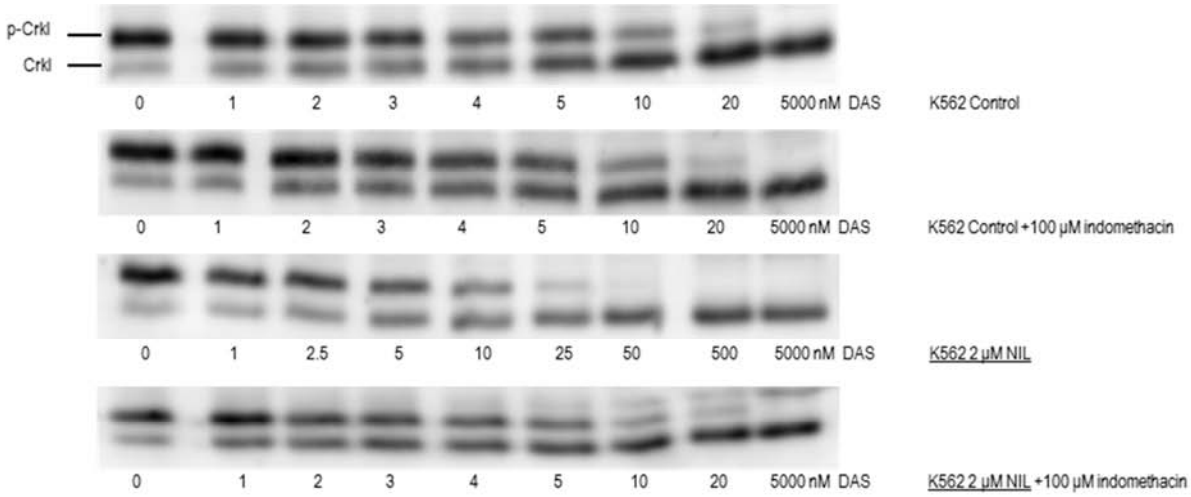
p-Crkl
Crkl
0 1 2 3 4 5 10 20 5000 nM DAS
K562 Control
0 1 2 3 4 5 10 20 5000 nM DAS
K562 Control +100 µM indomethacin
0 1 2.5 5 10 25 50 500 5000 nM DAS
K562 2 µM NIL
0 1 2 3 4 5 10 20 5000 nM DAS
K562 2 µM NIL +100 µM indomethacin

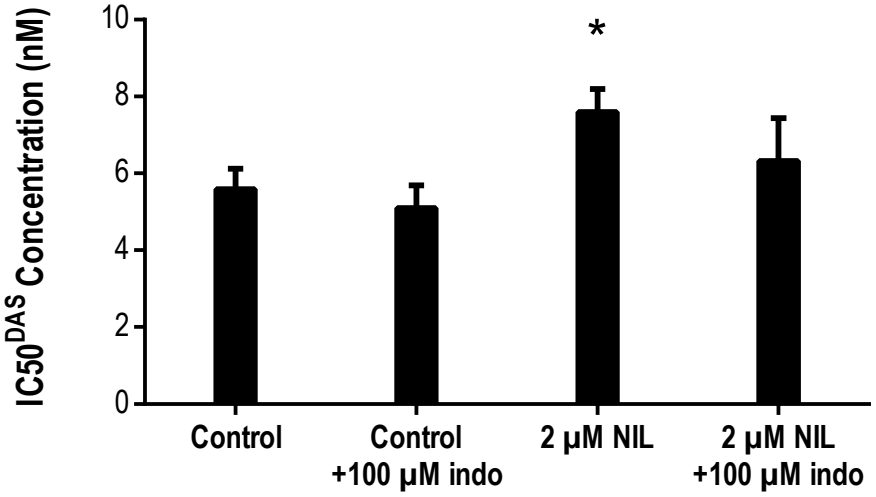
IC50DAS Concentration (nM)
10
8
6
4
2
0
*
Control
Control +100 µM indo
2 µM NIL
2 µM NIL +100 µM indo

7.3.9. Newly Diagnosed CML Patients Exhibit a Range of ABCC6 mRNA Expression Levels

Inhibition of ABCC6 in patient MNCs suggested ABCC6-mediated transport of nilotinib and dasatinib. Accordingly, ABCC6 mRNA levels were determined in 83 newly diagnosed CML patients receiving 300 mg upfront nilotinib twice daily to investigate whether a correlation exists between ABCC6 mRNA levels at diagnosis and response to therapy. Peripheral blood samples were used to determine baseline ABCC6 levels. Data demonstrated a large variation in ABCC6 mRNA levels from <1% to 40% with a median level of 3.2% (**Figure 7.13**). Patients were divided in half about the median and early molecular response at three months assessed (<10% Bcr-Abl). However, because nilotinib has a far greater potency compared with imatinib, the majority of patients achieved this landmark reduction in Bcr-Abl levels by three months thus making this time frame unsatisfactory for predicting long term response. Unfortunately, 12 month data is not yet available on a large enough cohort of patients for any conclusions to be drawn regarding long term major molecular response (MMR; <1% Bcr-Abl). However, achievement of a MMR at three months was assessed when considering the existence of a correlation between ABCB1 overexpression and ability to achieve MMR (**Chapter 6**). Hence, patient ABCC6 mRNA levels and short term response were examined to determine whether or not a correlation existed between these factors. Results demonstrated a weak correlation that may become stronger at 12 months: 78.6% of patients with low ABCC6 expression achieved MMR compared with 70.7% of patients with high ABCC6 expression.

7.3.10. ABCC6 mRNA Expression, in Conjunction with ABCB1 mRNA Expression, May be Used to Determine Response to Nilotinib Therapy

ABCB1 and ABCC6 have been demonstrated to work in concert during nilotinib resistance development (**Figure 7.14**). Thus, the predictive value of ABCB1 and ABCC6 mRNA levels, when assessed in combination, was determined in *de novo* CML patients. Patients were divided into four groups based on transporter mRNA levels: no overexpression, ABCB1 overexpression, ABCC6 overexpression and

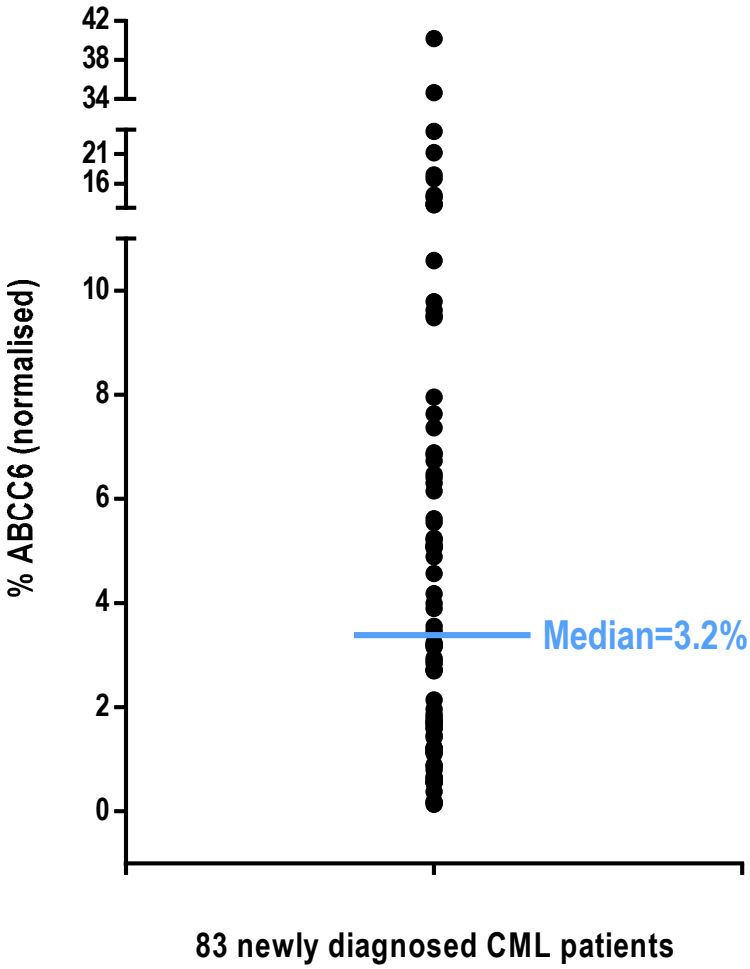

Figure 7.13: *De novo* CML patients exhibit diverse levels of ABCC6 mRNA

ABCC6 mRNA levels were assessed in the peripheral blood of 83 *de novo* CML patients prior to commencement of nilotinib therapy. Data demonstrate a wide variation in expression. Patients were divided in half about the median based on ABCC6 expression. mRNA expression was determined as a percentage of BCR and represents the mean of three independent experiments performed in triplicate. HepG2 cells (ABCC6 overexpressing) were used as a control for reproducibility in all assays. Experiments in which control results were inconsistent were repeated and the results were not included in the analysis.

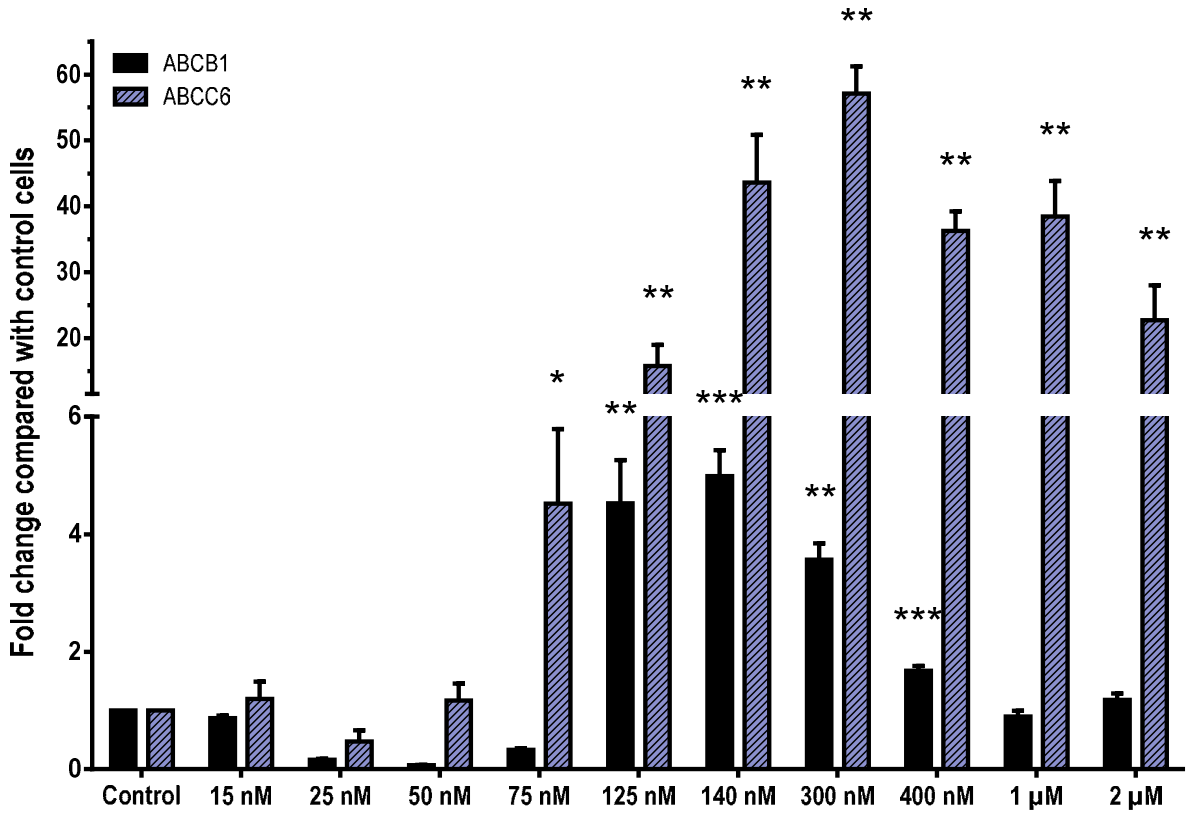

Figure 7.14: ABCB1 and ABCC6 mRNA levels increase in concert during development of nilotinib resistance in K562 cells

Expression levels of ABCB1 and ABCC6 mRNA were assessed in K562 resistance intermediates. Data demonstrate a significant increase in both ABCB1 and ABCC6 expression when cells are cultured in increasing concentrations of nilotinib. The mRNA expression represents the mean of six independent experiments performed in triplicate. Statistical analyses were performed on mRNA levels as a percentage of BCR using Student's *t*-test. Statistically significant *p*-values are denoted by asterisks (* $p<0.05$; ** $p<0.01$; *** $p<0.001$). Error bars represent SEM.

double overexpression and correlated with molecular response to nilotinib at 3 months (**Figure 7.15**). Results demonstrated that ABCC6 overexpression may be predictive of response to nilotinib therapy. Of those patients exhibiting ABCC6 overexpression, 52.6% achieved a MMR at 3 months, compared with 73.9% of patients exhibiting no overexpression or 85.0% of patients overexpressing ABCB1 only. Preliminary analyses of molecular response at 12 months for a small cohort of 29 patients appear to be even more predictive: 28.5% of patients exhibiting ABCC6 overexpression achieved a MMR compared with 44.4% of patients exhibiting no overexpression or overexpressing ABCB1 only. However, analysis of a much larger cohort is required in order to conclude whether a definitive correlation exists, and this will be completed once 12 month data for the remaining patients become available.

7.4. Discussion

We[354] and others[154,176] have previously implicated ABCB1 in the transport of nilotinib (**Chapters 4, 5** and **6**). For this reason, the effect of ABCB1 inhibition on $IC50^{NIL}$ in newly diagnosed CML patients was assessed using three known ABCB1 inhibitors: PSC-833, verapamil and pantoprazole. If nilotinib is indeed transported by ABCB1 one would expect the $IC50^{NIL}$ to decrease in the presence of ABCB1 inhibition. However, results were unexpected with only pantoprazole demonstrating a significant effect on $IC50^{NIL}$. There are two possible explanations for this; firstly, nilotinib is not transported by ABCB1. This seems unlikely given the large volume of *in vitro* data supporting ABCB1 transport. Alternatively, ABCB1 is not a relevant transporter in patient MNCs. This seems more plausible given the low protein expression levels our laboratory has observed in routine screening of *de novo* CML patients (unpublished data). This then casts doubt on the relevance of ABCB1 as a TKI transporter in the newly diagnosed setting. However, high expression of ABCB1 has been demonstrated in primitive $CD34^{+}CD38^{-}$ and $CD34^{+}CD38^{+}$ CML cells[355] as well as cells at the blood-brain barrier[145,356]. The ability of $CD34^{+}$ cells to effectively efflux the ABCB1 substrate rhodamine-123 has also been demonstrated[187]. Thus, ABCB1-mediated TKI efflux may predominantly occur in primitive subsets of cells and in cells at

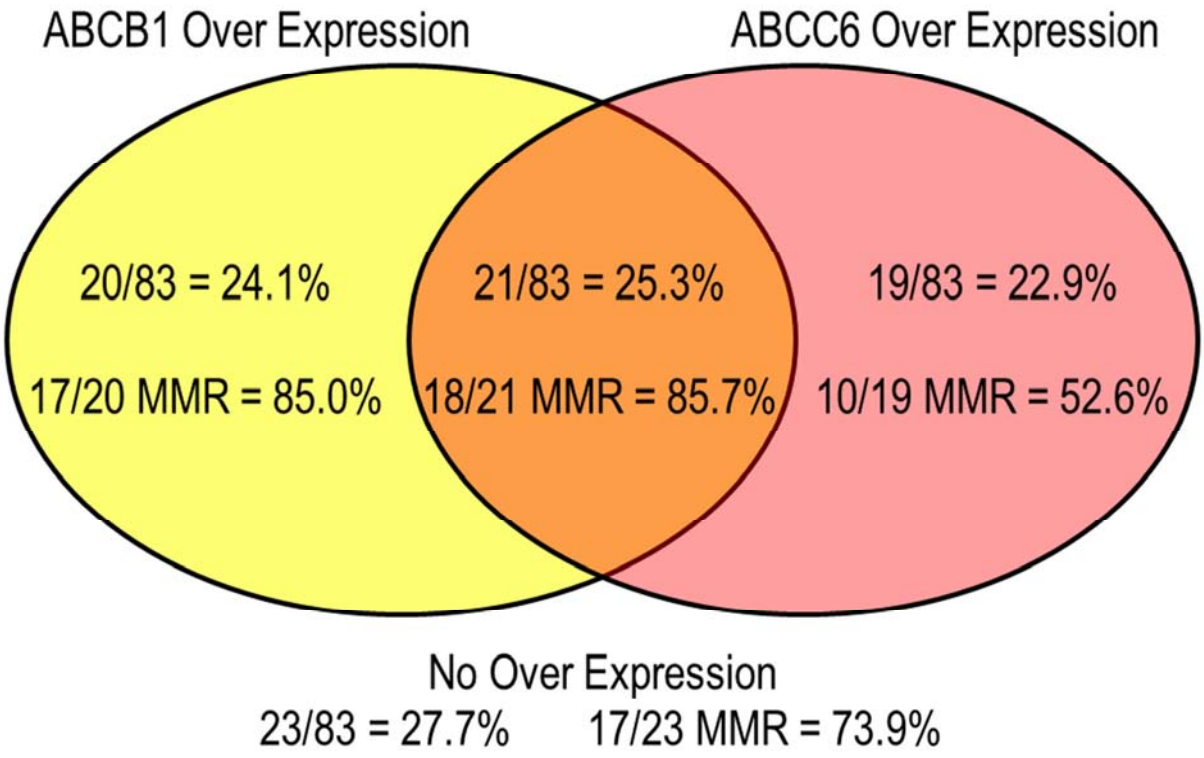

Figure 7.15: Schematic summary of ABCB1 and ABCC6 expression and corresponding patient response

mRNA levels of ABCB1 and ABCC6 were determined and correlated with whether or not a patient achieved <1% Bcr-Abl levels (Major Molecular Response, MMR) by 3 months. Patients were divided about the median for each transporter and separated into groups based on expression levels. Patients overexpressing **ABCB1**, **ABCC6** or **both** are contained within the **YELLOW**, **PINK** and **ORANGE** regions of the graph, respectively. Data demonstrate that those patients overexpressing ABCC6 have less chance of achieving a MMR by 3 months than those patients that do not overexpress either transporter or overexpress ABCB1.

blood-tissue barriers. ABCB1 overexpression may also be involved in progression of CML to more advanced phases of disease as well as exclusion of TKIs from sanctuary sites such as the CNS, brain and testes[318,357]. Furthermore, results described in **Chapter 4** comparing $IC50^{NIL}$ in K562 versus K562-Dox cells confirmed the relevance of ABCB1 overexpression in nilotinib-mediated Bcr-Abl inhibition. Therefore, ABCB1 should not be discounted as a relevant TKI transporter and concomitant administration of ABCB1 inhibitors may increase TKI concentrations in sanctuary sites where drug penetration is of paramount importance for the treatment of residual disease, although this would require *in vivo* testing. Future studies retrospectively assessing ABCB1 mRNA levels in patients who develop mutations, undergo disease progression or fail to achieve MMR while receiving up front imatinib will be conducted. ABCB1 mRNA and protein levels are also currently being assessed in newly diagnosed patients receiving up front nilotinib both at diagnosis as well as subsequent time points post therapy. These results will then be correlated with response once this data becomes available.

Previous studies have demonstrated that, upon exposure to certain xenobiotics, cells increase mRNA expression of transporters known to interact with the substrate under investigation[138,216-219]. The mRNA up regulation observed may be a direct result of exposure to the drug; alternatively, it could be the results of indirect mechanisms. The decreased levels of protein available for drug binding due to occupation of binding pockets by the xenobiotic under investigation may cause an increase in mRNA. Preliminary *in vitro* experiments comparing transporter expression in control cells versus those transiently exposed to nilotinib, revealed increased expression of various cellular transporters. Additional experiments comparing the transporter mRNA levels in nilotinib-sensitive versus nilotinib-resistant cell lines confirmed these results and highlighted several transporters of interest including ABCC6 and AQP1.

There are currently 13 known members of the Aquaporin family (AQP0–AQP12) and these proteins function as homotetramers[358-360]. AQPs are water channels capable of transporting glycerol, small molecules and ions through the cell membrane[360]. Thus, it is unlikely AQP1 would have any direct interaction with nilotinib which has a molecular weight of 529.52. Instead it is possible AQP1 acts as a marker for nilotinib sensitivity, with levels increasing upon nilotinib exposure and resistance development *in vitro*. Alternatively, AQP1 overexpression has previously been implicated in the pathogenesis of solid tumours and may play a role in cell cycle regulation[361,362] which could also affect development of nilotinib resistance.

ABCC6 belongs to the MRP family of efflux proteins which has been implicated in multidrug resistance[308]. ABCC6 is primarily expressed in the liver and kidney[309-311], both sites of drug extrusion, and confers resistance to a number of anti-cancer agents[312]. Thus, ABCC6 presents a likely and novel candidate to function as a TKI transporter. Accordingly, the role of ABCC6 in the transport of three TKIs currently approved for treatment of CML, nilotinib, imatinib and dasatinib, was investigated.

The levels of ABCC6 mRNA were determined in three different cell lines conferring resistance to 2 μM nilotinib with results demonstrating a correlation between expression and development of nilotinib resistance *in vitro*. Additionally, ABCC6 mRNA levels remained at least 20- and 6-fold greater in K562 2 μM NIL and K562-Dox 2 μM NIL cells respectively compared with control cells, whereas ABCB1 mRNA levels declined in both cell lines following continued nilotinib exposure (**Figure 7.14** and **Chapters 5** and **6**). This provides good evidence for a central role of ABCC6 in nilotinib resistance. Furthermore, inhibition of ABCC6 in patient MNCs by three different inhibitors, pantoprazole, indomethacin and probenecid, resulted in a significant decrease in $IC50^{NIL}$ indicating ABCC6 likely functions as a transporter of nilotinib. Subsequent investigation of the effect of ABCC6 inhibitors on $IC50^{DAS}$ and $IC50^{IM}$ revealed ABCC6 is also a likely transporter of dasatinib but not imatinib. The use of a panel of

inhibitors to confirm ABCC6 as a relevant TKI transporter was necessary, since many commonly used inhibitors have over lapping specificities. However, as demonstrated in **Table 7.6**, ABCC6 is the only transporter yielding consistent results. Other transporters inhibited by both indomethacin and probenecid (ABCC1 and ABCC4) are also inhibited by either PSC-833 or verapamil. Thus, one would anticipate an effect on IC50 in the presence of the latter two inhibitors which did not occur. ABCC2 and ABC11, which are also inhibited by both indomethacin and probenecid, are unlikely candidates of TKI transport given that there are no reports of pantoprazole interacting with either transporter. Additionally, no overexpression of ABCC2 was observed during nilotinib resistance development and ABCC11 is not expressed in tissues relevant to TKI absorption and extrusion.

IC50 experiments in K562 2 μM NIL cells proved difficult due to the other resistant mechanisms present in this cell line (**Chapter 5**). Calculation of $IC50^{NIL}$ was not possible, due, most likely, to Lyn overexpression. However, a clear difference in the concentration of nilotinib required for equal percentages of Crkl and p-Crkl proteins was apparent in the absence and presence of indomethacin. No change was observed in $IC50^{IM}$ in the absence or presence of indomethacin which was as expected since ABCC6 is not a candidate transporter of imatinib. Importantly, resistance to dasatinib was negated in the presence of indomethacin since both ABCC6 inhibition, and dasatinib-mediated Lyn inhibition, was occurring. These data support results from cytotoxicity experiments detailed in **Chapter 5**. Briefly, K562 2 μM NIL cells incubated with increasing concentrations of nilotinib and imatinib for 72 h demonstrated significantly increased survival when compared with control cells. Presumably this was due to no inhibition of either Lyn or ABCC6. However, when the same cells were incubated with increasing concentrations of dasatinib, which has inhibitory activity against Lyn, significant resistance was still observed; we propose this is most likely due to overexpression of ABCC6 through which dasatinib is transported. Significance was lost at the upper end of the dasatinib concentration range. This also supports ABCC6-mediated dasatinib transport since transporters such as these have a finite

Table 7.6: Summary of transporters of interest and inhibitors which are active against them

Transporter	Inhibitor				
	PSC-833	Verapamil	Pantoprazole	Indomethacin	Probenecid
Oct-1	×	✓	×	×	×
ABCB1	✓	✓	✓	×	×
ABCB4	✓	✓	×	×	×
ABCC1	✓	✓	×	✓	✓
ABCC2	×	×	×	✓	✓
ABCC3	×	✓	×	×	✓
ABCC4	✓	✓	×	✓	✓
ABCC5	×	×	×	×	✓
ABCC6	×	×	✓	✓	✓
ABCC11	×	×	×	✓	✓
ABCG2	×	✓	✓	×	×

transport capacity which would be overcome at high substrate concentrations (**Chapter 4**).

Finally, ABCC6 is known to transport substrates anionic in nature[363]. Imatinib predominantly exists *in vivo* as a cation owing to the large degree of protonation at physiological pH. In contrast, nilotinib and dasatinib exist as cations to a much lesser degree making nilotinib and dasatinib, but not imatinib, likely candidates for transport by ABCC6[364]. Accordingly, expression levels of ABCC6 in *de novo* CML patients at diagnosis may prove predictive of response to nilotinib therapy. ABCC6 mRNA levels were assessed in 83 *de novo* CML patients receiving up front nilotinib therapy. Results demonstrated large variation in ABCC6 expression; data comparing response at three months with ABCC6 expression demonstrated a weak correlation which may become stronger once 12 month data becomes available on a larger cohort of patients. Interestingly, when ABCC6 expression was assessed in conjunction with ABCB1 expression, results demonstrated those patients overexpressing ABCC6 only were far less likely to achieve MMR at 3 months when compared with those exhibiting no overexpression or ABCB1 overexpression. Preliminary analysis of a small cohort of patients suggests this prediction remains true for patients at 12 months; although it will be necessary to repeat the analyses on a larger cohort of patients once this data becomes available. Dependent on data at this later time point, patients exhibiting high levels of ABCC6 only at diagnosis may benefit from combination ABCC6 inhibitor:TKI therapy.

In conclusion, the findings detailed in this chapter strongly suggest that ABCC6 functions as a novel efflux transporter of nilotinib and dasatinib, but not imatinib in nilotinib resistant cell lines as well as patient MNCs. Inhibition of ABCC6 significantly decreases $IC50^{NIL}$ and $IC50^{DAS}$ in patient MNCs, most likely due to an increase in intracellular TKI concentrations. Additionally, experiments performed in nilotinib resistant cell lines confirm the likelihood of ABCC6-mediated nilotinib and dasatinib transport. Taken together with results from **Chapter 4**, it appears that while ABCB1 may not play a key role in

nilotinib transport in patient MNCs, in the context of overexpression, ABCB1 is likely to facilitate nilotinib transport (**Table 7.7**). Furthermore, it may be possible to use ABCC6 and ABCB1 mRNA levels in patients at diagnosis to predict response to TKI therapy. Subsequently, combination TKI:ABCC6 inhibitor therapy may offer an attractive option to enhance TKI efficacy.

Table 7.7: Summary of change in IC50 in the presence of the specified inhibitor when compared with the absence of inhibitor

	+10 μM PSC-833	+50 μM Verapamil	+200 μM Pantoprazole	+100 μM Indomethacin	+1 mM Probenecid
Patient MNC $IC50^{NIL}$	↔	↔	↓↓↓	↓↓↓	↓↓↓
Patient MNC $IC50^{IM}$	ND	ND	↔	↔	↔
Patient MNC $IC50^{DAS}$	ND	ND	↓	↓↓↓	↓↓↓
K562-Dox $IC50^{NIL}$	↓	↓	↓	ND	ND
K562 $IC50^{NIL}$	↔	↔	↓	↔	ND
K562 2 μM NIL $IC50^{NIL}$	ND	ND	ND	↓	ND
K562 $IC50^{IM}$	ND	ND	ND	↔	ND
K562 2 μM NIL $IC50^{IM}$	ND	ND	ND	↔	ND
K562 $IC50^{DAS}$	ND	ND	ND	↔	ND
K562 2 μM NIL $IC50^{DAS}$	ND	ND	ND	↓	ND

↔=no change; ↓=decrease; ND=not determined. The number of arrows delineates significance with ↓<0.05, ↓↓↓<0.001.

Chapter 8

Discussion

8.1. Introduction

Nilotinib is a highly potent second generation tyrosine kinase inhibitor (TKI) approved for use in chronic phase chronic myeloid leukaemia (CML) patients as both front line therapy as well as in chronic phase and accelerated phase individuals who have failed imatinib therapy[101]. Nilotinib has demonstrated superior patient response compared with imatinib, however, there still exists a group of patients who demonstrate primary resistance or intolerance to nilotinib therapy and a second group who develop secondary resistance following an initially successful treatment phase. Importantly, it may be possible to identify patients at risk of developing secondary resistance and intervene proactively. Thus, it is pertinent to investigate potential molecular predictors of response as well as methods by which TKI efficacy can be enhanced. Accordingly, the research described in this thesis aimed to generate *in vitro* models of nilotinib resistance such that a better understanding of *in vivo* resistance could be gained. Additionally, nilotinib transport and the relationship between nilotinib efflux and ABC transporters were examined. This resulted in identification of a previously undescribed transporter that may also be involved in nilotinib transport and resistance. Results from this research will provide a greater understanding of nilotinib transport, particularly with respect to ABC transporters. As we move into the era of customised treatment regimes for all patients, it becomes important to predict which patients are likely to respond to a given TKI such that treatment plans are tailored to the individual. The findings presented here may assist in developing new therapeutic strategies using TKIs in combination with other medications in order to enhance intracellular concentrations of TKI. Additionally, further insight into the modes of resistance to nilotinib, as well as the kinetics of resistance mechanism emergence, may assist in determining treatment options for CML patients.

8.2. Major Findings

8.2.1. Co-Administration of Nilotinib does not Adversely Affect Imatinib OCT-1 Activity

Previous research from our laboratory has demonstrated that the addition of nilotinib to radiolabelled

imatinib reduced the intracellular concentrations of imatinib, however, this reduction failed to reach statistical significance[194]. More recently it was proposed that the nilotinib-mediated reduction of intracellular imatinib was due to inhibition of the main imatinib influx pump: OCT-1[187]. This suggestion could have significant implications for imatinib/nilotinib combination therapies as well as adversely affecting the action of concomitantly administered medications transported by OCT-1, such as the diabetes drug metformin[213,214] and ranitidine[215] which inhibits the production of stomach acid. Thus, we sought to assess the effect of nilotinib on imatinib OCT-1 activity as this measurement is the key predictor of long term patient response[151]. As discussed in **Chapter 3**, while nilotinib does decrease what is most likely passive imatinib uptake, albeit insignificantly, no effect on OCT-1 activity was observed. Nilotinib also has no significant effect on uptake of the model OCT-1 substrate tetraethylammonium bromide. Therefore, nilotinib:imatinib combination therapy is still a viable option. This is contrary to the argument proposed by Davies *et al*, whereby nilotinib inhibits OCT-1 function and, when co-administered, may adversely affect the action of drugs transported by OCT-1[187]. The data presented in the current study are supported by recent case reports of patients who lost molecular response after cessation of imatinib therapy due to intolerance. Subsequent treatment with sub-therapeutic doses of imatinib and nilotinib in combination was well tolerated and resulted in rapid re-obtainment of molecular response[365,366]. The results described in this thesis, combined with other *in vitro* modelling[191,192] as well as the clinical observations from patients previously treated with TKIs, suggest that no adverse effect to patients will occur from the administration of nilotinib in combination with imatinib. In fact, patients may perform better with respect to decreased intolerance and emergence of kinase domain mutations when a cocktail of TKIs is administered. Thus, the findings presented here add to an increasing body of data suggesting clinical trials assessing upfront simultaneous administration of lower dose TKI therapy in order to reduce intolerance are warranted.

8.2.2. Nilotinib is Transported by ABCB1 but not ABCG2

The data described in **Chapter 3** strongly suggested that nilotinib enters the cell in a passive manner making it unlikely intracellular concentrations could be further improved by alteration of drug influx. Since this data also suggested active export, efflux transporters formed one of the main focus' of this thesis. A better understanding of how nilotinib is transported from the leukaemic cell may allow enhancement of drug retention via modulation of any drug transporters involved. Much conjecture exists in the literature about the nilotinib:ABCB1 and nilotinib:ABCG2 relationships with some studies concluding nilotinib is a substrate of these transporters, others suggesting nilotinib functions as an inhibitor. Furthermore, the reported TKI:ABC transporter relationships vary with methodologies and TKI concentrations used in individual studies. In order to overcome the discrepancies reported previously, the current study utilised Bcr-Abl kinase inhibition as the confirmatory readout for drug:transporter interactions. This is the first study to do so and because this approach measures actual target inhibition over a large concentration range, the relevant effects of TKI on Bcr-Abl kinase can be addressed directly. The *in vitro* data in Bcr-Abl positive cell lines reported in **Chapter 4** demonstrate that ABCB1, but not ABCG2, is involved in nilotinib efflux. Furthermore, the experiments described here highlight the importance of nilotinib concentration when assessing the interaction of TKIs with transporters. At low nanomolar concentrations, which more accurately reflect the clinical situation, intracellular nilotinib levels support ABCB1-mediated nilotinib efflux. However, higher micromolar concentrations resulted in the inhibition of both ABCB1 and ABCG2 function. The clear evidence of the concentration dependence of ABCB1-mediated nilotinib efflux provided likely explains the lack of consensus on this question in previous studies. From the clinical perspective, these findings suggest that nilotinib is likely to be susceptible to resistance mediated by overexpression of ABCB1. This would be particularly evident at points of drug extrusion (liver, kidney, intestine) and at the blood brain barrier where ABCB1 levels are high. Since nilotinib enters cells passively along a concentration gradient and efflux occurs actively, the net effect would be low intracellular nilotinib levels leading to inadequate Bcr-Abl inhibition. Thus, in

order to effectively target residual leukaemic cells, which have previously been hypothesised to cause TKI resistance and disease progression[40,357], patients may benefit from combined ABCB1 inhibitor:TKI therapy; although careful consideration would have to be given when determining correct TKI dose to prevent the occurrence of off target toxicity.

8.2.3. ABCB1 Acts as an Initiator of Nilotinib Resistance

In vitro models of nilotinib resistance were generated in Bcr-Abl positive cell lines, K562 and the ABCB1 overexpressing variant K562-Dox, by long term exposure to increasing concentrations of nilotinib (**Chapters 5** and **6**). In all resistant cell lines generated in this study, ABCB1 overexpression, at both the mRNA and protein level, was the initiating mechanism of resistance. Notably, this is the first report of ABCB1 overexpression in the K562 cell line in response to exposure to nilotinib. There are two mechanisms by which this could occur: firstly, clonal selection of cells within the population that have increased expression of ABCB1. Alternatively, up regulation of ABCB1 expression may have occurred as an immediate response following exposure to nilotinib. ABCB1 expression levels in newly thawed K562 2 μM NIL cells pre-nilotinib exposure and after 24 h culture in the presence of 2 μM nilotinib suggest the latter scenario is more likely (**Appendix 6A**). Importantly, $IC50^{NIL}$ was demonstrated to directly correlate with ABCB1 expression confirming the notion that nilotinib is an ABCB1 substrate and supporting results detailed in **Chapter 4**. No increase in ABCG2 protein was observed making it unlikely this transporter plays a role in the transport of, or development of resistance to, nilotinib, also confirming results described in **Chapter 4**. Continued culture in increasing concentrations of nilotinib resulted in a loss of ABCB1 expression in all cell lines, most likely by clonal selection, prior to the emergence of other resistance mechanisms. The fact that two distinct populations were present in K562-Dox 125 nM NIL #1 cells (**Chapter 6**) and that the ABCB1-negative population increased in size with a corresponding decrease in the ABCB1-positive population, suggests those cells with decreased ABCB1 expression had a growth advantage and were clonally selected over time. The same

phenomenon was observed in K562 50 nM NIL cells with ABCB1 expression decreasing gradually over time (**Chapter 5**). Continued exposure of K562 cells to increasing concentrations of nilotinib resulted in increased activity of the Src family kinase, Lyn. This resistance mechanism has previously been cited as Bcr-Abl *independent*[68,120]. However, in the current study, resistant K562 cells demonstrated increased IC50 which was unexpected if there was no involvement of Bcr-Abl. This, combined with the fact that Lyn reportedly regulates Bcr-Abl activity[123,158,160], suggests that Lyn overexpression is in fact a Bcr-Abl *dependent* mechanism of resistance, which is contrary to popular belief. Consequently, one could speculate that those patients initially exhibiting negligible levels of ABCB1 but who then demonstrate ABCB1 overexpression (as was observed in the K562 model of nilotinib resistance) may be at risk of developing Lyn overexpression. Such patients may benefit from monitoring of Lyn expression levels and a switch to dasatinib therapy, which has activity against Lyn and other Src family kinases, in the event that Lyn levels increase.

8.2.4. Prolonged Exposure to Nilotinib Results in Bcr-Abl Independent Resistance in K562-Dox Cells

Continued exposure of K562-Dox cells to nilotinib resulted in complete loss of ABCB1 expression and function and the emergence of a genuine Bcr-Abl *independent* mechanism of resistance (**Chapter 6**). K562-Dox cells have been stably expressing ABCB1 for over a decade and this is the first report of loss of ABCB1 expression back to levels observed in parental K562 cells. Interestingly, investigation of other previously reported nilotinib resistance mechanisms failed to determine the cause of resistance here. There was no overexpression or increased activity of Axl, Syk or Lyn nor was total tyrosine phosphorylation increased. Thus, it is likely a novel mechanism of resistance exists, possibly involving Bcr-Abl independent activation of PDGFR-β and decreased expression of MAP3K5. Previously, a small cohort of patients with demonstrated imatinib resistance were found to have adequate Bcr-Abl kinase inhibition[108]. Even though no confirmatory studies have been published subsequently, the long-term

treatment outcomes of nilotinib are yet to be defined and Bcr-Abl independent resistance may prove critical in this setting. Potentially, these cell lines could provide an *in vitro* model for patients with undetermined resistance. Additionally, this current model of nilotinib resistance suggests patients who exhibit ABCB1 overexpression initially may be prone to developing Bcr-Abl *independent* mechanisms of resistance. Thus, it may prove valuable to determine the expression levels of ABCB1 in such patients at both diagnosis and relapse and compare these with levels in resistant patients with kinase domain mutations to determine if this theory is also applicable *in vivo*. Taken together, these *in vitro* models highlight the importance of determining transporter expression at diagnosis and using this to monitor changes in expression while undergoing TKI therapy. An increase in levels of ABCB1 may serve as an easily transferrable and valuable early warning system for loss of response and possible development of resistance.

8.2.5. ABCC6 is a Novel Candidate Transporter of both Nilotinib and Dasatinib

The interaction of nilotinib with ABCB1 and ABCG2 has been studied comprehensively; however, the *in vitro* data described in **Chapter 4** suggested there may be another transporter/s with which nilotinib interacts. Thus, mRNA expression of a set of candidate cell transporters was investigated in cells that had been both transiently exposed to nilotinib as well as resistant cells cultured long term in nilotinib (**Chapter 7**). This approach has previously demonstrated mRNA levels of relevant transporters are up-regulated upon exposure to xenobiotics[138,216-219]. Results emphasised ABCC6 as a promising candidate: mRNA levels increased in both instances suggesting a role in transport of, and resistance to, nilotinib. To investigate this further, a panel of ABC transporter inhibitors was employed to determine the effect of ABCC6 inhibition in patient mononuclear cells (MNCs). Addition of three different ABCC6 inhibitors resulted in significantly increased nilotinib-mediated Bcr-Abl kinase inhibition supporting the notion that ABCC6 is involved in nilotinib transport. Cross referencing transporter and inhibition specificities validated ABCC6 as the only viable transporter. Similar experiments utilising dasatinib and

imatinib indicated that ABCC6 may also be involved in the transport of dasatinib, but is unlikely to be involved in imatinib transport. Importantly, *in vitro* data in resistant K562 cells which overexpress ABCC6 supported these hypotheses.

These results highlighted ABCC6 as important in the efflux of nilotinib from patient MNCs which was in contrast to the ABCB1:nilotinib interaction in these cells. Thus, it would appear ABCB1 expression levels may function as an indicator of loss of response or resistance development, while ABCC6 levels may potentially be used in order to predict those patients who will do poorly on nilotinib therapy. Comparing ABCB1 and ABCC6 mRNA levels in 83 *de novo* CML patients prior to initiation of nilotinib therapy supports this notion. Patients were divided into four groups based on transporter mRNA levels: no overexpression, ABCB1 overexpression, ABCC6 overexpression and double overexpression and correlated with major molecular response (MMR; <1% Bcr-Abl) to nilotinib at 3 months (**Chapter 7**). Results demonstrated that ABCC6 overexpression may be predictive of response to nilotinib therapy. Of those patients exhibiting ABCC6 overexpression, 52.6% achieved a MMR at 3 months, compared with 73.9% of patients exhibiting no overexpression or 85.0% of patients overexpressing ABCB1 only. Preliminary analysis of molecular response at 12 months for a small cohort of patients appears to be even more predictive: 28.5% of patients exhibiting ABCC6 overexpression achieved a MMR compared with 44.4% of patients exhibiting no overexpression or overexpressing ABCB1 only. However, analysis of a much larger cohort is required in order to conclude whether a definitive correlation exists, and this will be completed once data becomes available.

These data highlighted the rather perplexing observation that the predictive capability of ABCC6 mRNA expression is only valuable when analysed in conjunction with ABCB1 expression. If one were to look at ABBC6 expression in isolation, the correlation between high expression and inability to achieve MMR is considerably weaker (**Chapter 7**). Because we hypothesise that both ABCB1 and ABCC6 are

important in the transport of nilotinib, it was expected that those patients demonstrating overexpression of both transporters would exhibit an inferior response compared with patients exhibiting no overexpression or overexpression of one transporter only; however, this was not the case. As discussed earlier, ABCB1 is unlikely to be a major protein involved in nilotinib transport in MNCs. Instead, overexpression of this transporter may be a predictor of relapse or resistance development, since expression is high at sanctuary sites such as the brain and testes where it is hypothesised residual leukaemic cells remain[318,357]. In contrast, ABCC6 has been demonstrated as an important nilotinib transporter in patient MNCs (IC50 experiments in the absence and presence of ABCC6 inhibition, **Chapter 7**). It has also been demonstrated that continued exposure to nilotinib results in a sustained increase in ABCC6 mRNA (development of nilotinib resistance in K562 cells, **Chapter 7**). Therefore, one could speculate that patients exhibiting high initial levels of ABCC6 would further overexpress this transporter during nilotinib therapy leading to decreased intracellular nilotinib concentrations and a reduced probability of achieving MMR. However, this still does not explain why patients exhibiting high expression levels of both ABCB1 and ABCC6 do not have a decreased probability of achieving MMR when compared with patients exhibiting no overexpression. A potential explanation originates from examination of ABCB1 and ABCC6 expression during development of nilotinib resistance in K562-Dox cells. These cells initially overexpress ABCB1 and it was observed that early resistance intermediates, before development of overt resistance, demonstrated reduced expression of ABCC6 when compared with control cells, although ABCB1 levels remained constant (**Figure 8.1**). As discussed previously, ABCB1 is capable of modulating expression of ABCG2 (**Chapters 5** and **6**). Thus, we hypothesise that in the setting of ABCB1/ABCC6 overexpression, ABCC6 levels are modulated following nilotinib therapy such that patients originally overexpressing both transporters overexpress ABCB1 only, which, as discussed earlier, is unlikely to be a major nilotinib transporter in MNCs nor does overexpression appear to predict long term response to nilotinib. However, we acknowledge the artificiality of using a cell line system, and will seek to confirm these

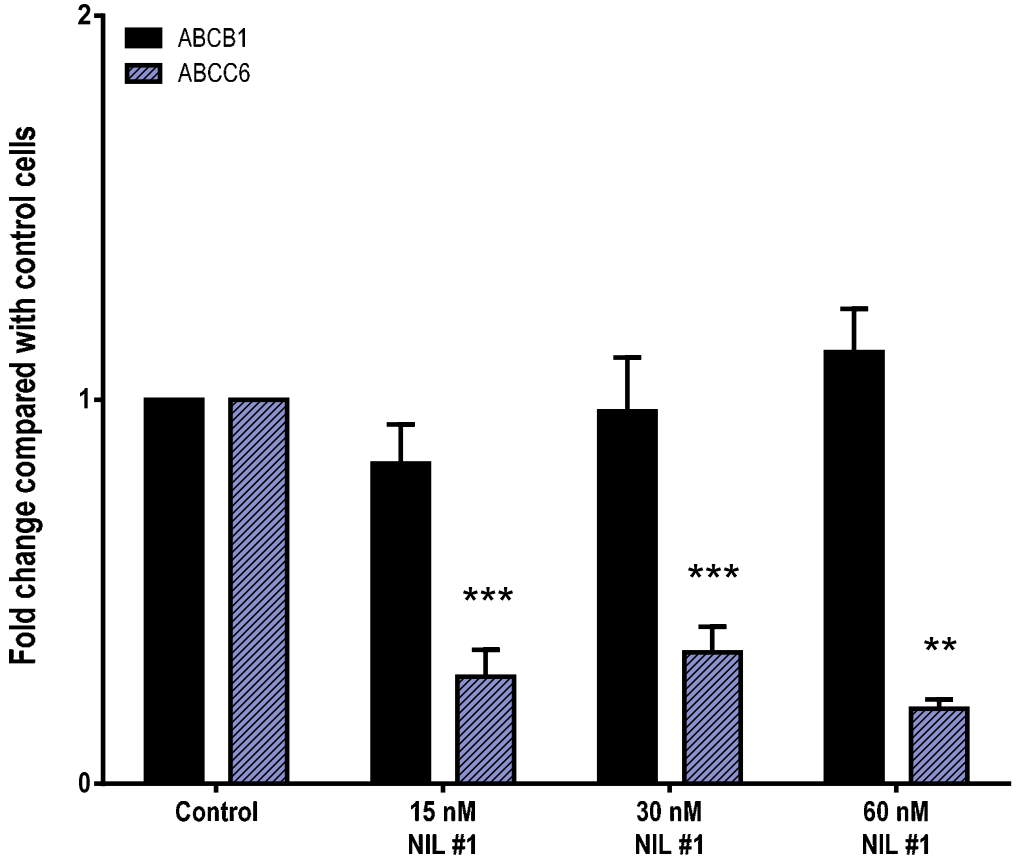

Figure 8.1: Early K562-Dox resistance intermediates demonstrate stable levels of ABCB1 mRNA and reduced levels of ABCC6 mRNA compared with control cells

Expression levels of ABCB1 and ABCC6 were assessed in K562-Dox nilotinib resistance intermediates. Data demonstrate no significant change in ABCB1 levels during early development of nilotinib resistance however a significant reduction in ABCC6 mRNA was observed. mRNA expression represents the mean of six independent experiments performed in triplicate. Statistical analyses were performed on mRNA levels as a percentage BCR using Student's *t*-test. Statistically significant *p*-values are denoted by asterisks (** $p<0.01$; *** $p<0.001$). Error bars represent SEM.

hypotheses by determining expression levels of ABCB1 and ABCC6 mRNA in patients following 12 months of nilotinib therapy once this data becomes available.

OCT-1 activity has been demonstrated as predictive of long term response to imatinib therapy[151,177], and has not yet been tested for nilotinib therapy; currently no other measure for predicting response to nilotinib has been defined. Having a reliable and easily disseminative predictor of response to TKI therapy at diagnosis is critical such that those patients likely to exhibit a suboptimal response are identified. Determination of ABCC6 and ABCB1 levels prior to initiation of TKI therapy may offer a quick and widely applicable diagnostic tool for predicting response to nilotinib. Additionally, this strategy may help identify those patients who would perform better on alternative TKI therapy or who may benefit from combined TKI:ABCC6 inhibitor therapy in order to improve response and prevent development of secondary resistance.

8.3. Summary

The use of TKIs in the treatment of CML has resulted in successful treatment outcomes for the majority of patients. However, the challenge now exists to induce the optimum response in all patients. The availability of second generation TKIs means there should no longer be a 'one treatment for all' approach. This, combined with the knowledge of relevant drug transporters for each of the TKIs, should allow customised treatment regimes where TKIs are combined with other drugs in order to enhance their efficacy.

This study investigated the interaction of nilotinib with major cellular drug transporters and assessed how altered expression or inhibition of these transporters affected nilotinib transport and efficacy. Additionally, three nilotinib resistant cell lines were generated and used to investigate the kinetics of nilotinib resistance mechanism emergence. Based on the findings presented in this thesis, **Figure 8.2**

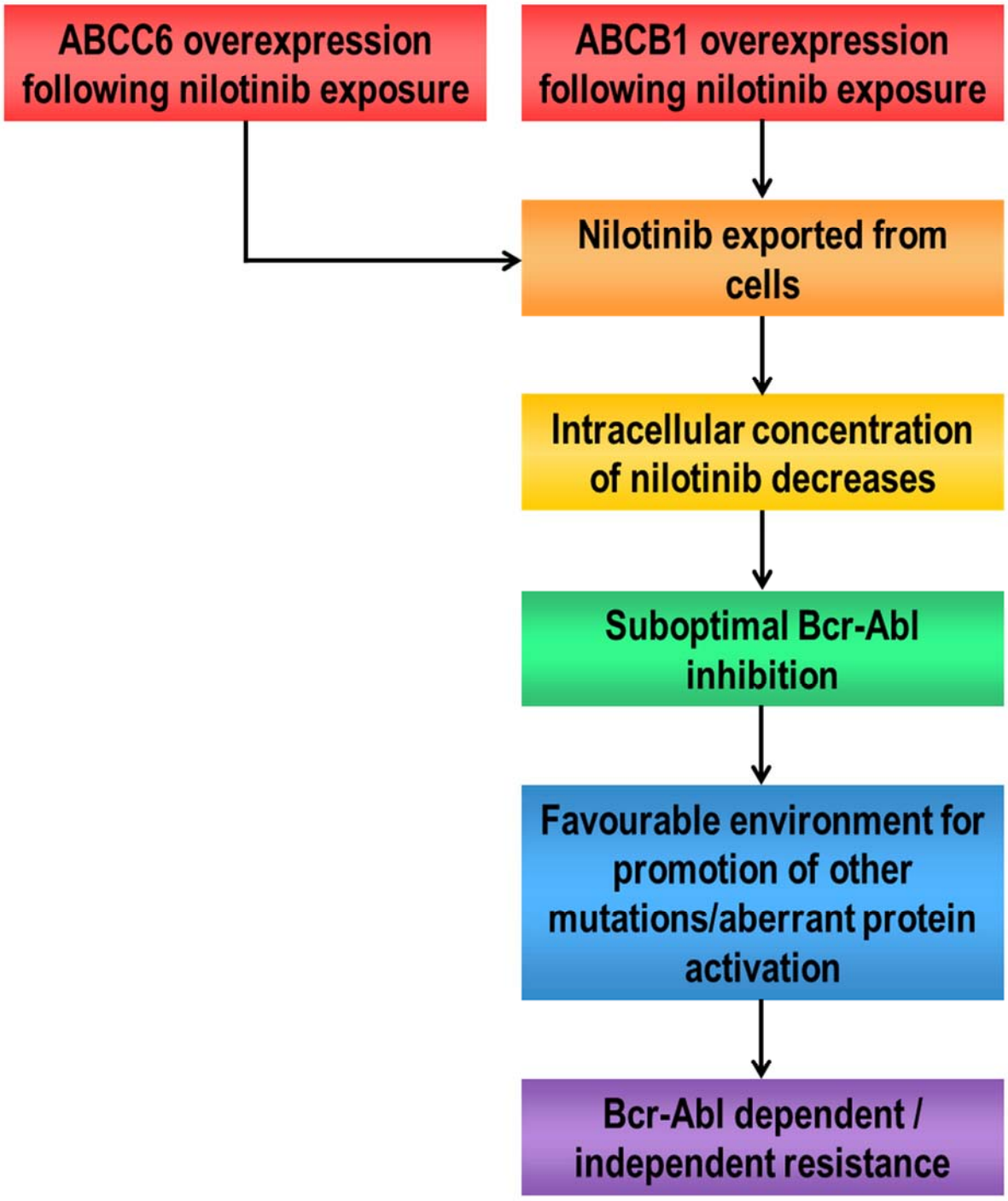

Figure 8.2: Schematic summary of involvement of ABC transporters in nilotinib resistance

Nilotinib is a substrate of both ABCB1 and ABCC6 and overexpression of these transporters causes a decreased level of intracellular nilotinib. This then results in inferior Bcr-Abl inhibition leading to a cellular environment that promotes further mutations/aberrant activation of proteins ultimately leading to Bcr-Abl *dependent* or *independent* mechanisms of resistance.

presents a current hypothesis for the role of cellular transporters in development of resistance to nilotinib. Nilotinib is a likely substrate of ABCB1 and ABCC6 and efflux by these transporters results in lower intracellular concentrations of nilotinib. In the context of resistance, overexpression of ABCB1 and/or ABCC6 creates a favourable environment in which mutations and aberrant expression of other proteins occurs.

ABCC6 was also found to interact with dasatinib, but not imatinib, and this represents the first time ABCC6 has been linked to TKI resistance and transport. *In vitro* experimentation in CML patient MNCs revealed a significant decrease in $IC50^{NIL}$ and $IC50^{DAS}$ in the presence of ABCC6 inhibition suggesting patients may benefit from concomitant administration of ABCC6 inhibitors to enhance nilotinib/dasatinib therapy, especially where there is high risk of emerging resistance. Additionally, mRNA expression levels of ABCB1 and ABCC6 at diagnosis may be used as a predictor of response to nilotinib. Alterations in expression of ABCB1 following therapy may also be used as an early warning for development of resistance to nilotinib.

8.4. Future Directions

As a result of the findings presented in this thesis, a number of lines of investigation have been proposed as essential for further understanding the development of nilotinib resistance and the role of ABCC6 in nilotinib efflux:

- In order to confirm the interaction between ABCC6 and nilotinib, dasatinib and imatinib, ABCC6 will be retrovirally overexpressed in cell lines; corresponding siRNA knockdown will also be performed. Collaborators with expertise in this field have initiated this project, however, ABCC6 was identified as a transporter of interest in the third year of study and complications in vector sequencing and ligation occurred, thus resulting in significant impediments to progress.

- Similarly, ABCC6 will be overexpressed in *xenopus* oocytes to determine whether a difference exists in concentrations of intracellular nilotinib in the absence versus the presence of ABCC6 inhibition. Oocytes do not express any cellular transporters thus, by engineering them to express ABCC6, any differences in intracellular nilotinib in the absence and presence of ABCC6 inhibitors will be due to transport mediated by ABCC6. Utilising oocytes will allow a definitive conclusion to be made regarding the nilotinib:ABCC6 relationship.
- A custom ABCC6 antibody will be manufactured (current commercially available antibodies are poor) and then used to assess ABCC6 protein levels in stored patient MNC lysates.
- Mutation analysis on PDGFR-β gene in K562-Dox resistant cell lines will be performed to determine if any activating mutations are present.
- Intracellular nilotinib levels will be assessed and compared with plasma levels by mass spectrometry. These data will be contrasted with those of imatinib and data used to compare *in vivo* kinase inhibition in patients receiving up front imatinib versus up front nilotinib.
- mRNA and protein levels of ABCB1 will be determined in patients who develop mutations, undergo disease progression or fail to achieve MMR while receiving up front imatinib or nilotinib. We hypothesise that ABCB1 overexpression plays a role in disease progression, resistance development and lack of response to therapy and thus expect these patients to exhibit increased levels of ABCB1 prior to onset of the adverse event.

8.5. Conclusion

In conclusion, while nilotinib entered the cell in a predominantly passive manner, efflux comprised an active component making moderation of export an attractive approach to enhance nilotinib efficacy. Nilotinib was found to be a substrate of ABCB1 but not ABCG2 but was capable of inhibiting both these transporters at high concentrations. Furthermore, the novel TKI transporter ABCC6 was identified, and was demonstrated to interact with both nilotinib and dasatinib, but not imatinib. Inhibition of ABCC6

increased nilotinib- and dasatinib-mediated Bcr-Abl kinase inhibition in patient MNCs. Accordingly, concomitant administration of ABCC6 inhibitors may increase TKI efficacy and prevent development of secondary resistance. Moreover, patients exhibiting ABCC6 overexpression at diagnosis may be at risk of failing to achieve a major molecular response by 12 months. Thus, examination of transporter mRNA levels in newly diagnosed CML patients, and continued monitoring during TKI therapy, could provide a useful indication for determining TKI and/or concomitant therapies.

Appendices

Table 1A: Summary of TKI concentrations with corresponding volumes for cytotoxicity assays

[TKI]	[stock]	Volume	[TKI]	[stock]	Volume	[TKI]	[stock]	Volume
Nilotinib (nM)			**Imatinib (μM)**			**Dasatinib (nM)**		
0	DMSO	4 μL	0	–	–	0	DMSO	4 μL
25	100 μM	1 μL	0.1	0.1 mM	4 μL	10	10 μM	4 μL
50	100 μM	2 μL	0.25	1 mM	1 μL	25	100 μM	1 μL
100	100 μM	4 μL	0.5	1 mM	2 μL	50	100 μM	2 μL
200	1 mM	0.8 μL	0.75	1 mM	3 μL	75	100 μM	3 μL
250	1 mM	1 μL	1	1 mM	4 μL	100	100 μM	4 μL
300	1 mM	1.2 μL	2.5	10 mM	1 μL	250	1 mM	1 μL
500	1 mM	2 μL	5	10 mM	2 μL	500	1 mM	2 μL
1000	1 mM	4 μL						
2000	10 mM	0.8 μL						
5000	10 mM	2 μL						

Fullmoon kinase array antibody list

ID	Antibody Name
1	LRRK2
2	BRAF
3	AHSA1
4	NTRK2
5	IRAK2
6	SLPI
7	STAT6
8	AXL
9	LIMK1
10	EPB41L3
11	PTK7
12	HIPK1
13	SGK2
14	STAT5A
15	GRK7
16	YARS
17	RPS6KC1
18	GRK4
19	MYO3A
20	ACVR1B
21	BCR
22	CDKL2
23	CDKL3
24	CDKL4
25	CDKL5
26	DYRK1A
27	DYRK4
28	EFNA1
29	EFNA5
30	FGFR1OP
31	FGFR1OP2
32	FRAP1
33	FLT1
34	FLT3LG
35	FLT4

ID	Antibody Name
36	GRAP2
37	ILK
38	IRAK1
39	LATS1
40	MAPK11
41	MAPK12
42	MAPK3
43	MAPK4
44	MAPK6
45	MAP2K1IP1
46	MAP2K3
47	MAP3K5
48	MAPKAPK5
49	MLKL
50	PAK4
51	PA2G4
52	PRKCBP1
53	PRKCZ
54	PRKD2
55	PRKD3
56	PRKAA1
57	PRKAG2
58	PRKACA
59	PRKDC
60	PRKRA
61	PTK2
62	PTK2B
63	PTK6
64	RET
65	SAB
66	TEK
67	TYK2
68	YES1
69	ROR2
70	CAMK2A

ID	Antibody Name
71	CAMK1D
72	CAMK4
73	CAMKK1
74	CAMKK2
75	CDC2L2
76	MAPKAPK3
77	MLL4
78	EFNA3
79	FES
80	LCK
81	PRKACB
82	ERBB2IP
83	MAPK14
84	PRKAR1B
85	EPHA5
86	EPHB2
87	EPHB4
88	MAPK8
89	CSNK1G1
90	BUB1B
91	CSNK1G2
92	HIPK2
93	RPS6KA6
94	GRK6
95	IKBKG
96	GRK1
97	MUSK
98	FGR
99	GRK5
100	MST1R
101	TIE1
102	ABL2
103	SYK
104	CDK5
105	FLT3

ID	Antibody Name
106	EPHA7
107	STK11
108	SGK3
109	ANP32A
110	FGFR2
111	EPHA4
112	CSF1
113	ZAP70
114	PDGFRA
115	ROCK1
116	RPS6KA3
117	INSRR
118	DMPK
119	EIF2AK2
120	TGFB1
121	PRKRIR
122	MYLK
123	EPB41
124	IKBKE
125	MYO7A
126	BMPR1A
127	STAT3
128	ATM
129	PRKAB2
130	EPHB1
131	MELK
132	EPHA2
133	RPS6KB2
134	PDGFRB
135	EGFR
136	RAF1
137	MAPK1
138	STAT1
139	CSF2RA
140	CSNK1D

ID	Antibody Name
141	CSNK1E
142	ROCK2
143	FGFR1
144	EPB41L1
145	ARG2
146	NTRK3
147	RPS6KA5
148	MYO9A
149	FGFR4
150	BMPR2
151	CSNK2A2
152	HIPK4
153	FGFRL1
154	PTK9L
155	EPB42
156	MAP2K1
157	RPS6KA2
158	PRIM2A
159	PRKCA
160	GSK3B
161	FUSIP1
162	WNK2
163	MYLIP
164	RPS6KA1
165	AKT2
166	CDC2
167	CDK5R1
168	CDK8
169	CHEK2
170	STAT2
171	STAT5B
172	MYO9B
173	RNASEL
174	CDC25A

ID	Antibody Name
175	MYLK2
176	HERC4
177	EPHX1
178	ACTR1B
179	CDK2
180	EPDR1
181	CDK6
182	CDK4
183	TYRO3
184	INS
185	TGFB1I1
186	CDK7
187	CSF2
188	IGFBP1
189	CDC25B
190	SRC
191	NPR2
192	EPM2A
193	MAP2K2
194	RNMT
195	CDK5RAP3
196	CDK3
197	CDKL1
198	DYRK1B
199	DYRK2
200	ILKAP
201	IRAK3
202	IRAK4
203	JAK3
204	MAST2
205	MASTL
206	MAPK10
207	MAPK13
208	MAP3K13

ID	Antibody Name
209	MAP3K15
210	MAP3K4
211	MAP4K5
212	MAPKAPK2
213	PAK3
214	PIM1
215	PIM3
216	PRKCABP
217	PRKAA2
218	PRKAB1
219	ERBB3
220	KDR
221	CAMK2D
222	CAMK1G
223	CAMK2B
224	ROR1
225	CDK9
226	MAP2K6
227	MAP3K1
228	MAP3K11
229	MAP3K3
230	PRKAR2A
231	PRKX
232	MAP4K4
233	ERBB2
234	PTK9
235	EPHB3
236	EPHB6
237	PRKCD
238	MAPK9
239	CHEK1
240	IKBKB
241	PAK2
242	SGK

ID	Antibody Name
243	RNASEH1
244	RPS6KB1
245	BUB1
246	AKT1
247	RNASEH2A
248	MAP2K5
249	PAK1
250	PRKG1
251	NEK2
252	CAMK1
253	BMPR1B
254	CSNK2A1
255	MAP3K7
256	CAMKV
257	CDC25C
258	PRKCSH
259	HERC3
260	PRKACG
261	RPS6
262	LIMK2
263	WNK3
264	MAP3K7IP1
265	IGFBP6
266	PLK1
267	IKBKAP
268	ANK1
269	STAT4
270	PRKCI
271	DYRK3
272	PLK4
273	FYN
274	CSF1R
275	MERTK
276	EPHA6

Fullmoon kinase array plate layout

Block 1

	c1	c2	c3	c4	c5	c6	c7	c8	c9	c10	c11	c12	c13	c14	c15	c16	c17	c18	c19	c20	c21	c22	c23	c24	c25	c26	c27	c28	c29	c30	c31	c32
r1	P	E	E	1	2	3	4	5	6	7	8	9	10	11	12	13	14	15	16	17	18	19	20	21	22	23	24	25	26	27	28	29
r2	P	E	E	1	2	3	4	5	6	7	8	9	10	11	12	13	14	15	16	17	18	19	20	21	22	23	24	25	26	27	28	29
r3	P	E	E	1	2	3	4	5	6	7	8	9	10	11	12	13	14	15	16	17	18	19	20	21	22	23	24	25	26	27	28	29
r4	P	E	E	1	2	3	4	5	6	7	8	9	10	11	12	13	14	15	16	17	18	19	20	21	22	23	24	25	26	27	28	29
r5	P	E	E	1	2	3	4	5	6	7	8	9	10	11	12	13	14	15	16	17	18	19	20	21	22	23	24	25	26	27	28	29
r6	P	E	E	1	2	3	4	5	6	7	8	9	10	11	12	13	14	15	16	17	18	19	20	21	22	23	24	25	26	27	28	29

Block 2

	c1	c2	c3	c4	c5	c6	c7	c8	c9	c10	c11	c12	c13	c14	c15	c16	c17	c18	c19	c20	c21	c22	c23	c24	c25	c26	c27	c28	c29	c30	c31	c32
r1	30	31	32	33	34	35	36	37	38	39	40	41	42	43	44	45	46	47	48	49	50	51	52	53	54	55	56	57	58	59	60	61
r2	30	31	32	33	34	35	36	37	38	39	40	41	42	43	44	45	46	47	48	49	50	51	52	53	54	55	56	57	58	59	60	61
r3	30	31	32	33	34	35	36	37	38	39	40	41	42	43	44	45	46	47	48	49	50	51	52	53	54	55	56	57	58	59	60	61
r4	30	31	32	33	34	35	36	37	38	39	40	41	42	43	44	45	46	47	48	49	50	51	52	53	54	55	56	57	58	59	60	61
r5	30	31	32	33	34	35	36	37	38	39	40	41	42	43	44	45	46	47	48	49	50	51	52	53	54	55	56	57	58	59	60	61
r6	30	31	32	33	34	35	36	37	38	39	40	41	42	43	44	45	46	47	48	49	50	51	52	53	54	55	56	57	58	59	60	61

Block 3

	c1	c2	c3	c4	c5	c6	c7	c8	c9	c10	c11	c12	c13	c14	c15	c16	c17	c18	c19	c20	c21	c22	c23	c24	c25	c26	c27	c28	c29	c30	c31	c32
r1	62	63	64	65	66	67	68	69	70	71	72	73	74	75	76	77	78	79	80	81	82	83	84	85	86	87	88	89	90	91	92	93
r2	62	63	64	65	66	67	68	69	70	71	72	73	74	75	76	77	78	79	80	81	82	83	84	85	86	87	88	89	90	91	92	93
r3	62	63	64	65	66	67	68	69	70	71	72	73	74	75	76	77	78	79	80	81	82	83	84	85	86	87	88	89	90	91	92	93
r4	62	63	64	65	66	67	68	69	70	71	72	73	74	75	76	77	78	79	80	81	82	83	84	85	86	87	88	89	90	91	92	93
r5	62	63	64	65	66	67	68	69	70	71	72	73	74	75	76	77	78	79	80	81	82	83	84	85	86	87	88	89	90	91	92	93
r6	62	63	64	65	66	67	68	69	70	71	72	73	74	75	76	77	78	79	80	81	82	83	84	85	86	87	88	89	90	91	92	93

Block 4

	c1	c2	c3	c4	c5	c6	c7	c8	c9	c10	c11	c12	c13	c14	c15	c16	c17	c18	c19	c20	c21	c22	c23	c24	c25	c26	c27	c28	c29	c30	c31	c32
r1	94	95	96	97	98	99	100	101	102	103	104	105	106	107	108	109	110	111	112	113	114	115	116	117	118	119	120	121	122	123	124	125
r2	94	95	96	97	98	99	100	101	102	103	104	105	106	107	108	109	110	111	112	113	114	115	116	117	118	119	120	121	122	123	124	125
r3	94	95	96	97	98	99	100	101	102	103	104	105	106	107	108	109	110	111	112	113	114	115	116	117	118	119	120	121	122	123	124	125
r4	94	95	96	97	98	99	100	101	102	103	104	105	106	107	108	109	110	111	112	113	114	115	116	117	118	119	120	121	122	123	124	125
r5	94	95	96	97	98	99	100	101	102	103	104	105	106	107	108	109	110	111	112	113	114	115	116	117	118	119	120	121	122	123	124	125
r6	94	95	96	97	98	99	100	101	102	103	104	105	106	107	108	109	110	111	112	113	114	115	116	117	118	119	120	121	122	123	124	125

Block 5

	c1	c2	c3	c4	c5	c6	c7	c8	c9	c10	c11	c12	c13	c14	c15	c16	c17	c18	c19	c20	c21	c22	c23	c24	c25	c26	c27	c28	c29	c30	c31	c32
r1	126	127	128	129	130	131	132	133	134	135	136	137	138	139	140	141	142	143	144	145	146	147	148	149	150	151	152	153	154	155	156	157
r2	126	127	128	129	130	131	132	133	134	135	136	137	138	139	140	141	142	143	144	145	146	147	148	149	150	151	152	153	154	155	156	157
r3	126	127	128	129	130	131	132	133	134	135	136	137	138	139	140	141	142	143	144	145	146	147	148	149	150	151	152	153	154	155	156	157
r4	126	127	128	129	130	131	132	133	134	135	136	137	138	139	140	141	142	143	144	145	146	147	148	149	150	151	152	153	154	155	156	157
r5	126	127	128	129	130	131	132	133	134	135	136	137	138	139	140	141	142	143	144	145	146	147	148	149	150	151	152	153	154	155	156	157
r6	126	127	128	129	130	131	132	133	134	135	136	137	138	139	140	141	142	143	144	145	146	147	148	149	150	151	152	153	154	155	156	157

Block 6

	c1	c2	c3	c4	c5	c6	c7	c8	c9	c10	c11	c12	c13	c14	c15	c16	c17	c18	c19	c20	c21	c22	c23	c24	c25	c26	c27	c28	c29	c30	c31	c32
r1	158	159	160	161	162	163	164	165	166	167	168	169	170	171	172	173	174	175	176	177	178	179	180	181	182	183	184	185	186	187	188	189
r2	158	159	160	161	162	163	164	165	166	167	168	169	170	171	172	173	174	175	176	177	178	179	180	181	182	183	184	185	186	187	188	189
r3	158	159	160	161	162	163	164	165	166	167	168	169	170	171	172	173	174	175	176	177	178	179	180	181	182	183	184	185	186	187	188	189
r4	158	159	160	161	162	163	164	165	166	167	168	169	170	171	172	173	174	175	176	177	178	179	180	181	182	183	184	185	186	187	188	189
r5	158	159	160	161	162	163	164	165	166	167	168	169	170	171	172	173	174	175	176	177	178	179	180	181	182	183	184	185	186	187	188	189
r6	158	159	160	161	162	163	164	165	166	167	168	169	170	171	172	173	174	175	176	177	178	179	180	181	182	183	184	185	186	187	188	189

Block 7

	c1	c2	c3	c4	c5	c6	c7	c8	c9	c10	c11	c12	c13	c14	c15	c16	c17	c18	c19	c20	c21	c22	c23	c24	c25	c26	c27	c28	c29	c30	c31	c32
r1	190	191	192	193	194	195	196	197	198	199	200	201	202	203	204	205	206	207	208	209	210	211	212	213	214	215	216	217	218	219	220	221
r2	190	191	192	193	194	195	196	197	198	199	200	201	202	203	204	205	206	207	208	209	210	211	212	213	214	215	216	217	218	219	220	221
r3	190	191	192	193	194	195	196	197	198	199	200	201	202	203	204	205	206	207	208	209	210	211	212	213	214	215	216	217	218	219	220	221
r4	190	191	192	193	194	195	196	197	198	199	200	201	202	203	204	205	206	207	208	209	210	211	212	213	214	215	216	217	218	219	220	221
r5	190	191	192	193	194	195	196	197	198	199	200	201	202	203	204	205	206	207	208	209	210	211	212	213	214	215	216	217	218	219	220	221
r6	190	191	192	193	194	195	196	197	198	199	200	201	202	203	204	205	206	207	208	209	210	211	212	213	214	215	216	217	218	219	220	221

Block 8

	c1	c2	c3	c4	c5	c6	c7	c8	c9	c10	c11	c12	c13	c14	c15	c16	c17	c18	c19	c20	c21	c22	c23	c24	c25	c26	c27	c28	c29	c30	c31	c32
r1	222	223	224	225	226	227	228	229	230	231	232	233	234	235	236	237	238	239	240	241	242	243	244	245	246	247	248	249	250	251	252	253
r2	222	223	224	225	226	227	228	229	230	231	232	233	234	235	236	237	238	239	240	241	242	243	244	245	246	247	248	249	250	251	252	253
r3	222	223	224	225	226	227	228	229	230	231	232	233	234	235	236	237	238	239	240	241	242	243	244	245	246	247	248	249	250	251	252	253
r4	222	223	224	225	226	227	228	229	230	231	232	233	234	235	236	237	238	239	240	241	242	243	244	245	246	247	248	249	250	251	252	253
r5	222	223	224	225	226	227	228	229	230	231	232	233	234	235	236	237	238	239	240	241	242	243	244	245	246	247	248	249	250	251	252	253
r6	222	223	224	225	226	227	228	229	230	231	232	233	234	235	236	237	238	239	240	241	242	243	244	245	246	247	248	249	250	251	252	253

Block 9

	c1	c2	c3	c4	c5	c6	c7	c8	c9	c10	c11	c12	c13	c14	c15	c16	c17	c18	c19	c20	c21	c22	c23	c24	c25	c26	c27	c28	c29	c30	c31	c32
r1	254	255	256	257	258	259	260	261	262	263	264	265	266	267	268	269	270	271	272	273	274	275	276	A	G	N	N	N	N	E	E	P
r2	254	255	256	257	258	259	260	261	262	263	264	265	266	267	268	269	270	271	272	273	274	275	276	A	G	N	N	N	N	E	E	P
r3	254	255	256	257	258	259	260	261	262	263	264	265	266	267	268	269	270	271	272	273	274	275	276	A	G	N	N	N	N	E	E	P
r4	254	255	256	257	258	259	260	261	262	263	264	265	266	267	268	269	270	271	272	273	274	275	276	A	G	N	N	N	N	E	E	P
r5	254	255	256	257	258	259	260	261	262	263	264	265	266	267	268	269	270	271	272	273	274	275	276	A	G	N	N	N	N	E	E	P
r6	254	255	256	257	258	259	260	261	262	263	264	265	266	267	268	269	270	271	272	273	274	275	276	A	G	N	N	N	N	E	E	P

N = Negative control **A = Beta actin** **E = Empty** **G = GAPDH** **P = Position marker**

Fullmoon cancer array antibody list

ID	Antibody Name
1	GSK3 beta (Phospho-Ser9)
2	c-Jun (Phospho-Ser73)
3	Elk1 (Phospho-Ser383)
4	PDK1 (Phospho-Ser241)
5	Raf1 (Phospho-Ser259)
6	GSK3 alpha (Phospho-Ser21)
7	MEK-2 (Phospho-Thr394)
8	NFkB-p65 (Phospho-Thr254)
9	NFkB-p100/p52 (Phospho-Ser865)
10	NFkB-p100/p52 (Phospho-Ser869)
11	NFkB-p105/p50 (Phospho-Ser893)
12	NFkB-p105/p50 (Phospho-Ser907)
13	Rel (Phospho-Ser503)
14	c-Jun (Phospho-Thr239)
15	c-Jun (Phospho-Ser243)
16	JunB (Phospho-Ser79)
17	JunB (Phospho-Ser259)
18	JunD (Phospho-Ser255)
19	Myc (Phospho-Thr58)
20	Myc (Phospho-Thr358)
21	Myc (Phospho-Ser373)
22	STAT1 (Phospho-Tyr701)
23	STAT3 (Phospho-Tyr705)
24	STAT3 (Phospho-Ser727)
25	STAT4 (Phospho-Tyr693)
26	STAT5A (Phospho-Tyr694)
27	STAT5A (Phospho-Ser780)
28	STAT6 (Phospho-Tyr641)
29	STAT6 (Phospho-Thr645)
30	CREB (Phospho-Ser133)
31	AKT (Phospho-Ser473)

ID	Antibody Name
32	AKT (Phospho-Thr308)
33	PTEN (Phospho-Ser380/Thr382/Thr383)
34	FAK (Phospho-Tyr861)
35	Integrin beta-3 (Phospho-Tyr773)
36	Chk2 (Phospho-Thr68)
37	BCL-2 (Phospho-Thr56)
38	BCL-2 (Phospho-Ser70)
39	BCL-XL (Phospho-Ser62)
40	BAD (Phospho-Ser112)
41	BAD (Phospho-Ser136)
42	BAD (Phospho-Ser155)
43	Estrogen Receptor-α (Phospho-Ser167)
44	HER2 (Phospho-Tyr877)
45	ICAM-1 (Phospho-Tyr512)
46	VEGFR2 (Phospho-Tyr951)
47	IGF-1R (Phospho-Tyr1161)
48	Caveolin-1 (Phospho-Tyr14)
49	Src (Phospho-Tyr418)
50	p53 (Phospho-Ser6)
51	p53 (Phospho-Ser315)
52	Tau (Phospho-Ser404)
53	FKHR (Phospho-Ser256)
54	Catenin beta (Phospho-Thr41/Ser45)
55	BRCA1 (Phospho-Ser1524)
56	CDC25C (Phospho-Ser216)
57	Chk1 (Phospho-Ser345)
58	FAK (Phospho-Tyr925)
59	AKT2 (Phospho-Ser474)
60	IKK-alpha (Phospho-Thr23)
61	Rb (Phospho-Ser780)
62	CDK2 (Phospho-Thr160)

ID	Antibody Name
63	CDC25A (Phospho-Ser75)
64	Chk1 (Phospho-Ser280)
65	Chk1 (Phospho-Ser317)
66	MKK3 (Phospho-Ser189)
67	Chk2 (Phospho-Ser516)
68	TYK2 (Phospho-Tyr1054)
69	JAK1 (Phospho-Tyr1022)
70	JAK2 (Phospho-Tyr221)
71	JAK2 (Phospho-Tyr1007)
72	IkB-alpha (Phospho-Ser32/36)
73	Src (Phospho-Tyr529)
74	MEK1 (Phospho-Ser221)
75	IkB-alpha (Phospho-Tyr42)
76	STAT1 (Phospho-Ser727)
77	HDAC8 (Phospho-Ser39)
78	HSP27 (Phospho-Ser15)
79	MSK1 (Phospho-Ser376)
80	Rac1/cdc42 (Phospho-Ser71)
81	MEK1 (Phospho-Ser217)
82	p21Cip1 (Phospho-Thr145)
83	p27Kip1 (Phospho-Ser10)
84	p27Kip1 (Phospho-Thr187)
85	Pyk2 (Phospho-Tyr402)
86	NFkB-p65 (Phospho-Ser529)
87	Catenin beta (Phospho-Ser33)
88	Catenin beta (Phospho-Ser37)
89	mTOR (Phospho-Ser2448)
90	4E-BP1 (Phospho-Thr36)
91	PDGF R beta (Phospho-Tyr751)
92	eIF4E (Phospho-Ser209)
93	Met (Phospho-Tyr1349)

ID	Antibody Name
94	FGFR1 (Phospho-Tyr154)
95	c-Kit (Phospho-Tyr721)
96	BRCA1 (Phospho-Ser1423)
97	CDC2 (Phospho-Tyr15)
98	p44/42 MAP Kinase (Phospho-Thr202)
99	p44/42 MAP Kinase (Phospho-Tyr204)
100	HSP27 (Phospho-Ser78)
101	SAPK/JNK (Phospho-Thr183)
102	NFkB-p105/p50 (Phospho-Ser932)
103	P38 MAPK (Phospho-Thr180)
104	P38 MAPK (Phospho-Tyr182)
105	HSF1 (Phospho-Ser303)
106	EGFR (Phospho-Tyr1110)
107	Histone H2A.X (Phospho-Ser139)
108	eIF2A (Phospho-Ser51)
109	Integrin beta-3 (Phospho-Tyr785)
110	P70S6K (Phospho-Ser424)
111	CaMKII (Phospho-Thr286)
112	MEK1 (Phospho-Thr291)
113	14-3-3 zeta (Phospho-Ser58)
114	AMPK1 (Phospho-Thr174)
115	HSP90B (Phospho-Ser254)
116	IkB-beta (Phospho-Ser23)
117	IkB-epsilon (Phospho-Ser22)
118	Keratin 18 (Phospho-Ser33)
119	Myc (Phospho-Ser62)
120	Shc (Phospho-Tyr349)
121	SHP-2 (Phospho-Tyr580)
122	Smad3 (Phospho-Ser425)
123	Trk B (Phospho-Tyr515)
124	CrkII (Phospho-Tyr221)

ID	Antibody Name
125	eEF2K (Phospho-Ser366)
126	GSK3 beta (Ab-9)
127	c-Jun (Ab-73)
128	Elk1 (Ab-383)
129	PDK1 (Ab-241)
130	Raf1 (Ab-259)
131	GSK3 alpha (Ab-21)
132	MEK-2 (Ab-394)
133	NFkB-p65 (Ab-254)
134	NFkB-p100/p52 (Ab-865)
135	NFkB-p100/p52 (Ab-869)
136	NFkB-p105/p50 (Ab-337)
137	NFkB-p105/p50 (Ab-893)
138	NFkB-p105/p50 (Ab-907)
139	Rel (Ab-503)
140	c-Jun (Ab-239)
141	c-Jun (Ab-243)
142	JunB (Ab-79)
143	JunB (Ab-259)
144	JunD (Ab-255)
145	Myc (Ab-58)
146	Myc (Ab-358)
147	Myc (Ab-373)
148	STAT1 (Ab-701)
149	STAT3 (Ab-705)
150	STAT3 (Ab-727)
151	STAT4 (Ab-693)
152	STAT5A (Ab-694)
153	STAT5A (Ab-780)
154	STAT6 (Ab-641)
155	STAT6 (Ab-645)

ID	Antibody Name
156	CREB (Ab-133)
157	AKT (Ab-473)
158	AKT (Ab-308)
159	PTEN (Ab-380/382/383)
160	BCL-2 (Ab-56)
161	BCL-2 (Ab-70)
162	BCL-XL (Ab-62)
163	BAD (Ab-112)
164	BAD (Ab-136)
165	BAD (Ab-155)
166	Estrogen Receptor-α (Ab-167)
167	HER2 (Ab-877)
168	FAK (Ab-861)
169	VEGFR2 (Ab-951)
170	IGF-1R (Ab-1161)
171	Integrin beta-3 (Ab-773)
172	p53 (Ab-6)
173	Chk2 (Ab-68)
174	p53 (Ab-315)
175	Tau (Ab-404)
176	Catenin beta (Ab-41/45)
177	ICAM-1 (Ab-512)
178	Rb (Ab-780)
179	CDK2 (Ab-160)
180	Caveolin-1 (Ab-14)
181	Chk1 (Ab-280)
182	Chk1 (Ab-317)
183	Src (Ab-418)
184	MKK3 (Ab-189)
185	Chk2 (Ab-516)
186	TYK2 (Ab-1054)

ID	Antibody Name
187	JAK1 (Ab-1022)
188	JAK2 (Ab-221)
189	JAK2 (Ab-1007)
190	IkB-alpha (Ab-32/36)
191	FKHR (Ab-256)
192	BRCA1 (Ab-1524)
193	HDAC8 (Ab-39)
194	HSP27 (Ab-15)
195	CDC25C (Ab-216)
196	Chk1 (Ab-345)
197	ATM (Ab-1981)
198	FAK (Ab-925)
199	p21Cip1 (Ab-145)
200	p27Kip1 (Ab-10)
201	p27Kip1 (Ab-187)
202	AKT2 (Ab-474)
203	IKK-alpha (Ab-23)
204	CDC25A (Ab-75)
205	Src (Ab-529)
206	MEK1 (Ab-221)
207	IkB-alpha (Ab-42)
208	STAT1 (Ab-727)
209	MSK1 (Ab-376)
210	Rac1/cdc42 (Ab-71)
211	MEK1 (Ab-217)
212	FAK (Ab-397)
213	Pyk2 (Ab-402)
214	NFkB-p65 (Ab-529)
215	Catenin beta (Ab-37)
216	mTOR (Ab-2448)
217	4E-BP1 (Ab-36)

ID	Antibody Name
218	PDGF R beta (Ab-751)
219	eIF4E (Ab-209)
220	Met (Ab-1349)
221	FGFR1 (Ab-154)
222	c-Kit (Ab-721)
223	BRCA1 (Ab-1423)
224	CDC2 (Ab-15)
225	p44/42 MAP Kinase (Ab-202)
226	p44/42 MAP Kinase (Ab-204)
227	HSP27 (Ab-78)
228	SAPK/JNK (Ab-183)
229	P38 MAPK (Ab-182)
230	HSF1 (Ab-303)
231	EGFR (Ab-1110)
232	Histone H2A.X (Ab-139)
233	eIF2A (Ab-51)
234	Integrin beta-3 (Ab-785)
235	P70S6K (Ab-424)
236	CaMKII (Ab-286)
237	MEK1 (Ab-291)
238	14-3-3 zeta (Ab-58)
239	AMPK1 (Ab-174)
240	HSP90B (Ab-254)
241	IkB-epsilon (Ab-22)
242	Keratin 18 (Ab-33)
243	Myc (Ab-62)
244	Shc (Ab-349)
245	SHP-2 (Ab-580)
246	Trk B (Ab-515)
247	CrkII (Ab-221)
248	eEF2K (Ab-366)

Fullmoon cancer array plate layout

Block 1

	c1	c2	c3	c4	c5	c6	c7	c8	c9	c10	c11	c12	c13	c14	c15	c16	c17	c18	c19	c20	c21	c22	c23	c24	c25	c26	c27	c28	c29	c30	c31	c32
r1	P	E	E	1	2	3	4	5	6	7	8	9	10	11	12	13	14	15	16	17	18	19	20	21	22	23	24	25	26	27	28	P
r2	P	E	E	1	2	3	4	5	6	7	8	9	10	11	12	13	14	15	16	17	18	19	20	21	22	23	24	25	26	27	28	P
r3	P	E	E	1	2	3	4	5	6	7	8	9	10	11	12	13	14	15	16	17	18	19	20	21	22	23	24	25	26	27	28	P
r4	P	E	E	1	2	3	4	5	6	7	8	9	10	11	12	13	14	15	16	17	18	19	20	21	22	23	24	25	26	27	28	P
r5	P	E	E	1	2	3	4	5	6	7	8	9	10	11	12	13	14	15	16	17	18	19	20	21	22	23	24	25	26	27	28	P
r6	P	E	E	1	2	3	4	5	6	7	8	9	10	11	12	13	14	15	16	17	18	19	20	21	22	23	24	25	26	27	28	P

Block 2

	c1	c2	c3	c4	c5	c6	c7	c8	c9	c10	c11	c12	c13	c14	c15	c16	c17	c18	c19	c20	c21	c22	c23	c24	c25	c26	c27	c28	c29	c30	c31	c32
r1	P	E	E	29	30	31	32	33	34	35	36	37	38	39	40	41	42	43	44	45	46	47	48	49	50	51	52	53	54	55	56	P
r2	P	E	E	29	30	31	32	33	34	35	36	37	38	39	40	41	42	43	44	45	46	47	48	49	50	51	52	53	54	55	56	P
r3	P	E	E	29	30	31	32	33	34	35	36	37	38	39	40	41	42	43	44	45	46	47	48	49	50	51	52	53	54	55	56	P
r4	P	E	E	29	30	31	32	33	34	35	36	37	38	39	40	41	42	43	44	45	46	47	48	49	50	51	52	53	54	55	56	P
r5	P	E	E	29	30	31	32	33	34	35	36	37	38	39	40	41	42	43	44	45	46	47	48	49	50	51	52	53	54	55	56	P
r6	P	E	E	29	30	31	32	33	34	35	36	37	38	39	40	41	42	43	44	45	46	47	48	49	50	51	52	53	54	55	56	P

Block 3

	c1	c2	c3	c4	c5	c6	c7	c8	c9	c10	c11	c12	c13	c14	c15	c16	c17	c18	c19	c20	c21	c22	c23	c24	c25	c26	c27	c28	c29	c30	c31	c32
r1	P	E	E	57	58	59	60	61	62	63	64	65	66	67	68	69	70	71	72	73	74	75	76	77	78	79	80	81	82	83	84	P
r2	P	E	E	57	58	59	60	61	62	63	64	65	66	67	68	69	70	71	72	73	74	75	76	77	78	79	80	81	82	83	84	P
r3	P	E	E	57	58	59	60	61	62	63	64	65	66	67	68	69	70	71	72	73	74	75	76	77	78	79	80	81	82	83	84	P
r4	P	E	E	57	58	59	60	61	62	63	64	65	66	67	68	69	70	71	72	73	74	75	76	77	78	79	80	81	82	83	84	P
r5	P	E	E	57	58	59	60	61	62	63	64	65	66	67	68	69	70	71	72	73	74	75	76	77	78	79	80	81	82	83	84	P
r6	P	E	E	57	58	59	60	61	62	63	64	65	66	67	68	69	70	71	72	73	74	75	76	77	78	79	80	81	82	83	84	P

Block 4

	c1	c2	c3	c4	c5	c6	c7	c8	c9	c10	c11	c12	c13	c14	c15	c16	c17	c18	c19	c20	c21	c22	c23	c24	c25	c26	c27	c28	c29	c30	c31	c32
r1	P	E	E	85	86	87	88	89	90	91	92	93	94	95	96	97	98	99	100	101	102	103	104	105	106	107	108	109	110	111	112	P
r2	P	E	E	85	86	87	88	89	90	91	92	93	94	95	96	97	98	99	100	101	102	103	104	105	106	107	108	109	110	111	112	P
r3	P	E	E	85	86	87	88	89	90	91	92	93	94	95	96	97	98	99	100	101	102	103	104	105	106	107	108	109	110	111	112	P
r4	P	E	E	85	86	87	88	89	90	91	92	93	94	95	96	97	98	99	100	101	102	103	104	105	106	107	108	109	110	111	112	P
r5	P	E	E	85	86	87	88	89	90	91	92	93	94	95	96	97	98	99	100	101	102	103	104	105	106	107	108	109	110	111	112	P
r6	P	E	E	85	86	87	88	89	90	91	92	93	94	95	96	97	98	99	100	101	102	103	104	105	106	107	108	109	110	111	112	P

Block 5

	c1	c2	c3	c4	c5	c6	c7	c8	c9	c10	c11	c12	c13	c14	c15	c16	c17	c18	c19	c20	c21	c22	c23	c24	c25	c26	c27	c28	c29	c30	c31	c32
r1	P	E	E	113	114	115	116	117	118	119	120	121	122	123	124	125	126	127	128	129	130	131	132	133	134	135	136	137	138	139	140	P
r2	P	E	E	113	114	115	116	117	118	119	120	121	122	123	124	125	126	127	128	129	130	131	132	133	134	135	136	137	138	139	140	P
r3	P	E	E	113	114	115	116	117	118	119	120	121	122	123	124	125	126	127	128	129	130	131	132	133	134	135	136	137	138	139	140	P
r4	P	E	E	113	114	115	116	117	118	119	120	121	122	123	124	125	126	127	128	129	130	131	132	133	134	135	136	137	138	139	140	P
r5	P	E	E	113	114	115	116	117	118	119	120	121	122	123	124	125	126	127	128	129	130	131	132	133	134	135	136	137	138	139	140	P
r6	P	E	E	113	114	115	116	117	118	119	120	121	122	123	124	125	126	127	128	129	130	131	132	133	134	135	136	137	138	139	140	P

Block 6

	c1	c2	c3	c4	c5	c6	c7	c8	c9	c10	c11	c12	c13	c14	c15	c16	c17	c18	c19	c20	c21	c22	c23	c24	c25	c26	c27	c28	c29	c30	c31	c32
r1	P	E	E	141	142	143	144	145	146	147	148	149	150	151	152	153	154	155	156	157	158	159	160	161	162	163	164	165	166	167	168	P
r2	P	E	E	141	142	143	144	145	146	147	148	149	150	151	152	153	154	155	156	157	158	159	160	161	162	163	164	165	166	167	168	P
r3	P	E	E	141	142	143	144	145	146	147	148	149	150	151	152	153	154	155	156	157	158	159	160	161	162	163	164	165	166	167	168	P
r4	P	E	E	141	142	143	144	145	146	147	148	149	150	151	152	153	154	155	156	157	158	159	160	161	162	163	164	165	166	167	168	P
r5	P	E	E	141	142	143	144	145	146	147	148	149	150	151	152	153	154	155	156	157	158	159	160	161	162	163	164	165	166	167	168	P
r6	P	E	E	141	142	143	144	145	146	147	148	149	150	151	152	153	154	155	156	157	158	159	160	161	162	163	164	165	166	167	168	P

Block 7

	c1	c2	c3	c4	c5	c6	c7	c8	c9	c10	c11	c12	c13	c14	c15	c16	c17	c18	c19	c20	c21	c22	c23	c24	c25	c26	c27	c28	c29	c30	c31	c32
r1	P	E	E	169	170	171	172	173	174	175	176	177	178	179	180	181	182	183	184	185	186	187	188	189	190	191	192	193	194	195	196	P
r2	P	E	E	169	170	171	172	173	174	175	176	177	178	179	180	181	182	183	184	185	186	187	188	189	190	191	192	193	194	195	196	P
r3	P	E	E	169	170	171	172	173	174	175	176	177	178	179	180	181	182	183	184	185	186	187	188	189	190	191	192	193	194	195	196	P
r4	P	E	E	169	170	171	172	173	174	175	176	177	178	179	180	181	182	183	184	185	186	187	188	189	190	191	192	193	194	195	196	P
r5	P	E	E	169	170	171	172	173	174	175	176	177	178	179	180	181	182	183	184	185	186	187	188	189	190	191	192	193	194	195	196	P
r6	P	E	E	169	170	171	172	173	174	175	176	177	178	179	180	181	182	183	184	185	186	187	188	189	190	191	192	193	194	195	196	P

Block 8

	c1	c2	c3	c4	c5	c6	c7	c8	c9	c10	c11	c12	c13	c14	c15	c16	c17	c18	c19	c20	c21	c22	c23	c24	c25	c26	c27	c28	c29	c30	c31	c32
r1	P	E	E	197	198	199	200	201	202	203	204	205	206	207	208	209	210	211	212	213	214	215	216	217	218	219	220	221	222	223	224	P
r2	P	E	E	197	198	199	200	201	202	203	204	205	206	207	208	209	210	211	212	213	214	215	216	217	218	219	220	221	222	223	224	P
r3	P	E	E	197	198	199	200	201	202	203	204	205	206	207	208	209	210	211	212	213	214	215	216	217	218	219	220	221	222	223	224	P
r4	P	E	E	197	198	199	200	201	202	203	204	205	206	207	208	209	210	211	212	213	214	215	216	217	218	219	220	221	222	223	224	P
r5	P	E	E	197	198	199	200	201	202	203	204	205	206	207	208	209	210	211	212	213	214	215	216	217	218	219	220	221	222	223	224	P
r6	P	E	E	197	198	199	200	201	202	203	204	205	206	207	208	209	210	211	212	213	214	215	216	217	218	219	220	221	222	223	224	P

Block 9

	c1	c2	c3	c4	c5	c6	c7	c8	c9	c10	c11	c12	c13	c14	c15	c16	c17	c18	c19	c20	c21	c22	c23	c24	c25	c26	c27	c28	c29	c30	c31	c32
r1	P	E	E	225	226	227	228	229	230	231	232	233	234	235	236	237	238	239	240	241	242	243	244	245	246	247	248	A	G	N	N	P
r2	P	E	E	225	226	227	228	229	230	231	232	233	234	235	236	237	238	239	240	241	242	243	244	245	246	247	248	A	G	N	N	P
r3	P	E	E	225	226	227	228	229	230	231	232	233	234	235	236	237	238	239	240	241	242	243	244	245	246	247	248	A	G	N	N	P
r4	P	E	E	225	226	227	228	229	230	231	232	233	234	235	236	237	238	239	240	241	242	243	244	245	246	247	248	A	G	N	N	P
r5	P	E	E	225	226	227	228	229	230	231	232	233	234	235	236	237	238	239	240	241	242	243	244	245	246	247	248	A	G	N	N	P
r6	P	E	E	225	226	227	228	229	230	231	232	233	234	235	236	237	238	239	240	241	242	243	244	245	246	247	248	A	G	N	N	P

N = Negative control **A = Beta actin** **E = Empty** **G = GAPDH** **P = Position marker**

	1	2	3	4	5	6	7	8	9	10	11	12
A	BCR std 6×10^{3}	BCR std 6×10^{3}	BCR std 6×10^{5}	BCR std 6×10^{6}					HeLa	Low	High	NTC
B												
C												
D												
E	b3a2 std 3.2×10^{1}	b3a2 std 3.2×10^{1}	b3a2 std 3.2×10^{2}	b3a2 std 3.2×10^{2}	b3a2 std 3.2×10^{3}	b3a2 std 3.2×10^{4}	b3a2 std 3.2×10^{5}	b3a2 std 3.2×10^{6}	HeLa	Low	High	NTC
F												
G												
H												

Taqman array gene list

Well	Context Sequence	Group	Gene Symbol	Gene Name	NCBI Reference
A01	TTGGAGGGCAAGTCTGGTGCCAGCA	Molecular function unclassified	18S	Eukaryotic 18S rRNA	X03205.1
A02	GGGCGCCTGGTCACCAGGGCTGCTT	Dehydrogenase	GAPDH	glyceraldehyde-3-phosphate dehydrogenase	NM_002046.3
A03	ATGGTCAAGGTCGCAAGCTTGCTGG	Glycosyltransferase	HPRT1	hypoxanthine phosphoribosyltransferase 1	NM_000194.2
A04	GACTGAACAGTCACCGACGAGAGTG	Galactosidase	GUSB	glucuronidase, beta	NM_000181.2
A05	TCGCCTTTGCCGATCCGCCGCCCGT	Actin family cytoskeletal protein	ACTB	actin, beta	NM_001101.3
A06	TTAAGTGGGATCGAGACATGTAAGC	Major histocompatibility complex antigen	B2M	beta-2-microglobulin	NM_004048.2
A07	GAAATGTTTCATTGTGGGAGCAGAC	Ribosomal protein	RPLP0	ribosomal protein, large, P0	NM_053275.3
A08	AATGCGGCTGCAACGGCGGAAGAAA	Deaminase	HMBS	hydroxymethylbilane synthase	NM_000190.3
A09	TGGGTTTTCCAGCTAAGTTCTTGGA	Molecular function unclassified	TBP	TATA box binding protein	M55654.1
A10	TGGGAACAAGGTTAAAGCCGAGCCA	Carbohydrate kinase	PGK1	phosphoglycerate kinase 1	NM_000291.3
A11	TGATCGTCACTTGACAATGCAGATC	Molecular function unclassified	UBC	ubiquitin C	NM_021009.4
A12	TCATCTGCACTGCCAAGACTGAGTG	Other isomerase	PPIA	peptidylprolyl isomerase A (cyclophilin A)	NM_021130.3
B01	CAACATGAATGCCATTTTCCAAATA	Atp-binding cassette (abc) transporter	ABCA1	ATP-binding cassette, sub-family A (ABC1), member 1	NM_005502.2
B02	AGTCTGGCTGCACAGCTCCTAATTC	Atp-binding cassette (abc) transporter	ABCA12	ATP-binding cassette, sub-family A (ABC1), member 12	NM_015657.3
B03	CCATGGGAGACGCCGTGGACCTGTC	Atp-binding cassette (abc) transporter	ABCA13	ATP-binding cassette, sub-family A (ABC1), member 13	NM_152701.2
B04	TCCTCAAGGCCAACGAGACTTTTGC	Atp-binding cassette (abc) transporter	ABCA2	ATP-binding cassette, sub-family A (ABC1), member 2	NM_001606.4
B05	CTCAGCTGGGCGAAGGTTTTCGGTA	Atp-binding cassette (abc) transporter	ABCA3	ATP-binding cassette, sub-family A (ABC1), member 3	NM_001089.2
B06	AGCCCAGGACTGATCTTTCACACCG	Atp-binding cassette (abc) transporter	ABCA4	ATP-binding cassette, sub-family A (ABC1), member 4	NM_000350.2
B07	GACCTTGTTGGAATGGCTCTTTTCA	Atp-binding cassette (abc) transporter	ABCA9	ATP-binding cassette, sub-family A (ABC1), member 9	NM_080283.3
B08	AGACATGACCAGGTATGCCTATTAT	Atp-binding cassette (abc) transporter	ABCB1	ATP-binding cassette, sub-family B (MDR/TAP), member 1	NM_000927.3
B09	TTCAAGGGGCTGCCGGCTCTCAGAT	Atp-binding cassette (abc) transporter	ABCB11	ATP-binding cassette, sub-family B (MDR/TAP), member 11	NM_003742.2
B10	ATCAGCAGCAAACAAAAAAGGAAAA	Atp-binding cassette (abc) transporter	ABCB4	ATP-binding cassette, sub-family B (MDR/TAP), member 4	NM_000443.3
B11	TTCAAGGAGCAACAGGTTCCAGGAT	Atp-binding cassette (abc) transporter	ABCB5	ATP-binding cassette, sub-family B (MDR/TAP), member 5	NM_178559.4
B12	GCTCAGCTACCTGGTGTTCAATGTC	Atp-binding cassette (abc) transporter	ABCB6	ATP-binding cassette, sub-family B (MDR/TAP), member 6	NM_005689.1
C01	TCGTGGCCAACAGGTGGCTGGCCGT	Atp-binding cassette (abc) transporter	ABCC1	ATP-binding cassette, sub-family C (CFTR/MRP), member 1	NM_004996.3
C02	GATGCGCGGGTTAAGCTTGTGACAG	Atp-binding cassette (abc) transporter	ABCC10	ATP-binding cassette, sub-family C (CFTR/MRP), member 10	NM_033450.2
C03	TGCTCTCAGGAACCATCAGATTCAA	Atp-binding cassette (abc) transporter	ABCC11	ATP-binding cassette, sub-family C (CFTR/MRP), member 11	NM_032583.3
C04	CCGCACCCGTGGCATTTAGTGTGAT	Atp-binding cassette (abc) transporter	ABCC12	ATP-binding cassette, sub-family C (CFTR/MRP), member 12	NM_033226.2
C05	CACCTCCAACAGGTGGCTTGCAATT	Atp-binding cassette (abc) transporter	ABCC2	ATP-binding cassette, sub-family C (CFTR/MRP), member 2	NM_000392.3
C06	TCCACAGCTGCTCAGCATCCTGATC	Molecular function unclassified	ABCC3	ATP-binding cassette, sub-family C (CFTR/MRP), member 3	AB010887.1
C07	AACAGCAAAACAGGTATACTTCAAA	Atp-binding cassette (abc) transporter	ABCC4	ATP-binding cassette, sub-family C (CFTR/MRP), member 4	NM_005845.3
C08	AACTCGACCGTTGGAATGCCAAGAT	Atp-binding cassette (abc) transporter	ABCC5	ATP-binding cassette, sub-family C (CFTR/MRP), member 5	NM_001023587.1

Well	Context Sequence	Group	Gene Symbol	Gene Name	NCBI Reference
C09	ACGCAGGAGAGAAGGTGGGCATCGT	Atp-binding cassette (abc) transporter	ABCC6	ATP-binding cassette, sub-family C (CFTR/MRP), member 6	NM_001171.5
C10	GGCCATGAGGTGGAGCTGGCCCTGC	Transporter	ABCD1	ATP-binding cassette, sub-family D (ALD), member 1	NM_000033.3
C11	GCAAAGAATGGCGATGGCAAGATTA	Transporter	ABCD3	ATP-binding cassette, sub-family D (ALD), member 3	NM_002858.3
C12	CGAAGTACGCAGTGCTTGATGAAGC	Transporter	ABCD4	ATP-binding cassette, sub-family D (ALD), member 4	NR_003256.2
D01	AAGCTGACACCGACCCATGGGGAAA	Atp-binding cassette (abc) transporter	ABCF1	ATP-binding cassette, sub-family F (GCN20), member 1	NM_001025091.1
D02	TGGAGGCAAATCTTCGTTATTAGAT	Transporter	ABCG2	ATP-binding cassette, sub-family G (WHITE), member 2	NM_004827.2
D03	CTGACTTCTATGTGGACCTGACCAG	Transporter	ABCG8	ATP-binding cassette, sub-family G (WHITE), member 8	NM_022437.2
D04	CGCAATGACCTGGCTGATGGTGTGA	Molecular function unclassified	AQP1	aquaporin 1 (Colton blood group)	NM_198098.1
D05	CCGGGCACAGGCGGTCCACCCGTGG	Other transporter	AQP7	aquaporin 7	NM_001170.1
D06	TCTTGATTGTCCTTGGATGTGGCTG	Molecular function unclassified	AQP9	aquaporin 9	NM_020980.3
D07	GACTATTCGTGGGCATGATCCTGAT	Cation transporter	ATP6V0C	ATPase, H+ transporting, lysosomal 16kDa, V0 subunit c	NM_001694.2
D08	CCTCATCACAGGGGAGGCAATGCCT	Cation transporter	ATP7A	ATPase, Cu++ transporting, alpha polypeptide	NM_000052.4
D09	AACATTGAGCTGACAATCACAGGGA	Cation transporter	ATP7B	ATPase, Cu++ transporting, beta polypeptide	NM_001005918.1
D10	TGGCCTACAACTGGCACTTTGAGGT	Ribonucleoprotein	MVP	major vault protein	NM_017458.2
D11	ATGAACCTCAGCATTGTGATGACCA	Cation transporter	SLC10A1	solute carrier family 10 (sodium/bile acid cotransporter family), member 1	NM_003049.2
D12	TTCTTAGGATTTTATGTGGCATACA	Cation transporter	SLC10A2	solute carrier family 10 (sodium/bile acid cotransporter family), member 2	NM_000452.2
E01	AGCAAACAGTGGGCCGAGTACATTC	Molecular function unclassified	SLC15A1	solute carrier family 15 (oligopeptide transporter), member 1	U21936.1
E02	GGTTGGGAAAATTCAAGACAATCAT	Other transporter	SLC15A2	solute carrier family 15 (H+/peptide transporter), member 2	NM_021082.2
E03	GGCCACCACTTTTAGGTCGGCTCAA	Other transporter	SLC16A1	solute carrier family 16, member 1 (monocarboxylic acid transporter 1)	NM_003051.3
E04	CTACTTGCAGGTCCTTTCCTTCCTG	Other transporter	SLC16A2	solute carrier family 16, member 2 (monocarboxylic acid transporter 8)	NM_006517.3
E05	CCCTTCGGGAGGCAAACTCCTGGAT	Other transporter	SLC16A3	solute carrier family 16, member 3 (monocarboxylic acid transporter 4)	NM_001042423.1
E06	GCGGGAGCAGGTCACGAACGAGATC	Other transporter	SLC19A1	solute carrier family 19 (folate transporter), member 1	NM_194255.1
E07	GAAATTACCACTCAGTTTTTGATCT	Other transporter	SLC19A2	solute carrier family 19 (thiamine transporter), member 2	NM_006996.2
E08	TATAACCATAGCAGTATTTCAGATT	Other transporter	SLC19A3	solute carrier family 19, member 3	NM_025243.3
E09	GATGTACCTGTGGTTCACGGACTCT	Cation transporter	SLC22A1	solute carrier family 22 (organic cation transporter), member 1	NM_153187.1
E10	CGAAAATATGCAAAGACCAAGAAAA	Cation transporter	SLC22A2	solute carrier family 22 (organic cation transporter), member 2	NM_003058.2
E11	AAAAACTTGGCAGTCCACATTCCTG	Cation transporter	SLC22A3	solute carrier family 22 (extraneuronal monoamine transporter), member 3	NM_021977.2
E12	TCTCCATGCTGTGGTTTGCCACTAG	Other transporter	SLC22A6	solute carrier family 22 (organic anion transporter), member 6	NM_153276.1
F01	CTCAGCCTCTGGTGGGTGCCTGAGT	Other transporter	SLC22A7	solute carrier family 22 (organic anion transporter), member 7	NM_153320.2
F02	CACCTTTGTGCCCTTGGACTTGCAG	Other transporter	SLC22A8	solute carrier family 22 (organic anion transporter), member 8	NM_004254.2
F03	GTCCTTTACGAGATTTGCAAACTTT	Other transporter	SLC22A9	solute carrier family 22 (organic anion transporter), member 9	NM_080866.2
F04	CTGGAGGCTGCGCTGGAGGCTCCCA	Calmodulin related protein	SLC25A13	solute carrier family 25, member 13 (citrin)	NM_014251.2

Well	Context Sequence	Group	Gene Symbol	Gene Name	NCBI Reference
F05	CTTCTCCAGATGGAGGAACCTGCAG	Other transporter	SLC28A1	solute carrier family 28 (sodium-coupled nucleoside transporter), member 1	NM_201651.1
F06	TACCAGAGGAGGAGTCGGTGGCCTT	Other transporter	SLC28A2	solute carrier family 28 (sodium-coupled nucleoside transporter), member 2	NM_004212.2
F07	GCCAAAGTCTGTTGAGCAGCACTGT	Other transporter	SLC28A3	solute carrier family 28 (sodium-coupled nucleoside transporter), member 3	NM_022127.1
F08	GCCTCAGGACAGATACAAAGCTGTC	Other transporter	SLC29A1	solute carrier family 29 (nucleoside transporters), member 1	NM_001078174.1
F09	TTCCTGTGGCCAGACGAGGACAGCC	Other transporter	SLC29A2	solute carrier family 29 (nucleoside transporters), member 2	NM_001532.2
F10	GCACTGCTGGAGCAGCTACCCTGGA	Carbohydrate transporter	SLC2A1	solute carrier family 2 (facilitated glucose transporter), member 1	NM_006516.2
F11	CTTGGAAGAATCAAAGCCATGTTAG	Carbohydrate transporter	SLC2A2	solute carrier family 2 (facilitated glucose transporter), member 2	NM_000340.1
F12	GGGGACACAGAAGGTCACCCCAGCT	Molecular function unclassified	SLC2A3	solute carrier family 2 (facilitated glucose transporter), member 3	M20681.1
G01	TGTTGGGCAACAGATGCTGAGCTTT	Cation transporter	SLC31A1	solute carrier family 31 (copper transporters), member 1	NM_001859.3
G02	AAAAGATTGGGGCTTTGTTCTTCCT	Other transporter	SLC38A2	solute carrier family 38, member 2	NM_018976.4
G03	GAGCTCTGCCGGCCCTCCAAGCGCA	Other transporter	SLC38A5	solute carrier family 38, member 5	NM_033518.2
G04	CCGGCAGATACAGGTTCATGGGGAC	Other transporter	SLC3A1	solute carrier family 3 (cystine, dibasic and neutral amino acid transporters), member 1	NM_000341.3
G05	GCTGCCCTTCCTGGACAGCCTATGG	Other miscellaneous function protein	SLC3A2	solute carrier family 3 (activators of dibasic and neutral amino acid transport), member 2	NM_001012661.1
G06	TGAAATAGAAACACAAGTTCCTGAG	Carbohydrate transporter	SLC5A1	solute carrier family 5 (sodium/glucose cotransporter), member 1	NM_000343.2
G07	TGATGGTGTTGAAGAAGATTATCCT	Carbohydrate transporter	SLC5A4	solute carrier family 5 (low affinity glucose cotransporter), member 4	NM_014227.2
G08	CATATGCTGGCTGGTTTTACCTCAA	Amino acid transporter	SLC7A11	solute carrier family 7, (cationic amino acid transporter, y+ system) member 11	NM_014331.3
G09	GCGTGCTGCTGCTCACGGCCGTGAA	Amino acid transporter	SLC7A5	solute carrier family 7 (cationic amino acid transporter, y+ system), member 5	NM_003486.5
G10	CTGTTCAATTGCACCATGGCACTCA	Amino acid transporter	SLC7A6	solute carrier family 7 (cationic amino acid transporter, y+ system), member 6	NM_001076785.1
G11	CTCTTCAATGGTATCATGGCATTGA	Amino acid transporter	SLC7A7	solute carrier family 7 (cationic amino acid transporter, y+ system), member 7	NM_001126105.1
G12	CCCCCGCCCCATCAAGATCAACCTG	Amino acid transporter	SLC7A8	solute carrier family 7 (cationic amino acid transporter, y+ system), member 8	NM_182728.1
H01	AGAAAATCTCAAAGCCGATTACCAT	Amino acid transporter	SLC7A9	solute carrier family 7 (cationic amino acid transporter, y+ system), member 9	NM_001126335.1
H02	GTTCTCTTGAGGTGTATGAAATCTG	Other transporter	SLCO1A2	solute carrier organic anion transporter family, member 1A2	NM_134431.3
H03	TTCCACATCATTTTCAAGGGTCTAC	Other transporter	SLCO1B1	solute carrier organic anion transporter family, member 1B1	NM_006446.3
H04	ACTTTTTGTTGGGAATCATAACCAT	Other transporter	SLCO1B3	solute carrier organic anion transporter family, member 1B3	NM_019844.2
H05	CTTGCTGGCCTGGCTGCCATCTCCA	Other transporter	SLCO2A1	solute carrier organic anion transporter family, member 2A1	NM_005630.2
H06	CTGCCAGGAAGGGCAAGGACTCTCC	Other transporter	SLCO2B1	solute carrier organic anion transporter family, member 2B1	NM_007256.2
H07	CTCGCTCTATATAGGAATCCTGTTC	Other transporter	SLCO3A1	solute carrier organic anion transporter family, member 3A1	NM_013272.2
H08	AGACCTGCCTCTCTCCATCTGGCTC	Other transporter	SLCO4A1	solute carrier organic anion transporter family, member 4A1	NM_016354.3
H09	GAACCAGACAGGTAACATCATGTCT	Transporter	TAP1	transporter 1, ATP-binding cassette, sub-family B (MDR/TAP)	NM_000593.5
H10	CGCCATCAGGAAGTGCTTCGGGAGA	Transporter	TAP2	transporter 2, ATP-binding cassette, sub-family B (MDR/TAP)	NM_000544.3
H11	TTCAGTGGTAGACTCGGGGAGAACT	Voltage-gated ion channel	VDAC1	voltage-dependent anion channel 1	NM_003374.1
H12	GCTGCAGTCCTGCAGTCACCTATAC	Voltage-gated ion channel	VDAC2	voltage-dependent anion channel 2	NM_003375.2

Taqman array plate layout

	1	2	3	4	5	6	7	8	9	10	11	12
A	18S	GAPDH	HPRT1	GUSB	ACTB	B2M	RPLP0	HMBS	TBP	PGK1	UBC	PPIA
B	ABCA1	ABCA12	ABCA13	ABCA2	ABCA3	ABCA4	ABCA9	ABCB1	ABCB11	ABCB4	ABCB5	ABCB6
C	ABCC1	ABCC10	ABCC11	ABCC12	ABCC2	ABCC3	ABCC4	ABCC5	ABCC6	ABCD1	ABCD3	ABCD4
D	ABCF1	ABCG2	ABCG8	AQP1	AQP7	AQP9	ATP6V0C	ATP7A	ATP7B	MVP	SLC10A1	SLC10A2
E	SLC15A1	SLC15A2	SLC16A1	SLC16A2	SLC16A3	SLC19A1	SLC19A2	SLC19A3	SLC22A1	SLC22A2	SLC22A3	SLC22A6
F	SLC22A7	SLC22A8	SLC22A9	SLC25A13	SLC28A1	SLC28A2	SLC28A3	SLC29A1	SLC29A2	SLC2A1	SLC2A2	SLC2A3
G	SLC31A1	SLC38A2	SLC38A5	SLC3A1	SLC3A2	SLC5A1	SLC5A4	SLC7A11	SLC7A5	SLC7A6	SLC7A7	SLC7A8
H	SLC7A9	SLCO1A2	SLCO1B1	SLCO1B3	SLCO2A1	SLCO2B1	SLCO3A1	SLCO4A1	TAP1	TAP2	VDAC1	VDAC2

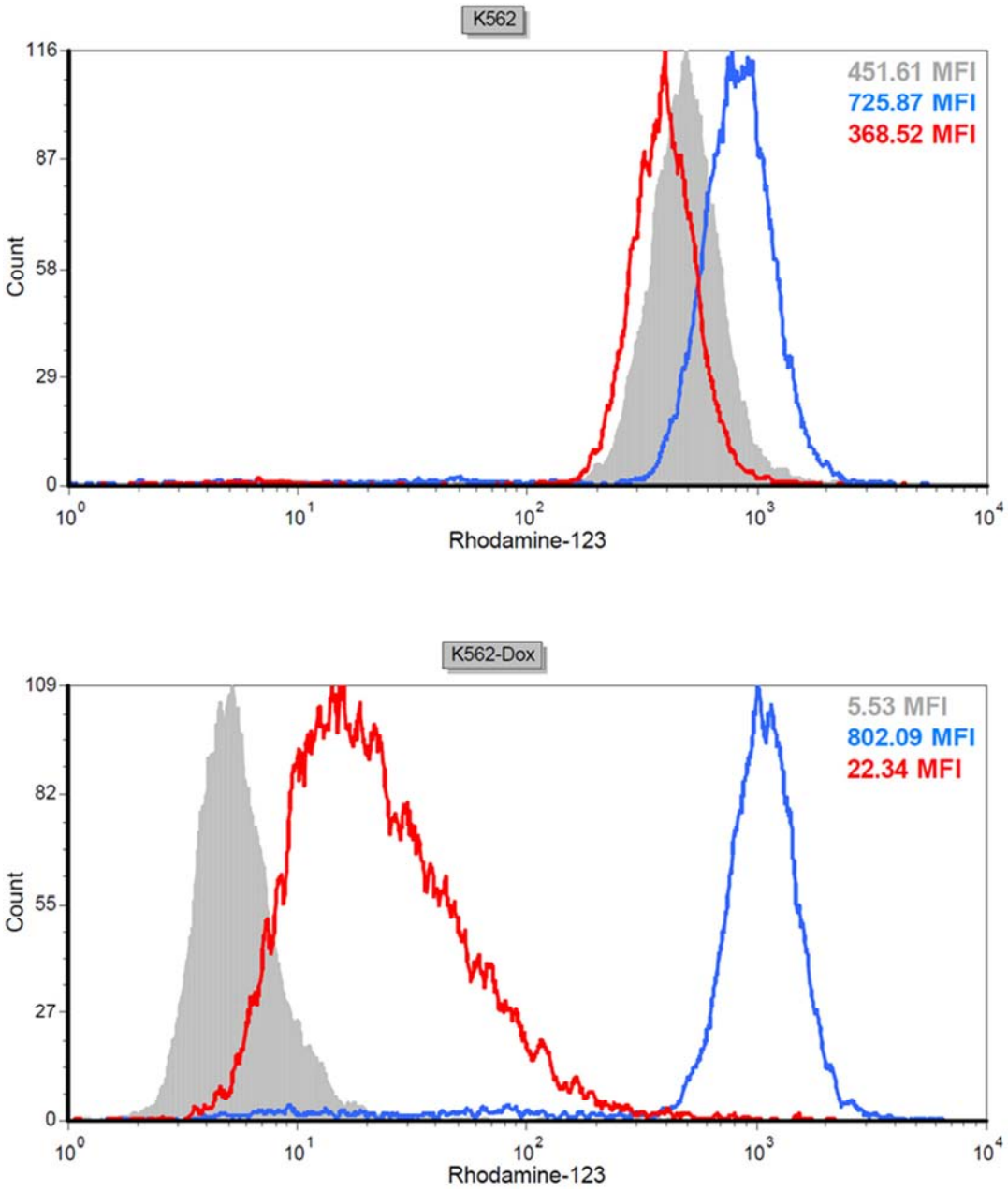

Figure 2A: PSC-833 and verapamil specifically inhibit ABCB1 function

K562 and K562-Dox cells were stained with rhodamine-123 and fluorescence determined in the absence and presence of PSC-833 and verapamil. Data demonstrate that in K562-Dox cells PSC-833 inhibits ABCB1 function. While not as potent an inhibitor of ABCB1, verapamil also inhibits ABCB1 and is thus a reliable and selective alternative. No significant effect of either inhibitor was observed in K562 cells which express negligible levels of ABCB1. Data are representative of typical MFI levels with the geometric mean of the peaks detailed. The **GREY** filled histograms represent **fluorescent substrate alone**, the **BLUE** and **RED** histograms represent **PSC-833** and the **verapamil** respectively.

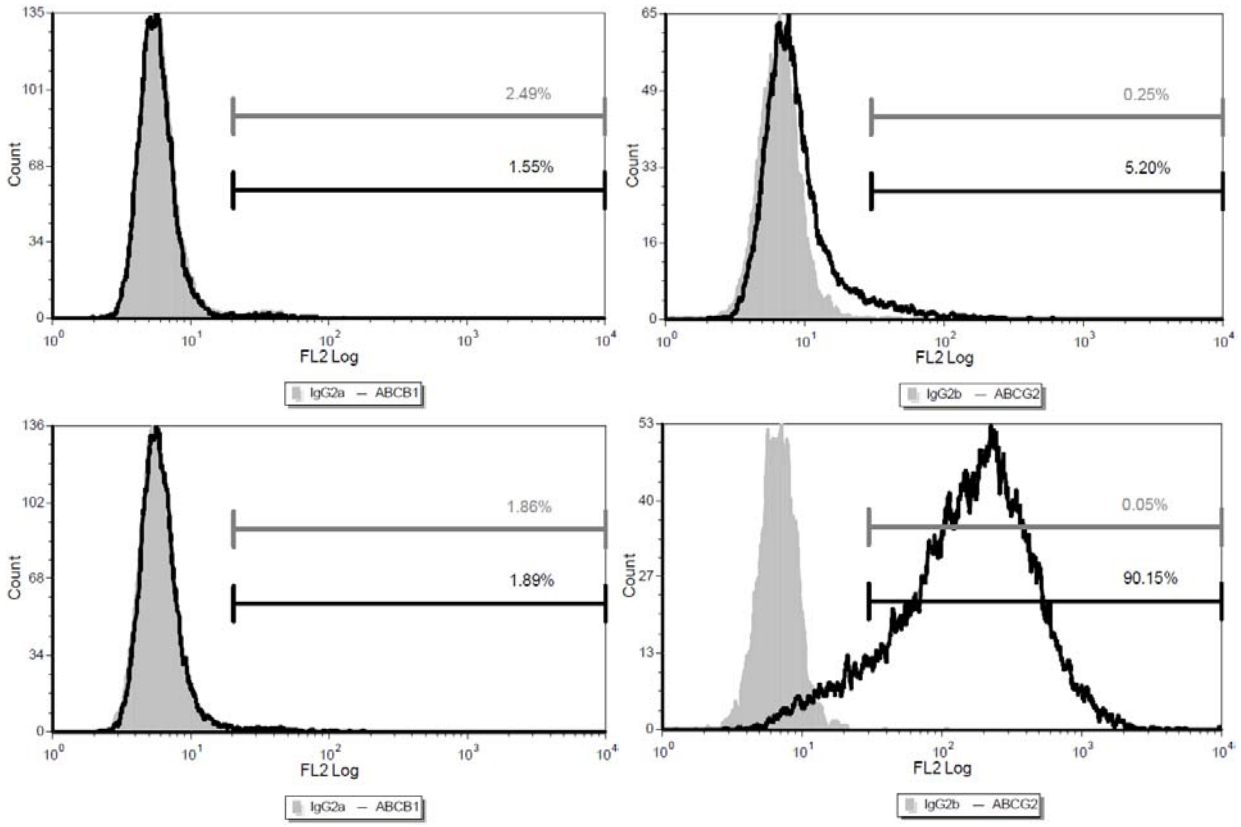

Figure 2B.1: ABCB1 and ABCG2 protein expression in K562 and K562-ABCG2 cells

K562 (a, b), and K562-ABCG2 (c, d) cells were stained with fluorescently labelled antibodies for ABCB1 (a, c) and ABCG2 (b, d) and transporter protein expression levels determined by flow cytometric analysis. The bold **BLACK** line represents cells stained with either **ABCB1-PE** or **ABCG2-PE** antibodies, while the **GREY** filled histogram represents cells stained with corresponding **isotype control** antibodies. The percentages displayed denote cells positive for transporter expression. Data are representative of typical expression levels following cell sorting for ABCG2.

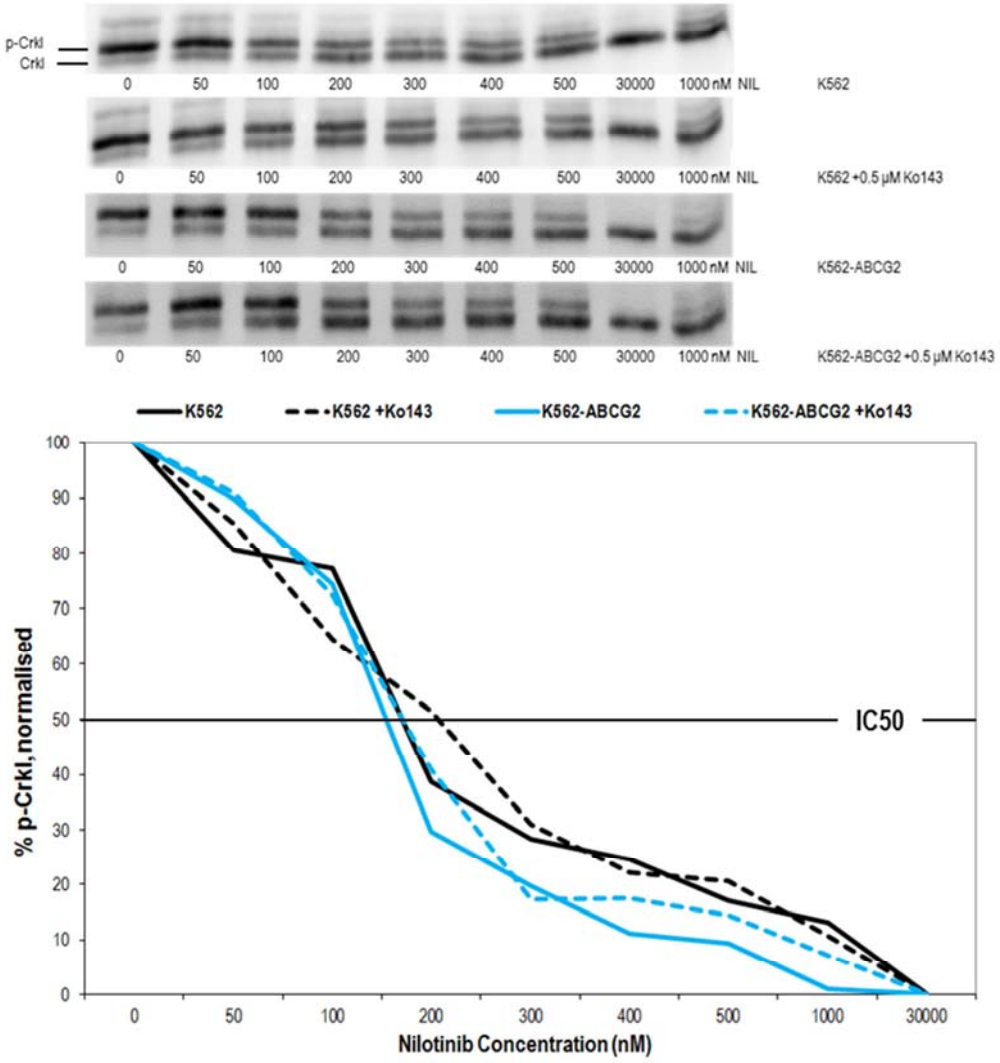

Figure 2B.2: High levels of ABCG2 have no significant effect on IC50NIL in Bcr-Abl positive cell lines

IC50 was determined via incubating cells for 2 h at 37°C in the absence and presence of 0.5 µM Ko143. Crkl western blot was performed to determine the concentration of nilotinib required to inhibit Bcr-Abl kinase activity by 50%. Data demonstrate that high levels of ABCG2 do not significantly increase IC50NIL. Similarly, IC50NIL does not significantly decrease upon ABCG2 inhibition in either K562-ABCG2 cells or K562 control cells. The western blot analysis shown is representative of two separate experiments with the corresponding densitometry analysis representing the mean. NIL=nilotinib.

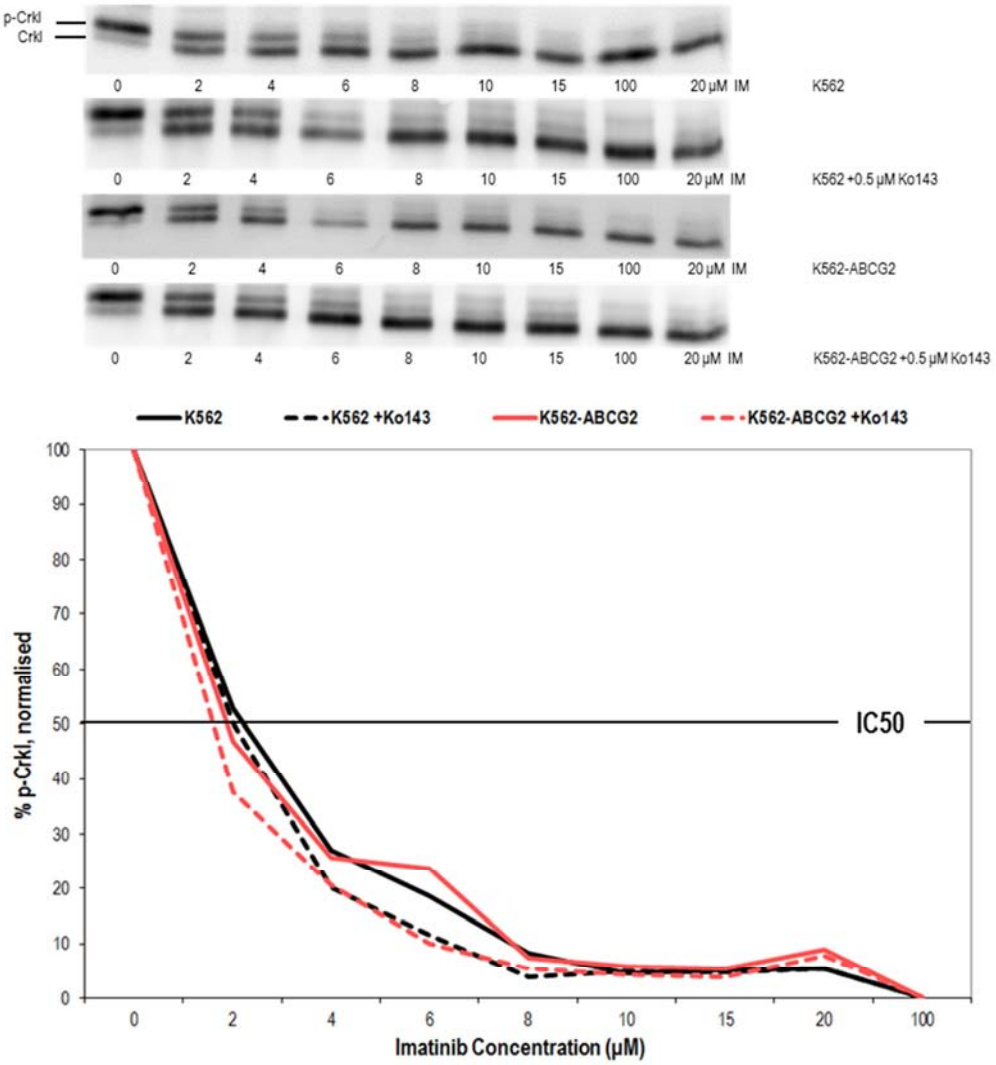

Figure 2B.3: High levels of ABCG2 have no significant effect on $IC50^{IM}$ in Bcr-Abl positive cell lines

IC50 was determined via incubating cells for 2 h at 37°C in the absence and presence of 0.5 µM Ko143. Crkl western blot was performed to determine the concentration of imatinib required to inhibit Bcr-Abl kinase activity by 50%. Data demonstrate that high levels of ABCG2 do not significantly increase $IC50^{IM}$. Similarly, $IC50^{IM}$ does not significantly decrease upon ABCG2 inhibition in either K562-ABCG2 cells or K562 control cells. The western blot analysis shown is representative of two separate experiments with the corresponding densitometry analysis representing the mean. IM=imatinib.

(a)

Figure 3A: K562 125 nM NIL and K562 2 µM NIL cells have significantly decreased TKI-mediated cell death

Cells were cultured for 72 h in increasing concentrations of a) nilotinib b) imatinib and c) dasatinib and cell viability assessed visually. Metabolic products from live cells turn the colour of the growth media from pink to yellow thus allowing a crude assessment of cell viability. Data demonstrate that K562 125 nM NIL cells and K562 2 µM NIL cells have significantly increased survival in the presence of nilotinib and imatinib when compared with control cells. Increased viability in the presence of dasatinib is not as obvious. The pictures shown are representative of at least three separate experiments performed in triplicate. The TKI concentrations are indicated.

(b)

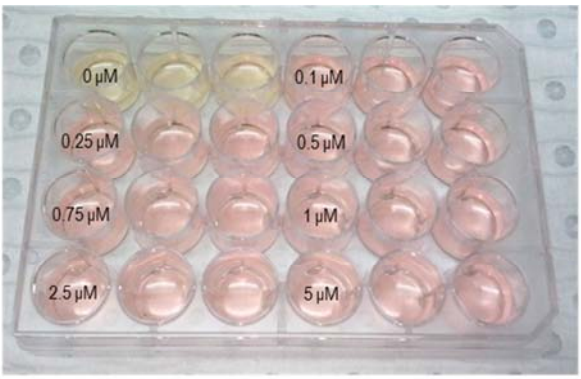
0 µM
0.1 µM
0.25 µM
0.5 µM
0.75 µM
1 µM
2.5 µM
5 µM

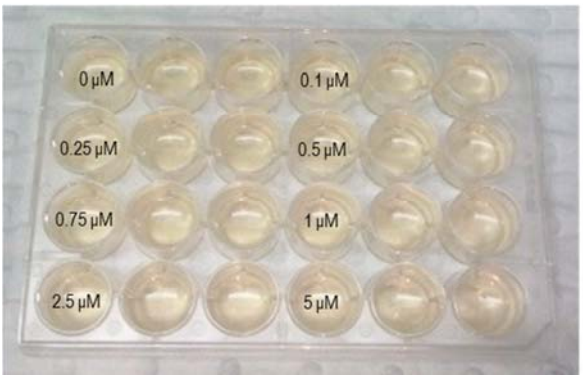
0 µM
0.1 µM
0.25 µM
0.5 µM
0.75 µM
1 µM
2.5 µM
5 µM

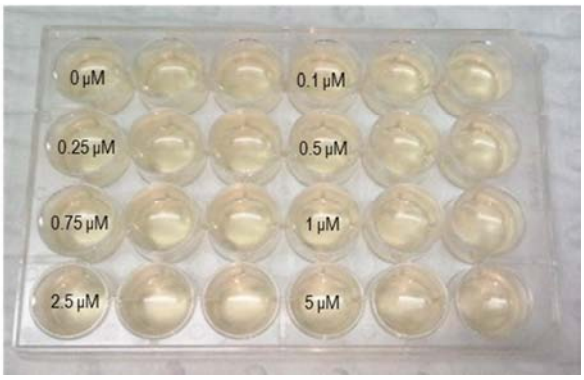
0 µM
0.1 µM
0.25 µM
0.5 µM
0.75 µM
1 µM
2.5 µM
5 µM

(c)

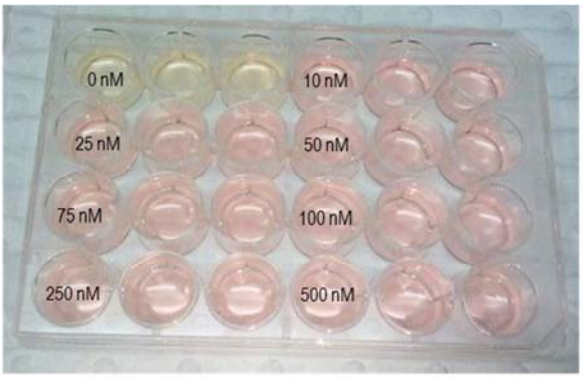
0 nM
10 nM
25 nM
50 nM
75 nM
100 nM
250 nM
500 nM

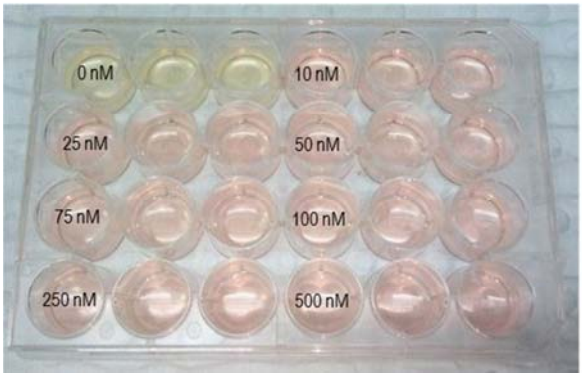
0 nM
10 nM
25 nM
50 nM
75 nM
100 nM
250 nM
500 nM

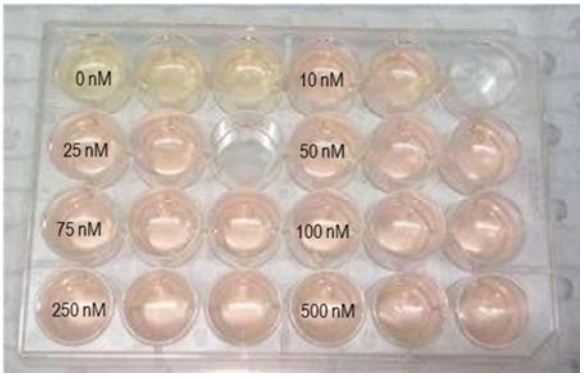
0 nM
10 nM
25 nM
50 nM
75 nM
100 nM
250 nM
500 nM

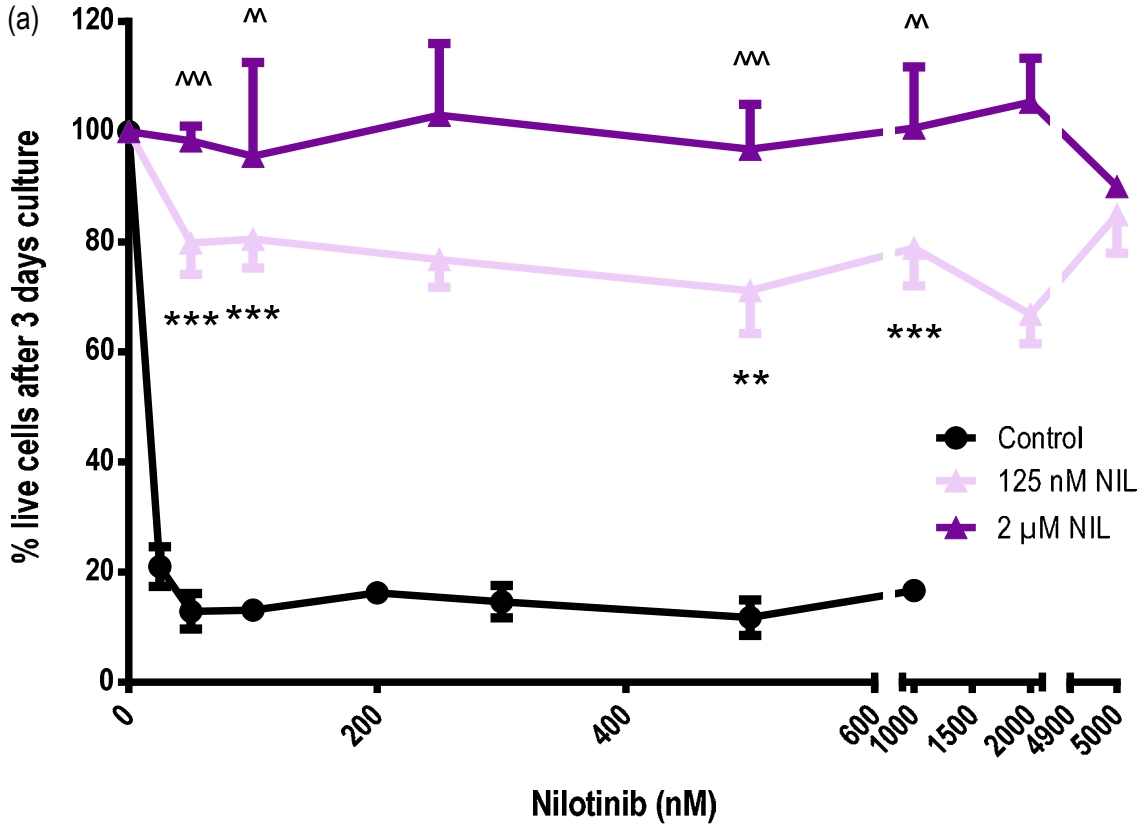

Figure 3B: K562 125 nM NIL and K562 2 µM NIL cells have significantly decreased TKI-mediated cell death

Cells were cultured for 72 h in increasing concentrations of a) nilotinib b) imatinib and c) dasatinib and cell death determined by trypan blue staining. Data demonstrate that K562 125 nM NIL cells and K562 2 µM NIL cells have significantly increased survival in the presence of TKIs when compared with control cells. It is important to note that while trypan blue counts following cytotoxicity assays demonstrate near complete cell death, Annexin V/7-AAD staining shows a maximum of 40% cell death even at the highest TKI concentrations. The data shown are representative of at least three separate experiments performed in triplicate with the corresponding survival curves representing the mean. Data were normalised to 0 nM TKI with the number of live cells in the absence of TKI set at 100%. Statistical analyses were performed using Student's *t*-test with statistically significant *p*-values denoted by asterisks and carets representing K562 125 nM NIL and K562 2 µM NIL cell lines respectively (* $p<0.05$; ** $p<0.01$; *** $p<0.001$). Error bars represent SEM. NIL=nilotinib.

(b)

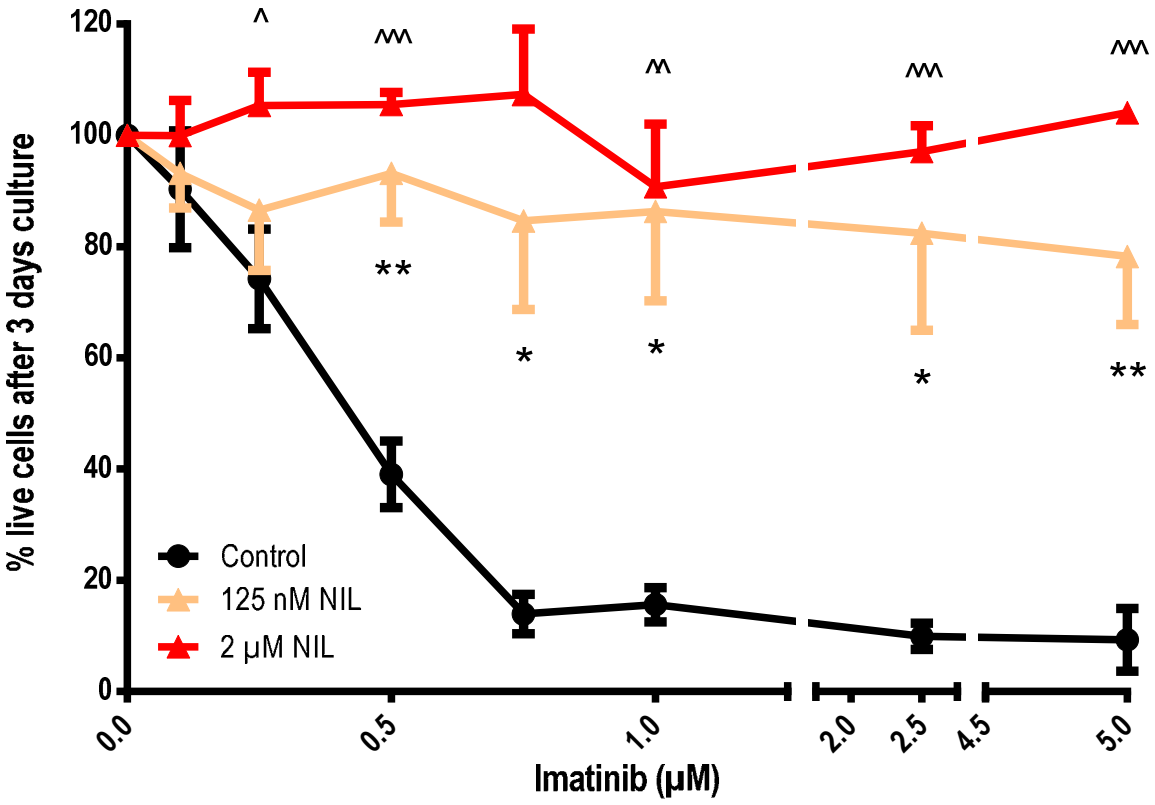
% live cells after 3 days culture
120
100
80
60
40
20
0
Control
125 nM NIL
2 µM NIL
0.0
0.5
1.0
2.0
2.5
4.5
5.0
Imatinib (µM)

(c)

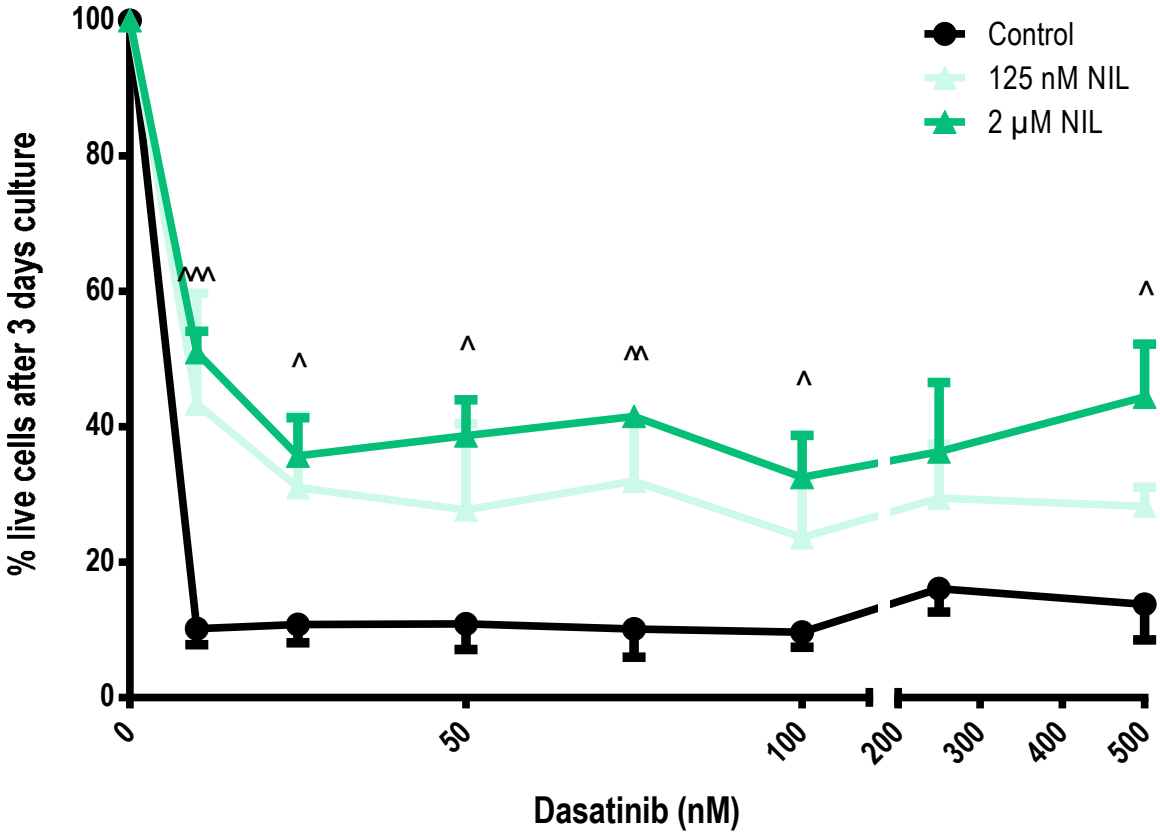
% live cells after 3 days culture
100
80
60
40
20
0
Control
125 nM NIL
2 µM NIL
0
50
100
200
300
400
500
Dasatinib (nM)

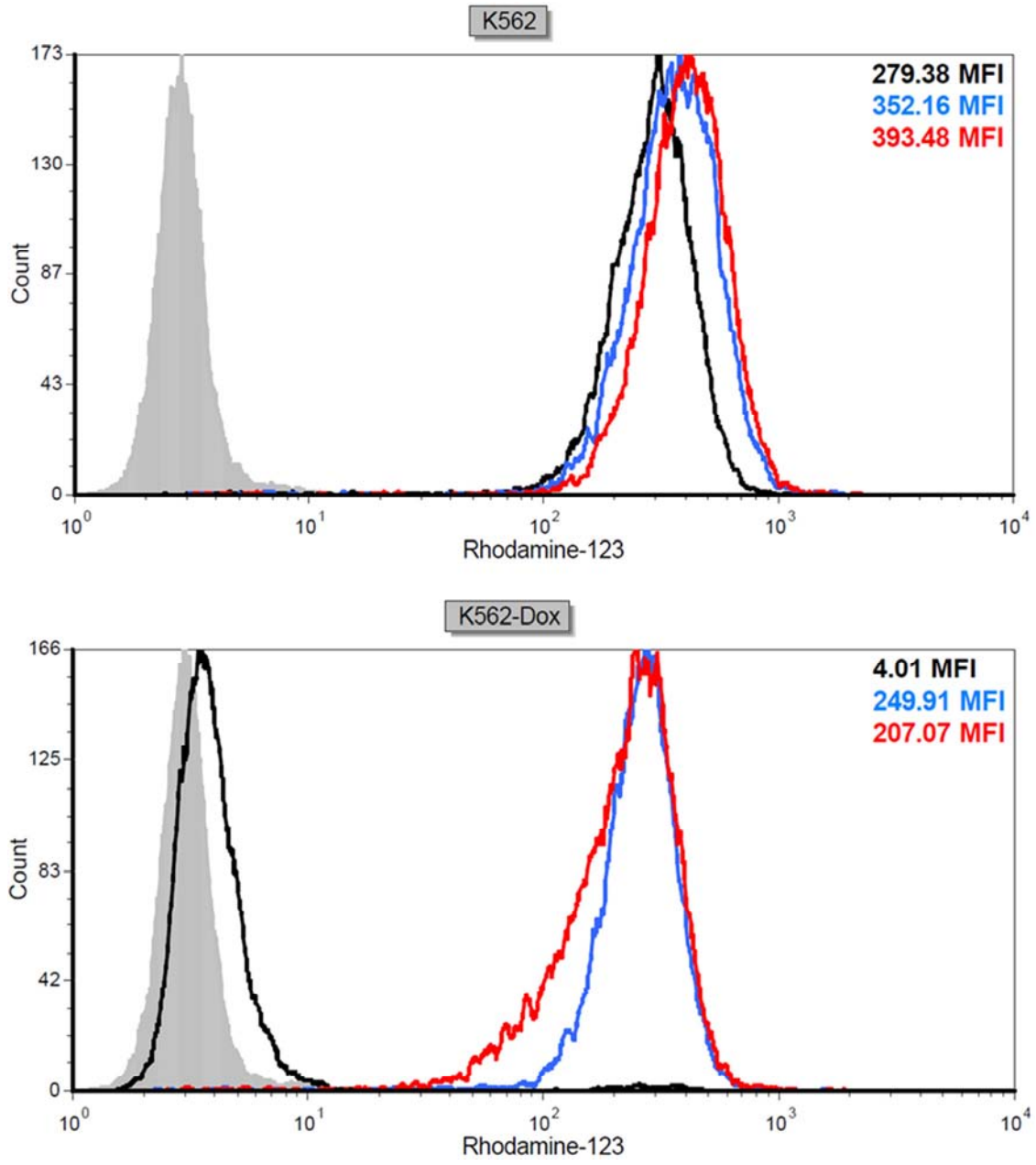

Figure 3C: Cyclosporin specifically inhibits ABCB1 function

K562 and K562-Dox cells were stained with rhodamine-123 and fluorescence determined in the absence and presence of PSC-833 (10 μM) and cyclosporine (10 μM). Data demonstrate that in K562-Dox cells cyclosporin inhibits ABCB1 function as effectively as PSC-833. No significant effect of either inhibitor was observed in K562 cells which express negligible levels of ABCB1. Data are representative of typical MFI levels with the geometric mean of the peaks detailed. The **GREY** filled histograms represent **unstained control** while the **BLACK**, **BLUE** and **RED** histograms represent **fluorescent substrate alone**, **PSC-833** and the **cyclosporin** respectively.

Figure 3D: K562 resistance intermediates do not carry any Bcr-Abl kinase domain mutations

DNA sequencing of the Bcr-Abl kinase domain of K562 control cells and resistance intermediates was conducted and compared with the GenBank ABL reference sequence. Data demonstrate that neither the control cells nor any of the resistance intermediates contain mutations. Data were analysed using Mutation Surveyor Version 3.24 with each peak representing a DNA base (A=Adenine; C=Cytosine; G=Guanine; T=Thymine) in the 5'-3' direction of the ABL sequence. The base number for both the reference sequence and the sequences of interest are indicated. The amino acid and corresponding residue number are also indicated. The amino acid sequences exactly match the reference sequence with none of the common kinase domain mutations summarised in **Figure 5.1** present.

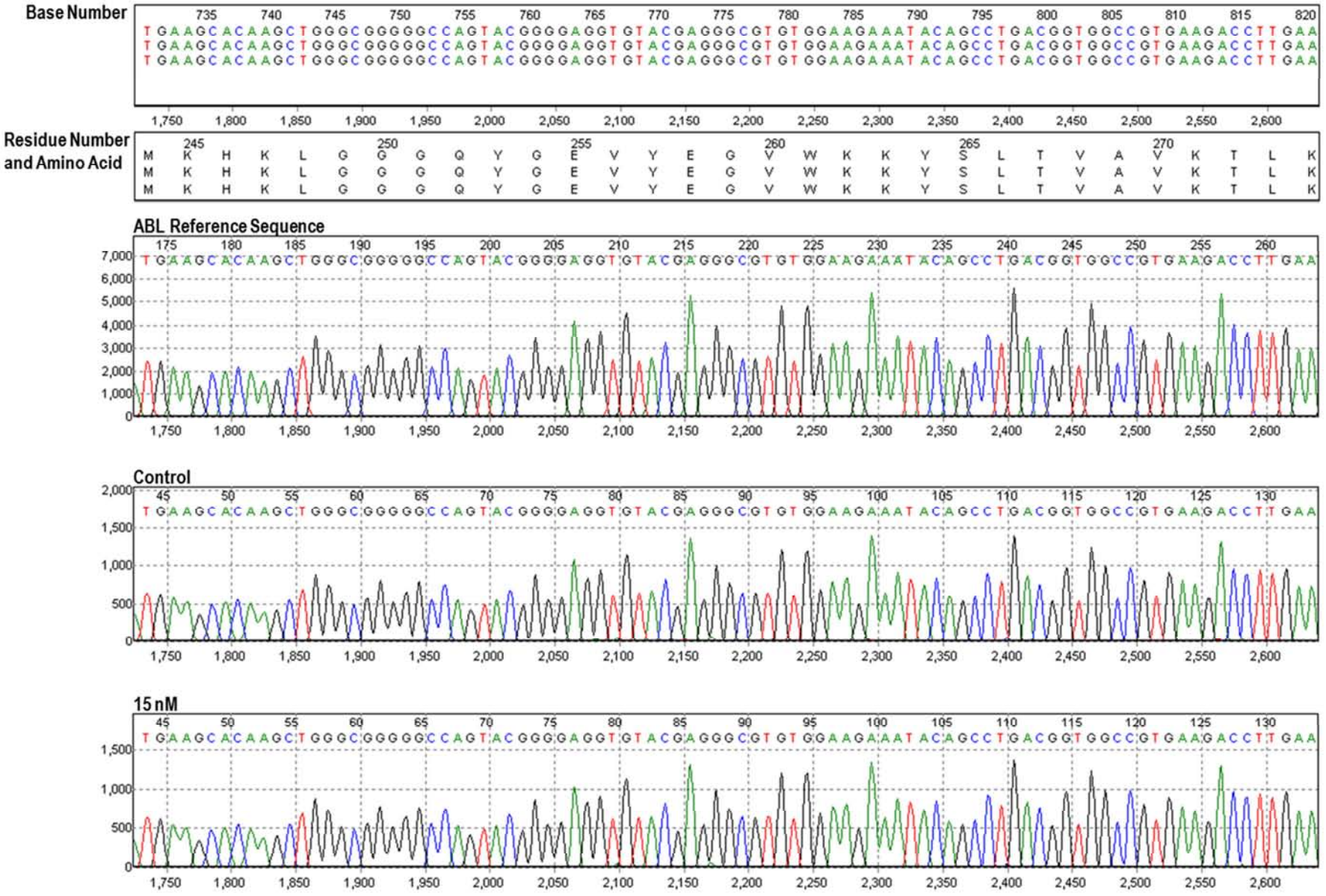
Base Number
Residue Number and Amino Acid
ABL Reference Sequence
Control
15 nM

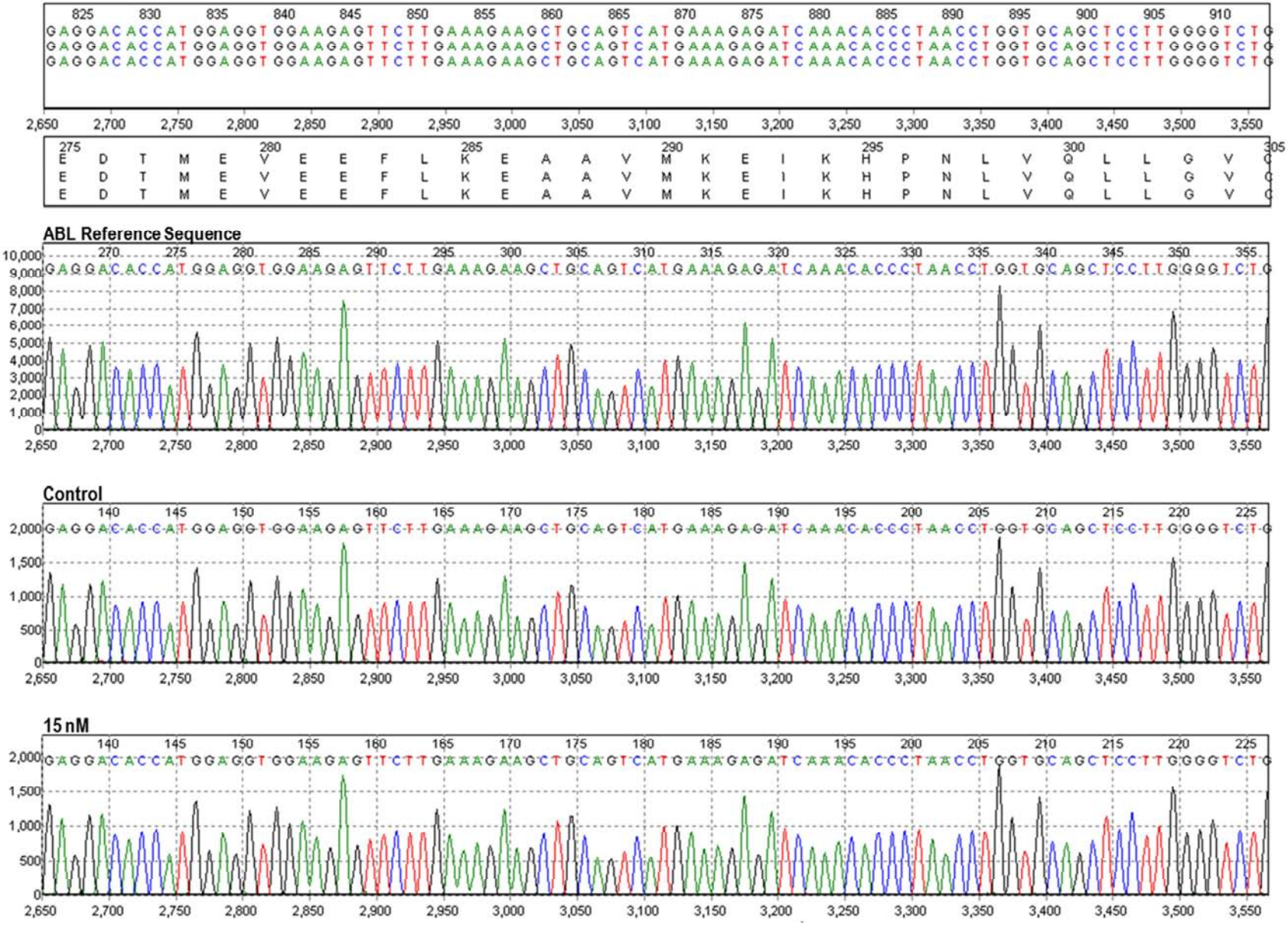
ABL Reference Sequence
Control
15 nM

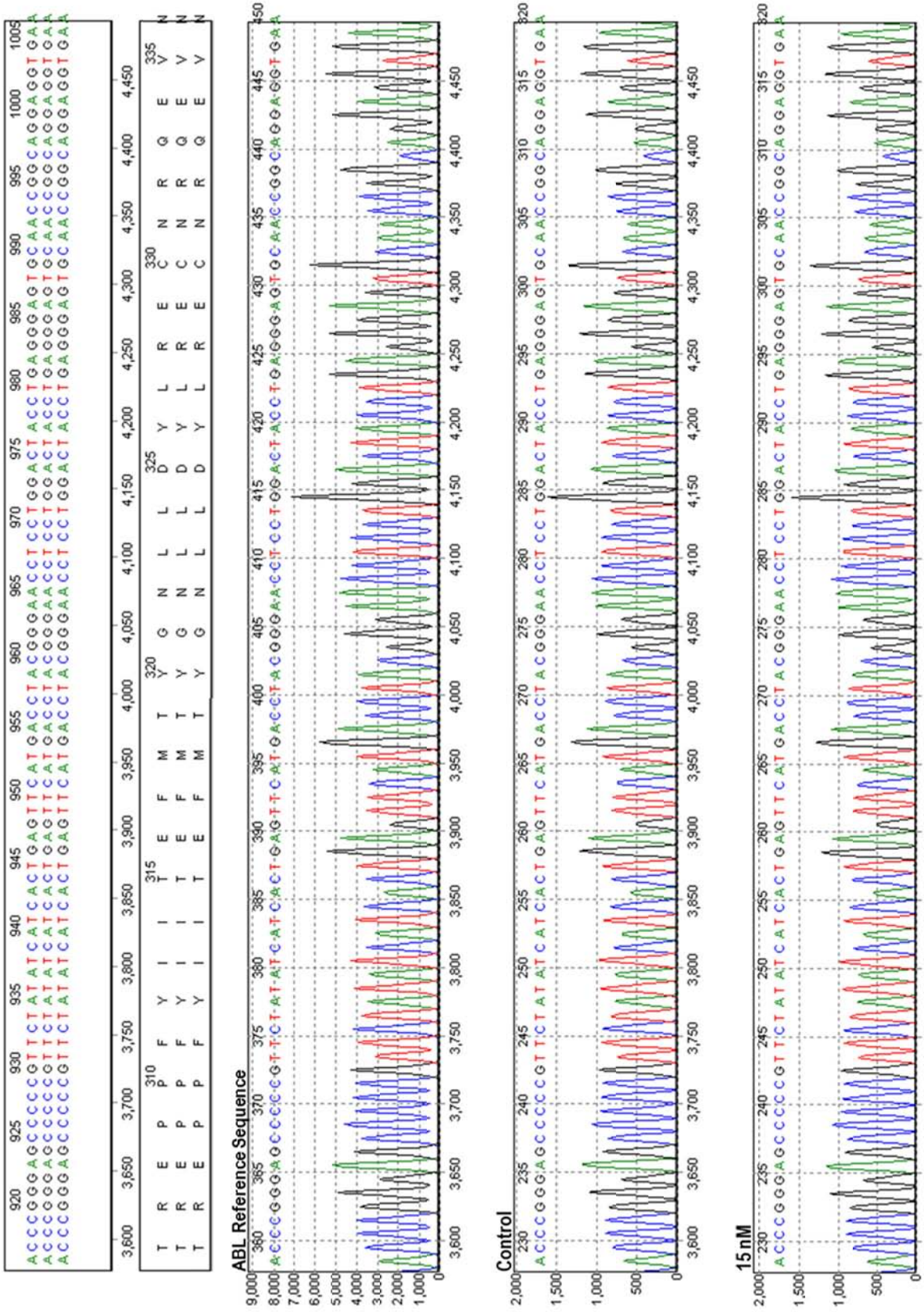
ABL Reference Sequence
Control
15 nM

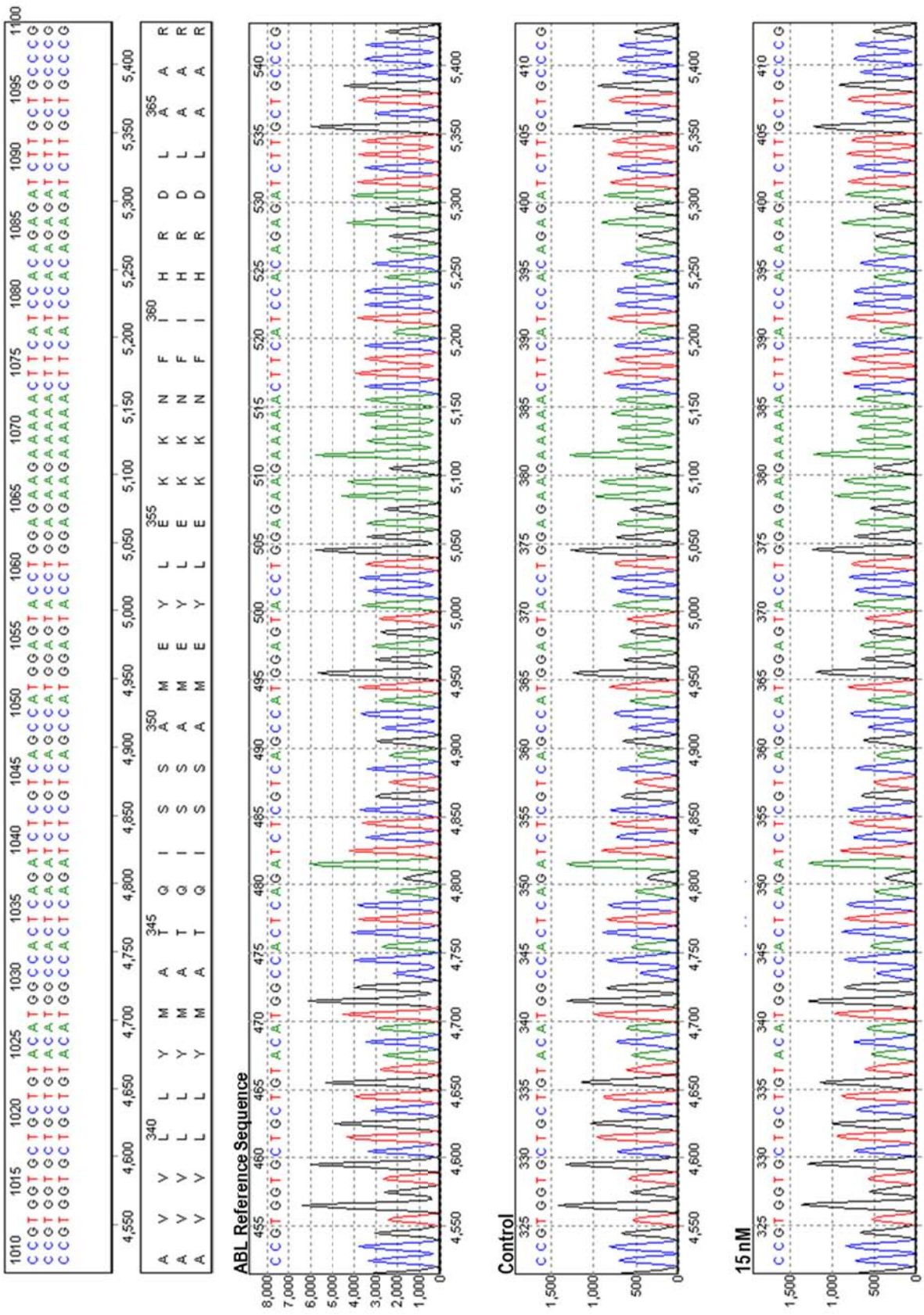
ABL Reference Sequence
Control
15 nM

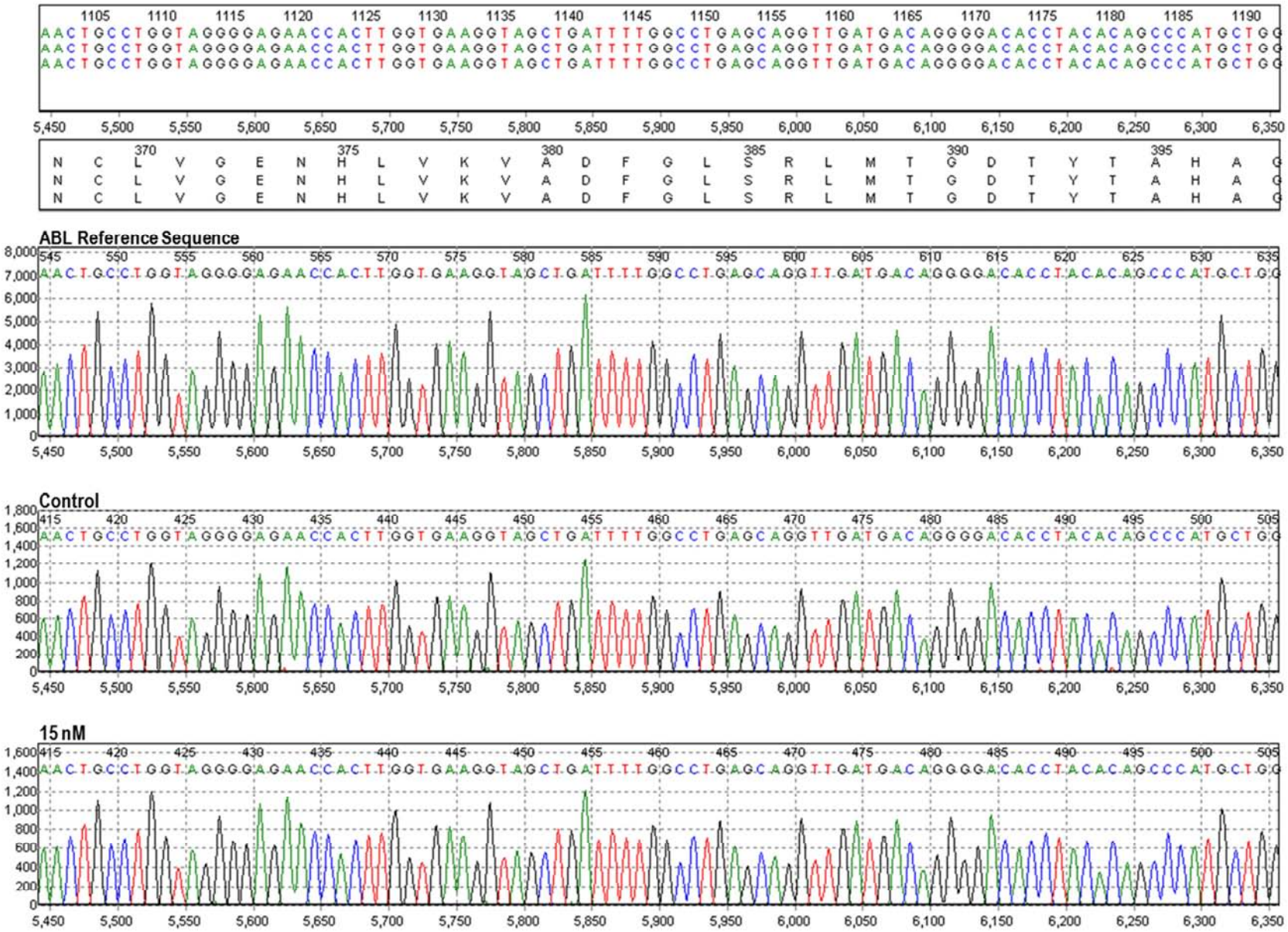
ABL Reference Sequence
Control
15 nM

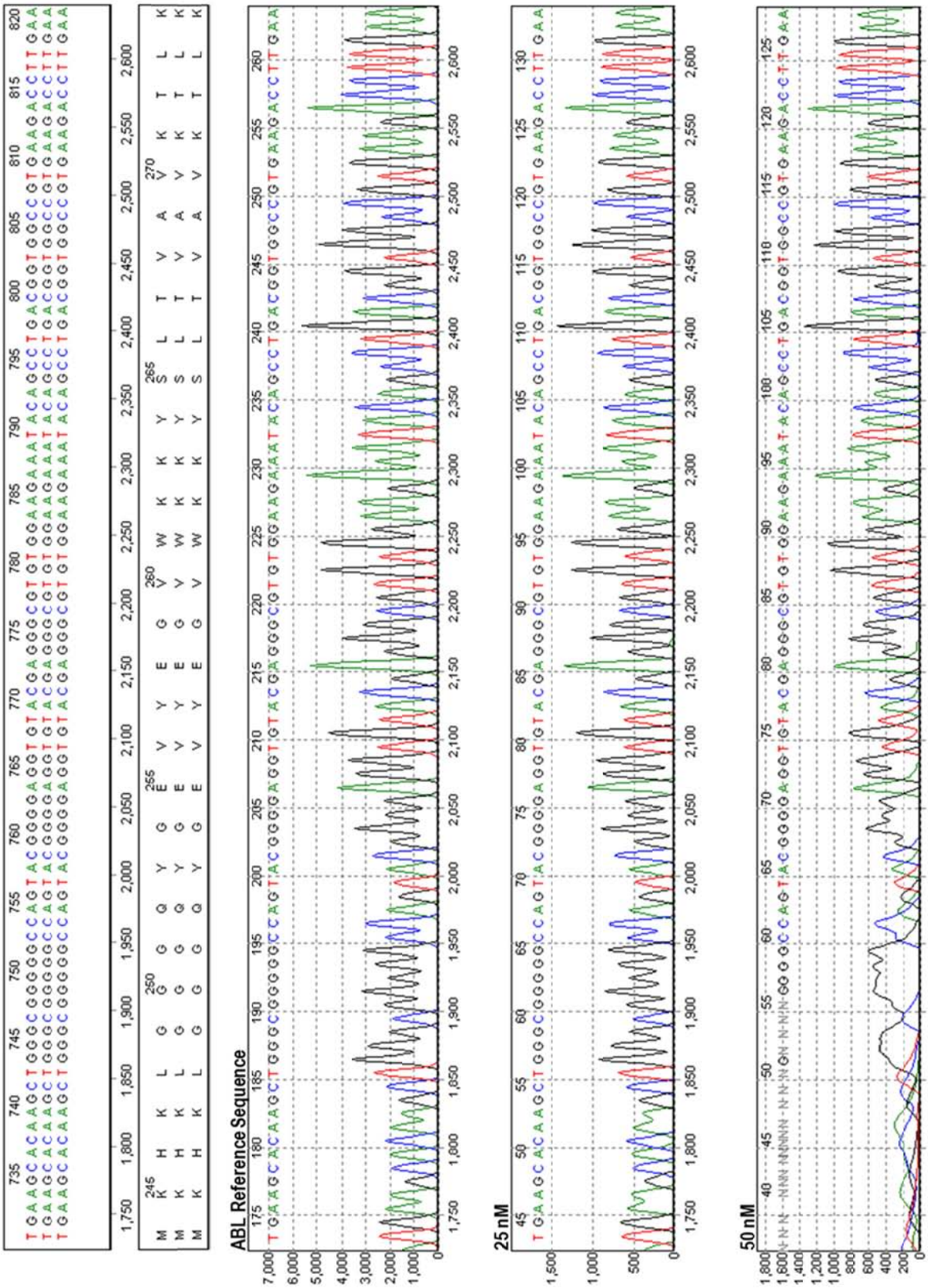
ABL Reference Sequence
25 nM
50 nM

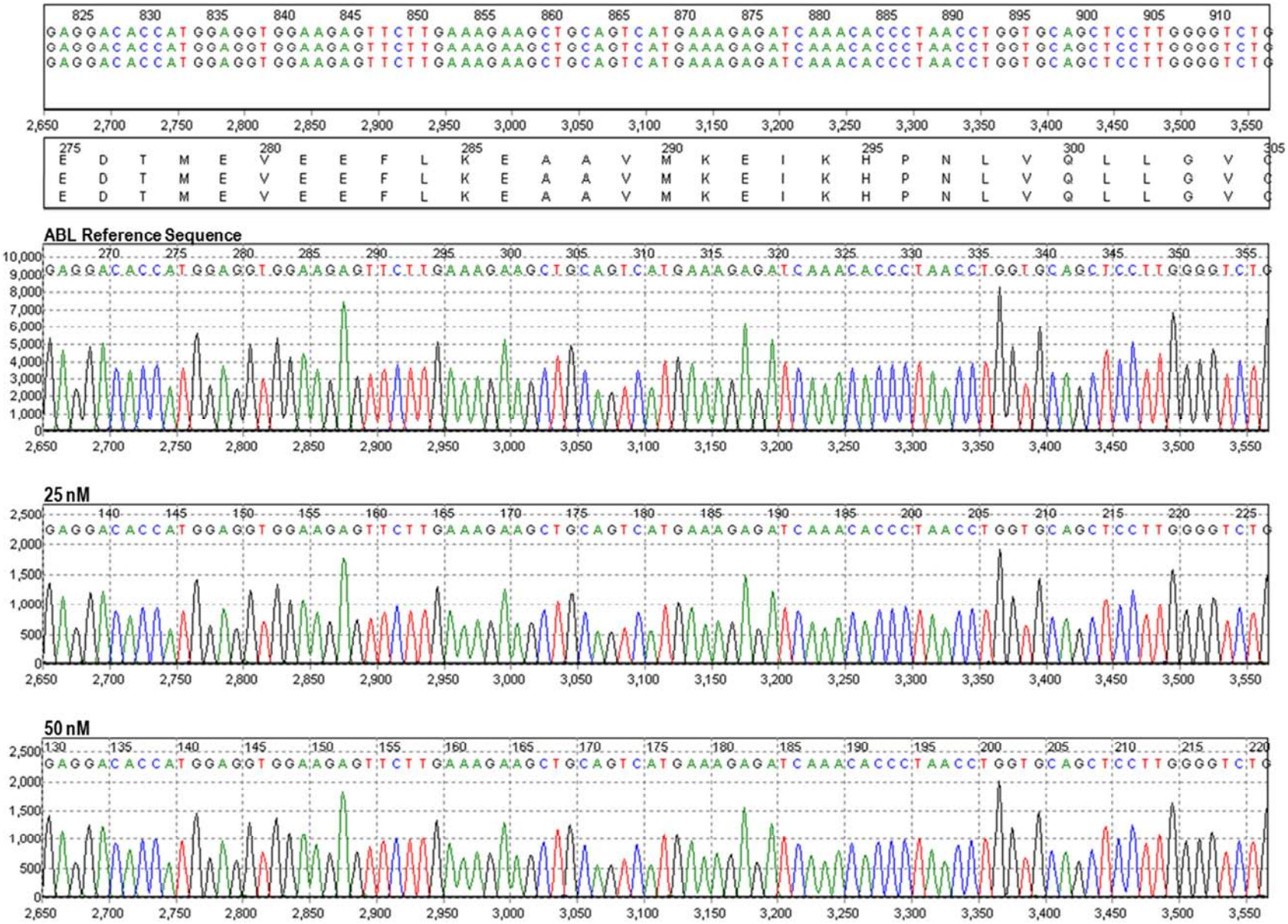
ABL Reference Sequence
25 nM
50 nM

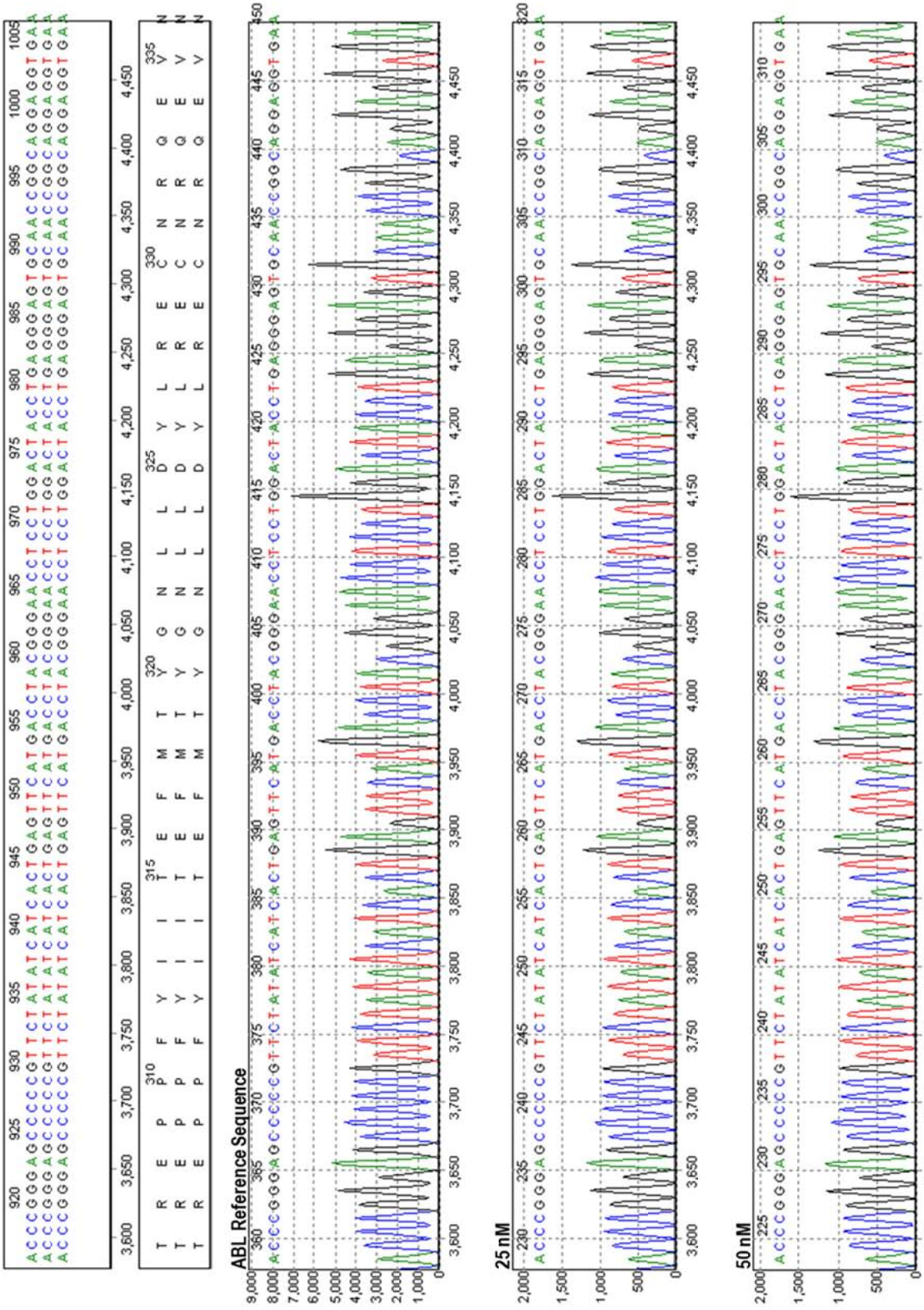
ABL Reference Sequence
25 nM
50 nM

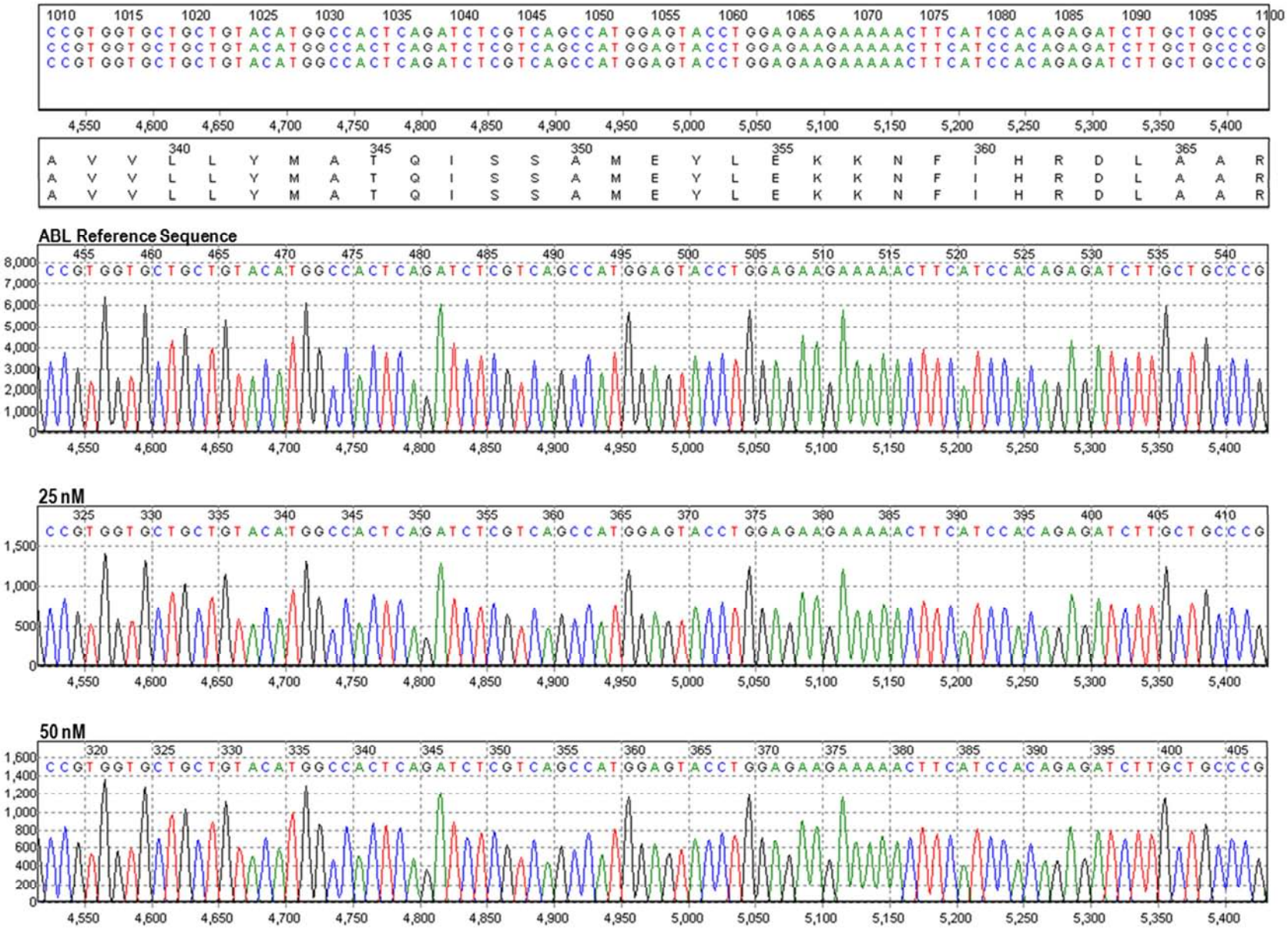
ABL Reference Sequence
25 nM
50 nM

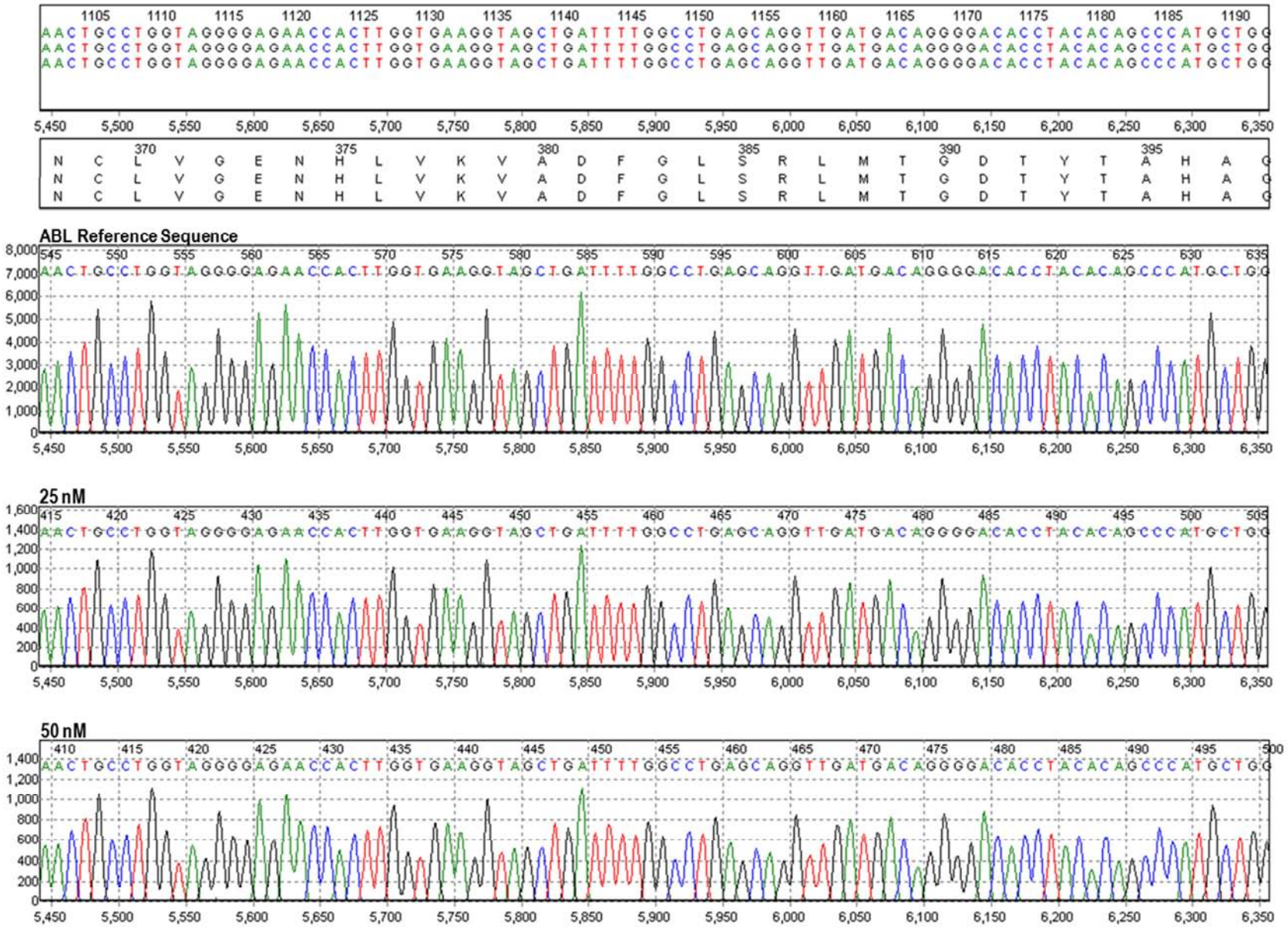
ABL Reference Sequence
25 nM
50 nM

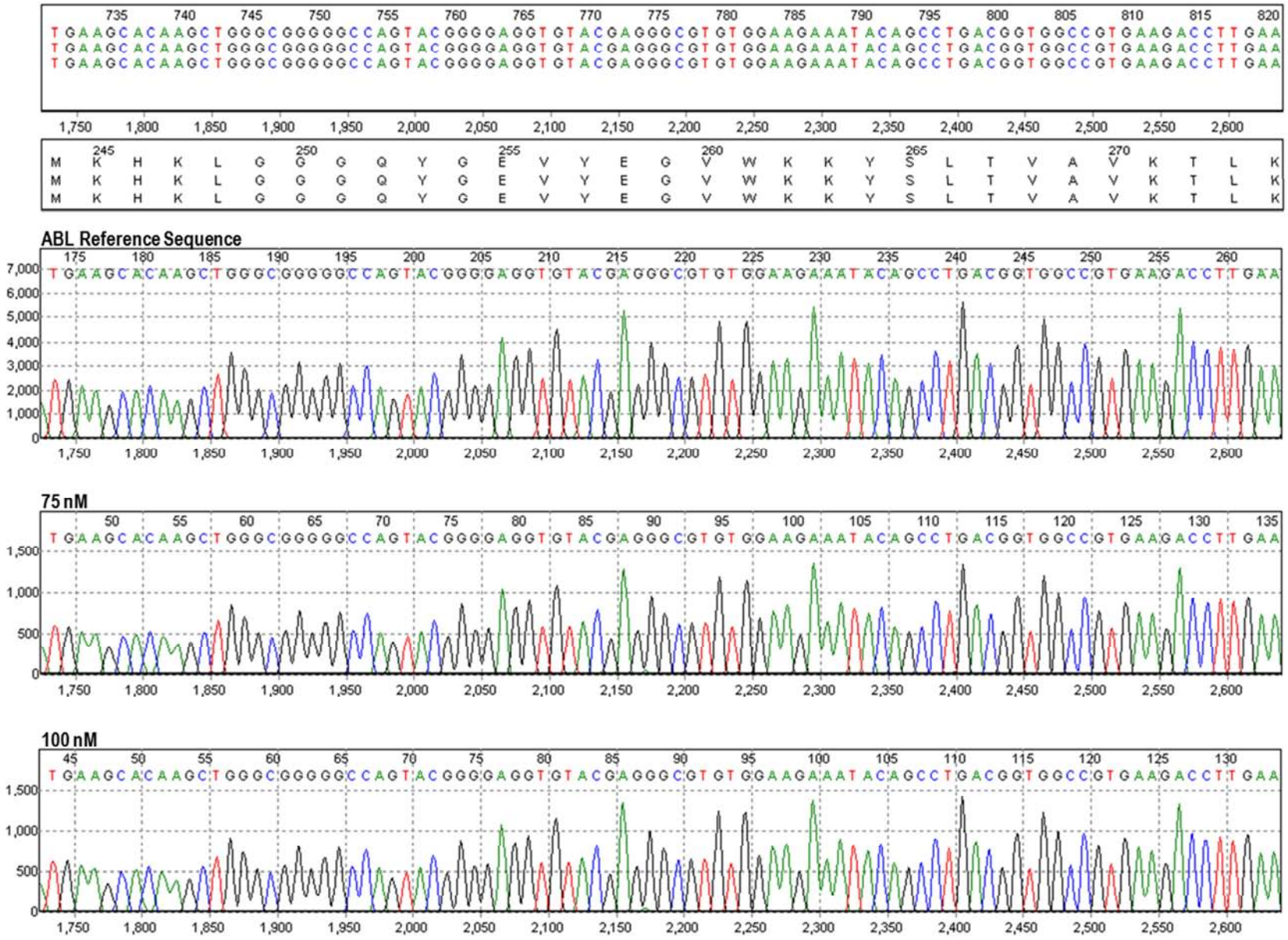
ABL Reference Sequence
75 nM
100 nM

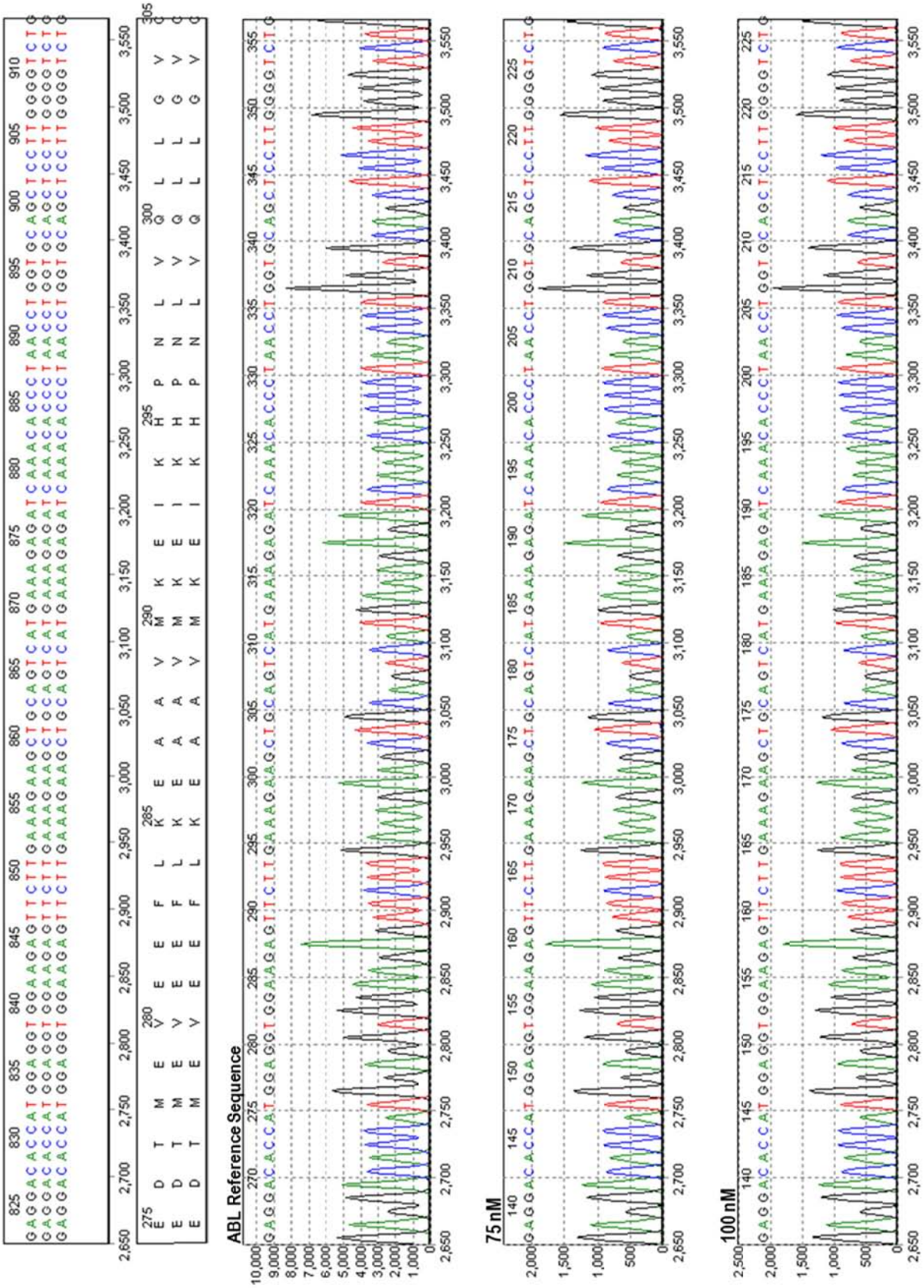
ABL Reference Sequence
75 nM
100 nM

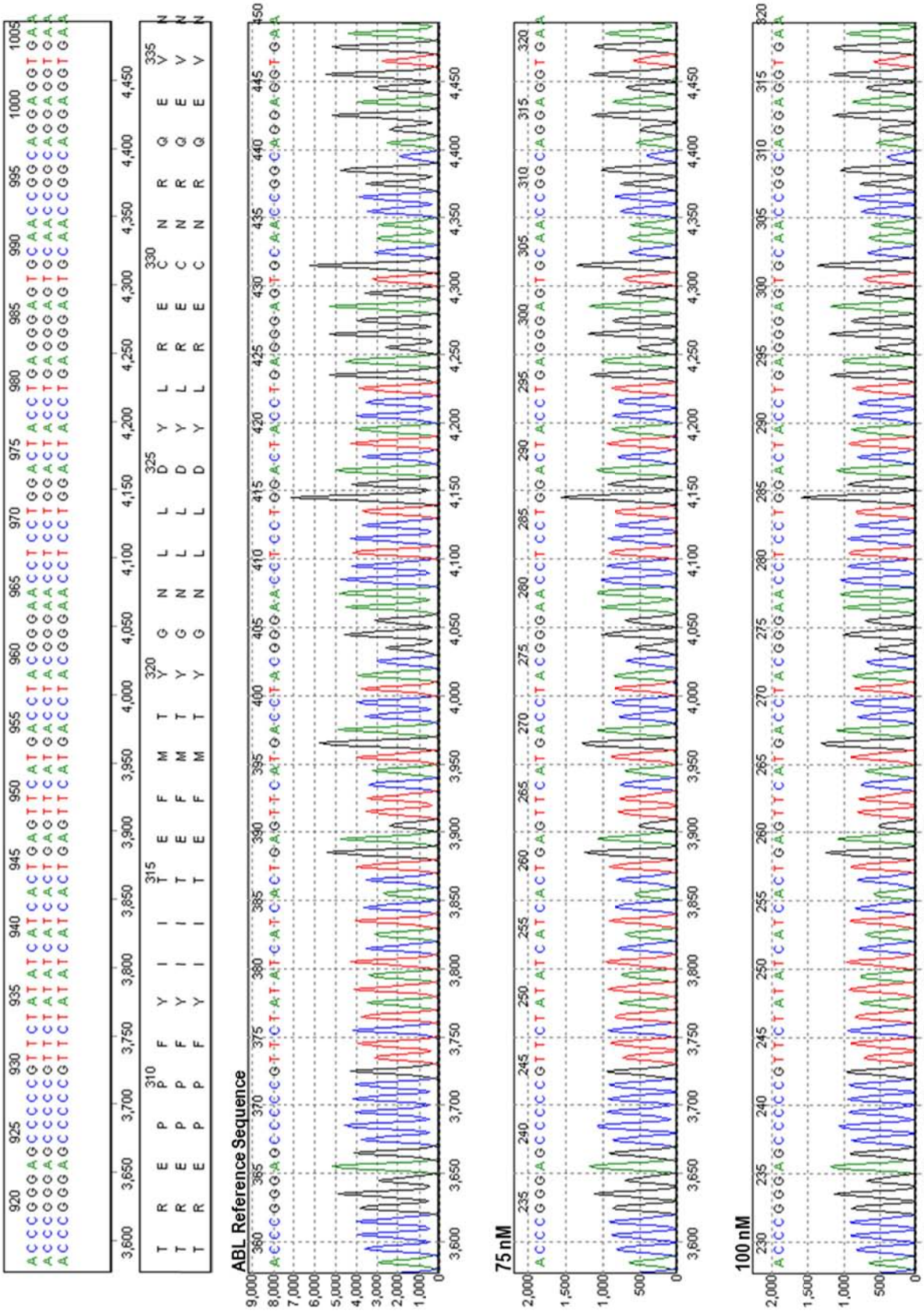
ABL Reference Sequence
75 nM
100 nM

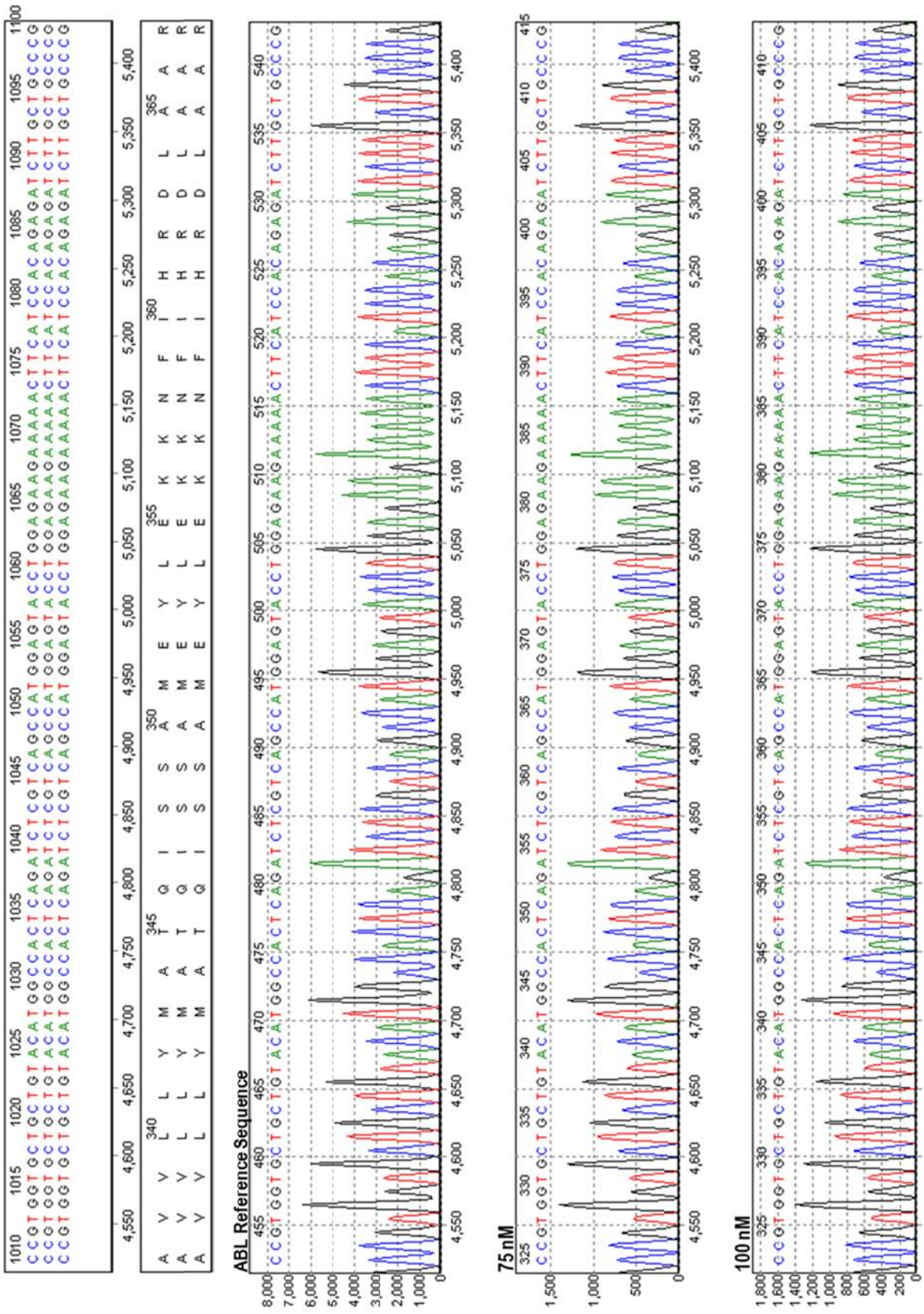
ABL Reference Sequence
75 nM
100 nM

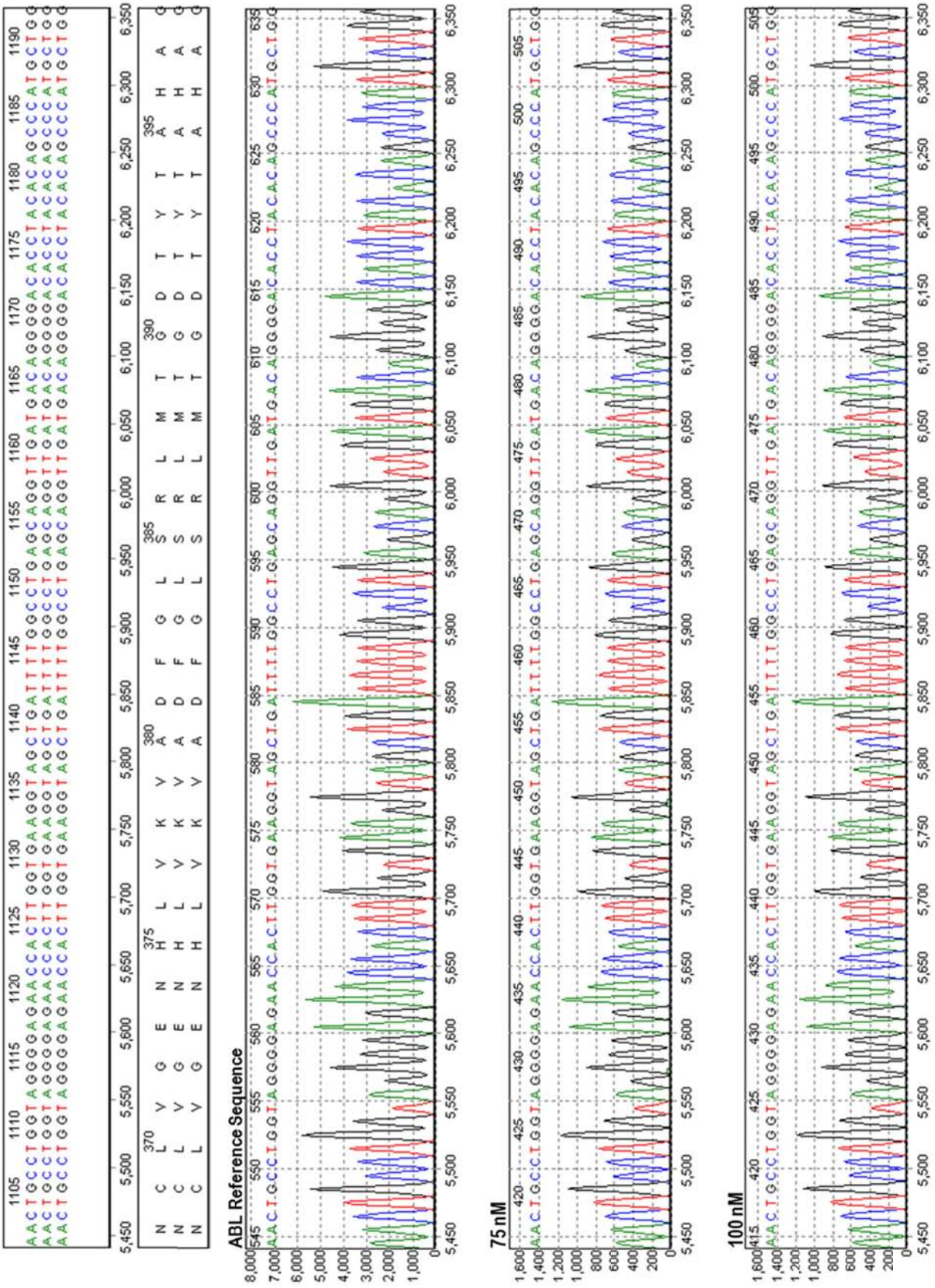
ABL Reference Sequence
75 nM
100 nM

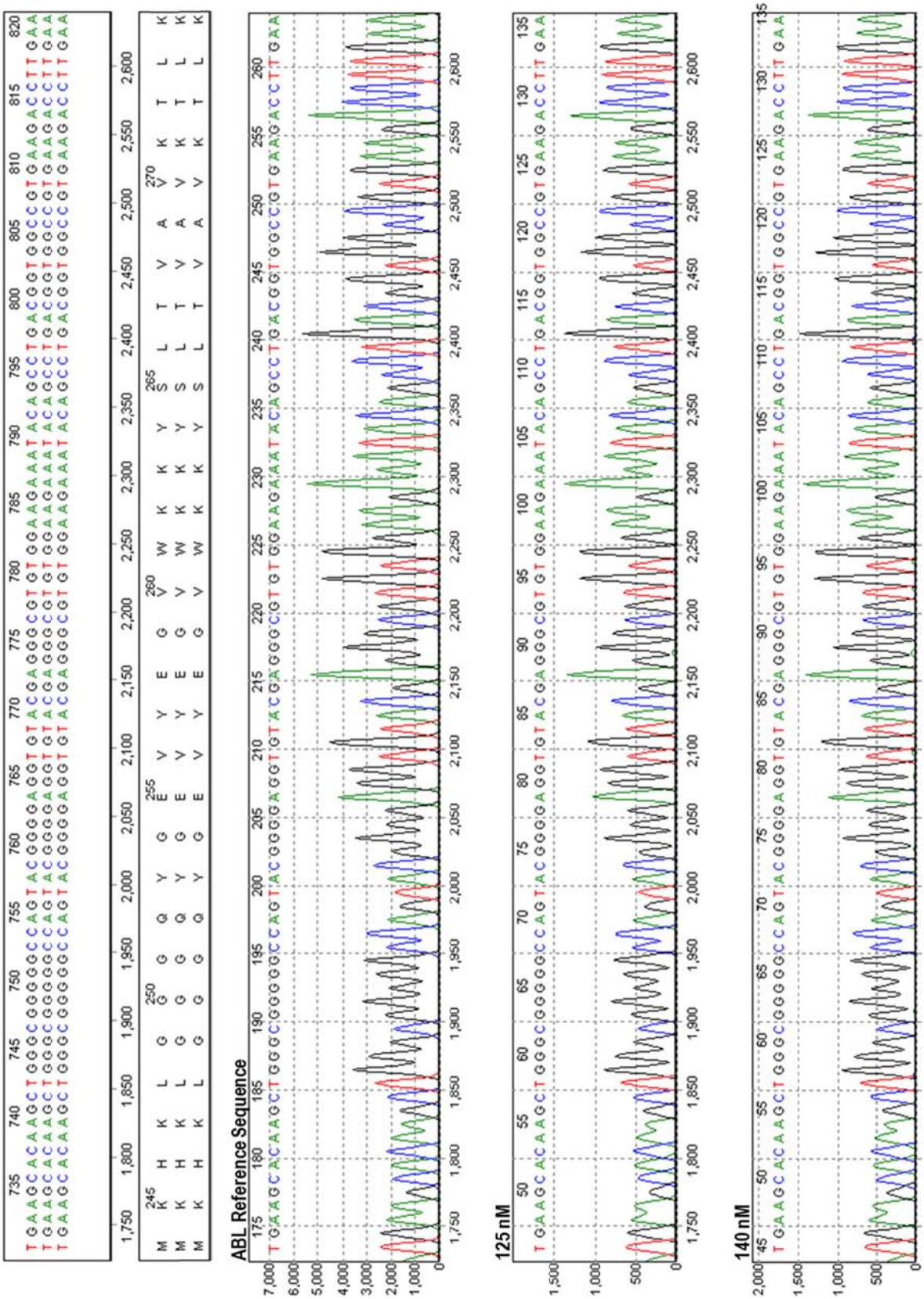
ABL Reference Sequence
125 nM
140 nM

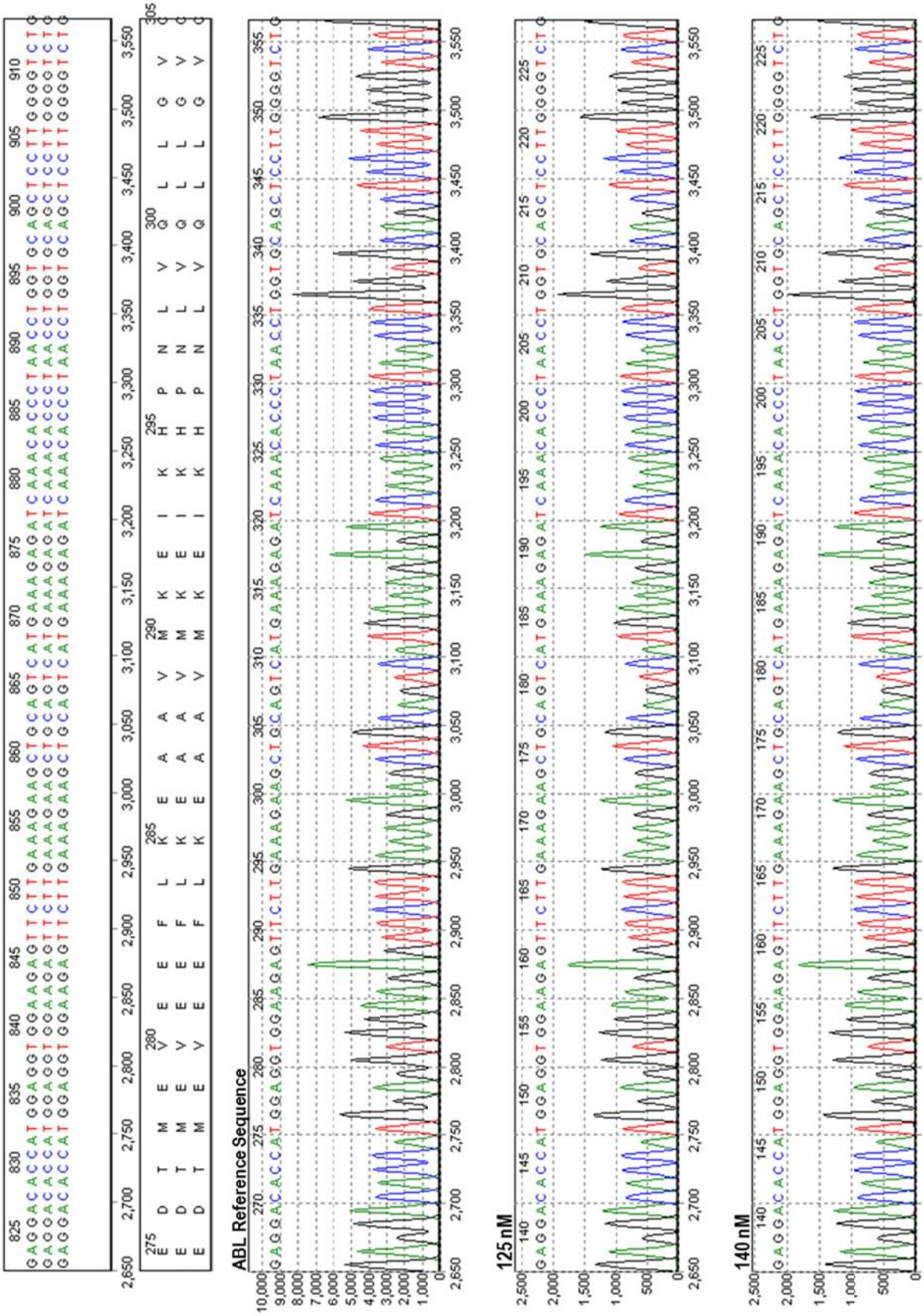
ABL Reference Sequence
125 nM
140 nM

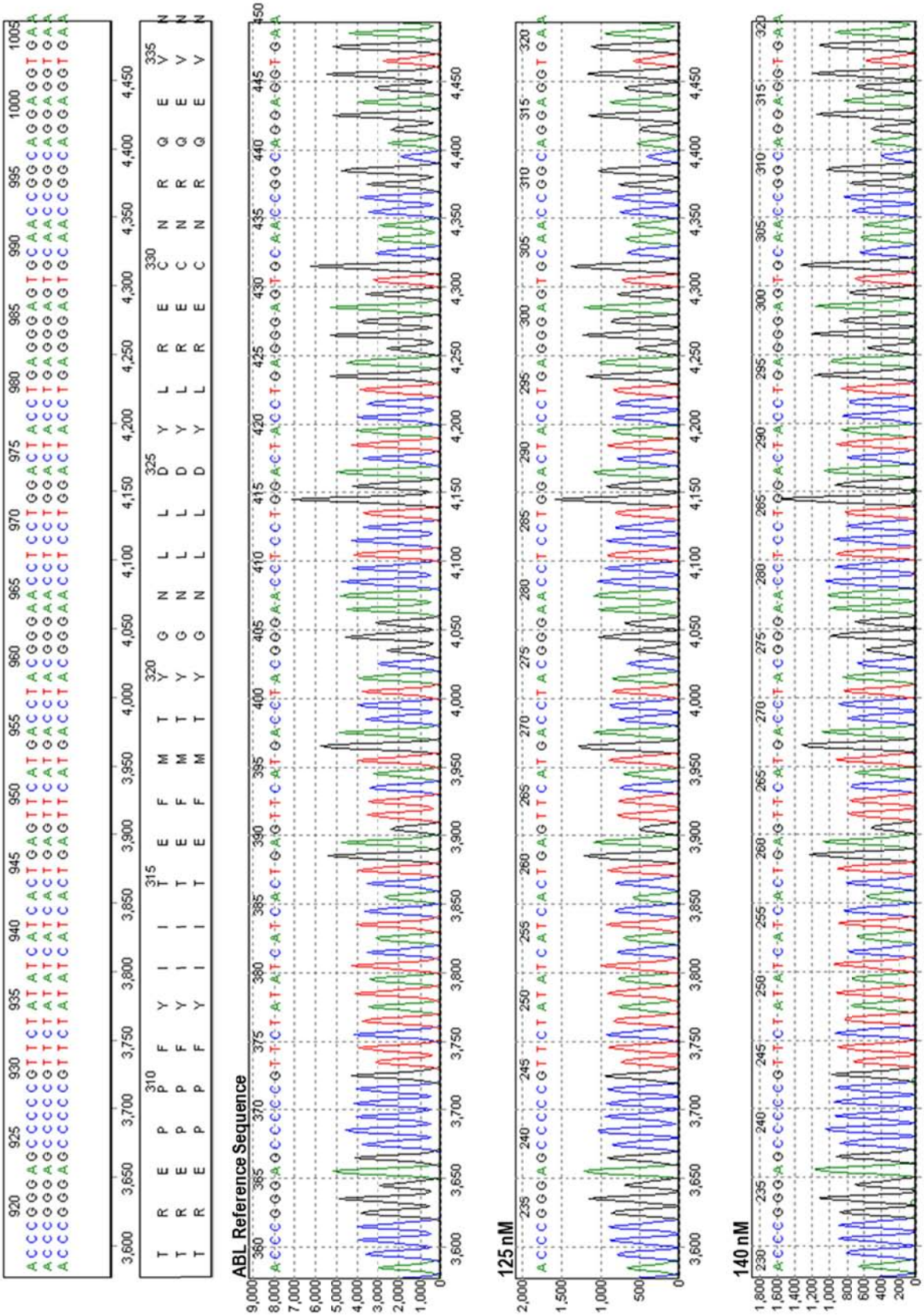
ABL Reference Sequence
125 nM
140 nM

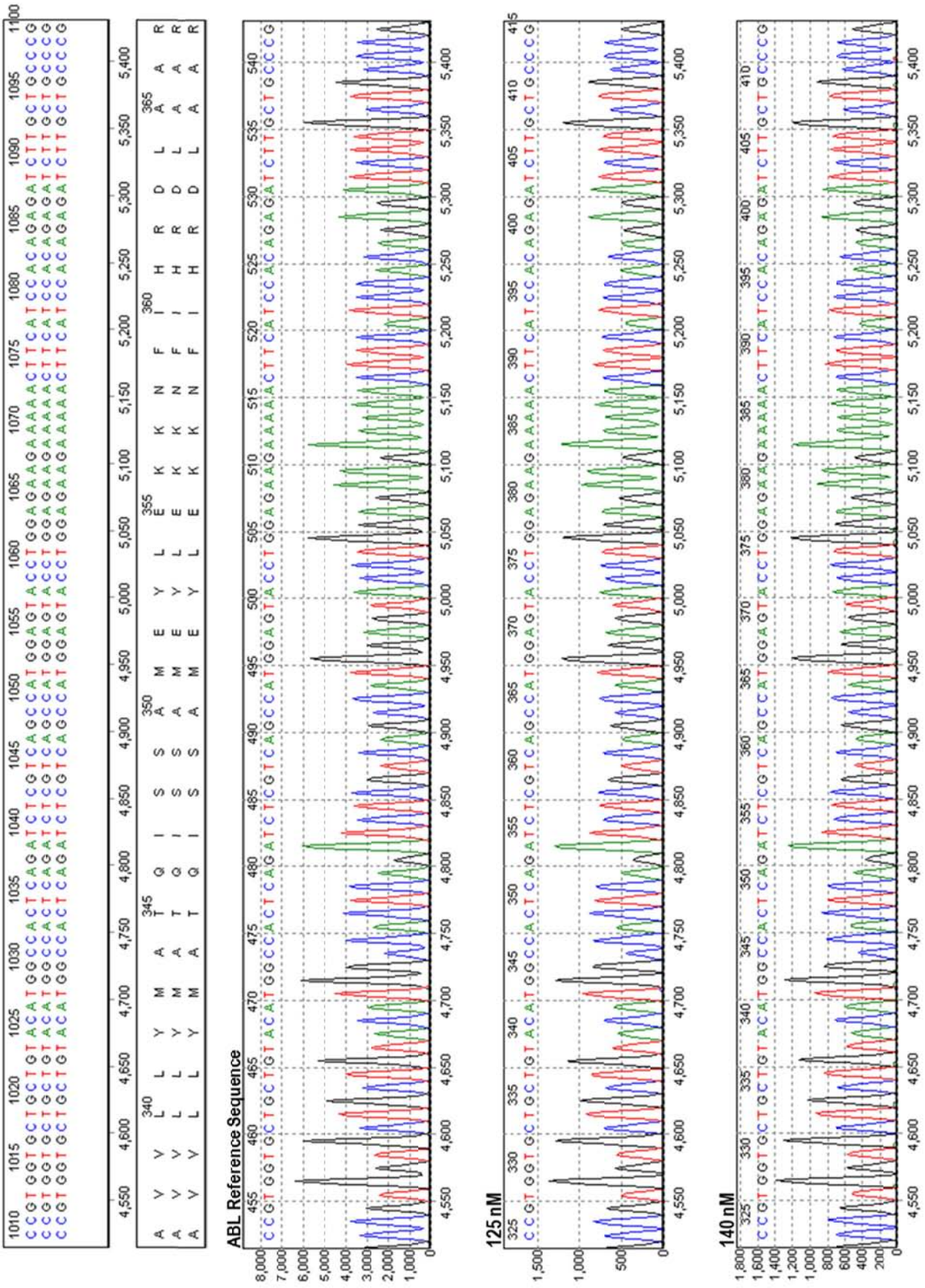
ABL Reference Sequence
125 nM
140 nM

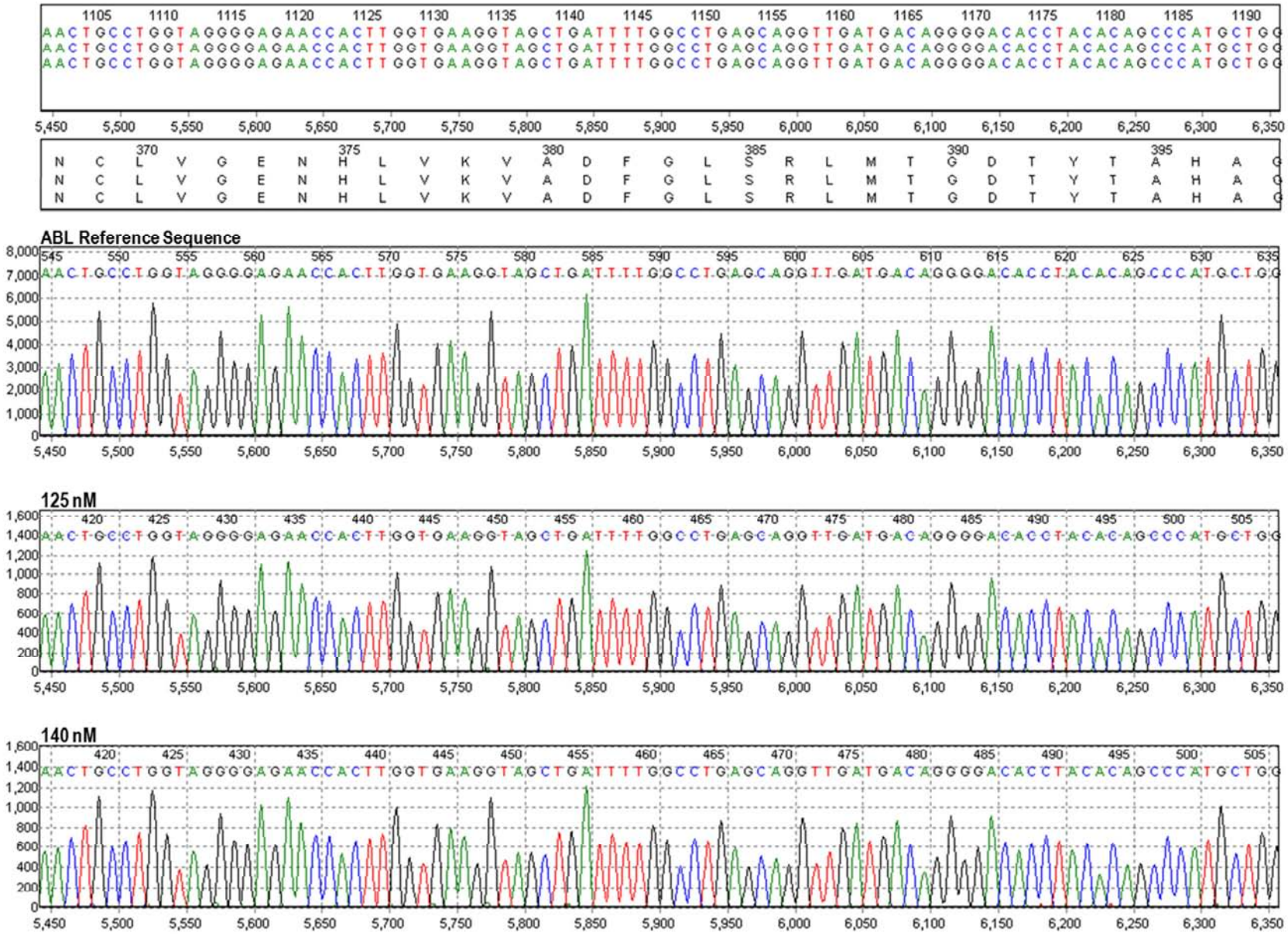
ABL Reference Sequence
125 nM
140 nM

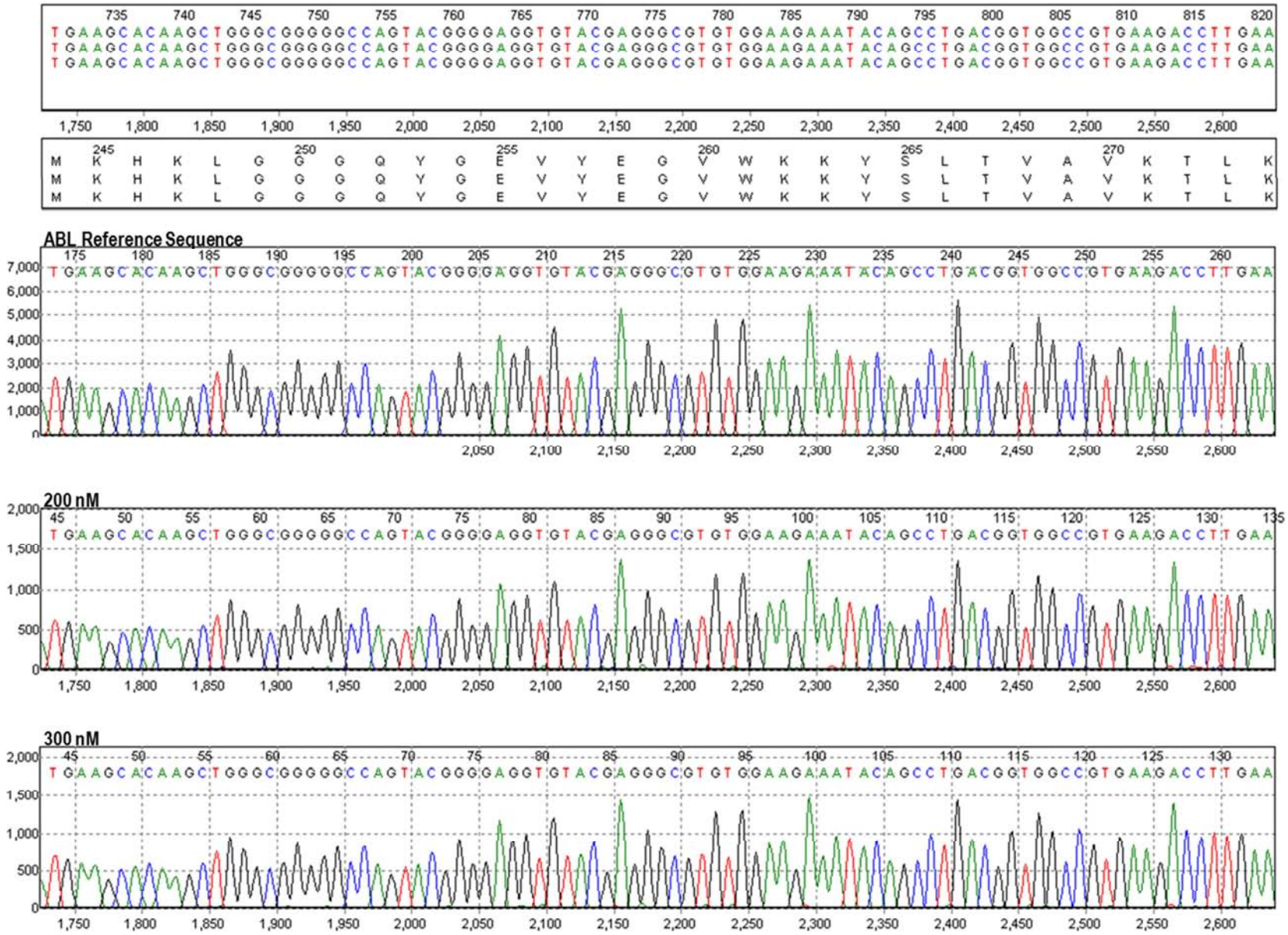
ABL Reference Sequence
200 nM
300 nM

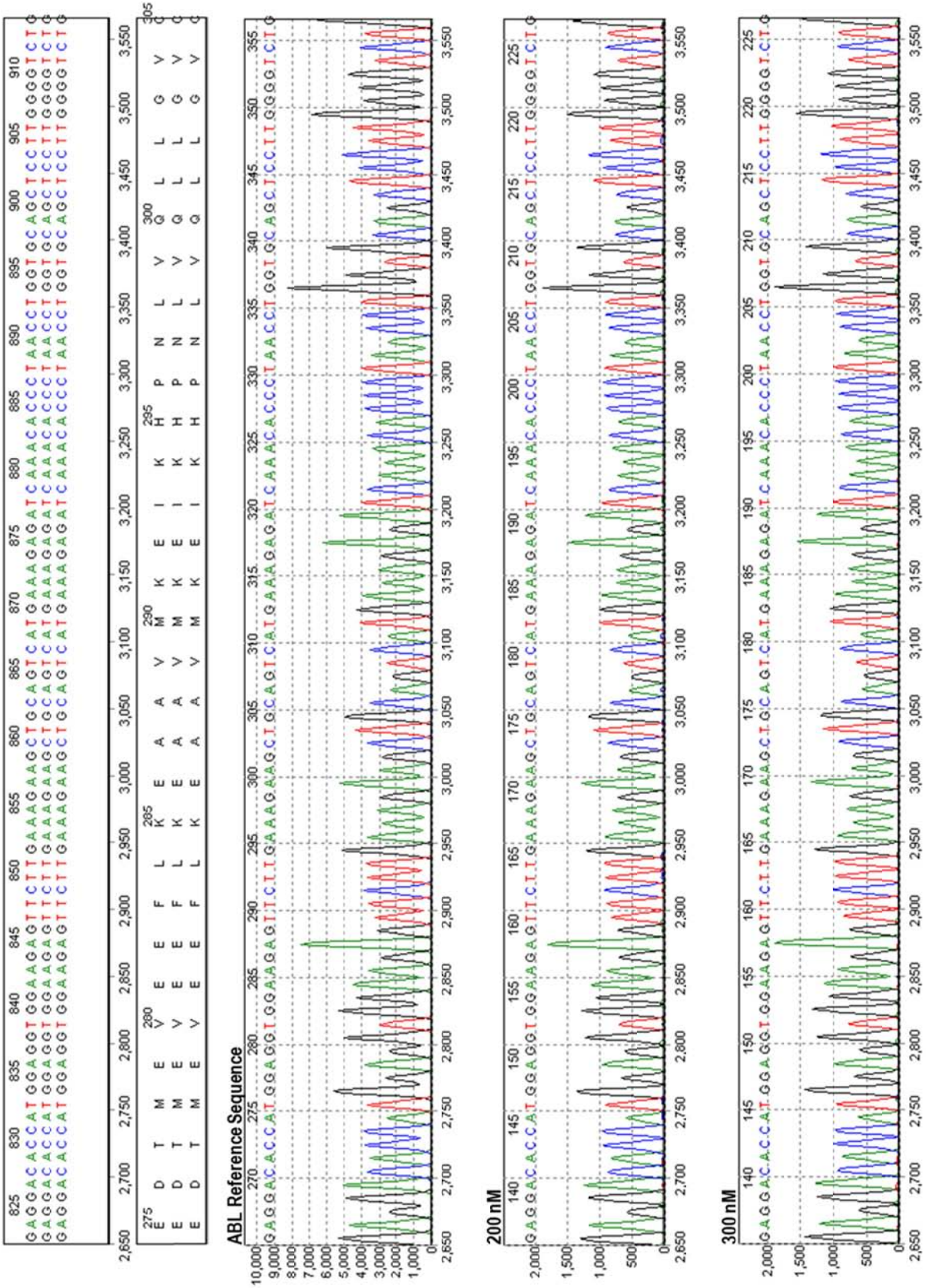
ABL Reference Sequence
200 nM
300 nM

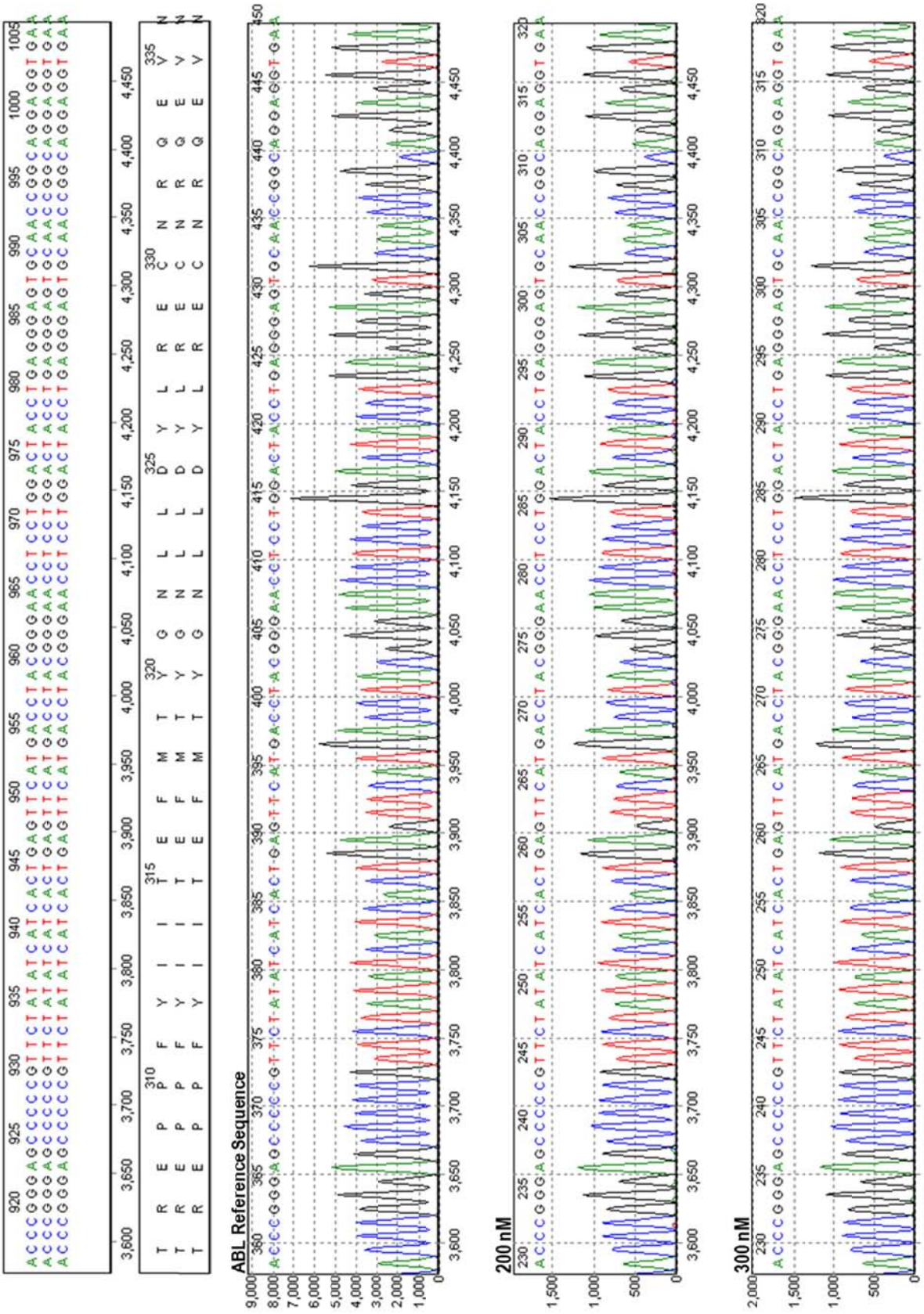
ABL Reference Sequence
200 nM
300 nM

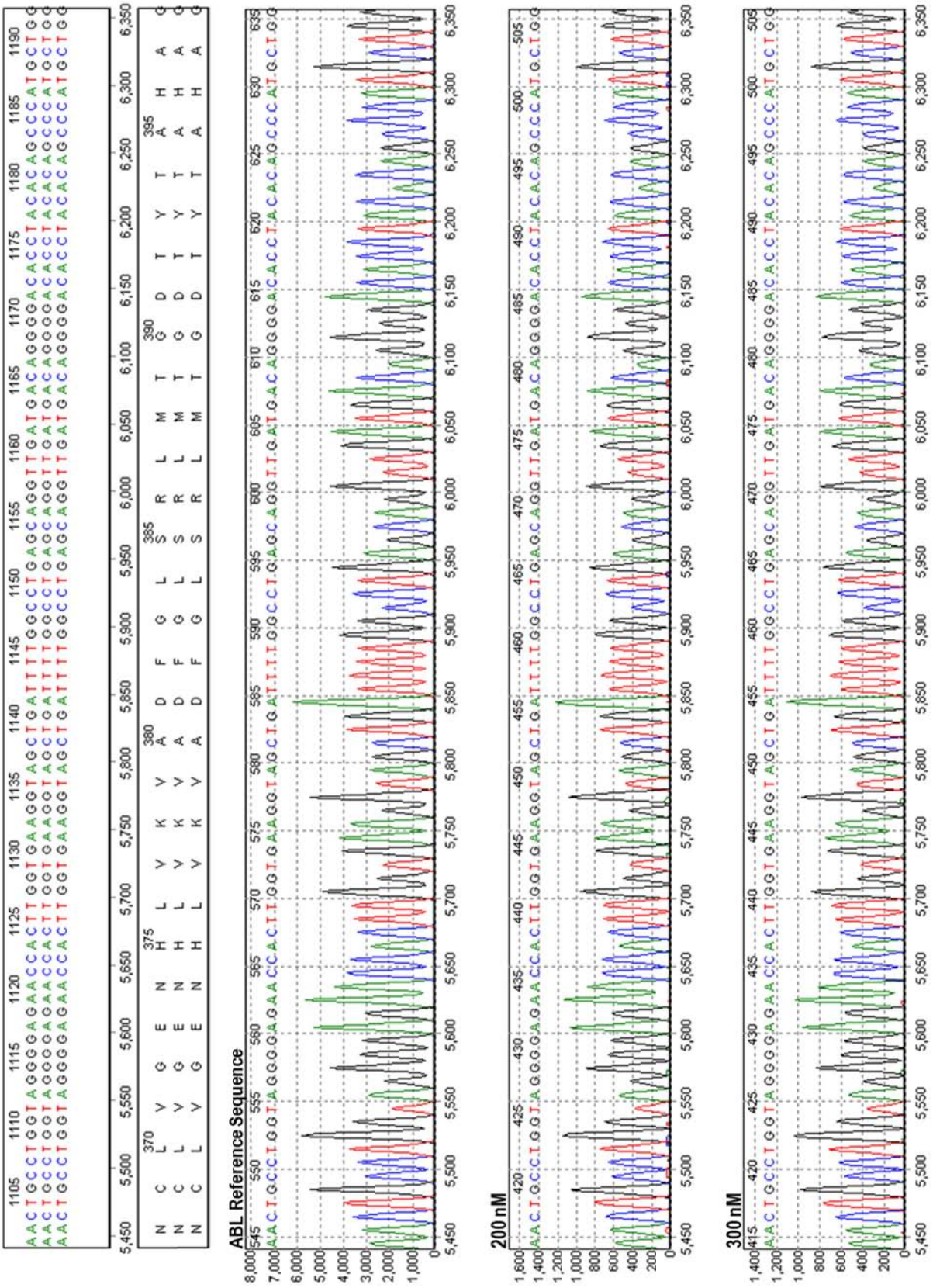
ABL Reference Sequence
200 nM
300 nM

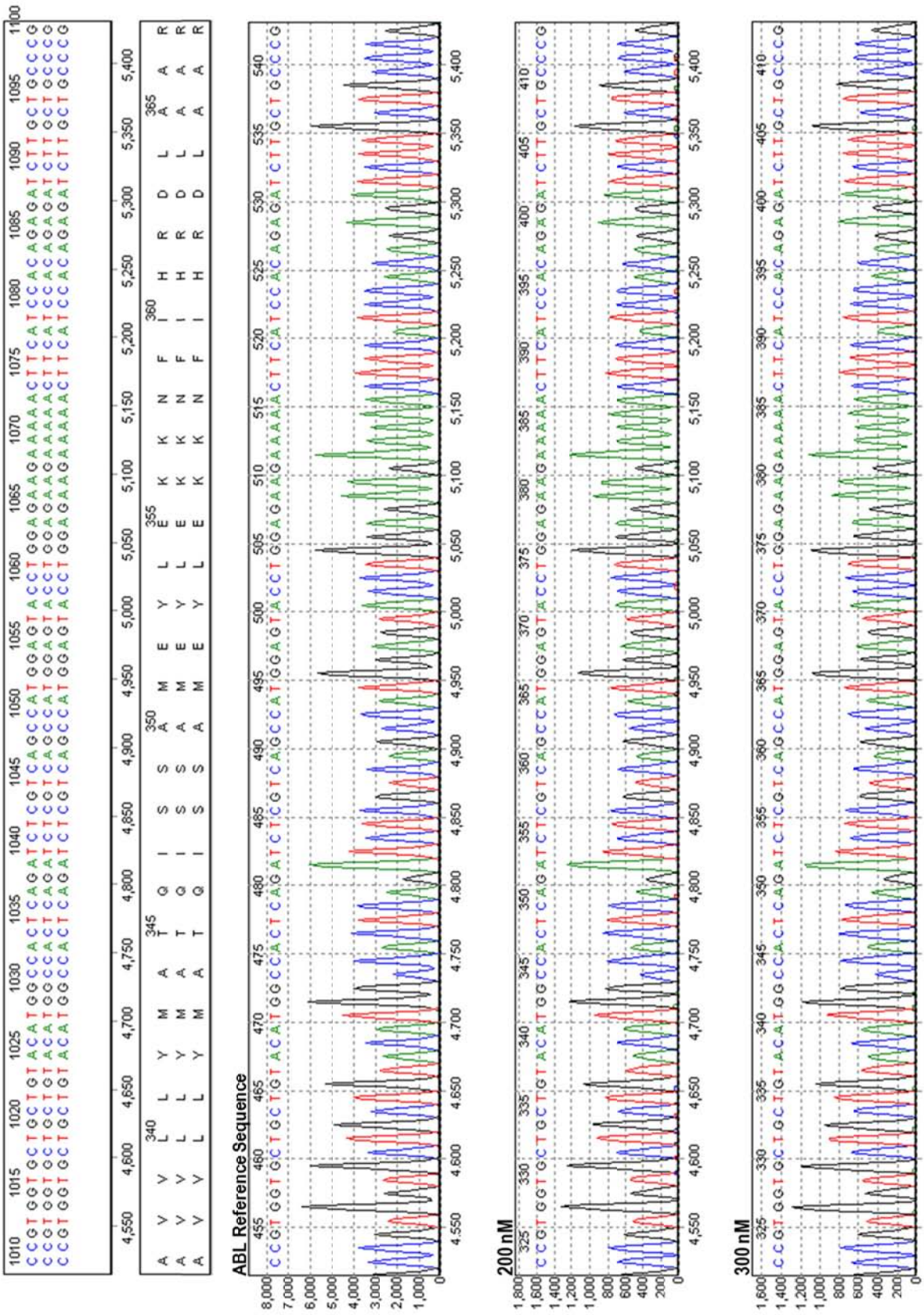
ABL Reference Sequence
200 nM
300 nM

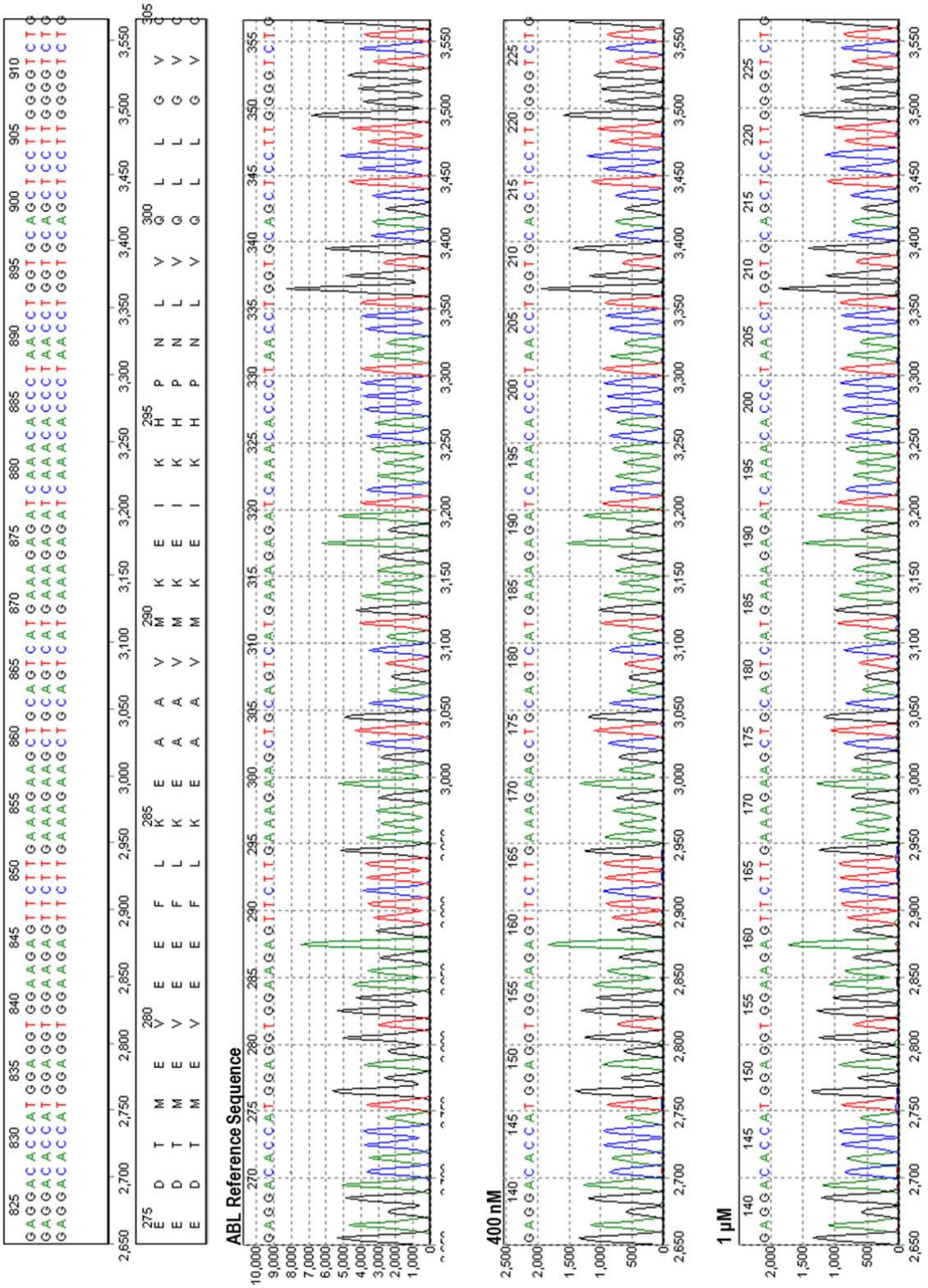
ABL Reference Sequence
400 nM
1 µM

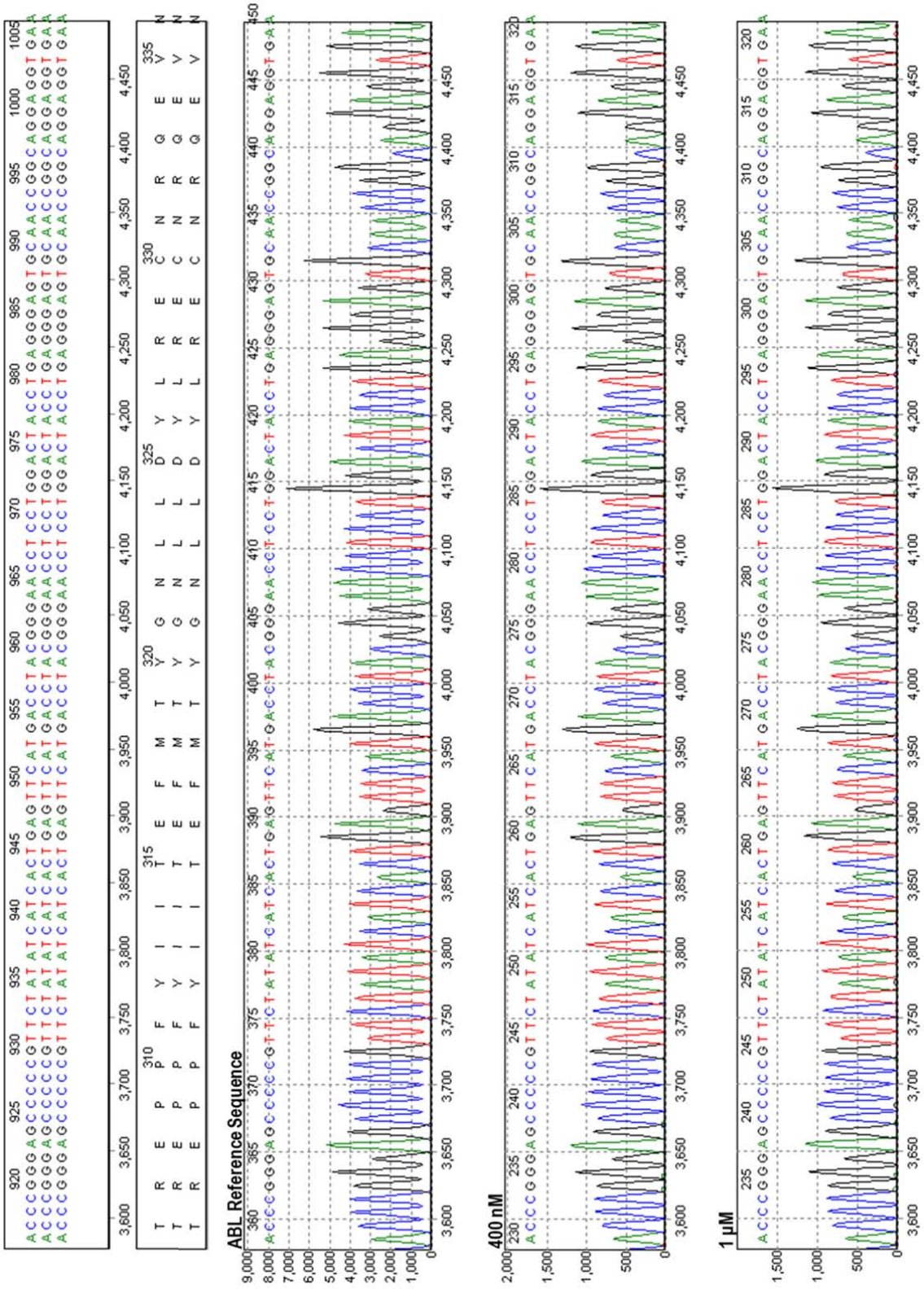
ABL Reference Sequence
400 nM
1 µM

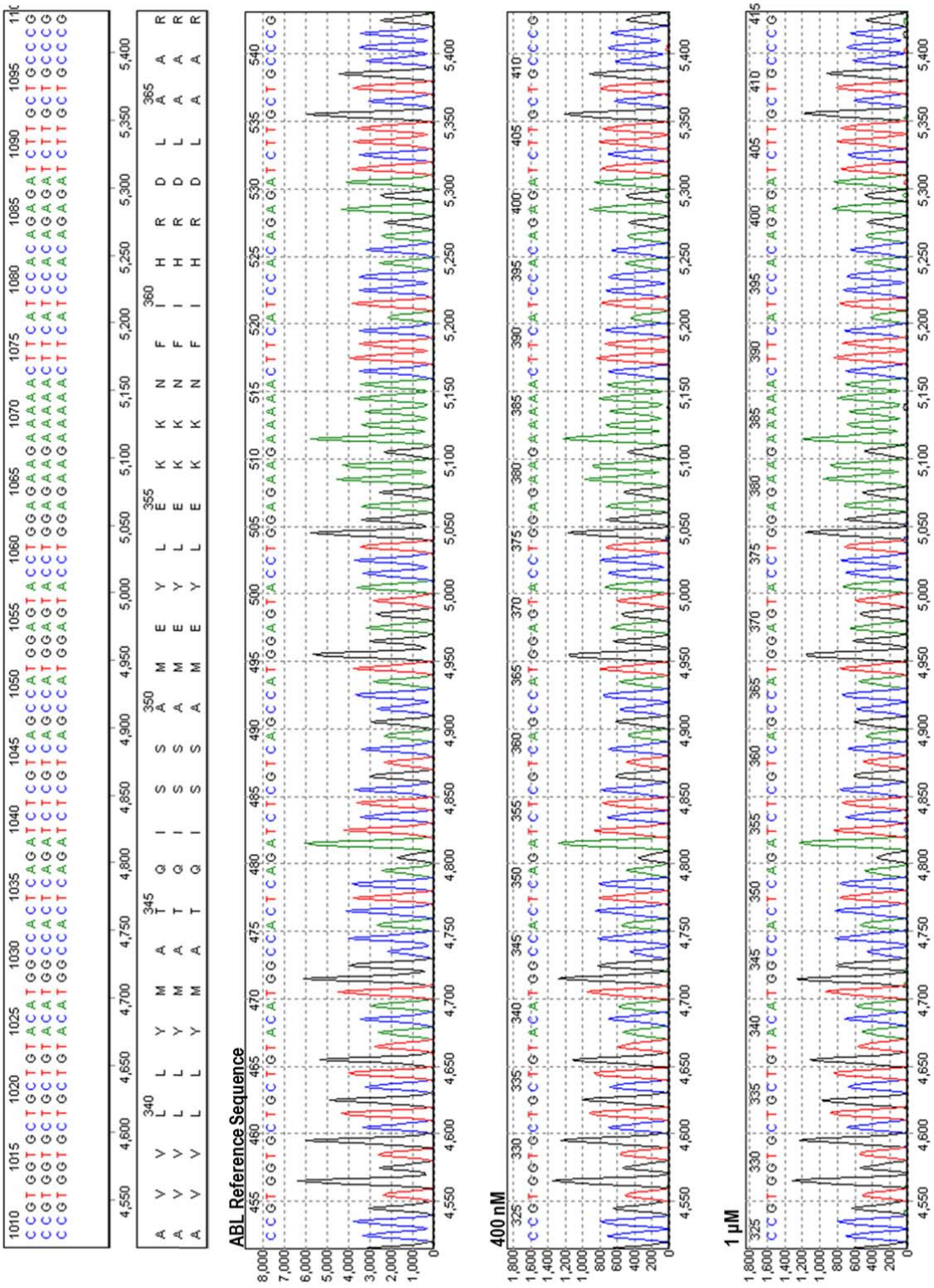
ABL Reference Sequence
400 nM
1 µM

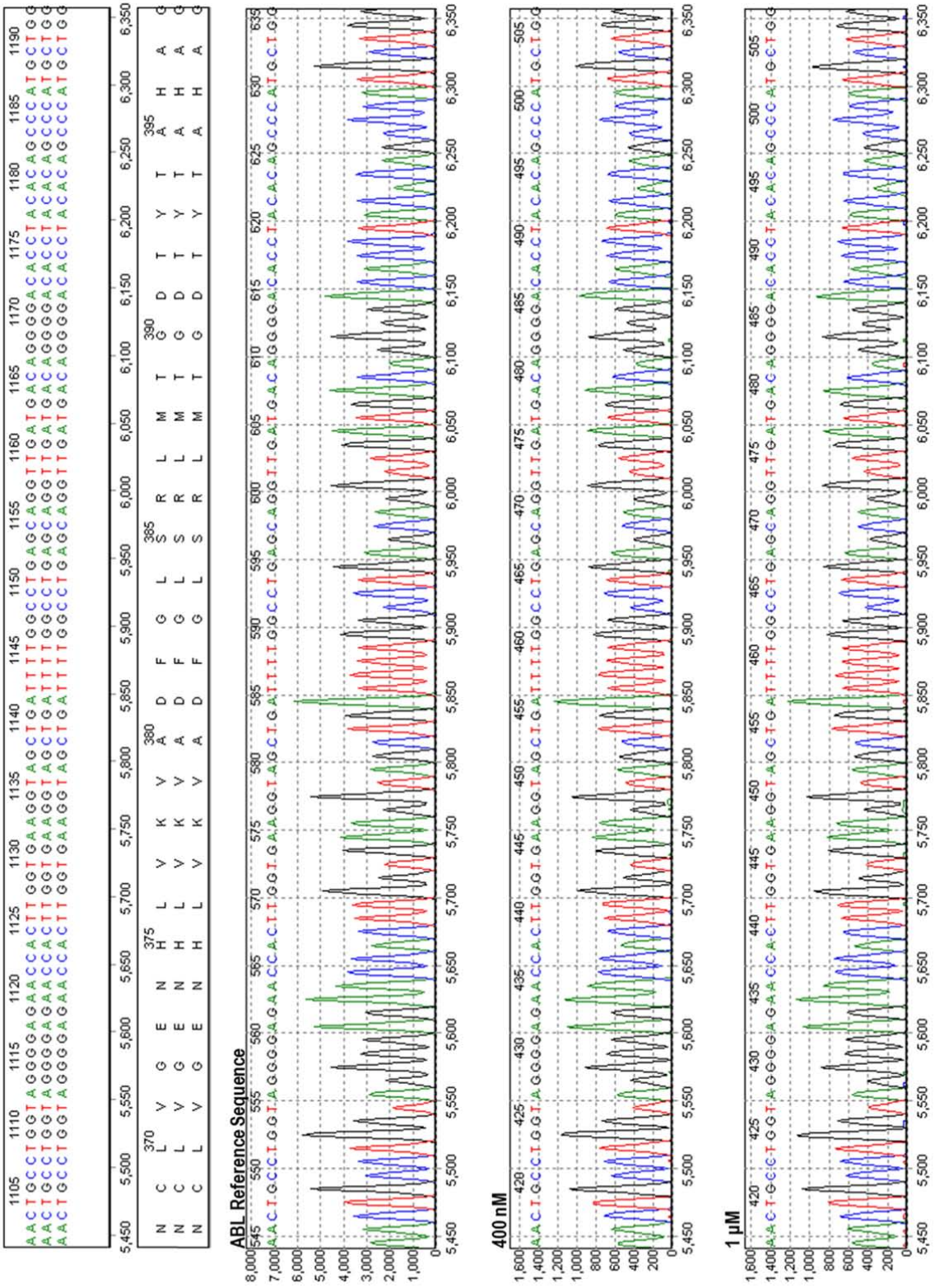
ABL Reference Sequence
400 nM
1 µM

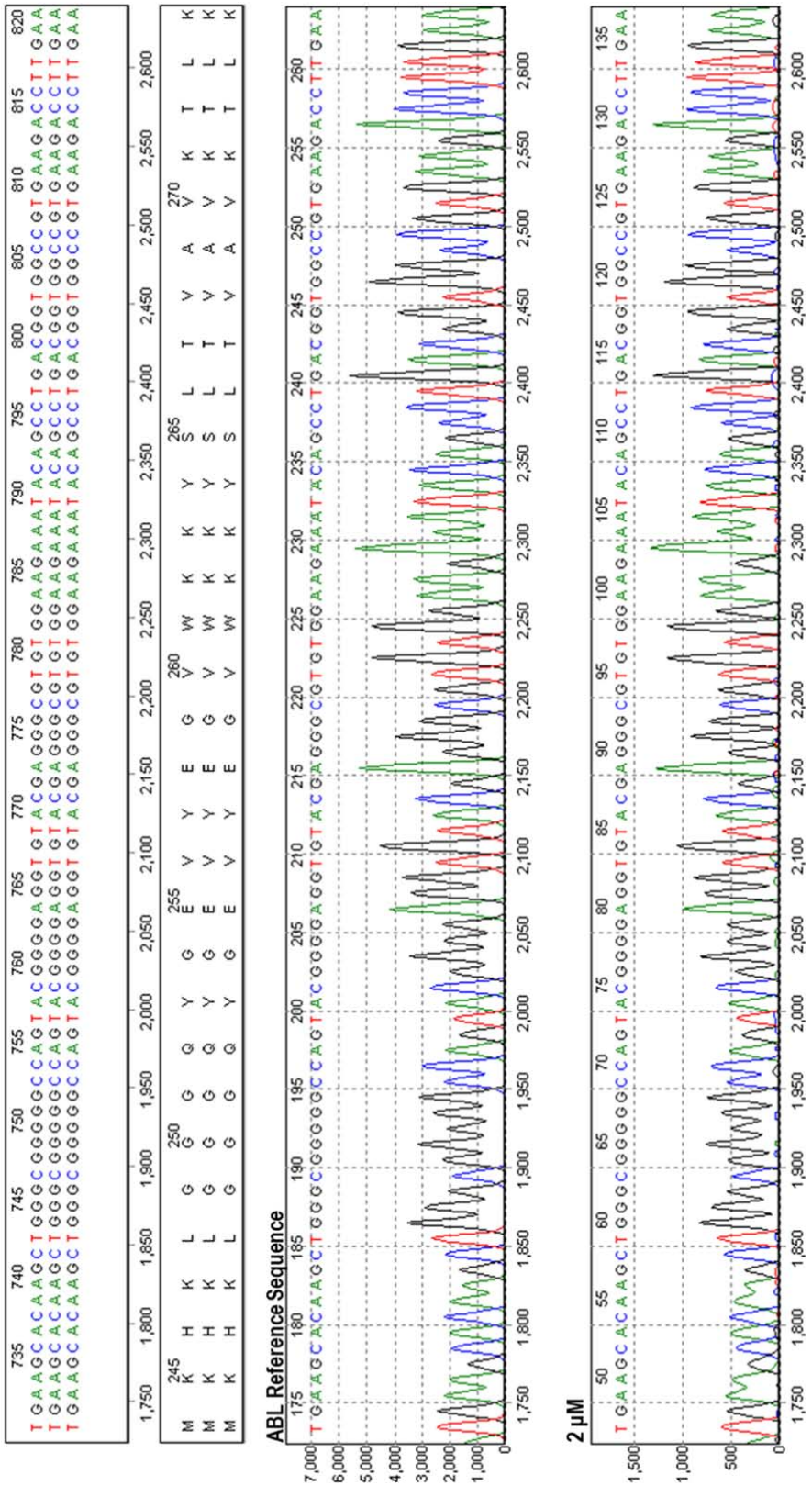
ABL Reference Sequence
2 µM

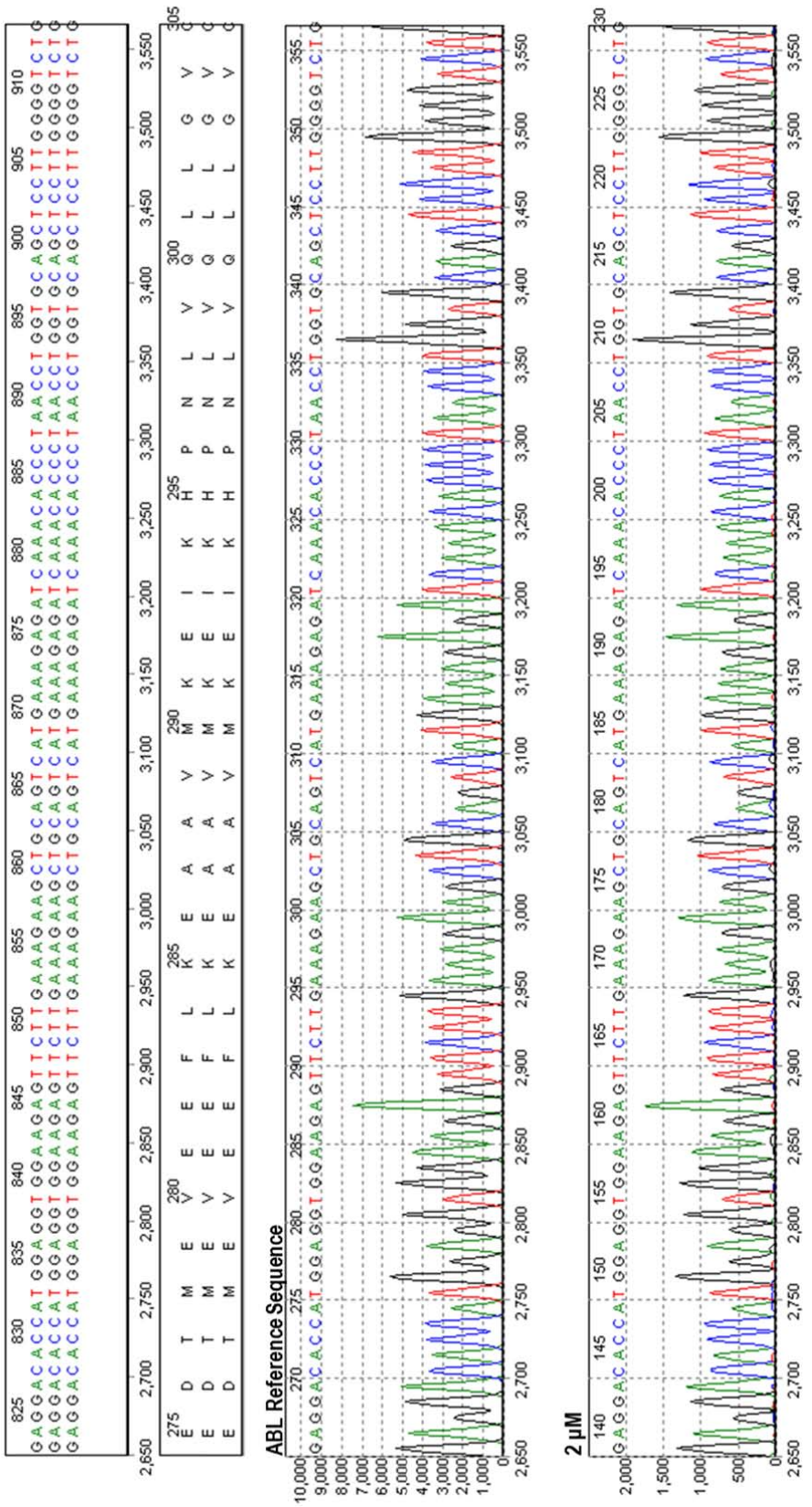
ABL Reference Sequence
2 µM

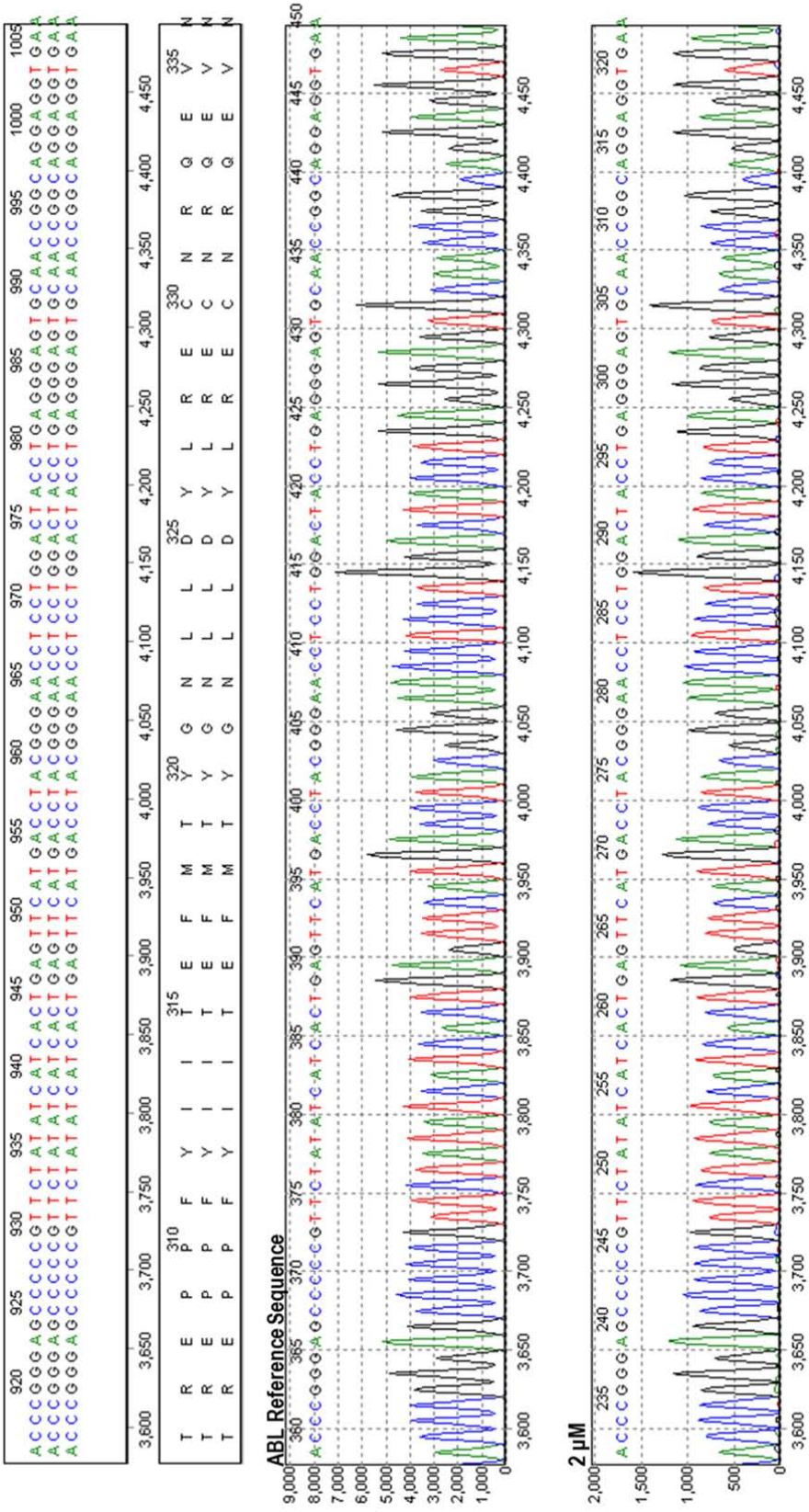
ABL Reference Sequence
2 µM

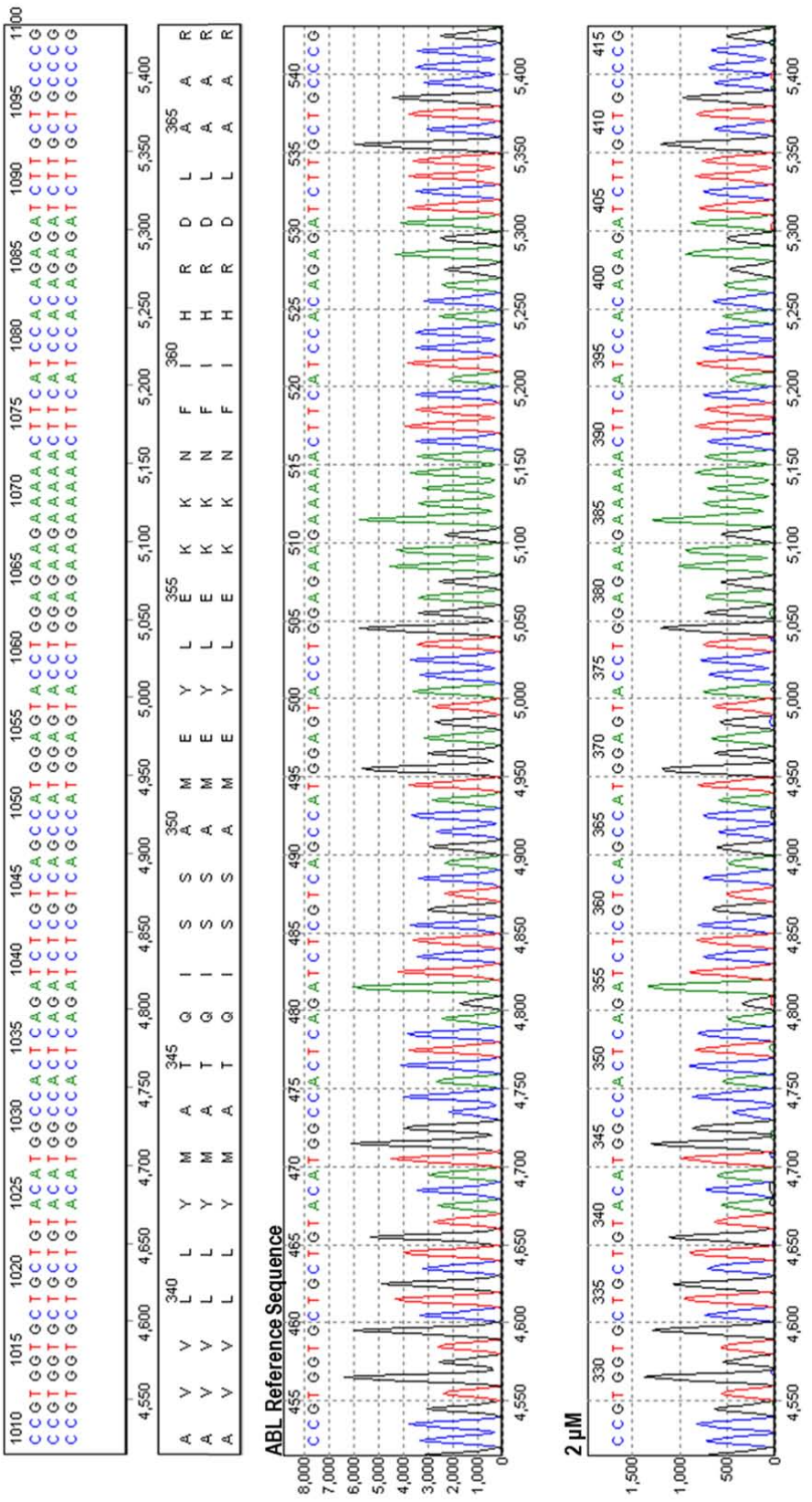
ABL Reference Sequence
2 µM

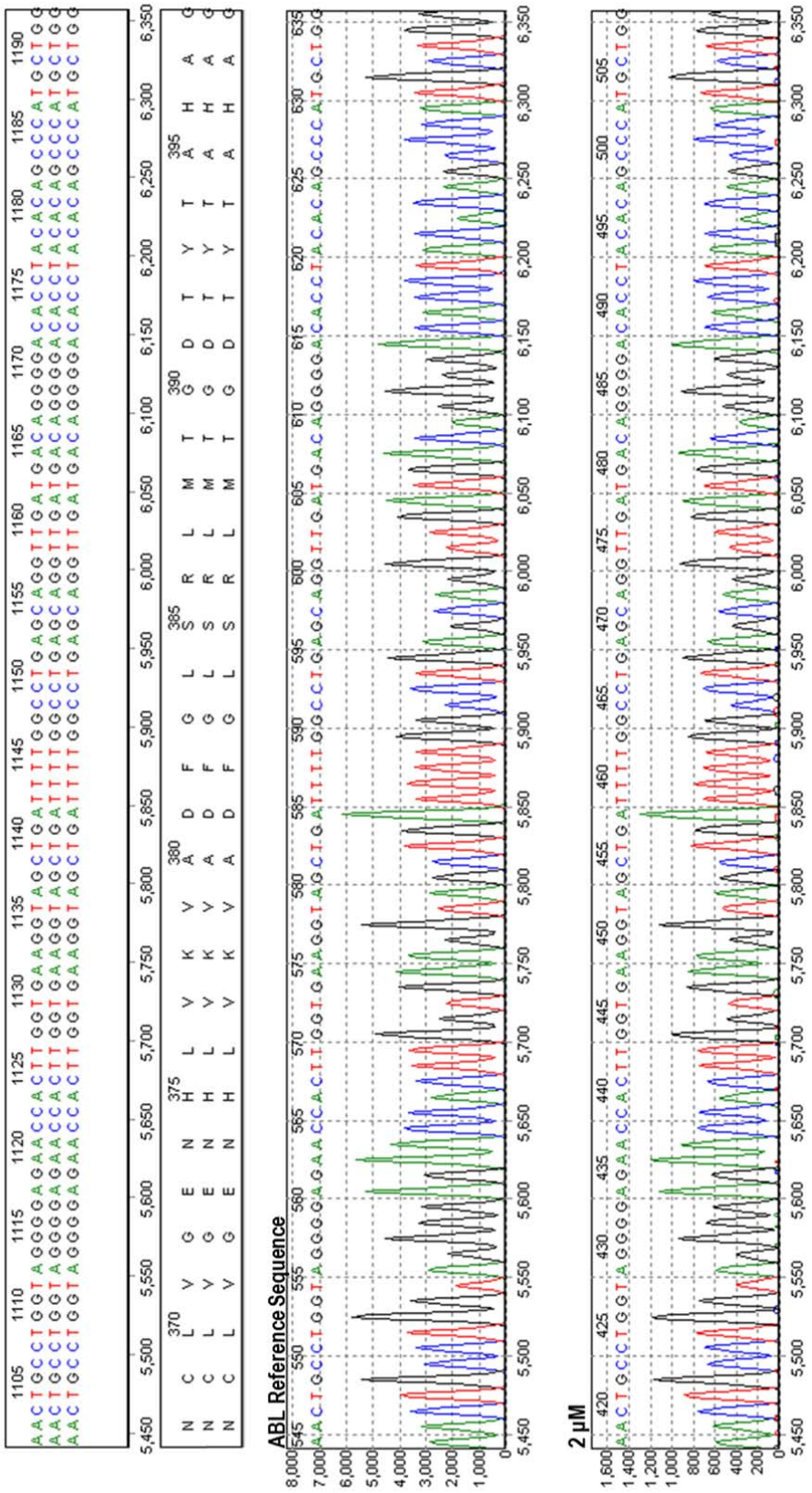
ABL Reference Sequence
2 µM

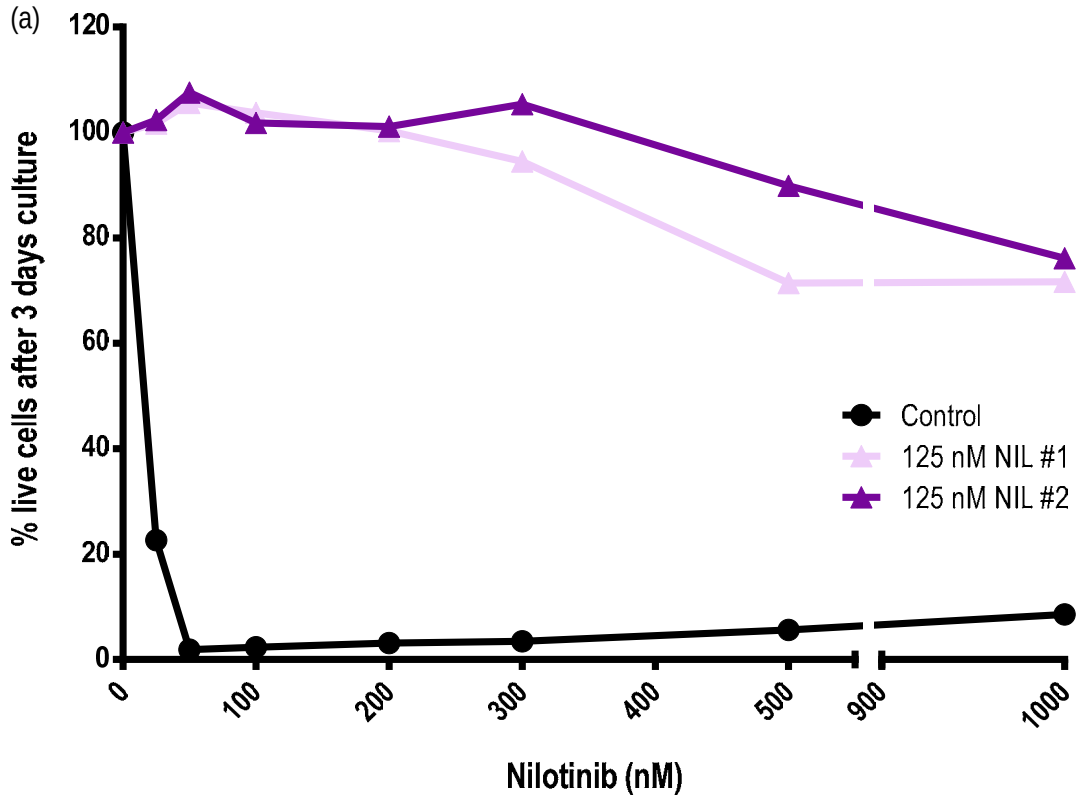

Figure 4A: K562-Dox 125 nM NIL #1 and K562-Dox 125 nM NIL #2 cells have significantly decreased TKI-mediated cell death

Cells were cultured for 72 h in increasing concentrations of a) nilotinib b) imatinib and c) dasatinib and cell death determined by trypan blue staining. Data demonstrate that K562-Dox 125 nM NIL #1 and K562-Dox 125 nM NIL #2 cells have significantly increased survival in the presence of TKIs when compared with control cells. It is important to note that while trypan blue counts following cytotoxicity assays demonstrate near complete cell death, Annexin V and 7-AAD staining shows a maximum of 40% cell death even at the highest TKI concentrations. The data shown represent one experiment performed in triplicate with the corresponding survival curves representing the mean. Data were normalised to 0 nM TKI with the number of live cells in the absence of TKI set at 100%. NIL=nilotinib

(b)

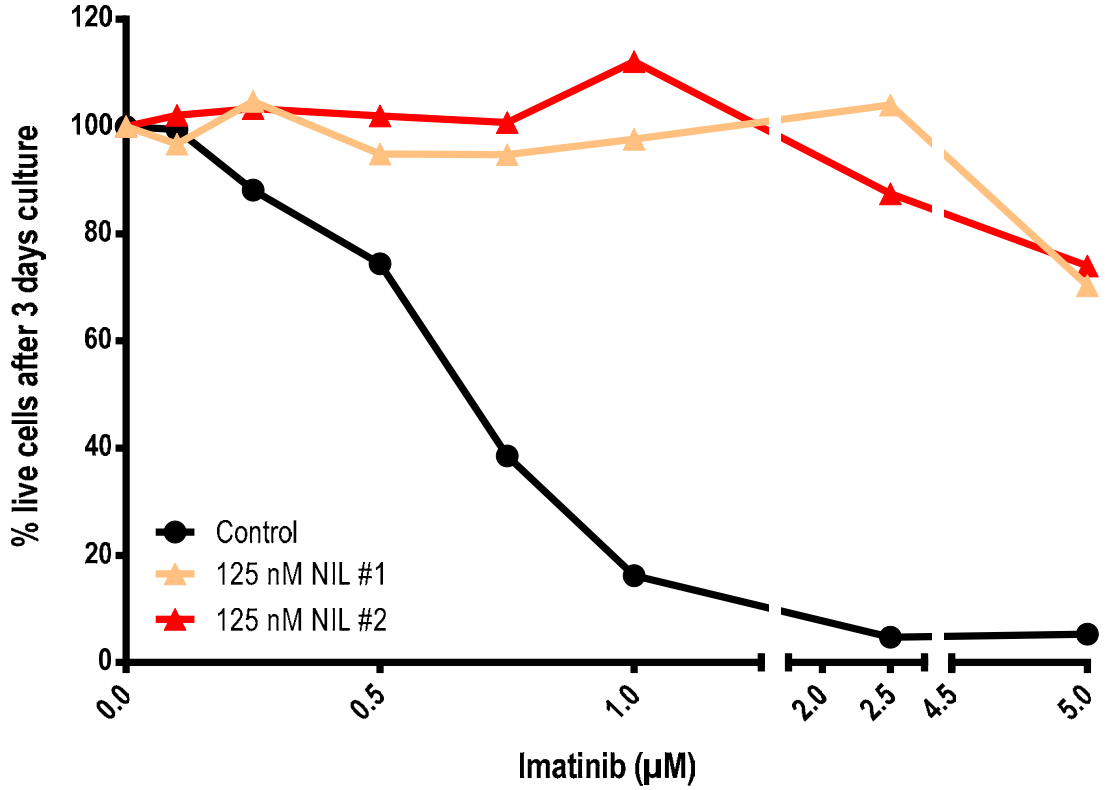
% live cells after 3 days culture
120
100
80
60
40
20
0
Control
125 nM NIL #1
125 nM NIL #2
0.0
0.5
1.0
2.0
2.5
4.5
5.0
Imatinib (µM)

(c)

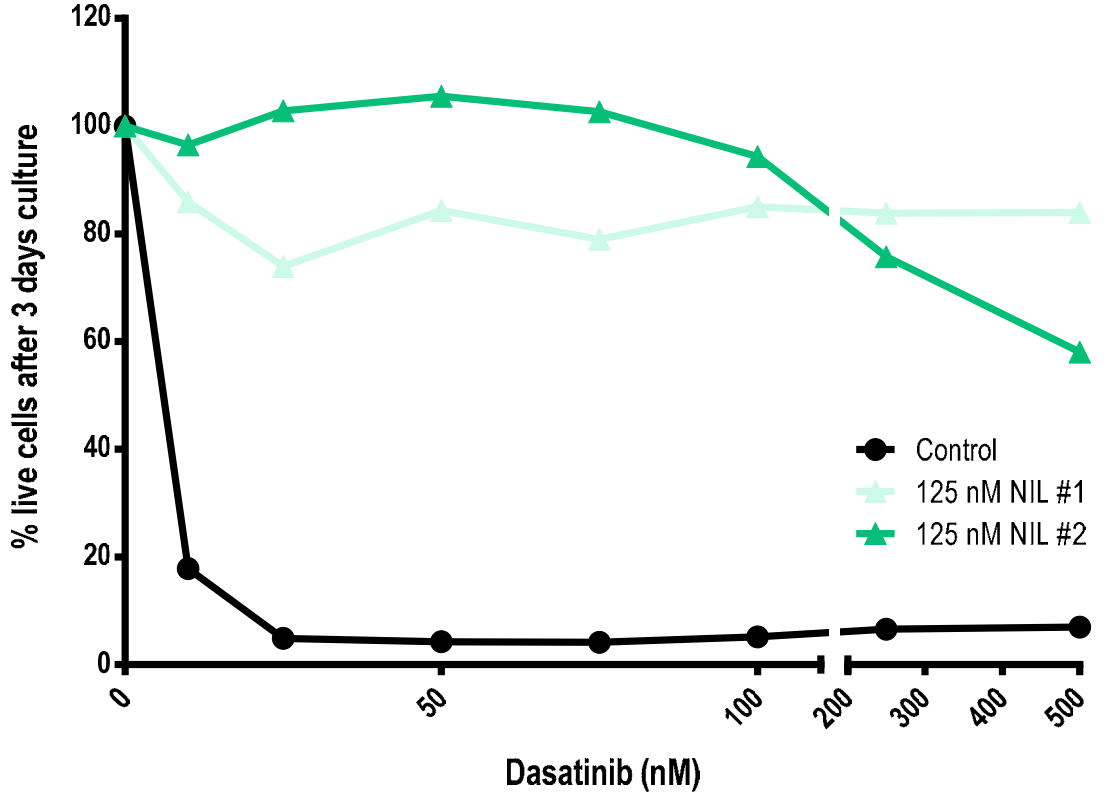
% live cells after 3 days culture
120
100
80
60
40
20
0
Control
125 nM NIL #1
125 nM NIL #2
0
50
100
200
300
400
500
Dasatinib (nM)

(a)

Figure 4B: K562-Dox 2 μM NIL #1 and K562-Dox 2 μM NIL #2 cells have significantly decreased TKI-mediated cell death

Cells were cultured for 72 h in increasing concentrations of a) nilotinib b) imatinib and c) dasatinib and cell viability assessed visually. Metabolic products from live cells turn the colour of the growth media from pink to yellow thus allowing a crude assessment of cell viability. Data demonstrate K562-Dox 2 μM NIL #1 cells and K562-Dox 2 μM NIL #2 cells have increased survival in the presence of nilotinib, imatinib and dasatinib when compared with control cells. The pictures shown are representative of at least three separate experiments performed in triplicate. The TKI concentrations are indicated.

Appendix 4B – Cell Death in K562-Dox 2 μM NIL #1 and NIL #2 Cells Determined by Visual Assessment of Growth Media

(b)

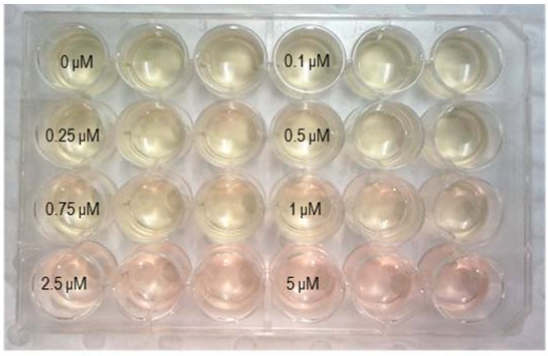

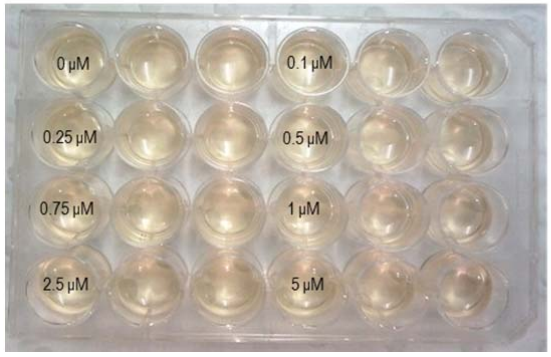

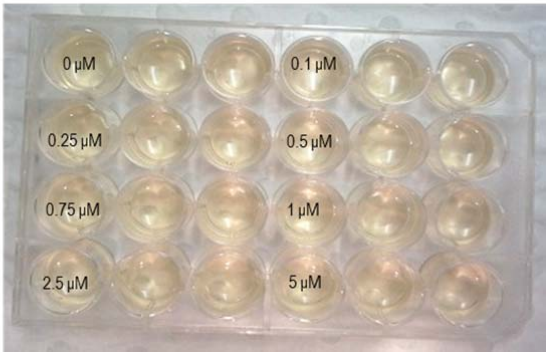

(c)

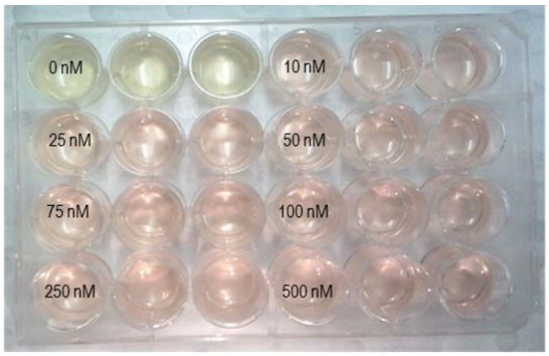

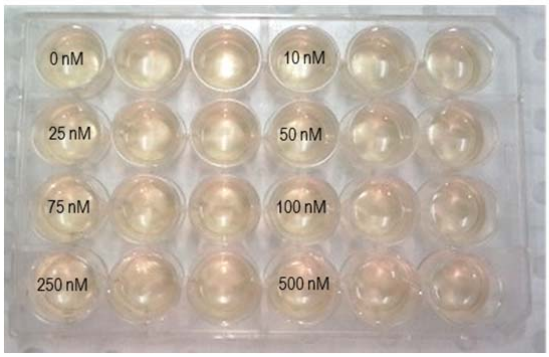

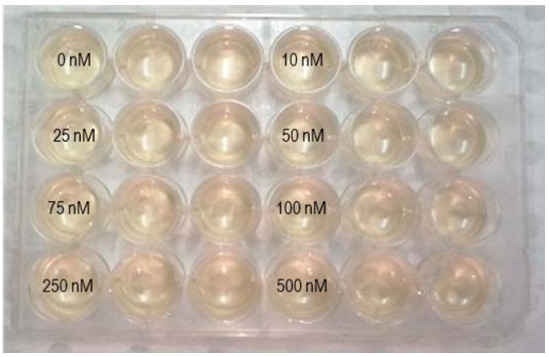

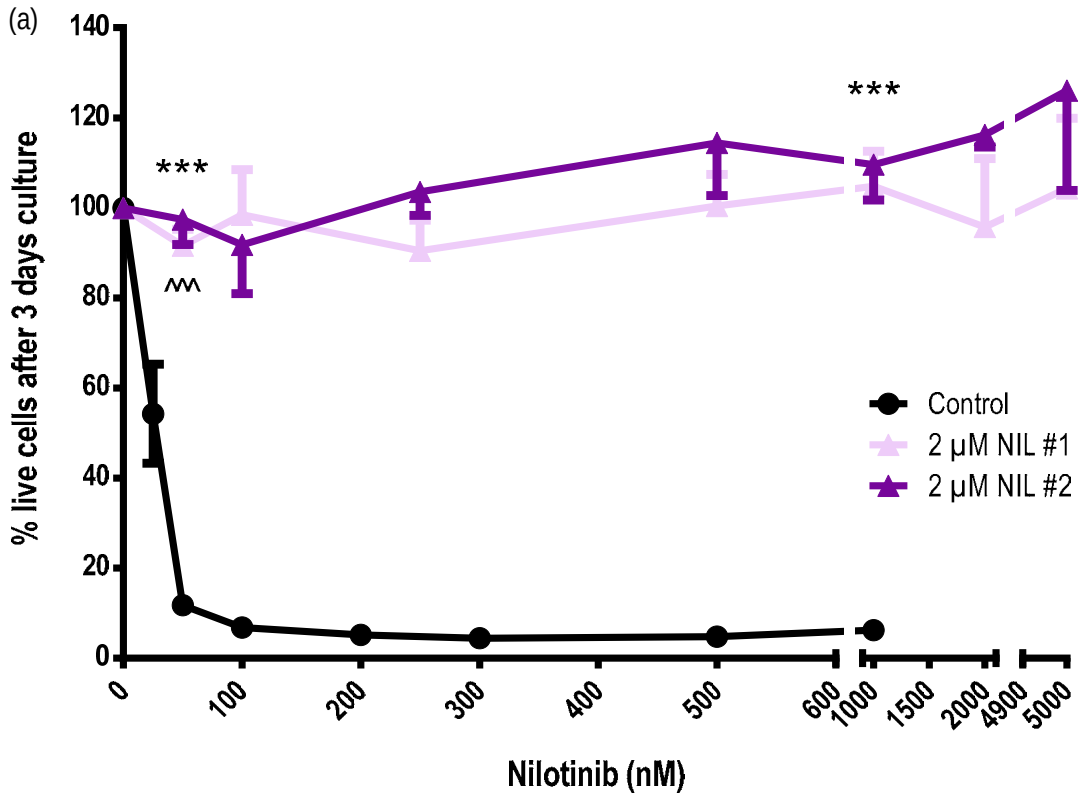

Figure 4C: K562-Dox 2 μM NIL #1 and K562-Dox 2 μM NIL #2 cells have significantly decreased TKI-mediated cell death

Cells were cultured for 72 h in increasing concentrations of a) nilotinib b) imatinib and c) dasatinib and cell death determined by trypan blue staining. Data demonstrate K562-Dox 2 μM NIL #1 cells and K562-Dox 2 μM NIL #2 cells have significantly increased survival in the presence of TKIs when compared with control cells. It is important to note that while trypan blue counts following cytotoxicity assays demonstrate near complete cell death, Annexin V/7-AAD staining shows a maximum of 80% cell death even at the highest TKI concentrations. The data shown are representative of at least three separate experiments performed in triplicate with the corresponding survival curves representing the mean. Data were normalised to 0 nM TKI with the number of live cells in the absence of TKI set at 100%. Statistical analyses were performed using Student's *t*-test with statistically significant *p*-values denoted by asterisks and carets representing K562-Dox 2 μM NIL #1 and K562-Dox 2 μM NIL #2 cell lines respectively (* $p<0.05$; ** $p<0.01$; *** $p<0.001$). Error bars represent SEM. NIL=nilotinib.

(b)

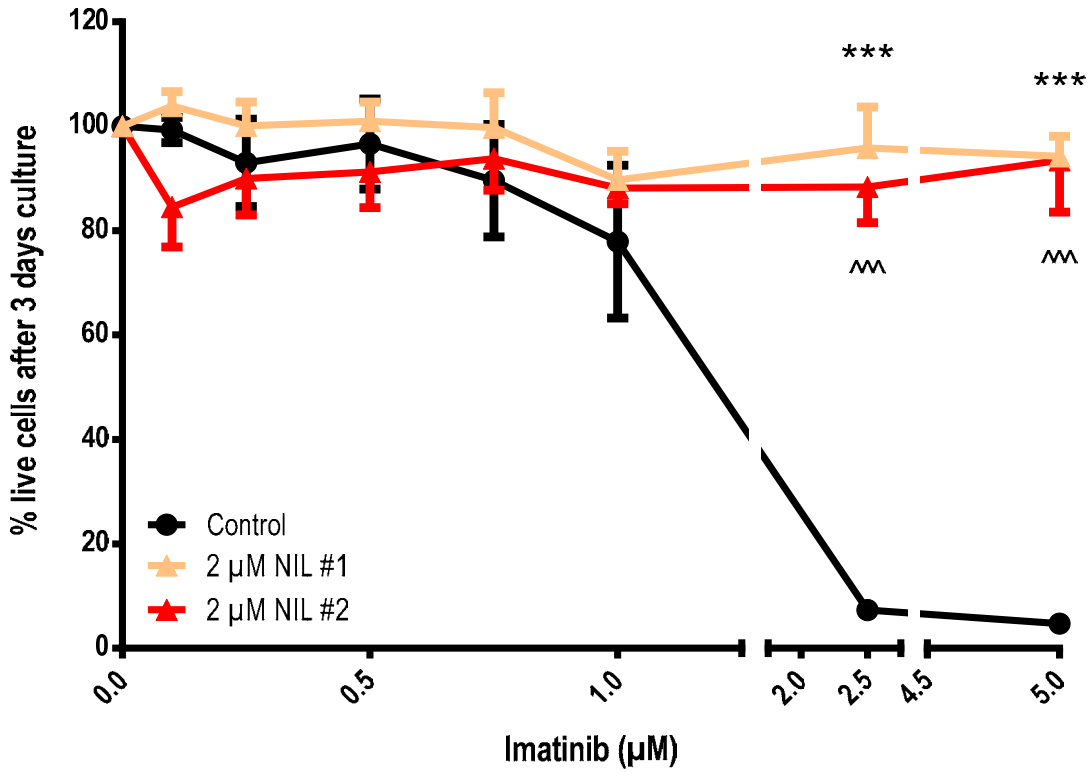
120
100
80
60
40
20
0
% live cells after 3 days culture
***
***
Control
2 µM NIL #1
2 µM NIL #2
0.0
0.5
1.0
2.0
2.5
4.5
5.0
Imatinib (µM)

(c)

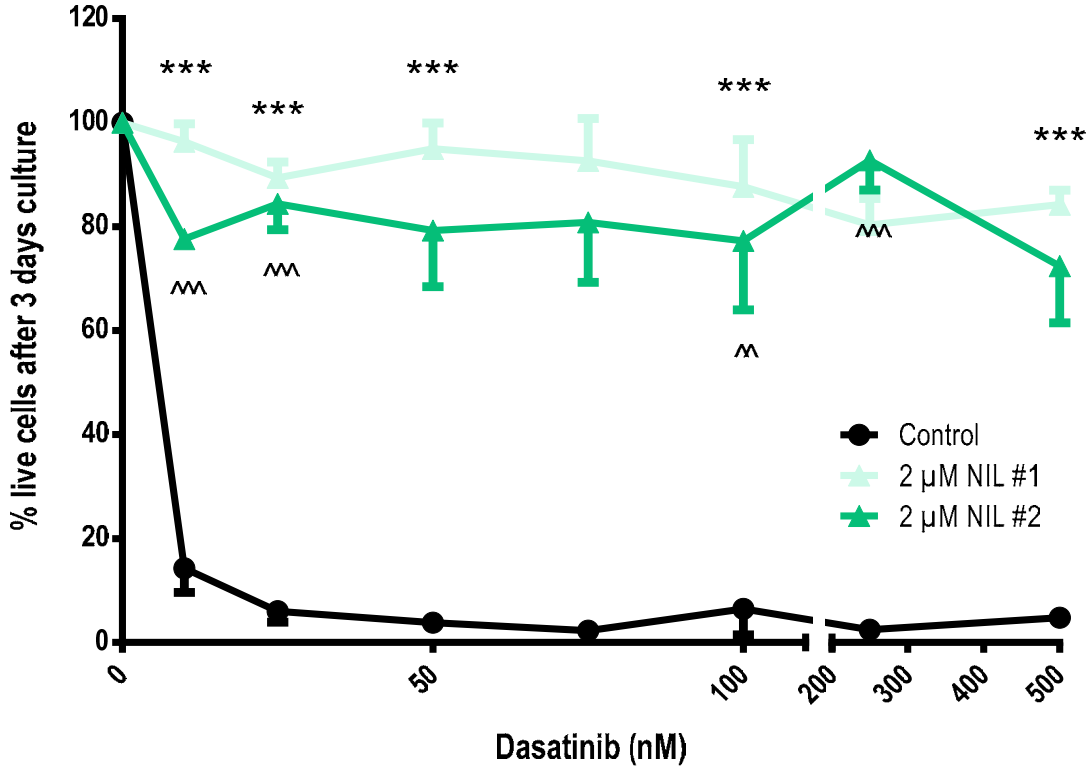
120
100
80
60
40
20
0
% live cells after 3 days culture
***
***
***
***
***
Control
2 µM NIL #1
2 µM NIL #2
0
50
100
200
300
400
500
Dasatinib (nM)

Figure 4D: K562-Dox 2 µM NIL resistant cells exhibit altered protein expression compared with K562-Dox control cells

Commercially available antibody array plates (Fullmoon Biosystems) were used to compare expression levels of various cellular kinases (a and c) and proteins involved in cancer signalling (b and d) in K562-Dox 2 µM NIL #1 and K562-Dox 2 µM NIL #2 cells compared with control cells. The arrays were analysed by Fullmoon Biosystems and the percentage change in expression levels determined. Proteins were then graded in descending order based on expression levels and the top ranked proteins chosen for further analysis. Proteins exhibiting >50% increase in expression in resistant cells are shown in PINK and proteins exhibiting >50% decrease in expression levels are shown in GREEN. Background expression levels were set at 2.5× greater than that of negative controls; proteins falling below this value were excluded from analysis (GREY SHADED).

(a)

Mean Signal	*457*	*490*
Average of -ve Controls	*82*	*92*
2.5x -ve Control values	205	230

Protein List	Average Signal Value of 6 Replicates on the Array		Data Normalized to Mean Signal on the Array		% Change
	K562-Dox Control	K562-Dox 2 µM NIL #1	K562-Dox Control	K562-Dox 2 µM NIL #1	Control – 2 µM NIL #1 ÷ 2 µM NIL #1
PRIM2A	*251*	*568*	0.55	1.16	110.99
PDGFRB	*580*	*1298*	1.27	2.65	108.61
CHEK2	*1004*	*2136*	2.20	4.36	98.46
RPS6KB2	*598*	*1186*	1.31	2.42	85.00
IGFBP6	*88*	*147*	0.19	0.30	56.19
MAP2K6	*192*	*295*	0.42	0.60	43.63
PRKAB2	*221*	*338*	0.48	0.69	42.68
EPHB3	*3952*	*5983*	8.64	12.21	41.23
EPHA6	*95*	*143*	0.21	0.29	40.76
PLK1	*74*	*110*	0.16	0.22	37.95
LIMK2	*144*	*205*	0.32	0.42	32.29
FGFR2	*290*	*403*	0.63	0.82	29.66
RPS6KB1	*100*	*138*	0.22	0.28	29.02
CAMK4	*80*	*110*	0.17	0.22	28.74
FLT3	*318*	*435*	0.70	0.89	27.48
IKBKAP	*82*	*109*	0.18	0.22	23.88
TEK	*220*	*282*	0.48	0.58	19.58
PRKAB1	*114*	*145*	0.25	0.30	18.49
DYRK1B	*160*	*204*	0.35	0.42	18.41
MERTK	*87*	*111*	0.19	0.23	18.40
SAB	*626*	*789*	1.37	1.61	17.68
CDC2L2	*196*	*247*	0.43	0.50	17.55
PAK2	*88*	*110*	0.19	0.22	16.31
STAT1	*6342*	*7880*	13.87	16.08	15.91
IKBKE	*95*	*118*	0.21	0.24	15.64
BUB1B	*115*	*142*	0.25	0.29	15.39
MAP3K3	*598*	*732*	1.31	1.49	14.20
CDK9	*276*	*338*	0.60	0.69	14.12
DYRK3	*80*	*97*	0.17	0.20	13.74
ERBB2	*111*	*134*	0.24	0.27	13.41
SRC	*1039*	*1262*	2.27	2.58	13.35
MAP2K1	*182*	*220*	0.40	0.45	13.17
NEK2	*97*	*118*	0.21	0.24	12.81
IRAK3	*126*	*152*	0.28	0.31	12.37
MELK	*108*	*129*	0.24	0.26	11.29
BCR	*284*	*339*	0.62	0.69	11.26
ANK1	*91*	*109*	0.20	0.22	11.20
WNK3	*113*	*135*	0.25	0.27	11.04
CDK5RAP3	*111*	*133*	0.24	0.27	11.03
ILKAP	*118*	*140*	0.26	0.29	10.84
PRKX	*95*	*113*	0.21	0.23	10.84
CDK4	*97*	*115*	0.21	0.23	10.76
RPS6KA3	*122*	*144*	0.27	0.29	10.24
MAP3K7IP1	*98*	*116*	0.21	0.24	10.11
RAF1	*121*	*143*	0.26	0.29	9.85
CSF1	*154*	*181*	0.34	0.37	9.77
EGFR	*207*	*243*	0.45	0.49	9.47
TIE1	*102*	*120*	0.22	0.24	9.42
CSNK1E	*7958*	*9332*	17.40	19.04	9.40
MAP3K11	*116*	*136*	0.25	0.28	9.24
CAMK1	*110*	*128*	0.24	0.26	8.86
MAP3K7	*90*	*105*	0.20	0.21	8.73
STAT3	*112*	*131*	0.25	0.27	8.52

CSNK1G2	133	154	0.29	0.31	8.41
PTK9	122	142	0.27	0.29	8.16
ROR1	106	122	0.23	0.25	8.03
MAP3K1	233	269	0.51	0.55	7.93
MAP4K4	131	152	0.29	0.31	7.85
MST1R	123	142	0.27	0.29	7.85
CAMKK1	102	118	0.22	0.24	7.80
TGFB1I1	2847	3281	6.23	6.69	7.54
MAPK1	94	108	0.20	0.22	7.24
EPHB1	127	145	0.28	0.30	7.18
CSNK1G1	132	152	0.29	0.31	7.07
MAPK9	103	118	0.23	0.24	7.03
MAP2K2	91	104	0.20	0.21	7.01
MAPKAPK2	125	143	0.27	0.29	6.57
AKT2	99	113	0.22	0.23	6.49
MUSK	3971	4529	8.68	9.24	6.41
EPHA2	125	142	0.27	0.29	6.37
ROR2	265	302	0.58	0.62	6.37
ERBB3	114	130	0.25	0.27	6.37
RET	220	251	0.48	0.51	6.30
CSNK2A1	115	130	0.25	0.27	5.88
PRKCI	87	99	0.19	0.20	5.80
CDK2	103	117	0.23	0.24	5.80
PRKCA	116	132	0.25	0.27	5.76
MAPK13	92	105	0.20	0.21	5.75
FLT1	120	135	0.26	0.28	5.65
FUSIP1	96	109	0.21	0.22	5.58
JAK3	174	197	0.38	0.40	5.46
RNASEH1	117	132	0.26	0.27	5.37
ANP32A	459	518	1.00	1.06	5.28
MYO7A	99	112	0.22	0.23	5.23
EPDR1	102	115	0.22	0.23	5.16
TYRO3	9578	10770	20.95	21.97	4.90
GSK3B	116	130	0.25	0.26	4.87
PTK6	109	123	0.24	0.25	4.83
MAP3K13	91	102	0.20	0.21	4.76
CDKL1	119	133	0.26	0.27	4.68
RPS6KA6	109	122	0.24	0.25	4.56
IRAK4	111	124	0.24	0.25	4.22
NPR2	105	117	0.23	0.24	4.14
PTK2	91	102	0.20	0.21	3.85
DYRK1A	133	148	0.29	0.30	3.81
PLK4	97	108	0.21	0.22	3.71
ATM	121	135	0.26	0.27	3.69
DYRK2	120	133	0.26	0.27	3.53
HIPK2	8060	8934	17.63	18.23	3.40
CAMK2B	102	113	0.22	0.23	3.39
PIM1	92	102	0.20	0.21	3.28
PTK2B	99	109	0.22	0.22	3.24
BMPR1A	219	243	0.48	0.49	3.15
EPHA5	110	122	0.24	0.25	3.03
CDK5	111	122	0.24	0.25	2.99
EFNA5	7509	8288	16.42	16.91	2.97
TGFB1	463	511	1.01	1.04	2.96
PAK1	98	108	0.21	0.22	2.83
FGFR1OP2	106	117	0.23	0.24	2.83
CDC2	108	119	0.24	0.24	2.82
RPS6KA5	139	153	0.30	0.31	2.67
MYO9A	135	149	0.30	0.30	2.60
SGK3	98	108	0.21	0.22	2.49

MYLIP	107	117	0.23	0.24	2.49
ROCK2	203	223	0.44	0.45	2.41
PRKCSH	98	107	0.21	0.22	2.22
FGR	118	129	0.26	0.26	2.15
YES1	104	114	0.23	0.23	2.11
MYO3A	126	138	0.28	0.28	1.94
CDK3	113	124	0.25	0.25	1.80
MAPK14	105	115	0.23	0.23	1.57
PRKACG	104	113	0.23	0.23	1.50
RNMT	108	118	0.24	0.24	1.49
MAPKAPK3	116	126	0.25	0.26	1.47
RNASEH2A	103	112	0.23	0.23	1.42
HERC3	97	105	0.21	0.21	1.35
FGFRL1	83	89	0.18	0.18	1.02
WNK2	115	125	0.25	0.25	0.99
AKT1	125	136	0.27	0.28	0.98
IGFBP1	93	101	0.20	0.21	0.96
PRKDC	97	104	0.21	0.21	0.87
STAT2	103	111	0.23	0.23	0.84
PTK9L	110	119	0.24	0.24	0.81
RPS6KA1	102	110	0.22	0.22	0.62
GRK5	130	139	0.28	0.28	0.38
CDKL5	95	102	0.21	0.21	0.20
CSF1R	140	150	0.31	0.31	0.19
MAST2	113	121	0.25	0.25	0.17
CSNK1D	130	139	0.29	0.28	-0.27
EFNA1	95	101	0.21	0.21	-0.30
INSRR	116	124	0.25	0.25	-0.42
MLL4	107	114	0.23	0.23	-0.46
CDK7	110	117	0.24	0.24	-0.46
MAP2K5	99	105	0.22	0.21	-0.57
CDKL2	109	116	0.24	0.24	-0.69
STAT4	125	132	0.27	0.27	-0.84
EPM2A	11655	12384	25.49	25.27	-0.87
GRK1	122	129	0.27	0.26	-0.96
ROCK1	109	116	0.24	0.24	-0.99
PDGFRA	107	113	0.23	0.23	-1.03
GRK6	110	116	0.24	0.24	-1.04
PRKACA	98	104	0.21	0.21	-1.16
PRKAR2A	116	123	0.25	0.25	-1.36
CAMKV	95	101	0.21	0.21	-1.48
CAMKK2	146	155	0.32	0.32	-1.50
PAK3	111	118	0.24	0.24	-1.54
BUB1	124	131	0.27	0.27	-1.57
MAP4K5	159	167	0.35	0.34	-1.70
CAMK1D	203	214	0.44	0.44	-1.74
PRKAA2	144	152	0.31	0.31	-1.85
FES	106	111	0.23	0.23	-1.85
IKBKG	96	101	0.21	0.21	-2.03
RPS6KA2	130	136	0.28	0.28	-2.04
EPHA7	108	113	0.24	0.23	-2.24
PRKAA1	97	101	0.21	0.21	-2.36
IKBKB	687	718	1.50	1.46	-2.50
LRRK2	120	125	0.26	0.25	-2.68
ABL2	130	135	0.28	0.28	-2.87
EPHA4	118	123	0.26	0.25	-2.88
EIF2AK2	145	151	0.32	0.31	-2.95
EPB41	105	109	0.23	0.22	-3.15
CAMK2A	245	254	0.54	0.52	-3.21
PRKAG2	99	102	0.22	0.21	-3.24

FGFR4	132	136	0.29	0.28	-3.28
IRAK2	114	118	0.25	0.24	-3.44
EPHX1	133	137	0.29	0.28	-3.67
MAPK8	115	118	0.25	0.24	-4.00
TYK2	118	121	0.26	0.25	-4.06
PIM3	5658	5816	12.37	11.87	-4.10
PRKRA	110	113	0.24	0.23	-4.16
CDC25C	95	98	0.21	0.20	-4.26
STAT5B	128	131	0.28	0.27	-4.40
FGFR1	165	169	0.36	0.34	-4.44
MAP2K3	109	112	0.24	0.23	-4.57
ACVR1B	105	108	0.23	0.22	-4.64
KDR	169	172	0.37	0.35	-4.77
CDC25B	97	99	0.21	0.20	-4.78
FRAP1	106	108	0.23	0.22	-4.80
PRKAR1B	183	186	0.40	0.38	-4.83
ERBB2IP	121	123	0.26	0.25	-5.16
CAMK1G	131	133	0.29	0.27	-5.28
MASTL	197	200	0.43	0.41	-5.45
CDK5R1	138	140	0.30	0.28	-5.47
CSF2RA	159	161	0.35	0.33	-5.54
RPS6	108	109	0.24	0.22	-5.70
AHSA1	217	219	0.47	0.45	-5.92
LATS1	119	120	0.26	0.24	-5.92
GRAP2	112	113	0.24	0.23	-6.01
PRKRIR	113	113	0.25	0.23	-6.57
PRKACB	112	112	0.25	0.23	-7.26
EPHB6	280	278	0.61	0.57	-7.32
LCK	126	125	0.27	0.25	-7.33
ARG2	173	172	0.38	0.35	-7.34
PRKD3	123	122	0.27	0.25	-7.34
MAPK3	97	96	0.21	0.20	-7.35
GRK4	135	134	0.30	0.27	-7.74
MAPKAPK5	96	95	0.21	0.19	-8.01
PRKCD	150	148	0.33	0.30	-8.16
EPHB2	129	127	0.28	0.26	-8.27
MAPK4	104	102	0.23	0.21	-8.35
CDK6	104	102	0.23	0.21	-8.36
GRK7	131	129	0.29	0.26	-8.37
STAT6	215	211	0.47	0.43	-8.38
DYRK4	110	108	0.24	0.22	-8.40
MAP2K1IP1	102	100	0.22	0.20	-8.69
PRKCBP1	101	99	0.22	0.20	-9.17
IRAK1	142	139	0.31	0.28	-9.22
MYO9B	735	713	1.61	1.45	-9.52
MYLK2	126	122	0.27	0.25	-9.55
INS	112	109	0.25	0.22	-9.76
SGK	430	416	0.94	0.85	-9.89
EFNA3	110	106	0.24	0.22	-9.95
PA2G4	117	112	0.25	0.23	-10.31
STK11	178	170	0.39	0.35	-10.56
FLT3LG	140	134	0.31	0.27	-10.61
HIPK4	377	359	0.82	0.73	-11.21
BRAF	124	118	0.27	0.24	-11.35
CDK8	144	137	0.32	0.28	-11.56
AXL	117	111	0.26	0.23	-11.62
MAPK12	136	129	0.30	0.26	-11.64
MAPK6	208	197	0.45	0.40	-11.65
ILK	137	129	0.30	0.26	-12.16
EPB41L1	3620	3403	7.92	6.94	-12.31

CSF2	139	130	0.30	0.27	-12.32
SGK2	904	848	1.98	1.73	-12.44
YARS	127	119	0.28	0.24	-12.59
CDKL4	110	103	0.24	0.21	-12.64
MYLK	144	135	0.31	0.27	-12.86
DMPK	205	191	0.45	0.39	-13.08
PTK7	131	121	0.29	0.25	-13.26
SLPI	178	165	0.39	0.34	-13.45
ACTR1B	158	146	0.35	0.30	-13.88
PRKD2	137	125	0.30	0.26	-14.34
MLKL	132	121	0.29	0.25	-14.48
CDKL3	2415	2200	5.28	4.49	-15.03
HERC4	308	280	0.67	0.57	-15.05
LIMK1	123	111	0.27	0.23	-15.59
MAPK10	144	130	0.31	0.26	-15.91
EPB41L3	138	124	0.30	0.25	-15.96
RPS6KC1	128	114	0.28	0.23	-17.01
EPHB4	972	844	2.13	1.72	-18.96
FGFR1OP	176	153	0.39	0.31	-19.23
RNASEL	215	186	0.47	0.38	-19.30
FLT4	488	420	1.07	0.86	-19.80
NTRK2	169	143	0.37	0.29	-21.10
CAMK2D	393	331	0.86	0.67	-21.54
PRKCZ	333	280	0.73	0.57	-21.64
CSNK2A2	845	707	1.85	1.44	-21.98
SYK	171	141	0.37	0.29	-22.91
STAT5A	188	155	0.41	0.32	-23.30
CDC25A	306	251	0.67	0.51	-23.63
NTRK3	224	183	0.49	0.37	-23.99
BMPR2	249	199	0.54	0.41	-25.52
MAPK11	559	442	1.22	0.90	-26.34
GAPDH	325	256	0.71	0.52	-26.49
HIPK1	173	136	0.38	0.28	-26.64
PRKCABP	495	376	1.08	0.77	-29.14
FYN	571	426	1.25	0.87	-30.37
MAP3K15	824	596	1.80	1.22	-32.44
PRKG1	886	623	1.94	1.27	-34.42
EPB42	401	256	0.88	0.52	-40.46
CHEK1	1528	970	3.34	1.98	-40.77
BMPR1B	272	167	0.60	0.34	-42.73
PAK4	572	327	1.25	0.67	-46.73
ZAP70	662	311	1.45	0.63	-56.21
MAP3K5	752	344	1.64	0.70	-57.30
Beta-Actin	1356	560	2.96	1.14	-61.47
MAP3K4	1915	164	4.19	0.33	-92.03

(b)

Mean Signal	*634*	*1032*
Average of -ve Controls	411	490
2.5× -ve Control values	1028	1225

Protein List	Average Signal Value of 6 Replicates on the Array		Data Normalized to Mean Signal on the Array		% Change
	K562-Dox Control	K562-Dox 2 µM NIL #1	K562-Dox Control	K562-Dox 2 µM NIL #1	Control – 2 µM NIL #1 ÷ 2 µM NIL #1
Histone H2A.X(Ab-139)	*3348*	*13608*	5.28	13.19	149.69
cdc25C(Ab-216)	*1394*	*5559*	2.20	5.39	144.91
BRCA1(Ab-1423)	*5569*	*20714*	8.79	20.08	128.46
Src(Phospho-Tyr418)	*439*	*1363*	0.69	1.32	90.59
PTEN(Phospho-Ser380/Phospho-Thr382/Thr383)	*355*	*1056*	0.56	1.02	82.80
cdc25C(Phospho-Ser216)	*340*	*952*	0.54	0.92	71.93
Keratin 18(Ab-33)	*2405*	*6590*	3.79	6.39	68.34
Catenin beta (Ab-37)	*1734*	*4705*	2.74	4.56	66.64
HSP27(Phospho-Ser15)	*480*	*1298*	0.76	1.26	66.12
p27Kip1(Phospho-Thr187)	*601*	*1580*	0.95	1.53	61.41
NF kappa B-p65(Ab-254)	*805*	*2005*	1.27	1.94	53.10
Rac1/cdc42(Ab-71)	*443*	*1103*	0.70	1.07	52.92
c-Jun(Phospho-Ser243)	*475*	*1180*	0.75	1.14	52.77
Beta actin	*645*	*1575*	1.02	1.53	49.95
NF kappa B p100/p52(phospho Ser865)	*388*	*915*	0.61	0.89	44.76
Catenin beta (Phospho-Thr41/Phospho-Ser45)	*698*	*1583*	1.10	1.53	39.19
Met(Phospho-Tyr1349)	*177*	*397*	0.28	0.38	38.03
BAD(Phospho-Ser112)	*462*	*1014*	0.73	0.98	34.84
MEK1(Phospho-Ser221)	*776*	*1661*	1.22	1.61	31.59
p27Kip1(Ab-10)	*189*	*397*	0.30	0.38	28.91
STAT6(Phospho-Tyr641)	*366*	*765*	0.58	0.74	28.44
c-Kit(Phospho-Tyr721)	*4284*	*8896*	6.76	8.62	27.54
CaMKII (Phospho-Thr286)	*416*	*862*	0.66	0.84	27.33
p44/42 MAP Kinase(Phospho-Tyr204)	*595*	*1224*	0.94	1.19	26.38
STAT3(Phospho-Ser727)	*516*	*1054*	0.81	1.02	25.59
Integrin beta-3(Phospho-Tyr785)	*643*	*1268*	1.01	1.23	21.18
CDC2(Ab-15)	*355*	*694*	0.56	0.67	19.97
MEK1(Phospho-Thr291)	*699*	*1363*	1.10	1.32	19.67
BAD(Ab-155)	*209*	*397*	0.33	0.38	16.77
JAK1(Phospho-Tyr1022)	*401*	*762*	0.63	0.74	16.60
Trk B(Ab-515)	*397*	*751*	0.63	0.73	16.32
NF kappa B-p100/p52(Ab-869)	*581*	*1081*	0.92	1.05	14.26
STAT6(Ab-645)	*869*	*1609*	1.37	1.56	13.70
TYK2(Phospho-Tyr1054)	*275*	*509*	0.43	0.49	13.69
PDGF Receptor Beta(Ab-751)	*562*	*1035*	0.89	1.00	13.08
p53(Phospho-Ser315)	*525*	*961*	0.83	0.93	12.40
eEF2K(Ab-366)	*463*	*842*	0.73	0.82	11.62
p70 S6 Kinase (Phospho-Ser424)	*594*	*1071*	0.94	1.04	10.78
STAT5A (Phospho-Tyr694)	*438*	*788*	0.69	0.76	10.46
BAD(Ab-112)	*370*	*665*	0.58	0.64	10.34
Myc(Ab-358)	*514*	*921*	0.81	0.89	10.19
HSP90B(Ab-254)	*380*	*679*	0.60	0.66	9.73
GSK3-beta(Ab-9)	*276*	*490*	0.44	0.47	9.04
STAT5A (Phospho-Ser780)	*592*	*1050*	0.93	1.02	8.91
STAT5A (Ab-694)	*225*	*397*	0.35	0.38	8.62
JunB(Phospho-Ser79)	*485*	*855*	0.77	0.83	8.34
Myc(Ab-62)	*511*	*891*	0.81	0.86	7.19
HSP27(Ab-15)	*274*	*477*	0.43	0.46	7.00
NF kappa B-p100/p52(Ab-865)	*1430*	*2480*	2.26	2.40	6.57
GSK3-beta(Phospho-Ser9)	*401*	*694*	0.63	0.67	6.41
CrkII(Ab-221)	*515*	*889*	0.81	0.86	6.07
HSF1(Phospho-Ser303)	*468*	*808*	0.74	0.78	6.03
c-Kit(Ab-721)	*498*	*860*	0.79	0.83	6.00
Rac1/cdc42(Phospho-Ser71)	*803*	*1377*	1.27	1.33	5.40
FAK(Ab-861)	*374*	*642*	0.59	0.62	5.36
p21Cip1(Phospho-Thr145)	*341*	*584*	0.54	0.57	5.25
eIF4E(Ab-209)	*383*	*654*	0.60	0.63	5.03
JAK2(Phospho-Tyr1007)	*378*	*645*	0.60	0.62	4.83

Chk2(Phospho-Ser516)	538	915	0.85	0.89	4.45
MEK1(Phospho-Ser217)	478	807	0.75	0.78	3.81
Caveolin-1(Phospho-Tyr14)	235	397	0.37	0.38	3.77
Akt(Ab-308)	306	516	0.48	0.50	3.51
STAT4(Phospho-Tyr693)	323	544	0.51	0.53	3.47
mTOR(Ab-2448)	433	728	0.68	0.71	3.32
BCL-XL(Ab-62)	411	688	0.65	0.67	2.75
Shc(Ab-349)	377	630	0.59	0.61	2.64
I-kappa-B-epsilon(Ab-22)	345	577	0.54	0.56	2.64
BAD(Ab-136)	356	593	0.56	0.57	2.40
Tau(Phospho-Ser404)	509	841	0.80	0.82	1.61
BCL-2(Ab-70)	350	576	0.55	0.56	1.05
Estrogen Receptor-alpha (Phospho-Ser167)	997	1632	1.57	1.58	0.59
eIF2 alpha(Phospho-Ser51)	1093	1789	1.73	1.73	0.50
NF kappa B-p105/p50(Phospho-Ser932)	484	791	0.76	0.77	0.49
BRCA1(Ab-1524)	383	624	0.60	0.60	0.08
Chk1(Ab-345)	289	469	0.46	0.45	-0.30
VEGFR2(Phospho-Tyr951)	1104	1783	1.74	1.73	-0.79
FGF Receptor 1(Ab-154)	522	836	0.82	0.81	-1.67
4E-BP1(Ab-36)	309	494	0.49	0.48	-1.73
Myc(Phospho-Ser373)	398	637	0.63	0.62	-1.75
p27Kip1(Phospho-Ser10)	647	1032	1.02	1.00	-2.04
PDK1(Ab-241)	2131	3391	3.36	3.29	-2.24
BCL-2(Ab-56)	289	459	0.46	0.44	-2.39
JAK2(Ab-221)	297	471	0.47	0.46	-2.46
Estrogen Receptor-alpha (Ab-167)	434	688	0.69	0.67	-2.68
I-kappa-B-alpha(Phospho-Ser32/Phospho-Ser36)	782	1235	1.23	1.20	-3.05
AMPK1(Ab-174)	313	492	0.49	0.48	-3.44
I-kappa-B-alpha(Phospho-Tyr42)	701	1093	1.11	1.06	-4.24
c-Jun(Phospho-Ser73)	605	941	0.95	0.91	-4.42
CREB(Phospho-Ser133)	350	544	0.55	0.53	-4.54
FKHR(Ab-256)	549	850	0.87	0.82	-4.87
Myc(Phospho-Thr358)	496	766	0.78	0.74	-5.11
IKK alpha(Phospho-Thr23)	997	1538	1.57	1.49	-5.18
NF kappa B-p105/p50(Ab-907)	337	520	0.53	0.50	-5.22
JunD(Phospho-Ser255)	805	1242	1.27	1.20	-5.29
NF kappa B-p100/p52(Phospho-Ser869)	384	590	0.61	0.57	-5.62
BRCA1(Phospho-Ser1524)	523	802	0.82	0.78	-5.70
HER2(Ab-877)	383	587	0.60	0.57	-5.82
NF kappa B-p105/p50(Ab-337)	260	397	0.41	0.38	-6.21
EGFR(Phospho-Tyr1110)	765	1162	1.21	1.13	-6.73
MSK1(Phospho-Ser376)	755	1145	1.19	1.11	-6.83
Akt(Phospho-Thr308)	526	794	0.83	0.77	-7.27
NF kappa B-p105/p50(Ab-893)	311	469	0.49	0.45	-7.54
HSP27(Ab-78)	264	397	0.42	0.38	-7.63
HDAC8(Phospho-Ser39)	927	1394	1.46	1.35	-7.68
NF kappa B-p65(Ab-529)	315	473	0.50	0.46	-7.90
Histone H2A.X(Phospho-Ser139)	1259	1886	1.99	1.83	-7.97
NF kappa B-p105/p50(Phospho-Ser893)	734	1095	1.16	1.06	-8.35
Elk-1(Phospho-Ser383)	648	966	1.02	0.94	-8.39
CREB(Ab-133)	280	414	0.44	0.40	-8.98
Akt(Ab-473)	385	570	0.61	0.55	-9.06
SHP-2(Ab-580)	405	599	0.64	0.58	-9.24
FKHR(Phospho-Ser256)	665	979	1.05	0.95	-9.52
ICAM-1(Phospho-Tyr512)	724	1066	1.14	1.03	-9.53
PTEN(Ab-380/382/383)	399	584	0.63	0.57	-10.08
FAK(Ab-925)	272	397	0.43	0.38	-10.29
JAK2(Phospho-Tyr221)	496	722	0.78	0.70	-10.62
NF kappa B-p105/p50(Phospho-Ser907)	443	644	0.70	0.62	-10.71
STAT3(Phospho-Tyr705)	704	1024	1.11	0.99	-10.73
JAK2(Ab-1007)	303	439	0.48	0.42	-11.16
NF kappa B-p65(Phospho-Thr254)	441	638	0.70	0.62	-11.25
JunB(Phospho-Ser259)	593	854	0.94	0.83	-11.57
Myc(Phospho-Thr58)	935	1345	1.48	1.30	-11.69
p70 S6 Kinase (Ab-424)	471	675	0.74	0.65	-11.89

Raf1(Ab-259)	551	790	0.87	0.77	-11.95
STAT1(Ab-701)	279	397	0.44	0.38	-12.44
Chk1(Phospho-Ser345)	326	464	0.51	0.45	-12.59
P38 MAPK(Phospho-Tyr182)	959	1363	1.51	1.32	-12.72
HSF1(Ab-303)	334	474	0.53	0.46	-12.76
cdc25A (Phospho-Ser75)	692	978	1.09	0.95	-13.24
I-kappa-B-epsilon(Phospho-Ser22)	541	763	0.85	0.74	-13.33
JAK1(Ab-1022)	401	565	0.63	0.55	-13.41
MEK1(Ab-291)	331	463	0.52	0.45	-14.13
P38 MAPK(Ab-182)	307	428	0.48	0.42	-14.21
Rel(Ab-503)	740	1030	1.17	1.00	-14.47
Integrin beta-3(Ab-785)	517	719	0.82	0.70	-14.58
c-Jun(Ab-73)	4801	6670	7.58	6.46	-14.66
STAT6(Phospho-Thr645)	818	1134	1.29	1.10	-14.77
BCL-XL(Phospho-Ser62)	417	578	0.66	0.56	-14.97
Rb(Phospho-Ser780)	288	397	0.45	0.38	-15.18
Raf1(Phospho-Ser259)	688	948	1.09	0.92	-15.40
JunD(Ab-255)	292	397	0.46	0.38	-16.58
c-Jun(Phospho-Thr239)	330	448	0.52	0.43	-16.59
Met(Ab-1349)	1008	1368	1.59	1.33	-16.59
Src(Ab-418)	451	610	0.71	0.59	-16.95
Src(Phospho-Tyr529)	720	970	1.14	0.94	-17.25
ICAM-1(Ab-512)	295	397	0.47	0.38	-17.29
Rel(Phospho-Ser503)	472	635	0.74	0.62	-17.32
HSP90B(Phospho-Ser254)	438	588	0.69	0.57	-17.63
JunB(Ab-79)	297	397	0.47	0.38	-17.80
Pyk2(Ab-402)	566	755	0.89	0.73	-17.98
STAT1(Phospho-Ser727)	716	956	1.13	0.93	-18.03
Chk1(Ab-280)	298	398	0.47	0.39	-18.07
FAK(Phospho-Tyr925)	341	453	0.54	0.44	-18.34
Akt(Phospho-Ser473)	334	443	0.53	0.43	-18.51
MKK3(Phospho-Ser189)	387	512	0.61	0.50	-18.68
HER2(Phospho-Tyr877)	844	1115	1.33	1.08	-18.86
BCL-2(Phospho-Ser70)	1074	1412	1.70	1.37	-19.26
STAT4(Ab-693)	318	415	0.50	0.40	-19.85
STAT1(Phospho-Tyr701)	626	815	0.99	0.79	-19.98
TYK2(Ab-1054)	446	579	0.70	0.56	-20.15
FAK(Phospho-Tyr861)	839	1087	1.32	1.05	-20.40
BCL-2(Phospho-Thr56)	389	503	0.61	0.49	-20.55
STAT3(Ab-705)	321	415	0.51	0.40	-20.57
Myc(Ab-373)	394	509	0.62	0.49	-20.67
GSK3-alpha(Phospho-Ser21)	733	945	1.16	0.92	-20.83
EGFR(Ab-1110)	371	478	0.59	0.46	-20.91
MSK1(Ab-376)	384	493	0.61	0.48	-21.29
SAPK/JNK(Phospho-Thr183)	957	1221	1.51	1.18	-21.59
BAD(Phospho-Ser136)	1141	1456	1.80	1.41	-21.61
c-Jun(Ab-239)	361	459	0.57	0.45	-21.76
MKK3(Ab-189)	389	496	0.61	0.48	-21.79
STAT3(Ab-727)	386	491	0.61	0.48	-21.95
Chk2(Ab-68)	343	436	0.54	0.42	-22.00
PDK1(Phospho-Ser241)	457	579	0.72	0.56	-22.11
I-kappa-B-alpha(Ab-32/36)	464	588	0.73	0.57	-22.12
MEK-2(Ab-394)	769	974	1.21	0.94	-22.20
SAPK/JNK(Ab-183)	391	495	0.62	0.48	-22.33
Chk2(Phospho-Thr68)	390	492	0.61	0.48	-22.46
FAK(Ab-397)	612	765	0.97	0.74	-23.24
CDC2(Phospho-Tyr15)	628	781	0.99	0.76	-23.64
IGF-1R (Phospho-Tyr1161)	592	731	0.93	0.71	-24.18
Chk1(Ab-317)	396	489	0.62	0.47	-24.18
Keratin 18(Phospho-Ser33)	323	397	0.51	0.38	-24.46
Integrin beta-3(Phospho-Tyr773)	762	935	1.20	0.91	-24.62
Caveolin-1(Ab-14)	335	408	0.53	0.39	-25.17
p53(Phospho-Ser6)	959	1165	1.51	1.13	-25.40
BAD(Phospho-Ser155)	902	1094	1.42	1.06	-25.52
Myc(Ab-58)	424	514	0.67	0.50	-25.54

HDAC8(Ab-39)	388	468	0.61	0.45	-25.88
P38 MAPK(Phospho-Thr180)	695	836	1.10	0.81	-26.12
HSP27(Phospho-Ser78)	859	1027	1.36	1.00	-26.54
I-kappa-B-alpha(Ab-42)	463	548	0.73	0.53	-27.22
STAT1(Ab-727)	555	656	0.88	0.64	-27.34
Chk1(Phospho-Ser280)	592	700	0.93	0.68	-27.37
MEK-2(Phospho-Thr394)	748	882	1.18	0.85	-27.52
IGF-1R (Ab-1161)	472	552	0.74	0.53	-28.13
14-3-3 Zeta(Ab-58)	825	965	1.30	0.93	-28.19
Catenin beta (Phospho-Ser33)	542	631	0.85	0.61	-28.50
FGF Receptor 1(Phospho-Tyr154)	605	703	0.95	0.68	-28.58
Chk1(Phospho-Ser317)	828	953	1.31	0.92	-29.26
BRCA1(Phospho-Ser1423)	1027	1177	1.62	1.14	-29.61
p44/42 MAP Kinase(Phospho-Thr202)	577	661	0.91	0.64	-29.67
MEK1(Ab-221)	501	568	0.79	0.55	-30.47
eIF4E(Phospho-Ser209)	532	601	0.84	0.58	-30.69
p44/42 MAP Kinase(Ab-204)	405	456	0.64	0.44	-30.81
p21Cip1(Ab-145)	462	518	0.73	0.50	-31.08
MEK1(Ab-217)	551	614	0.87	0.60	-31.56
GSK3-alpha(Ab-21)	456	508	0.72	0.49	-31.57
STAT6(Ab-641)	392	436	0.62	0.42	-31.59
AMPK1(Phospho-Thr174)	473	525	0.75	0.51	-31.82
ATM(Ab-1981)	358	397	0.57	0.38	-31.95
CaMKII (Ab-286)	797	881	1.26	0.85	-32.10
Akt2(Phospho-Ser474)	928	1011	1.46	0.98	-33.05
VEGFR2(Ab-951)	1239	1350	1.96	1.31	-33.06
IKK alpha(Ab-23)	751	818	1.18	0.79	-33.11
STAT5A (Ab-780)	591	637	0.93	0.62	-33.77
CrkII(Phospho-Tyr221)	1099	1177	1.73	1.14	-34.24
CDK2(Ab-160)	505	537	0.80	0.52	-34.64
14-3-3 Zeta(Phospho-Ser58)	443	470	0.70	0.46	-34.88
NF kappa B-p65(Phospho-Ser529)	586	620	0.92	0.60	-35.00
p53(Ab-6)	384	400	0.61	0.39	-35.99
p53(Ab-315)	402	418	0.63	0.41	-36.08
Elk-1(Ab-383)	627	645	0.99	0.62	-36.83
Myc(Phospho-Ser62)	481	495	0.76	0.48	-36.90
4E-BP1(Phospho-Thr36)	801	822	1.26	0.80	-36.91
eEF2K(Phospho-Ser366)	790	810	1.25	0.78	-37.02
Rb(Ab-780)	710	723	1.12	0.70	-37.45
Shc(Phospho-Tyr349)	805	817	1.27	0.79	-37.63
p27Kip1(Ab-187)	470	474	0.74	0.46	-38.12
eIF2 alpha(Ab-51)	530	525	0.84	0.51	-39.21
p44/42 MAP Kinase(Ab-202)	471	464	0.74	0.45	-39.55
PDGF Receptor beta(Phospho-Tyr751)	788	764	1.24	0.74	-40.43
Chk2(Ab-516)	730	706	1.15	0.68	-40.58
Catenin beta (Phospho-Ser37)	625	602	0.99	0.58	-40.81
CDK2(Phospho-Thr160)	567	539	0.89	0.52	-41.57
Smad3(Phospho-Ser425)	444	420	0.70	0.41	-41.85
JunB(Ab-259)	482	455	0.76	0.44	-42.02
c-Jun(Ab-243)	555	519	0.87	0.50	-42.55
Tau(Ab-404)	534	497	0.84	0.48	-42.85
Pyk2(Phospho-Tyr402)	595	551	0.94	0.53	-43.15
I-kappa-B-beta(Phospho-Ser23)	685	622	1.08	0.60	-44.25
Akt2(Ab-474)	594	497	0.94	0.48	-48.59
Src(Ab-529)	1064	877	1.68	0.85	-49.40
mTOR(Phospho-Ser2448)	767	584	1.21	0.57	-53.23
cdc25A (Ab-75)	747	545	1.18	0.53	-55.20
GAPDH	796	574	1.26	0.56	-55.68
Trk B(Phospho-Tyr515)	904	638	1.43	0.62	-56.70
SHP-2(Phospho-Tyr580)	728	478	1.15	0.46	-59.66
Catenin beta (Ab-41/45)	809	466	1.28	0.45	-64.63
Integrin beta-3(Ab-773)	1007	458	1.59	0.44	-0.72

(c)

Mean Signal	*457*	*607*
Average of -ve Controls	*82*	*115*
2.5x -ve Control values	205	288

Protein List	Average Signal Value of 6 Replicates on the Array		Data Normalized to Mean Signal on the Array		% Change
	K562-Dox Control	K562-Dox 2 µM NIL #2	K562-Dox Control	K562-Dox 2 µM NIL #2	Control – 2 µM NIL #2 ÷ 2 µM NIL #2
CHEK2	*1004*	*2720*	2.20	4.48	104.17
STAT5B	*128*	*339*	0.28	0.56	99.40
PDGFRB	*580*	*1522*	1.27	2.51	97.57
HIPK4	*377*	*810*	0.82	1.33	61.90
DMPK	*205*	*437*	0.45	0.72	60.69
EPB42	*401*	*782*	0.88	1.29	47.00
IGFBP6	*88*	*166*	0.19	0.27	42.28
PLK1	*74*	*136*	0.16	0.22	38.17
RPS6KB2	*598*	*1096*	1.31	1.81	38.10
TGFB1	*463*	*843*	1.01	1.39	37.12
EPHA6	*95*	*168*	0.21	0.28	33.12
TYRO3	*9578*	*16732*	20.95	27.57	31.63
BMPR2	*249*	*414*	0.54	0.68	25.37
TGFB1I1	*2847*	*4732*	6.23	7.80	25.25
RPS6KB1	*100*	*165*	0.22	0.27	24.74
LIMK2	*144*	*239*	0.32	0.39	24.60
DYRK1B	*160*	*265*	0.35	0.44	24.46
IKBKAP	*82*	*134*	0.18	0.22	23.54
IRAK3	*126*	*201*	0.28	0.33	19.59
EPHB3	*3952*	*6175*	8.64	10.18	17.73
MERTK	*87*	*136*	0.19	0.22	17.48
STAT1	*6342*	*9800*	13.87	16.15	16.43
CAMK4	*80*	*123*	0.17	0.20	16.41
PRKX	*95*	*146*	0.21	0.24	15.74
CSNK2A2	*845*	*1292*	1.85	2.13	15.16
SGK	*430*	*657*	0.94	1.08	15.00
WNK3	*113*	*172*	0.25	0.28	14.92
DYRK3	*80*	*122*	0.17	0.20	14.84
ILKAP	*118*	*179*	0.26	0.29	14.46
PRKAB1	*114*	*173*	0.25	0.29	14.40
CSNK1E	*7958*	*12015*	17.40	19.80	13.76
MAP3K15	*824*	*1219*	1.80	2.01	11.57
ERBB2	*111*	*162*	0.24	0.27	10.70
MAP3K7IP1	*98*	*144*	0.21	0.24	10.46
JAK3	*174*	*254*	0.38	0.42	9.96
SRC	*1039*	*1510*	2.27	2.49	9.53
DYRK2	*120*	*174*	0.26	0.29	9.15
AKT2	*99*	*143*	0.22	0.24	8.97
IKBKB	*687*	*993*	1.50	1.64	8.89
MAP2K1	*182*	*261*	0.40	0.43	8.36
ANK1	*91*	*131*	0.20	0.22	8.27
FLT3	*318*	*456*	0.70	0.75	7.82
PRKCI	*87*	*124*	0.19	0.20	7.69
MAP3K11	*116*	*165*	0.25	0.27	7.07
PIM3	*5658*	*8033*	12.37	13.24	6.98
EPM2A	*11655*	*16529*	25.49	27.24	6.87
CDC2L2	*196*	*278*	0.43	0.46	6.78
PLK4	*97*	*137*	0.21	0.23	6.55
PTK9	*122*	*173*	0.27	0.28	6.35
PAK2	*88*	*123*	0.19	0.20	5.52
PRKAB2	*221*	*309*	0.48	0.51	5.24
CDKL1	*119*	*164*	0.26	0.27	4.10
FGFR2	*290*	*400*	0.63	0.66	4.04

CDC2	108	149	0.24	0.24	3.93
MAPK1	94	129	0.20	0.21	3.77
CDK9	276	380	0.60	0.63	3.73
PRKAR2A	116	160	0.25	0.26	3.63
HERC3	97	133	0.21	0.22	3.46
PIM1	92	126	0.20	0.21	3.39
CDK5RAP3	111	153	0.24	0.25	3.33
MAP4K4	131	180	0.29	0.30	3.08
FGFR4	132	180	0.29	0.30	3.05
EPHA5	110	150	0.24	0.25	2.82
MAP2K6	192	262	0.42	0.43	2.78
CAMKK1	102	139	0.22	0.23	2.61
CDK5R1	138	187	0.30	0.31	2.44
RET	220	298	0.48	0.49	1.95
PRKACG	104	140	0.23	0.23	1.39
EGFR	207	278	0.45	0.46	1.36
RNASEH1	117	157	0.26	0.26	1.08
RAF1	121	163	0.26	0.27	1.06
MAPK9	103	138	0.23	0.23	0.96
IRAK4	111	149	0.24	0.24	0.81
RNASEH2A	103	138	0.23	0.23	0.75
ROR1	106	141	0.23	0.23	0.71
ANP32A	459	611	1.00	1.01	0.22
IKBKE	95	125	0.21	0.21	-1.33
PRKCSH	98	128	0.21	0.21	-1.34
RPS6	108	141	0.24	0.23	-1.36
AKT1	125	164	0.27	0.27	-1.50
TEK	220	287	0.48	0.47	-1.64
MYO7A	99	129	0.22	0.21	-1.69
FRAP1	106	139	0.23	0.23	-1.70
PTK6	109	142	0.24	0.23	-1.87
CDK3	113	148	0.25	0.24	-1.93
DYRK1A	133	173	0.29	0.29	-1.99
PAK1	98	127	0.21	0.21	-2.06
INSRR	116	151	0.25	0.25	-2.16
MAP3K7	90	116	0.20	0.19	-2.66
TIE1	102	132	0.22	0.22	-2.77
STAT2	103	133	0.23	0.22	-2.82
SGK3	98	126	0.21	0.21	-2.86
CDK5	111	143	0.24	0.23	-2.97
FLT1	120	154	0.26	0.25	-3.00
MAP2K5	99	127	0.22	0.21	-3.17
EPHB6	280	360	0.61	0.59	-3.22
MAPKAPK2	125	161	0.27	0.27	-3.31
CSNK1G1	132	169	0.29	0.28	-3.34
MAPK8	115	147	0.25	0.24	-3.40
FGFRL1	83	106	0.18	0.17	-3.64
NEK2	97	124	0.21	0.20	-3.71
EPHB2	129	165	0.28	0.27	-3.75
TYK2	118	150	0.26	0.25	-3.94
CAMK2B	102	129	0.22	0.21	-4.14
CAMK1	110	140	0.24	0.23	-4.18
PTK2B	99	125	0.22	0.21	-4.25
FGR	118	150	0.26	0.25	-4.26
MAST2	113	144	0.25	0.24	-4.31
ROCK2	203	257	0.44	0.42	-4.46
BUB1B	115	145	0.25	0.24	-4.50
MAP3K3	598	757	1.31	1.25	-4.61
STAT3	112	142	0.25	0.23	-4.64
EPHB1	127	159	0.28	0.26	-5.09

RPS6KA2	130	153	0.28	0.25	-11.11
PRKCBP1	101	119	0.22	0.20	-11.12
MAP3K1	233	274	0.51	0.45	-11.21
PRKCA	116	136	0.25	0.22	-11.44
PRKCD	150	176	0.33	0.29	-11.49
CSF1R	140	164	0.31	0.27	-11.52
MYO9B	735	863	1.61	1.42	-11.53
RNMT	108	127	0.24	0.21	-11.53
DYRK4	110	129	0.24	0.21	-11.54
MST1R	123	144	0.27	0.24	-11.66
IRAK1	142	166	0.31	0.27	-12.03
GRK5	130	151	0.28	0.25	-12.04
RPS6KC1	128	150	0.28	0.25	-12.22
IGFBP1	93	109	0.20	0.18	-12.27
MUSK	3971	4621	8.68	7.61	-12.31
PRKD2	137	159	0.30	0.26	-12.32
CAMK1G	131	152	0.29	0.25	-12.33
EPB41L1	3620	4206	7.92	6.93	-12.46
ILK	137	159	0.30	0.26	-12.53
CDC25B	97	112	0.21	0.18	-12.70
EPHA4	118	136	0.26	0.22	-12.82
BMPR1A	219	254	0.48	0.42	-12.91
CSNK2A1	115	133	0.25	0.22	-12.95
FES	106	122	0.23	0.20	-13.00
PA2G4	117	135	0.25	0.22	-13.01
GAPDH	325	375	0.71	0.62	-13.08
EIF2AK2	145	167	0.32	0.27	-13.10
CDK7	110	126	0.24	0.21	-13.41
PTK2	91	105	0.20	0.17	-13.51
CSF2RA	159	183	0.35	0.30	-13.52
MLL4	107	122	0.23	0.20	-13.85
MAPK3	97	110	0.21	0.18	-13.98
CDKL5	95	108	0.21	0.18	-14.02
CDK6	104	118	0.23	0.19	-14.11
GRK7	131	150	0.29	0.25	-14.13
LATS1	119	135	0.26	0.22	-14.26
EPHX1	133	151	0.29	0.25	-14.36
ABL2	130	147	0.28	0.24	-14.48
CDK8	144	164	0.32	0.27	-14.54
MAPKAPK3	116	132	0.25	0.22	-14.58
STAT6	215	243	0.47	0.40	-14.70
ACVR1B	105	119	0.23	0.20	-14.99
LRRK2	120	135	0.26	0.22	-15.20
CDKL2	109	122	0.24	0.20	-15.27
ARG2	173	195	0.38	0.32	-15.29
ROCK1	109	122	0.24	0.20	-15.30
STAT5A	188	212	0.41	0.35	-15.31
PRKRA	110	123	0.24	0.20	-15.50
CDKL4	110	124	0.24	0.20	-15.53
MAP2K3	109	122	0.24	0.20	-15.55
MAPK4	104	117	0.23	0.19	-15.59
ERBB2IP	121	135	0.26	0.22	-15.70
BRAF	124	138	0.27	0.23	-15.94
MAP2K1IP1	102	114	0.22	0.19	-16.02
PTK9L	110	122	0.24	0.20	-16.18
EFNA5	7509	8350	16.42	13.76	-16.21
PTK7	131	145	0.29	0.24	-16.37
MAPK12	136	150	0.30	0.25	-16.69
FGFR1	165	182	0.36	0.30	-16.79
PRKACB	112	123	0.25	0.20	-17.48

YARS	127	139	0.28	0.23	-17.62
EFNA3	110	120	0.24	0.20	-17.81
PDGFRA	107	117	0.23	0.19	-17.83
FGFR1OP	176	192	0.39	0.32	-18.10
CAMK1D	203	221	0.44	0.36	-18.29
LCK	126	136	0.27	0.22	-18.45
ROR2	265	286	0.58	0.47	-18.82
FLT3LG	140	150	0.31	0.25	-19.07
AHSA1	217	233	0.47	0.38	-19.33
CAMK2A	245	262	0.54	0.43	-19.37
MLKL	132	141	0.29	0.23	-19.70
MYLK2	126	134	0.27	0.22	-19.85
MAPK6	208	221	0.45	0.36	-20.06
MAPK10	144	151	0.31	0.25	-20.63
AXL	117	123	0.26	0.20	-20.90
MYLK	144	150	0.31	0.25	-21.60
Beta-Actin	1356	1402	2.96	2.31	-22.06
CSF2	139	143	0.30	0.24	-22.11
SAB	626	646	1.37	1.06	-22.22
SLPI	178	183	0.39	0.30	-22.53
PRKAR1B	183	186	0.40	0.31	-23.07
LIMK1	123	125	0.27	0.21	-23.11
CDKL3	2415	2438	5.28	4.02	-23.95
EPHB4	972	978	2.13	1.61	-24.17
NTRK2	169	169	0.37	0.28	-24.43
RNASEL	215	210	0.47	0.35	-26.34
PRKG1	886	864	1.94	1.42	-26.49
PRKCABP	495	482	1.08	0.79	-26.55
CAMK2D	393	382	0.86	0.63	-26.89
HIPK1	173	168	0.38	0.28	-27.11
HERC4	308	295	0.67	0.49	-27.75
SYK	171	163	0.37	0.27	-28.25
FYN	571	541	1.25	0.89	-28.63
NTRK3	224	212	0.49	0.35	-28.69
EPB41L3	138	130	0.30	0.21	-29.20
SGK2	904	829	1.98	1.37	-30.86
FLT4	488	444	1.07	0.73	-31.54
CDC25A	306	278	0.67	0.46	-31.54
MASTL	197	172	0.43	0.28	-34.27
PRKCZ	333	246	0.73	0.41	-44.40
BMPR1B	272	188	0.60	0.31	-47.89
MAP3K5	752	462	1.64	0.76	-53.67
PAK4	572	343	1.25	0.56	-54.91
ZAP70	662	286	1.45	0.47	-67.46
MAP3K4	1915	208	4.19	0.34	-91.80

(d)

Mean Signal	*634*	*1102*
Average of -ve Controls	411	443
2.5x -ve Control values	1028	1108

Protein List	Average Signal Value of 6 Replicates on the Array		Data Normalized to Mean Signal on the Array		% Change
	K562-Dox Control	K562-Dox 2 µM NIL #2	K562-Dox Control	K562-Dox 2 µM NIL #2	Control – 2 µM NIL #2 ÷ 2 µM NIL #2
PTEN(Phospho-Ser380/Phospho-Thr382/Thr383)	*355*	*1092*	0.56	0.99	77.00
CaMKII (Phospho-Thr286)	*416*	*1260*	0.66	1.14	74.14
p44/42 MAP Kinase(Phospho-Tyr204)	*595*	*1742*	0.94	1.58	68.38
NF kappa B-p105/p50(Ab-907)	*337*	*951*	0.53	0.86	62.33
I-kappa-B-epsilon(Phospho-Ser22)	*541*	*1461*	0.85	1.33	55.23
JAK2(Phospho-Tyr1007)	*378*	*980*	0.60	0.89	49.05
HSP27(Ab-15)	*274*	*694*	0.43	0.63	45.76
Rb(Phospho-Ser780)	*288*	*726*	0.45	0.66	45.20
HER2(Ab-877)	*383*	*960*	0.60	0.87	44.20
STAT6(Phospho-Tyr641)	*366*	*913*	0.58	0.83	43.39
CDK2(Ab-160)	*505*	*1249*	0.80	1.13	42.32
HSF1(Phospho-Ser303)	*468*	*1151*	0.74	1.04	41.37
Estrogen Receptor-alpha (Ab-167)	*434*	*1068*	0.69	0.97	41.31
CDC2(Ab-15)	*355*	*857*	0.56	0.78	38.59
p21Cip1(Ab-145)	*462*	*1109*	0.73	1.01	38.13
Myc(Ab-62)	*511*	*1225*	0.81	1.11	37.86
p27Kip1(Phospho-Thr187)	*601*	*1442*	0.95	1.31	37.85
eEF2K(Ab-366)	*463*	*1107*	0.73	1.00	37.35
JAK2(Phospho-Tyr221)	*496*	*1184*	0.78	1.07	37.25
CREB(Phospho-Ser133)	*350*	*833*	0.55	0.76	36.85
HDAC8(Ab-39)	*388*	*921*	0.61	0.84	36.56
p21Cip1(Phospho-Thr145)	*341*	*810*	0.54	0.73	36.56
FAK(Ab-861)	*374*	*880*	0.59	0.80	35.25
Raf1(Ab-259)	*551*	*1295*	0.87	1.17	35.03
TYK2(Phospho-Tyr1054)	*275*	*641*	0.43	0.58	33.89
p53(Ab-315)	*402*	*932*	0.63	0.85	33.28
Myc(Ab-58)	*424*	*980*	0.67	0.89	32.91
p70 S6 Kinase (Phospho-Ser424)	*594*	*1371*	0.94	1.24	32.74
Shc(Ab-349)	*377*	*870*	0.59	0.79	32.71
Histone H2A.X(Ab-139)	*3348*	*7582*	5.28	6.88	30.19
Rb(Ab-780)	*710*	*1606*	1.12	1.46	30.03
mTOR(Ab-2448)	*433*	*978*	0.68	0.89	29.97
Chk1(Ab-345)	*289*	*652*	0.46	0.59	29.70
FGF Receptor 1(Ab-154)	*522*	*1167*	0.82	1.06	28.55
BAD(Phospho-Ser112)	*462*	*1028*	0.73	0.93	27.93
STAT5A (Ab-780)	*591*	*1310*	0.93	1.19	27.50
c-Kit(Ab-721)	*490*	*1102*	0.79	1.00	27.20
Src(Ab-418)	*451*	*998*	0.71	0.90	27.10
JunB(Ab-259)	*482*	*1065*	0.76	0.97	27.02
Chk1(Ab-317)	*396*	*873*	0.62	0.79	26.78
ATM(Ab-1981)	*358*	*789*	0.57	0.72	26.52
P38 MAPK(Ab-182)	*307*	*671*	0.48	0.61	25.78
CrkII(Ab-221)	*515*	*1125*	0.81	1.02	25.64
BRCA1(Ab-1423)	*5569*	*12145*	8.79	11.02	25.35
p70 S6 Kinase (Ab-424)	*471*	*1026*	0.74	0.93	25.33
Trk B(Ab-515)	*397*	*863*	0.63	0.78	25.04
AMPK1(Phospho-Thr174)	*473*	*1027*	0.75	0.93	24.94
c-Jun(Ab-243)	*555*	*1201*	0.87	1.09	24.47
STAT5A (Phospho-Tyr694)	*438*	*948*	0.69	0.86	24.44
4E-BP1(Ab-36)	*309*	*667*	0.49	0.60	24.19
SHP-2(Ab-580)	*405*	*871*	0.64	0.79	23.60
Myc(Ab-373)	*394*	*847*	0.62	0.77	23.56
Tau(Ab-404)	*534*	*1141*	0.84	1.03	22.76
HSF1(Ab-303)	*334*	*711*	0.53	0.64	22.38
BAD(Ab-112)	*370*	*786*	0.58	0.71	22.14
GSK3-beta(Phospho-Ser9)	*401*	*850*	0.63	0.77	22.03
MSK1(Ab-376)	*384*	*812*	0.61	0.74	21.48
JAK2(Ab-221)	*297*	*625*	0.47	0.57	21.18

CDC2(Phospho-Tyr15)	628	1324	0.99	1.20	21.15
NF kappa B-p65(Ab-529)	315	663	0.50	0.60	20.81
Akt(Ab-308)	306	643	0.48	0.58	20.80
I-kappa-B-alpha(Ab-42)	463	970	0.73	0.88	20.59
c-Jun(Ab-239)	361	756	0.57	0.69	20.53
eIF4E(Ab-209)	383	802	0.60	0.73	20.45
PDGF Receptor Beta(Ab-751)	562	1176	0.89	1.07	20.32
eIF4E(Phospho-Ser209)	532	1107	0.84	1.00	19.56
cdc25C(Phospho-Ser216)	340	700	0.54	0.63	18.27
MKK3(Ab-189)	389	801	0.61	0.73	18.25
Catenin beta (Phospho-Ser33)	542	1112	0.85	1.01	18.03
I-kappa-B-epsilon(Ab-22)	345	708	0.54	0.64	18.00
MKK3(Phospho-Ser189)	387	794	0.61	0.72	17.99
Akt(Ab-473)	385	786	0.61	0.71	17.39
NF kappa B-p65(Ab-254)	805	1637	1.27	1.48	16.97
BCL-XL(Phospho-Ser62)	417	849	0.66	0.77	16.97
Chk2(Phospho-Ser516)	538	1091	0.85	0.99	16.50
NF kappa B-p105/p50(Ab-893)	311	627	0.49	0.57	15.80
Chk1(Ab-280)	298	600	0.47	0.54	15.74
JAK1(Ab-1022)	401	805	0.63	0.73	15.55
Keratin 18(Phospho-Ser33)	323	648	0.51	0.59	15.30
PTEN(Ab-380/382/383)	399	798	0.63	0.72	15.07
MEK1(Ab-217)	551	1099	0.87	1.00	14.59
TYK2(Ab-1054)	446	887	0.70	0.80	14.39
Rac1/cdc42(Ab-71)	443	879	0.70	0.80	14.04
Integrin beta-3(Ab-785)	517	1022	0.82	0.93	13.66
eEF2K(Phospho-Ser366)	790	1561	1.25	1.42	13.65
FAK(Ab-925)	272	537	0.43	0.49	13.56
Rel(Ab-503)	740	1461	1.17	1.33	13.56
FAK(Ab-397)	612	1208	0.97	1.10	13.48
BCL-2(Ab-70)	350	690	0.55	0.63	13.36
Pyk2(Ab-402)	566	1115	0.89	1.01	13.29
Caveolin-1(Ab-14)	335	659	0.53	0.60	13.22
FKHR(Ab-256)	549	1079	0.87	0.98	13.10
Catenin beta (Ab-41/45)	809	1588	1.28	1.44	12.79
BRCA1(Ab-1524)	383	748	0.60	0.68	12.39
EGFR(Phospho-Tyr1110)	765	1495	1.21	1.36	12.28
p27Kip1(Ab-187)	470	917	0.74	0.83	12.10
Integrin beta-3(Phospho-Tyr785)	643	1252	1.01	1.14	11.95
Keratin 18(Ab-33)	2405	4648	3.79	4.22	11.12
JAK1(Phospho-Tyr1022)	401	775	0.63	0.70	10.94
AMPK1(Ab-174)	313	603	0.49	0.55	10.80
cdc25A (Phospho-Ser75)	692	1331	1.09	1.21	10.54
HSP90B(Phospho-Ser254)	438	841	0.69	0.76	10.34
BCL-XL(Ab-62)	411	785	0.65	0.71	9.84
Chk1(Phospho-Ser280)	592	1130	0.93	1.02	9.68
GSK3-beta(Ab-9)	276	525	0.44	0.48	9.48
MEK1(Phospho-Ser221)	776	1472	1.22	1.34	9.13
Pyk2(Phospho-Tyr402)	595	1127	0.94	1.02	8.87
STAT3(Ab-727)	386	730	0.61	0.66	8.60
JunB(Ab-79)	297	559	0.47	0.51	8.22
Akt2(Ab-474)	594	1117	0.94	1.01	8.16
STAT1(Phospho-Ser727)	716	1335	1.13	1.21	7.19
Elk-1(Phospho-Ser383)	648	1198	1.02	1.09	6.32
JunD(Ab-255)	292	540	0.46	0.49	6.09
NF kappa B-p65(Phospho-Ser529)	586	1080	0.92	0.98	5.92
STAT3(Ab-705)	321	590	0.51	0.54	5.60
IGF-1R (Phospho-Tyr1161)	592	1088	0.93	0.99	5.57
Myc(Phospho-Ser62)	481	877	0.76	0.80	4.70
Raf1(Phospho-Ser259)	688	1250	1.09	1.13	4.41
ICAM-1(Ab-512)	295	535	0.47	0.49	4.38
NF kappa B-p100/p52(Ab-869)	581	1053	0.92	0.95	4.17
CREB(Ab-133)	280	505	0.44	0.46	3.83
FGF Receptor 1(Phospho-Tyr154)	605	1091	0.95	0.99	3.77
P38 MAPK(Phospho-Thr180)	695	1245	1.10	1.13	3.01

STAT4(Ab-693)	318	569	0.50	0.52	2.97
I-kappa-B-beta(Phospho-Ser23)	685	1222	1.08	1.11	2.51
MEK1(Ab-221)	501	894	0.79	0.81	2.51
IKK alpha(Ab-23)	751	1339	1.18	1.21	2.50
STAT1(Ab-727)	555	987	0.88	0.89	2.21
CaMKII (Ab-286)	797	1413	1.26	1.28	1.91
STAT3(Phospho-Ser727)	516	914	0.81	0.83	1.87
I-kappa-B-alpha(Ab-32/36)	464	820	0.73	0.74	1.61
EGFR(Ab-1110)	371	653	0.59	0.59	1.28
p44/42 MAP Kinase(Ab-204)	405	707	0.64	0.64	0.35
MEK1(Phospho-Ser217)	478	833	0.75	0.76	0.30
Catenin beta (Phospho-Ser37)	625	1087	0.99	0.99	0.09
Chk1(Phospho-Ser317)	828	1438	1.31	1.30	-0.11
SAPK/JNK(Phospho-Thr183)	957	1660	1.51	1.51	-0.24
BRCA1(Phospho-Ser1423)	1027	1782	1.62	1.62	-0.28
eIF2 alpha(Ab-51)	530	920	0.84	0.83	-0.29
p44/42 MAP Kinase(Phospho-Thr202)	577	1000	0.91	0.91	-0.42
SAPK/JNK(Ab-183)	391	678	0.62	0.61	-0.43
STAT4(Phospho-Tyr693)	323	559	0.51	0.51	-0.43
BAD(Ab-136)	356	615	0.56	0.56	-0.63
Chk2(Ab-68)	343	591	0.54	0.54	-1.13
Chk2(Ab-516)	730	1253	1.15	1.14	-1.31
STAT6(Ab-641)	392	671	0.62	0.61	-1.45
p44/42 MAP Kinase(Ab-202)	471	808	0.74	0.73	-1.46
I-kappa-B-alpha(Phospho-Ser32/Phospho-Ser36)	782	1340	1.23	1.22	-1.53
BCL-2(Phospho-Thr56)	389	664	0.61	0.60	-1.75
cdc25A (Ab-75)	747	1275	1.18	1.16	-1.84
BCL-2(Ab-56)	289	491	0.46	0.44	-2.38
CDK2(Phospho-Thr160)	567	962	0.89	0.87	-2.44
c-Jun(Phospho-Ser73)	605	1026	0.95	0.93	-2.48
STAT6(Ab-645)	869	1475	1.37	1.34	-2.49
GSK3-alpha(Ab-21)	456	771	0.72	0.70	-2.78
Myc(Ab-358)	514	864	0.81	0.78	-3.24
HSP90B(Ab-254)	380	638	0.60	0.58	-3.60
Smad3(Phospho-Ser425)	444	741	0.70	0.67	-3.98
MEK-2(Ab-394)	769	1283	1.21	1.16	-4.07
Met(Phospho-Tyr1349)	177	294	0.28	0.27	-4.28
FKHR(Phospho-Ser256)	665	1100	1.05	1.00	-4.81
STAT6(Phospho-Thr645)	818	1348	1.29	1.22	-5.21
Chk2(Phospho-Thr68)	390	642	0.61	0.58	-5.25
p27Kip1(Phospho-Ser10)	647	1065	1.02	0.97	-5.45
Akt2(Phospho-Ser474)	928	1524	1.46	1.38	-5.55
Myc(Phospho-Ser373)	398	654	0.63	0.59	-5.69
JAK2(Ab-1007)	303	497	0.48	0.45	-5.73
MEK1(Ab-291)	331	542	0.52	0.49	-5.82
FAK(Phospho-Tyr861)	839	1371	1.32	1.24	-6.08
BAD(Ab-155)	209	341	0.33	0.31	-6.27
Src(Phospho-Tyr529)	720	1171	1.14	1.06	-6.51
14-3-3 Zeta(Ab-58)	825	1338	1.30	1.21	-6.80
CrkII(Phospho-Tyr221)	1099	1762	1.73	1.60	-7.84
JunB(Phospho-Ser259)	593	950	0.94	0.86	-7.96
Rac1/cdc42(Phospho-Ser71)	803	1284	1.27	1.16	-8.00
Estrogen Receptor-alpha (Phospho-Ser167)	997	1594	1.57	1.45	-8.08
HSP27(Phospho-Ser78)	859	1372	1.36	1.24	-8.16
P38 MAPK(Phospho-Tyr182)	959	1531	1.51	1.39	-8.21
IKK alpha(Phospho-Thr23)	997	1590	1.57	1.44	-8.29
Integrin beta-3(Ab-773)	1007	1599	1.59	1.45	-8.72
Beta actin	645	1022	1.02	0.93	-8.94
4E-BP1(Phospho-Thr36)	801	1267	1.26	1.15	-9.03
PDGF Receptor beta(Phospho-Tyr751)	788	1244	1.24	1.13	-9.23
MSK1(Phospho-Ser376)	755	1190	1.19	1.08	-9.35
Elk-1(Ab-383)	627	988	0.99	0.90	-9.43
HDAC8(Phospho-Ser39)	927	1460	1.46	1.32	-9.49
Src(Phospho-Tyr418)	439	688	0.69	0.62	-9.99
BAD(Phospho-Ser155)	902	1394	1.42	1.26	-11.14

NF kappa B-p100/p52(phospho-Ser865)	388	599	0.61	0.54	-11.28
NF kappa B-p105/p50(Phospho-Ser907)	443	682	0.70	0.62	-11.48
HSP27(Phospho-Ser15)	480	734	0.76	0.67	-12.15
Chk1(Phospho-Ser345)	326	497	0.51	0.45	-12.29
Myc(Phospho-Thr358)	496	756	0.78	0.69	-12.31
GSK3-alpha(Phospho-Ser21)	733	1116	1.16	1.01	-12.46
ICAM-1(Phospho-Tyr512)	724	1096	1.14	0.99	-12.98
NF kappa B-p100/p52(Phospho-Ser869)	384	578	0.61	0.52	-13.42
14-3-3 Zeta(Phospho-Ser58)	443	666	0.70	0.60	-13.68
Tau(Phospho-Ser404)	509	762	0.80	0.69	-13.89
Catenin beta (Ab-37)	1734	2590	2.74	2.35	-14.14
HSP27(Ab-78)	264	393	0.42	0.36	-14.50
Met(Ab-1349)	1008	1498	1.59	1.36	-14.52
JunD(Phospho-Ser255)	805	1189	1.27	1.08	-15.10
Shc(Phospho-Tyr349)	805	1187	1.27	1.08	-15.25
p53(Ab-6)	384	566	0.61	0.51	-15.32
PDK1(Ab-241)	2131	3125	3.36	2.83	-15.69
Integrin beta-3(Phospho-Tyr773)	762	1111	1.20	1.01	-16.24
SHP-2(Phospho-Tyr580)	728	1057	1.15	0.96	-16.48
STAT1(Ab-701)	279	404	0.44	0.37	-16.68
HER2(Phospho-Tyr877)	841	1224	1.33	1.11	-16.69
eIF2 alpha(Phospho-Ser51)	1093	1579	1.73	1.43	-16.99
STAT5A (Ab-694)	225	323	0.35	0.29	-17.21
NF kappa B-p65(Phospho-Thr254)	441	632	0.70	0.57	-17.70
c-Jun(Phospho-Ser243)	475	674	0.75	0.61	-18.30
NF kappa B-p105/p50(Ab-337)	260	369	0.41	0.33	-18.38
Catenin beta (Phospho-Thr41/Phospho-Ser45)	698	989	1.10	0.90	-18.60
c-Jun(Ab-73)	4801	6794	7.58	6.16	-18.64
NF kappa B-p100/p52(Ab-865)	1430	2017	2.26	1.83	-18.88
PDK1(Phospho-Ser241)	457	633	0.72	0.57	-20.30
Akt(Phospho-Ser473)	334	458	0.53	0.41	-21.30
p53(Phospho-Ser315)	525	718	0.83	0.65	-21.44
MEK-2(Phospho-Thr394)	748	1013	1.18	0.92	-22.10
FAK(Phospho-Tyr925)	341	461	0.54	0.42	-22.11
Histone H2A.X(Phospho-Ser139)	1259	1699	1.99	1.54	-22.42
VEGFR2(Ab-951)	1239	1667	1.96	1.51	-22.68
BCL-2(Phospho-Ser70)	1074	1438	1.70	1.30	-23.04
mTOR(Phospho-Ser2448)	767	1010	1.21	0.92	-24.26
STAT5A (Phospho-Ser780)	592	777	0.93	0.71	-24.54
MEK1(Phospho-Thr291)	699	915	1.10	0.83	-24.81
p27Kip1(Ab-10)	189	247	0.30	0.22	-25.09
Trk B(Phospho-Tyr515)	904	1174	1.43	1.06	-25.39
IGF-1R (Ab-1161)	472	608	0.74	0.55	-25.89
BAD(Phospho-Ser136)	1141	1456	1.80	1.32	-26.63
NF kappa B-p105/p50(Phospho-Ser932)	484	603	0.76	0.55	-28.29
JunB(Phospho-Ser79)	485	602	0.77	0.55	-28.68
c-Jun(Phospho-Thr239)	330	408	0.52	0.37	-28.80
BRCA1(Phospho-Ser1524)	523	639	0.82	0.58	-29.73
Rel(Phospho-Ser503)	472	576	0.74	0.52	-29.89
Caveolin-1(Phospho-Tyr14)	235	278	0.37	0.25	-32.08
Src(Ab-529)	1064	1257	1.68	1.14	-32.10
Akt(Phospho-Thr308)	526	613	0.83	0.56	-33.03
I-kappa-B-alpha(Phospho-Tyr42)	701	768	1.11	0.70	-37.01
NF kappa B-p105/p50(Phospho-Ser893)	734	803	1.16	0.73	-37.07
STAT3(Phospho-Tyr705)	704	765	1.11	0.69	-37.55
STAT1(Phospho-Tyr701)	626	679	0.99	0.62	-37.65
VEGFR2(Phospho-Tyr951)	1104	1156	1.74	1.05	-39.82
c-Kit(Phospho-Tyr721)	4284	4056	6.76	3.68	-45.57
Myc(Phospho-Thr58)	935	877	1.48	0.80	-46.11
cdc25C(Ab-216)	1394	1274	2.20	1.16	-47.48
p53(Phospho-Ser6)	959	726	1.51	0.66	-56.50
GAPDH	796	515	1.26	0.47	-62.82

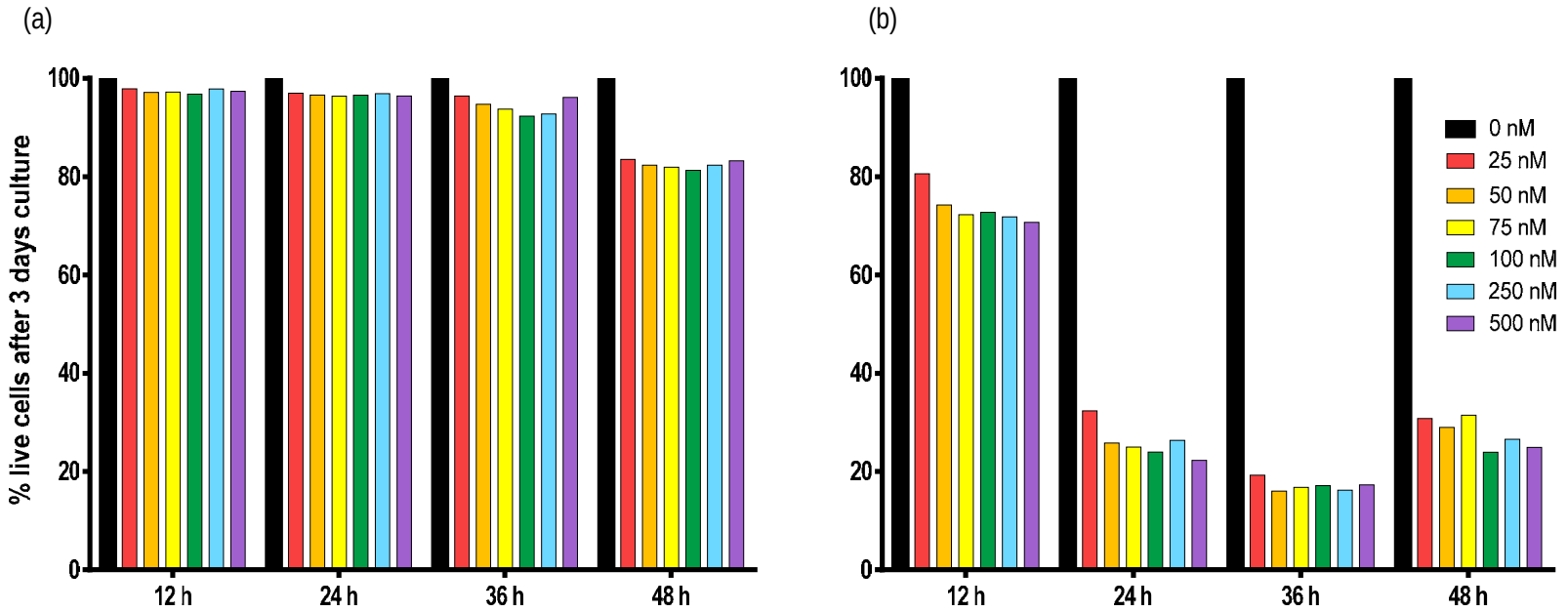

Figure 5A.1: Summary of K562 and KU812 cell death following incubation in increasing concentrations of nilotinib

a) K562 and b) KU812 cells were cultured for time points ranging 12–48 h in increasing concentrations of nilotinib and cell death determined by Annexin V/ 7-AAD staining. Data demonstrate that K562 cell death occurs following incubation for 36 h and 48 h; KU812 cells are more sensitive with substantial cell death occurring following incubation greater than 12 h. However, there is minimal impact on K562 cell viability following incubation for 24 h in 75 nM nilotinib when compared with control cells. Similarly, there is minimal impact on KU812 cell viability following incubation for 12 h in 100 nM nilotinib when compared with control cells. Annexin V/7-AAD was performed in duplicate with the corresponding survival plots representing the mean. Data represent one experiment and were normalised to 0 nM nilotinib with control values set at 100% live cells. NIL=nilotinib.

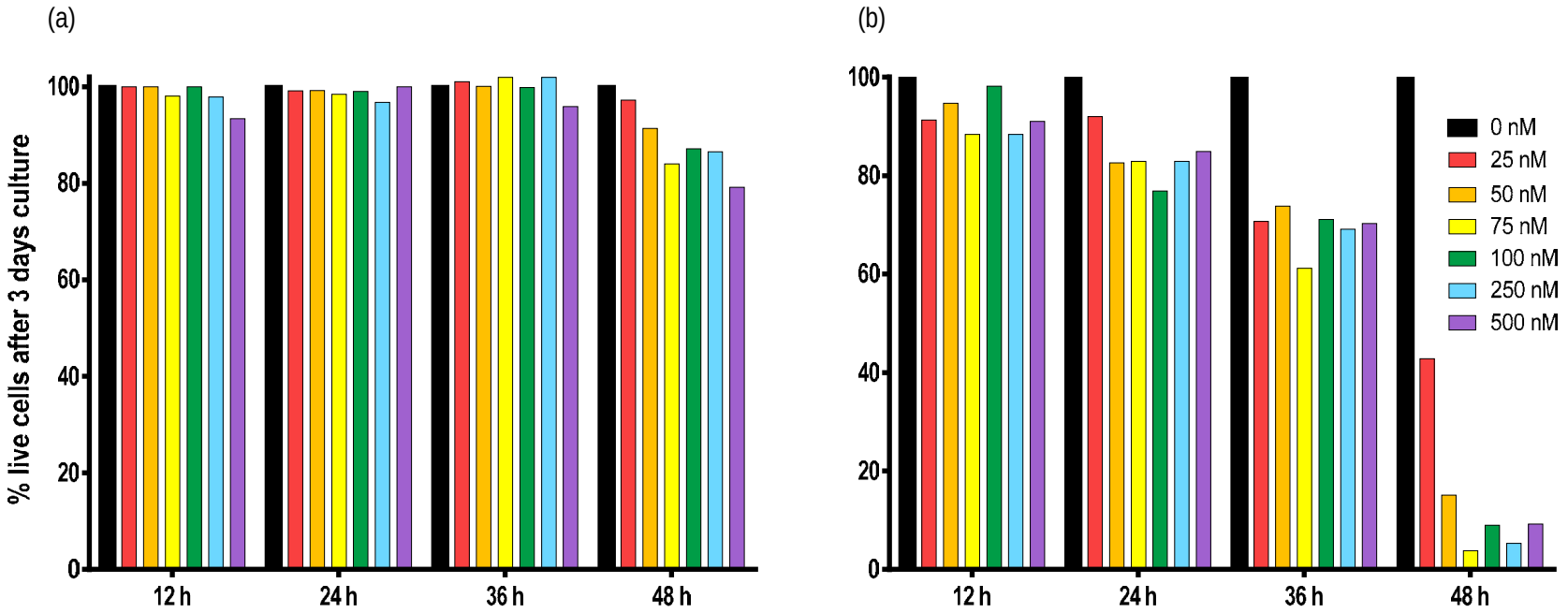

Figure 5A.2: Summary of K562 and KU812 cell death following incubation in increasing concentrations of nilotinib

a) K562 and b) KU812 cells were cultured for time points ranging 12–48 h in increasing concentrations of nilotinib and cell death determined by trypan blue staining. Data demonstrate that K562 cell death occurs following incubation for 48 h; KU812 cells are more sensitive with substantial cell death occurring following incubation greater than 12 h. However, there is minimal impact on K562 cell viability following incubation for 24 h in 75 nM nilotinib when compared with control cells. Similarly, there is minimal impact on KU812 cell viability following incubation for 12 h in 100 nM nilotinib when compared with control cells. Data represent one experiment and were normalised to 0 nM nilotinib with control values set at 100% live cells. NIL=nilotinib.

Table 5B.1: Summary of fold changes in transporter mRNA expression in K562 cells incubated for 24 h in the presence versus the absence of 75 nM nilotinib

Transporter Gene	Type	0 nM NIL (Ct)	+75 nM NIL (Ct)	Fold Change
18S	Control	8.8	9.0	1.0
ABCA1	Target	37.2	34.3	8.7
ABCA12	Target	35.3	37.1	0.4
ABCA13	Target	31.5	31.0	1.8
ABCA2	Target	28.9	28.4	1.7
ABCA3	Target	26.6	26.9	1.0
ABCA4	Target	36.5	35.9	1.8
ABCA9	Target	36.9	32.8	20.7
ABCB1	Target	31.1	34.0	0.2
ABCB11	Target	35.7	34.9	2.0
ABCB4	Target	36.0	35.1	2.1
ABCB5	Target	36.9	33.0	17.9
ABCB6	Target	27.0	25.8	2.7
ABCC1	Target	27.0	27.9	0.6
ABCC10	Target	27.9	28.0	1.1
ABCC11	Target	37.3	34.4	8.5
ABCC12	Target	40.0	37.0	9.1
ABCC2	Target	35.6	36.0	0.9
ABCC3	Target	37.0	36.9	1.4
ABCC4	Target	25.0	25.3	0.9
ABCC5	Target	25.0	25.3	0.9
ABCC6	Target	40.0	36.9	9.7
ABCD1	Target	31.0	29.9	2.4
ABCD3	Target	25.7	27.0	0.5
ABCD4	Target	27.8	28.1	0.9
ABCF1	Target	24.9	27.0	0.3
ABCG2	Target	32.9	30.5	6.1
ABCG8	Target	37.1	36.4	1.9
ACTB	Control	20.4	21.9	0.4
AQP1	Target	27.0	23.9	10.0

AQP7	Target	37.1	33.9	10.3
AQP9	Target	37.0	40.0	0.1
ATP6V0C	Target	25.0	25.9	0.6
ATP7A	Target	25.9	26.2	0.9
ATP7B	Target	24.9	24.6	1.4
B2M	Control	20.9	21.5	0.8
GAPDH	Control	19.0	19.9	0.6
GUSB	Control	24.9	25.0	1.1
HMBS	Control	24.9	25.5	0.8
HPRT1	Control	22.9	24.0	0.6
MVP	Target	34.6	33.0	3.6
PGK1	Control	20.8	22.9	0.3
PPIA	Control	18.7	19.9	0.5
RPLP01	Control	18.9	18.9	1.1
SLC10A1	Target	36.1	29.9	86.9
SLC10A2	Target	40.0	37.0	9.4
SLC15A1	Target	37.2	40.0	0.2
SLC15A2	Target	32.6	30.9	3.7
SLC16A1	Target	23.0	24.7	0.3
SLC16A2	Target	40.0	40.0	1.2
SLC16A3	Target	30.9	31.8	0.6
SLC19A1	Target	24.9	28.0	0.1
SLC19A2	Target	25.9	27.9	0.3
SLC19A3	Target	36.9	40.0	0.1
SLC22A1	Target	34.0	32.3	3.6
SLC22A2	Target	37.3	40.0	0.2
SLC22A3	Target	37.2	40.0	0.7
SLC22A6	Target	40.0	40.0	1.2
SLC22A7	Target	40.0	40.0	1.2
SLC22A8	Target	40.0	40.0	1.2
SLC22A9	Target	40.0	40.0	1.2
SLC25A13	Target	24.9	26.0	0.6
SLC28A1	Target	37.2	36.3	2.1
SLC28A2	Target	37.1	36.3	1.9

SLC28A3	Target	37.2	34.0	10.7
SLC29A1	Target	23.9	23.6	1.5
SLC29A2	Target	26.0	28.0	0.3
SLC2A1	Target	24.0	23.0	2.3388
SLC2A2	Target	8.5	32.2	0.0
SLC2A3	Target	23.0	30.4	0.0
SLC31A1	Target	24.7	24.9	1.0
SLC38A2	Target	23.9	25.5	0.4
SLC38A5	Target	23.0	24.1	0.5
SLC3A1	Target	37.1	36.1	2.4
SLC3A2	Target	23.9	24.3	0.9
SLC5A1	Target	40.0	37.0	9.3
SLC5A4	Target	36.7	36.9	1.0
SLC7A11	Target	26.1	25.9	1.3
SLC7A5	Target	23.6	26.0	0.2
SLC7A6	Target	25.7	28.0	0.3
SLC7A7	Target	34.9	34.0	2.1
SLC7A8	Target	26.8	27.0	1.1
SLC7A9	Target	37.2	35.6	3.7
SLCO1A2	Target	30.9	28.0	8.7
SLCO1B1	Target	35.9	34.1	3.9
SLCO1B3	Target	40.0	40.0	1.2
SLCO2A1	Target	38.0	40.0	0.3
SLCO2B1	Target	28.8	31.9	0.1
SLCO3A1	Target	35.9	34.9	2.4
SLCO4A1	Target	26.0	29.9	0.1
TAP1	Target	30.0	30.0	1.1
TAP2	Target	25.9	28.7	0.2
TBP	Control	24.7	25.9	0.5
UBC	Control	21.6	22.9	0.5
VDAC1	Target	21.9	23.9	0.3
VDAC2	Target	25.7	26.9	0.5

Table 5B.2: Summary of fold changes in transporter mRNA expression in KU812 cells incubated for 12 h in the presence versus the absence of 100 nM nilotinib

Transporter Gene	Type	0 nM NIL (Ct)	+100 nM NIL (Ct)	Fold Change
18S	Control	11.0	10.5	1.6
ABCA1	Target	28.9	28.6	1.5
ABCA12	Target	36.6	37.1	0.8
ABCA13	Target	40.0	40.0	1.2
ABCA2	Target	27.4	27.9	0.8
ABCA3	Target	36.9	35.4	3.3
ABCA4	Target	36.0	34.8	2.8
ABCA9	Target	37.0	21.5	53879.0
ABCB1	Target	29.6	29.9	0.9
ABCB11	Target	34.9	35.4	0.9
ABCB4	Target	30.7	28.9	3.8
ABCB5	Target	36.9	34.5	6.3
ABCB6	Target	26.8	26.9	1.1
ABCC1	Target	27.0	27.9	0.6
ABCC10	Target	27.9	27.9	1.2
ABCC11	Target	36.9	35.8	2.5
ABCC12	Target	37.2	33.2	17.8
ABCC2	Target	32.9	33.3	0.9
ABCC3	Target	40.0	40.0	1.2
ABCC4	Target	25.0	25.4	0.9
ABCC5	Target	25.0	24.9	1.2
ABCC6	Target	40.0	37.0	9.5
ABCD1	Target	31.8	31.9	1.1
ABCD3	Target	25.0	25.9	0.6
ABCD4	Target	28.6	27.9	1.8
ABCF1	Target	24.7	26.0	0.5
ABCG2	Target	31.0	31.0	1.2
ABCG8	Target	37.0	40.0	0.1
ACTB	Control	21.0	22.9	0.3
AQP1	Target	33.0	29.0	18.6

AQP7	Target	37.2	36.2	2.5
AQP9	Target	37.1	40.0	0.2
ATP6V0C	Target	25.9	27.2	0.5
ATP7A	Target	26.8	27.0	1.0
ATP7B	Target	24.6	23.9	1.8
B2M	Control	24.0	24.7	0.7
GAPDH	Control	19.5	20.0	0.8
GUSB	Control	26.9	27.7	0.7
HMBS	Control	27.5	27.9	0.9
HPRT1	Control	25.7	27.0	0.5
MVP	Target	32.9	31.9	2.4
PGK1	Control	23.0	24.7	0.4
PPIA	Control	20.0	21.2	0.5
RPLP01	Control	20.9	20.9	1.2
SLC10A1	Target	40.0	40.0	1.2
SLC10A2	Target	34.3	36.8	0.2
SLC15A1	Target	40.0	40.0	1.2
SLC15A2	Target	31.4	30.9	1.7
SLC16A1	Target	23.1	23.9	0.7
SLC16A2	Target	37.0	34.3	7.9
SLC16A3	Target	32.0	33.8	0.3
SLC19A1	Target	27.0	29.6	0.2
SLC19A2	Target	27.9	28.9	0.6
SLC19A3	Target	40.0	40.0	1.2
SLC22A1	Target	36.0	35.6	1.5
SLC22A2	Target	40.0	40.0	1.2
SLC22A3	Target	38.0	40.0	0.3
SLC22A6	Target	40.0	40.0	1.2
SLC22A7	Target	40.0	38.0	4.7
SLC22A8	Target	29.0	28.9	1.2
SLC22A9	Target	40.0	40.0	1.2
SLC25A13	Target	26.9	28.2	0.5
SLC28A1	Target	40.0	40.0	1.2

SLC28A2	Target	37.1	40.0	0.2
SLC28A3	Target	37.0	33.0	18.6
SLC29A1	Target	23.9	27.1	0.1
SLC29A2	Target	26.7	28.9	0.3
SLC2A1	Target	24.8	25.0	1.1
SLC2A2	Target	40.0	40.0	1.2
SLC2A3	Target	26.0	29.9	0.1
SLC31A1	Target	27.0	27.6	0.7
SLC38A2	Target	25.9	27.0	0.5
SLC38A5	Target	24.9	27.0	0.3
SLC3A1	Target	37.0	36.3	1.8
SLC3A2	Target	25.9	26.9	0.6
SLC5A1	Target	37.1	40.0	0.2
SLC5A4	Target	40.0	40.0	1.2
SLC7A11	Target	28.9	30.2	0.5
SLC7A5	Target	27.6	30.0	0.2
SLC7A6	Target	27.8	29.9	0.3
SLC7A7	Target	36.7	37.0	1.0
SLC7A8	Target	26.0	26.7	0.7
SLC7A9	Target	36.8	37.0	1.0
SLCO1A2	Target	30.9	28.6	5.9
SLCO1B1	Target	38.0	36.0	4.6
SLCO1B3	Target	36.9	37.1	1.1
SLCO2A1	Target	37.3	35.8	3.3
SLCO2B1	Target	35.9	34.7	2.7
SLCO3A1	Target	4.8	35.3	0.0
SLCO4A1	Target	27.4	32.0	0.0
TAP1	Target	29.9	28.5	3.1
TAP2	Target	28.0	28.9	0.6
TBP	Control	25.0	25.8	0.7
UBC	Control	22.9	23.4	0.8
VDAC1	Target	23.9	26.0	0.3
VDAC2	Target	32.4	33.0	0.8

Table 5B.3: Summary of fold changes in transporter mRNA expression in K562 cells cultured long term in the presence of 300 nM nilotinib compared with control cells

Transporter Gene	Type	Control (Ct)	+300 nM NIL (Ct)	Fold Change
18S	Control	14.7	14.3	1.4
ABCA1	Target	37.0	34.9	4.9
ABCA12	Target	36.9	36.3	1.6
ABCA13	Target	29.7	27.4	5.2
ABCA2	Target	27.4	25.9	3.0
ABCA3	Target	25.1	26.1	0.6
ABCA4	Target	32.4	31.6	1.9
ABCA9	Target	37.0	34.5	5.9
ABCB1	Target	29.6	25.4	19.9
ABCB11	Target	32.9	34.2	0.5
ABCB4	Target	34.9	34.3	1.6
ABCB5	Target	37.7	36.7	2.2
ABCB6	Target	25.1	24.6	1.6
ABCC1	Target	24.7	24.8	1.1
ABCC10	Target	25.3	25.9	0.7
ABCC11	Target	35.2	36.5	0.4
ABCC12	Target	40.0	39.0	2.1
ABCC2	Target	34.8	35.7	0.6
ABCC3	Target	38.4	36.1	5.2
ABCC4	Target	24.8	24.8	1.1
ABCC5	Target	23.2	24.3	0.5
ABCC6	Target	37.4	31.6	64.5
ABCD1	Target	28.7	27.9	1.9
ABCD3	Target	24.5	25.3	0.6
ABCD4	Target	26.9	27.9	0.6
ABCF1	Target	23.8	24.2	0.8
ABCG2	Target	32.6	34.7	0.3
ABCG8	Target	37.9	36.4	3.1
ACTB	Control	21.0	21.2	0.9
AQP1	Target	30.8	26.9	16.2

AQP7	Target	35.6	36.5	0.6
AQP9	Target	33.6	34.5	0.6
ATP6V0C	Target	22.3	22.6	0.8
ATP7A	Target	26.5	27.5	0.5
ATP7B	Target	24.2	23.8	1.5
B2M	Control	19.5	19.7	1.0
GAPDH	Control	17.8	18.1	0.9
GUSB	Control	22.0	22.0	1.0
HMBS	Control	22.4	23.1	0.7
HPRT1	Control	22.5	23.1	0.7
MVP	Target	29.7	29.7	1.1
PGK1	Control	20.6	20.8	0.9
PPIA	Control	18.0	18.7	0.7
RPLP0	Control	16.8	17.1	0.9
SLC10A1	Target	40.0	34.3	58.2
SLC10A2	Target	40.0	40.0	1.1
SLC15A1	Target	35.8	40.0	0.1
SLC15A2	Target	31.9	29.2	6.6
SLC16A1	Target	21.8	22.7	0.6
SLC16A2	Target	40.0	40.0	1.1
SLC16A3	Target	30.7	27.3	11.2
SLC19A1	Target	25.3	25.3	1.1
SLC19A2	Target	24.9	25.1	1.0
SLC19A3	Target	40.0	40.0	1.1
SLC22A1	Target	32.6	31.1	3.1
SLC22A2	Target	40.0	40.0	1.1
SLC22A3	Target	40.0	40.0	1.1
SLC22A6	Target	40.0	40.0	1.1
SLC22A7	Target	40.0	38.8	2.4
SLC22A8	Target	40.0	39.8	1.3
SLC22A9	Target	40.0	39.9	1.2
SLC25A13	Target	23.1	23.1	1.1
SLC28A1	Target	40.0	40.0	1.1

SLC28A2	Target	40.0	40.0	1.1
SLC28A3	Target	37.9	33.7	20.3
SLC29A1	Target	22.5	21.7	1.9
SLC29A2	Target	25.6	25.0	1.7
SLC2A1	Target	21.8	20.9	2.0
SLC2A2	Target	40.0	40.0	1.1
SLC2A3	Target	21.9	23.9	0.3
SLC31A1	Target	21.9	23.0	0.5
SLC38A2	Target	22.1	22.4	0.9
SLC38A5	Target	23.0	23.2	0.9
SLC3A1	Target	39.1	37.3	3.6
SLC3A2	Target	20.2	21.2	0.5
SLC5A1	Target	37.8	37.0	1.9
SLC5A4	Target	40.0	40.0	1.1
SLC7A11	Target	22.5	23.2	0.7
SLC7A5	Target	21.7	23.5	0.3
SLC7A6	Target	23.7	24.3	0.7
SLC7A7	Target	32.6	32.1	1.5
SLC7A8	Target	25.0	26.0	0.5
SLC7A9	Target	37.5	40.0	0.2
SLCO1A2	Target	27.3	29.7	0.2
SLCO1B1	Target	32.0	40.0	0.0
SLCO1B3	Target	40.0	40.0	1.1
SLCO2A1	Target	40.0	40.0	1.1
SLCO2B1	Target	31.1	26.7	22.7
SLCO3A1	Target	32.6	32.7	1.0
SLCO4A1	Target	27.8	27.7	1.1
TAP1	Target	26.8	27.7	0.6
TAP2	Target	24.2	25.8	0.4
TBP	Control	23.6	24.1	0.8
UBC	Control	19.9	19.9	1.1
VDAC1	Target	21.4	22.1	0.7
VDAC2	Target	26.6	27.1	0.8

Table 5B.4: Summary of fold changes in transporter mRNA expression in K562 cells cultured long term in the presence of 2 µM nilotinib compared with control cells

Transporter Gene	Type	Control (Ct)	+2 µM NIL (Ct)	Fold Change
18S	Control	10.0	10.0	1.0
ABCA1	Target	35.9	36.9	0.5
ABCA12	Target	37.0	37.0	1.0
ABCA13	Target	31.9	29.9	4.0
ABCA2	Target	26.9	27.0	1.0
ABCA3	Target	26.9	28.0	0.5
ABCA4	Target	32.0	34.0	0.3
ABCA9	Target	35.9	36.0	1.0
ABCB1	Target	31.0	29.0	4.0
ABCB11	Target	34.0	34.9	0.5
ABCB4	Target	31.9	36.9	0.0
ABCB5	Target	36.9	36.9	1.0
ABCB6	Target	27.9	27.0	1.9
ABCC1	Target	27.0	27.0	1.0
ABCC10	Target	27.9	27.9	1.0
ABCC11	Target	35.9	37.0	0.5
ABCC12	Target	37.1	36.9	1.2
ABCC2	Target	36.0	35.9	1.0
ABCC3	Target	37.0	37.3	0.8
ABCC4	Target	25.0	26.0	0.5
ABCC5	Target	26.0	26.0	1.0
ABCC6	Target	37.0	33.9	8.1
ABCD1	Target	30.0	29.0	2.0
ABCD3	Target	26.0	26.0	1.0
ABCD4	Target	28.0	29.0	0.5
ABCF1	Target	25.0	25.0	1.0
ABCG2	Target	36.0	35.9	1.0
ABCG8	Target	36.9	40.0	0.1
ACTB	Control	22.9	23.0	1.0
AQP1	Target	30.0	27.0	7.9

AQP7	Target	37.2	37.0	1.2
AQP9	Target	30.9	35.0	0.1
ATP6V0C	Target	25.0	24.9	1.0
ATP7A	Target	26.9	27.0	1.0
ATP7B	Target	24.9	24.9	1.0
B2M	Control	20.9	21.0	1.0
GAPDH	Control	20.0	20.0	1.0
GUSB	Control	24.0	23.9	1.0
HMBS	Control	24.9	24.9	1.0
HPRT1	Control	24.0	24.0	1.0
MVP	Target	31.0	32.0	0.5
PGK1	Control	21.9	22.0	1.0
PPIA	Control	20.0	20.0	1.0
RPLP0	Control	17.9	17.9	1.0
SLC10A1	Target	40.0	32.0	248.3
SLC10A2	Target	40.0	40.0	1.0
SLC15A1	Target	37.1	37.0	1.0
SLC15A2	Target	31.9	30.9	2.0
SLC16A1	Target	23.0	24.0	0.5
SLC16A2	Target	40.0	37.1	7.5
SLC16A3	Target	33.0	29.0	16.0
SLC19A1	Target	27.0	27.0	1.0
SLC19A2	Target	26.9	26.9	1.0
SLC19A3	Target	40.0	13.2	119997543.9
SLC22A1	Target	34.0	33.0	2.0
SLC22A2	Target	36.9	37.1	0.8
SLC22A3	Target	36.9	37.1	0.8
SLC22A6	Target	40.0	40.0	1.0
SLC22A7	Target	37.5	37.2	1.2
SLC22A8	Target	37.0	7.7	621847739.5
SLC22A9	Target	40.0	40.0	1.0
SLC25A13	Target	25.0	25.0	1.0
SLC28A1	Target	36.8	40.0	0.1

SLC28A2	Target	37.2	40.0	0.1
SLC28A3	Target	37.0	35.9	2.0
SLC29A1	Target	23.9	22.9	2.0
SLC29A2	Target	25.9	25.9	1.0
SLC2A1	Target	25.0	24.0	2.0
SLC2A2	Target	40.0	40.0	1.0
SLC2A3	Target	23.9	25.9	0.3
SLC31A1	Target	23.9	26.0	0.2
SLC38A2	Target	23.9	23.9	1.0
SLC38A5	Target	24.9	24.0	1.9
SLC3A1	Target	36.9	36.9	1.0
SLC3A2	Target	22.9	23.9	0.5
SLC5A1	Target	36.9	38.0	0.5
SLC5A4	Target	32.9	33.0	0.9
SLC7A11	Target	24.9	25.9	0.5
SLC7A5	Target	23.9	26.0	0.2
SLC7A6	Target	25.9	27.0	0.5
SLC7A7	Target	32.9	32.9	1.0
SLC7A8	Target	27.0	26.9	1.0
SLC7A9	Target	36.9	36.9	1.0
SLCO1A2	Target	28.9	31.9	0.1
SLCO1B1	Target	34.9	37.2	0.2
SLCO1B3	Target	40.0	40.0	1.0
SLCO2A1	Target	37.1	40.0	0.1
SLCO2B1	Target	29.0	26.0	8.3
SLCO3A1	Target	32.0	36.0	0.1
SLCO4A1	Target	30.0	29.0	2.0
TAP1	Target	29.0	29.0	1.0
TAP2	Target	27.0	26.9	1.0
TBP	Control	26.0	24.9	2.1
UBC	Control	20.9	20.9	1.0
VDAC1	Target	23.0	23.0	1.0
VDAC2	Target	28.0	29.0	0.5

Table 5C: Summary of Ct values for cellular transporters in K562 cells during development of resistance to nilotinib

Resistance Intermediate	Average Ct			
	ABCA9	ABCC12	SLC10A1	SLC28A3
Positive Control	–	–	–	25.1
Control	31.4	38.5	33.5	36.2
15 nM	ND	38.3	33.9	34.8
25 nM	ND	NEG	35.8	35.6
50 nM	ND	38.6	33.5	35.0
75 nM	ND	37.8	37.6	32.4
100 nM	ND	36.8	33.1	34.4
125 nM	30.5	35.1	31.6	30.7
140 nM	ND	37.0	30.0	30.6
200 nM	ND	37.7	30.5	31.4
300 nM	27.9	38.3	30.2	31.0
400 nM	ND	38.2	31.0	31.0
1 μM	ND	39.6	31.0	31.8
2 μM	31.1	37.7	32.7	32.6

ND=not determined; NEG=negative expression levels; Ct=cycle threshold (the number of cycles required for the fluorescent signal to exceed background level).

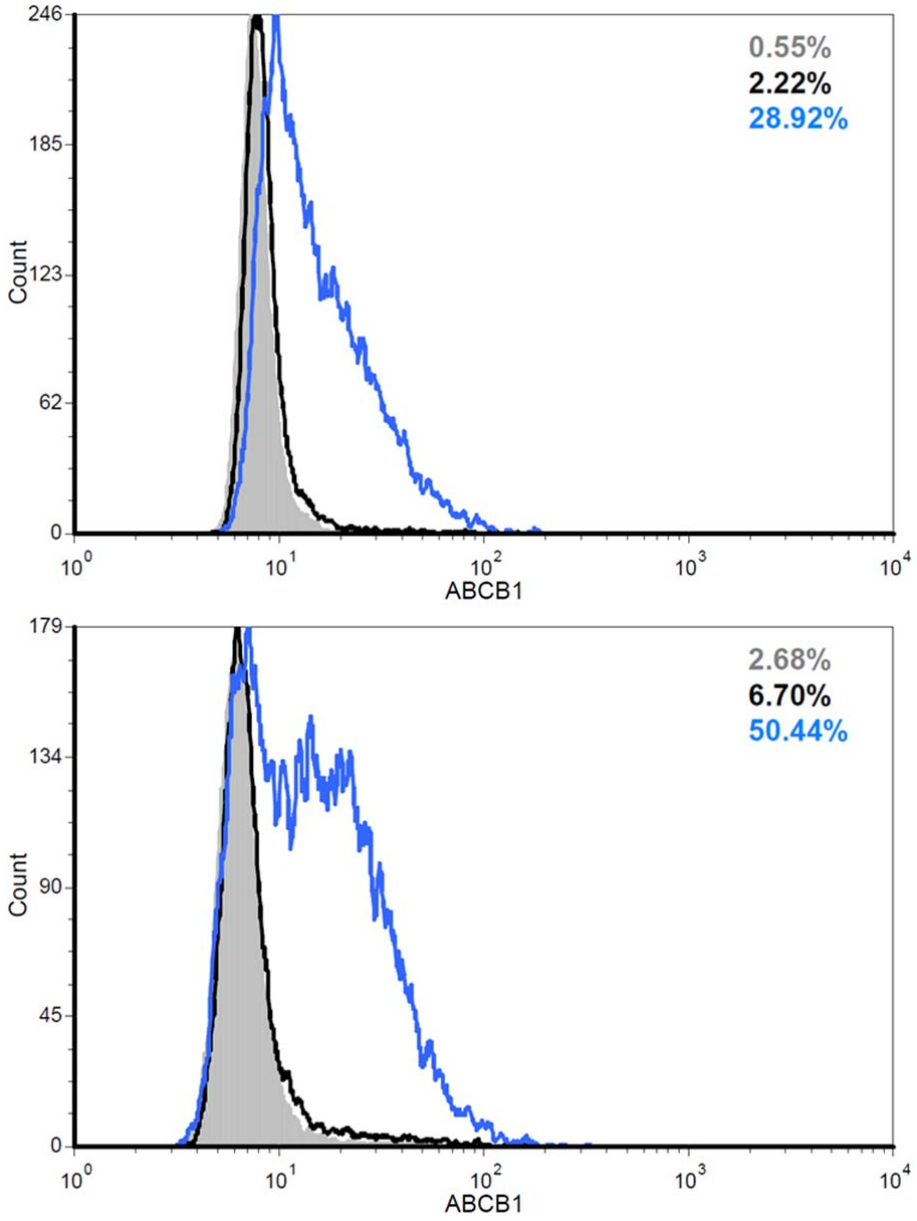

Figure 6A: ABCB1 protein expression in K562 cells pre- and 24 h post-nilotinib exposure

K562 control and newly thawed K562 2 µM NIL cells were stained with fluorescently labelled antibodies for ABCB1 a) pre-nilotinib exposure and b) 24 h post-nilotinib exposure and transporter protein expression levels determined by flow cytometric analysis. Data demonstrate up-regulation of ABCB1 expression immediately following exposure to 2 µM nilotinib. The bold BLACK and BLUE lines represent control and 2 µM NIL resistant cells respectively stained with ABCB1-PE antibody. The GREY filled histogram represents cells stained with corresponding isotype control antibody. The percentages displayed denote cells positive for transporter expression.

Publications Arising from this Thesis

Statement of Authorship

Title of Paper	Nilotinib does not significantly reduce imatinib OCT-1 activity in either cell lines or primary CML cells
Publication Status	◉ Published, ○ Accepted for Publication, ○ Submitted for Publication, ○ Publication style
Publication Details	Leukemia, 24 (4): 855-857. Impact factor: 9.561.

Author Contributions

By signing the Statement of Authorship, each author certifies that their stated contribution to the publication is accurate and that permission is granted for the publication to be included in the candidate's thesis.

Name of Principal Author (Candidate)	Laura Eadie		
Contribution to the Paper	Wrote the manuscript Designed and performed the experiments Analysed the data		
Signature		Date	14/7/13

Name of Co-Author	Timothy Hughes		
Contribution to the Paper	Edited the manuscript		
Signature		Date	10/7/13

Name of Co-Author	Deborah White		
Contribution to the Paper	Edited the manuscript Designed the experiments		
Signature		Date	10/7/13

Name of Co-Author			
Contribution to the Paper			
Signature		Date	

Eadie, L., Hughes, T.P. & White, D.L. (2010) Nilotinib does not significantly reduce imatinib OCT-1 activity in either cell lines or primary CML cells.
Leukemia, v. 24, pp. 855-857

Statement of Authorship

Title of Paper	Degree of kinase inhibition achieved in vitro by imatinib and nilotinib is decreased by high levels of ABCB1 but not ABCG2
Publication Status	◉ Published, ○ Accepted for Publication, ○ Submitted for Publication, ○ Publication style
Publication Details	Leukemia and Lymphoma, 54 (3): 569-578. Impact factor: 2.580

Author Contributions

By signing the Statement of Authorship, each author certifies that their stated contribution to the publication is accurate and that permission is granted for the publication to be included in the candidate's thesis.

Name of Principal Author (Candidate)	Laura Eadie		
Contribution to the Paper	Wrote the manuscript Designed and performed the experiments Analysed the data		
Signature		Date	14/7/13

Name of Co-Author	Verity Saunders		
Contribution to the Paper	Edited the manuscript Designed and performed the experiments Analysed the data		
Signature		Date	10/7/13

Name of Co-Author	Timothy Hughes		
Contribution to the Paper	Edited the manuscript		
Signature		Date	10/7/13

Name of Co-Author	Deborah White		
Contribution to the Paper	Edited the manuscript Designed the experiments		
Signature		Date	10/7/13.

Eadie, L.N., Saunders, V.A., Hughes, T.P. & White, D.L. (2013) Degree of kinase inhibition achieved *in vitro* by imatinib and nilotinib is decreased by high levels of ABCB1 but not ABCG2. *Leukemia and Lymphoma v. 54(3), pp. 569-578*

References

1. Moorhead PS, Nowell PC, Mellman WJ, Battips DM, Hungerford DA. Chromosome preparations of leukocytes cultured from human peripheral blood. *Exp Cell Res*. 1960;20:613-616.

2. Nowell PC, Hungerford DA. Chromosome studies on normal and leukemic human leukocytes. *J Natl Cancer Inst*. 1960;25:85-109.

3. Nowell PC, Hungerford DA. A Minute Chromosome in Human Chronic Granulocytic Leukemia. *Science*. 1960;132:1497.

4. Baikie AG, Court-Brown WM, Buckton KE, Harnden DG, Jacobs PA, Tough IM. A possible specific chromosome abnormality in human chronic myeloid leukaemia. *Nature*. 1960;188:1165-1166.

5. Rowley JD. Letter: A new consistent chromosomal abnormality in chronic myelogenous leukaemia identified by quinacrine fluorescence and Giemsa staining. *Nature*. 1973;243(5405):290-293.

6. Bartram CR, de Klein A, Hagemeijer A, et al. Translocation of c-ab1 oncogene correlates with the presence of a Philadelphia chromosome in chronic myelocytic leukaemia. *Nature*. 1983;306(5940):277-280.

7. de Klein A, van Kessel AG, Grosveld G, et al. A cellular oncogene is translocated to the Philadelphia chromosome in chronic myelocytic leukaemia. *Nature*. 1982;300(5894):765-767.

8. Heisterkamp N, Groffen J, Stephenson JR, et al. Chromosomal localization of human cellular homologues of two viral oncogenes. *Nature*. 1982;299(5885):747-749.

9. Clarkson B, Strife A, Wisniewski D, Lambek CL, Liu C. Chronic myelogenous leukemia as a paradigm of early cancer and possible curative strategies. *Leukemia*. 2003;17(7):1211-1262.

10. Ben-Neriah Y, Daley GQ, Mes-Masson AM, Witte ON, Baltimore D. The chronic myelogenous leukemia-specific P210 protein is the product of the bcr/abl hybrid gene. *Science*. 1986;233(4760):212-214.

11. Groffen J, Stephenson JR, Heisterkamp N, de Klein A, Bartram CR, Grosveld G. Philadelphia chromosomal breakpoints are clustered within a limited region, bcr, on chromosome 22. *Cell*. 1984;36(1):93-99.

12. Chissoe SL, Bodenteich A, Wang YF, et al. Sequence and analysis of the human ABL gene, the BCR gene, and regions involved in the Philadelphia chromosomal translocation. *Genomics*. 1995;27(1):67-82.

13. Melo JV. The diversity of BCR-ABL fusion proteins and their relationship to leukemia phenotype. *Blood*. 1996;88(7):2375-2384.

14. Pane F, Frigeri F, Sindona M, et al. Neutrophilic-chronic myeloid leukemia: a distinct disease with a specific molecular marker (BCR/ABL with C3/A2 junction). *Blood*. 1996;88(7):2410-2414.

15. Russo C, Carroll A, Kohler S, et al. Philadelphia chromosome and monosomy 7 in childhood acute lymphoblastic leukemia: a Pediatric Oncology Group study. *Blood*. 1991;77(5):1050-1056.

16. Saglio G, Guerrasio A, Rosso C, et al. New type of Bcr/Abl junction in Philadelphia chromosome-positive chronic myelogenous leukemia. *Blood*. 1990;76(9):1819-1824.

17. Suryanarayan K, Hunger SP, Kohler S, et al. Consistent involvement of the bcr gene by 9;22 breakpoints in pediatric acute leukemias. *Blood*. 1991;77(2):324-330.

18. Westbrook CA, Hooberman AL, Spino C, et al. Clinical significance of the BCR-ABL fusion gene in adult acute lymphoblastic leukemia: a Cancer and Leukemia Group B Study (8762). *Blood*. 1992;80(12):2983-2990.

19. McLaughlin J, Chianese E, Witte ON. In vitro transformation of immature hematopoietic cells by the P210 BCR/ABL oncogene product of the Philadelphia chromosome. *Proc Natl Acad Sci U S A*. 1987;84(18):6558-6562.

20. Daley GQ, Baltimore D. Transformation of an interleukin 3-dependent hematopoietic cell line by the chronic myelogenous leukemia-specific P210bcr/abl protein. *Proc Natl Acad Sci U S A*. 1988;85(23):9312-9316.

21. Daley GQ, Van Etten RA, Baltimore D. Induction of chronic myelogenous leukemia in mice by the P210bcr/abl gene of the Philadelphia chromosome. *Science*. 1990;247(4944):824-830.

22. Savage DG, Szydlo RM, Goldman JM. Clinical features at diagnosis in 430 patients with chronic myeloid leukaemia seen at a referral centre over a 16-year period. *Br J Haematol*. 1997;96(1):111-116.

23. Elefanty AG, Hariharan IK, Cory S. bcr-abl, the hallmark of chronic myeloid leukaemia in man, induces multiple haemopoietic neoplasms in mice. *EMBO J*. 1990;9(4):1069-1078.

24. Voncken JW, Kaartinen V, Pattengale PK, Germeraad WT, Groffen J, Heisterkamp N. BCR/ABL P210 and P190 cause distinct leukemia in transgenic mice. *Blood*. 1995;86(12):4603-4611.

25. Konopka JB, Witte ON. Detection of c-abl tyrosine kinase activity in vitro permits direct comparison of normal and altered abl gene products. *Mol Cell Biol*. 1985;5(11):3116-3123.

26. Lugo TG, Pendergast AM, Muller AJ, Witte ON. Tyrosine kinase activity and transformation potency of bcr-abl oncogene products. *Science*. 1990;247(4946):1079-1082.

27. McWhirter JR, Wang JY. Activation of tyrosinase kinase and microfilament-binding functions of c-abl by bcr sequences in bcr/abl fusion proteins. *Mol Cell Biol*. 1991;11(3):1553-1565.

28. Daley GQ, Ben-Neriah Y. Implicating the bcr/abl gene in the pathogenesis of Philadelphia chromosome-positive human leukemia. *Adv Cancer Res*. 1991;57:151-184.

29. Sonoyama J, Matsumura I, Ezoe S, et al. Functional cooperation among Ras, STAT5, and phosphatidylinositol 3-kinase is required for full oncogenic activities of BCR/ABL in K562 cells. *J Biol Chem*. 2002;277(10):8076-8082.

30. Bedi A, Zehnbauer BA, Barber JP, Sharkis SJ, Jones RJ. Inhibition of apoptosis by BCR-ABL in chronic myeloid leukemia. *Blood*. 1994;83(8):2038-2044.

31. Sawyers CL, McLaughlin J, Witte ON. Genetic requirement for Ras in the transformation of fibroblasts and hematopoietic cells by the Bcr-Abl oncogene. *J Exp Med*. 1995;181(1):307-313.

32. Skorski T, Kanakaraj P, Ku DH, et al. Negative regulation of p120GAP GTPase promoting activity by p210bcr/abl: implication for RAS-dependent Philadelphia chromosome positive cell growth. *J Exp Med*. 1994;179(6):1855-1865.

33. Jain SK, Susa M, Keeler ML, Carlesso N, Druker B, Varticovski L. PI 3-kinase activation in BCR/abl-transformed hematopoietic cells does not require interaction of p85 SH2 domains with p210 BCR/abl. *Blood*. 1996;88(5):1542-1550.

34. Frank DA, Varticovski L. BCR/abl leads to the constitutive activation of Stat proteins, and shares an epitope with tyrosine phosphorylated Stats. *Leukemia*. 1996;10(11):1724-1730.

35. Li S, Ilaria RL, Jr., Million RP, Daley GQ, Van Etten RA. The P190, P210, and P230 forms of the BCR/ABL oncogene induce a similar chronic myeloid leukemia-like syndrome in mice but have different lymphoid leukemogenic activity. *J Exp Med*. 1999;189(9):1399-1412.

36. Goldman JM, Melo JV. Chronic myeloid leukemia--advances in biology and new approaches to treatment. *N Engl J Med*. 2003;349(15):1451-1464.

37. Carlesso N, Frank DA, Griffin JD. Tyrosyl phosphorylation and DNA binding activity of signal transducers and activators of transcription (STAT) proteins in hematopoietic cell lines transformed by Bcr/Abl. *J Exp Med*. 1996;183(3):811-820.

38. Ilaria RL, Jr., Van Etten RA. P210 and P190(BCR/ABL) induce the tyrosine phosphorylation and DNA binding activity of multiple specific STAT family members. *J Biol Chem*. 1996;271(49):31704-31710.

39. Baskiewicz-Masiuk M, Machalinski B. The role of the STAT5 proteins in the proliferation and apoptosis of the CML and AML cells. *Eur J Haematol*. 2004;72(6):420-429.

40. Bhatia R, Holtz M, Niu N, et al. Persistence of malignant hematopoietic progenitors in chronic myelogenous leukemia patients in complete cytogenetic remission following imatinib mesylate treatment. *Blood*. 2003;101(12):4701-4707.

41. Holtz MS, Slovak ML, Zhang F, Sawyers CL, Forman SJ, Bhatia R. Imatinib mesylate (STI571) inhibits growth of primitive malignant progenitors in chronic myelogenous leukemia through reversal of abnormally increased proliferation. *Blood*. 2002;99(10):3792-3800.

42. Jonuleit T, Peschel C, Schwab R, et al. Bcr-Abl kinase promotes cell cycle entry of primary myeloid CML cells in the absence of growth factors. *Br J Haematol*. 1998;100(2):295-303.

43. Tokarski JS, Newitt JA, Chang CY, et al. The structure of Dasatinib (BMS-354825) bound to activated ABL kinase domain elucidates its inhibitory activity against imatinib-resistant ABL mutants. *Cancer Res*. 2006;66(11):5790-5797.

44. Ogawa M, Fried J, Sakai Y, Strife A, Clarkson BD. Studies of cellular proliferation in human leukemia. VI. The proliferative activity, generation time, and emergence time of neutrophilic granulocytes in chronic granulocytic leukemia. *Cancer*. 1970;25(5):1031-1049.

45. Deutsch E, Dugray A, AbdulKarim B, et al. BCR-ABL down-regulates the DNA repair protein DNA-PKcs. *Blood*. 2001;97(7):2084-2090.

46. Deutsch E, Jarrousse S, Buet D, et al. Down-regulation of BRCA1 in BCR-ABL-expressing hematopoietic cells. *Blood*. 2003;101(11):4583-4588.

47. Jasin M. Homologous repair of DNA damage and tumorigenesis: the BRCA connection. *Oncogene*. 2002;21(58):8981-8993.

48. Starita LM, Parvin JD. The multiple nuclear functions of BRCA1: transcription, ubiquitination and DNA repair. *Curr Opin Cell Biol*. 2003;15(3):345-350.

49. Calabretta B, Perrotti D. The biology of CML blast crisis. *Blood*. 2004;103(11):4010-4022.

50. Kantarjian HM, Keating MJ, Talpaz M, et al. Chronic myelogenous leukemia in blast crisis. Analysis of 242 patients. *Am J Med*. 1987;83(3):445-454.

51. Spiers AS. The clinical features of chronic granulocytic leukaemia. *Clin Haematol*. 1977;6(1):77-95.

52. Champlin RE, Golde DW. Chronic myelogenous leukemia: recent advances. *Blood*. 1985;65(5):1039-1047.

53. Sandberg AA. The cytogenetics of chronic myelocytic leukemia (CML): chronic phase and blastic crisis. *Cancer genetics and cytogenetics*. 1980;1:217.

54. Furet P, Caravatti G, Lydon N, et al. Modelling study of protein kinase inhibitors: binding mode of staurosporine and origin of the selectivity of CGP 52411. *J Comput Aided Mol Des*. 1995;9(6):465-472.

55. Buchdunger E, Zimmermann J, Mett H, et al. Inhibition of the Abl protein-tyrosine kinase in vitro and in vivo by a 2-phenylaminopyrimidine derivative. *Cancer Res*. 1996;56(1):100-104.

56. Carroll M, Ohno-Jones S, Tamura S, et al. CGP 57148, a tyrosine kinase inhibitor, inhibits the growth of cells expressing BCR-ABL, TEL-ABL, and TEL-PDGFR fusion proteins. *Blood*. 1997;90(12):4947-4952.

57. Druker BJ, Tamura S, Buchdunger E, et al. Effects of a selective inhibitor of the Abl tyrosine kinase on the growth of Bcr-Abl positive cells. *Nat Med*. 1996;2(5):561-566.

58. Buchdunger E, Cioffi CL, Law N, et al. Abl protein-tyrosine kinase inhibitor STI571 inhibits in vitro signal transduction mediated by c-kit and platelet-derived growth factor receptors. *J Pharmacol Exp Ther*. 2000;295(1):139-145.

59. Heinrich MC, Griffith DJ, Druker BJ, Wait CL, Ott KA, Zigler AJ. Inhibition of c-kit receptor tyrosine kinase activity by STI 571, a selective tyrosine kinase inhibitor. *Blood*. 2000;96(3):925-932.

60. Dewar AL, Zannettino AC, Hughes TP, Lyons AB. Inhibition of c-fms by imatinib: expanding the spectrum of treatment. *Cell Cycle*. 2005;4(7):851-853.

61. Okuda K, Weisberg E, Gilliland DG, Griffin JD. ARG tyrosine kinase activity is inhibited by STI571. *Blood*. 2001;97(8):2440-2448.

62. Nagar B, Bornmann WG, Pellicena P, et al. Crystal structures of the kinase domain of c-Abl in complex with the small molecule inhibitors PD173955 and imatinib (STI-571). *Cancer Res*. 2002;62(15):4236-4243.

63. Schindler T, Bornmann W, Pellicena P, Miller WT, Clarkson B, Kuriyan J. Structural mechanism for STI-571 inhibition of abelson tyrosine kinase. *Science*. 2000;289(5486):1938-1942.

64. Deininger MW, Goldman JM, Lydon N, Melo JV. The tyrosine kinase inhibitor CGP57148B selectively inhibits the growth of BCR-ABL-positive cells. *Blood*. 1997;90(9):3691-3698.

65. Gambacorti-Passerini C, le Coutre P, Mologni L, et al. Inhibition of the ABL kinase activity blocks the proliferation of BCR/ABL+ leukemic cells and induces apoptosis. *Blood Cells Mol Dis*. 1997;23(3):380-394.

66. le Coutre P, Mologni L, Cleris L, et al. In vivo eradication of human BCR/ABL-positive leukemia cells with an ABL kinase inhibitor. *J Natl Cancer Inst*. 1999;91(2):163-168.

67. Druker BJ, Talpaz M, Resta DJ, et al. Efficacy and safety of a specific inhibitor of the BCR-ABL tyrosine kinase in chronic myeloid leukemia. *N Engl J Med*. 2001;344(14):1031-1037.

68. Melo JV, Chuah C. Resistance to imatinib mesylate in chronic myeloid leukaemia. *Cancer Lett*. 2007;249(2):121-132.

69. Deininger M, Buchdunger E, Druker BJ. The development of imatinib as a therapeutic agent for chronic myeloid leukemia. *Blood*. 2005;105(7):2640-2653.

70. Druker BJ, Sawyers CL, Kantarjian H, et al. Activity of a specific inhibitor of the BCR-ABL tyrosine kinase in the blast crisis of chronic myeloid leukemia and acute lymphoblastic leukemia with the Philadelphia chromosome. *N Engl J Med*. 2001;344(14):1038-1042.

71. Kantarjian H, Sawyers C, Hochhaus A, et al. Hematologic and cytogenetic responses to imatinib mesylate in chronic myelogenous leukemia. *N Engl J Med*. 2002;346(9):645-652.

72. Ottmann OG, Druker BJ, Sawyers CL, et al. A phase 2 study of imatinib in patients with relapsed or refractory Philadelphia chromosome-positive acute lymphoid leukemias. *Blood*. 2002;100(6):1965-1971.

73. Sawyers CL, Hochhaus A, Feldman E, et al. Imatinib induces hematologic and cytogenetic responses in patients with chronic myelogenous leukemia in myeloid blast crisis: results of a phase II study. *Blood*. 2002;99(10):3530-3539.

74. Talpaz M, Silver RT, Druker BJ, et al. Imatinib induces durable hematologic and cytogenetic responses in patients with accelerated phase chronic myeloid leukemia: results of a phase 2 study. *Blood*. 2002;99(6):1928-1937.

75. Guilhot F, Druker B, Larson RA, et al. High rates of durable response are achieved with imatinib after treatment with interferon {alpha} plus cytarabine: results from the International Randomized Study of Interferon and STI571 (IRIS) trial. *Haematologica*. 2009.

76. Hughes TP, Kaeda J, Branford S, et al. Frequency of major molecular responses to imatinib or interferon alfa plus cytarabine in newly diagnosed chronic myeloid leukemia. *N Engl J Med*. 2003;349(15):1423-1432.

77. O'Brien SG, Guilhot F, Larson RA, et al. Imatinib compared with interferon and low-dose cytarabine for newly diagnosed chronic-phase chronic myeloid leukemia. *N Engl J Med*. 2003;348(11):994-1004.

78. Imatinib (Glivec ®) [Prescribing Information]. *East Hanover, New Jersey: Novartis Pharmaceuticals Corporation*. 2001.

79. Das J, Chen P, Norris D, et al. 2-aminothiazole as a novel kinase inhibitor template. Structure-activity relationship studies toward the discovery of N-(2-chloro-6-methylphenyl)-2-[[6-[4-(2-hydroxyethyl)-1- piperazinyl)]-2-methyl-4-pyrimidinyl]amino)]-1,3-thiazole-5-carboxamide (dasatinib, BMS-354825) as a potent pan-Src kinase inhibitor. *J Med Chem*. 2006;49(23):6819-6832.

80. Lombardo LJ, Lee FY, Chen P, et al. Discovery of N-(2-chloro-6-methyl- phenyl)-2-(6-(4-(2-hydroxyethyl)- piperazin-1-yl)-2-methylpyrimidin-4- ylamino)thiazole-5-carboxamide (BMS-354825), a dual Src/Abl kinase inhibitor with potent antitumor activity in preclinical assays. *J Med Chem*. 2004;47(27):6658-6661.

81. O'Hare T, Walters DK, Stoffregen EP, et al. In vitro activity of Bcr-Abl inhibitors AMN107 and BMS-354825 against clinically relevant imatinib-resistant Abl kinase domain mutants. *Cancer Res*. 2005;65(11):4500-4505.

82. Vajpai N, Strauss A, Fendrich G, et al. Solution conformations and dynamics of ABL kinase-inhibitor complexes determined by NMR substantiate the different binding modes of imatinib/nilotinib and dasatinib. *J Biol Chem*. 2008;283(26):18292-18302.

83. Shah NP, Tran C, Lee FY, Chen P, Norris D, Sawyers CL. Overriding imatinib resistance with a novel ABL kinase inhibitor. *Science*. 2004;305(5682):399-401.

84. Kantarjian H, Shah NP, Hochhaus A, et al. Dasatinib versus imatinib in newly diagnosed chronic-phase chronic myeloid leukemia. *N Engl J Med*. 2010;362(24):2260-2270.

85. Cortes J, Rousselot P, Kim DW, et al. Dasatinib induces complete hematologic and cytogenetic responses in patients with imatinib-resistant or -intolerant chronic myeloid leukemia in blast crisis. *Blood*. 2007;109(8):3207-3213.

86. Cortes J, Kim DW, Raffoux E, et al. Efficacy and safety of dasatinib in imatinib-resistant or -intolerant patients with chronic myeloid leukemia in blast phase. *Leukemia*. 2008;22(12):2176-2183.

87. Guilhot F, Apperley J, Kim DW, et al. Dasatinib induces significant hematologic and cytogenetic responses in patients with imatinib-resistant or -intolerant chronic myeloid leukemia in accelerated phase. *Blood*. 2007;109(10):4143-4150.

88. Hochhaus A, Kantarjian HM, Baccarani M, et al. Dasatinib induces notable hematologic and cytogenetic responses in chronic-phase chronic myeloid leukemia after failure of imatinib therapy. *Blood*. 2007;109(6):2303-2309.

89. Kantarjian H, Pasquini R, Hamerschlak N, et al. Dasatinib or high-dose imatinib for chronic-phase chronic myeloid leukemia after failure of first-line imatinib: a randomized phase 2 trial. *Blood*. 2007;109(12):5143-5150.

90. Ottmann O, Dombret H, Martinelli G, et al. Dasatinib induces rapid hematologic and cytogenetic responses in adult patients with Philadelphia chromosome positive acute lymphoblastic leukemia with resistance or intolerance to imatinib: interim results of a phase 2 study. *Blood*. 2007;110(7):2309-2315.

91. Dasatinib (Sprycel ®) [Prescribing Information]. *Princeton New Jersey: Bristol Myers Squibb Company*. 2006.

92. Weisberg E, Manley PW, Breitenstein W, et al. Characterization of AMN107, a selective inhibitor of native and mutant Bcr-Abl. *Cancer Cell*. 2005;7(2):129-141.

93. Manley PW, Breitenstein W, Bruggen J, et al. Urea derivatives of STI571 as inhibitors of Bcr-Abl and PDGFR kinases. *Bioorg Med Chem Lett*. 2004;14(23):5793-5797.

94. Golemovic M, Verstovsek S, Giles F, et al. AMN107, a novel aminopyrimidine inhibitor of Bcr-Abl, has in vitro activity against imatinib-resistant chronic myeloid leukemia. *Clin Cancer Res*. 2005;11(13):4941-4947.

95. Saglio G, Kim DW, Issaragrisil S, et al. Nilotinib versus imatinib for newly diagnosed chronic myeloid leukemia. *N Engl J Med*. 2010;362(24):2251-2259.

96. Giles FJ, Larson RA, Kantarjian HM, et al. Nilotinib in patients with Philadelphia chromosome-positive chronic myelogenous leukemia in blast crisis (CML-BC) who are resistant or intolerant to imatinib. *J Clin Oncol (Meeting Abstracts)*. 2008;26(15_suppl):7017-.

97. Kantarjian H, Giles F, Wunderle L, et al. Nilotinib in imatinib-resistant CML and Philadelphia chromosome-positive ALL. *N Engl J Med*. 2006;354(24):2542-2551.

98. le Coutre P, Ottmann OG, Giles F, et al. Nilotinib (formerly AMN107), a highly selective BCR-ABL tyrosine kinase inhibitor, is active in patients with imatinib-resistant or -intolerant accelerated-phase chronic myelogenous leukemia. *Blood*. 2008;111(4):1834-1839.

99. Ottmann O, Kantarjian H, Larson R, et al. A Phase II Study of Nilotinib, a Novel Tyrosine Kinase Inhibitor Administered to Imatinib Resistant or Intolerant Patients with Chronic Myelogenous Leukemia (CML) in Blast Crisis (BC) or Relapsed/Refractory Ph+ Acute Lymphoblastic Leukemia (ALL). *ASH Annual Meeting Abstracts*. 2006;108(11):1862-.

100. Kantarjian HM, Giles F, Gattermann N, et al. Nilotinib (formerly AMN107), a highly selective BCR-ABL tyrosine kinase inhibitor, is effective in patients with Philadelphia chromosome-positive chronic myelogenous leukemia in chronic phase following imatinib resistance and intolerance. *Blood*. 2007;110(10):3540-3546.

101. Nilotinib (Tasigna ®) [Prescribing Information]. *East Hanover, New Jersey: Novartis Pharmaceuticals Corporation*. 2007.

102. Giles FJ, le Coutre PD, Pinilla-Ibarz J, et al. Nilotinib in imatinib-resistant or imatinib-intolerant patients with chronic myeloid leukemia in chronic phase: 48-month follow-up results of a phase II study. *Leukemia*. 2013;27(1):107-112.

103. Khorashad JS, Kelley TW, Szankasi P, et al. BCR-ABL1 compound mutations in tyrosine kinase inhibitor-resistant CML: frequency and clonal relationships. *Blood*. 2013;121(3):489-498.

104. Storey S. Chronic myelogenous leukaemia market. *Nat Rev Drug Discov*. 2009;8(6):447.

105. Deininger M. Imatinib - an overview. *Haematologica reports*. 2005;Vol. 1(8):20 - 27.

106. Hochhaus A, La Rosee P, Muller MC, Ernst T, Cross NC. Impact of BCR-ABL mutations on patients with chronic myeloid leukemia. *Cell Cycle*. 2011;10(2):250-260.

107. Tang C, Schafranek L, Watkins DB, et al. Tyrosine kinase inhibitor resistance in chronic myeloid leukemia cell lines: investigating resistance pathways. *Leuk Lymphoma*. 2011;52(11):2139-2147.

108. Hochhaus A, Kreil S, Corbin AS, et al. Molecular and chromosomal mechanisms of resistance to imatinib (STI571) therapy. *Leukemia*. 2002;16(11):2190-2196.

109. Gorre ME, Mohammed M, Ellwood K, et al. Clinical resistance to STI-571 cancer therapy caused by BCR-ABL gene mutation or amplification. *Science*. 2001;293(5531):876-880.

110. O'Hare T, Eide CA, Deininger MW. Bcr-Abl kinase domain mutations, drug resistance, and the road to a cure for chronic myeloid leukemia. *Blood*. 2007;110(7):2242-2249.

111. Mahon FX, Deininger MW, Schultheis B, et al. Selection and characterization of BCR-ABL positive cell lines with differential sensitivity to the tyrosine kinase inhibitor STI571: diverse mechanisms of resistance. *Blood*. 2000;96(3):1070-1079.

112. le Coutre P, Tassi E, Varella-Garcia M, et al. Induction of resistance to the Abelson inhibitor STI571 in human leukemic cells through gene amplification. *Blood*. 2000;95(5):1758-1766.

113. Campbell LJ, Patsouris C, Rayeroux KC, Somana K, Januszewicz EH, Szer J. BCR/ABL amplification in chronic myelocytic leukemia blast crisis following imatinib mesylate administration. *Cancer Genet Cytogenet*. 2002;139(1):30-33.

114. Gambacorti-Passerini C, Barni R, le Coutre P, et al. Role of alpha1 acid glycoprotein in the in vivo resistance of human BCR-ABL(+) leukemic cells to the abl inhibitor STI571. *J Natl Cancer Inst*. 2000;92(20):1641-1650.

115. Mahon FX, Belloc F, Lagarde V, et al. MDR1 gene overexpression confers resistance to imatinib mesylate in leukemia cell line models. *Blood*. 2003;101(6):2368-2373.

116. Mahon FX, Hayette S, Lagarde V, et al. Evidence that resistance to nilotinib may be due to BCR-ABL, Pgp, or Src kinase overexpression. *Cancer Res*. 2008;68(23):9809-9816.

117. Gromicho M, Dinis J, Magalhaes M, et al. Development of imatinib and dasatinib resistance: dynamics of expression of drug transporters ABCB1, ABCC1, ABCG2, MVP, and SLC22A1. *Leuk Lymphoma*. 2011;52(10):1980-1990.

118. Illmer T, Schaich M, Platzbecker U, et al. P-glycoprotein-mediated drug efflux is a resistance mechanism of chronic myelogenous leukemia cells to treatment with imatinib mesylate. *Leukemia*. 2004;18(3):401-408.

119. Grosso S, Puissant A, Dufies M, et al. Gene expression profiling of imatinib and PD166326-resistant CML cell lines identifies Fyn as a gene associated with resistance to BCR-ABL inhibitors. *Mol Cancer Ther*. 2009;8(7):1924-1933.

120. Dai Y, Rahmani M, Corey SJ, Dent P, Grant S. A Bcr/Abl-independent, Lyn-dependent form of imatinib mesylate (STI-571) resistance is associated with altered expression of Bcl-2. *J Biol Chem*. 2004;279(33):34227-34239.

121. Donato NJ, Wu JY, Stapley J, et al. BCR-ABL independence and LYN kinase overexpression in chronic myelogenous leukemia cells selected for resistance to STI571. *Blood*. 2003;101(2):690-698.

122. Okabe S, Tauchi T, Tanaka Y, Ohyashiki K. Dasatinib preferentially induces apoptosis by inhibiting Lyn kinase in nilotinib-resistant chronic myeloid leukemia cell line. *J Hematol Oncol*. 2011;4(1):32.

123. Wu J, Meng F, Lu H, et al. Lyn regulates BCR-ABL and Gab2 tyrosine phosphorylation and c-Cbl protein stability in imatinib-resistant chronic myelogenous leukemia cells. *Blood*. 2008;111(7):3821-3829.

124. Okabe S, Tauchi T, Ohyashiki K. 16th Congress of the European Hematology Association, London, United Kingdom, June 9–12, 2011. *Haematologica*. 2011;96(supplement 2):498-499.

125. Wu J, Meng F, Kong LY, et al. Association between imatinib-resistant BCR-ABL mutation-negative leukemia and persistent activation of LYN kinase. *J Natl Cancer Inst*. 2008;100(13):926-939.

126. Gioia R, Leroy C, Drullion C, et al. Quantitative phosphoproteomics revealed interplay between Syk and Lyn in the resistance to nilotinib in chronic myeloid leukemia cells. *Blood*. 2011;118(8):2211-2221.

127. Dufies M, Jacquel A, Belhacene N, et al. Mechanisms of AXL overexpression and function in Imatinib-resistant chronic myeloid leukemia cells. *Oncotarget*. 2011;2(11):874-885.

128. Pene-Dumitrescu T, Smithgall TE. Expression of a Src family kinase in chronic myelogenous leukemia cells induces resistance to imatinib in a kinase-dependent manner. *J Biol Chem*. 2010;285(28):21446-21457.

129. Quentmeier H, Eberth S, Romani J, Zaborski M, Drexler HG. BCR-ABL1-independent PI3Kinase activation causing imatinib-resistance. *J Hematol Oncol*. 2011;4:6.

130. Apperley JF. Part I: mechanisms of resistance to imatinib in chronic myeloid leukaemia. *Lancet Oncol*. 2007;8(11):1018-1029.

131. Branford S, Rudzki Z, Walsh S, et al. High frequency of point mutations clustered within the adenosine triphosphate-binding region of BCR/ABL in patients with chronic myeloid leukemia or Ph-positive acute lymphoblastic leukemia who develop imatinib (STI571) resistance. *Blood*. 2002;99(9):3472-3475.

132. Shah NP, Nicoll JM, Nagar B, et al. Multiple BCR-ABL kinase domain mutations confer polyclonal resistance to the tyrosine kinase inhibitor imatinib (STI571) in chronic phase and blast crisis chronic myeloid leukemia. *Cancer Cell*. 2002;2(2):117-125.

133. Hofmann WK, Jones LC, Lemp NA, et al. Ph(+) acute lymphoblastic leukemia resistant to the tyrosine kinase inhibitor STI571 has a unique BCR-ABL gene mutation. *Blood*. 2002;99(5):1860-1862.

134. Barnes DJ, Palaiologou D, Panousopoulou E, et al. Bcr-Abl expression levels determine the rate of development of resistance to imatinib mesylate in chronic myeloid leukemia. *Cancer Res*. 2005;65(19):8912-8919.

135. Modi H, McDonald T, Chu S, Yee JK, Forman SJ, Bhatia R. Role of BCR/ABL gene-expression levels in determining the phenotype and imatinib sensitivity of transformed human hematopoietic cells. *Blood*. 2007;109(12):5411-5421.

136. Cowan-Jacob SW, Guez V, Fendrich G, et al. Imatinib (STI571) resistance in chronic myelogenous leukemia: molecular basis of the underlying mechanisms and potential strategies for treatment. *Mini Rev Med Chem*. 2004;4(3):285-299.

137. von Bubnoff N, Schneller F, Peschel C, Duyster J. BCR-ABL gene mutations in relation to clinical resistance of Philadelphia-chromosome-positive leukaemia to STI571: a prospective study. *Lancet*. 2002;359(9305):487-491.

138. Burger H, van Tol H, Brok M, et al. Chronic imatinib mesylate exposure leads to reduced intracellular drug accumulation by induction of the ABCG2 (BCRP) and ABCB1 (MDR1) drug transport pumps. *Cancer Biol Ther*. 2005;4(7):747-752.

139. Hirayama C, Watanabe H, Nakashima R, et al. Constitutive overexpression of P-glycoprotein, rather than breast cancer resistance protein or organic cation transporter 1, contributes to acquisition of imatinib-resistance in K562 cells. *Pharm Res*. 2008;25(4):827-835.

140. Widmer N, Colombo S, Buclin T, Decosterd LA. Functional consequence of MDR1 expression on imatinib intracellular concentrations. *Blood*. 2003;102(3):1142.

141. Ferrao PT, Frost MJ, Siah SP, Ashman LK. Overexpression of P-glycoprotein in K562 cells does not confer resistance to the growth inhibitory effects of imatinib (STI571) in vitro. *Blood*. 2003;102(13):4499-4503.

142. Zong Y, Zhou S, Sorrentino BP. Loss of P-glycoprotein expression in hematopoietic stem cells does not improve responses to imatinib in a murine model of chronic myelogenous leukemia. *Leukemia*. 2005;19(9):1590-1596.

143. Gardner ER, Sparreboom A, Verweij J, Figg WD. Lack of ABC transporter autoinduction in mice following long-term exposure to imatinib. *Cancer Biol Ther*. 2008;7(3):412-415.

144. Breedveld P, Pluim D, Cipriani G, et al. The effect of Bcrp1 (Abcg2) on the in vivo pharmacokinetics and brain penetration of imatinib mesylate (Gleevec): implications for the use of breast cancer resistance protein and P-glycoprotein inhibitors to enable the brain penetration of imatinib in patients. *Cancer Res*. 2005;65(7):2577-2582.

145. Dai H, Marbach P, Lemaire M, Hayes M, Elmquist WF. Distribution of STI-571 to the brain is limited by P-glycoprotein-mediated efflux. *J Pharmacol Exp Ther*. 2003;304(3):1085-1092.

146. Nakanishi T, Shiozawa K, Hassel BA, Ross DD. Complex interaction of BCRP/ABCG2 and imatinib in BCR-ABL-expressing cells: BCRP-mediated resistance to imatinib is attenuated by imatinib-induced reduction of BCRP expression. *Blood*. 2006;108(2):678-684.

147. Thomas J, Wang L, Clark RE, Pirmohamed M. Active transport of imatinib into and out of cells: implications for drug resistance. *Blood*. 2004;104(12):3739-3745.

148. Wang L, Giannoudis A, Lane S, Williamson P, Pirmohamed M, Clark RE. Expression of the uptake drug transporter hOCT1 is an important clinical determinant of the response to imatinib in chronic myeloid leukemia. *Clin Pharmacol Ther*. 2008;83(2):258-264.

149. Crossman LC, Druker BJ, Deininger MW, Pirmohamed M, Wang L, Clark RE. hOCT 1 and resistance to imatinib. *Blood*. 2005;106(3):1133-1134; author reply 1134.

150. White DL, Saunders VA, Dang P, et al. OCT-1-mediated influx is a key determinant of the intracellular uptake of imatinib but not nilotinib (AMN107): reduced OCT-1 activity is the cause of low in vitro sensitivity to imatinib. *Blood*. 2006;108(2):697-704.

151. White DL, Dang P, Engler J, et al. Functional activity of the OCT-1 protein is predictive of long-term outcome in patients with chronic-phase chronic myeloid leukemia treated with imatinib. *J Clin Oncol*. 2010;28(16):2761-2767.

152. White DL, Radich J, Soverini S, et al. Chronic phase chronic myeloid leukemia patients with low OCT-1 activity randomised to high-dose imatinib achieve better responses, and lower failure rates, than those randomized to standard-dose. *Haematologica*. 2011.

153. Brendel C, Scharenberg C, Dohse M, et al. Imatinib mesylate and nilotinib (AMN107) exhibit high-affinity interaction with ABCG2 on primitive hematopoietic stem cells. *Leukemia*. 2007;21(6):1267-1275.

154. Dohse M, Scharenberg C, Shukla S, et al. Comparison of ATP-binding cassette transporter interactions with the tyrosine kinase inhibitors imatinib, nilotinib, and dasatinib. *Drug Metab Dispos*. 2010;38(8):1371-1380.

155. Hegedus C, Ozvegy-Laczka C, Apati A, et al. Interaction of nilotinib, dasatinib and bosutinib with ABCB1 and ABCG2: implications for altered anti-cancer effects and pharmacological properties. *Br J Pharmacol*. 2009;158(4):1153-1164.

156. Yeatman TJ. A renaissance for SRC. *Nat Rev Cancer*. 2004;4(6):470-480.

157. Lionberger JM, Wilson MB, Smithgall TE. Transformation of myeloid leukemia cells to cytokine independence by Bcr-Abl is suppressed by kinase-defective Hck. *J Biol Chem*. 2000;275(24):18581-18585.

158. Warmuth M, Bergmann M, Priess A, Hauslmann K, Emmerich B, Hallek M. The Src family kinase Hck interacts with Bcr-Abl by a kinase-independent mechanism and phosphorylates the Grb2-binding site of Bcr. *J Biol Chem*. 1997;272(52):33260-33270.

159. Danhauser-Riedl S, Warmuth M, Druker BJ, Emmerich B, Hallek M. Activation of Src kinases p53/56lyn and p59hck by p210bcr/abl in myeloid cells. *Cancer Res*. 1996;56(15):3589-3596.

160. Meyn MA, 3rd, Wilson MB, Abdi FA, et al. Src family kinases phosphorylate the Bcr-Abl SH3-SH2 region and modulate Bcr-Abl transforming activity. *J Biol Chem*. 2006;281(41):30907-30916.

161. Hayette S, Chabane K, Michallet M, et al. Longitudinal studies of SRC family kinases in imatinib- and dasatinib-resistant chronic myelogenous leukemia patients. *Leuk Res*. 2011;35(1):38-43.

162. O'Bryan JP, Frye RA, Cogswell PC, et al. axl, a transforming gene isolated from primary human myeloid leukemia cells, encodes a novel receptor tyrosine kinase. *Mol Cell Biol*. 1991;11(10):5016-5031.

163. Caligiuri MA, Briesewitz R, Yu J, et al. Novel c-CBL and CBL-b ubiquitin ligase mutations in human acute myeloid leukemia. *Blood*. 2007;110(3):1022-1024.

164. Sargin B, Choudhary C, Crosetto N, et al. Flt3-dependent transformation by inactivating c-Cbl mutations in AML. *Blood*. 2007;110(3):1004-1012.

165. Miyoshi-Akiyama T, Aleman LM, Smith JM, Adler CE, Mayer BJ. Regulation of Cbl phosphorylation by the Abl tyrosine kinase and the Nck SH2/SH3 adaptor. *Oncogene*. 2001;20(30):4058-4069.

166. Deckert M, Elly C, Altman A, Liu YC. Coordinated regulation of the tyrosine phosphorylation of Cbl by Fyn and Syk tyrosine kinases. *J Biol Chem*. 1998;273(15):8867-8874.

167. Howlett CJ, Bisson SA, Resek ME, Tigley AW, Robbins SM. The proto-oncogene p120(Cbl) is a downstream substrate of the Hck protein-tyrosine kinase. *Biochem Biophys Res Commun*. 1999;257(1):129-138.

168. Pasquet JM GR, Treogat C, Lagarde V, Prouzet-Mauléon V, Lippert E, Sirvent A, Roche S, Mahon FX,. CBL downregulation plays a critical role in the increase of AXL and LYN tyrosine kinase levels mediating resistance of chronic myeloid leukemia cells to nilotinib. *EHA Meeting Abstracts*. 2012;97(Supplement 1):65.

169. Gambacorti-Passerini C, Zucchetti M, Russo D, et al. Alpha1 acid glycoprotein binds to imatinib (STI571) and substantially alters its pharmacokinetics in chronic myeloid leukemia patients. *Clin Cancer Res*. 2003;9(2):625-632.

170. Tanaka C, Yin OQ, Sethuraman V, et al. Clinical pharmacokinetics of the BCR-ABL tyrosine kinase inhibitor nilotinib. *Clin Pharmacol Ther*. 2010;87(2):197-203.

171. Hughes T, Saglio G, Branford S, et al. Impact of baseline BCR-ABL mutations on response to nilotinib in patients with chronic myeloid leukemia in chronic phase. *J Clin Oncol*. 2009;27(25):4204-4210.

172. Szakacs G, Varadi A, Ozvegy-Laczka C, Sarkadi B. The role of ABC transporters in drug absorption, distribution, metabolism, excretion and toxicity (ADME-Tox). *Drug Discov Today*. 2008;13(9-10):379-393.

173. Rees DC, Johnson E, Lewinson O. ABC transporters: the power to change. *Nat Rev Mol Cell Biol*. 2009;10(3):218-227.

174. Scharenberg CW, Harkey MA, Torok-Storb B. The ABCG2 transporter is an efficient Hoechst 33342 efflux pump and is preferentially expressed by immature human hematopoietic progenitors. *Blood*. 2002;99(2):507-512.

175. Zhou S, Schuetz JD, Bunting KD, et al. The ABC transporter Bcrp1/ABCG2 is expressed in a wide variety of stem cells and is a molecular determinant of the side-population phenotype. *Nat Med*. 2001;7(9):1028-1034.

176. Hegedus T, Orfi L, Seprodi A, Varadi A, Sarkadi B, Keri G. Interaction of tyrosine kinase inhibitors with the human multidrug transporter proteins, MDR1 and MRP1. *Biochim Biophys Acta*. 2002;1587(2-3):318-325.

177. White DL, Saunders VA, Dang P, et al. Most CML patients who have a suboptimal response to imatinib have low OCT-1 activity: higher doses of imatinib may overcome the negative impact of low OCT-1 activity. *Blood*. 2007;110(12):4064-4072.

178. Ozvegy-Laczka C, Hegedus T, Varady G, et al. High-affinity interaction of tyrosine kinase inhibitors with the ABCG2 multidrug transporter. *Mol Pharmacol*. 2004;65(6):1485-1495.

179. Burger H, van Tol H, Boersma AW, et al. Imatinib mesylate (STI571) is a substrate for the breast cancer resistance protein (BCRP)/ABCG2 drug pump. *Blood*. 2004;104(9):2940-2942.

180. Houghton PJ, Germain GS, Harwood FC, et al. Imatinib mesylate is a potent inhibitor of the ABCG2 (BCRP) transporter and reverses resistance to topotecan and SN-38 in vitro. *Cancer Res*. 2004;64(7):2333-2337.

181. Jordanides NE, Jorgensen HG, Holyoake TL, Mountford JC. Functional ABCG2 is overexpressed on primary CML CD34+ cells and is inhibited by imatinib mesylate. *Blood*. 2006;108(4):1370-1373.

182. Liu W, Baer MR, Bowman MJ, et al. The tyrosine kinase inhibitor imatinib mesylate enhances the efficacy of photodynamic therapy by inhibiting ABCG2. *Clin Cancer Res*. 2007;13(8):2463-2470.

183. Hiwase DK, Saunders V, Hewett D, et al. Dasatinib cellular uptake and efflux in chronic myeloid leukemia cells: therapeutic implications. *Clin Cancer Res*. 2008;14(12):3881-3888.

184. Giannoudis A, Davies A, Lucas CM, Harris RJ, Pirmohamed M, Clark RE. Effective dasatinib uptake may occur without human organic cation transporter 1 (hOCT1): implications for the treatment of imatinib-resistant chronic myeloid leukemia. *Blood*. 2008;112(8):3348-3354.

185. Lagas JS, van Waterschoot RA, van Tilburg VA, et al. Brain accumulation of dasatinib is restricted by P-glycoprotein (ABCB1) and breast cancer resistance protein (ABCG2) and can be enhanced by elacridar treatment. *Clin Cancer Res*. 2009;15(7):2344-2351.

186. Chen Y, Agarwal S, Shaik NM, Chen C, Yang Z, Elmquist WF. P-glycoprotein and breast cancer resistance protein influence brain distribution of dasatinib. *J Pharmacol Exp Ther*. 2009;330(3):956-963.

187. Davies A, Jordanides NE, Giannoudis A, et al. Nilotinib concentration in cell lines and primary CD34(+) chronic myeloid leukemia cells is not mediated by active uptake or efflux by major drug transporters. *Leukemia*. 2009.

188. Hiwase DK, White D, Zrim S, Saunders V, Melo JV, Hughes TP. Nilotinib-mediated inhibition of ABCB1 increases intracellular concentration of dasatinib in CML cells: implications for combination TKI therapy. *Leukemia*. 2010;24(3):658-660.

189. Tiwari AK, Sodani K, Wang SR, et al. Nilotinib (AMN107, Tasigna) reverses multidrug resistance by inhibiting the activity of the ABCB1/Pgp and ABCG2/BCRP/MXR transporters. *Biochem Pharmacol*. 2009;78(2):153-161.

190. Hazarika M, Jiang X, Liu Q, et al. Tasigna for chronic and accelerated phase Philadelphia chromosome--positive chronic myelogenous leukemia resistant to or intolerant of imatinib. *Clin Cancer Res*. 2008;14(17):5325-5331.

191. Bradeen HA, Eide CA, O'Hare T, et al. Comparison of imatinib mesylate, dasatinib (BMS-354825), and nilotinib (AMN107) in an N-ethyl-N-nitrosourea (ENU)-based mutagenesis screen: high efficacy of drug combinations. *Blood*. 2006;108(7):2332-2338.

192. Komarova NL, Wodarz D. Combination therapies against chronic myeloid leukemia: short-term versus long-term strategies. *Cancer Res*. 2009;69(11):4904-4910.

193. Weisberg E, Catley L, Wright RD, et al. Beneficial effects of combining nilotinib and imatinib in preclinical models of BCR-ABL+ leukemias. *Blood*. 2007;109(5):2112-2120.

194. White DL, Saunders VA, Quinn SR, Manley PW, Hughes TP. Imatinib increases the intracellular concentration of nilotinib, which may explain the observed synergy between these drugs. *Blood*. 2007;109(8):3609-3610.

195. Burgess MR, Skaggs BJ, Shah NP, Lee FY, Sawyers CL. Comparative analysis of two clinically active BCR-ABL kinase inhibitors reveals the role of conformation-specific binding in resistance. *Proc Natl Acad Sci U S A*. 2005;102(9):3395-3400.

196. Kantarjian HM, Baccarani M, Jabbour E, Saglio G, Cortes JE. Second-generation tyrosine kinase inhibitors: the future of frontline CML therapy. *Clin Cancer Res*. 2011;17(7):1674-1683.

197. Luciani F, Spada M, De Milito A, et al. Effect of proton pump inhibitor pretreatment on resistance of solid tumors to cytotoxic drugs. *J Natl Cancer Inst*. 2004;96(22):1702-1713.

198. Pauli-Magnus C, Rekersbrink S, Klotz U, Fromm MF. Interaction of omeprazole, lansoprazole and pantoprazole with P-glycoprotein. *Naunyn Schmiedebergs Arch Pharmacol*. 2001;364(6):551-557.

199. Suzuki K, Doki K, Homma M, et al. Co-administration of proton pump inhibitors delays elimination of plasma methotrexate in high-dose methotrexate therapy. *Br J Clin Pharmacol*. 2009;67(1):44-49.

200. White D, Saunders V, Quinn S, Manley P, Hughes T. Proton pump inhibitors interact with transport of both imatinib and nilotinib. *AACR Meeting Abstracts*. 2007;2007(1_Annual_Meeting):1635-.

201. Bogman K, Peyer AK, Torok M, Kusters E, Drewe J. HMG-CoA reductase inhibitors and P-glycoprotein modulation. *Br J Pharmacol*. 2001;132(6):1183-1192.

202. Sieczkowski E, Lehner C, Ambros PF, Hohenegger M. Double impact on p-glycoprotein by statins enhances doxorubicin cytotoxicity in human neuroblastoma cells. *International Journal of Cancer*. 2010;126(9):2025-2035.

203. Glodkowska-Mrowka E, Mrowka P, Winiarska M, et al. Statins Increase Antileukemic Potency of Imatinib Through the Inhibition of MDR/ABCB1 and BCRP/ABCG2 Drug Transporters Activity. *ASH Annual Meeting Abstracts*. 2011;118(21):2742-.

204. Lozzio CB, Lozzio BB. Human chronic myelogenous leukemia cell-line with positive Philadelphia chromosome. *Blood*. 1975;45(3):321-334.

205. Kubonishi I, Miyoshi I. Establishment of a Ph1 chromosome-positive cell line from chronic myelogenous leukemia in blast crisis. *Int J Cell Cloning*. 1983;1(2):105-117.

206. Kishi K. A new leukemia cell line with Philadelphia chromosome characterized as basophil precursors. *Leuk Res*. 1985;9(3):381-390.

207. Scherer WF, Syverton JT, Gey GO. Studies on the propagation in vitro of poliomyelitis viruses. IV. Viral multiplication in a stable strain of human malignant epithelial cells (strain HeLa) derived from an epidermoid carcinoma of the cervix. *J Exp Med*. 1953;97(5):695-710.

208. Knowles BB, Aden, David P. Human hepatoma derived cell line, process for preparation thereof, and uses therefor. US Patent 4,393,133. United States of America: The Wistar Institute Of Anatomy And Biology; 1983

209. Miller E. Apoptosis measurement by annexin v staining. *Methods Mol Med*. 2004;88:191-202.

210. White D, Saunders V, Lyons AB, et al. In vitro sensitivity to imatinib-induced inhibition of ABL kinase activity is predictive of molecular response in patients with de novo CML. *Blood*. 2005;106(7):2520-2526.

211. Branford S, Hughes TP, Rudzki Z. Monitoring chronic myeloid leukaemia therapy by real-time quantitative PCR in blood is a reliable alternative to bone marrow cytogenetics. *Br J Haematol*. 1999;107(3):587-599.

212. Branford S, Rudzki Z, Walsh S, et al. Detection of BCR-ABL mutations in patients with CML treated with imatinib is virtually always accompanied by clinical resistance, and mutations in the ATP phosphate-binding loop (P-loop) are associated with a poor prognosis. *Blood*. 2003;102(1):276-283.

213. Ahlin G, Chen L, Lazorova L, et al. Genotype-dependent effects of inhibitors of the organic cation transporter, OCT1: predictions of metformin interactions. *Pharmacogenomics J*. 2011;11(6):400-411.

214. Choi MK, Jin QR, Jin HE, et al. Effects of tetraalkylammonium compounds with different affinities for organic cation transporters on the pharmacokinetics of metformin. *Biopharm Drug Dispos*. 2007;28(9):501-510.

215. Bourdet DL, Pritchard JB, Thakker DR. Differential substrate and inhibitory activities of ranitidine and famotidine toward human organic cation transporter 1 (hOCT1; SLC22A1), hOCT2 (SLC22A2), and hOCT3 (SLC22A3). *J Pharmacol Exp Ther*. 2005;315(3):1288-1297.

216. Abolhoda A, Wilson AE, Ross H, Danenberg PV, Burt M, Scotto KW. Rapid activation of MDR1 gene expression in human metastatic sarcoma after in vivo exposure to doxorubicin. *Clin Cancer Res*. 1999;5(11):3352-3356.

217. Chaudhary PM, Roninson IB. Induction of multidrug resistance in human cells by transient exposure to different chemotherapeutic drugs. *J Natl Cancer Inst*. 1993;85(8):632-639.

218. Herzog CE, Tsokos M, Bates SE, Fojo AT. Increased mdr-1/P-glycoprotein expression after treatment of human colon carcinoma cells with P-glycoprotein antagonists. *J Biol Chem*. 1993;268(4):2946-2952.

219. Riva MA, Tascedda F, Lovati E, Racagni G. Regulation of NMDA receptor subunit messenger RNA levels in the rat brain following acute and chronic exposure to antipsychotic drugs. *Brain Res Mol Brain Res*. 1997;50(1-2):136-142.

220. Eytan GD, Regev R, Oren G, Assaraf YG. The role of passive transbilayer drug movement in multidrug resistance and its modulation. *J Biol Chem*. 1996;271(22):12897-12902.

221. Chen CJ, Chin JE, Ueda K, et al. Internal duplication and homology with bacterial transport proteins in the mdr1 (P-glycoprotein) gene from multidrug-resistant human cells. *Cell*. 1986;47(3):381-389.

222. Ambudkar SV, Dey S, Hrycyna CA, Ramachandra M, Pastan I, Gottesman MM. Biochemical, cellular, and pharmacological aspects of the multidrug transporter. *Annu Rev Pharmacol Toxicol*. 1999;39:361-398.

223. Gottesman MM, Fojo T, Bates SE. Multidrug resistance in cancer: role of ATP-dependent transporters. *Nat Rev Cancer*. 2002;2(1):48-58.

224. Sauna ZE, Ambudkar SV. Evidence for a requirement for ATP hydrolysis at two distinct steps during a single turnover of the catalytic cycle of human P-glycoprotein. *Proc Natl Acad Sci U S A*. 2000;97(6):2515-2520.

225. Garrigos M, Mir LM, Orlowski S. Competitive and non-competitive inhibition of the multidrug-resistance-associated P-glycoprotein ATPase--further experimental evidence for a multisite model. *Eur J Biochem*. 1997;244(2):664-673.

226. Shapiro AB, Ling V. Positively cooperative sites for drug transport by P-glycoprotein with distinct drug specificities. *Eur J Biochem*. 1997;250(1):130-137.

227. Martin C, Berridge G, Higgins CF, Mistry P, Charlton P, Callaghan R. Communication between multiple drug binding sites on P-glycoprotein. *Mol Pharmacol*. 2000;58(3):624-632.

228. Dey S, Ramachandra M, Pastan I, Gottesman MM, Ambudkar SV. Evidence for two nonidentical drug-interaction sites in the human P-glycoprotein. *Proc Natl Acad Sci U S A*. 1997;94(20):10594-10599.

229. Aller SG, Yu J, Ward A, et al. Structure of P-glycoprotein reveals a molecular basis for poly-specific drug binding. *Science*. 2009;323(5922):1718-1722.

230. Higgins CF. Multiple molecular mechanisms for multidrug resistance transporters. *Nature*. 2007;446(7137):749-757.

231. Doyle LA, Yang W, Abruzzo LV, et al. A multidrug resistance transporter from human MCF-7 breast cancer cells. *Proc Natl Acad Sci U S A*. 1998;95(26):15665-15670.

232. Staud F, Pavek P. Breast cancer resistance protein (BCRP/ABCG2). *Int J Biochem Cell Biol*. 2005;37(4):720-725.

233. Eckford PD, Sharom FJ. ABC efflux pump-based resistance to chemotherapy drugs. *Chem Rev*. 2009;109(7):2989-3011.

234. Dezi M, Fribourg PF, Di Cicco A, et al. The multidrug resistance half-transporter ABCG2 is purified as a tetramer upon selective extraction from membranes. *Biochim Biophys Acta*. 2010;1798(11):2094-2101.

235. McDevitt CA, Collins RF, Conway M, et al. Purification and 3D structural analysis of oligomeric human multidrug transporter ABCG2. *Structure*. 2006;14(11):1623-1632.

236. Xu J, Liu Y, Yang Y, Bates S, Zhang JT. Characterization of oligomeric human half-ABC transporter ATP-binding cassette G2. *J Biol Chem*. 2004;279(19):19781-19789.

237. Hazai E, Bikadi Z. Homology modeling of breast cancer resistance protein (ABCG2). *J Struct Biol*. 2008;162(1):63-74.

238. Clark R, Kerr ID, Callaghan R. Multiple drugbinding sites on the R482G isoform of the ABCG2 transporter. *Br J Pharmacol*. 2006;149(5):506-515.

239. Evers R, de Haas M, Sparidans R, et al. Vinblastine and sulfinpyrazone export by the multidrug resistance protein MRP2 is associated with glutathione export. *Br J Cancer*. 2000;83(3):375-383.

240. Flanagan SD, Cummins CL, Susanto M, Liu X, Takahashi LH, Benet LZ. Comparison of furosemide and vinblastine secretion from cell lines overexpressing multidrug resistance protein (P-glycoprotein) and multidrug resistance-associated proteins (MRP1 and MRP2). *Pharmacology*. 2002;64(3):126-134.

241. Doige CA, Yu X, Sharom FJ. ATPase activity of partially purified P-glycoprotein from multidrug-resistant Chinese hamster ovary cells. *Biochim Biophys Acta*. 1992;1109(2):149-160.

242. Raaijmakers MH, de Grouw EP, van der Reijden BA, de Witte TJ, Jansen JH, Raymakers RA. ABCB1 modulation does not circumvent drug extrusion from primitive leukemic progenitor cells and may preferentially target residual normal cells in acute myelogenous leukemia. *Clin Cancer Res*. 2006;12(11 Pt 1):3452-3458.

243. Ozvegy C, Litman T, Szakacs G, et al. Functional characterization of the human multidrug transporter, ABCG2, expressed in insect cells. *Biochem Biophys Res Commun*. 2001;285(1):111-117.

244. Boesch D, Gaveriaux C, Jachez B, Pourtier-Manzanedo A, Bollinger P, Loor F. In vivo circumvention of P-glycoprotein-mediated multidrug resistance of tumor cells with SDZ PSC 833. *Cancer Res*. 1991;51(16):4226-4233.

245. Boesch D, Muller K, Pourtier-Manzanedo A, Loor F. Restoration of daunomycin retention in multidrug-resistant P388 cells by submicromolar concentrations of SDZ PSC 833, a nonimmunosuppressive cyclosporin derivative. *Exp Cell Res*. 1991;196(1):26-32.

246. Blume H, Donath F, Warnke A, Schug BS. Pharmacokinetic drug interaction profiles of proton pump inhibitors. *Drug Saf*. 2006;29(9):769-784.

247. Breedveld P, Zelcer N, Pluim D, et al. Mechanism of the pharmacokinetic interaction between methotrexate and benzimidazoles: potential role for breast cancer resistance protein in clinical drug-drug interactions. *Cancer Res*. 2004;64(16):5804-5811.

248. Pauli-Magnus C, Murdter T, Godel A, et al. P-glycoprotein-mediated transport of digitoxin, alpha-methyldigoxin and beta-acetyldigoxin. *Naunyn Schmiedebergs Arch Pharmacol*. 2001;363(3):337-343.

249. Shi Z, Tiwari AK, Shukla S, et al. Sildenafil Reverses ABCB1- and ABCG2-Mediated Chemotherapeutic Drug Resistance. *Cancer Res*;71(8):3029-3041.

250. Dohse M, Scharenberg C, Shukla S, et al. Comparison of ATP-binding cassette transporter interactions with the tyrosine kinase inhibitors imatinib, nilotinib, and dasatinib. *Drug Metab Dispos*;38(8):1371-1380.

251. Hiwase DK, White D, Zrim S, Saunders V, Melo JV, Hughes TP. Nilotinib-mediated inhibition of ABCB1 increases intracellular concentration of dasatinib in CML cells: implications for combination TKI therapy. *Leukemia*;24(3):658-660.

252. Kerns EH, Di L. Drug-like properties : concepts, structure design and methods : from ADME to toxicity optimization. Amsterdam ; Boston: Academic Press; 2008.

253. White D, Dang P, Venables A, et al. ABCB1 Overexpression May Predispose Imatinib Treated CML Patients to the Development of Abl Kinase Domain Mutations, and May Be an Important Contributor to Acquired Resistance. *ASH Annual Meeting Abstracts*. 2006;108(11):2144-.

254. Druker BJ, Guilhot F, O'Brien SG, et al. Five-year follow-up of patients receiving imatinib for chronic myeloid leukemia. *N Engl J Med*. 2006;355(23):2408-2417.

255. De Braekeleer E, Douet-Guilbert N, Le Bris MJ, Morel F, De Braekeleer M. Translocation 3;21, trisomy 8, and duplication of the Philadelphia chromosome: a rare but recurrent cytogenetic pathway in the blastic phase of chronic myeloid leukemia. *Cancer Genet Cytogenet*. 2007;179(2):159-161.

256. Marega M, Piazza RG, Pirola A, et al. BCR and BCR-ABL regulation during myeloid differentiation in healthy donors and in chronic phase/blast crisis CML patients. *Leukemia*. 2010;24(8):1445-1449.

257. Morel F, Bris MJ, Herry A, et al. Double minutes containing amplified bcr-abl fusion gene in a case of chronic myeloid leukemia treated by imatinib. *Eur J Haematol*. 2003;70(4):235-239.

258. Barker PE. Double minutes in human tumor cells. *Cancer Genet Cytogenet*. 1982;5(1):81-94.

259. Jabbour E, Kantarjian H, Jones D, et al. Frequency and clinical significance of BCR-ABL mutations in patients with chronic myeloid leukemia treated with imatinib mesylate. *Leukemia*. 2006;20(10):1767-1773.

260. Muller MC, Cortes JE, Kim DW, et al. Dasatinib treatment of chronic-phase chronic myeloid leukemia: analysis of responses according to preexisting BCR-ABL mutations. *Blood*. 2009;114(24):4944-4953.

261. Ingley E. Src family kinases: regulation of their activities, levels and identification of new pathways. *Biochim Biophys Acta*. 2008;1784(1):56-65.

262. Summy JM, Gallick GE. Treatment for Advanced Tumors: Src Reclaims Center Stage. *Clinical Cancer Research*. 2006;12(5):1398-1401.

263. Okada M, Nada S, Yamanashi Y, Yamamoto T, Nakagawa H. CSK: a protein-tyrosine kinase involved in regulation of src family kinases. *Journal of Biological Chemistry*. 1991;266(36):24249-24252.

264. Sun G, Ramdas L, Wang W, Vinci J, McMurray J, Budde RJ. Effect of autophosphorylation on the catalytic and regulatory properties of protein tyrosine kinase Src. *Arch Biochem Biophys*. 2002;397(1):11-17.

265. Sun G, Sharma AK, Budde RJ. Autophosphorylation of Src and Yes blocks their inactivation by Csk phosphorylation. *Oncogene*. 1998;17(12):1587-1595.

266. Tegtmeyer N, Backert S. Role of Abl and Src family kinases in actin-cytoskeletal rearrangements induced by the Helicobacter pylori CagA protein. *Eur J Cell Biol*. 2011;90(11):880-890.

267. Liu E, Hjelle B, Bishop JM. Transforming genes in chronic myelogenous leukemia. *Proc Natl Acad Sci U S A*. 1988;85(6):1952-1956.

268. Neubauer A, Fiebeler A, Graham DK, et al. Expression of axl, a transforming receptor tyrosine kinase, in normal and malignant hematopoiesis. *Blood*. 1994;84(6):1931-1941.

269. Janssen JW, Schulz AS, Steenvoorden AC, et al. A novel putative tyrosine kinase receptor with oncogenic potential. *Oncogene*. 1991;6(11):2113-2120.

270. Hafizi S, Dahlback B. Signalling and functional diversity within the Axl subfamily of receptor tyrosine kinases. *Cytokine Growth Factor Rev*. 2006;17(4):295-304.

271. Craven RJ, Xu LH, Weiner TM, et al. Receptor tyrosine kinases expressed in metastatic colon cancer. *Int J Cancer*. 1995;60(6):791-797.

272. Zantek ND, Walker-Daniels J, Stewart J, et al. MCF-10A-NeoST: a new cell system for studying cell-ECM and cell-cell interactions in breast cancer. *Clin Cancer Res*. 2001;7(11):3640-3648.

273. Hafizi S, Alindri F, Karlsson R, Dahlback B. Interaction of Axl receptor tyrosine kinase with C1-TEN, a novel C1 domain-containing protein with homology to tensin. *Biochem Biophys Res Commun*. 2002;299(5):793-800.

274. Duta F, Ulanova M, Seidel D, et al. Differential expression of spleen tyrosine kinase Syk isoforms in tissues: Effects of the microbial flora. *Histochem Cell Biol*. 2006;126(4):495-505.

275. Hahn EA, Glendenning GA, Sorensen MV, et al. Quality of life in patients with newly diagnosed chronic phase chronic myeloid leukemia on imatinib versus interferon alfa plus low-dose cytarabine: results from the IRIS Study. *J Clin Oncol*. 2003;21(11):2138-2146.

276. Efremov DG, Laurenti L. The Syk kinase as a therapeutic target in leukemia and lymphoma. *Expert Opin Investig Drugs*. 2011;20(5):623-636.

277. Kurosaki T, Johnson SA, Pao L, Sada K, Yamamura H, Cambier JC. Role of the Syk autophosphorylation site and SH2 domains in B cell antigen receptor signaling. *J Exp Med*. 1995;182(6):1815-1823.

278. Zhang J, Kimura T, Siraganian RP. Mutations in the activation loop tyrosines of protein tyrosine kinase Syk abrogate intracellular signaling but not kinase activity. *J Immunol*. 1998;161(8):4366-4374.

279. Kurosaki T, Takata M, Yamanashi Y, et al. Syk activation by the Src-family tyrosine kinase in the B cell receptor signaling. *J Exp Med*. 1994;179(5):1725-1729.

280. Lupher ML, Jr., Rao N, Lill NL, et al. Cbl-mediated negative regulation of the Syk tyrosine kinase. A critical role for Cbl phosphotyrosine-binding domain binding to Syk phosphotyrosine 323. *J Biol Chem*. 1998;273(52):35273-35281.

281. van der Kolk DM, de Vries EG, Muller M, Vellenga E. The role of drug efflux pumps in acute myeloid leukemia. *Leuk Lymphoma*. 2002;43(4):685-701.

282. Rautio J, Humphreys JE, Webster LO, et al. In vitro p-glycoprotein inhibition assays for assessment of clinical drug interaction potential of new drug candidates: a recommendation for probe substrates. *Drug Metab Dispos*. 2006;34(5):786-792.

283. Shah NP, Sawyers CL. Mechanisms of resistance to STI571 in Philadelphia chromosome-associated leukemias. *Oncogene*. 2003;22(47):7389-7395.

284. Cisternino S, Mercier C, Bourasset F, Roux F, Scherrmann JM. Expression, up-regulation, and transport activity of the multidrug-resistance protein Abcg2 at the mouse blood-brain barrier. *Cancer Res*. 2004;64(9):3296-3301.

285. Garg RJ, Kantarjian H, O'Brien S, et al. The use of nilotinib or dasatinib after failure to 2 prior tyrosine kinase inhibitors: long-term follow-up. *Blood*. 2009;114(20):4361-4368.

286. Traer E, MacKenzie R, Snead J, et al. Blockade of JAK2-mediated extrinsic survival signals restores sensitivity of CML cells to ABL inhibitors. *Leukemia*. 2012;26(5):1140-1143.

287. Nair RR, Tolentino JH, Argilagos RF, Zhang L, Pinilla-Ibarz J, Hazlehurst LA. Potentiation of Nilotinib-mediated cell death in the context of the bone marrow microenvironment requires a promiscuous JAK inhibitor in CML. *Leuk Res*. 2012;36(6):756-763.

288. Burchert A, Wang Y, Cai D, et al. Compensatory PI3-kinase/Akt/mTor activation regulates imatinib resistance development. *Leukemia*. 2005;19(10):1774-1782.

289. Wang Y, Cai D, Brendel C, et al. Adaptive secretion of granulocyte-macrophage colony-stimulating factor (GM-CSF) mediates imatinib and nilotinib resistance in BCR/ABL+ progenitors via JAK-2/STAT-5 pathway activation. *Blood*. 2007;109(5):2147-2155.

290. O'Hare T, Deininger MW, Eide CA, Clackson T, Druker BJ. Targeting the BCR-ABL signaling pathway in therapy-resistant Philadelphia chromosome-positive leukemia. *Clin Cancer Res*. 2011;17(2):212-221.

291. Lipka DB, Wagner MC, Dziadosz M, et al. Intracellular retention of ABL kinase inhibitors determines commitment to apoptosis in CML cells. *PLoS One*. 2012;7(7):e40853.

292. Ostman A, Heldin CH. Involvement of platelet-derived growth factor in disease: development of specific antagonists. *Adv Cancer Res*. 2001;80:1-38.

293. Apperley JF, Gardembas M, Melo JV, et al. Response to imatinib mesylate in patients with chronic myeloproliferative diseases with rearrangements of the platelet-derived growth factor receptor beta. *N Engl J Med*. 2002;347(7):481-487.

294. White DL, Eadie LN, Saunders VA, Hiwase DK, Hughes TP. Proton pump inhibitors significantly increase the intracellular concentration of nilotinib, but not imatinib in target CML cells. *Leukemia*. 2012.

295. Yin OQ, Giles FJ, Baccarani M, et al. Concurrent use of proton pump inhibitors or H2 blockers did not adversely affect nilotinib efficacy in patients with chronic myeloid leukemia. *Cancer Chemother Pharmacol*. 2012;70(2):345-350.

296. Oda T, Heaney C, Hagopian JR, Okuda K, Griffin JD, Druker BJ. Crkl is the major tyrosine-phosphorylated protein in neutrophils from patients with chronic myelogenous leukemia. *J Biol Chem*. 1994;269(37):22925-22928.

297. White D, Saunders V, Grigg A, et al. Measurement of in vivo BCR-ABL kinase inhibition to monitor imatinib-induced target blockade and predict response in chronic myeloid leukemia. *J Clin Oncol*. 2007;25(28):4445-4451.

298. La Rosee P, Holm-Eriksen S, Konig H, et al. Phospho-CRKL monitoring for the assessment of BCR-ABL activity in imatinib-resistant chronic myeloid leukemia or Ph+ acute lymphoblastic leukemia patients treated with nilotinib. *Haematologica*. 2008;93(5):765-769.

299. Shibata M, Ezoe S, Oritani K, et al. Predictability of the response to tyrosine kinase inhibitors via in vitro analysis of Bcr-Abl phosphorylation. *Leuk Res*. 2011;35(9):1205-1211.

300. Heinrich MC, Corless CL, Duensing A, et al. PDGFRA activating mutations in gastrointestinal stromal tumors. *Science*. 2003;299(5607):708-710.

301. Erben P, Gosenca D, Muller MC, et al. Screening for diverse PDGFRA or PDGFRB fusion genes is facilitated by generic quantitative reverse transcriptase polymerase chain reaction analysis. *Haematologica*. 2010;95(5):738-744.

302. Baxter EJ, Hochhaus A, Bolufer P, et al. The t(4;22)(q12;q11) in atypical chronic myeloid leukaemia fuses BCR to PDGFRA. *Hum Mol Genet*. 2002;11(12):1391-1397.

303. Gotlib J, Cools J, Malone JM, 3rd, Schrier SL, Gilliland DG, Coutre SE. The FIP1L1-PDGFRalpha fusion tyrosine kinase in hypereosinophilic syndrome and chronic eosinophilic leukemia: implications for diagnosis, classification, and management. *Blood*. 2004;103(8):2879-2891.

304. Cassier PA, Fumagalli E, Rutkowski P, et al. Outcome of Patients with Platelet-Derived Growth Factor Receptor Alpha-Mutated Gastrointestinal Stromal Tumors in the Tyrosine Kinase Inhibitor Era. *Clin Cancer Res*. 2012;18(16):4458-4464.

305. Lyle AN, Griendling KK. Modulation of vascular smooth muscle signaling by reactive oxygen species. *Physiology (Bethesda)*. 2006;21:269-280.

306. Ichijo H, Nishida E, Irie K, et al. Induction of apoptosis by ASK1, a mammalian MAPKKK that activates SAPK/JNK and p38 signaling pathways. *Science*. 1997;275(5296):90-94.

307. Yamamoto K, Ichijo H, Korsmeyer SJ. BCL-2 is phosphorylated and inactivated by an ASK1/Jun N-terminal protein kinase pathway normally activated at G(2)/M. *Mol Cell Biol*. 1999;19(12):8469-8478.

308. Sodani K, Patel A, Kathawala RJ, Chen ZS. Multidrug resistance associated proteins in multidrug resistance. *Chin J Cancer*. 2012;31(2):58-72.

309. Kool M, van der Linden M, de Haas M, Baas F, Borst P. Expression of human MRP6, a homologue of the multidrug resistance protein gene MRP1, in tissues and cancer cells. *Cancer Res*. 1999;59(1):175-182.

310. Scheffer GL, Hu X, Pijnenborg AC, Wijnholds J, Bergen AA, Scheper RJ. MRP6 (ABCC6) detection in normal human tissues and tumors. *Lab Invest*. 2002;82(4):515-518.

311. Nishimura M, Naito S. Tissue-specific mRNA expression profiles of human ATP-binding cassette and solute carrier transporter superfamilies. *Drug Metab Pharmacokinet*. 2005;20(6):452-477.

312. Belinsky MG, Chen ZS, Shchaveleva I, Zeng H, Kruh GD. Characterization of the drug resistance and transport properties of multidrug resistance protein 6 (MRP6, ABCC6). *Cancer Res*. 2002;62(21):6172-6177.

313. Chen ZS, Tiwari AK. Multidrug resistance proteins (MRPs/ABCCs) in cancer chemotherapy and genetic diseases. *FEBS J*. 2011;278(18):3226-3245.

314. Fulop K, Barna L, Symmons O, Zavodszky P, Varadi A. Clustering of disease-causing mutations on the domain-domain interfaces of ABCC6. *Biochem Biophys Res Commun*. 2009;379(3):706-709.

315. Dean M, Annilo T. Evolution of the ATP-binding cassette (ABC) transporter superfamily in vertebrates. *Annu Rev Genomics Hum Genet*. 2005;6:123-142.

316. De Milito A, Luciani F, Fais S. How to Overcome Cisplatin Resistance Through Proton Pump Inhibitors. In: Bonetti A, Leone R, Muggia F, Howell S, eds. Platinum and Other Heavy Metal Compounds in Cancer Chemotherapy: Humana Press; 2009:109-114.

317. Senn-Bilfinger J, Sturm E. The Development of a New Proton-Pump Inhibitor: The Case History of Pantoprazole. Analogue-based Drug Discovery: Wiley-VCH Verlag GmbH & Co. KGaA; 2006:115-136.

318. Oostendorp RL, Buckle T, Beijnen JH, van Tellingen O, Schellens JH. The effect of P-gp (Mdr1a/1b), BCRP (Bcrp1) and P-gp/BCRP inhibitors on the in vivo absorption, distribution, metabolism and excretion of imatinib. *Invest New Drugs*. 2009;27(1):31-40.

319. Marchetti S, Oostendorp RL, Pluim D, et al. In vitro transport of gimatecan (7-t-butoxyiminomethylcamptothecin) by breast cancer resistance protein, P-glycoprotein, and multidrug resistance protein 2. *Mol Cancer Ther*. 2007;6(12 Pt 1):3307-3313.

320. Zhang L, Schaner ME, Giacomini KM. Functional characterization of an organic cation transporter (hOCT1) in a transiently transfected human cell line (HeLa). *J Pharmacol Exp Ther*. 1998;286(1):354-361.

321. Choo EF, Leake B, Wandel C, et al. Pharmacological inhibition of P-glycoprotein transport enhances the distribution of HIV-1 protease inhibitors into brain and testes. *Drug Metab Dispos*. 2000;28(6):655-660.

322. Mayer U, Wagenaar E, Dorobek B, Beijnen JH, Borst P, Schinkel AH. Full blockade of intestinal P-glycoprotein and extensive inhibition of blood-brain barrier P-glycoprotein by oral treatment of mice with PSC833. *J Clin Invest*. 1997;100(10):2430-2436.

323. Smith AJ, van Helvoort A, van Meer G, et al. MDR3 P-glycoprotein, a phosphatidylcholine translocase, transports several cytotoxic drugs and directly interacts with drugs as judged by interference with nucleotide trapping. *J Biol Chem*. 2000;275(31):23530-23539.

324. Luo FR, Paranjpe PV, Guo A, Rubin E, Sinko P. Intestinal transport of irinotecan in Caco-2 cells and MDCK II cells overexpressing efflux transporters Pgp, cMOAT, and MRP1. *Drug Metab Dispos*. 2002;30(7):763-770.

325. Leier I, Jedlitschky G, Buchholz U, Cole SP, Deeley RG, Keppler D. The MRP gene encodes an ATP-dependent export pump for leukotriene C4 and structurally related conjugates. *J Biol Chem*. 1994;269(45):27807-27810.

326. Wong IL, Chan KF, Tsang KH, et al. Modulation of multidrug resistance protein 1 (MRP1/ABCC1)-mediated multidrug resistance by bivalent apigenin homodimers and their derivatives. *J Med Chem*. 2009;52(17):5311-5322.

327. Zeng H, Chen ZS, Belinsky MG, Rea PA, Kruh GD. Transport of methotrexate (MTX) and folates by multidrug resistance protein (MRP) 3 and MRP1: effect of polyglutamylation on MTX transport. *Cancer Res*. 2001;61(19):7225-7232.

328. Chen ZS, Lee K, Walther S, et al. Analysis of methotrexate and folate transport by multidrug resistance protein 4 (ABCC4): MRP4 is a component of the methotrexate efflux system. *Cancer Res*. 2002;62(11):3144-3150.

329. Bai J, Lai L, Yeo HC, Goh BC, Tan TM. Multidrug resistance protein 4 (MRP4/ABCC4) mediates efflux of bimane-glutathione. *Int J Biochem Cell Biol*. 2004;36(2):247-257.

330. Hong J, Lambert JD, Lee SH, Sinko PJ, Yang CS. Involvement of multidrug resistance-associated proteins in regulating cellular levels of (-)-epigallocatechin-3-gallate and its methyl metabolites. *Biochem Biophys Res Commun*. 2003;310(1):222-227.

331. Ilias A, Urban Z, Seidl TL, et al. Loss of ATP-dependent transport activity in pseudoxanthoma elasticum-associated mutants of human ABCC6 (MRP6). *J Biol Chem*. 2002;277(19):16860-16867.

332. Bakos E, Evers R, Sinko E, Varadi A, Borst P, Sarkadi B. Interactions of the human multidrug resistance proteins MRP1 and MRP2 with organic anions. *Mol Pharmacol*. 2000;57(4):760-768.

333. Issandou M, Grand-Perret T. Multidrug resistance P-glycoprotein is not involved in cholesterol esterification. *Biochem Biophys Res Commun*. 2000;279(2):369-377.

334. Horikawa M, Kato Y, Tyson CA, Sugiyama Y. The potential for an interaction between MRP2 (ABCC2) and various therapeutic agents: probenecid as a candidate inhibitor of the biliary excretion of irinotecan metabolites. *Drug Metab Pharmacokinet*. 2002;17(1):23-33.

335. Nozaki Y, Kusuhara H, Kondo T, et al. Species difference in the inhibitory effect of nonsteroidal anti-inflammatory drugs on the uptake of methotrexate by human kidney slices. *J Pharmacol Exp Ther*. 2007;322(3):1162-1170.

336. Zamek-Gliszczynski MJ, Xiong H, Patel NJ, Turncliff RZ, Pollack GM, Brouwer KL. Pharmacokinetics of 5 (and 6)-carboxy-2',7'-dichlorofluorescein and its diacetate promoiety in the liver. *J Pharmacol Exp Ther*. 2003;304(2):801-809.

337. Reid G, Wielinga P, Zelcer N, et al. The human multidrug resistance protein MRP4 functions as a prostaglandin efflux transporter and is inhibited by nonsteroidal antiinflammatory drugs. *Proc Natl Acad Sci U S A*. 2003;100(16):9244-9249.

338. Reid G, Wielinga P, Zelcer N, et al. Characterization of the transport of nucleoside analog drugs by the human multidrug resistance proteins MRP4 and MRP5. *Mol Pharmacol*. 2003;63(5):1094-1103.

339. Rius M, Nies AT, Hummel-Eisenbeiss J, Jedlitschky G, Keppler D. Cotransport of reduced glutathione with bile salts by MRP4 (ABCC4) localized to the basolateral hepatocyte membrane. *Hepatology*. 2003;38(2):374-384.

340. van Aubel RA, Smeets PH, Peters JG, Bindels RJ, Russel FG. The MRP4/ABCC4 gene encodes a novel apical organic anion transporter in human kidney proximal tubules: putative efflux pump for urinary cAMP and cGMP. *J Am Soc Nephrol*. 2002;13(3):595-603.

341. Jedlitschky G, Burchell B, Keppler D. The multidrug resistance protein 5 functions as an ATP-dependent export pump for cyclic nucleotides. *J Biol Chem*. 2000;275(39):30069-30074.

342. Chen ZS, Guo Y, Belinsky MG, Kotova E, Kruh GD. Transport of bile acids, sulfated steroids, estradiol 17-beta-D-glucuronide, and leukotriene C4 by human multidrug resistance protein 8 (ABCC11). *Mol Pharmacol*. 2005;67(2):545-557.

343. Jain KS, Shah AK, Bariwal J, et al. Recent advances in proton pump inhibitors and management of acid-peptic disorders. *Bioorg Med Chem*. 2007;15(3):1181-1205.

344. Slater LM, Sweet P, Stupecky M, Gupta S. Cyclosporin A reverses vincristine and daunorubicin resistance in acute lymphatic leukemia in vitro. *J Clin Invest*. 1986;77(4):1405-1408.

345. Tsuruo T, Iida H, Tsukagoshi S, Sakurai Y. Overcoming of vincristine resistance in P388 leukemia in vivo and in vitro through enhanced cytotoxicity of vincristine and vinblastine by verapamil. *Cancer Res*. 1981;41(5):1967-1972.

346. Friedenberg WR, Rue M, Blood EA, et al. Phase III study of PSC-833 (valspodar) in combination with vincristine, doxorubicin, and dexamethasone (valspodar/VAD) versus VAD alone in patients with recurring or refractory multiple myeloma (E1A95). *Cancer*. 2006;106(4):830-838.

347. Fox E, Bates SE. Tariquidar (XR9576): a P-glycoprotein drug efflux pump inhibitor. *Expert Rev Anticancer Ther*. 2007;7(4):447-459.

348. Belpomme D, Gauthier S, Pujade-Lauraine E, et al. Verapamil increases the survival of patients with anthracycline-resistant metastatic breast carcinoma. *Ann Oncol*. 2000;11(11):1471-1476.

349. Millward MJ, Cantwell BM, Munro NC, Robinson A, Corris PA, Harris AL. Oral verapamil with chemotherapy for advanced non-small cell lung cancer: a randomised study. *Br J Cancer*. 1993;67(5):1031-1035.

350. Wattel E, Solary E, Hecquet B, et al. Quinine improves the results of intensive chemotherapy in myelodysplastic syndromes expressing P glycoprotein: results of a randomized study. *Br J Haematol*. 1998;102(4):1015-1024.

351. List AF, Kopecky KJ, Willman CL, et al. Benefit of cyclosporine modulation of drug resistance in patients with poor-risk acute myeloid leukemia: a Southwest Oncology Group study. *Blood*. 2001;98(12):3212-3220.

352. Geus WP, Mathot RA, Mulder PG, Lamers CB. Pharmacodynamics and kinetics of omeprazole MUPS 20 mg and pantoprazole 40 mg during repeated oral administration in Helicobacter pylori-negative subjects. *Aliment Pharmacol Ther*. 2000;14(8):1057-1064.

353. Wohrer S, Bartsch R, Hejna M, Drach J, Raderer M. Routine application of the proton-pump inhibitor pantoprazole in patients with gastric lymphoma undergoing chemotherapy. *Scand J Gastroenterol*. 2005;40(10):1222-1225.

354. Eadie LN, Saunders VA, Hughes TP, White DL. Degree of kinase inhibition achieved in vitro by imatinib and nilotinib is decreased by high levels of ABCB1 but not ABCG2. *Leuk Lymphoma*. 2012.

355. Jiang X, Zhao Y, Smith C, et al. Chronic myeloid leukemia stem cells possess multiple unique features of resistance to BCR-ABL targeted therapies. *Leukemia*. 2007;21(5):926-935.

356. Loscher W, Potschka H. Blood-brain barrier active efflux transporters: ATP-binding cassette gene family. *NeuroRx*. 2005;2(1):86-98.

357. Altintas A, Cil T, Kilinc I, Kaplan MA, Ayyildiz O. Central nervous system blastic crisis in chronic myeloid leukemia on imatinib mesylate therapy: a case report. *J Neurooncol*. 2007;84(1):103-105.

358. Murata K, Mitsuoka K, Hirai T, et al. Structural determinants of water permeation through aquaporin-1. *Nature*. 2000;407(6804):599-605.

359. Sui H, Han BG, Lee JK, Walian P, Jap BK. Structural basis of water-specific transport through the AQP1 water channel. *Nature*. 2001;414(6866):872-878.

360. Wspalz T, Fujiyoshi Y, Engel A. The AQP Structure and Functional Implications. In: Beitz E, ed. Aquaporins. Vol. 190: Springer Berlin Heidelberg; 2009:31-56.

361. Hoque MO, Soria JC, Woo J, et al. Aquaporin 1 is overexpressed in lung cancer and stimulates NIH-3T3 cell proliferation and anchorage-independent growth. *Am J Pathol*. 2006;168(4):1345-1353.

362. Moon C, Soria JC, Jang SJ, et al. Involvement of aquaporins in colorectal carcinogenesis. *Oncogene*. 2003;22(43):6699-6703.

363. Zhou SF, Wang LL, Di YM, et al. Substrates and inhibitors of human multidrug resistance associated proteins and the implications in drug development. *Curr Med Chem*. 2008;15(20):1981-2039.

364. Szakacs Z, Beni S, Varga Z, Orfi L, Keri G, Noszal B. Acid-base profiling of imatinib (gleevec) and its fragments. *J Med Chem*. 2005;48(1):249-255.

365. Gomez-Almaguer D, Tarin-Arzaga L, Cantu-Rodriguez O, Ceballos-Lopez A. More about Imatinib and Nilotinib Combination Therapy in Chronic Myeloid Leukemia. *Acta Haematol*. 2013;129(1):18-19.

366. Zhu GR, Ji O, Ji JM, et al. Combining nilotinib and imatinib improves the outcome of imatinib-resistant blast phase CML. *Acta Haematol*. 2012;127(3):152-155.